Implications of Airflow Dynamics and Soft-Tissue Reconstructions for the Heat Exchange Potential of Dinosaur Nasal Passages

A dissertation presented to

the faculty of

the College of Arts and Sciences of Ohio University

In partial fulfillment

of the requirements for the degree

Doctor of Philosophy

Jason Michael Bourke

December 2015

This dissertation titled

Implications of Airflow Dynamics and Soft-Tissue Reconstructions for the Heat Exchange Potential of Dinosaur Nasal Passages

by

JASON MICHAEL BOURKE

has been approved for

the Department of Biological Sciences

and the College of Arts and Sciences by

Lawrence M. Witmer

Professor of Biomedical Sciences

Robert Frank

Dean, College of Arts and Sciences

ABSTRACT

BOURKE, JASON MICHAEL, Ph.D., December 2015, Biological Sciences

Implications of Airflow Dynamics and Soft-Tissue Reconstructions for the Heat Exchange Potential of Dinosaur Nasal Passages

Director of Dissertation: Lawrence M. Witmer

This study seeks to restore the internal anatomy within the nasal passages of dinosaurs via the use of comparative anatomical methods along with computational fluid dynamic simulations. Nasal airway descriptions and airflow simulations are described for extant birds, crocodylians, and lizards. These descriptions served as a baseline for airflow within the nasal passages of diapsids. The presence of shared airflow and soft-tissue properties found in the nasal passages of extant diapsids, were used to restore soft tissues within the airways of dinosaurs, under the assumption that biologically unfeasible airflow patterns (e.g., lack of air movement in olfactory recess) can serve as signals for missing soft tissues. This methodology was tested on several dinosaur taxa. Restored airways in some taxa, revealed the potential presence and likely shape of nasal turbinates. Heat transfer efficiency was tested in two dinosaur species with elaborated nasal passages. Results of that analysis revealed that dinosaur noses were efficient heat exchangers that likely played an integral role in maintaining cephalic thermoregulation. Brain cooling via nasal expansion appears to have been necessary for dinosaurs to have achieved their immense body sizes without overheating their brains.

DEDICATION

This work is dedicated to my love, Sydney, who supported and encouraged me through the most difficult parts of this endeavour. To my mother, Joan Page, and the rest of my family who always encouraged me to fulfill my dream. Lastly to Chip, who has shared in this adventure from the start.

ACKNOWLEDGMENTS

This work would not have been possible without the wisdom, guidance and generosity of my advisor and friend, Larry Witmer. He took a chance on me despite the non-traditional way in which I joined the lab. His support and attention to detail—both on the page and in the images—helped make me into the professional that I am today. Thanks to my dissertation committee members: Larry Witmer, Patrick O'Connor, Steve Reilly, and John Cotton for ushering me through the dissertation process. For donation of specimens I would like to thank S. Reilly, P. O'Connor, W. Roosenburg, S. Montuelle, E. Schachner, T. Lyson, P. Bell, and C.G. Farmer. Many thanks to the Rockefeller Wildlife Refuge and Miami Metro Zoo for donations of specimens. I wish to extend thanks to the many collections managers and curators who provided access to fossils and wet specimens, all of which were invaluable to this study. P. Sereno, R. Masek (U. Chicago), M. Norell, and C. Mehling (AMNH), D. Berman and A. Henrichi (CM), K. Padian and P. Holroyd (UCMP), J. Gauthier and D. Brinkman (YPM), G. Watkin-Colwell (YPM), W. Simpson (FMNH), M. Carrano and M.K. Brett-Surman (NMNH), R. Irmis (NHMU), and K. Seymour and D. Evans (ROM). Special thanks to H. Rockhold (Ohio Health O'Blenness) and R. Ridgely (OUμCT) for access to and help with CT scanning. Thanks to WitmerLab members: D. Dufeau, W.R. Porter, E. Snively, A. Morhardt, C. Early, D. Cerio, J. Nassif. for useful discussions and help with hypothesis testing and synthesizing. Thanks to D. Harper for helping with some equations. Thanks to E. Gorscak, R. Felice, H. O'Brien and the rest of the BIOS graduate students for providing useful discussions and a welcoming atmosphere of collaboration and comradery. Funding for this project

was provided by a National Science Foundation Graduate Research Fellowship, Jurassic Foundation Grant, Welles Fund, Ohio University Student Enhancement Award, and Original Work Grants.

TABLE OF CONTENTS

Page

LIST OF TABLES

LIST OF FIGURES

CHAPTER 1 : RECONSTRUCTING DINOSAUR NASAL AIRFLOW AND TESTING ITS EFFICACY AT HEAT TRANSFER DURING RESPIRATION

Abstract

Dinosaur nasal passages show signs of enhancement and elaboration that appear to relate to the evolution of large body sizes. Previous research has suggested that this relationship was connected to handling the thermal stresses associated with large body size. In contrast, other authors have argued that dinosaur nasal passages were too small to house respiratory turbinates, leading these authors to conclude that dinosaur noses were probably ineffective heat exchange devices. Testing these hypotheses requires knowledge of how air moves through the nasal passages of the extant relatives of dinosaurs (birds, crocodylians, and lizards). We used computational fluid dynamics to simulate the movement of air through the nasal passages of extant diapsids where we observed similar airflow patterns that could be used to aid reconstructions of dinosaur noses. Using these data, we analyzed airflow patterns in the pachycephalosaurian dinosaur *Stegoceras validum*. Both anatomical evidence and fluid dynamic analysis revealed the potential presence of a soft-tissue respiratory turbinate in this taxon. Moreover, heat transfer analysis was performed on two large armored dinosaurs, *Panoplosaurus mirus* and *Euoplocephalus tutus*. Results of these analyses found support for the hypothesis that nasal passage elaboration played an integral role in conditioning the respired air field. Heat and water savings in these large dinosaurs were found to be on par with many extant amniotes, suggesting that nasal passage elongation and convolution is a viable alternative to respiratory turbinates. The unique body plan of dinosaurs—large bodies with small

brains—likely necessitated the evolution of a highly effective air conditioning system as a means of keeping dinosaur brains from overheating. Our results suggest that dinosaurs did have low ventilation rates, but that ventilation rate may be more suggestive of a particular respiration style rather than metabolism. Nasal elaboration for brain cooling may have been exapted for auxiliary functions in some dinosaur groups such as hadrosaurs.

Glossary

Bony-bounded nasal passage: A reconstructed nasal passage that is based solely on the outer, bony boundaries of the nasal passage.

Bony narial aperture: The bony rim of the nasal cavity that houses the nostril and portions of the nasal passage (Baumel 1993; Waibl et al. 2012).

Cavum nasi proprium: The portion of the nasal passage between the nasal vestibule and the nasopharyngeal duct (Figure 1-1; Parsons 1959). The cavum nasi proprium (CNP; "nasal cavity proper" in English) houses most of the nasal conchae as well as the olfactory recess.

Concha: Mucociliated structures that cloak the underlying turbinates. Conchae directly interact with the respired air field.

Ectonaris: The portion of the nasal cavity that includes both the bony narial aperture as well as the narial fossa on the surrounding bones, equivalent to the bony nostril sensu Witmer (2001).

Endonaris: Equivalent to the bony narial aperture (see bony narial aperture).

Laminarity: The orderly arrangement of fluid streams caused by a dominance of viscous forces over inertial forces.

Mucosa: A well-vascularized lining of epithelia and connective tissue that aids in retaining body moisture and provides protection against pathogens.

Naris: The fleshy nostril sensu Witmer (2001) and comprised of the opening in the skin leading into the nasal vestibule (Baumel 1993; Waibl et al. 2012).

Narial fossa: A depression located on the bones surrounding the rostroventral portion of the bony narial aperture, forming an extension of the nasal passage.

Nasal airway: The inner-most region of the nasal passage, where the respired air field travels.

Nasal capsule: The cartilaginous housing for the nasal passage. Located immediately deep to the bones forming the nasal cavity and covered internally by the nasal mucosa.

Nasal cavity: In the context of this project, we refer only to the hard-tissue boundaries of the nasal passage (i.e., the bones comprising the nasal passage) as the "nasal cavity," although the same term has been applied to the soft-tissue components (FCAT 1998) and both the hard and soft-tissue components (Baumel 1993; Waibl et al. 2012).

Nasal passage: The portion of the respiratory system consisting of the soft and hard tissues between the nostril and choana, bounded by bones of the premaxillae, maxillae, nasals, palatines, vomers, prefrontal, and lacrimals.

Nasal vestibule: The rostralmost portion of the nasal passage, just deep to the nostril (Figure 1-1; Parson, 1959). Often tubular in shape, the nasal vestibule varies in length

and complexity from species to species. The caudal terminus of the nasal vestibule is the entrance to the cavum nasi proprium.

Nasopharyngeal duct: The structure located between the CNP and the choana (Figure 1-1; Parsons, 1959). Nasopharyngeal duct length varies between species.

Olfactory recess: A portion of the CNP that strictly houses olfactory epithelium. The olfactory recess is variably located away from the main flow of air, forming a cul-de-sac of the nasal passage where olfaction can take place (Figure 1-1).

Reynolds Number: A dimensionless ratio between the viscous and inertial forces in a fluid dynamic system (Vogel 1994). The Reynolds number provides an estimate of when a fluid flow will be laminar or turbulent.

Soft-tissue bounded nasal passage: A reconstructed nasal passage that uses both the hard- and soft-tissue boundaries of the nasal passage (i.e., how the airway looks in life).

Turbinate: Thin scrolls of bone or cartilage that invade the nasal passage, increasing available surface area for mucosa. Turbinates function as scaffolding for conchae.

Turbulence: The chaotic movement of a fluid caused by an imbalance between inertial and viscous forces. Turbulent fluids form random vortices that impede a fluid's forward motion by increasing fluid resistance.

Introduction

A hallmark of Dinosauria is the immense body size of many of its members. Many species of dinosaur routinely reached body mass estimates in excess of 2 tonnes, greatly surpassing average body mass estimates for other amniote groups in any time in Earth history. Dinosauria as a whole has shown a trend towards large body size

(O'Gorman and Hone 2012). Witmer and Sampson (1999; see also Witmer 2001) observed a similar trend in dinosaur nasal passages. Large dinosaur species tended to have enhanced nasal passages as indicated by the expansion of the nasal cavity, especially the rostral portions of the nasal cavity (Figure 1-2). Enhanced nasal passages evolved at least four different times within Dinosauria (Hadrosauroidea, Ceratopsidae, Ankylosauria, and Eusauropoda), suggesting the presence of a common evolutionary pressure. Previous hypotheses, such as snorkels (Romer 1945; Colbert 1955), or trunks (Bakker 1971, 1986; Coombs 1975) have neither been validated on anatomical grounds, nor do they explain why so many disparate dinosaur lineages underwent nasal expansion. Witmer and Sampson (1999) proposed that thermal stress may have been the driving force behind nasal passage expansion in large dinosaurs. Massive bodies stay warm easily due to their low surface areas and large volumes (Schmidt-Nielsen 1984). This physical arrangement slows the release of metabolically generated heat from the body core. Similarly, vascular supply to the skin allows larger bodies to absorb massive quantities of heat from the environment (largely radiant heat from the sun) yet slow that heat from escaping back into the environment as the environment cools (Spotila et al. 1973, 1991; Paladino et al. 1990). The thermal inertia associated with large body size allows large-bodied animals to stay warm relatively easily. However, this also places large-bodied animals at risk of overheating. This overheating problem would necessitate the evolution of specialized anatomical structures to dissipate that heat such as the well-vascularized ears of elephants, which have been shown to offer a cooling function during heat stress (Rowe 2012; Rowe et al. 2013).

Could nasal passage enhancement have provided a thermal buffer for large dinosaur species? The nasal passages are known to offer an important air conditioning function in extant amniotes (Jackson and Schmidt-Nielsen 1964; Schmidt-Nielsen et al. 1970; Murrish and Schmidt-Nielsen 1970; Murrish 1973; Langman et al. 1979). The placement of well-vascularized mucosa—often lofted on bony or cartilaginous turbinates—next to the respired air field allows nasal passages to warm and humidify air prior to reaching the lungs. Warming and humidifying air comes at the expense of the adjacent mucosa, cooling (via evaporation) and drying it. Upon expiration the now warmed and humidified air from the lungs passes back over the dried and cooled mucosa, transferring some of the heat and moisture (via condensation) back onto the nasal passage prior to exiting into the environment. This temporal counter-current heat exchanger provides a critical role in both maintaining heat balance and reducing respiratory evaporative water loss (REWL; Jackson and Schmidt-Nielsen 1964; Schmidt-Nielsen et al. 1970). The alternate ability of the nose to dump excess heat from the body core into the environment has been observed and extensively studied in artiodactyl mammals (Taylor 1970; Taylor and Lyman 1972; Johnsen and Folkow 1988; Kuhnen 1997; Jessen 1998; Caputa 2004; Robertshaw 2006), where it plays an important role in brain cooling. Wheeler (1978) suggested that dinosaurs may have used their nasal passages for a similar brain-cooling function. In contrast, Ruben et al. (1996, 1998) suggested that dinosaur noses were not sufficiently competent at reducing REWL. They based their inferences on cross sections taken through the nasal passages of the dinosaurs *Ornithomimus*, *Nanotyrannus* (cf. *Tyrannosaurus*), and *Hypacrosaurus*. The authors compared cross-

sectional area of the nasal passage to similar cross-sectional areas taken from the nasal passages of mammals, birds, and crocodylians. Ruben et al. (1996) argued that the small cross-sectional areas of dinosaur noses would not have provided enough room for respiratory turbinates, and thus dinosaurs would likely have had low ventilation rates similar to those of extant, bradymetabolic reptiles (Ruben et al. 1996, 1998; Hillenius and Ruben 2004). The data on dinosaur nasal passages thus appear to offer two radically different interpretations for nasal function in this group.

The Problem of Restoring Airflow…and a Solution

The problem with interpretations of dinosaur nasal passage function is that they are dependent on the soft-tissue structures within. The process of fossilization, however, tends to preserve only hard tissues such as bone and teeth. Soft-tissue preservation is extremely rare. Soft tissues in the nose include the nasal mucosa, the underlying nasal neurovasculature, nasal cartilages, and the nasal gland (Figure 1-3). Of these three structures, the mucosa is the most varied. Studies on extant mammals have found that the mucosa often takes on radically different shapes from those implied by the underlying turbinates (Clifford and Witmer 2004). Furthermore, the presence of cavernous tissue (erectile swell-bodies) in the conchae of mammals and nasal vestibule of crocodilians allows for dynamic shape change within the nasal passage (Dawes and Prichard 1953; Bellairs and Shute 1953; Bojsen-Møller and Fahrenkrug 1971), and presents another class of soft tissue that is not directly preserved in most animals. Nasal reconstructions in dinosaurs generally have relied on the external, bony boundaries, for nasal passage shape. These reconstructions are enhanced by incorporation of likely soft tissues sharing the

same space (i.e., neurovasculature, nasolacrimal duct, and the nasal gland), which can be fairly reliably placed using the extant phylogenetic bracketing method (EPB, Witmer 1995a). This methodology, when coupled with non-destructive techniques such as CT scanning, produces the most accurate interpretations of soft-tissue anatomy in extinct animals to date (Witmer 1995b, 1997; Snively and Russell 2007; Witmer and Ridgely 2008, 2009; Holliday 2009; Hieronymus et al. 2009; Evans et al. 2009; Tsuihiji 2010; Schachner et al. 2011). Nonetheless, the lack of information on the physiologically important internal structures of the nasal passage, places limits on interpretations of nasal passage shape and physiological function.

As the nasal passage is an organ that functions in modifying respired air, a potential means of determining aspects of the internal structure of extinct animal noses is to move air through these nasal reconstructions and see how it behaves relative to extant animals with known and "complete" soft-tissue noses. As it turns out, this is no mean feat. Air is a colorless fluid, which makes it very difficult to visualize. Further compounding this difficulty is the enclosed nature of animal noses. Many researchers have tried to visualize the movements of air, with varying degrees of success (Dawes 1952; Hornung et al. 1987; Morgan et al. 1991; Hahn et al. 1993). The most common method is to produce scaled up, physical models of the nasal passage. These models are typically made from acrylic or similarly clear solids. Air is often replaced with a saline solution and pushed through the nose using a pump system. The velocity of the flow field is adjusted to match the targeted Reynolds number of the air, producing equivalent results to air movement via the principle of similitude (Graebel 2001). These physical modeling

processes are often expensive and difficult to validate. With the advent of ever more potent computer processing power, computational fluid dynamics (CFD) has emerged as a viable alternative to physical modeling. CFD uses well-known physical properties to describe the motion of fluids in and around digital models. The use of digital models allows for full-scale tests of structures as diverse as airplanes, racecars, and building ventilation (Agarwal 1999; Brzustowicz et al. 2002; Yam et al. 2011). Relatively recently, CFD has been successfully applied to biological systems, where the use of radiological techniques such as computed tomography (CT) and magnetic resonance (MR) imaging allow for non-invasive views inside the bodies of living animals. 3D models constructed from CT and MR datasets, can be imported into CFD programs where fluid movement can be simulated. As digital models, the user is given the freedom to view fluid movements from a variety of angles by manipulating the models in 3D space, allowing for unprecedented access to difficult to observe anatomical structures (Hoi et al. 2004; Guilherme et al. 2007). Moreover, the use of digital models allows researchers to nondestructively manipulate anatomy (e.g., adding and removing anatomical elements, changing relative sizes of different structures, etc.), providing a means to conduct sensitivity analyses that assess the effects of different anatomical structures on airflow (e.g., Chen et al. 2009; Eiting et al. 2014; Bourke et al. 2014; Chapters 2–6).

Using CFD on extinct animals is more difficult than using it on extant animals. In extant taxa, one simulates fluid movement and uses flow patterns in those fluids to determine how anatomical geometry is affecting fluid motion (e.g., vortex shedding off

the trailing edge of bird wings [Hedenström and Sunada 1999]). In the nasal passages of extinct animals, however, that anatomical geometry is rarely ever present due to the processes of decomposition and fossilization. Thus, to determine the location of soft tissues within the nasal passage, we must reverse-engineer the flow field, which we did by exploiting a key property of fluids, which is that they conform to the shape of their containers. For instance, inspired air will move around obstacles imposed by the anatomy of the nasal passage, which produces a "fluid cast" of the air field within the nasal passage. By comparing the "fluid casts" of extant animals to their bony-bounded airway reconstructions, we potentially can detect the locations of soft-tissue structures within the nose; moreover, if these extant airflow patterns are phylogenetically conservative (Chapter 2), further weight is provided to the inference in extinct species (see Bourke et al. 2014). This methodology can be applied to the bony-bounded reconstructions of the nasal passages of extinct animals by using fluid flow patterns in extant animals as a benchmark by which to test the validity of the extinct animal's reconstructed nose. Areas where the bony-bounded reconstruction differs from soft-tissue airflow patterns suggest the location of soft tissues. This process can be used to refine bony-bounded models until they produce results more in line with what is observed in the soft-tissue airways (Figure 1-4). This process represents a version of Rudwick's "paradigm approach," in which function is used to determine form (Rudwick 1964).

Analyzing the Extant

However, this reverse-engineering of dinosaur nasal passages can only work if the extant relatives of dinosaurs preserve phylogenetically conserved airflow patterns.

Airflow through the noses of the extant relatives of dinosaurs—birds, crocodylians, and lizards—has been an untested area of study. Recent CFD work on airflow through the trachea and lungs of birds and lizards has been done (Maina et al. 2009; Cieri et al. 2014), but the nasal passage had remained an untouched area of study. To address this gap, we looked at a representative crocodylian (*Alligator mississippiensis*), two bird species representing basal branches of Aves (*Meleagris gallopavo* and *Struthio camelus*) as well as two divergent squamate species (*Iguana iguana* and *Varanus exanthematicus*) (see Chapter 2). The goal of this study was to document the fluid flow patterns observed during both parts of respiration (i.e., inspiration and expiration). As archosaurs, birds and crocodylians represent the closest living relatives to dinosaurs, and thus similar airflow patterns observed between these two groups can be hypothesized to have existed in dinosaurs with a higher degree of certainty than similar patterns between birds and mammals (Witmer 1995a), which may involve a high degree of convergence (Farmer 2000). Squamates represent an earlier diverging branch of Diapsida from archosaurs and can offer further support for soft-tissue reconstructions in dinosaurs as shared airflow patterns between squamates, birds, and crocodylians would suggest an even deeper homology (Witmer 1995a). Squamates may also retain more plesiomorphic patterns that could have been lost in crocodylians or birds. This knowledge can aid in determining the pattern of character acquisition by polarizing those characters (e.g., a character shared by birds and lizards, but not crocodylians could indicate secondary loss of the character in the lineage leading to crocs, rather than apomorphic acquisition of that character in birds).

Shared Airflow Patterns Among Extant Diapsids

CFD analyses of diapsid airflow (see Chapter 2) revealed that in spite of vast differences in lifestyles, thermophysiology, and nasal passage shape, there were gross airflow patterns that are conserved among extant diapsids. For instance, even flowing air streams (laminar flow) were present in all the taxa tested. This conservation of laminar airflow has also been observed in humans and other animals during restful breathing (Zhao et al. 2006; Hörschler et al. 2006; Craven et al. 2010). Such a finding is not entirely unexpected in that the physiology of most animals largely limits them to internal flow patterns (blood and air) that fall in the Reynolds number ranges that encompass laminar flow (Vogel 1994). However, there are energetic reasons for promoting laminar airflow as well, such as the greater efficiency in fluid transport in laminar flowing fluid as opposed to chaotic or turbulent airflow (Vogel 1994). Under a laminar flow regime, the cost of transport (i.e., as measured by airway resistance) increases linearly with increases in velocity. For turbulent flowing fluid, this cost increases by the square of velocity. Thus, animals may incorporate anatomical structures or behaviors that promote laminar airflow, such as mouth breathing during moderate to intense exercise in humans and dogs (McCaffrey et al. 1979; Saibene et al. 1981) or airway dilation during running in horses (Lafortuna et al. 2003). Even the scrolled and branched respiratory turbinates found in birds appear to promote laminar airflow, as turbinates reduce the caliber of the nasal airways, increasing nasal wall surface area, which compresses the air field such that it becomes more difficult for individual air streams to fall out of line and produce turbulent vortices (see Chapter 3).

Further evidence of shared airflow patterns was observed in the olfactory recess (Figure 1-5), which tended to reside in a portion of the nasal passage that was somewhat separated from the choana. During inspiration, negative pressure caused by expansion of the trunk, produces a strong pressure gradient between the lungs and the environment, resulting in the rushing in of air to fill the lungs. In the nasal passage, this negative pressure drop manifests at the choana. By placing the olfactory recess away from the choana, it becomes partially removed from the drop in pressure produced during inspiration, which turns the olfactory recess into a cul-de-sac where a relatively high-pressure zone is maintained. Maintaining a shallower pressure gradient between the olfactory recess and the outside environment results in slower moving air streams. The importance of slow-moving air streams appears to be important in olfaction, as it gives odorant molecules more time to attach to odorant receptors along the olfactory epithelia lining the olfactory recess (Mozell 1970; Schoenfeld and Cleland 2005; Craven et al. 2010). Animals with strong senses of smell (macrosmatic) show a further elaboration of the olfactory recess, incorporating anatomical structures (e.g., the lamina transversa; Cave 1967; Craven et al. 2010; Chapters 2, 6) that block the ability for air to enter the olfactory recess during expiration, thus forming a unidirectional airflow through the olfactory recess during respiration. Unidirectional, stop-and-start flow appears to play an important role in separating odorant molecules (Mozell 1970) and can be used to distinguish macrosmatic animals from animals with weaker olfactory abilities (i.e., microsmatic; Craven et al. 2010). The disadvantage of placing the olfactory chamber away from the main flow of air in the nasal passage is that it becomes a challenge to

move air into this region during respiration. Although intense, ballistic breathing patterns such as sniffing and, potentially, buccal pumping, are capable of bringing air into the olfactory recess (Craven et al. 2009, 2010), it is important to remember that sniffing is a behavior done only after an odorant has been detected (Dial and Schwenk 1996; Craven et al. 2010). For this to happen, at least some air needs to make it into the olfactory recess during a restful breath. Indeed in our study (see Chapter 2), olfactory flow was observed during restful breathing in all our study specimens (Figure 1-5). Further evidence in found in other CFD analyses that have shown similar patterns in mammals (Jiang and Zhao 2010; Eiting et al. 2014). How do animals get air into their olfactory recess without sniffing? The answer resides with the soft-tissue structures within the nose. For all of the diapsids in our CFD sample, we observed the presence of mucosal constrictions lining the nasal passage just prior to the olfactory recess (Figure 1-5). These mucosal constrictions greatly decreased the caliber of the nasal passage in this region. Bernoulli's law states that the air moving through these constrictions will experience a steeper pressure gradient, resulting in a sudden increase in air stream velocity. In the CFD models, this produced a Venturi effect that jetted inspired air into the olfactory region. In birds and lizards, this mucosal constriction (= crista nasalis in birds and postvestibular ridge in squamates) was located immediately at the junction of the nasal vestibule and the cavum nasi proprium. This similarity suggests that these two structures may have had a common origin. Unlike the birds and lizards, no such ridge-like structure was observed at the junction of the nasal vestibule and cavum nasi proprium of crocodylians, but this absence is likely due to the apomorphic elongation of the cavum nasi proprium in crocodylians. In

crocodylians, the nasal vestibule is a small, reduced structure (see Chapter 4), whereas the cavum nasi proprium comprises the majority of the nasal passage. Although, there is no crista nasalis-like structure in crocodylians, a unique mucosal constriction was still observed at the junction of the olfactory recess and the nasopharyngeal duct. The repeated presence of these mucosal constrictions near the olfactory recess of diapsids strongly suggests a biophysical requirement for increasing air velocity just prior to the olfactory recess. Removing these structures, as was done for bony-bounded reconstructions of the nasal passage for crocodylians (Chapter 2) or in a step-wise fashion for turkeys (Chapter 3), resulted in weak airflow to the olfactory recess. These findings indicate that soft-tissue constrictions of the nasal passage were likely present at the junction of the nasal vestibule and cavum nasi proprium of dinosaurs, as well, based on arguments of both parsimony (presence of probably homologous constrictions in birds and lizards, with presumed apomorphic loss in crocodylians) and biophysics (such a constriction is so functionally necessary that crocodylians apparently re-evolved it in the biophysically appropriate location).

Soft-Tissue Correction

What of the rest of the nasal passage? CFD simulations of airflow in the nasal passages of extant diapsids (Chapters 2–3) revealed that the airway is remarkably compressed throughout the nasal passage. To determine if there is an overall nasal passage pattern to airway compression, we looked at a diverse collection of extant birds, crocodylians, and lizards (see Chapter 4). Comparisons of bony-bounded nasal passage volumes to their soft-tissue counterparts revealed a remarkable consistency across

Diapsida (Figure 1-6). Soft-tissue airways in all groups comprised approximately 50% of the bony-bounded nasal passage. Regional variation throughout the nasal passage indicated that the nasal vestibule had a very high degree of variability, with soft tissue composing over 90% of the available vestibular space in alligators as opposed to 22% for ostriches. In contrast, the cavum nasi proprium proved to be far more stable with soft tissues routinely filling 40–60% of this region of the nasal passage. The greater variability of the nasal vestibule in diapsids appears to correlate with the amount of hard-tissue boundaries present. Large, complicated nasal vestibules were correlated with large ectonares in all diapsid taxa. Somewhat counterintuitively, this finding suggests that complicated airways in diapsids require less bony scaffolding than more well-bounded regions of the nasal passage. Alternatively, removal of the bony walls of the nasal cavity might be a requirement to free up sufficient space for nasal elaboration to take place. Regardless, this reduction in bone makes reconstructions of the elaborate nasal vestibules of some dinosaurs (e.g., sauropods and hadrosaurids) more difficult as fewer osteological correlates are available. Along with the airway comprising a relatively small proportion of nasal passage volume, a survey of extant mammal, bird, and reptile nasal passages revealed that all amniote airways remain extremely compressed. Constriction of the nasal passages is imposed by either the mucosal walls or the mucosa-covered conchae. The result is a remarkable consistency in the compression of the nasal passage. The radial distance from the center of the air field to the nearest nasal wall rarely exceeded 5 mm regardless of the taxon or its body size (Figure 1-7). For instance a small 150 gram Tokay gecko (*Gekko gecko*) had an average radial airway distance of 0.48 mm, whereas a

74,000 gram subadult ostrich (*Struthio camelus*)—which is over two orders of magnitude more massive than the gecko—had an average radial airway distance that was only 3.75 times greater (Figure 1-7). This consistency of nasal passage constriction exists across phylogenetically disparate taxa and across body masses spanning multiple orders of magnitude (e.g., a 600 kg giraffe has a radial distance of 2 mm [Langman et al. 1979], whereas a 2 tonne rhino has a distance of 3.9 mm [this study]), strongly suggesting that there is strong selective pressure for maintaining small airway distances.

That selective pressure was likely related to two of the nasal passage's most important functions: heat transfer and olfaction. Both of these functions rely on bulk flow in the form of diffusion and convection (Vogel 2003), and both are limited to act over very small distances. As described by Schmidt-Nielsen et al. (1970), effective heat transfer in the nasal passages is a function of (1) surface area across which heat can be conducted, (2) the velocity of the air field over that surface, and (3) the distance from the center of the air field to the nearest mucosal wall. Mathematically, this produces the following relationship:

$$Heat\ transfer\ \propto \frac{surface\ area}{(velocity * radius)}$$

Although other properties of the nasal passage, such as location of adjacent vasculature along with density and thermal conductivity of the mucosa, blood, and air field, will all affect the efficacy of the nasal passage at heat transfer, we can nonetheless obtain some general insight into nasal morphology based on the three criteria shown above. For effective heat transfer to occur, nasal passages should show large surface areas with low velocity air moving through nasal passages with very small radii. Similar

requirements are seen for olfaction (Schoenfeld and Cleland 2005). Amniote nasal passages conform to these requirements. Indeed, the variability observed in amniote nasal passages appears largely to be a byproduct of maintaining the requirements listed above as body mass increases.

Breathing Life into a Dinosaur

Using these data, we set out to reconstruct the airway of the small pachycephalosaurian dinosaur *Stegoceras validum*. The appeal of this species was that it is known from an extremely well-preserved skull (Gilmore 1924). This skull revealed evidence of hypermineralization, or the calcification and/or ossification of soft tissues that typically do not mineralize and hence no not fossilize. This hypermineralization extended into the nasal cavity where evidence of mineralized olfactory turbinates was present along with portions of the nasal capsule walls and a ridge suggestive of the presence of other soft tissues (e.g., respiratory turbinates [see Chapter 5]). These allowed for a more accurate reconstruction of the soft-tissue boundaries in *Stegoceras*. Mass estimates placed this *Stegoceras* specimen in the 10–40 kg range (Peczkis 1995), making it approximately the size of a German shepherd. The appeal of starting with a smaller dinosaur was that it allowed for more accurate estimations of its respiratory variables, as it fell within the mass range of many extant animals for which respiratory data are available. Estimations of respiratory variables were taken from the extensive dataset in Frappell et al. (2001). Initial airflow simulations were performed on a bony-bounded version of the nasal passage in *Stegoceras*, which was done to determine areas in which soft tissue likely had been present. The results of that bony-bounded analysis revealed

multiple regions of unrealistic airflow including very little olfactory flow and a very large caudal-to-rostral current of air running along the lateral aspect of the nasal passage (Figure 1-8A). These unrealistic flow patterns indicated that soft tissue likely filled these areas. A re-analysis of the nasal passage in *Stegoceras* revealed a dorsolateral ridge running along the underside of the nasals. Ridges within the nasal cavity typically act as mucosal anchors, especially turbinate anchors, and have been commonly cited as evidence for the presence of turbinates in extinct synapsids (Hillenius 1992, 1994; Ruben et al. 1996, 1998). Multiple versions of the nasal passage of *Stegoceras* were constructed to account for variation in turbinate shape, as well as alternative structures such as a cartilaginous septum separating the nasal passage from an extended antorbital sinus (Chapter 5). These different anatomical reconstructions represented hypotheses or sensitivity tests that evaluated the sensitivity of the air field to different anatomical conformations. Running these alternative models produced more realistic results in all cases, suggesting that even modest additions of soft tissue can have dramatic effects on airflow properties. Of the four alternative airway models tested, the airway that performed the most realistically—as determined by the presence of substantial airflow in the olfactory recess—was a model that incorporated a branched respiratory turbinate (Figure 1-8B, Chapter 5), although adding a turbinate of any shape dramatically improved airflow realism in comparison to the bony-bounded airway. This study represented the first time that airflow patterns had detected a potential soft-tissue structure within the nasal passages of an extinct animal. The presence of a respiratory turbinate was required to move air into the olfactory recess, and the preservation of the

bony ridge for such a turbinate within the nasal cavity of *Stegoceras* provided the hard evidence for its presence. These results agreed with our previous analyses of turbinate placement in turkeys (Chapter 3), which found that respiratory turbinates can act as important airway baffles, pushing portions of the air field into different regions of the nasal passage. The inference of extensive vasculature within the nasal passage of *Stegoceras* (Porter 2015) suggested that these turbinates would have offered an air conditioning function similar to that observed in extant amniotes. Certainly the addition of a branched turbinate model greatly increased available surface area while simultaneously reducing the radial distance from the center of the air field (Chapter 5). As such, these changes would have likely increased the efficiency of the nasal passage at heat transfer.

Heat Transfer in the Nasal Passages of Large Dinosaurs

Although successful in reconstructing some of the soft tissue within the nasal passage of *Stegoceras*, these results did little to answer the bigger question of whether enhanced dinosaur nasal passages offered thermal benefits. To answer this question, we turned to a larger group of dinosaurs, the armored ankylosaurs (see Chapter 6). Much like *Stegoceras*, ankylosaurs were chosen for their tendency to mineralize, and thus preserve, soft tissues throughout their bodies. This tendency to hypermineralize tissues extended into the nasal passage where, as with *Stegoceras*, the presence of olfactory turbinates and nasal walls were observed. Furthermore, Ankylosauria is known to be one of the dinosaur groups that show this trend of enhanced nasal passages with body size, although it may not look that way on the outset. The ectonaris of ankylosaurs is deceptively small. This is

largely due to extensive osteoderm placement across the skull, covering practically all of the nasal passage (Hill et al. 2003; Witmer and Ridgely 2008). This extensive mineralization preserved much of the original shape of the nasal passage in ankylosaurs, making them particularly amenable to soft-tissue reconstruction. Two well-preserved ankylosaurs, the nodosaurid *Panoplosaurus mirus* and the ankylosaurid *Euoplocephalus tutus*, were used for CFD analysis. Unlike the much smaller *Stegoceras*, respiratory variables for the ankylosaurs were more difficult to obtain using the equations from Frappell et al. (2001). Reynolds numbers based on estimated volumetric flow rates through the nasal passage indicated the presence of substantial turbulence within the nasal passages during both phases of respiration, which seemed unlikely for a resting animal, as discussed above. To alleviate this potential turbulence problem, we rearranged our Reynolds number equation to solve for flow rate at a given Reynolds number. Our "Reverse-Reynolds" approach (Chapter 6) was used to determine the maximum flow rate that could be achieved within the nasal passage prior to transitioning into turbulence (i.e., at a Reynolds number of 2000). To determine heat transfer efficiency within the nasal passages, we modeled the flow of air at 15°C and 50% relative humidity (r. h.) being inspired into a nasal passage that had a body temperature of 35°C. The body temperature chosen was largely arbitrary, but reflected body temperatures observed in many large, terrestrial animals today, regardless of thermophysiology (Chapter 6). To ensure this methodology was reliable we first validated our process in a pigeon, using data from Geist (2000). CFD analysis of heat transfer through the elaborated nasal passages of ankylosaurs revealed extensive capacity to modify the heat content of the respired air

field (Figure 1-9). Furthermore, the ability to modify the heat content of the respired air field increased with body size (Figure 1-9). Using estimated tidal volumes for *Panoplosaurus* and *Euoplocephalus*, we calculated the caloric cost to heat and humidify a single breath of ambient air at 15°C and 50% r.h. to 35°C and 100% r.h. as would be experienced in the lung (Chapter 6). The total caloric cost for *Panoplosaurus* and *Euoplocephalus* was estimated to be 833 and 1568 thermal calories (= 0.8 and 1.6 nutritional calories), respectively. On exhalation, the enhanced nasal passages of both ankylosaurs were able to cool the temperature of the respired air field substantially below body temperature (Chapter 6), producing caloric savings on par with those of many extant amniotes (Chapter 6).

Physiological Effects of Nasal Passage Enhancement in Dinosaurs

The results of our project support the hypothesis that nasal passage elaboration played an integral role in thermoregulation in dinosaurs. These data agree well with work from previous authors (Witmer 2001; Porter 2015) that indicated that the nasal passages of dinosaurs were efficient sites of thermal exchange. In our ankylosaur examples, the nasal passages of *Panoplosaurus* and *Euoplocephalus* were able to warm air by 19°C and 20°C, respectively. This heating of the airway would have come at the cost of the nasal mucosa temperature which accordingly would have been cooled. Cooled mucosa would have thereby cooled the underlying nasal vasculature. Porter (2015) found that an extensive venous network exited the nasal passage and was diverted to the endocranial cavity and brain. Our data agree with Wheeler's (1978) and Porter's (2015) assessment that the nasal passage acted as a thermal sink, allowing large dinosaurs to dump heat from

the body core into the environment. Having blood cooled in the nasal cavity return to the brain would have provided a significant thermal buffer for hot blood coming from the body core. Porter (2015) found strong evidence to suggest that large dinosaurs not only enhanced their nasal passages, but also the associated nasal vasculature, which suggests that nasal cooling of blood may have been paramount for large dinosaurs. Why was that true?

We suspect that the unique body plan of dinosaurs may explain this association. Although many dinosaurs grew to enormous sizes, they generally retained remarkably small brains. Small brains have large surface areas to relatively small volumes. This meant that dinosaur brains could change temperature relatively quickly as opposed to their much larger, more thermally stable bodies. This unique combination of small brains with large bodies would have placed dinosaur brains at a constant risk of heat stress. By enhancing the nasal apparatus, dinosaurs were able to buffer their brains from hot blood coming from the body core, as well as environmentally acquired heat conducted directly from the skull.

Interestingly, theropods appear to be the exceptions among dinosaurs. Theropod nasal passages do not show signs of enhancement with increasing body size. It appears that theropods solved their potential brain overheating problem in a different manner altogether, potentially by enlisting their much enhanced paranasal sinus system. Unlike other amniotes, the antorbital sinus in theropods—both extant avian theropods and apparently also nonavian theropods—has the capacity to be actively ventilated (Witmer 1997, 1999; Sedlmayr 2002). Extensive vasculature associated with the antorbital sinus

(Porter, 2015), coupled with active ventilation of this structure, could have provided the necessary blood and brain cooling for this dinosaur group. Future analyses will test the efficacy of this structure at modifying the air field.

Interestingly, nasal passage enhancement in many dinosaur species appears to have occurred via elongation of the nasal vestibule, which created an elongated, serial-arranged airway. This arrangement is in contrast to the method employed by almost all mammals and most birds, in which an enlarged nasal passage is filled with turbinates, separating the air field into a series of smaller, parallel channels. The results of our analysis on ankylosaurs indicate that both serial and parallel methods produce equivalent results. Serial nasal passages offer advantages in that they are able to condition respired air with only small increases in nasal resistance (Figure 1-10). This is due to the well-known relationship between fluid resistance (R) in enclosed spaces as described by the resistance equation for fluid flow in a pipe (the Hagen-Poiseuille equation):

$$R \propto \frac{8\mu L}{\pi r^4},$$

where μ is the dynamic viscosity of the fluid, L is the characteristic length of the pipe, and r is the radius of the pipe. According to the Hagen-Poiseuille resistance equation, fluid flow resistance will increase in direct proportion to the length of the nasal passage, but will increase by the 4th power for any reduction in nasal passage radius. Thus, by increasing nasal passage length, dinosaurs were able to reduce the energetic costs of breathing as compared to reducing the nasal passage diameter (Figure 1-10). There is a caveat to evolving a serial-based approach to air conditioning. Serially-arranged nasal passages must treat the entire bolus of air at once, and longer nasal passages increase the

dead space that must be overcome to avoid rebreathing spent air. This places a limit on ventilation (breathing) rates. In contrast, turbinate-filled nasal passages, although having to deal with a dramatic increase in airway resistance (partially offset by treating the air field in parallel), they are able to treat the same volume of air faster by partitioning it into smaller channels. Thus, turbinate-filled nasal passages offer the ability to treat the same volume of air in a much smaller anatomical space and more rapidly (for more on this, see Chapters 3 and 6).

This partitioning of the air field may explain why respiratory turbinates are nearly universal for mammals. As tachymetabolic endotherms with tidal breathing patterns (Crosfill and Widdicombe 1961; Stahl 1967; Frappell et al. 2001), mammals have high ventilation rates. These high ventilation rates require fast processing times for air conditioning to reduce REWL while simultaneously fueling high basal metabolic rates. Note that there are a few notable exceptions to turbinate air conditioning in mammals. Elephants and whales use serially-constructed nasal passages to treat air on the way to and from the lungs. Both animals are extremely large and are characterized by low ventilation rates (Stahl 1967; Worthington et al. 1991), and even periods of extensive apnea in the case of whales (Blix et al. 1995; Shaffer et al. 1997). Thus, after a certain size, mammals seem capable of taking advantage of serial-based nasal air conditioning.

In contrast, although respiratory turbinates are commonplace among birds, their role in reducing REWL is not as well established (Tieleman et al. 1999; Geist 2000; Michaeli and Pinshow 2001). Although extant birds are tachymetabolic endotherms, their unidirectional breathing patterns allow them to maintain the same low ventilation rates

observed in other diapsids (Bennett 1973; Frappell et al. 2001). These breathing rates are roughly one-third as often as a similar-sized mammal. The evolution of respiratory turbinates in birds may have been spurred more by competition for space with other sensory systems (i.e., the eyes) than the need to reduce REWL (see Chapter 3). That the respiratory system of birds is more than capable of handling a serial-constructed air conditioning system can be seen in the much elongated trachea of many bird species (Hinds and Calder 1971; Fitch 1999). Our knowledge of sauropsid respiration has grown extensively in the past few years, and it now appears that unidirectional airflow in the lungs may be an ancestral trait for Diapsida (Farmer and Sanders 2010; Sanders and Farmer 2012; Schachner et al. 2013a,b; Farmer 2015), if not Sauropsida. As with birds, unidirectional airflow allows diapsids to breathe much slower. This provides the opportunity for the evolution of elongated, serially-arranged nasal passages. Ironically, the results of our analysis support the original assertion of Ruben et al. (1996) that the nasal passages of dinosaurs indicate low ventilation rates. However, as shown with extant birds, low ventilation rates do not necessarily indicate low basal metabolic rates. Instead, they may suggest the presence of unidirectional respiration.

This project offers the first functional test of the thermoregulatory hypothesis for nasal passage elaboration in dinosaurs. Results of our work support this hypothesis and suggest that the low ventilation rates estimated for dinosaurs allowed for the evolution of serially-elongated nasal passages. Elongating the nasal vestibules in response to the need for brain cooling may have opened up the potential for exaptation of these expanded nasal passages for other purposes, such as the evolution of nasal crests in lambeosaurine

hadrosaurs (Figure 1-11), along with potential trumpeting in this group (Weishampel 1981, 1997; Evans et al. 2009).

Acknowledgments

We would like to thank members of WitmerLab (Ohio University) W. Ruger Porter, Ryan Ridgely, Ashley Morhardt, Don Cerio, and Catherine Early; Farmerlab (University of Utah) members C.G. Farmer and E. R. Schachner; and Rex Lab (University of Wisconsin-La Crosse) member E. Snively. We wish to thank Ruth Elsey of the Rockefeller Wildlife Refuge, the Miami Metro Zoo, Willem M. Roosenburg, Stephen M. Reilly, S. Montuelle, and P. Currie for providing some of the specimens used in this project. We wish to thank H. Rockhold and OhioHealth O'Bleness Hospital (Athens, OH) as well as C. Gerrard, G. Hatch, C. Pilbro, and T. Williamson for CT scanning of specimens. For specimen access we wish to thank C. Mehling and M. Norell for AMNH material as well as D. Evans and K. Seymour for access to ROM material. Bourke's work was funded by a National Science Foundation Graduate Research Fellowship along with a Jurassic Foundation Grant, Doris O. and Samuel P. Welles Research Fund, and an Ohio University Student Enhancement Award.

References

Agarwal, R. 1999. Computational fluid dynamics of whole body aircraft. Annu Rev Fluid Mech. 31:125–169.

Bakker, R.T. 1986. The Dinosaur Heresies: New Theories Unlocking the Mystery of the Dinosaurs and their Extinction. New York. William Morrow and Co.

Bakker, R.T. 1971. Ecology of the Brontosaurs. Nature. 229:172–174.

Baumel, J.J. 1993. Handbook of Avian Anatomy: Nomina Anatomica Avium. Cambridge, MA: Nuttall Ornithological Club. New York. Academic Press.

Bellairs, AD'A., Shute, C. C. D. 1953. Observations on the narial musculature of Crocodilia and its innervation from the sympathetic system. J Anat. 87(pt 4):367–378.

Bennett, A.F. 1973. Ventilation in two species of lizards during rest and activity. Comp Biochem Physiol. 46A:653–671.

Blix, A.S., Folkow, L.P. 1995. Daily energy expenditure in free living minke whales. Acta Physiol Scand. 153:61–66.

Bojsen-Møller, F., Fahrenkrug, J. 1971. Nasal swell-bodies and cyclic changes in the air passage of the rat and rabbit nose. J Anat. 110(1):25–37.

Brzustowicz, J.P., Lounsberry, T.H., Esclafer de la Rode, J.M. 2002.Experimental and computational simulations utilized during the aerodynamic development of the Dodge Intrepid R/T race car. SAE 2002-01–3334.

Cave, A.J.E. 1967. The nature and function of the mammalian epipharynx. J Zool Lond. 153:277–289.

Cieri, R.L., Craven, B.A., Schachner, E.R., Farmer, C.G. 2014. New insight into the evolution of the vertebrate respiratory system and the discovery of unidirectional airflow in iguana lungs. PNAS. 111(48):17218–17233.

Chen, X.B.B.E, Lee, P.H., Chong, V.F.H., Wang, D.Y. 2009. Assessment of septal deviation effects on nasal air flow: a computational fluid dynamics model. Laryngoscope. 119:1730–1736.

Clifford, A.B., Witmer, L.M. 2004. Case studies in novel narial anatomy: 2. The enigmatic nose of moose (Artiodactyla: Cervidae: *Alces alces*). J Zool Lond. 262:339–360.

Colbert, E.H. 1955. Evolution of the Vertebrates. New York. John Wiley and Sons.

Coombs. W.P. 1975. Sauropod habits and habitats. Palaeogeo Palaeoclim Palaeoeco. 17:1–33.

Craven, B.A., Paterson, E.G., Settles, G.S. 2010. The fluid dynamics of canine olfaction: Unique nasal airflow patterns as an explanation of macrosmia. J R Soc Interface. 7:933–943.

Craven, B.A., Patterson, E.G., Settles, G.S., Lawson, M.J. 2009. Development and verification of a high-fidelity computational fluid dynamics models of canine nasal airflow. J Biomech Engin. 131:091002–1.

Crosfill, M.L., Widdicombe, J.G. 1961. Physical characteristics of the chest and lungs and the work of breathing in different mammalian species. J Physiol. 158:1–14.

Dawes, J.D.K. 1952. The course of the nasal airstreams. J Laryng Oto. 66(12):583–593.

Dawes, J.D.K., Prichard, M.M.L. 1953. Studies of the vascular arrangements of the nose. J Anat. 87:311–322.

Dial, B.E., Schwenk, K. 1996. Olfaction and predator detection in *Coleonyx brevis* (Squamata: Eublepharidae), with comments on the functional significance of buccal pulsing in geckos. J Exp Zool. 276:415–424.

Evans, D., Witmer, L.M., Ridgely, R.C. 2009. Endocranial anatomy of lambeosaurine dinosaurs: a sensorineural perspective on cranial crest function. Anat Rec. 292:1315–1337.

Farmer, C.G. 2015. Unidirectional flow in lizard lungs: A paradigm shift in our understanding of lung evolution in Diapsida. Zoology.

Farmer, C.G. 2000. Parental care: The key to understanding endothermy and other convergent features in birds and mammals. Am Nat. 155(3):326–334.

Farmer, C.G., Sanders, K. 2010. Unidirectional airflow in the lungs of alligators. Science. 327:338–340.

FCAT. 1998. Terminologia Anatomica: International Anatomical Terminology. Stuttgart, New York: Thieme

Fitch, W.T. 1999. Acoustic exaggeration of size in birds via tracheal elongation: Comparative and theoretical analyses. J Zool Lond. 248:31–48.

Frappell, P.B., Hinds, D.S., Boggs, D.F. 2001. Scaling of respiratory variables and the breathing pattern in birds: an allometric and phylogenetic approach. Phys Biochem Zool. 74:75–89.

Eiting, T.P., Smith, T.D., Perot, J.B., Dumont, E.R. 2014. The role of the olfactory recess in olfactory airflow. J Exp Biol. 217:1799–1803.

Geist, N.R. 2000. Nasal respiratory turbinate function in birds. Physiol Biochem Zool. 73:581–589.

Gilmore, C.W. 1924. On *Troodon validus*: An orthopodous dinosaur from the Belly River Cretaceous of Alberta, Canada. Bull Alberta Univ. 1:1–43.

Graebel, W. 2001. Engineering Fluid Mechanics. New York, NY. CRC press. Taylor and Francis Group

Guilherme, J.M.G., Bailie, N., Martins, D.A., Kimbell, J.S. 2007. Atrophic rhinitis: a CFD study of air conditioning in the nasal cavity. J Appl Physiol. 103:1082–1092.

Hahn, I., Scherer, P.w., Mozell, M.M. 1993. Velocity profiles measured for airflow through a large-scale model of the human nasal cavity. J App Physiol. 75(5):2273–2287.

Hedenström, A., Sunada, S. 1999. On the aerodynamics of moult gaps in birds. J Exp Biol. 202:67–76.

Hieronymus, T.L., Witmer, L.M., Tanke, D.H., Currie, P.J. 2009. The facial integument of centrosaurine ceratopsids: Morphological and histological correlates of novel skin structures. Anat Rec. 292:1370–1396.

Hill, R.V., Witmer, L.M., Norell, M.A. 2003. A new specimen of *Pinacosaurus grangeri* (Dinosauria: Ornithischia) from the Late Cretaceous of Mongolia: Ontogeny and phylogeny of ankylosaurs. Am Mus Novit. 3395:1–29.

Hillenius, W.J. 1992. The evolution of nasal turbinates and mammalian endothermy. Paleobiology. 18:17–29.

Hillenius, W.J. 1994. Turbinates in therapsids: evidence for Late Permian origins of mammalian endothermy. Evolution. 48: 207–229.

Hillenius, W.J., Ruben, J.A. 2004. The evolution of endothermy in terrestrial vertebrates: Who? when? why? Phys Biochem Zool. 77:1019–1042.

Hinds, D.S., Calder, W.A. 1971. Tracheal dead space in the respiration of birds. Evolution. 25(2):429–440.

Hoi, Y., Meng, H., Woodward, S.H., Bendok, B.R., Hanel, R.A., Guterman, L.R., Hopkins, L.N. 2004. Effects of arterial geometry on aneurysm growth: three-dimensional computational fluid dynamics study. J Neurosurg. 101:676–681.

Holliday, C.M. 2009. New insights into dinosaur jaw muscle anatomy. Anat Rec. 292:1246–1265.

Hornung, D.E., Leopold, D.A., Youngentob, S.L., Sheehe, P.R., Gagne, G.M., Thomas, F.D., Mozell, M.M.. 1987. Airflow patterns in a human nasal model. Arch Otol Head Neck Surg. 113:169-172.

Hörschler, I., Brücker, Ch., Schröder, W., Meinke, M. 2006. Investigation of the impact of the geometry on the nose flow. Eu J Mech B/Fluids. 25:471–490.

Jackson, D.C., Schmidt-Nielsen, K. 1964. Countercurrent heat exchange in the respiratory passages. Physiology. 51:1192–1197.

Jessen, C., 1998. Brain cooling: an economy mode of temperature regulation in artiodactyls. News Physiol. Sci. 13, 281–286.

Jiang, J., Zhao, K. 2010. Airflow and nanoparticle deposition in rat nose under various breathing and sniffing conditions. J Aerosol Sci. 41:1030–1043.

Johnsen, H. K. & Folkow, L. P. (1988). Vascular control of brain cooling in reindeer. Am. J. Physiol. 254: R730–R739.

Kuhnen, G. (1997). Selective brain cooling reduces respiratory water loss during heat stress. Comp. Biochem. Physiol. 118: 891–895.

Lafortuna, C.L., Saibene, F., Albertini, M., Clement, M.G. 2003. The regulation of respiratory resistance in exercising horses. Eur. J. Appl. Physiol. 90:396-–404.

Langman, V.A, Maloiy, G.M.O., Schmidt-Nielsen, K., Schroter, R.C. 1979. Nasal heat exchange in the giraffe and other large mammals. Respir Physiol. 37:325–333.

Maina, J.N., Sing, P., Moss, E.A. 2009. Inspiratory aerodynamic valving occurs in the ostrich, *Struthio camelus* lung: A computational fluid dynamics study under resting unsteady state inhalation. Resp Physiol Neurobiol. 169:262–270.

McCaffrey, T.V., Kern, E.B. 1979. Response of nasal airway resistance to hypercapnia and hypoxia in the dog. Acta Oto. 87:545-–553.

Michaeli, G., Pinshow, B. 2001. Respiratory water loss in free-flying pigeons. J Exp Biol. 204:3803–3814.

Morgan, K.T., Kimbell, J.S., Monticello, T.M., Patra, A.L., Fleishman, A. 1991. Studies of inspiratory airflow patterns in the nasal passages of the F344 rat and rhesus monkey using nasal molds: Relevant to formaldehyde toxicity. Tox App Pharm. 110:223–240.

Mozell, M.M. 1970. Evidence for a chromatographic model of olfaction. J Gen Physiol. 56:46–63.

Murrish, D.E. 1973. Respiratory heat and water exchange in penguins. Resp. Physiol. 19:262–270.

Murrish , D.E., Schmidt-Nielsen, K. 1970. Exhaled air temperature and water conservation in lizards. Resp Phys. 10:151–158.

O'Gorman, E.J., Hone, D.W.E. 2012. Body size distribution of the dinosaurs. PLOS One. 7:e51925. doi:10.1371/journal.pone.0051925.

Paladino, F.V., O'Connor, M.P., Spotila, J.R. 1990. Metabolism of leatherback turtles, gigantothermy, and thermoregulation of dinosaurs. Nature. 344:858–860.

Parsons, T.S. 1959. Nasal anatomy and the phylogeny of reptiles. Evolution. 13:175–187.

Peczkis, J. 1995. Implications for body-mass estimates for dinosaurs. J Vert Paleo. 14:520–533.

Porter, W.R. 2015. Physiological implications of dinosaur cephalic vascular systems. Unpublished doctoral dissertation, Ohio University. 433 pp.

Robertshaw, D., 2006. Mechanisms for the control of respiratory evaporative heat loss in panting animals. J. Appl. Physiol. 101, 664–668.

Romer, A.S. 1945. Vertebrate Paleontology. (2nd ed.). Chicago. Univ. Chicago Press.

Rowe, M.F., Bakken, G.S., Ratliff, J.J., Langman, V.A. 2013. Heat storage in Asian elephants during submaximal exercise: behavioral regulation of thermoregulatory constraints on activity in endothermic gigantotherms. J Exp Biol. 216:1774–1785.

Rowe, M.F. 2012. Seasonal biophysical variations in resting and exercising elephants: Energetic, thermoregulatory, and behavioral adaptations. Unpublished Ph. D dissertation.

Ruben, J.A., Hillenius, W.J., Geist, N.R., Leitch, A., Jones, T.D., Currie, P.J., Horner, J.R., Espe III, G. 1996. The metabolic status of some Late Cretaceous dinosaurs. Science. 273:1204–1207.

Ruben, J.A., Jones, T.D., Geist, N.R. 1998. Respiratory physiology of the dinosaurs. BioEssays. 20:852–859.

Rudwick MJS. 1964. The inference of function from structure in fossils. Br J Philos Sci. 15:27–40.

Saibene, F., Aguggini, M.G., Clement, M.G. 1981. Work of breathing in dog during exercise. J. Appl. Physiol. 50:1087–1092.

Sanders, R.K., Farmer, C.G. 2012. The pulmonary anatomy of *Alligator mississippiensis* and its similarity to the avian respiratory system. Anat Rec. 295(4):699–714.

Schachner, E.R., Cieri, R.L., Butler, J.P., Farmer, C.G. 2013. Unidirectional pulmonary airflow patterns in the savannah monitor lizard. Nature. 506:367–370.

Schachner ER, Farmer CG, McDonald AT, Dodson P. 2011. Evolution of the dinosauriform respiratory apparatus: new evidence from the postcranial axial skeleton. Anat Rec. 294:1532–1547.

Schachner, E.R., Hutchinson, J.R., Farmer, C.G. 2013. Pulmonary anatomy in the Nile crocodile and the evolution of unidirectional airflow in Archosauria. PeerJ. 1:e60.

Schmidt-Nielsen, K. 1984. Scaling: Why is animal size so important? Cambridge, MA. Cambridge U Press.

Schmidt-Nielsen, K., Hainsworth, R.F., Murrish, D. 1970. Counter-current heat exchange in the respiratory passages: Effect on water and heat balance. Resp Physiol. 9:263–276.

Schoenfeld, T.A., Cleland, T.A. 2005. The anatomical logic of smell.Trends Neurosci. 28:620–627.

Sedlmayr, J.C. 2002. Anatomy, evolution, and functional significance of cephalic vasculature in Archosauria. Unpublished doctoral dissertation, Ohio University. 498 pp.

Shaffer, S.A., Costa, D.P., Williams, T.M., Ridgway, S.H. 1997. Diving and swimming performance of white whales, *Delphinapterus leucas*: An assessment of plasma lactate and blood gas levels and respiratory rates. J Exp Biol. 200:3091–3099.

Snively, E., Russell, A.P. 2007. Functional variation of neck muscles and their relation to feeding style in Tyrannosauridae and other large theropod dinosaurs. Anat Rec. 290:934–957.

Spotila, J.R., Lommen, P.W., Bakken, G.S., Gates, D.M. 1973. A mathematical model for body temperatures of large reptiles: Implications for dinosaur ecology. Am Nat. 107 (955):391–404.

Spotila, J. R., O'Connor, M. P., Dodson, P. and Paladino, F. V. (1991). Hot and cold running dinosaurs: body size, metabolism and migration. Mod. Geol. 16, 203-227.

Stahl, W.R. 1967. Scaling of respiratory variables in mammals. J Appl Physiol. 22:453–460.

Taylor, C.R., 1970. Dehydration and heat: effects on temperature regulation of East African ungulates. Am. J. Physiol. 219, 1136–1138.

Taylor, C.R., Lyman, C.P., 1972. Heat storage in running antelopes: independence of brain and body temperatures. Am. J. Physiol. 222, 114–117.

Tieleman, B.I, Williams, J.B, Michaeli, G., Pinshow, B. 1999. The role of the nasal passages in the water economy of crested larks and desert larks. Physiol Biochem Zool. 72:219–226.

Tsuihiji, T. 2010. Reconstructions of the axial muscle insertions in the occipital region of dinosaurs: evaluations of past hypotheses on Marginocephalia and Tyrannosauridae using the extant phylogenetic bracket approach. Anat Rec. 293:1360–1386.

Vogel, S. 2003. Comparative Biomechanics: Life's Physical World. New Jersey. Princeton University Press.

Vogel, S. 1994. Life in Moving Fluids. 2nd ed. New Jersey: Princeton University Press.

Waibl, H., Gasse, H., Hashimoto, Y., Burdas, K-D., Constantinescu, G.M., Saber, A.S., Simoens, P., Salazar, I., Sotonyi, P., Augsburger, H., Bragulla, H. 2012. Nomina anatomica veterinaria. 5th ed. International Committee on Veterinary Gross Anatomical Nomenclature. World Association of Veterinary Anatomists. Columbia, Missouri.

Weishampel, D.B. 1997. Dinosaurian cacophany. Bioscience. 47(3):150–159.

Weishampel, D.B. 1981. The nasal cavity of Lambeosaurine hadrosaurids (Reptilia: Ornithischia): Comparative anatomy and homologies. J Paleo. 55(5):1046 –1057.

Wheeler, P. 1978. Elaborate CNS cooling structures in large dinosaurs. Nature. 275:441–443.

Witmer, L.M. 1995a. The extant phylogenetic bracket and the importance of reconstructing soft tissues in fossils. In: Thomason JJ, editor. Functional

morphology in vertebrate paleontology. New York: Cambridge University Press. pp:19–33.

Witmer, L.M. 1995b. Homology of facial structures in extant archosaurs (birds and crocodilians), with special reference to paranasal pneumaticity and nasal conchae. J Morphol. 225:269–327.

Witmer, L.M. 1997. The evolution of the antorbital cavity of archosaurs: a study in soft-tissue reconstruction in the fossil record with an analysis of the function of pneumaticity. J Vert Paleo. 17 (1 supp):1–73.

Witmer, L.M. 1999. The phylogenetic history of paranasal air sinuses. in: Koppe, T., Nagai, H., Alt, K.W. (eds). The paranasal sinuses of higher primates: development, function and evolution. Chicago. Quintessence. pp:21–34.

Witmer, L.M. 2001. Nostril position in dinosaurs and other vertebrates and its significance for nasal function. Science. 293:850–853.

Witmer, L.M., Ridgely, R.C. 2008. The paranasal air sinuses of predatory and armored dinosaurs (Archosauria: Theropoda and Ankylosauria) and their contribution to cephalic architecture. Anat Rec. 291:1362–1388.

Witmer, L.M., Ridgely, R.C. 2009. New insights into the brain, braincase, and ear region of tyrannosaurs (Dinosauria, Theropoda), with implications for sensory organization and behavior. Anat Rec. 292:1266–1296.

Witmer, L.M., Sampson, S.D. 1999. Nasal conchae and blood supply in some dinosaurs: physiological implications. J Vert Paleo. 19(3 supp):85A. Japan.

Worthington, J., Young, I.S., Altringham, J.D. 1991. The relationship between body mass and ventilation rate in mammals. J Exp Biol. 161: 533–536.

Yam, R., Yuen, P.L., Yung, R., Choy, T. 2011. Rethinking hospital general ward ventilation design using computational fluid dynamics. J Hosp Infect. 77:31–36.

Zhao, K., Dalton, P., Yang, G.C., Scherer, P.W. 2006. Numerical modeling of turbulent and laminar airflow and odorant transport during sniffing in the human and rat nose. Chem Senses. 31:107–118.

CHAPTER 2 : THE IMPACT OF SOFT TISSUES ON NASAL AIRFLOW IN DIAPSIDS: IMPLICATIONS FOR DINOSAURS

Abstract

The nasal passages are involved in a variety of important functions including olfaction and thermoregulation. These functions were likely as important in the past as they are today. However, the vagaries of fossil preservation tend to provide only low-resolution views of the structures that were once present in the nasal passages of extinct animals. To test the effects of these lower resolution models on interpretations of nasal function, we performed a broadly comparative analysis of the nasal passages in representative extant diapsids (alligator, turkey, ostrich, iguana, and monitor lizard). Using a computational fluid dynamic approach, it was possible to simulate airflow through 3D reconstructed models of these different nasal passages. We compared these soft-tissue-bounded results to similar analyses of airways that only incorporated the bony boundaries, as typically preserved in fossils. Airflow patterns in bony-bounded, low-resolution, airways were more homogeneous and overall slower moving than those of their soft-tissue counterparts. These data indicate that bony-bounded airway reconstructions are far too conservative and result in placing physiological limitations on extinct taxa that would not have been present in the living animals. Similarities in airflow patterns across this diverse assemblage of diapsids revealed shared features of the nasal capsule that can be reasonably inferred to exist on phylogenetic grounds in the nasal passages of extinct diapsids such as dinosaurs.

Abbreviations

at co, atrial nasal concha; caud co, caudal nasal concha; caud meat, caudal nasal meatus; ch, choana; cnp, cavum nasi proprium; co, nasal concha; co meat, nasal conchal meatus; cr nas, crista nasalis; cup, cupola; dist L, distal limb; f ex, fenestra exochoanalis; m ex, medial expansion; mid co, middle nasal concha; mid meat, middle nasal meatus; n, naris; npd, ductus nasopharyngeus; olf, olfactory chamber; postco, nasal postconcha; postco meat, nasal postconchal meatus; post ridge, postvestibular ridge; preco meat, nasal preconchal meatus; preco, nasal preconcha; preco rec, preconchal recess; prim ch, primary choana; prox L, proximal limb; ro meat, rostral nasal meatus; ros co, rostral nasal concha; sc, spherical capsule; sec ch, secondary choana; sep co, septal nasal concha; sm, septomaxilla; vest, vestibulum nasi, vest fl, floor of vestibulum nasi.

Introduction

Nasal passages serve a variety of vital functions in most extant amniotes. The nasal passage—along with the trachea and primary bronchi—forms the air conducting portion of the respiratory system (Kierszenbaum 2007), delivering air from the environment to the lungs for gas exchange. Epithelial mucosa in the nasal passages acts as air conditioners, modifying the heat and water content of respired air and reducing respiratory evaporative water loss (Jackson & Schmidt-Nielsen 1964, Murrish & Schmidt-Nielsen 1970, Schmidt-Nielsen et al. 1970, Hillenius 1992, Nelson et al. 2007). Moreover, airborne olfactorant molecules are analyzed in the nasal passages, providing an odorant discrimination function. Nasal passages may also act as resonators,

influencing the timbre of exhaled air and providing a role in communication (Roberts 1973, Brackenbury 1982, Nowicki 1987, Frey et al. 2007).

All of the aforementioned functions are present in extant archosaurs and were likely present in extinct archosaurs, as well. The presence of extensive nasal passage development in a variety of dinosaur lineages suggests that one or more of these functions were selected for in dinosaur evolution (Weishampel 1981, Witmer & Ridgely 2008, Evans et al. 2009, Miyashita et al. 2011). Determining which of these functions were highlighted in dinosaurs requires a deeper understanding of nasal anatomy within this group. Unfortunately, preservational biases limit our knowledge of dinosaur nasal passages to the bony-outer boundaries of the cartilaginous nasal capsule (Figure 2-1). Previous attempts at restoring dinosaur nasal anatomy have relied extensively on these outer boundaries coupled with their placement next to other inferred soft-tissues such as the paranasal sinuses (Witmer & Ridgely 2008). Results from these reconstructions show the hard outer limits of the nasal capsule. However the inner boundaries of the nasal capsule—where the physiologically relevant mucosa reside—remain unknown. To better determine where these inner boundaries reside in extinct taxa a detailed understanding of nasal capsule morphology and physiology in extant animals is required. As Dinosauria is deeply nested within Diapsida (Benton 2005, Nesbitt 2011, Brusatte 2012), a better understanding of nasal physiology in dinosaurs would benefit from knowledge of nasal anatomy and physiology in extant diapsids.

Vertebrate nasal passage morphology has been investigated extensively (Seydel 1896, Hoppe 1934, Negus 1958). Nasal passage physiology in mammals has been and is

currently a ripe area of study (Kimbell et al. 1997; Van Valkenburgh et al. 2004; Rakesh et al. 2008; Craven et al. 2009, 2010; Green et al. 2012), especially as it pertains to humans (Gizurarson 1993, Hahn et al. 1993, Mygind & Dahl 1998, Doorly et al. 2008, Elad et al. 2008, Chen et al. 2009). Conversely, whereas nasal passage morphology has been extensively surveyed in diapsids (Stebbins 1943, 1948; Parsons, 1959, 1970; Bang 1964, 1966, 1971: Gabe & Saint Girons 1976, Bang & Wenzel 1985), nasal passage physiology has been investigated in only a handful of studies (Prange & Schmidt-Nielsen 1969; Schmidt-Nielsen et al. 1970; Murrish & Schmidt-Nielsen 1970; Schwenk 1993; Tieleman et al. 1999; Geist 2000; Michaeli & Pinshow 2001; Tattersall et al. 2006). All of these works have relied on inferences of nasal airflow based on anatomy, behavioral analyses, and basic fluid dynamics (e.g, Bang 1971, Schwenk 1993). To date there has been no attempt to visualize air moving through these nasal passages.

Here we set out to describe airflow dynamics within representative nasal passages of extant diapsids. A mix of gross dissection, computed tomographic (CT) imagery, and 3D segmentation were used to visualize the anatomy. To understand how airflow interacts with the soft tissues of the nasal passages, specimens of each species were subjected to a computational fluid dynamics analysis (CFD). This engineering technique has been extensively used in the fields of industry (Agarwal 1999; Brzustowicz et al. 2002, 2003; Mirade and Daudin 2006; Yam et al. 2011) as well as medicine (Hoi et al. 2004, Garcia et al. 2007, Chen et al 2009). CFD offers the ability to simulate fluid flow in a digital environment, which reduces the costs associated with creating elaborate flume structures or with acquiring and maintaining expensive machinery such as those used for

digital particle image velocimetry (Lauder et al. 2003). The limiting factor for CFD is computational power, which is ultimately determined by the complexity and size of the model used. For CFD models that must simulate very fine details such as the maxillo- and ethmoturbinates of carnivoran mammals, model size can be prohibitively large (>14 million elements) and require the use of multiple networked computers (Craven et al 2009). Diapsid nasal passages are not as heavily subdivided as in many mammals, making it possible to create models that are substantially simpler and smaller in size (e.g., the models used in this study ranged from 1.6–2.9 million elements) and thus require much less computational power to solve.

To understand how soft-tissue affects the respired air field, we observed airflow patterns seen in diapsid nasal passages that retained their soft tissues and compared them to models that had these soft tissues digitally removed, leaving only the bony-bounded (BB) airway behind. These bony-bounded airways represent the type of nasal passages that are typically preserved in fossils.

Anatomy and Terminology

The nasal passage can be divided into a series of successive layers, each with their own boundaries (Figure 2-1).

Bony nasal cavity—We use this general term to incorporate the outermost border of the bony nasal passage and everything within it. It is bounded by the bones of the facial skeleton, which for diapsids commonly consist of the premaxilla, maxilla, nasal, prefrontal, lacrimal, palatine, and vomer. Its rostral-most extent ends at the bony nasal

aperture whereas the caudal extent usually ends at the lacrimal, prefrontal, and palatines (extending as far back as the pterygoids in crocodylians).

Bony and fleshy nostril—The bony nostril is the rostral opening of the bony nasal cavity, bounded by the premaxilla, nasal, and maxilla. The formal term is bony nasal aperture (apertura nasi ossea [Baumel and Witmer, 1993]; International Committee on Veterinary Gross Anatomical Nomenclature, 2012). The fleshy nostril resides within the confines of the bony nasal aperture and is referred to as the naris (Witmer 2001).

Bony and fleshy choana—The choana, or "internal nostril," represents the exit of air from the nasal capsule during inspiration and its entry from the glottis during expiration. As with the nostril, there is both a bony and a fleshy choana. The bony choana has been referred to as the fenestra exochoanalis (Jarvik 1942, Bellairs 1949). It is bordered laterally by the maxilla, rostrally by the maxilla and vomer, medially by the vomer and palatines, and caudally by the palatines. The evolution of an extensive bony secondary palate in crocodylians has pushed the entire fenestra exochoanalis caudally where it is encapsulated by the pterygoids (Witmer 1995a). These bony boundaries often result in an extensive opening that may cover much of the roof of the oral cavity. Soft tissue from the nasal capsule and oral roof obscure much of the choana in extant diapsids such that the rostral opening of the choana may be partially or completely covered in a sheet of oral mucosa (Rieppel et al. 2008, Crole and Soley 2010). In birds, fleshy papillae on these choanal flaps may act to block food particles from entering the nasal capsule during swallowing (Gussekloo 2006). This much smaller and caudally placed opening for the fleshy choana has been referred to as the fenestra endochoanalis (Jarvik 1942, Bellairs

1949). For the purposes of this paper we will restrict "choana" to the fleshy choana only. The bony choana will be referred to as the fenestra exochoanalis.

Nasal capsule—This cartilaginous structure is deep to the bony nasal cavity and serves as the main point of attachment or outgrowth for most of the soft tissues inside the nasal passage (e.g., turbinates, mucosa, conchae). The rostral extent of the nasal capsule may continue as a cartilaginous extension beyond the bony borders of the bony nasal aperture as external nasal cartilages.

Conchae and turbinates—The terms turbinate (or turbinal) and concha are often used interchangeably, but we prefer to separate the two. The turbinates are the cartilaginous outgrowths of the nasal capsule that project into the nasal cavity, whereas the conchae comprise the overlying mucosa that covers the turbinates. Turbinates can be viewed as the internal support of the conchae, although sometimes conchae can be entirely mucosal with no internal support (Nickel et al. 1986, Witmer et al. 1999). Turbinates often take the form of thin scrolls or lamellae (branched or unbranched) of cartilage that sometimes mineralize and thus are occasionally preserved within the bony nasal cavity in dried skulls and fossils, providing some indication of the presence and disposition of the conchal mucosa. Functionally, the conchae are more important, being the physiological players that increase the available surface area over which the respired air passes, allowing them to function in countercurrent heat exchange as well as odorant analysis. The functions of conchae vary depending on location in the nasal passage and what epithelial layers they support (e.g., respiratory vs. olfactory epithelium).

Mucosal layer—Resting on the inner surfaces of the nasal capsule and conchae is the nasal epithelium. Various epithelial types and their corresponding submucosal neurovascular bundles are found here. Three basic epithelial types can be distinguished in the nasal passage, in roughly rostral to caudal order: variably cornified stratified squamous epithelium, ciliated columnar (respiratory) epithelium, and olfactory epithelium (identified by the presence olfactory receptor neurons and Bowman's glands).

Airway—This is the deepest space within the nasal passage and is where respired air travels. The nasal airway passes from the fleshy nostril to the fleshy choana.

Divisions of the nasal passages—Diapsid nasal passages received special attention in the works of Parsons (1959, 1967, 1970), Bang (1960, 1971), Bang and Wenzel (1985), and Witmer (1995b). Diapsid nasal passages vary greatly in size and shape, but their gross underlying structure shows consistent and predictable morphologies. This structure allows for separation of the nasal capsule into the following three compartments. (1) Vestibulum nasi: the nasal vestibule is the rostralmost portion of the nasal capsule just deep to the fleshy nostril. It is typically a tubular region that is smaller in diameter than the succeeding cavum nasi proprium. (2) Cavum nasi proprium (CNP): continuing caudally from the vestibulum nasi and rostral to the ductus nasopharyngeus, the cavum nasi proprium (= main nasal cavity) usually occupies a more spacious portion of the nasal capsule. Conchae, both respiratory and olfactory, tend to lie within the CNP. The olfactory chamber resides within the cavum nasi proprium at its caudal-most extent and is typically outside of the main respiratory flow. (3) Ductus nasopharyngeus: following the terminology of Parsons (1970), the nasopharyngeal duct is

defined as any connection from the cavum nasi proprium that leads to the choana. It varies in length and complexity between taxa.

Materials and Methods

Study Taxa

All specimens, with the exception of data contributed by C. G. Farmer and E. R. Schachner, were acquired post-mortem from various sources and are housed in a public repository, the Ohio University Vertebrate Collections (OUVC). Specimen condition varied depending on acquisition. Alligators, ostriches, and turkeys had only their heads preserved, requiring mass estimates based on regression equations taken from the literature (Coulson et al. 1973 for alligators, Hinds & Calder 1971 for birds). Squamates were often preserved in total and could be directly weighed. All specimens were cadaveric salvage specimens obtained from legal sources, and the animals' deaths were independent of this project, the researchers, or Ohio University. They are legally housed in the OUVC under the terms of permit #14-2762 issued by the Ohio Division of Wildlife.

Crocodylians: Various specimens of American alligator (*Alligator mississippiensis*) were examined with CT and/or dissection. The specimen used for CFD modeling was OUVC 10389, a hatchling male American alligator approximately 468 grams in mass. The specimen was acquired as a salvage specimen from the Rockefeller Wildlife Refuge in Louisiana.

Birds: Multiple specimens of wild turkey (*Meleagris gallapovo*) and farmed ostrich (*Struthio camelus*) were examined with CT and/or dissection. Specimens used for

CFD modeling were OUVC 10636, a subadult ostrich of approximately 74 kg in mass, and OUVC 10599, an adult wild turkey approximately 4.9 kg in mass. The heads of the turkeys were obtained from local hunters as part of a legal controlled hunt and donated to the OUVC, whereas the ostriches were obtained as salvage specimens from a commercial processing center (Nutri-Tech, LLC, Beaver City, Nebraska).

Squamates: Multiple specimens of green iguana (*Iguana iguana*) and savannah monitor (*Varanus exanthematicus*) were examined with CT scan and/or dissection. Specimens used for CFD modeling were OUVC 10603, a juvenile green iguana with a mass of 870 grams, obtained from the Miami Metro Zoo in Miami, Florida, as a salvage specimen generated by the zoo's feral pest eradication program. The monitor specimen used for CFD modeling was OUVC 10675, a young adult male, 1.73 kg in mass, whose body was donated to our study following a previous, unrelated study (McElroy and Reilly 2009). CT data used for comparison in this study were contributed by C. G. Farmer and E. R. Schachner, based on live animal data acquired from an unrelated study (Schachner et al. 2013).

Dissections

The nasal capsules of squamates, birds, and crocodylians were dissected to directly observe the anatomical relationships of the structures within the nasal cavity. Dissections were either performed on whole specimens or on heads that were hemisected, allowing access through the medial wall (septum) of the nasal capsule. In certain instances, the nasal capsule was physically excised from the nasal cavity by removal of surrounding bone to better observe anatomical relationships within the capsule.

Computed Tomography

The heads of juvenile alligators, turkeys, iguanas, and monitor lizards were scanned using the Ohio University MicroCT Scanning Facility (OUμCT). The scanner used was an eXplore Locus MicroCT scanner by General Electric. Specimens were scanned at 60kv at 450μA with a slice thickness of 45–90μm. Data were exported in DICOM format for segmentation in Avizo 6.3–7.1 (Visualization Science Group). Ostrich and large alligator heads were scanned using a Toshiba Aquilion 64 slice CT scanner at OhioHealth O'Bleness Hospital in Athens, Ohio.

Model Reconstruction

DICOM data were read in Avizo 6.3–7.1. The left airway of each taxon was segmented using Avizo's segmentation tools. The singular exception to this was the savannah monitor, which preserved a better right airway than left. The existence of a complete nasal septum in all the taxa studied obviated the need to model both nasal passages as the septum would maintain complete separation of airflow up to the choana. Each nasal capsule was segmented into two models. The first model took into account the soft tissue that encompassed each airway, creating a cast of the airway in the nasal capsule, showing all the places that the air field could travel. The second model took only the bony-boundaries of the nasal cavity into account. Boundaries of the nasal capsule that could be inferred from osteological correlates for other soft-tissue structures, such as sinuses, were also incorporated (Figure 2-2)

Segmented models were cleaned of scanning and segmentation artifacts using the cleaning functions in Geomagic Studios 10 (3D Systems Geomagic, Rock Hill, SC).

Cleaning and refining served to reduce triangle skew, producing models that were more amenable to tetrahedral meshing. Models were assigned a series of boundary conditions that would induce physiologically-realistic airflow through them (i.e., pressure-driven flow from nostril to choana during inspiration and vice versa during expiration). Three boundary conditions were placed on the model (Figure 2-3B). These boundaries were the following: (1) a pressure inlet located at either the naris or choana for inspiration and expiration, respectively; (2) a pressure outlet located at either the choana or naris for inspiration and expiration; and (3) an impermeable wall boundary condition assigned to the rest of the nasal capsule. After cleaning and boundary condition assignment, models were converted into tetrahedral meshes for fluid dynamic analysis. For the purpose of the grid refinement study (see below), multiple grid resolutions were created (Figure 2-3C).

Physiological Parameters

Resting respiration was simulated in all four models. To best approximate physiological relevance, volumetric flow rate during resting respiration for each species was obtained from the literature when available (Table 2-1). Respiration data for squamates is limited. Despite numerous studies that have looked at factorial scope, blood PH, and other aspects of metabolism in squamates, we could only find one published study that attempted to survey respiratory variables in this group (Bennett 1973). Further complicating matters were the lack of data on the non-ventilatory period (NVP) for the animals being studied. Most reptiles and amphibians exhibit diphasic breathing in which air is first expired then inspired and held within the lungs for some variable length of time (Milsom 1988, 1991). Mechanical analyses suggest that diphasic breathing evolved as an

adaptation to minimize the costs of ventilation in animals whose metabolic demands did not require continuous breathing to satisfy oxygen requirements (Milsom 1984, Vitalis & Milsom 1986). NVP varies between species, individuals, and individual breathing bouts, making documentation of NVP durations extremely important for a variety of physiological variables such as metabolic rate (Thompson & Withers 1997). For this study, NVP knowledge was necessary for calculating inspiratory drive (= tidal volume / inspiration time). Without this knowledge, calculations of volumetric flow rate would be exceedingly low, producing results that would not accurately reflect the shape of the air field during resting respiration. Thus, we used estimates of breathing frequency from the literature and incorporated an 80% NVP. This proportion was based on previous literature values that have recorded NVP in reptiles (Milsom 1984, Vitalis & Milsom 1986, Thompson & Withers 1997, Frappell et al. 2002). Whereas this proportion would likely change depending on the animal and the situation in which it was measured, incorporating an 80% NVP into data taken from the literature served to reduce respiratory cycle time down to 1-2 seconds/breath; resulting in "burst" breathing rates that fell in line with literature values on reptiles that had incorporated this apnoeic period (Milsom 1988, Vitalis and Milsom 1986).

Fluid Dynamic Analysis

Fluid dynamic analysis was accomplished using the CFD program Fluent 13 (ANSYS Inc., Canonsburg, PA). A 3-dimensional double-precision, pressure-based solver was used. Fluid dynamic modeling requires that some initial assumptions be made prior to running an analysis. These assumptions determine the type of flow patterns that

are expected to be observed. Determining these gross patterns ahead of time aids in selecting the appropriate algorithms to solve the fluid dynamic problems and decreases computation time. Determining the type of flow pattern that is likely to be observed was done by calculating the dimensionless Reynolds and Womersley numbers for the airway. Typically, biological systems—in particular, blood circulation and respiration—are subjected to orderly, laminar flow regimes (Vogel 1994). This is in part due to the small sizes and volumes of fluid being moved during each cycle, but may also come about due to anatomical structures that promote laminarity as laminar bulk flow is the most efficient (Vogel 1994). Reynolds numbers are used to roughly determine when a flow should be laminar and when it should be chaotic or turbulent. Reynolds numbers below 2000 suggest laminar flow whereas turbulent flow is expected at Reynolds numbers above 4000. Flows that exist between 2000–4000 lie in a transitional zone where secondary flows (vortices) may be present. It is difficult to calculate Reynolds numbers for biological systems as the fractal nature of the shapes involved rarely approach the more simplistic geometries used in engineering. One way around this problem is to borrow a technique from civil engineering and take the volumetric flow rate and compare it to the wetted perimeter of the object in question (Holmes et al. 2011) according to the following equation for Reynolds number (Re):

$$\mathrm{Re} = \frac{4\mathrm{Q}}{\mathrm{Pv}}$$

where Q = the volumetric flow rate measured in m^3/s, P = the wetted perimeter in meters (Foss 1998), and v = the kinematic viscosity of air ($1.6036e^{-05}$ m^2/s at 30°C).

Reynolds numbers were calculated from cross sections taken roughly every 3 mm along a path parallel to the respired air field. Wetted perimeter and area measurements were taken directly using the built-in tools in Avizo 6.3–7.1. Reynolds calculations indicated that laminar flow was the most likely state for the three reptile taxa and the turkey (Table 2-2). The potential for some transitional flow existed in the nasal capsule of the ostrich model (Table 2-2). For the reptile and turkey models the default laminar viscosity model was chosen. The ostrich model incorporated a Wilcox two equation κ-ω turbulence model as this model has been found to work best with dynamic flows within the nasal capsule (Liu et al. 2007, Craven et al. 2009). A shear stress transport model was incorporated to deal with the transition zone from laminar to turbulent flow (Chen et al. 2009). The second assumption that needed to be met was the steadiness of the flow field. The steadiness of a flow determines how often it is able to assume the classic parabolic profile under oscillating conditions (e.g., the pulsation of blood flow or the pendular pattern of breathing). To determine this we used the dimensionless Womersley number (Wo; Womersley, 1955), as defined for the respiratory system (Craven et al., 2009) in the following equation:

$$\mathrm{Wo} = \frac{\mathrm{Dh}}{2}\sqrt{\frac{2\,\pi\,\mathrm{f}}{\mathrm{v}}}$$

where f = the frequency of oscillation (Hz), and Dh is the hydraulic diameter of the airway defined as (Foss, 1998):

$$\mathrm{Dh} = \frac{4\mathrm{A}}{\mathrm{P}}$$

where A = the area of the cross section being measured (m^2).

The Womersley number is a function of a structure's size, the frequency of oscillation, and the kinematic viscosity of the fluid being moved (Loudon and Tordesillas, 1998). At Wo ≤ 1, the flow field may be considered to exist in a quasi-steady state, which suggests that the fluid is capable of reaching and maintaining the standard parabolic profile. This implies that instantaneous flow rate can be determined by the corresponding instantaneous pressure gradient (Loudon and Tordesillas, 1998), allowing for a steady-state solution to be modeled, eliminating the need for time-steps. As Wo increasingly deviates from unity, the flow becomes more unsteady. At Wo > 10 inertial forces dominate once more, forcing a flattened "plug" profile to the fluid flow (Ku, 1997). This flow type is considered to be completely unsteady, making its shape for a given pressure gradient unknown a priori, necessitating the use of a transient model for flow calculations.

Womersley numbers were calculated from the same cross sections used to obtain the Reynolds number. Results indicated that a quasi-steady flow was present in all of our taxa (Table 2-2), suggesting that results obtained from a steady-state analysis should be valid.

Standard sea-level atmospheric pressure (101,325 Pa) was used for the area surrounding the nostrils. The wall boundary incorporated a no-slip boundary condition indicating a lack of movement at the solid-fluid boundary (a standard assumption for laminar flow). Although the mucous and cilia that comprise the respiratory epithelia will contribute to some movement of the air field, these movements are often so slow (≤1cm/min) and their thickness so slight that they can essentially be ignored (Craven et

al. 2009). To determine the pressure and speed at which air must move through the nasal passage to match empirically determined volumetric flow rates, the "target-mass-flow-rate" option in Fluent was used for the pressure outlet boundary. A segregated pressure-based PISO (pressure implicit with splitting of operator) algorithm was used to solve the steady-state continuity and Navier-Stokes equations. A node-based discretization gradient was used on all models. A second-order accurate spatial discretization scheme was used for both pressure and momentum (Fluent 2006). Iterative models ran until all normalized residuals of error had converged to $1.0x10^{-4}$. Point surface monitors placed at various locations on the models were employed as a secondary means of determining convergence independent of continuity and momentum. Results were analyzed using Fluent 13 and Avizo Wind 7.1. Models were tested during resting inspiration and expiration.

To ensure that results remained grid-independent (i.e., grid size did not influence the solution) a three grid convergence index (GCI) for each model was calculated using a grid refinement ratio of 2 (i.e., the coarsest model was half the resolution of the intermediate model which was half the resolution of the finest model). GCI calculations followed the methods of Roache (1994) and Craven et al. (2009).

Results

Grid Independence

We used the area weighted average for pressure drop at the choana as our converged variable of interest. Grid independence was verified for our finest resolution airways, with GCI results indicating errors of less than 10% for most models (Table 2-3).

Soft-tissue airways typically required more tetrahedra than bony-bounded airways in order to accurately reflect the geometry of the nasal capsule.

Morphological Comparisons of the Soft-Tissue Airways

Vestibulum nasi—In *Alligator*, as with all extant crocodylians, the vestibulum nasi was a small, J-shaped structure that extended ventrally a short distance from the naris before curving caudally to join the cavum nasi proprium (Figure 2-4).

In contrast, the vestibulum nasi was much larger in both the bird and lizard taxa examined. In both the turkey and the ostrich, the vestibulum nasi was a spacious structure that housed the rostral and atrial (turkey only) nasal conchae (Figure 2-5, Figure 2-6). These conchae reduced the aperture of the airway in this region. In the turkey, the presence of an operculum over much of the bony narial aperture, along with the atrial concha, served to further reduce the airway dimensions in this region (Figure 2-5C). In contrast, the ostrich naris (fleshy nostril) was very large, resembling the air scoops seen in many sports cars. In both taxa, the caudal extent of the vestibulum nasi was demarcated by a raised ridge—the crista nasalis—separating it from the cavum nasi proprium (Figure 2-5C, Figure 2-6C).

Both the iguana and savannah monitor presented elongate and tubular nasal vestibules (Figure 2-7). In the iguana, an expansion of the vestibulum was observed just deep to the naris (Figure 2-7B). This medial expansion of the vestibulum acts as a reservoir for the hypersaline products released by the nasal gland (Murrish & Schmidt-Nielsen 1970). In the savannah monitor, the vestibulum nasi was composed of a proximal and distal limb (Figure 2-7C, D). The distal limb extended from the caudally placed

nostrils, rostral to the tip of the snout where it formed an expanded cupola (Bellairs 1949). The proximal limb extended caudally from the cupola where the vestibulum nasi became rounder in cross section. A berry-shaped spherical expansion of the vestibulum was observed just prior to the terminus of the vestibulum nasi (Figure 2-7D). In both lizards, as with both birds, the vestibulum nasi was demarcated by the presence of a raised mucosal ridge akin to the crista nasalis. In lizards, this structure is referred to as the postvestibular ridge (Parsons 1970, Figure 2-7).

Cavum nasi proprium—This portion of the nasal cavity is extensively developed in crocodylians. The rostral expansion of the cavum nasi proprium, along with the presence of the preconcha in this region, mirrored the well developed vestibulum nasi in birds and lizards. The olfactory chamber rested caudodorsal to the ductus nasopharyngeus, placing it well away from the path of the respired airfield (Figure 2-4). The concha in *Alligator* was a semi-scrolled structure residing in the olfactory chamber. Crocodylians have a third concha known as the postconcha. As with the concha, the preconcha resided in the olfactory chamber, where its medial wall served as the lateral boundary to the airway (Figure 2-4).

The cavum nasi proprium of both birds contained the remaining conchae. The middle concha was well developed in both taxa. Its shape was either scrolled (turkey, Figure 2-5) or branched (ostrich, Figure 2-6). The medial aspect of the middle concha led directly into the caudal concha. This caudal concha rested caudodorsally to the middle concha. It was a curved structure in both taxa. Partial scrolling was observed in the caudal concha of the ostrich (Figure 2-6).

The cavum nasi proprium of *Iguana* was a spacious structure that housed a single enlarged concha (Figure 2-7A, B). In the savannah monitor the cavum nasi proprium was a much more abbreviated structure featuring a rostrocaudally compressed, dorsoventrally elongated concha (Figure 2-7C, D). The concha curved ventrally towards the ductus nasopharyngeus.

Ductus nasopharyngeus—This region is extremely well developed in crocodylians. In the alligator the ductus nasopharyngeus extended caudally from the primary choana to the secondary choana within the enclosed pterygoids (Figure 2-4).

In both the bird and lizard taxa, the ductus nasopharyngeus was variably developed. In both birds, the ductus nasopharyngeus started at either the caudal half (ostrich) or the caudal 1/4th (turkey) of the middle concha. It was a fairly short, wide structure in ostriches, whereas in turkeys the ductus nasopharyngeus extended a fair distance away from the cavum nasi proprium prior to reaching the choana (Figure 2-5, Figure 2-6).

In *Iguana,* the ductus nasopharyngeus was better developed caudally than rostrally. This resulted in direct access to the choana from the rostral half of the concha whereas the caudal half of the concha remained separated from the choana via a medial shelf (Figure 2-7A). The choana itself was a long, teardrop-shaped structure that ran much of the length of the tooth row. The widest end of the choana was at its caudal terminus. A similar architecture of the ductus nasopharyngeus was observed in the savannah monitor (Figure 2-7C). As with the iguana, a medial shelf separated a portion of the concha. However, given the smaller rostrocaudal dimensions of the cavum nasi

proprium in this taxon, this duct was noticeably smaller than it was in the iguana. The ductus nasopharyngeus arched ventromedially towards the choana. The choana of the savannah monitor was a fairly small, though rostrocaudally elongated, structure that opened into the oral cavity near the distal-most maxillary teeth.

Soft-Tissue and Bony-Bounded Nasal Capsule Morphology

Bony-bounded nasal capsules in all taxa studied were much less defined than were their soft-tissue counterparts (Figure 2-8). The largest differences were observed in the shape of the vestibulum nasi and the removal of conchae. Whereas the vestibulum nasi was enlarged in all the study specimens, it showed a substantial increase in volume in the alligator (Figure 2-8A). Large increases in volume were observed in both bird airways as the removal of conchae removed any partitioning within the nasal capsule (Figure 2-8B, C; see Chapter 3). Portions of the vestibulum nasi extended beyond the boundaries of the bony nasal aperture in both lizards (Figure 2-8D, E; Figure 2-9) which resulted in slight to substantial decreases in length from the soft-tissue nasal capsule. The savannah monitor's vestibulum nasi was further decreased in length (and substantially increased in volume) by the removal of the mucosal barrier that separated the proximal and distal limbs of the vestibulum nasi. The cavum nasi proprium was represented by an enlarged open space in all taxa (Figure 2-8). The ductus nasopharyngeus was the least affected of the nasal structures. In the alligator, the entrance from the primary choana to the ductus nasopharyngeus increased. However the remainder of the structure differed little from its soft-tissue counterpart (Figure 2-8A). Similar limits were seen in the turkey and ostrich, as palatal processes aided in maintaining shape for the ductus

nasopharyngeus (Figure 2-8B, C). Duct shape was less preserved in the two lizard species. In the iguana, the cartilage composing the medial shelf was obliterated, providing direct access from the cavum nasi proprium to the choana. The overall shape of the choana remained the same. In the savannah monitor, the placement of the vomer ventral to the medial shelf aided in maintaining this structure's original shape. However, the lack of soft tissue made the arc into the choana shallower than the soft-tissue nasal capsule. The rostrocaudal length of the choana remained largely intact, but soft-tissue removal made the choana substantially wider.

Airflow in Soft-Tissue Nasal Capsules

Vestibulum nasi—In the alligator, inspired air passed quickly through this abbreviated structure prior to jetting into the somewhat more spacious preconchal meatus. Expiration showed the same pattern albeit in reverse.

Vorticity was observed in the vestibulum nasi of both squamates and birds, though the cause of the vortices was quite different. In the avian taxa, vorticity and flow separation were the result of contact with the rostral and atrial (turkey) nasal conchae. The initial vortex was invoked by air banking off the rostral concha of both birds. Air moved medially around the rostral concha where it was directed caudodorsally into the cavum nasi proprium and the more intricate middle concha of the turkey. Air moving laterally along the turkey's rostral concha was forced to wrap around the concha's caudal edge, as the raised crista nasalis formed a barrier (Figure 2-10A). On the medial side, the air field joined with medial airstreams where they launched off the crista nasalis, producing a jetting action (Figure 2-10C). Upon expiration, air proceeded along the

medial and lateral side of the rostral concha, with lateral airstreams forced into a slight mediolateral spiral caused by the proximity of the atrial concha to the rostral concha. Air entering the ostrich nasal capsule came into contact with the large, snowshoe-shaped rostral concha. The concha diverted the inspired air field into lateral and medial streams. Similarly to the turkey, the lateral airstream curved mediolaterally before entering the cul-de-sac created by the crista nasalis (Figure 2-10B). Air in this lateral stream wrapped ventrally around the rostral concha and arced caudodorsally over the hillock comprised of the septal concha (Figure 2-10D bottom) where it entered the CNP. During expiration, airflow along the dorsal aspect of the nasal capsule predominantly moved along the medial side of the rostral concha prior to exiting the nostril. A slightly greater pressure gradient along the caudolateral aspect of the rostral concha resulted in a portion of the air field exiting the middle meatus where it arced under the rostral concha and proceeded along its lateral aspect towards the nostril.

In the iguana nasal capsule, the geometry of the vestibulum nasi, coupled with the laterally placed nostril, imparted a mediolateral spiral to the inspired air (Figure 2-11A2), resulting in the most air streams preferentially staying in the medial half of the nasal vestibule. On expiration this was reversed, with more air moving over the lateral end of the vestibule (Figure 2-11A3). As with inspiration, a vortex formed within the air field upon expiration. A portion of the air field passed over the medial expansion of the vestibulum nasi during both inspiration and expiration (Figure 2-11A insets). The vestibulum nasi in the savannah monitor was greatly elongated, with the caudally placed nostrils forming an extra limb to the vestibulum nasi, making for a broad, u-shaped

vestibule (Figure 2-11B1). Air moved around the expanded cupola, creating a standing vortex in its rostroventral half (Figure 2-11B1). Just prior to the postvestibular ridge, the vestibulum nasi formed a spherical capsule with constrictions on either end. These constrictions greatly sped up the inspired air causing it to jet into the more spacious cavum nasi proprium (Figure 2-11B2). On expiration, this spherical capsule functioned as a mixing chamber, creating a swirling jet of outgoing air into the proximal limb of the vestibulum nasi, which formed a vortex that wrapped around the cupola prior to exiting through the distal limb and naris (Figure 2-11B3). No vorticity was observed in the rostroventral half of the cupola upon expiration.

Cavum nasi proprium —Straight, laminar airflow dominated the preconchal meatus. A noticeable increase in air velocity was observed at the junction of the primary choana and the olfactory chamber. This jetting effect was caused by a mucosal constriction at this junction, followed by a sudden expansion caused by the preconchal recess. This jetting effect produced stationary vortices on both the lateral and the medial sides of the nasal capsule wall (Figure 2-12). These were counter-rotating vortices. When observed dorsally (Figure 2-12B), the lateral vortex moved clockwise whereas the more caudomedial vortex moved counter-clockwise. Air streams from both vortices drained into the ductus nasopharyngeus. Airflow in the olfactory chamber moved unidirectionally with air entering medially to the concha and exiting lateral to it in the postconchal meatus (Figure 2-13A). No evidence of secondary flow in the olfactory chamber was observed during inspiration, nor was there any flow within the postconcha itself. Flow during expiration was largely similar but with no airflow in the olfactory chamber (Figure

2-13B). Some slight secondary flow was noted at the junction of the primary choana and the olfactory chamber (Figure 2-13B).

Inspiratory airflow in the cavum nasi proprium of the turkey quickly split into lateral and medial airstreams as it contacted the coiled middle concha. The lateral airstreams continued through the middle concha where they further split, producing lateral-to-medial vortices that eventually exited at the entrance to the ductus nasopharyngeus (Figure 2-14A). The medial stream ran alongside the middle concha, fanning out across it. Dorsal-most streamlines meandered towards the olfactory chamber and the caudal concha (Figure 2-14B). Air passed over the convex caudal concha before continuing caudoventrally towards the ductus nasopharyngeus (Figure 2-14B). During expiration the olfactory chamber showed complete washout with air speeding through the chamber at similar velocities observed during inspiration. The air field appeared to cross the middle concha more medially than laterally during expiration, though air movement was still present throughout. In the ostrich, medial and lateral air streams coming from the rostral concha took different paths upon contact with the complicated middle concha (Figure 2-15). Banking and branching of the airway was noted in the ostrich middle meatus, with most branches converging at the entrance of the nasopharyngeal duct. The single exception to this pattern was the medial branch of the middle concha. Air in this region was under higher pressure than elsewhere in the middle meatus, resulting in a substantial slowdown in the air field (Figure 2-15). This medial branch of the air field meandered dorsally into the olfactory chamber and the caudal meatus. Air passed both dorsally and ventrally between the semi-scrolled caudal concha (Figure 2-15). Airflow in

the olfactory chamber was unidirectional with the returning airstreams moving along the medial side of the caudal concha. An enlarged, capsular extension dorsal to the caudal concha remained almost entirely clear of airflow and showed no evidence of a functional role during inspiration (Figure 2-16A). Upon expiration, the air field traveled predominantly along the lateral aspect of the middle concha. Two major airstreams were detected (Figure 2-16B, C). A ventrally located airstream moved from the lateral to medial side of the middle meatus where it arced over the septal concha and entered the rostral meatus. The second airstream included a ventromedial branch that moved along the outside of the middle concha before entering its lateral branch and moving into the rostral meatus (Figure 2-16B). A miniscule third airstream was observed running along the dorsomedial aspect of the middle meatus before anastomosing with the second airstream in the lateral branch of the middle concha. Little to no air movement was observed in the olfactory chamber, its dorsal extension, nor the medial branch of the middle concha during expiration (Figure 2-16B, C).

Airflow was not homogeneous across the conchae of either squamate species in the sample. The majority of airflow in the cavum nasi proprium of the iguana took a caudoventral path towards the ductus nasopharyngeus (Figure 2-17A), with a slower path of air moving around the caudolateral aspect of the concha (Figure 2-17B). In the savannah monitor, the formation of a medial ridge coming off the concha served to split the air field into caudal and rostral streams (Figure 2-18). Upon expiration the majority of the air field passed over the rostral—respiratory—region of the iguana concha, leaving the olfactory region relatively untouched, although slow air movement was still observed

(Figure 2-17C). Greater olfactory washout was noticed in the savannah monitor during expiration (Figure 2-18B).

Ductus nasopharyngeus and choana—In the alligator, air dipped from the primary choana into the ductus nasopharyngeus where it continued straight and laminarly through to the secondary choana. A similar pattern, albeit reversed, was noted during expiration. For the turkey, air entered into the ductus nasopharyngeus via all aspects of the middle meatus. Olfactory flow rejoined the main air field via a communication between the caudal meatus and the ductus nasopharyngeus. Flow pattern was much the same during expiration. In the ostrich all respired air entered and exited the ductus nasopharyngeus from the middle meatus. No contribution from the olfactory chamber was seen. The cartilage composing the ductus nasopharyngeus in the iguana imparted a vortex to the inspired air field. This resulted in air taking a more circuitous route towards the choana. Despite being a long, open structure, the caudal position of the pressure drop (coming from the glottis and ultimately the lungs) as well as the vortex imposed on the air field by the cartilage of the ductus nasopharyngeus, resulted in the majority of inspired air exiting from the expanded, caudal terminus of the choana (Figure 2-19). During expiration, air entered the choana from all along its length. Rostral-most airstreams proceeded dorsally into the cavum nasi proprium whereas air entering from the caudal, teardrop-shaped, end was directed rostrodorsally. This resulted in all airstreams converging on the rostroventral region of the iguana concha. The ductus nasopharyngeus in the savannah monitor contained a medial shelf where inspired air from the cavum nasi proprium would enter before arcing lateroventrally into the choana. Inspired air entered

the oral cavity across much of the choana, though a slight caudal draw to the air field was observed. Expiration revealed little air movement within the medial shelf as expired air made a straighter path dorsally into the cavum nasi proprium.

Airflow in Bony-Bounded Nasal Capsules

Bony-bounded nasal capsules had pressure drops and respiratory velocities that were fractions of their soft-tissue counterparts. The large empty spaces within the nasal capsules resulted in more homogeneous air fields. The largest pressure drops, and fastest flow speeds were present in the ductus nasopharyngeus for all species. No separation of airflow into olfactory and respiratory streams was observed in any of the taxa. Some aspects of the air field unique to each taxon, are discussed below.

The more open olfactory chamber in the alligator resulted in substantially slower air movement (Figure 2-20C), with large sections of the chamber containing stagnant air. This pattern was true for both inspiration and expiration (Figure 2-20A, B), with larger portions of the olfactory chamber containing stagnant air during expiration than during inspiration (Figure 2-20B).

Despite a lack of soft-tissues to redirect airflow, a similar set of spiraling airstreams was observed in the turkey's bony-bounded nasal capsule during inspiration (Figure 2-21A, B). This spiraling took place in the region that housed the rostral meatus in the ST airway. These vortices were less developed than the vortices seen in the soft-tissue nasal capsule. Spiraling continued caudally into the rostral portion of the middle meatus before dissipating. A generally homogeneous distribution of airflow was observed during both inspiration and expiration (Figure 2-21A, C). In the ostrich airway, a

dorsoventral velocity gradient was observed, with more dorsally located airstreams moving slower than more ventrally located airstreams. This was not unexpected as the ventral regions of the nasal capsule contained the pressure inlets and outlets. The more homogeneous flow in the bony-bounded ostrich nasal capsule resulted in slightly more air movement within the sinus dorsal to the caudal concha (Figure 2-22), though airflow to this region was still low overall.

As with the turkey, similar spiraling motions to the soft-tissue nasal capsule were observed in the iguana. Lateral nostril placement coupled with the raised septomaxilla imparted spiraling motion to the inspired air field (Figure 2-23A). The pressure gradient present along the bony-bounded nasal capsule during expiration resulted in air jetting up into the cavum nasi proprium before arcing mediolaterally prior to contacting the tectum nasi and then proceeding rostroventrally towards the nostril, which resulted in lateral airstreams moving straight towards the nostril whereas medial airstreams—partially blocked by the septomaxilla—made a corkscrew spiral towards the nostril (Figure 2-23B). The rough placement of the nostril in the bony-bounded nasal capsule of the savannah monitor resulted in air spraying across the nasal capsule during inspiration (Figure 2-24A). Portions of the air field moved caudally immediately upon entering the nasal capsule. Surprisingly, a fairly large portion of the air field followed the same route from the nostril as in the soft-tissue-bounded nasal capsule, taking a rostromedial route from the nostril before arcing caudally towards the cavum nasi proprium (Figure 2-24A). The bony-bounded nasal capsule lacked any separation between the airway and the chamber housing the vomeronasal organ. This resulted in some air passing into the

vomeronasal chamber (Figure 2-24C). As this cavity was out of the main airflow path, only negligible air movement was noted (typically < 3 mm/s). Some vorticity was observed in the cavum nasi proprium as air from the spacious vestibulum nasi arced down towards the ductus nasopharyngeus (Figure 2-24A). This spiraling occurred approximately at the junction of the postvestibular ridge and the concha. Most of the air field coming off this vortex continued ventrally into the choana. Airflow during expiration was similar to inspiration. No spiraling was observed as the air field made a fairly direct path towards the nostril (Figure 2-24B). Little airflow was observed in the olfactory chamber. The pressure gradient within the nasal capsule was such that very little airflow was seen near the cavity leading to the vomeronasal organ.

Discussion

Despite vast differences in morphology and physiology, grossly similar airflow patterns were observed in all the taxa studied. Laminar flow dominated the air field under resting conditions for all taxa studied, including the ostrich, which was the only species for which Reynolds number data suggested may have had transitional flow patterns. Secondary flows (laminar vortices) were observed, but were limited to small sections of the airway in all taxa. Prior studies have found laminar flow to be the dominant airflow pattern during resting respiration (Craven et al. 2009, Jiang and Zhao 2010, Holmes et al 2011). Laminarity is partly a result of the generally low Reynolds numbers present in most of the airways in this study (Table 2-2). However, there are energetic reasons associated with laminar and turbulent fluid flow that indicate that laminar flow may have been selected for during nasal passage evolution. The nasal passage is a contained

structure that moves air between the nostrils and choanae. This makes the flow of fluid (air) through this system, akin to fluid flow through a pipe. The physics of fluid flow through enclosed structures such as pipes tells us that, for a given length of pipe, the resistance of a fluid to movement within that pipe will be inversely related to the radius of the pipe's cross section raised to the fourth power (viz. Hagen-Poiseuille's Law; Vogel 1994). Under a laminar flow regime, this resistance will further increase in proportion to velocity (Swift 1982, Vogel 1994). In contrast, under turbulent conditions, local pressure drops caused by regional vorticity greatly increase resistance of the fluid to forward momentum. Now instead of increasing in direct proportion to the velocity gradient, turbulent fluid flow in a pipe increases its resistance by the square of velocity (Swift 1982). Thus, pipes with turbulent fluid flow require an overall steeper pressure gradient to maintain the same flow rate as pipes with laminar flowing fluids (Vogel 1994). Physiologically, this relationship means that pushing turbulent air through a nasal passage will require more energy. As a result, perhaps it is not surprising to find evidence of anatomical and physiological strategies that appear to promote laminarity in the airways, such as airway dilation and a switch to oropharyngeal breathing during moderate to intense exercise in many taxa (McCaffrey & Kern 1979, Saibene et al. 1981, England & Bartlett 1982, Lafortuna et al. 2003).

The paranasal sinus system of archosaurs is extensively developed (Witmer 1995a) with many of these sinuses having ostia that open directly into the nasal capsule. Most of these sinuses were not incorporated into these models. The cul-de-sac nature of the sinuses coupled with ostia that are often perpendicular to the direction of the respired

air field suggest that these are not well ventilated regions. Incorporating them would have resulted in needless complexity. However, we did perform an exploratory test involving a model of the alligator airway that incorporated all of its paranasal sinuses. Results confirmed the presence of stagnant air within the multiple sinuses surrounding the nasal capsule. Similarly, models of the ostrich and savannah monitor both incorporated structures that were suspected of being sinuses. For the ostrich, there was a dorsal extension from the caudal concha that formed an inflated bulla within the skull (Figure 2-16A, Figure 2-25A). For the savannah monitor, the potential paranasal sinus was a ventral extension off the caudal limb of the vestibulum nasi (Figure 2-7C, Figure 2-25B). The bilateral symmetry of these structures in the monitor lizard and ostrich, coupled with their presence in multiple specimens, validated that they were not artifacts of preservation. Stagnant airflow in both structures (Figure 2-25) further suggested that both should be considered sinuses. However, the structure of these sinuses was very different between the two species. Witmer and Ridgely (2008) figured the bulla in ostriches as part of the olfactory recess, largely due its placement near the olfactory bulbs and associated nerves. Histologically, olfactory epithelia were observed in this bulla. However, the bulla resided substantially dorsal to the caudal (olfactory) concha, where it inflated the overlying frontals and nasals. This hard-tissue pneumatization is a hallmark of the paranasal sinuses in archosaurs and mammals (Witmer 1995a, 1999), and may indicate that the bulla developed as an opportunistic invasion of the surrounding bone (Witmer 1997). However, since this sinus developed from within the nasal cavity, as opposed to the extracapsular origin of paranasal sinuses (Witmer 1995b, 1997), it would have

brought with it, epithelia from the olfactory recess. It remains possible that this olfactory bulla is simply an extension of the olfactory recess and that under a more intense breathing regime (e.g., sniffing) air could cycle through it. Further investigation will be needed to determine the origin of this structure.

In contrast, the sinus observed in our varanid was a soft-tissue only evagination of the vestibulum nasi. The structure of this sinus was somewhat similar to the extraconchal recess, which is the only nasal structure previously considered to be a potential paranasal sinus in lizards (Bellairs 1949, Parsons 1970 [= subconchal recess], Bellairs and Kamal 1981, Witmer 1999). As with the extraconchal recess, the structure that we observed evaginating ventrally from the vestibulum nasi was a soft-tissue-only structure with no associated bone pneumatization. In the monitor lizard, these sinuses appear to be an epiphenomenon caused by an incompletely floored nasal capsule (Bellairs 1949).

The partitioning of the air field into multiple channels was observed in all the taxa studied. Air field partitioning varied between taxa, with the two birds exhibiting the most divisions. For most of the taxa there was at least one airstream that consisted of slower moving air which flowed towards the olfactory chamber. The single exception to this was the turkey, which split its air field but did not show signs of airflow velocity reduction in the olfactory chamber. For the other taxa the presence of slower, olfactory flow mirrored observations in other taxa (Negus 1958, Craven et al. 2009) showing that nasal capsule soft-tissue anatomy functions in creating air field heterogeneity.

In crocodylians the greatly elongated nasopharyngeal duct separated the olfactory chamber from the main pressure drop in the nasal capsule. Sequestration of the ductus

nasopharyngeus by the pterygoids formed the equivalent of the *lamina transversa* in macrosmatic mammals (Craven et al. 2010). This resulted in air traveling unidirectionally through the olfactory chamber during inspiration, but remaining stagnant during expiration. A similar setup was observed in ostriches, which separated their olfactory chamber using the cartilaginous body of the middle concha, allowing access via the medial branch of the middle concha only. In contrast, the olfactory chamber of the turkey remained patent to the main airway via a caudal connection between the olfactory concha and the choana. This connection to the choana in the turkey allowed bidirectional flow of air within the olfactory chamber, resulting in olfactory washout during expiration. These results suggest that turkeys have much lower potential to sift and analyze airborne particles than ostriches. This interpretation agrees well with behavioral observations of wild turkeys (Pelham and Dickson 1992).

It was somewhat surprising to observe airflow separation in the nasal capsule of the squamates studied. The cavum nasi proprium in squamates does not, on the surface, appear to offer a means of isolating olfactory airflow from respiratory airflow, resulting in what should be uniform pressure drop and airflow across the entire concha. However the results of our fluid dynamic analyses suggest that there is heterogeneous flow within the cavum nasi proprium. For iguanas, this separation of airflow occurred over the caudodorsal region of the concha. This appears to have been afforded by the spiral-shaped cartilage of the ductus nasopharyngeus. Its spiral shape produced a medial shelf that served to isolate the caudal region of the concha from the choana, producing a higher pressure cul-de-sac region. This separation from the main airway also reduced (but did

not eliminate) olfactory washout during expiration. A similar flow pattern was noted in the savannah monitor, which presented a medial ridge along its concha. This ridge served to separate flow from the rostral and caudal aspects of the concha. Regionalization of the concha lined up well with distribution of epithelia types on squamate conchae (Gabe and Saint-Girones 1976, Rehorek et al. 2000) and agrees with prior anatomical studies of squamate nasal architecture (Kratzing 1975, Bellairs 1949, Bellairs & Boyd 1950, Bernstein 1999). Together they suggest that previous interpretations of squamate (and reptile) conchae as strictly olfactory in function (Hillenius 1992; Ruben et al. 1998, 2012) have oversimplified the function of these structures.

Another similarity observed in all the taxa studied was the presence of constrictions along the airway. In squamates and birds, the diameter of the airway showed a consistent constriction at the junction of the vestibulum nasi and the cavum nasi proprium. This constriction took the form of the crista nasalis in birds and the postvestibular ridge in squamates. The short vestibulum in the alligator had no constrictions prior to entering the much elongated cavum nasi proprium. However, airway constriction did occur further caudally at the junction of the primary choana and the ductus nasopharyngeus. Over the course of crocodylian evolution the airway was extended via stretching of the cavum nasi proprium rather than the vestibulum nasi as in other diapsids (Figure 2-4–7). The preconchal meatus of crocodylians appears to function aerodynamically as an elongate vestibulum nasi, complete with a constriction at its caudal terminus just prior to entering the olfactory chamber.

The results of each taxon's airway constriction was a localized pressure drop that pushed air through at a higher velocity prior to jetting out into the more spacious cavum nasi proprium or, in the case of the birds, following conchal tracts. This Venturi effect imparted extra momentum on the airborne particles pushing them further into olfactory chamber. The presence of two counter-rotating vortices on either side of the olfactory chamber in the alligator (Figure 2-12B) may have further aided in pushing air further into the olfactory chamber.

Airflow in bony-bounded nasal capsules was markedly different from that of their soft-tissue counterparts. Bony-bounded nasal capsules produced slower moving, more homogeneous air, with airway stagnation being more commonplace in all the taxa studied. Surprisingly, respired air in the bony-bounded airways did occasionally show similar, albeit cruder, patterns to their soft-tissue counterparts. In the turkey, iguana, and varanid, the air field in the bony-bounded nasal capsule reproduced certain spiral motions of the air field that were also observed in the soft-tissue nasal capsule (Figure 2-21A, Figure 2-23A, Figure 2-24). These results indicate that aspects of the bony-outer boundaries are responsible for some components of the respired air field and that the soft tissue acts more to augment and refine these characteristics. This phenomenon is perhaps best exemplified in the savannah monitor. The bony-bounded nasal capsule of the savannah monitor produced the same arching flow pattern within the vestibulum nasi as was observed in the soft-tissue nasal capsule (Figure 2-24). The doming of the septomaxilla appears to be responsible for this similarity. Doming effectively separated the rostral region of the nasal capsule from the caudal region. A prominent ridge on the

medial aspect of the septomaxilla enhanced this regionalization. This septomaxillary ridge left a medial trough within the nasal capsule which served as a low pressure tunnel that funneled air rostrally from the nostril, through a medial arch and caudally towards the choana (Figure 2-26). In life, this ridge is covered in a large slab of well vascularized mucosa. This mucosa completely separates the lateral vestibulum nasi from its medial limb, producing a much more pronounced arching pattern to the inspired airflow. Similarity was also observed in regions where air did not flow, such as the olfactory bulla in the ostrich and the vomeronasal chamber in the savannah monitor (Figure 2-16, Figure 2-22, Figure 2-24).

Results from the bony-bounded nasal capsule comparisons have immediate implications for airflow reconstruction in extinct taxa. Airflow simulation in currently reconstructed, bony-bounded nasal capsules of extinct taxa are likely underestimating the physiological abilities of the animals being studied due to the larger, more empty nasal regions reconstructed. However, the presence of certain flow patterns in even these "low-resolution" models of nasal anatomy has the potential to illuminate the true flow patterns that would have been present in the living animals. Thus, airflow reconstruction in extinct taxa can benefit from these first pass, low-resolution studies as they can help identify regions of airflow that may be real.

Accounting for Missing Soft Tissue

Comparing the soft-tissue nasal capsules to their bony-bounded counterparts illustrates just how much airway shape is dictated by soft tissues (Figure 2-27). A preliminary survey of soft tissue proportions in the nasal capsule revealed substantial

variation between nasal regions across taxa (Figure 2-28). However a general pattern did emerge. The vestibulum nasi had the most variable amount of soft tissue (Figure 2-28). This agrees will with general anatomical studies which have shown this region of the nasal capsule to be the most structurally labile (Stebbins 1948, Bang and Wenzel 1985, Witmer 1995b). Surprisingly, this proved true in the alligator as well despite its rather miniscule vestibulum nasi. The large collection of soft-tissue filling the space of the alligator vestibulum nasi is related to the unique narial musculature of crocodylians (Bellairs and Shute 1953) coupled with extensive erectile tissue that may be further elaborated into visual and auditory structures as in gharials (Martin & Bellairs 1977). For some taxa, such as the two lizards, the bony-bounded nasal capsule did not completely encapsulate the length of the soft-tissue nasal capsule due to soft-tissue extensions that went beyond the border of the bony nasal aperture. These soft-tissue extensions represented a significant proportion of the nasal capsule in the varanid, with over half of the convoluted vestibulum nasi extending beyond the borders of the bony narial aperture (Figure 2-9).

The cavum nasi proprium proved to be the least variable region in terms of soft-tissue proportions (Figure 2-28). Despite vast differences in conchal shape and number between the study taxa, the proportion of soft tissues comprising this region was fairly steady at 44%–66% (mean 54%). The relatively static cavum nasi proprium, compared to other nasal regions, suggests that the CNP is more restricted in relative expansion compared to other regions of the nasal passage. It's possible that the location of the CNP to other sensory and functional systems within the skull (e.g., the eyes and jaw muscles),

forces a compromise on CNP expansion, limiting the extent to which new soft tissues can excavate space within the skull.

When comparing the bony-bounded and soft-tissue nasal capsules it became readily apparent just how small the airway was in relation to the potential space that it could encompass (Figure 2-27). In the soft-tissue nasal passages of all five specimens the average distance from the center of the air field to the nearest mucosal wall was less than 2.5 mm, with most areas less than 1.5 mm (Table 2-4). These small distances agree well with previous comparative nasal studies on mammals (Jackson and Schmidt-Nielsen 1964, Langman et al. 1979), birds (Schmidt-Nielsen et al. 1970), and reptiles (Murrish and Schmidt-Nielsen 1970). These incredibly small distances from the air field to the mucosa of the nasal passage can be explained by the process in which heat, moisture, and odorants are transferred throughout the nasal passage. All of these processes are diffusion dependent. Diffusion is a rather slow and inefficient process by itself (Vogel 1994). However, the efficiency of this process can be boosted by increasing the surface area of the substrate relative to its volume, and by increasing the transit time of the molecules moving through the structure (Schmidt-Nielsen et al. 1970, Collins et al. 1971, Vogel 1994). Anatomically, this can be accomplished by separating the nasal passage into multiple smaller compartments. Birds and mammals do this with their various scrolled or branched conchae. An alternative method is to compress and extend the overall length of the nasal passage as squamates and crocodylians have done.

It is noteworthy that even large taxa such as the 74 kg ostrich used in this study, or the 600 kg giraffes and oxen used by Langman et al. (1979), had radial distances from

the center of their air fields to the mucosal wall of approximately 2 mm. This remarkable conservation of nasal passage caliber suggests that the physical limitations of diffusion are not overwhelmed by increases in body mass. Thus, even large animals should be expected to have extremely narrow nasal passages. Diversity in nasal passage shape becomes a byproduct, in part, from the different ways in which taxa solve this diffusion problem.

Airway proportions and the remarkable stability of airway distance within the nasal passages suggest that previous nasal passage reconstructions in dinosaurs and other extinct taxa, grossly overestimated airway size. These enlarged airways will have direct consequences for any analyses that use them to determine aspects of physiology such as olfactory sensitivity (Ostrom 1962), air conditioning capacity (Wheeler 1978), or even metabolic rate (Ruben et al. 1996).

Conclusions

Fluid dynamic analyses of the airways in a variety of extant diapsids have revealed heretofore unknown flow patterns and characteristics for this diverse assemblage of extant tetrapods. Despite large differences in life history between birds, crocodylians, and lizards, some common airflow patterns were observed between all five taxa. The most notable commonality was a constriction within the airway near the region of the olfactory chamber.

Comparing soft-tissue and bony-bounded nasal capsules in extant animals along with the use of computational fluid dynamics to simulate fluid movements, revealed the extent to which the soft tissues affect airflow. Models devoid of all soft-tissue boundaries

produced very different results from their soft-tissue counterparts and resulted in unrealistic flow patterns within regions of the nasal capsule (in particular, the olfactory chamber). These results indicate that previous soft-tissue reconstructions of the nasal passages in extinct taxa such as dinosaurs are likely overly conservative, resulting in an underestimation of the physiological abilities for this region of anatomy. A preliminary survey of soft-tissue proportions within the nasal capsule suggests that the cavum nasi proprium is the least variable region of the nasal capsule, and thus has the potential to be the best region of nasal anatomy for soft-tissue reconstruction in extinct animals.

Acknowledgments

WitmerLab members W. Ruger Porter, Ashley Morhardt, Ryan Ridgely, Don Cerio, and Catherine Early. FarmerLab members: C.G. Farmer and Emma Schachner. Rex Lab member: Eric Snively. We wish to thank Ruth Elsey of the Rockefeller Wildlife Refuge, the Miami Metro Zoo, Willem M. Roosenburg, and Stephen M. Reilly for providing the specimens used in this study.

Funding

This project was made possible through the National Science Foundation Graduate Research Fellowship and a Student Enhancement Award provided by Ohio University.

References

Agarwal, R. 1999. Computational Fluid Dynamics of Whole Body Aircraft. Annu Rev Fluid Mech. 31:125–169.

Bang, B.G. 1971. Functional anatomy of the olfactory system in 23 orders of birds. Acta Anat. 79(58):1–76.

Bang, B.G. 1966. The olfactory apparatus of tubenosed birds (Procellariiformes). Acta Anat. 65:391–415.

Bang, B.G., 1964. The nasal organs of the black and turkey vultures; A comparative study of the cathartid species *Coragryps atratus atratus* and *Cathartes aura septentrionalis* (with notes on *Cathartes aura falklandica*, *Psudogyps bengalensis*, and *Neophoron percnopterus*). J Morph. 115:153–184.

Bang, B.G., Wenzel, B.M. 1985. Nasal cavity and olfactory system. in King, A.S., McLelland, J. (eds). Form and Function in Birds. Vol. 3. Academic Press. New York. pp:195–225.

Bertmar, G. 1969. The vertebrate nose, remarks on its structural and functional adaptation and evolution. Evolution. 23(1):131–152.

Bellairs, A.D'A. 1950. Observations on the cranial anatomy of *Anniella*, and a comparison with that of other burrowing lizards. Proc Zool Soc Lond. 119(4):887–904.

Bellairs, A.D'A. 1949. Observations on the snout of *Varanus*, and a comparison with that of other lizards and snakes. J Anat. 83(pt2):116–146.

Bellairs, A.D'A. Boyd, J.D. 1950. The lachrymal apparatus in lizards and snakes—II. The anterior part of the lachrymal duct and its relationship with the palate and with the nasal and vomeronasal organs. Proc Zool Soc Lond. 120:269–310.

Bellairs, A.D'A., Kamal, A. 1981. The chondrocranium and development of the skull in Recent reptiles. in Gans, C. Parsons, T.S. (eds). Biology of the Reptilia: Volume 11: Morphology. F. New York: Academic Press. pp:1–264.

Benton, M.J. 2005. Vertebrate Paleontology. Wiley-Blackwell. Malden, MA.

Bernstein, P. 1999. Morphology of the nasal capsule of *Heloderma suspectum* with comments on the systematic position of helodermatids (Squamata: Helodermatidae). Act Zool. 80:219–230.

Bertmar, G. 1969. The Vertebrate Nose, Remarks on Its Structural and Functional Adaptation and Evolution. Evolution. 23(1):131–152.

Brackenbury, J.H. 1982. The structural basis of voice production and its relationship to sound characteristics. in Kroodsma, D.E., Miller, E.H., Ouellet, H. (eds.). Acoustic Communication in Birds. Vol. 1. Academic Press, New York. pp:53–73.

Brusatte, S.L. 2012. Dinosaur Paleobiology. Wiley-Blackwell, Hoboken, NJ.

Brzustowicz, J.P., Lounsberry, T.H., Esclafer de la Rode, J.M. 2002. Experimental and computational simulations utilized during the aerodynamic development of the Dodge Intrepid R/T race car. SAE 2002-01-3334.

Brzustowicz, J., Lounsberry, T., Esclafer de la Rode, J.M. 2003. Improving racecar aerodynamics. SAE Automot Eng. 111(5):95–98.

Busch, C.H. 1898. Beitrag zur Kenntniss der Gaumenbildung bei den Reptilien. Zool Jb Abt Anat. 11:441-500.

Chen, X.B.B.E., Lee, P.H., Chong, V.F.H., Wang, D.Y. 2009. Assessment of Septal Deviation Effects on nasal Air Flow; A Computational Fluid Dynamics Model. Laryngoscope. 119:1730–1736.

Churchill, S.E., Shackelford, L.L. Georgi, N., Black, M.T. 2004. Morphological Variation and Airflow Dynamics in the Human Nose. Am J Hum Biol. 16:625–638.

Collins, J.C., Pilkington, T.C., Schmidt-Nielsen, K. 1971. A model of respiratory heat transfer in a small mammal. Biophys J. 11:886–914.

Coulson, R.A., Hernandez, T. 1983. Alligator Metabolism. Studies on Chemical Reactions In Vivo. Comp Biochem Physiol B. 74(1):1–182.

Coulson, T.D., Coulson, R.A., Hernandez, T. 1973. Some observations on the growth of captive alligators. Zoologica. 58(2):47–52.

Craven, B. A. 2008. A fundamental study of the anatomy, aerodynamics, and transport phenomena of canine olfaction. University Park, PA: The Pennsylvania State University.

Craven, B.A., Neuberger, T., Paterson, E.G., Webb, A.G., Josephson, E.M., Morrison, E.E., Settles, G.S. 2007. Reconstruction and Morphometric Analysis of the Nasal Airway of the Dog (*Canis familiaris*) and Implications Regarding Olfactory Airflow. Anat Rec. 290:1325–1340.

Craven, B.A., Paterson, E.G., Settles, G.S. 2010. The fluid dynamics of canine olfaction: unique nasal airflow patterns as an explanation of macrosmia. J R Soc Interface. 7:933–943.

Craven, B.A., Paterson, E.G., Settles, G.S., Lawson, M.J. 2009. Development and Verification of a High-Fidelity Computational Fluid Dynamics Model of Canine Nasal Airflow. J Biomech Engin. 131:91002-1—11.

Dawes, J.D.K. 1952. The course of nasal airstreams. J Laryn Oto. 66:583–593.

Doorly, D.J., Taylor, D.J., Schroter, R.C. 2008. Mechanics of airflow in the human nasal airways. Resp Phys Neuro. 163:100–110.

Elad, D., Liebenthal, R., Wenig, B.L., Einav, S. 1993. Analysis of Air Flow Patterns in the Human Nose. Med Biol Engin Comput. 31:585–592.

Elad. D., Wolf, M., Keck. T. 2008. Air-conditioning in the human nasal cavity. Resp Phys Neuro. 163:121–127.

England, S.J., Bartlett Jr., D. 1982. Changes in respiratory movements of the human vocal cords during hyperpnea. J Appl Physiol. 52:780–785.

Erickson, G.M., Lappin, K.A., Vilet, K.A. 2003. The Ontogeny of Bite-Force Performance in American Alligator (*Alligator mississippiensis*). J Zool. 260(3):317–327.

Evans, D., Witmer, L.M., Ridgely, R.C. 2009. Endocranial anatomy of lambeosaurine dinosaurs: a sensorineural perspective on cranial crest function. Anat Rec. 292:1315–1337.

Farmer, C.G., Carrier, D.R. 2000a. Pelvic Aspiration in the American Alligator (*Alligator mississippiensis*). J Exp Biol. 203:1679–1687.

Farmer, C.G., Carrier, D.R. 2000b. Ventilation and Gas Exchange During Treadmill Locomotion in the American Alligator (*Alligator mississippiensis*). J Exp Biol. 203:1671–1678.

Farmer, C.G., Sanders, K. 2010. Unidirectional Airflow in the Lungs of Alligators. Science. 327:338–340.

Fletcher, C.A.J. 1991. Theoretical Background. in Glowinski, R., Holt, M., Hut, P., Keller, H.B., Killeen, J., Orszag, S.A., Rusanov V.V. (eds). Computational Techniques for Fluid Dynamics 1: Fundamental and General Techniques. Springer-Verlag. New York, NY.

Fluent. 2006. Fluent 13 Getting Started Guide. Fluent Inc.

Foss, J.F. 1998. Basic Engineering of Fluid Mechanics. in Johnson, R.W. (ed). The Handbook of Fluid Dynamics. CRC Press. Boca Raton, Fl.

Frappell. P.B., Schultz, T.J., Christian, K.A. 2002. The respiratory system in varanid lizards: determinants of O2 transfer. Comp Biochem Physiol. 133A:239–258.

Frappell. P.B., Hinds, D.S., Boggs, D.F. 2001. Scaling of respiratory variables and the breathing pattern in birds: an allometric and phylogenetic approach. Phys Biochem Zool. 74(1):75–89.

Freitas, C. 1993. Journal of Fluids Engineering Editorial Policy Statement on the Control of Numerical Accuracy. ASME J Fluids Engin. 115:339–34.

Frey, R., Volodin, I., Volodina, E. 2007. A nose that roars: Anatomical specializations and behavioural features of rutting male saiga. J Anat. 211:717–736.

Gabe, M., Saint Girons, H. 1976. Contribution a la morphologie comparee des fosses nasales et de leurs annexes chez les lepidosoriens. Memoires du museum national d'histoire naturelle series A: Zoologie.

Garcia, G.J.M., Bailie, N., Martins, D.A., Kimbell, J.S. 2007. Atrophic Rhinitis: A CFD Study of Air conditioning in the Nasal Cavity. J Appl Physiol. 103:1082–1092.

Gatesy, S.M. 2009. Hind Limb Movements of the American Alligator (*Alligator mississippiensis*) and Postural Grades. J Zool. 224(4):577–588.

Geist, N.R. 2000. Nasal respiratory turbinate function in birds. Physiol Biochem Zool. 73(5):581–589.

Giordano, R.V., Jackson, D.C. 1973. The effect of temperature on ventilation in the green iguana (*Iguana iguana*). Comp Biochem Physiol. 45A:235–238.

Girardin, M., Bilgen, E. Arbour, P. 1983. Experimental Study of Velocity Fields in a Human Nasal Fossa by Laser Anemometry. Ann Otol Rhino Laryngol. 92:231–236.

Gizurarson, S. 1993. The relevance of nasal physiology to the design of drug absorption studies. Adv Drug Deliv Rev. 11:329–347.

Green, P.A., Van Valkenburgh, B., Pang, B., Bird, D., Rowe, T., Curtis, A. 2012. Respiratory and olfactory turbinal size in canid and arctoid carnivorans. J Anat. 221(6):609–621.

Gussekloo, S.W.S. 2006. Feeding structures in birds. in Bels, V. (ed). Feeding in Domestic Vertebrates: From Structure to Behaviour. Cambridge, MA. CABI Publishing.

Hahn, I., Sherer, P.W., Mozell, M.M. 1993. Velocity Profiles Measured for Airflow through a Large-Scale Model of the Human Nasal Cavity. J App Physiol. 75(5):2273–2287.

Hicks, J.W., Farmer, C.G. 1999. Gas Exchange Potential in Reptilian Lungs: Implications for the Dinosaur-Avian Connection. Resp Physiol. 117:73–83.

Hieronymus, T. L., Witmer, L.M., Tanke, D.H., Currie, P.J. 2009. The facial integument of centrosaurine ceratopsids: morphological and histological correlates of novel skin structures. Anat Rec. 292:1370–1396.

Hillenius, W. 1992. The evolution of nasal turbinates and mammalian endothermy. Paleobiol. 18(1):17–29.

Hinds, D.S., Calder, W.A. 1971. Tracheal dead space in the respiration of birds. Evolution. 25(2):429–440.

Hoi, Y., Meng, H., Woodward, S.H., Bendok, B.R., Hanel, R.A., Guterman, L.R., Hopkins, L.N. 2004. Effects of Arterial Geometry on Aneurysm Growth: Three-Dimensional Computational Fluid Dynamics Study. J Neurosurg. 101:676–681.

Holliday, C.M., Ridgely, R.C., Sedlmayr, J.C., Witmer, L.M.. 2010. Cartilaginous epiphyses in extant archosaurs and their implications for reconstructing limb function in dinosaurs. PLOS ONE. 5(9):e1312.

Holliday, C.M. Witmer, L.M. 2007. Archosaur adductor chamber evolution: integration of musculoskeletal and topological criteria in jaw muscle homology. J Morph. 268:457–484.

Holmes, W.M., Cotton, R., Xuan, V.B., Rygg, A.D., Craven, B.A., Abel, R.L., Slack, R., Cox, J.P.L. 2011. Three-Dimensional Structure of the Nasal Passageway of a Hagfish and its Implications for Olfaction. Anat Rec. 294:1045–1056.

Hoppe, G. 1934. Das Geruchsorgan von *Hatteria punctata*. Z Anat Entwickl. 102:434–461.

Jackson, D.C., Schmidt-Nielsen, K. 1964. Countercurrent Heat Exchange in the Respiratory Passages. Physiol. 51:1192–1197.

Jiang, J., Zhao, K 2010. Airflow and nanoparticle deposition in rat nose under various breathing and sniffing conditions. J Aerosol Sci. 41(11):1030–1043.

Kepler, G.M., Richardson, R.B., Morgan, K.T., Kimbell, J.S. 1998. Computer Simulation of Inspiratory Nasal Airflow and Inhaled Gas Uptake in a Rhesus Monkey. Tox App Pharm. 150:1–11.

Kierszenbaum, A.L. 2007. Respiratory System in Histology and Cell Biology: An Introduction to Pathology. 2nd ed. Elsevier. Philadelphia, PA.

Kimbell, J.S., Godo, M.N., Gross, E.A., Joyner, D.R., Richardson, R.B., Morgan, K.T. 1997. Computer simulation of inspiratory airflow in all regions of the F344 rat nasal passages. Tox App Pharm. 145:388–398.

Kratzing, J.E. 1975. The fine structure of the olfactory and vomeronasal organs of a lizard (*Tiliqua scincoides scincoides*). Cell Tiss Res. 156:239–252.

Lafortuna, C.L., Saibene, F., Albertini, M., Clement, M.G. 2003. The regulation of respiratory resistance in exercising horses. Eur J Appl Physiol. 90:396–404.

Lakjer, T. 1927. Studien uber die Gaumenregion bei Sauriern im Vergleich mit Anamniern und primitiven Sauropsiden. Zool Jb (Anat. Abt.). 49:57–356.

Langman, V.A., Maloiy, G.M.O., Schmidt-Nielsen, K., Schroter, R.C. 1979. Nasal heat exchange in the giraffe and other large mammals. Resp Physiol. 37:325–333.

Lauder, G. V., Drucker, E.G., Nauen, J.C., Wilga, C.D. 2003. Experimental Hydrodynamics and Evolution: Caudal Fin Locomotion in Fishes. in Bels, V.L., Gasc, J-P., Casinos, A. (eds) Vertebrate Biomechanics and Evolution. Oxford: BIOS Scientific Publishers. pp:117–135.

Liu, Y., Matida, E.A., Gu, J., Johnson, M.R. 2007. Numerical simulation of aerosol deposition in a 3-D human nasal cavity using RANS, RANS/EIM, and LES. Aero Sci. 38:383–700.

Loudon, C., Tordesillas, A. 1998. The Use of the Dimensionless Womersley Number to Characterize the Unsteady Nature of Internal Flow. J Theor Biol. 191(1):63–78.

McCaffrey, T.V., Kern, E.B. 1979. Response of nasal airway resistance to hypercapnia and hypoxia in the dog. Acta Oto. 87:545–553.

McElroy, E.J., Reilly, S.M. 2009. The relationship between limb morphology, kinematics, and force during running: the evolution of locomotor dynamics in lizards. Biol J Linn Soc. 97:634–651.

McHenry, C.R., Clausen, P.D., Daniel, W.J.T., Meers, M.B., Pendharkar, A. 2006. Biomechanics of the Rostrum in Crocodilians: A comparative Analysis using Finite-Element Modeling. Anat Rec. 288A:827–849.

Michaeli, G., Pinshow, B. 2001. Respiratory water loss in free-flying pigeons. J Exp Biol. 204:3803–3814.

Milsom, W.K. 1984. The interrelationship between pulmonary mechanics and the spontaneous breathing pattern in the Tokay lizard, *Gekko gecko*. J Exp Biol. 113:203–214.

Milsom, W.K. 1988. Control of arrhythmic breathing in aerial breathers. Can J Zool. 66(1):99–108.

Milsom, W.K. 1991. Intermittent breathing in vertebrates. Annu Rev Physiol. 53:87–105.

Mirade, P.S., Daudin, J-D. 2006. Computational Fluid Dynamics Prediction and Validation of Gas Circulation in a Cheese-Ripening Room. Int Dairy J. 16(8):920–930.

Miyashita, T., Arbour, V.M., Witmer, L.M., Currie, P.J. 2011. The internal cranial morphology of an armoured dinosaur *Euoplocephalus* corroborated by X-ray computed tomographic reconstruction. J Anat. 219(6):661–675.

Morgan, K.T., Kimbell, J.S., Monticello, T.M. Patra, A.L., Fleishman, A. 1991. Studies of inspiratory airflow patterns in the nasal passages of the F344 Rat and rhesus monkey using nasal molds. Relevance to formaldehyde toxicity. Tox App Pharm. 110:223–240.

Murrish, D.E. and Schmidt-Nielsen, K. 1970. Exhaled air temperature and water conservation in lizards. Resp Phys. 10(2):151–158.

Mygind, N., Dahl, R. 1998. Anatomy, physiology and function of the nasal cavities in health and disease. Adv Drug Deliv Rev. 29:3–12.

Negus, V.E. 1958. The comparative anatomy and physiology of the nose and paranasal sinuses. E&S Livingstone Ltd. Edinburgh, Scotland.

Nelson, J.E., Christian, K.A., Baudinette, R.V. 2007. Anatomy of the nasal passages of three species of Australian bats in relation to water loss. Aus J Zool. 55:57–62.

Nowicki, S. 1987. Vocal tract resonance in oscine bird sound production: evidence from birdsongs in a helium atmosphere. Nature. 325:53–55.

Ostrom, J.H. 1962. The cranial crests of hadrosaurian dinosaurs. Postilla. 62:1–29.

Parsons, T.S. 1970. The nose and Jacobson's organ. in Gans, C., Parsons, T.S. (eds). Biology of the Reptilia Vol. 2. New York: Academic Press. pp:99-191.

Parsons, T.S. 1967. Evolution of the nasal structure in the lower tetrapods. Am Zool. 7:397–413.

Parsons, T.S. 1959. Nasal anatomy and the phylogeny of reptiles. Evolution. 13:175–187.

Pelham, PH., Dickson, J.G. 1992. Physical Characteristics. in Dickson, J.G. (ed). The Wild Turkey: Biology and Management. Stackpole Books. Mechanicsburg PA. p:37.

Prange, H.D., Schmidt-Nielsen, K. 1969. Evaporative water loss in snakes. Comp Biochem Physiol. 28:973–975.

Pratt, C.W. McE. 1948. The morphology of the ethmoidal region of *Sphenodon* and lizards. Proc Zool Soc Lond. 118(1):171–201.

Proctor, D.F. 1966. Airborne disease and the upper respiratory tract. Bact Rev. 30(3):498–513.

Rakesh, V., Datta, A.K., Ducharme, N.G., Pease, A.P. 2008. Simulation of turbulent airflow using a CT based upper airway model of a racehorse. J Biomech Engin. 130:031011-1– 13.

Rayfield, E.J., Milner, A.C., Xuan, V.B., Young, P.G. 2007. Functional Morphology of Spinosaur "Crocodile-Mimic" Dinosaurs. J Vert Paleo. 27(4):892–901.

Rehorek, S.J., Firth, B.T., Hutchinson, M.N. 2000. The structure of the nasal chemosensory system in squamate reptiles. 1. The olfactory organ, with special reference to olfaction in geckos. J Biosci. 25(2):173–179.

Roache, P.J. 1997. Quantification of uncertainty in computational fluid dynamics. Annu Rev Fluid Mech. 29:123–160.

Roberts, L. H. (1973). Cavity resonances in the production of orientation cries. Periodicum Biologorum. 75:27–32.

Ruben, J.A., Hillenius, W.J., Kemp, T.S., Quick, D.E. 2012. The evolution of mammalian endothermy. in Chinsamy, A. (ed). Forerunners of Mammals: Radiation, Histology, Biology. Indiana University Press, Bloomington. pp:273–286.

Ruben, J.A., Jones, T.D., Geist, N.R. 1998. Respiratory physiology of the dinosaurs. BioEssays 20:852–859.

Saibene, F., Aguggini, M.G., Clement, M.G. 1981. Work of breathing in dog during exercise. J Appl Physiol. 50:1087–1092.

Schachner, E.R., Cieri, R.L., Butler, J.P., Farmer, C.G. 2013. Unidirectional pulmonary airflow patterns in the savannah monitor lizard. Nature. 506:367–370.

Schmidt-Nielsen, K. 1997. Animal Physiology. 5th ed. Cambridge: Cambridge University Press.

Schmidt-Nielsen, K., Hainsworth, R.F., Murrish, D. 1970. Counter-current heat exchange in the respiratory passages: Effect on water and heat balance. Resp Physiol. 9:263–276.

Schwenk, K. 1993. Are geckos olfactory specialists? J Zool Lond. 229:289–302.

Segal, R.A., Kepler, G.M., Kimbell, J.S. 2008. Effects of differences in nasal anatomy on airflow distribution: A comparison of four individuals at rest. Annals Biomed Engin. 36(11):1870–1882.

Seydel, O. 1896. Uber die Nasenhohle und das Jacobson'sche Organ der Land-und Sumpf-schildkrijten. Eine vergleichend-anatomische Untersuchung. in Festschrift zum 70sten Geburtstage von Carl Gegenbaur. W. Engel-mann, Leipzig, 2:385–486.

Seymour, R.S., Bennett-Stamper, C.L., Johnston, S.D., Carrier, D.R., Grigg, G.C. 2004. Evidence for endothermic ancestors of crocodiles at the stem of archosaur evolution. Phys Biol Zool. 77(6):1051–1067.

Shelton, G., Jones, D.R. 1991. The physiology of the alligator heart. The cardiac cycle. J Exp Biol. 158:539–564.

Stebbins, R.C. 1943. Adaptations in the nasal passages for sand burrowing in the saurian genus *Uma*. Am Nat. 77(768):38–52.

Stebbins, R.C. 1948. Nasal structure in lizards with reference to olfaction and conditioning of the inspired air. Am J Anat. 83(2):183-221.

Swift, D.L. 1982. Physical principles of airflow and transport phenomena influencing air modification. in Proctor, D.F., Anderson, I. (eds). The Nose, Upper Airway Physiology and the Atmospheric Environment. Amsterdam, the Netherlands: Elsevier Science Publishers. pp:337–349.

Tattersall, G.J., Cadena, V., Skinner, M.C. 2006. Respiratory cooling and thermoregulatory coupling in reptiles. Resp Physiol Neuro. 154:302–318.

Templeton, J.R. 1964. Nasal salt excretion in terrestrial lizards. Comp Biochem Physiol. 11:223–229.

Thompson, G.G., Withers, P.C. 1997. Patterns of gas exchange and extended non-ventilatory periods in small goannas (Squamata: Varanidae). Comp Biochem Physiol. 118A(4):1411–1417.

Tieleman, B.I., Williams, J.B., Michaeli, G., Pinshow, B. 2001. The role of the nasal passages in the water economy of crested larks and desert larks. Physiol Biochem Zool. 70(2):219–226.

Van Valkenburgh, B., Theodor, J., Friscia, A., Pollack, A., Rowe, T. 2004. Respiratory turbinates of canids and felids: a quantitative comparison. J Zool Lond. 264:281–293.

Vitalis, T.Z., Milsom, W.K. 1986. Mechanical analysis of spontaneous breathing in the semi-aquatic turtle, *Pseudemys scripta*. J Exp Biol. 125:157–171.

Vogel S. 1994. Life in Moving Fluids. 2nd ed. Princeton: Princeton University Press.

Weishampel, D.B. 1981. The nasal cavity of lambeosaurine hadrosaurids (Reptilia: Ornithischia): Comparative anatomy and homologies. J Vert Paleo. 55(5):1046–1057.

Wheeler, P.E. 1978. Elaborate CNS cooling structures in large dinosaurs. Nature. 275:441–443.

Witmer, L. M. 2001. Nostril position in dinosaurs and other vertebrates and its significance for nasal function. Science. 293:850–853.

Witmer, L.M. 1999. The phylogenetic history of paranasal air sinuses. in: Koppe, T., Nagai, H., Alt, K.W. (eds). The paranasal sinuses of higher primates: development, function and evolution. Chicago. Quintessence. pp:21–34.

Witmer, L.M. 1995a. Homology of facial structures in extant archosaurs (birds and crocodilians), with special reference to paranasal pneumaticity and nasal conchae. J Morph. 225:269–327.

Witmer, L.M. 1995b. The Extant Phylogenetic Bracket and the importance of reconstructing soft tissues in fossils. in Thomason, J.J.(ed): Functional Morphology in Vertebrate Paleontology. New York: Cambridge University Press. pp:19–33.

Witmer, L.M., Ridgely, R.C. 2008. The paranasal air sinuses of predatory and armored dinosaurs (Archosauria: Theropoda and Ankylosauria) and their contribution to cephalic structure. Anat Rec. 291:1362–1388.

Womersley, J.R. 1955. Method for the calculation of velocity, rate of flow and viscous drag in arteries when the pressure gradient is known. J Physiol. 127:553–563.

Yam, R. Yuen, P.L., Yung, R., Choy, T. 2011. Rethinking hospital general ward ventilation design using computational fluid dynamics. J Hosp Inf. 77(1):31–36.

CHAPTER 3 : NASAL CONCHAE FUNCTION AS AERODYNAMIC BAFFLES: AN EXPERIMENTAL COMPUTATIONAL FLUID DYNAMIC ANALYSIS IN THE NOSE OF TURKEYS (AVES: GALLIFORMES)

Abstract

Nasal concha function in birds has largely been attributed to reducing respiratory evaporative water loss. However, discrepancies in empirical studies of conchae in birds suggest that these structures may have evolved for different functions than the conchae of mammals. An alternative hypothesis for the evolution of avian conchae is that of an aerodynamic baffle. The convoluted shapes of conchae offer the potential to channel air to different regions of the nasal capsule during respiration. To test this hypothesis, we used CT data from an adult turkey (*Meleagris gallopavo*) to construct 3D models of its nasal capsule. A series of digital "turbinectomies" was performed on these models. Models were subjected to a computational fluid dynamic analysis to simulate resting inspiration. They were compared to their wild type control. Results of our analysis revealed that the four conchae found in turkeys, along with the crista nasalis, alter the flow of inspired air in ways that can be considered baffle-like. However, these baffle-like functions are remarkably limited or local in their areal extent, indicating that avian conchae are more functionally independent than originally hypothesized. Our results found the conchae of birds to be efficient baffles that—along with heat and moisture transfer—serve to efficiently move air to specific regions of the nasal passage. This alternate function of conchae has implications for their evolution in birds and other amniotes.

List of Abbreviations

ad olf = aditus olfactorius; aat co = atrial nasal concha; at meat = atrial meatus; caud co = caudal nasal concha; caud meat = caudal meatus; ch = choana: cnp = cavum nasi proprium; cr nas = crista nasalis; mid co = middle nasal concha; mid meat = middle meatus; olf = olfactory chamber; ros co = rostral nasal concha; ros meat = rostral meatus; vest = vestibulum nasi.

Introduction

Conchae are projections of the nasal mucosa lining the nasal passages of most extant amniotes. They vary in complexity from species to species, ranging from simple, hill-shaped evaginations of the nasal capsule to scrolled or variably branched structures arising from either a cartilaginous or mineralized skeleton (turbinates; Negus 1956, 1958). Conchae increase the surface area of the nasal mucosa, which aids in physiologically relevant functions such as olfaction and thermoregulation (Hillenius 1992).

The function of conchae garnered extensive interest in the 1960s and 1970s with the seminal works of Jackson et al. (1964), Schmidt-Nielsen et al. (1970), and Collins et al. (1971) laying the groundwork for nasal passage function and the role of respiratory conchae in maintaining heat and water balance. Several studies later validated these conchal functions across a broad range of species within Amniota (Schmidt-Nielsen et al. 1969; Murrish and Schmidt-Nielsen 1970; Murrish 1973; Langman et al. 1979; Schmidt-Nielsen et al. 1981; Schroter and Watkins 1986). The role of conchae in maintaining body temperature and reducing respiratory evaporative water loss (REWL), coupled with

the generally more complicated conchae observed in mammals and birds led to the hypothesis that respiratory conchae—and the turbinates on which they rest—may be a necessity for the evolution of tachymetabolic endothermy (Hillenius 1992, 1994; Ruben 1995; Ruben et al. 1996; Hillenius and Ruben 2004). Whereas this hypothesis has received continued support from studies on mammals (Van Valkenburgh 2004, 2011; Green et al. 2012), support in birds has been less consistent (Tieleman et al. 1999; Geist 2000; Michaeli and Pinshow 2001). This inconsistency led us to question if avian conchae had an alternate function beyond just heat and water exchange.

Although there is some variation in their number and placement, most avian nasal passages consist of three conchae: a rostral, middle, and caudal concha (Bang 1971, Bang and Wenzel 1985, Witmer 1995, Figure 3-1). The physiological functions of conchae in olfaction and thermoregulation are due to the increased surface area that they provide for these diffusion-based processes (Schmidt-Nielsen et al. 1970; Gretchell et al. 1980; Hillenius 1992). However, by simply being in the path of the respired air field, conchae also have the potential to function as baffles, redirecting air to specific regions of the nasal capsule. This aerodynamic baffling function can be particularly beneficial for olfaction in that odorant absorption requires slower airflow speeds for odorant particles to bind to odorant receptors (Mozell et al. 1973; Craven et al. 2009a). In contrast, oxygen requirements of the body necessitate faster air speeds that reduce air transport time between the environment and lungs. These dichotomous demands of the nasal passage can be met by anatomically separating the respired air field into a low-pressure, fast-moving respiratory stream and a higher-pressure, slower-moving olfactory stream.

Having anatomical structures in the nose that can direct air to various regions of the nasal capsule can thus be advantageous. Prior work on mammalian noses have observed that the nasoturbinate in carnivorans and the inferior turbinate of humans and other primates both function as airway baffles, redirecting air to the olfactory chamber and middle meatus respectively (Elad et al. 1993; Churchill et al. 2004; Wexler et al. 2005; Craven et al. 2009a, b). Bang (1971) proposed that the atrial (when present) and rostral conchae were chiefly airway baffles. We sought to functionally test this hypothesis along with related hypotheses pertaining to the other conchae and soft-tissue structures within a representative bird.

To test the function of avian conchae in redirecting airflow, we produced a series of 3D models based on CT scans of the airway in an adult turkey (*Meleagris gallopavo*). As members of the basal-branching group Galliformes, turkeys serve as useful model organisms for avian nasal passages. The conchae shape of turkeys are representative of many avian orders (Bang 1971) and may be close to the ancestral neognathan nasal conchae arrangement. Results obtained from this study can thus be generalized to a variety of different bird groups, making turkeys ideal candidates for nasal passage airflow analysis. Multiple airway models were created, differing only in which conchae were removed. Models were subjected to a computational fluid dynamic (CFD) analysis that simulated the flow of air through the nasal passage during restful inspiration. If conchae played an appreciable role in redirecting airflow then the removal of those conchae should produce detectable—and presumably physiologically detrimental—effects on air field characteristics.

Materials and Methods

Specimen

To test the effects of conchae on nasal airflow, we used an adult wild turkey (*Meleagris gallopavo*). The animal had an estimated mass of 4.94 kg. The animal was legally harvested in southeastern Ohio completely independently from the authors or Ohio University, and the head of the turkey was later obtained from the hunter as a salvage specimen. It was accessioned into a public repository, the Ohio University Vertebrate Collections (OUVC), as OUVC 10599 under the terms of permit #14-2762 issued by the Ohio Division of Wildlife.

CT Scanning

The head of OUVC 10599 was CT scanned using Ohio University's MicroCT scanning facility (OUμCT). The scanner used was an eXplore Locus MicroCT scanner by General Electric. The specimen was scanned at 60kv at 450μA with a slice thickness of 90μm. Data were exported in DICOM format for segmentation in Avizo 7.1 (FEI Visualization Sciences Group, Burlington, MA.). Nasal passage data were compared to those of other turkeys found in the collections (e.g., OUVC 10624, 10362); it was determined that OUVC 10599 had conchae representative of turkeys in general.

Model Creation

Model creation and boundary condition assignment followed the procedures detailed in Chapter 2. Briefly, DICOM data from the microCT scan of OUVC 10599 were used to segment out the left airway of the animal. We chose to segment only one side as the presence of a complete nasal septum ensured that each nasal passage would

act independently of the other. The segmented airway served as a cast, indicating every possible place that air could enter within the nasal passage. Nasal conchae were segmented out as well, to better visualize how air moved past these structures. 3D models were converted into volumetric meshes using the program ICEM CFD (ANSYS Inc., Canonsburg, PA). However, unlike our previous study, the volumetric models used in this study incorporated a tetrahedral-hexahedral (tet-hex) hybrid mesh (Figure 3-2). Hexahedral meshes are preferred over tetrahedral meshes for CFD analyses as they are capable of obtaining the same results as their tetrahedral counterparts at a fraction of the element size, thus reducing computational costs (Aftosmis et al., 1994; Biswas and Strawn, 1998). Unfortunately, hexahedral mesh generation is more time consuming and meticulous than tetrahedral meshing. It is often very difficult to fit hexahedra to unstructured grids such as those of organic structures (Blacker, 2001; Ruiz-Gironés, 2011). To alleviate this problem, we used a tet-hex hybrid mesh. The outer shell of the model was composed of tetrahedra to better capture the anatomical detail whereas the inner core incorporating most of the air field was composed of hexahedral cells. This hybrid design allowed for automated mesh generation with only a marginal increase in computational cost compared to a hexahedral-only mesh.

The boundary conditions given to each model consisted of a pressure inlet located at the nostril, a pressure outlet located at the choana, and an impermeable wall boundary. Boundary conditions were used to induce physiologically-realistic airflow through the models (Figure 3-2).

To ensure grid independence, we performed a solution-based adaptive mesh refinement on each airway model (Table 3-1, Prakash 1999; Prakash and Ethier 2000). This process uses data from a fairly converged solution (see "convergence" below) to determine regions of the mesh where cell count is too low to accurately resolve the flow field. These regions are marked and refined by the program (e.g., by splitting each tetrahedral or hexahedral cell into eight daughter cells). The refined model is then re-run using the same criteria as in the original mesh, and the results are compared between meshes. This process is repeated until the refined mesh returns values that are approximately the same (falling below a predetermined margin of error), at which point they are considered to be mesh-independent (Prakash and Ethier 2000). This method of grid refinement is similar to a standard multi-grid convergence index (Roache 1994; Craven et al. 2009b). However, by using fluid flow criteria and localized refinement, it reduces the need to re-mesh the entire model multiple times, which greatly reduces processing time and saves on computational costs by only refining poorly resolved regions of the model. Using mean velocity magnitude we ran a solution-based AMR until our grids had returned errors <5%.

Digital "Turbinectomies"

To test the effects that the various conchae had on airflow, we digitally removed each concha, accounting for most possible permutations (Table 3-2). A grid-independent bony-bounded model (2,600,494 cells) of OUVC 10599 (Chapter 2) was used to represent airflow through a completely emptied airway with no conchae. Digital removal

was accomplished by ignoring the soft-tissue boundaries for the conchae in question and "painting" over them using the segmentation tools in Avizo 7.1.

Analysis

CFD analysis was performed on each model using the commercial software Fluent (ANSYS Inc., Canonsburg, PA.). Inspiratory flow was modeled as steady state under a laminar flow regime. Air material properties reflected air at sea level and 30°C. The laminar viscous model was chosen for this analysis based on Reynolds and Womersely number calculations from cross sections of the airway as described previously (chapter 2). Given that flow rate has never been recorded in vivo for turkeys, we used body mass to estimate flow rate using the phylogenetically corrected allometric equation for inspiratory flow from Frappell et al. (2001).

Convergence

CFD analysis is an iterative process. As such, the values of the variables being calculated will change from iteration to iteration. The difference in these values between iterations reflects imbalances in the calculation. These imbalances are referred to as the residuals of error (Tu et al. 2012). The lower the residual of error for the variables of interest, the more refined the solution and the closer it is to its "true" value (i.e., residual of error = 0). Residual error is often measured in orders of magnitude, such that a residual of error of $10e^{-1}$ is roughly equivalent to 10% error (accurate to 1 significant digit), $10e^{-2}$ is around 1% (accurate to 2 significant digits), and so on. Depending on the variable being measured, the acceptable amount of error will vary. In general, global errors for momentum and pressure are considered acceptable at a level of $10e^{-3}$ (Tu et al. 2012).

However, for physiological simulations, a level of $10e^{-4}$ is preferred (Craven et al. 2009b). When the residuals of error have reached a designated level of acceptability, the simulation is considered converged. Although global variables such as momentum and continuity can provide a superficial view of how converged an analysis is, it is generally recommended that one directly monitor the convergence of one's flow variables of interest (Fluent 2006. Tu et al. 2012), which can be accomplished by using custom monitoring surfaces that are designed to record data from a single location (point surfaces).

For our analysis, convergence was determined when the residuals of error for momentum and continuity had fallen below 10^{-4}. Surface point models were placed along the models to further monitor convergence of specific criteria (velocity magnitude and pressure). A "flatlining" of these surface point values indicated a lack of change between iterations and, thus, convergence.

Data Comparisons

Velocity and pressure data were compared using area-weighted average surface integrals of specific regions within the nasal capsule using Fluent. The CFD module for Avizo (Avizo Wind) was used for post-processing and visual analysis of the Fluent data. For specific velocity magnitude comparisons, a region-of-interest (ROI) box was placed around specific portions of the nasal capsule (e.g., just the nasal vestibule) and the average velocity magnitude was calculated using the built-in functions of Avizo Wind 7.1.

Results

Anatomy

The nasal passage in turkeys houses four nasal conchae (Figure 3-1). Just deep to the nostril, inside the nasal vestibule (vestibulum nasi), there is the short, partially coiled (approximately one-half of a scroll) atrial nasal concha. Deep to that is the larger rostral nasal concha. This concha retains the same shape as the atrial concha, albeit at a larger scale such that the atrial concha rests inside the lateral aspect of the rostral concha (Figure 3-1). Both conchae are covered in stratified squamous epithelium similar to skin, but the rostral concha may still be well vascularized (Bang 1971). Immediately caudal to the rostral concha, at the terminus of the nasal vestibule, the floor of the nasal passage (solum nasi) rises up to form a fleshy crest known as the crista nasalis (Bang 1971). This structure constricts the passage between the nasal vestibule and the cavum nasi proprium (CNP). Inside the CNP resides the more complicated middle nasal concha. The middle concha in turkeys is a well vascularized structure that scrolls 1.5 times before exiting into the short nasopharyngeal duct (ductus nasopharyngeus, Figure 3-1). The middle concha is covered by mucociliated respiratory epithelium (Bang 1971). The final concha found in turkeys is the olfactory-based caudal nasal concha. It resides in the caudodorsal region of the CNP dorsal to the middle concha. It forms a bubble-shaped hillock within the olfactory chamber of the nasal passage (Figure 3-1). As expected for a structure located in the olfactory chamber, the caudal concha is covered in olfactory epithelium (Bang 1971).

Air Speed and Pressure Distribution

Air movement through the nasal passage is the result of changes in local pressure between the lungs and the environment. Contraction of the respiratory muscles creates a negative air space inside the lungs. This low-pressure gradient between the lungs and the outside environment forces air to rush in to fill the vacuum. When the mouth is closed, the avian glottis slots into the choana located in the caudal portion of the roof of the mouth (Crole and Solely 2010), thus creating a direct connection between the lungs and the nasal passage. Following Bernoulli's Principle (Vogel 1994), air speed through the nasal passage will be dependent on the changes in pressure that occur as the caliber of the nasal passage changes shape throughout its length. In order to satisfy the law of continuity (i.e., conservation of mass), a specified volume of air needs to move faster through a small caliber tube than it does a larger caliber tube. Doing so requires having a steeper pressure gradient (high to low) between the larger tubes and the smaller tubes. This results in small caliber tubes having relatively low pressures, whereas larger, more spacious containers tend to have higher pressures (Vogel 1994).

Comparisons of air speed between the various permutations of the turkey nasal capsule (Table 3-3) revealed variability in velocity distribution with the removal of different conchae. This variability caused by jetting and vorticity within newly opened regions of the nasal capsule. In general, as more soft-tissues were removed the increased space within the nasal capsule resulted in shallower pressure gradients and lower air speeds within the nasal passage. These reductions reached their zenith in the bony-

bounded airway model which had the most homogenous pressure distribution and air velocities of all the models tested.

Atrial Concha Removal (A model)

Removal of the atrial concha resulted in an over four-fold increase in pressure within this region of the nasal vestibule (Figure 3-3). Inspired air produced a swirling effect along the lateral aspect of the rostral concha (Figure 3-3). This swirling, coupled with the increased pressure, slowed down the velocity of the inspired air (Table 3-3), increasing its transit time through the nasal capsule. Airflow across the lateral aspect of the rostral concha was more restricted upon removal of the atrial concha, with an airflow vortex localizing air along the central portion of the lateral aspect of the rostral concha (Figure 3-3). In contrast, with the atrial concha in place the pressure gradient increased, resulting in air moving faster and more evenly across the majority of the lateral aspect of the rostral concha (Figure 3-3). Atrial concha removal resulted in some air passing ventrally along the rostral portion of the rostral concha. Air passing ventrally and caudoventrally along the rostral concha appeared the same regardless of atrial concha removal, indicating that the atrial concha's effect on airflow was limited to its local region.

Rostral Concha Removal (R model)

Removing the rostral concha resulted in a large drop in velocity magnitude (Table 3-3) caused by a doubling of local pressure within the nasal vestibule (Figure 3-4.). The continued presence of the atrial concha in the R model produced a splitting of the air field into lateral and medial streams very similar to what we observed in the wild type model.

However, unlike the wild type model, this splitting of the air field was not maintained. In the R model, air passed medially over the atrial concha where it formed a slight vortex as it continued caudoventrally to the lateral aspect of the rostral meatus (Figure 3-4). This vorticity continued into the entrance of the middle meatus of the CNP. A portion of the air field passed dorsomedially over the atrial concha where it hugged the medial wall of the nasal capsule and entered the CNP medially. These medial air streams represented the olfactory flow and were the biggest difference between the R model and the wild type model. In the wild type model a medial channel of air was maintained throughout the majority of the nasal vestibule. Few air streams were observed crossing back under the rostral concha. As air proceeded caudally, it passed medially around the base of the crista nasalis prior to entering the CNP. In contrast, the R model revealed no crista nasalis flow during inspiration. In the R model maintenance of a medial, olfactory channel of air was weak with large portions of the air field continuing ventrolaterally after banking off the medial wall of the nasal vestibule. Airflow between the wild type and R models only became equivalent upon entrance into the CNP, indicating the limits of the rostral concha's effect on air flow.

Atrial and Rostral Concha Removal (AR model)

Ablation of both atrial and rostral conchae produced a drop in velocity magnitude that was greater than either the A or R model (Table 3-3). Pressure within the nasal vestibule was 3.3x higher in the AR model vs. the wild type (Figure 3-5). Air in the nasal vestibule of the AR model swirled across the nasal capsule, producing a large vortex (Figure 3-5). Air entered the laterally-placed nostril where it banked off the nasal

capsule's medial wall and continued to arc across the rostral meatus. In the wild type model the shape of the rostral concha split the airfield immediately into a large medial channel and a smaller lateral channel (Figure 3-5). Air passed the lateral aspect of the rostral concha, banking medially around the cul-de-sac formed by the crista nasalis. In contrast, the AR model produced homogenous airflow throughout the rostral meatus (Figure 3-5) with some ventral air streams entering the cul-de-sac of the crista nasalis from a medial aspect and exiting laterally. As with the A and R model, airflow in the AR and wild type models became equivalent at the level of the CNP, suggesting limited influence of these conchae on the inspired air field.

Middle Concha Removal (M model)

Airflow traveled through the middle meatus of the M model at lower velocity than air in the same region of the wild type model (Table 3-3). Although the air field did receive a noticeable bump in velocity as it passed from the nasal vestibule into the CNP, due to the Venturi effect formed by the sudden opening of the airway caudal to the crista nasalis (Figure 3-6), this jetting effect was short-lived and airstreams throughout much of the middle meatus were noticeably slower than similar airstreams in the wild type model. The air field within the nasal vestibule was undisturbed by middle concha ablation. Under the wild type condition, the air field was tightly constrained by the shape of the coiled middle concha, producing strong separations of medial and lateral air streams. With the middle concha removed, the air field was "free" to span the entire volume of the middle meatus.

Despite this freedom, the air field proved to be remarkably limited, with evidence of velocity stratification within the middle meatus. Most air channels were localized to the center of the middle meatus (Figure 3-6). The ventral portion of the middle meatus contained recirculating air streams that ran in a caudal to rostral direction, producing a barrier to entry for much of the rest of the air field, causing a stratified velocity field within the CNP. Air entering from the nasal vestibule moved in a fairly straight path caudally towards the nasopharyngeal duct. A noticeable mediolateral angling of the airfield was noticed as air, banking off the medial and ventral aspect of the rostral concha, would enter the CNP medially and proceed caudolaterally towards the nasopharyngeal duct. This airflow pattern held true for all of the air field minus some of the more medial streams, which drifted into the olfactory chamber. Surprisingly, air that entered the olfactory chamber traversed it nearly identically in both the M model and the wild type model (Figure 3-6), albeit at slower speeds in the M model as opposed to the wild type (25 cm/s vs. 36 cm/s, respectively).

Caudal Concha Removal (C model)

Unlike the other airway models, there was a noticeable increase in air field velocity upon ablation of the caudal concha (Table 3-3). Removal of the hillock-shaped caudal concha increased the volume of the olfactory chamber by 44%. This increased volume acted as a reservoir for inspired olfactory air, drawing most of the air field into it (Figure 3-7). In the wild type model, air entered the caudal meatus where it proceeded across the caudal concha caudomedially (Figure 3-7). A slightly raised region of the nasal passage, on the dorsal surface of the middle concha—which we refer to as the entrance to

the olfactory chamber (aditus olfactorius)—partially split incoming olfactory air into medial and lateral streams. These streams anastomosed within the olfactory chamber (containing the caudal concha, Figure 3-7). In the ablated model, olfactory air entered the caudal meatus similarly to the wild type model, but with a larger lateral component due to the increased volume of the olfactory chamber. The pressure draw from the nasopharyngeal duct resulted in multiple air streams moving caudoventrally from the lateral stream (Figure 3-7). The air splitting caused by the aditus olfactorius remained separated for a greater distance in the wild type model compared to the C model. Unlike with previous models removal of the caudal concha actually decreased the pressure within the olfactory chamber (Figure 3-7). Pressure in the C model decreased by 13%, producing a noticeable increase in olfactory flow over the wild type model (60 cm/s vs. 39 cm/s, respectively).

Middle and Caudal Concha Removal (MC model)

Removal of both conchae within the CNP resulted in a noticeable decrease in velocity magnitude (Table 3-3). Air field patterns were very different from what was observed in the wild type model (Figure 3-8). In the MC model, a relatively slow moving air stream ran along the medial wall of the nasal capsule. Air entering from the nasal vestibule continued caudally in a mediolateral spiral towards the nasopharyngeal duct (Figure 3-8). Airway stratification was evident and similar to that observed in the M model (Figure 3-6, Figure 3-8). The majority of the air field stayed localized to the center of the middle meatus. Airway stratification was more exaggerated in the MC model compared to the M model. Dorsal-most air streams entered the olfactory chamber where,

as in the C model, the air streams continued laterally across the chamber before diving ventrally back into the rest of the CNP (Figure 3-8). However, unlike in the C model, airflow through the olfactory chamber formed a large ventrally-directed vortex. In the absence of both middle and caudal conchae a substantial portion of the air field moved in a counterintuitive direction during inspiration (Figure 3-8). As with the M model, this slower-moving, recirculating air stream acted as a barrier for much of the inspired air field, keeping it from filling up the ventral portion of the middle meatus.

Only Crista Nasalis Present (CN model)

Airflow through the CN model was remarkably consistent with airflow through the original bony-bounded model previously reported for this specimen (Chapter 2, Figure 3-9). The arcing effect imposed by the crista nasalis was most evident when compared to the original bony-bounded model (Figure 3-9). In the absence of the crista nasalis, air was free to pass directly to the nasopharyngeal duct. This resulted in fewer air streams within the olfactory chamber. In contrast, the presence of the crista nasalis resulted in more air reaching the olfactory chamber due to air launching off this structure (Figure 3-9).

Discussion

The atrial and rostral conchae in birds are composed of stratified squamous epithelium (Bang 1971) rather than ciliated or respiratory epithelium. This suggests that these conchae may have an alternate function than simply warming inspired air. We hypothesized, as others have before us (Bang 1971), that the atrial and rostral conchae would be the most likely to act as baffles for redirecting air through the nasal passage.

We found support for this hypothesis upon removal of the atrial concha. This concha provided a strong directional force for inspired air and maintained a distinctive lateral channel of air across the rostral concha (Figure 3-3). This channel of air traversed more of the nasal vestibule than it would have otherwise, banking off the crista nasalis prior to entering the CNP. A similarly strong baffling function was observed in the rostral concha, as its presence produced a distinct medial channel of air. This channel of air ultimately made its way into the olfactory chamber. This maintenance of airflow separation during inspiration may be advantageous for odor discrimination. Interestingly, the rostral concha appeared necessary for air to move around the crista nasalis (Figure 3-10). The crista nasalis receives the products of the nasal gland and acts like a reservoir (vestibular cisterna, Bang and Wenzel 1985). Dry air passing over this reservoir vaporizes the fluid, partially humidifying the air prior to entering the CNP. When the rostral concha was removed no moving air passed over this reservoir (Figure 3-10). These results indicate that the baffle function of the rostral concha is necessary to help humidify incoming air streams and that rostral concha removal may significantly alter the moisture content of inspired air.

Within the CNP, airflow separation was produced solely by the middle and caudal conchae regardless of the flow patterns imparted by the more rostral conchae. This indicated that airflow baffling is a more localized process than we had previously suspected. The only observed effect of the rostral conchae on CNP airflow was on the speed and strength of the incoming air jet. The smaller calibers of the airway in the wild type nasal vestibule imparted a higher airway velocity, which translated into an overall

greater Venturi effect for the air field entering the CNP. When the middle concha was present, this jetting effect was delayed until the air field reached the nasopharyngeal duct. When the middle concha was removed, the air field jetted immediately from the nasal vestibule into the CNP. With only the crista nasalis present in the M and MC models, this air jet traveled quickly along the surface of the crista nasalis. However, the relatively sharp corners of this nasal structure, compared to the more canal-like conchae, resulted in a deceleration zone immediately caudal to the crista nasalis, followed by flow separation and vortex formation. This vortex-shedding zone became a barrier for air passing through the CNP, resulting in the majority of inspired air traveling through the mid-portion of the middle meatus, with the ventral portion containing relatively slowly recirculating flow (Figure 3-6, Figure 3-8). This fluid dynamic pattern was reminiscent of airflow over non-aerodynamic trucks (e.g., Wang et al. 2009; Ha et al. 2010).

Ablation of the crista nasalis, as was done in a previous experiment (see Chapter 2, Figure 3-9), removed this vortex-shedding zone and produced nearly completely homogenous flow throughout the nasal passage during inspiration, with resulting low olfactory flow. These results suggest that, along with aiding air humidification during inspiration, the crista nasalis functions as a ramp to launch air from the nasal vestibule into the vaulted olfactory chamber.

Although turkeys are not renowned for their olfactory prowess (Pelham 1992), and our previous analyses of airflow through the turkey nose revealed high flow speeds and olfactory washout upon expiration (Chapter 2), the relatively simple caudal concha of turkeys still produced noticeable—and physiologically important—differences in the air

field when it was present. Unlike some other birds and many other macrosmatic animals such as dogs and crocodylians (Weldon et al. 1993; Craven et al. 2009a), turkeys do not have a blind olfactory chamber. The caudoventral end of the olfactory chamber is confluent with the nasopharyngeal duct, allowing the full draw of pressure from the lungs to affect air flow within the olfactory region as well as olfactory washout as air leaves the lungs and passes over the olfactory epithelia during expiration (Chapter 2). Nonetheless, the presence of the caudal concha did provide a buffer to this pressure drop. The dorsolateral portion of the caudal concha formed a pocket of relatively high-pressure air that was buffered from the effects of the nasopharyngeal duct (Figure 3-7). This high-pressure region of the olfactory chamber slowed down air molecules passing through it, providing more time for odorant molecules to bind to olfactory receptors. Much like the crista nasalis, it was impressive that these rather simplistic geometries were sufficient to produce noticeable differences in pressure and concomitant olfactory flow within the nasal capsule.

The nasal anatomy of turkeys is characteristic of Galliformes and many other avian orders (Bang 1971). Thus, the results obtained from our experimental simulations can broadly be applied to many other bird groups. Our analyses support the hypothesis that avian conchae do have a baffle-like function, minimally in turkeys but probably in other birds, as well. This ability to partition and redirect air to certain regions of the nose is beneficial for the various physiological functions of the nasal capsule. In turkeys, medial air channels have the capacity to move air at slower speeds through to the olfactory chamber (Chapter 2) where pressure buffering from the caudal concha can

further slow down air around some of the olfactory epithelium. Lateral air channels can move at a higher speed, decreasing transit time through the nose and into the lungs for oxygenation of the body. These results agree well with previous analyses that have observed a baffle-like function for some of the conchae in mammals (Elad et al. 1993; Churchill et al. 2004; Craven et al. 2009 a,b). Whether conchae evolved as baffles or were exapted for this function is beyond the scope of this analysis. Regardless, the benefits of this function are readily observable.

Our results further revealed the presence of largely laminar flow through the nasal capsule, a result that is in agreement with other resting respiration studies (Schmidt-Nielsen et al. 1970; Hahn et al. 1993; Craven et al. 2009b; Jiang and Zhao 2010). Similar to previous authors (Churchill et al. 2004), we observed that respiratory conchae/turbinates—counter to their name—seem to reduce turbulence rather than promote it. The presence of conchae in the nasal capsule greatly decreases airway caliber which decreases local pressure while simultaneously increasing the speed of airflow through the nasal capsule. These small airway calibers promote stability of the flow field via increased nasal wall surface area. These characteristics promote laminar flow through the nose, which may seem counterintuitive for thermoregulation. Laminar flow is less efficient at heat transfer as compared to turbulent flow due to the presence of a non-motile boundary layer at the nasal-wall-air interface, which creates an obstacle to energy transfer from the air to the mucosa (Vogel 1994). In contrast, turbulent flow breaks up this boundary layer, promoting greater heat transfer at the air-wall boundary. However, the chaotic nature of turbulent flow is more costly in terms of nasal resistance. Under

laminar flow, resistance increases linearly with velocity (Vogel 1994). With turbulent flow, the localized pressure drops that occur during vortex formation cause resistance to increase by the square of velocity in narrow passageways such as the nasal capsule. Higher resistance greatly increases the energetic cost of moving air through the nose (Swift 1982; Vogel 1994). It appears that the costs of moving turbulent air through the nasal passage outweigh any potential thermoregulatory benefits. Instead, birds likely incorporate other, less energetically demanding means of reducing boundary layer thickness, such as increasing airfield velocity, which will have an inverse effect on boundary layer thickness (Vogel 1994). Similarly, the small caliber of the airways between these conchae, coupled with their increased surface area partially caused by the curving of the conchae, further promotes diffusive heat transfer in laminar flowing air (Schmidt-Nielsen et al. 1970), ultimately producing an efficient heat exchange mechanism with only a minimal cost in respiratory energetics.

A further benefit of conchae is that they partition the air field into multiple parallel channels. On the outset, this partitioning of the air field into multiple, smaller caliber airways seems detrimental as resistance of the airway should increase in a manner described by the Hagen-Poiseuille equation (Vogel 1994):

$$R = \frac{8\mu l}{\pi r^4},$$

where R = resistance, μ = dynamic viscosity, l = the length of the "pipe" and r = the radius of the "pipe." Resistance is highly sensitive to the radius of the structure through which a fluid flows. As indicated by the exponent in the denominator, decreasing airway caliber by half would increase resistance of fluid flow by 16 fold (Vogel 1994). This

highly sensitive aspect of fluid resistance is offset, in conchae, by the breaking of the air field into multiple, parallel streams. Parallel fluid streams act similar to parallel electrical current in a circuit and can best be described using mathematical notation from that field:

$$R_{total} = \sum \frac{1}{\frac{1}{R_1} + \frac{1}{R_2} + \frac{1}{R_3} \ldots},$$

where subscripts indicate each individual airway segment. In a parallel arrangement, decreasing airway caliber by half and spreading those half-caliber airways across four parallel segments only increases airway resistance by 4. Splitting the half caliber airways across six parallel segments increases resistance by 2.6 and so on. This phenomenon of fluid flow allows conchae to partition the air field in a way that provides extensive physiological surface area with only a slight increase in nasal resistance (Figure 3-11).

In contrast, long convoluted airways should provide the same heat transfer benefits as a concha-partitioned airways and at a reduced cost in nasal resistance. However, the cost in anatomical real estate is greater, and the serial arrangement of the air field limits the amount of air that can be processed at any one time (Figure 3-11). Using the channeling ability of conchae to redirect air to different regions of the nasal capsule allows for aerodynamic segregation of the nasal passage without the need for hard-tissue excavations such as a dedicated olfactory chamber. This could be beneficial for birds, which may pay a high cost—aerodynamically—for increases in cranial mass (Gussekloo and Cubo 2013). Baffle-like conchae may have evolved as a means to compensate for the increasingly larger eyes of birds, many of which "squeeze" out the more typical olfactory recesses seen in extant amniotes (Witmer 1995). Though conchae

have been largely associated with the evolution of high resting metabolism (Hillenius 1992, 1994; Geist 2000, Hillenius and Ruben 2004) the results of our analyses indicate that conchae do have other functions. These alternate functions should be taken into consideration when investigating the evolution of these structures in amniotes.

Acknowledgments

This work was funded by a National Science Foundation Graduate Research Fellowship, as well as in-house funding from Ohio University. We would like to thank Willem Roosenburg for access to specimens, Eric Snively for modeling help and respiration information, as well as WitmerLab members: Ryan Ridgely, Ruger Porter, Ashley Morhardt, Don Cerio, and Catherine Early.

References

Aftosmis, M., Gaitonde, D., Tavares, T.S. 1994. On the accuracy, stability and monotonicity of various reconstruction algorithms for unstructured meshes. AIAA Pap. 94–0415.

Bang, B.G. 1971. Functional anatomy of the olfactory system in 23 orders of birds. Acta Anat. 79(58):1–76.

Bang, B.G., Wenzel, B.M. 1985. Nasal cavity and olfactory system. In: King AS., McLelland J, editors. Form and Function in Birds Volume 3. Elsevier. p 195–225.

Biswas, R., Strawn, R.C. 1998. Tetrahedral and hexahedral mesh adaptation for CFD problems. App Num Math. 26:135–151.

Blacker, T. 2001. Automated conformal hexahedral meshing constraints, challenges and opportunities. Engin Comp. 17:201–210.

Churchill, S.E., Shackelford, L.L., Georgi, N., Black, M.T. 2004. Morphological variation and airflow dynamics in the human nose. Am J Hum Biol. 16:625–638.

Collins, J.C., Pilkington, T.C., Schmidt-Nielsen, K. 1971. A model of respiratory heat transfer in a small mammal. Biophys J. 11:886–914.

Craven, B.A., Neuberger, T., Paterson, E.G., Webb, A.G., Josephson, E.M., Morrison, E.E., Settles, G.S. 2007. Reconstruction and morphometric analysis of the nasal airway of the dog (*Canis familiaris*) and implications regarding olfactory airflow. Anat Rec. 290:1325–1340.

Craven, B.A., Paterson, E.G., Settles, G.S. 2009a. The fluid dynamics of canine olfaction: Unique nasal airflow patterns as an explanation of macrosmia. J R Soc Interface. rsif.2009.0490v1–rsif20090490.

Craven, B.A., Paterson, E.G., Settles, G.S., Lawson, M.J. 2009b. Development and verification of a high-fidelity computational fluid dynamics model of canine nasal airflow. J Biomech Engin. 131:91002-1–91002-11.

Crole, M.R., Soley, J.T. 2010. Gross morphology of the intra-oral rhampotheca, oropharynx and proximal oesophagus of the emu (*Dromaius novaehollandiae*). Anat Hist Embryol. 39:207–218.

Elad, D., Liebenthal, R., Wenig, B.L., Einav, S. 1993. Analysis of air flow patterns in the human nose. Med Biol Eng Comput. 31:585–592.

Fluent. 2006. Fluent 13 Getting Started Guide. Fluent Inc.

Geist, N.R. 2000. Nasal respiratory turbinate function in birds. Physiol Biochem Zool. 73(5):581–589.

Green, P.A., Van Valkenburgh, B., Pang, B., Bird, D., Rowe, T., Curtis, A. 2012. Respiratory and olfactory turbinal size in canid and arctoid carnivorans. J Anat. 221(6):609–621.

Gussekloo, S.W.S., Cubo, J. 2013. Flightlessness affects cranial morphology in birds. Zoology. 116:75–84.

Ha, J., Jeong, S., Obayashi, S. 2010. Flow characteristics of a pickup truck with regard to the bed geometry variation. Proc IMechE. 224D:881–891.

Hahn, I., Scherer, P.W., Mozell, M.M. 1993. Velocity profiles measured for airflow through a large-scale model of the human nasal cavity. J App Physiol. 75:2273–2287.

Hillenius, W.J. 1994. Turbinates in therapsids: Evience for Late Permian origins of mammalian endothermy. Evolution. 48(2):207–229.

Hillenius, W.J. 1992. The evolution of nasal turbinates and mammalian endothermy. Paleobiology. 18(1):17–29.

Hillenius, W.J., Ruben, J.A. 2004. The evolution of endothermy in terrestrial vertebrates: Who? When? Why? Physiol Biochem Zool. 77(6):1019–1042.

Michaeli, G., Pinshow, B. 2001. Respiratory water loss in free-flying pigeons. J. Exp. Biol. 204:3803-3814.

Mozell, M.M., Jadodowicz, M. 1973. Chromatographic separation of odorants by the nose: Retention times measured across in vivo olfactory mucosa. Science. 181(4106):1247–1249.

Murrish, D.E. 1973. Respiratory heat and water exchange in penguins. Resp Phys. 19:262–270.

Murrish, D.E., Schmidt-Nielsen, K. 1970. Exhaled air temperature and water conservation in lizards. Resp Phys. 10:151–158.

Negus, V. 1956. The air-conditioning mechanism of the nose. Br Med J. 1(4693):367–371.

Negus, V.E. 1958. The comparative anatomy and physiology of the nose and paranasal sinuses. Livingstone, London, England.

Jackson, D.C., Schmidt-Nielsen, K. 1964. Countercurrent heat exchange in the respiratory passages. Phys. 51:1192–1197.

Jiang, J., Zhao, K. 2010. Airflow and nanoparticle deposition in rat nose under various breathing and sniffing conditions. J Aerosol Sci. 41(11):1030–1043.

Langman, V.A., Maloiy, G.M.O., Schmidt-Nielsen, K., Schroter, R.C. 1979. Nasal heat exchange in the giraffe and other large mammals. Resp Phys. 37:325–333.

Prakash, S. 1999. Adaptive mesh refinement for finite element flow modeling in complex geometries, Ph.D. Thesis.

Prakash, S., Ethier, C.R. 2001. Enhanced error estimator for adaptive finite element analysis of 3D incompressible flow. Comput Meth Appl Mech Engrg. 190:5413–5426.

Pelham, PH., Dickson, J.G. 1992. "Physical characteristics" in Dickson, J.G. (ed). The Wild Turkey: Biology and Management. Mechanicsburg PA. Stackpole Books. p.37.

Roache, P.J. 1994. Perspective: A method of uniform reporting of grid refinement studies. J Fluid Engin. 116:405–413.

Ruben, J. 1995. The evolution of endothermy in mammals and birds: From physiology to fossils. Annu Rev Physiol. 57:69–95.

Ruben, J.A., Hillenius, W.J., Geist, N.R., Leitch, A., Jones, T.D., Currie, P.J., Horner, J.R., Espe III, G. 1996. The metabolic status of some Late Cretaceous dinosaurs. Science. 273:1204–1207.

Ruiz-Gironés, E. 2011. Automatic hexahedral meshing algorithms: From structured to unstructured meshes. Ph.D. Dissertation, Universitat Politècnica de Catalunya, Barcelona Spain.

Schmidt-Nielsen, K., Hainsworth, F.R., Murrish, D.E. 1970. Counter-current heat exchange in the respiratory passages: Effect on water and heat balance. Resp Phys. 9:263–276.

Schmidt-Nielsen, K., Kanwisher, J., Lasiewski, R.C., Cohn, J.E., Bretz, W.L. 1969. Temperature regulation and respiration in the ostrich. Condor. 71(4):341–352.

Schmidt-Neilsen, K., Schroter, R.C., Shkolnik, A. 1981. Desaturation of exhaled air in camels. Proc R Soc B. 211(1184):305–319.

Schroter, R.C., Watkins, N.V. 1986. Respiratory heat exchange in mammals. Resp Physiol. 78:357–368.

Swift, D.L. 1982. Physical principles of airflow and transport phenomena influencing air modification. in Proctor DF, Anderson, I. (eds). The Nose, Upper Airway Physiology and the Atmospheric Environment. Amsterdam, The Netherlands. Elsevier Science Publishers pps: 337–349.

Tieleman, B.I., Williams, J.B., Michaeli, G., Pinshow, B. 2001. The role of the nasal passages in the water economy of crested larks and desert larks. Physiol Biochem Zool. 70(2):219–226.

Tu, J., Yeoh, GH., Liu, C. 2012. Computational Fluid Dynamics, Second Edition: A practical Approach. United Kingdom: Butterworth-Heinemann.

Van Valkenburgh, B., Curtis, A., Samuels, J.X., Bird, D., Fulkerson, B., Meachen-Samuels, J., Slater, G.J. 2011. Aquatic adaptations in the nose of carnivorans: Evidence from the turbinates. J Anat. 218(3):298–310.

Van Valkenburgh, B., Theodor, J., Friscia, A., Pollack, A., Rowe, T. 2004. Respiratory turbinates of canids and felids: a quantitative comparison. J Zool Lond. 264:281–293.

Wang, M., Dengfeng, Q.L., Yang, C., Zhao, J., Wen, G. 2009. The air-deflector and the drag: A case study of low drag cab styling for a heavy truck. CAID & CD 2009. IEEE 10th International Conference. pp:1025–1030.

Weldon, P.J., Ferguson, M.W.J. 1993. Chemoreception in crocodilians: Anatomy, natural history, and empirical results. Brain Behaviour Evolution. 41(3–5):239–245.

Wexler, D., Segal, R, Kimbell, J. 2005. Aerodynamic effects of inferior turbinate reduction: Computational fluid dynamics simulation. Arch Octolaryngol Head Neck Surg. 131:1102–1107.

Witmer, L.M. 1995. Homology of facial structures in extant archosaurs (birds and crocodilians), with special reference to paranasal pneumaticity and nasal conchae. J Morph. 225:269–327.

CHAPTER 4 : SOFT-TISSUE CORRECTION FACTORS IMPACT NASAL PASSAGE SHAPE AND FUNCTIONAL EFFICIENCY IN DINOSAURS AND OTHER EXTINCT ANIMALS

Abstract

The nasal passages of extinct animals have typically been reconstructed using only their bony-boundaries as proxies for shape. Lack of preservational detail forced these reconstructions to ignore the physiologically relevant inner boundaries of the nasal capsule comprised of the mucous membranes. Such bony-bounded reconstructions may greatly overestimate the extent of the airway within the nasal passage. To determine the magnitude of difference such reconstructions can make we surveyed the nasal passages of extant sauropsids. Using 3D segmentation we made digital models of the soft-tissue airways as well as their bony-bounded counterparts. Results of our survey indicated that bony-bounded reconstructions roughly double the volume of the airway. The increased caliber of these airways greatly reduces the efficiency of the nasal passage at transferring, heating, humidifying, and analyzing respired air. Radial measurements from the center of the air field within the nasal passages of a variety of sauropsids indicated that nasal passages rarely exceed 2 mm in radius at any one spot. These data, coupled with data from surveys of extant mammals indicate that nasal airway constriction remains true regardless of size or phylogenetic distance. Using these data, we reconstructed the nasal passages of the theropod *Majungasaurus crenatissimus* and the sauropod *Camarasaurus grandis* using these "soft-tissue corrections." Reconstructing the airway of the theropod was easier than the sauropod due to better-preserved hard-tissue boundaries for the nasal

passage. Applying airway constrictions to the bony-bounded nasal passages provided details on potential soft-tissue morphologies that may have been present in the living animals. Accounting for the effects of soft-tissue on the airways of extinct animals provides more realistic interpretations of how these nasal passages would have functioned in life, allowing for future functional tests of physiological potential in these animals.

Introduction

Reconstructing soft tissues in extinct animals is necessary for tackling important questions regarding their natural history. Questions of metabolism (Ruben et al. 1996; Gunga et al. 1998; Wedel 2003; Franz et al. 2009), growth rate (Erickson and Tumanova 2000; Hutchinson et al. 2011, 2014), locomotion (Hutchinson and Gatesy 2000; Hutchinson and Garcia 2002; Hutchinson 2004), feeding (Meers 2002; Holliday 2009; Bates and Falkingham 2012), cognitive functions (Evans et al. 2009; Witmer and Ridgely 2009; Zelenitsky et al. 2011; Lautenschlager et al. 2012), and behavior (Dimond et al. 2011) are all reliant on inferences of soft-tissue anatomy. However, soft-tissue reconstructions are hampered by the limited data provided to us by the fossil record. Soft-tissue reconstructions require us to fill in missing data from the fossil record with data obtained from living relatives of the animals in which we are interested. The extant phylogenetic bracket (EPB) has been successfully employed as a means of limiting inferences based on shared characteristics of animals that are closely related to the extinct taxa (Witmer 1995a, 1997). This soft-tissue reconstruction methodology has produced the most realistic depictions of extinct animal soft-tissues to date (O'Connor 2006; Witmer et

al. 2008; Evans et al. 2009; Hieronymus et al. 2009; Holliday 2009; Tsuihiji 2010; Schachner et al. 2011).

The efficacy of the EPB in soft-tissue reconstructions depends on the anatomical region being modeled. Muscle reconstructions are often the most rigorous and true to life as the attachment sites of muscle to bone, coupled with the known mechanics of muscle function, provide hard limits for muscle size and shape (Holliday 2009; Tsuihiji 2010; Snively et al. 2013). In contrast, integumental structures are often the most difficult to reconstruct as the epidermis and its associated derivatives (i.e., scales, hair, and feathers) are often not attached directly to the underlying endoskeleton. Barring relatively rare cases of bone-integument interaction (Turner et al. 2007; Hieronymus et al. 2009), this disconnect between the endoskeleton and the epidermis forces these soft-tissue interpretations to rely on either prime-level inferences (Witmer 1995a) or extrapolations from uniquely well preserved specimens (e.g., Quanguo et al. 2012). The nasal capsules of dinosaurs fall somewhere between these two extremes. Much of the nasal capsule is bounded by the bones of the nasal cavity. These bones serve as scaffolding for the cartilaginous walls and invaginations of the nasal capsule. Nasal cavity bones further function as hard limits to nasal capsule shape and extent, allowing researchers to faithfully determine the outer limits of the nasal capsule. In contrast, the internal borders of the nasal capsule—where the functional part of the nasal passage resides—do not touch bone and often use soft-tissue structures (i.e., mucosa) to create the internal geometry of the nasal passage. These soft-tissue structures rarely preserve in the fossil record, leaving this inner portion of the nasal passage a black box for reconstruction.

To determine how much the soft-tissue boundaries of the nasal passage affect interpretations of nasal anatomy, we segmented the nasal passages of a diversity of birds, crocodylians, and lizards to create 3D models of the corresponding nasal airways. Nasal passage segmentation followed a two-pass approach. The first pass segmented the airway as it was in life, based on soft-tissue boundaries for the nasal passage. The second pass replicated the situation in fossils by using only the bony boundaries of the nasal passage as a proxy for the extent of the airway. Bony-bounded airways were compared to their soft-tissue counterparts in terms of volume to determine how much soft-tissue resided within the nasal passage. We further divided the nasal passages into their different anatomical regions so as to determine which portions of the nasal passage were most variable in regards to soft tissues.

Anatomy

The nasal passage in sauropsids can be divided into four regions (Figure 4-1) based on certain soft-tissue anatomical characters (Parsons 1970). The entrance to the nasal passage, just deep to the naris is referred to as the nasal vestibule (vestibulum nasi). It is typically a grossly tubular region of relatively small diameter. The nasal vestibule varies in shape and length, depending on the species studied (Figure 4-1). In general, birds and lizards show enhancement of the nasal vestibule whereas crocodylians show reduction (Witmer 1995b). The caudal extent of the nasal vestibule is demarcated by the placement of the duct of the nasal gland (glandula nasalis). Although fairly innocuous in crocodylians, the duct of the nasal gland is often associated with a raising of the nasal floor (solum nasi) into a ridge. This ridge is referred to as the crista nasalis in birds

(Witmer 1995b, Schwelle in older literature [e.g., Bang 1971])) and the postvestibular ridge in lizards (Parsons 1970). Caudal to the nasal vestibule the nasal passage expands into a large chamber referred to as the nasal cavity proper (cavum nasi proprium [CNP], Figure 4-1). The CNP houses the majority of the conchae in sauropsids (except the rostral and [when present] atrial conchae in birds). The CNP can be subdivided into a main "respiratory" chamber and a caudal or caudodorsal olfactory recess (Bang & Wenzel 1985, Figure 4-1). Ventral to caudoventral from the CNP is the nasopharyngeal duct (ductus nasopharyngeus, Figure 4-1). Following the terminology of Parsons (1970), this area is defined here as any connection from the CNP that leads to the choana. This substructure varies in length and complexity between taxa, with some birds and lizards having no appreciable separation between the two.

The outer rim of the nasal cavity is often referred to as the naris, external naris, or bony naris in the literature (e.g., Jacobs et al. 1993; Xu et al. 2002; Clifford and Witmer 2004). This anatomical reference is confusing as the naris is defined as the fleshy nostril of the living animal (Baumel 1993; Waibl et al. 2012). The bones that rim the rostral opening of the nasal cavity make up the bony narial (or nasal) aperture (apertura nasi ossea, Baumel and Witmer 1993, Figure 4-2). The bony narial aperture (bna) similarly does not fully describe the limits of the nasal passage as it is in life, but instead roughly represents the entrance of the nasal vestibule into the nasal cavity proper. Outside of the bony narial aperture resides a variably deep depression known as the narial fossa (Witmer 2001, Figure 4-2). The narial fossa houses portions of the nasal apparatus (blood vessels, nasal cartilages, portions of the nasal passage, cavernous tissue) and can be viewed as an

extension of the bony narial aperture. To differentiate between these structures when referencing the bony naris, the use of endonaris and ectonaris may be employed (e.g., Loewen et al. 2009; Farke 2011; Sampson et al. 2013, Figure 4-2). The endonaris represents the extent of the bony narial aperture, and may be synonymized with it. The ectonaris includes both the bony narial aperture as well as the associated narial fossa. Thus, the ectonaris contains the endonaris. This definition makes the ectonaris equivalent to the "bony nostril," as described by Witmer (2001).

Institutional and Anatomical Abbreviations

Institutions: CM, Carnegie Museum of Natural History; FMNH, Field Museum of Natural History; GMNH-PV, Gunma Museum of Natural History Vertebrate Paleontology; OUVC, Ohio University Vertebrate Collections; TM, Transvaal Museum; YPM R, Yale Peabody Museum of Natural History, Reptiles collection.

Anatomical: bna, bony narial aperture; ch, choana; max, maxilla; npd, nasopharyngeal duct; pmax, premaxilla; smax, septomaxilla; vest, vestibulum

Materials and Methods

Taxa

Multiple species of crocodylians, birds, and lizards were examined via CT segmentation (Table 4-1). Taxa varied in ontogenetic development from young juveniles to adult animals. Animals were acquired post mortem from registered museum collections or as salvage specimens from legal sources. No animals were collected or euthanized for this study and no live animals were studied. Sex of the animals was

ignored for this study as many specimens were either difficult to sex or the option was simply not available (e.g., having only isolated heads).

CT Methods

Scanning methods varied between specimens, requiring varying degrees of resampling to obtain usable 3D digital casts of the airways (see Segmentation). Many species were scanned using Ohio University's MicroCT scanning facility (OUμCT). The scanner used was an eXplore Locus MicroCT scanner by General Electric. Specimens were scanned at 60 kV at 450 μA with a slice thickness of 45 or 90μm. Larger specimens were scanned at OhioHealth O'Bleness Hospital in Athens, Ohio using a Toshiba Aquilion 64 CT scanner with a slice thickness of 300 μm at 120–140 kV and 100–400 mA. Specimens provided by E. Schachner and C.G. Farmer were scanned using a 100 kV, 400 μA CT scanner in Salt Lake City, UT, with a slice thickness of 400–600 μm.

Segmentation

CT data were exported in DICOM format and brought into the 3D segmentation program Avizo 7.1 (FEI Visualization Sciences Group, Burlington, MA), where the airway was segmented from the surrounding soft and hard tissues. For relatively low resolution scans (e.g., a 600 μm full body scan of one or two individuals) the nasal passage was isolated as a region of interest (ROI). This ROI was then resampled such that the voxels composing the CT images were equidimensional across the X, Y, and Z planes (i.e., isotropic voxels). This upsampling procedure does not add new data to the image, but the resulting interpolation serves to "smooth" the voxels composing the DICOM

images, providing for smoother segmentations with reduced aliasing or "stair-stepping" artifacts.

Each nasal passage underwent a two-pass segmentation (Figure 4-3). The first segmentation used the boundaries of the airway as they appear in life, which was referred to as the Soft-Tissue Airway (ST). The second segmentation ignored all soft-tissue boundaries for the airway and used only the bony-boundaries of the nasal passage as a proxy for nasal passage extent (Figure 4-4). This was deemed the Bony-Bounded airway (BB) and is intended to replicate the condition in fossils in which only the bones and no soft tissues are present. The rostral extent of the BB airway was delimited by the rim of the ectonaris (Figure 4-3). The caudal extent of the BB airway was delimited by the fenestra exochoanalis (Figure 4-3). The same smoothing and contrast-enhancing algorithms that were used for the ST airway were also used on the BB airway so as to reduce errors that may arise from using different methodologies on the same data set.

Volumetric Comparisons

Volume measurements were obtained using the built-in features of Avizo 7.1. Both whole airway volume comparisons and regional comparisons were taken. Soft-tissue anatomical correlates for the extent of each anatomical region were used to determine the limits of each region for volumetric comparison. ST and BB airways were divided at the same location for each region. Regional division was done using Avizo 7.1 and Geomagic 10 (3D Systems Geomagic, Rock Hill, SC).

Airway Radial Distance and Other Measurements

Nasal passage measurements were taken in Avizo using the program's built-in tools. Measurements of radial distance from the center of the air field to the nearest mucosal wall were performed by taking the mean of multiple measurements from cross sections throughout the left and right nasal passages (Figure 4-5). Nasal passage regions were demarcated based on anatomical correlates for each anatomical location (i.e., nasal vestibule, cavum nasi proprium, and nasopharyngeal duct). Multiple cross sections were taken from each region. Cross section numbers varied depending on length of region and degree of anatomical change between slices. Airway radii were measured for each airway side within the same cross section (Figure 4-5). Measurement number varied from 1–15 per side, and were dependent on anatomical complexity within each cross section (Figure 4-5). For instance, a simple tubular cross section of roughly even radial distance throughout could be measured with one to two measurements. In contrast, a heavily partitioned nasal passage (e.g., the turbinate-filled airway of an ostrich) may have multiple regions of the airway that are separated into "zones" of various sizes and shapes, thus requiring more measurements to accurately capture the average radial airway distance (Figure 4-5).

Results

Global volumetric comparisons between ST and BB airways found the ST airway comprised between 40–60% of the entire nasal passage (Figure 4-6). Regional variation indicated that the CNP was the least variable region of the nasal passage (Table 4-2). In contrast, the nasal vestibule exhibited extreme variation in volume, reaching its lowest in

crocodylians (5% of available space). The nasal vestibule in all taxa extended beyond the limits of the bony narial aperture to encompass the rim of the narial fossa. The fleshy nostril in some taxa (e.g., *Iguana iguana*) extended slightly further, beyond the limits of the skull. The degree of extension varied from modest in turkeys and crocodylians to substantial in lizards (Figure 4-7). This was especially noticeable in the varanids, as the largely open ectonaris in these taxa are roofed completely by soft-tissues. Relying on strictly bony boundaries for these taxa resulted in removal of large portions of the nasal vestibule (Figure 4-7).

Radial distances across the nasal passage were remarkably consistent for all the taxa measured (Figure 4-8), with radial distances rarely exceeding 2 mm across the airway. Radial distance to the nearest mucosal wall was smallest within the confines of the CNP, whereas radial distance was greatest within the nasopharyngeal duct.

Discussion

As in our previous work (Chapter 2), this study provides further support for the hypothesis that bony-bounded airways do not accurately capture the shape of the nasal passage in life. Despite the various shapes and sizes of nasal passages in extant sauropsids, the nasal passage appears to fill a remarkably consistent portion of the nasal cavity (~50% ± 10%). Looking at the nasal passage more regionally revealed that the nasal vestibule was the most labile portion of the nasal passage. Nasal vestibule shape is largely dictated by soft-tissue structures such as cartilage and mucosa. These structures often extended beyond the limits of the skull and showed little evidence of their interaction with the bone. These factors make the nasal vestibule the most difficult region

of the nasal passage to reconstruct in extinct animals. In contrast, the CNP shows remarkable constraint in its volume, with nasal tissues filling 52–66% of the nasal cavity proper. The CNP is more or less completely surrounded by the bones of the skull in all the taxa examined. This encapsulation of the CNP may enforce a hard limit on CNP size. Physiologically, the CNP receives pretreated air from the nasal vestibule. Receiving pretreated air during inspiration results in less time required to bring air up to body temperature and humidity. This may alleviate some selective pressure to expand this region of the nasal passage, which may explain the relatively consistent nasal proportions of this region of the nose. Alternatively, the more caudal location of the CNP may force a compromise on expansion vs. other structural needs of the skull and adjacent tissues such as the orbits and teeth. Nasopharyngeal duct size and shape was difficult to separate from the nasal passage in some taxa (in particular, the lizards), making volumetric comparisons difficult to measure in a repeatable way.

Osteological Correlates for the Nasal Vestibule

The nasal passage can be divided into four anatomical regions using soft-tissue correlates for their boundaries. Previous research has indicated that there may also be hard-tissue correlates for some of these boundaries (Witmer 2001; Evans 2006). The nasal vestibule is separated from the cavum nasi proprium via the ostium of the duct of the nasal gland along with (when present) an associated raised ridge (Bang and Wenzel 1985; Witmer 1995b). Neither structure leaves behind osteological correlates as both are completely encased within the cartilage of the nasal capsule. However, an examination of the nasal vestibule and the corresponding bones of the nasal cavity did reveal some

correspondence. In archosaurs, the size of the ectonaris appears to correlate with the length of the nasal vestibule. Birds with elongate nasal vestibules such as gulls (*Larus*) and hummingbirds (*Calypte*) had correspondingly elongate ectonares (Figure 4-9). Birds with small nasal vestibules such as hornbills (*Buceros*) and pelicans (*Pelicanus*) had similarly reduced ectonares (Figure 4-10). Pelecaniformes and Suliformes are particularly interesting groups as many species have walled over their ectonaris and only have short, truncated nasal vestibules (Figure 4-10B). A similar relationship of the nasal vestibule to the ectonaris was seen in crocodylians (Figure 4-11). In crocodylians, the nasal vestibule is the smallest anatomical region of the nasal passage. The ectonaris (comprised mostly of the endonaris) is fairly large in comparison to the nasal vestibule, though still small relative to the entire skull. Apomorphic nasal rotation in crocodylians (Witmer 1995b) redirected the nasal vestibule, causing it to take a largely vertical trek into the nasal passage rather than a more horizontal one as in most sauropsids. When we accounted for nasal rotation we found the nasal vestibule extended 72% of the largest diameter of the endonaris in crocodylians (Figure 4-11). Although the nasal vestibule does not strictly adhere to the limits of the endonaris in crocodylians it is noteworthy that it never exceeds it. Thus, as with birds, it seems reasonable to use the ectonaris as a proxy for the maximum rostrocaudal distance of the nasal vestibule in archosaurs.

The relationship between the ectonaris and the nasal vestibule was less well maintained in squamates. In lizards, as with birds, the nasal vestibule varies substantially in size and shape (Stebbins 1948; Parsons 1970; Witmer 1995b). Many squamates (e.g., *Varanus* and *Uromastyx,* Figure 4-12) showed a similar relationship of the nasal vestibule

to the ectonaris as was observed in archosaurs. Such a relationship was observed in multiple species of *Varanus* (*V. gouldii, V. exanthematicus*), although it was not as tightly linked as what was observed in birds (e.g., in *V. exanthematicus* the junction of the vestibule and CNP was slightly caudal to the rim of the endonaris). Iguanids and geckonids did not exhibit this relationship. In these taxa, the nasal vestibule continued substantially past the relatively small endonaris (Figure 4-13). Instead of being constrained by the rim of the endonaris, the nasal vestibule in these taxa appeared to track better with the septomaxilla (Figure 4-13). Both iguanids and geckonids have spire-like septomaxillae that form a shelf for either the medial or lateral wall of the nasal vestibule to rest on (Figure 4-13). Thus, the junction of the nasal vestibule and the CNP in iguanids and geckos winds up tracking better with the caudal extent of their septomaxillae rather than their ectonaris. In contrast, the septomaxillae in varanids are more dome-shaped and appear to function primarily in segregating the vomeronasal organ from the nasal passage. Processes off these septomaxillae do contribute to the boundary of the elongate nasal vestibule in these taxa, but do not seem to offer as much space for attachment as the endonaris. Interestingly, the iguanids and gecko in this study had relatively short and simple nasal vestibules compared to the elaborated nasal vestibules of both *Uromastyx* and *Varanus* (cf. Figure 4-10–11). It appears that expansion of the ectonaris may be necessary for substantial expansion of the nasal vestibule to occur. A similar relationship is seen in mammals, in which the endonaris is greatly enlarged and the nasal vestibule extends rostrally from it using only soft-tissues (Witmer et al. 1999; Witmer 2001; Clifford and Witmer 2004a, b.)

Soft-Tissue Correction

The results of our anatomical survey indicate that the bony-bounded nasal passages reconstructed for dinosaurs and other extinct animals (e.g., Witmer and Ridgely 2008; Evans et al. 2009) overestimate the size of the soft-tissue airway by as much as two times.

Reconstructions based on soft-tissue dimensions obtained from extant animals indicate that the cavum nasi proprium is the best-bounded portion of the nasal capsule. Reductions in bony-bounded airway size of 44%–53% within the CNP (based on archosaur-only data) would be necessary to achieve more accurate airway proportions in extinct archosaurs. Reconstructing the nasal vestibule is a more difficult prospect due to its greater degree of variation compared to the rest of the nasal passage. Our survey of extant sauropsids indicates that the caudal limit of the endonaris can be used as an approximate osteological correlate for a level 1 inference for the caudal limit of the nasal vestibule in archosaurs. Reconstructions of nasal passages in extinct lepidosaurs and other reptiles that retain the septomaxilla, requires knowledge of the shape of the septomaxilla in these taxa, as this bone appears to be a more reliable indicator of the caudal limit of the nasal vestibule than the ectonaris. Regardless of taxon, elaborated nasal vestibules do appear to track well with enlarged ectonares. Although the size of the ectonaris may be used to infer an elaborated nasal vestibule, the lack of a complete bony roof for this portion of the nasal passage limits inferences on shape and lateral extent of this anatomical structure. Reconstructing the nasopharyngeal duct can be inferred based on the shape of the palate and the location of anatomical correlates for the choana, such

as the fossa exochoanalis (see Chapters 5 and 6). This fossa, coupled with the extent of the shelf-like structures that separate the olfactory recess from the rest of the nasal passage, may be used to approximate the length of the nasopharyngeal duct.

More interesting were the results of the airway radial distance analysis. The radial distance from the center of the air field to the nearest wall throughout the nasal passage routinely hovered around an average of 2 mm, with an average distance of 0.7–1.3 mm within the CNP. Constricted airways are beneficial for maintaining laminar flow throughout the nasal passage (Churchill et al. 2004; Chapter 3), which reduces the energetic costs of moving air into the lungs. Small caliber airways are beneficial for heat transfer and humidification of inspired air as well as analysis of odorant particles (Jackson and Schmidt-Nielsen 1964; Collins et al. 1971; Schoenfeld and Cleland 2005). Our survey of extant sauropsids, coupled with data from extant mammals across a mass range of over four orders of magnitude (Jackson and Schmidt-Nielsen 1964; Langman et al. 1979), suggests that the biophysical limits of diffusion transcend phylogeny. The only apparent exception to this trend appears to be in saiga antelope (*Saiga tatarica*), which have an apomorphically enlarged nasal vestibule (Clifford and Witmer 2004a). The function of this enlarged nasal vestibule remains enigmatic and may be related to the unique sound production in this species (Frey et al. 2007) and/or the removal of the dust particles that are heavily prevalent during its foraging mode (Frey and Hoffman 1997; Clifford and Witmer 2004a). Setting the unique nasal anatomy of saiga aside, a safe, biophysically conservative inference is that even multi-tonne sauropods would have had airways that rarely exceeded 10 mm in diameter at any one spot along the nasal passage.

These biophysical constraints provide more refined reconstructions of the anatomy of extinct animals.

Using the above criteria, we reconstructed the nasal passages of *Majungasaurus crenatissimus* (FMNH PR 2100, Figure 4-14) and *Camarasaurus grandis* (GMNH-PV101, Figure 4-15). Extensive metaplastic ossification of the dermis in *Majungasaurus* offered hard evidence for the limits of the nostril in life (Sampson and Witmer 2007). The rather simple airway, save for a greatly expanded olfactory chamber, provided limits on airway shape that allowed for a fairly robust interpretation of the nasal passage as it would have been in life (Figure 4-14). The capaciousness of the olfactory chamber allowed for two possible nasal morphologies. The first was an enlarged, hillock-shaped concha similar to the caudal concha in many birds and the concha in most crocodylians (Witmer 1995b, Figure 4-14C2). In these taxa, the concha is usually hollowed out by an expansion of the antorbital sinus into the olfactory cavity. Alternatively, the ample size of the olfactory recess could have housed a coiled olfactory concha similar in shape to the concha observed in olfactory-specialized birds such as turkey vultures (*Cathartes aura*, Figure 4-14C3). Airway reconstruction in *Camarasaurus* proved much more difficult. The relatively reduced CNP, with its small olfactory recess, provides some hard-tissue limits for nasal passage shape in this region. However, the much enlarged nasal vestibule and lack of a bony roof made it more difficult to determine overall nasal passage shape (Figure 4-15A–C). The large size of the bony nostril was similar to the enlarged bony nostril of varanids (Figure 4-15D). In varanids such as *Varanus exanthematicus* (Figure 4-15D), the large ectonaris is filled with a variably contorted nasal vestibule. In

Camarasaurus, premaxillary processes extending from the maxillae form a bony lamina that separated the vestibular region of the nasal passage from the more caudal CNP. If the nasal passage anatomy in *Camarasaurus* followed a similar pattern as that of varanids, then we might expect this bony lamina to have supported a much larger cartilaginous lamina or mucosal sheet (Figure 4-15C). Some evidence for this cartilaginous lamina may be seen in one specimen of *C. lentus* (CM 12020). This lamina would reduce the diameter of the nasal passage, bringing it closer to the 10 mm or smaller diameter observed in extant animals. In varanids, the rim of the narial fossa serves as an attachment site for a large mucosal barrier that helps contort the nasal vestibule (Chapter 2). A ridge rising from the septomaxilla acts as support for a much larger mucosal covering that served to contort the vestibule (Figure 4-15D). The ascending processes of the maxillae in *Camarasaurus* along with the premaxillary processes, may both have housed extensive mucosal coverings that would have pinched the nasal vestibule medially (Figure 4-15B,C). Although the rostral limit of the nasal vestibule cannot be directly determined, it is doubtful that the nasal vestibule extended much more rostral than the limits of the narial fossa, as it appears not to do so in any of the extant sauropsids that we have observed. Dorsal and lateral limits of the nasal vestibule, however, are less restricted (Figure 4-7, Chapter 2 fig. 9). This allows for many potential morphologies for the enlarged nasal vestibule of *Camarasaurus* (Figure 4-15A, B). If the nasal vestibule in *Camarasaurus* showed a similar arrangement to that observed in varanids then it was possible that the entire rostrum extended dorsally beyond the limits of the nasal processes

of the premaxillae, resulting in an even more box-shaped head than the skull of this taxon already suggests (Figure 4-15A).

These refined dinosaur nasal passage restorations provide us with better interpretations of the nasal passage in life, which provides a more solid foundation for tackling in-depth physiological questions related to the nasal passage, such as olfactory sensitivity, thermoregulatory efficiency, and acoustic production..

Acknowledgments

We would like to thank E.R. Schachner and C.G. Farmer for use of specimens and scan data. We would like to thank S. Montuelle for acquisition of Tokay gecko data. We thank WitmerLab members R.C. Ridgely, Wm. R. Porter, A. Morhardt, D. Cerio, and C. Early for support and help with the manuscript. This work was funded by a National Science Foundation Graduate Research Fellowship, a Jurassic Foundation Grant, Welles Grant, and a Student Enhancement Award from Ohio University.

References

Bang, B.G. 1971. Functional anatomy of the olfactory system in 23 orders of birds. Acta. Anat. 79 (58 supp):1–76.

Bang, B.G., Wenzel, B.M. 1985. Nasal cavity and olfactory system. in: King, A.S., McLelland, J. (eds). Form and Function in Birds. Vol. 3. Academic Press. New York. pp 195-225.

Bates, K.T., Falkingham, P.L. 2012. Estimating maximum bite performance in *Tyrannosaurus rex* using multi-body dynamics. Biol Lett rsbl20120056

Baumel, J.J. 1993. Handbook of Avian Anatomy: Nomina Anatomica Avium. Cambridge, MA: Nuttall Ornithological Club. New York. Academic Press.

Baumel, J.J., Witmer, L.M. 1993. Osteologia. in Baumel, J.J., King, A.S., Breazile, J.E., Evans, H.E., Vanden Berge, J.C., (eds). Handbook of Avian Anatomy: Nomina Anatomica Avium. Publications of the Nuttall Ornithological Club. No. 23. pp:45–132.

Churchill SE, Shackelford LL, Georgi, N., Black, M.T. 2004. Morphological variation and airflow dynamics in the human nose. Am J Hum Biol. 16:625–638.

Clifford, A.B., Witmer, L.M. 2004a. Case studies in novel narial anatomy: 2. The enigmatic nose of moose (Artiodactyla: Cervidae: *Alces alces*). J Zool Lond. 262:339–360.

Clifford, A.B., Witmer, L.M. 2004b. Case studies in novel narial anatomy: 3. Structure and function of the nasal cavity of saiga (Artiodactyla: Bovidae: *Saiga tatarica*). J Zool Lond. 264:217–230.

Dimond, C.C., Cabin, R.J., Brooks, J.S. 2011. Feathers, dinosaurs, and behavioral cues: Defining the visual display hypothesis for the adaptive function of feathers in non-avian theropods. Bios. 82(3):58–63.

Erickson, G.M., Tumanova, T.A. 2000. Growth curve of *Psittacosaurus mongoliensis* Osborn (Ceratopsia: Psittacosauridae) inferred from long bone histology. Zool J Linn Soc. 130:551–556.

Evans, D.C. 2006. Nasal cavity homologies and cranial crest function in lambeosaurine dinosaurs. Paleobiology. 32(1):109–125.

Evans, D., Witmer L.M., Ridgely, R.C. 2009. Endocranial anatomy of lambeosaurine dinosaurs: a sensorineural perspective on cranial crest function. Anat Rec. 292:1315–1337.

Farke, A.A. 2011. Anatomy and taxonomic status of the chasmosaurine ceratopsid *Nedoceratops hatcheri* from the Upper Cretaceous Lance Formation of Wyoming, U.S.A. PLOS One. 6(1):e161196.

Franz, R., Hummel, J., Kienzle, E., Kolle, P., Gunga, H-C., Clauss, M. 2009. Allometry of visceral organs in living amniotes and its implications for sauropod dinosaurs. Proc R Soc B. 276:1731–1736.

Frey, R. Hofmann, R. R. 1997. Skull, proboscis musculature and preorbital gland in the saiga antelope and Guenther's dikdik (Mammalia, Artiodactyla, Bovidae). Zool Anz. 235:183–199.

Frey, R., Volodin, I., Volodina, E. 2007. A nose that roars: Anatomical specializations and behavioural features of rutting male saiga. J Anat. 211:717–736.

Gunga, H-C., Kirsch, K., Rittweger, J., Rocker, L., Clarke, A., Albertz, J., Wiedemann, A., Mokry, S., Suthau, T., Wehr, A., Heinrich, W-D., Schultze, H-P. 1998. Body size and body volume distribution in two sauropods from the Upper Jurassic of Tendaguru (Tanzania). Mitt Mus Nat Kd Berl Geowiss Reihe. 3:91–102.

Hieronymus, T.L., Witmer, L.M., Tanke, D.H., Currie, P.J. 2009. The facial integument of centrosaurine ceratopsids: Morphological and histological correlates of novel skin structures. Anat Rec. 292:1370–1396.

Holliday, C.M. 2009. New insights into dinosaur jaw muscle anatomy. Anat Rec. 292:1246–1265.

Hutchinson, J.R. 2004. Biomechanical modeling and sensitivity analysis of bipedal running ability. II. Extinct taxa. J Morph. 262:441–461.

Hutchinson, J.R., Bates, K.T., Molnar, J., Allen, V., Makovicky, P.J. 2011. A computational analysis of limb and body dimensions in *Tyrannosaurus rex* with Implications for locomotion, ontogeny, and growth. PLOS ONE. 6(10):e26037.

Hutchinson, J.R., Bates, K.T., Molnar, J., Allen, V., Makovicky, P.J. 2014. Correction: A computational analysis of limb and body dimension in *Tyrannosaurus rex* with implications for locomotion, ontogeny, and growth. PLOS ONE. 9(5):e97055.

Hutchinson, J.R., Garcia, M. 2002. *Tyrannosaurus* was not a fast runner. Nature. 415:1018–1021.

Hutchinson, J.R., Gatesy, S.M. 2000. Adductors, abductors, and the evolution of archosaur locomotion. Paleobiol. 26(4):734–751.

Jackson, D.C., Schmidt-Nielsen, K. 1964. Countercurrent heat exchange in the respiratory passages. Physiology. 51:1192–1197.

Jacobs, L.L., Winkler, D.A., Downs, W.R., Gomani, E.M. 1993. New material of an Early Cretaceous titanosaurid sauropod dinosaur from Malawi. Paleontology. 36(3):523–534.

Langman, V.A., Maloiy, G.M.O., Schmidt-Nielsen, K., Schroter, R.C. 1979. Nasal heat exchange in the giraffe and other large mammals. Respir Physiol. 37:325–333.

Lautenschlager, S., Rayfield, E.J., Altangerel, P., Zanno, L.E., Witmer, L.M. 2012. The endocranial anatomy of Therizinosauria and its implications for sensory and cognitive function. PLOS ONE. 7(12):e52289.

Loewen, M.A., Sampson, S.D., Lund, E.K., Farke, A.A., Aguillón-Martínez, M.C., De Leon, C.A., Rodríguez-De La Rosa, R.A., Getty, M.A., Eberth, D.A. 2009. Horned dinosaurs (Ornithischia: Ceratopsidae) from the Upper Cretaceous (Campanian) Cerro del Pueblo Formation, Coahuila, Mexico. in Ryan, M.J., Chinnery-Allgeier, B.J., Eberth, D.A. (eds). New Perspectives on Horned Dinosaurs. Bloomington, IN. Indiana University Press. pps:99–116.

Meers, M.B. 2002. Maximum bite force and prey size of *Tyrannosaurus rex* and their relationships to the inference of feeding behavior. Hist Biol. 16(1):1–12.

O'Connor, P.M. 2006. Postcranial pneumaticity: An evaluation of soft-tissue influences on the postcranial skeleton and the reconstruction of pulmonary anatomy in archosaurs. J Morphol. 267:1199–1226.

Parsons, T.S. 1970. The nose and Jacobson's organ. in C. Gans and T.S. Parsons (eds): Biology of the Reptilia, Vol. 2. New York: Academic Press, pps:99-191.

Quanguo, L., Ke-Qin, G., Qingijin, M., Clarke, J.A., Shawkey, M.O., Rui, P., Ellison, M., Norell, M.A., Vinther, J., D'Alba, L. 2012. Reconstruction of *Microraptor* and the evolution of iridescent plumage. Science. 335(6073):1215–1219.

Ruben J.A., Hillenius, W.J., Geist, N.R., Leitch, A., Jones, T.D., Currie, P.J., Horner, J.R., Espe III, G. 1996. The metabolic status of some Late Cretaceous dinosaurs. Science. 273:1204–1207.

Sampson, S.D., Lund, E.K., Loewen, M.A., Farke, A.A., Clayton, K.E. 2013. A remarkable short-snouted horned dinosaur from the Late Cretaceous (Late Campanian) of southern Laramidia. Proc R Soc B. 280:20131186.

Sampson, S.D., Witmer, L.M. 2007. Craniofacial anatomy of *Majungasaurus crenatissimus* (Theropoda: Abelisauridae) from the Late Cretaceous of Madagascar. J Vert Paleo. 27:32–102.

Schachner, E.R., Farmer, C.G., McDonald, A.T., Dodson, P. 2011.Evolution of the dinosauriform respiratory apparatus: new evidence from the postcranial axial skeleton. Anat Rec. 294:1532–1547.

Schoenfeld, T.A., Cleland, T.A. 2005. The anatomical logic of smell. Trends Neuro. 28(11):620–627.

Snively, E., Cotton, J.R., Ridgely, R., Witmer, L.M. 2013. Multibody dynamics model of head and neck function in *Allosaurus* (Dinosauria, Theropoda). Paleo Electronic. 16(2):11A.

Stebbins, R.C. 1948. Nasal structure in lizards with reference to olfaction and conditioning of the inspired air. Am J Anat. 83(2):183–221.

Tsuihiji, T. 2010. Reconstructions of the axial muscle insertions in the occipital region of dinosaurs: evaluations of past hypotheses on Marginocephalia and Tyrannosauridae using the extant phylogenetic bracket approach. Anat Rec. 293:1360–1386.

Turner, A.H., Makovicky, P.J., Norell, M.A. 2007. Feather quill knobs in *Velociraptor*. Science. 317:1721.

Waibl H, Gasse H, Hashimoto Y, Burdas K-D, Constantinescu GM, Saber AS, Simoens P, Salazar I, Sotonyi P, Augsburger H, Bragulla H. 2012. Nomina anatomica veterinaria. 5th ed. International Committee on Veterinary Gross Anatomical Nomenclature. World Association of Veterinary Anatomists. Columbia, Missouri.

Wedel, M.J. 2003. Vertebral pneumaticity, air sacs, and the physiology of sauropod dinosaurs. Paleobiol. 29(2):243–255.

Witmer, L.M. 1995a. The extant phylogenetic bracket and the importance of reconstructing soft tissues in fossils. In: Thomason JJ, editor. Functional morphology in vertebrate paleontology. New York: Cambridge University Press. p 19–33.

Witmer, L.M. 1995b. Homology of facial structures in extant archosaurs (birds and crocodilians), with special reference to paranasal pneumaticity and nasal conchae. J Morphol. 225:269–327.

Witmer, L.M. 1997. The evolution of the antorbital cavity of archosaurs: a study in soft-tissue reconstruction in the fossil record with an analysis of the function of pneumaticity. J Vertebr Paleontol. 17 (1 supp):1–73.

Witmer, L.M. 2001. Nostril position in dinosaurs and other vertebrates and its significance for nasal function. Science. 293:850–853.

Witmer, L.M., Ridgely, R.C., 2008. The paranasal air sinuses of predatory and armored dinosaurs (Archosauria: Theropoda and Ankylosauria) and their contribution to cephalic architecture. Anat Rec. 291:1362–1388.

Witmer, L.M., Ridgely, R.C.,. 2009. New insights into the brain, braincase, and ear region of tyrannosaurs (Dinosauria, Theropoda), with implications for sensory organization and behavior. Anat Rec. 292:1266–1296.

Witmer, L.M., Ridgely, R.C., Dufeau, D.L, Semones, M.C. 2008. Using CT to peer into the past: 3D visualization of the brain and ear regions of birds, crocodiles, and nonavian dinosaurs. In: Endo H, Frey R, editors. Anatomical Imaging: Towards a New Morphology. Springer. p 67–87.

Witmer, L.M., Sampson, S.D., Solounias, N. 1999. The proboscis of tapirs (Mammalia: Perissodactyla): A case study in novel narial anatomy. J Zool Lond. 249:249–267.

Xu, X., Norell, M.A., Wang, X-L., Makovicky, P.J., Wu, X-C. 2002. A basal troodontid from the Early Cretaceous of China. Nature. 415:780–784.

Zelenitsky, D.K., Therrien, F., Ridgely, R.C., McGee, A.R., Witmer, L.M. 2011. Evolution of olfaction in non-avian theropod dinosaurs and birds. Proc R Soc B. 278:3625–3634.

CHAPTER 5 : BREATHING LIFE INTO DINOSAURS: TACKLING CHALLENGES OF SOFT-TISSUE RESTORATION AND NASAL AIRFLOW IN EXTINCT SPECIES

Abstract

The nasal region plays a key role in sensory, thermal, and respiratory physiology, but exploring its evolution is hampered by a lack of preservation of soft-tissue structures in extinct vertebrates. As a test case, we investigated members of the "bony-headed" ornithischian dinosaur clade Pachycephalosauridae (particularly *Stegoceras validum*) because of their small body size (which mitigated allometric concerns) and their tendency to preserve nasal soft tissues within their hypermineralized skulls. Hypermineralization directly preserved portions of the olfactory turbinates and also preserved an internal nasal ridge that we regard as potentially an osteological correlate (OC) for respiratory conchae. Fossil specimens were CT-scanned, and nasal cavities were segmented and restored. Soft-tissue reconstruction of the nasal capsule was functionally tested in a virtual environment using computational fluid dynamics (CFD) by running air through multiple models differing in nasal soft-tissue conformation: a bony-bounded model (i.e., skull without soft tissue) and then models with soft tissues added, such as a paranasal septum, a scrolled concha, a branched concha, and a model combining the paranasal septum with a concha. Deviations in fluid flow in comparison to a phylogenetically constrained sample of extant diapsids were used as indicators of missing soft tissue. Models that restored aspects of airflow found in extant diapsids, such as appreciable airflow in the olfactory chamber, were judged as more likely. The model with a branched concha produced airflow patterns closest to those of extant diapsids. These results from both

paleontological observation and airflow modeling indicate that *S. validum* and other pachycephalosaurids could have had both olfactory and respiratory conchae. Although respiratory conchae have been linked to endothermy, such conclusions require caution in that our re-evaluation of the reptilian nasal apparatus indicates that respiratory conchae may be more widespread than originally thought, and other functions, such as selective brain temperature regulation, could be important.

Abbreviations

acPM, anastomotic canal in premaxilla; aEth, ethmoid artery; air, airway*;* anas, anastomosis between palatine, lateral nasal, and dorsal alveolar vessels; aSO+LN, anastomosis between supraorbital and lateral nasal vessels; aSph, sphenopalatine artery; at, potential accessory turbinate; bch, bony choana (fenestra exochoanalis); bLN, branches of lateral nasal vessels; bMN, branches of medial nasal vessels; cap, cartilaginous nasal capsule; caud co, caudal concha; cDA, dorsal alveolar canal; ch, choana (fenestra endochoanalis); cLN, canal for lateral nasal vessels; cMN, canal for medial nasal vessels; co, concha; cPM, canal in premaxilla; cSO+LN, canal for anastomosis between supraorbital and lateral nasal vessels; cSO canal for supraorbital vessels; DA, dorsal alveolar vessels; f, frontal; fSO, suborbital fenestra; gLN, groove for lateral nasal vessels; j, jugal; lac, lacrimal; Lc, lacrimal canal; LN, lateral nasal vessels; max, maxilla; mid co, middle concha; MN, medial nasal vessels; mu, mucosa; nar, naris; nas, nasal; nc, nasal capsule; ng, nasal gland; npd, ductus nasopharyngeus; ns, nasal septum; ob, olfactory bulb; OfC, olfactory conchal vessels; olf e, olfactory epithelium; om, olfactory meatus; ot, olfactory turbinate; p, parietal; PA, palatine vessels; pl,

palatine; pm, premaxilla; po, postorbital; post, postvestibular ridge; preco, preconcha; preco rec, preconchal recess; prf, prefrontal; ps, parasphenoid rostrum; pt, pterygoid; q, quadrate; qj, quadratojugal; RC, respiratory conchal vessels; res e, respiratory epithelium; sDS, dorsal sagittal sinus; so1, supraorbital 1; so2, supraorbital 2; som, supraorbital bone (mineralized supraorbital membrane); sOf, olfactory sinus; SO, supraorbital vessels; sq, squamosal; t, tongue; turb, turbinate; v, vomer; vest, vestibulum nasi; vp, ventromedian process.

Introduction

Dinosaur nasal cavities present a diverse array of shapes and sizes, ranging from seemingly simple nostril-to-throat passages, all the way to elaborate convoluted pathways (Coombs, 1978; Witmer, 2001; Vickaryous and Russell, 2003; Witmer and Ridgely, 2008a; Evans et al., 2009; Miyashita et al., 2011). A number of functions have been proposed for this elaboration of the nasal apparatus including thermoregulatory benefits (Maryańska, 1977; Wheeler, 1978; Witmer and Sampson, 1999), enhanced olfaction (Ostrom, 1961, 1962; Miyashita et al., 2011), phonation (Weishampel, 1981; Evans et al., 2009), and osmoregulation (Osmólska, 1974). None of these functions are mutually exclusive, and the diversity of dinosaurs throughout the Mesozoic makes it likely that different species emphasized different functions.

Early dinosaur nasal reconstructions focused on specimens that represented extremes of narial architecture such as sauropods (Osborn, 1898; Romer, 1933; Coombs, 1975) and hadrosaurs (Ostrom, 1961, 1962; Weishampel, 1981). Soft-tissue reconstruction in extinct animals has relied heavily on the bony features of fossils along

with comparative anatomy of similar, related taxa (e.g., Romer, 1922, 1924; Simpson and Elftman, 1928; Colbert, 1946; Haas, 1955). Much of this work has focused on muscle reconstruction as the relationship between muscle and bone is often the most observable. However, other soft tissues have also been reconstructed in this fashion, including blood vessels (Lehman, 1996) and general neuromorphology (Hopson, 1979). Incorporation of the extant phylogenetic bracket with its inverted pyramid of inference (Witmer, 1995a) greatly increased the confidence of soft-tissue reconstructions by providing a stable, evolutionarily-grounded framework. Reconstructions that have followed from it have produced the most accurate inferences of soft tissues in extinct animals to date (Witmer, 1997a; Carrano and Hutchinson, 2002; Snively and Russell, 2007; Holliday and Witmer, 2008; Witmer et al., 2008; Witmer and Ridgely, 2008a, b, 2009; Holliday, 2009; Hieronymus et al., 2009; Evans et al., 2009; Tsuihiji, 2010; Schachner et al., 2011a).

Despite these improvements, the soft-tissue relations of the nasal region remain elusive due to the preservational biases of the fossil record. Whereas the nasal cavity is composed of bone, its contents—the cartilaginous nasal capsule and associated structures (turbinates, mucosa, etc.)—are mostly composed of soft tissues that rarely fossilize (Figure 5-1). These soft tissues support critical, physiologically relevant functions in extant taxa. Reconstructions have typically used the internal bony boundaries of the nasal cavity to determine the shape of the nasal capsule (Witmer and Ridgely, 2008a; Evans et al., 2009). These results have produced nasal cavity shapes that faithfully represent the outermost extent of the nasal capsule adjacent to the bone, but leave the inner boundaries adjacent to the air spaces unresolved, producing a large empty shell (Figure 5-2). Our

previous work comparing the effects of shape between bony-bounded nasal capsules and soft-tissue nasal capsules of extant diapsids has shown that not taking into account these missing soft tissues greatly changes the patterns of respired airflow, resulting in underestimated physiological capabilities in the animals studied (Bourke and Witmer, 2011). Study of the osteological correlates for these missing tissues has not received adequate attention previously, limiting our understanding of extinct animal physiology.

One potential means of testing hypotheses on the possible locations of nasal soft-tissue structures in extinct taxa is to use airflow patterns through the nasal capsule as a guide. Shared nasal airflow patterns observed in the extant relatives (birds, crocodylians, and lizards) of extinct dinosaurs provide evidence for phylogenetic constraint, highlighting regions of similarity among taxa. Given the causative role that nasal soft tissues play in determining airflow patterns, hypotheses of soft tissues in the nasal cavities of extinct taxa can be tested via their effects on modeled airflow in comparison to phylogenetically conserved airflow patterns present in extant outgroups. This method of soft-tissue reconstruction is somewhat similar to Rudwick's (1964) 'paradigm approach' in which one assesses the function of a structure in an animal or animal group, by comparing it to its "idealized" form. However, unlike Rudwick's paradigm, we do not assume that the nasal capsule is optimized for any particular function. The nose serves a variety of functions, all of which are phylogenetically constrained and some of which conflict with one another (e.g., respiration vs. olfaction), thus limiting the optimality of any one function. Instead of optimization, airways of extinct animals are judged based on how consistent their airflow pattern is compared to observed or modeled airflow patterns

in extant animals. As a trivial example, given that inspired air travels from nostril to throat in all extant outgroups, any soft-tissue hypotheses in dinosaurs that disallowed such flow would be falsified on phylogenetic grounds. As a more sophisticated example, the hypothesis that the caudodorsal region of the nasal capsule adjacent to the olfactory bulb of the brain was ventilated in extinct dinosaurs may be tested by studying airflow patterns in extant outgroups with similar associations. Should these outgroups show airflow in this olfactory region, any nasal-capsule soft-tissue hypotheses in dinosaurs that fail to produce olfactory airflow would be falsified. Thus, phylogenetically constrained airflow patterns can be used as a standard by which airflow in extinct taxa can be compared, tested, and potentially restored. Unlike many functional properties that rely on a suite of attributes that do not preserve in the fossil record (e.g., the detailed functioning of the feeding apparatus depends on attributes like muscle architecture and neural motor activation patterns), airflow is ultimately the outcome of fairly well-understood physical parameters (fluid dynamics), making it useful for soft-tissue reconstruction. To simulate airflow, models can be subjected to a computational fluid dynamic (CFD) analysis. CFD is an engineering technique used extensively in industry (Agarwal, 1999; Brzustowicz et al., 2002, 2003; Mirade and Daudin, 2006; Yam et al., 2011), as well as in medicine (Hoi et al., 2004; Garcia et al., 2007; Chen et al., 2009). CFD uses numerical simulation techniques that typically utilize either the finite element or finite volume method. Models are broken into thousands, or even millions of discrete elements collectively referred to as a computational mesh. Governing equations for fluid flow are discretized and then numerically solved across this mesh. The ability of CFD to simulate fluid flow in a digital

environment reduces the costs associated with creating elaborate flume structures or from acquiring and maintaining the machinery needed for digital particle image velocimetry (Lauder et al., 2003). The largest limiting factor for CFD comes down to computational power.

Even with airflow-aided nasal reconstructions, the fidelity of reconstructed airflow achievable in extinct species will be limited by the taxa chosen, quality of fossil preservation, and overall skull architecture. For instance, the nasal capsule of many theropod dinosaurs was only partially bounded by the bones of the nasal cavity, leaving large areas of the nasal capsule bounded only by other soft tissues. The same limitation is seen in large sauropods (Figure 5-3). Although evidence for a rostrally extended nasal vestibule has been discovered in sauropods (Witmer, 2001), these results only indicated rostrocaudal extent, leaving the nasal roof, or tectum nasi, completely unbounded and potentially quite variable. Further complicating matters are the large sizes of most dinosaur species (O'Gorman and Hone, 2012), many of which were larger than any terrestrial animal today. These large size discrepancies make it problematic to predict physiological parameters for dinosaurs based on the osteology of extant animals as such predictions require extrapolation beyond the empirical data.

Nasal soft-tissue reconstructions benefit from a "best case" scenario that utilizes taxa that fall within the size range of extant animals while also having nasal passages that are osteologically well defined. Pachycephalosaurs appear to provide this ideal case (Figure 5-1). The group is composed of small to moderate sized species (Maryańska and Osmólska, 1974). Although much focus has been placed on the enlarged domes and their

role in paleobiology (Fastovsky and Weishampel, 2005; Snively and Cox, 2008; Horner and Goodwin, 2009; Schott et al., 2011; Snively and Theodor, 2011), pachycephalosaurs are also known for extensive mineralization of soft tissues, contributing to the supraorbital ridge on the skull (Maidment and Porro, 2009) and continuing to the tail where mineralized myosepta have recently been discovered (Brown and Russell, 2012). Few pachycephalosaurs preserve much more than a dome, but skulls or partial skulls are known for some species. Computerized Tomography (CT) scan data of the exceptionally well preserved holotype skull of *Stegoceras validum* (UALVP 2) revealed the presence of mineralized olfactory turbinates in the nasal cavity (Figure 5-1E, F). Similar turbinates were also found in two specimens of the derived pachycephalosaur *Sphaerotholus* spp.: *S. edmontonensis* (MRF 360, Figure 5-1B) and *S. goodwini* (NMMNH P-27403, Figure 5-1D). Moreover, as is discussed below, ridges preserved on the nasal bones of both *Stegoceras* (Figure 5-1F) and two specimens of *Sphaerotholus edmontonensis* may represent the mineralized bases of respiratory turbinate or conchal structures. Mineralization of these turbinates provides a rare glimpse of the soft tissues that were present in the nasal passages of a dinosaur. They also allow for direct comparisons with other diapsids, testing hypotheses of turbinate shape in dinosaurs. Such well defined structures make the nasal cavity of pachycephalosaurs the most amenable for soft-tissue reconstruction. Other published examples of mineralized olfactory turbinates (e.g., ankylosaurs; Witmer and Ridgely, 2008a) or mineralized olfactory and respiratory turbinates (e.g., tyrannosaurids; Witmer and Ridgely, 2010) come from large dinosaurs

outside the range of extant empirical data, and so pachycephalosaurs may indeed provide our strongest case for restoring and interpreting nasal function in extinct dinosaurs.

The work presented here is an extension of prior work that has been conducted on a variety of extant diapsid species including crocodylians (Bourke and Witmer, 2010), birds (Bourke and Witmer, 2011) and lizards. This work has been extended to dinosaurs previously, with preliminary models of airflow in *Majungasaurus, Diplodocus*, and *Camarasaurus* (Bourke and Witmer, 2012). The use of pachycephalosaurs in this study provides the most complete reconstruction of nasal soft tissues in a dinosaur to date.

Approach

We set out to test the effects of soft-tissue configurations in the nasal capsule of pachycephalosaurs. We started by first reconstructing the most conservative interpretation of the nasal anatomy, which was accomplished using CT-scan data and segmentation software to reconstruct the nasal capsule based on only the bony-boundaries of the surrounding nasal cavity. The result produced a nasal capsule that hugged the surrounding bones and was reminiscent of previous soft-tissue nasal capsule reconstructions in extinct animals (e.g., Witmer & Ridgely 2008). From this original model, the nasal capsule was progressively modified by the addition of potential soft-tissue structures—including turbinates—based on the shapes observed in the extant relatives of dinosaurs. CFD was used to assess the functional implications of these different anatomical variants by comparing nasal flow patterns between the different models and against previous CFD models of related extant animals.

Terminology

Bony nasal cavity.—We use this general term to incorporate the outermost border of the bony nasal passage and everything within it. It is bounded by the bones of the facial skeleton, which for diapsids typically consist of the premaxilla, maxilla, nasal, prefrontal, lacrimal, palatine, and vomer. Its rostralmost extent ends at the bony narial aperture (*apertura nasi* ossea) whereas the caudal extent usually ends at the lacrimal, prefrontal, and palatines (extending as far back as the pterygoids in crocodylians).

Bony and fleshy nostril.—The bony nostril is the rostral opening of the bony nasal cavity, bounded by the premaxilla, nasal, and maxilla. This bony structure is often called the "naris" by paleontologists, but that term technically refers to the fleshy nostril and the formal term is bony nasal aperture (apertura nasi ossea [Baumel and Witmer, 1993]; Waibl et al. 2012). The distinction is important here as we will use the terms fleshy and bony nostril (Witmer, 2001).

Bony and fleshy choana.— As with nostrils, the term choana has often been applied to both the bony opening of the nasal cavity within the palate as well as the fleshy opening of the nasal cavity into the pharynx. However, these are two structurally distinct anatomical features. The bony choana is the skeletal structure surrounding the smaller fleshy choana (fenestrae exochoanalis and endochoanalis, respectively [Jarvik, 1942; Bellairs, 1949]). Rarely are these two structures identical. As such, we will distinguish between the two when necessary.

Nasal capsule.—This cartilaginous structure is deep to the bony nasal cavity and serves as the main point of attachment or outgrowth for most of the soft tissues inside the

nasal passage (e.g., turbinates, mucosa, conchae). The rostral extent of the nasal capsule may continue as a cartilaginous extension beyond the bony borders of the bony narial aperture as external nasal cartilages.

Conchae and turbinates.—The terms turbinate (or turbinal) and concha are often used interchangeably, but we prefer to separate the two. The turbinates are the cartilaginous outgrowths of the nasal capsule that project into the nasal cavity, whereas the conchae comprise the overlying mucosa that covers the turbinates. Turbinates can be viewed as the internal support of the conchae, although sometimes conchae can be entirely mucosal with no internal support. Turbinates often take the form of thin scrolls or lamellae (branched or unbranched) of cartilage that sometimes mineralize and thus are occasionally preserved within the bony nasal cavity in dried skulls and fossils, providing some indication of the presence and disposition of the conchal mucosa. Functionally, the conchae are more important, being the physiological players that increase the available surface area for respired air to pass over, allowing them to function in countercurrent heat exchange as well as odorant analysis. The functions of conchae vary depending on location in the nasal passage and what epithelial layers they support (e.g., respiratory vs. olfactory epithelium).

Mucosal layer.—Resting on the inner surfaces of the nasal capsule and conchae is the nasal epithelium. Various epithelial types and their corresponding submucosal neurovascular bundles are found here. Three basic epithelial types can be distinguished in the nasal passage, in roughly rostral to caudal order: cornified stratified epithelium,

ciliated columnar (respiratory) epithelium, and olfactory epithelium (identified by the presence olfactory receptor neurons and Bowman's glands).

Airway.—This is the deepest space within the nasal passage and is occupied by respired air. The nasal airway passes from the fleshy nostril to the fleshy choana.

Divisions of the Nasal Passages

Diapsid nasal passages received special attention in the works of Parsons (1959, 1967, 1970), Bang (1960, 1971), Bang and Wenzel (1985), and Witmer (1995b). Diapsid nasal passages vary greatly in size and shape, but their gross underlying structure shows consistent and predictable morphologies. This structure allows for separation of the nasal capsule into the following three compartments. (1) Vestibulum nasi: The nasal vestibule is the rostralmost portion of the nasal capsule just deep to the fleshy nostril. It is typically a tubular region that is smaller in diameter than the succeeding cavum nasi proprium. (2) Cavum nasi proprium (CNP): Continuing caudally from the vestibulum nasi and rostral to the ductus nasopharyngeus, the cavum nasi proprium (= main nasal cavity) typically occupies a more capacious portion of the nasal capsule. Conchae, both respiratory and olfactory, tend to lie within the CNP. The olfactory chamber resides within the cavum nasi proprium at its caudalmost extent and is typically outside of the main respiratory flow. (3) Ductus nasopharyngeus: Following the terminology of Parsons (1970), the nasopharyngeal duct is defined as any connection from the cavum nasi proprium that leads to the choana. It varies in length and complexity between taxa.

Institutional Abbreviations

MRF, Marmarth Research Foundation, Marmath, ND; NMMNH, New Mexico Museum of Natural History, Albuquerque, NM; OUVC, Ohio University Vertebrate Collections, Athens, OH; UALVP, University of Alberta Laboratory for Vertebrate Paleontology, Edmonton, AB; ZPAL, Institute of Paleobiology, Polish Academy of Sciences, Warsaw.

Fossil Specimens and CT Scanning

We primarily focused on two pachycephalosaurid species, *Stegoceras validum* and *Sphaerotholus edmontonensis*, supplemented with data from another species of *Sphaerotholus* (*S. goodwini*; Williamson and Carr, 2002) and *Prenocephale prenes* (Maryańska and Osmólska, 1974). Sullivan (2003, 2006) formally referred the two species of *Sphaerotholus* to the Mongolian genus *Prenocephale*, and this assignment was followed by Schott et al. (2009) and Watabe et al. (2011). The name *Sphaerotholus*, however, was retained by Maryańska et al. (2004), Longrich et al. (2010), and Evans et al. (2013), and we follow this taxonomy. Likewise, some workers synonymize *Sphaerotholus edmontonensis* with *S. buchholtzae* (Williamson and Carr, 2002), but we provisionally follow Sullivan (2003, 2006), Schott et al. (2009), Longrich et al. (2010) , and Watabe et al. (2011) in accepting the validity of the species *edmontonensis*. All recent authors regard *Stegoceras* as a relatively basal pachycephalosaurid and *Sphaerotholus* as part of a diverse clade of more advanced pachycephalosaurine taxa including *Prenocephale* (Sereno, 2000; Williamson and Carr, 2002; Sullivan, 2003, 2006; Maryańska et al., 2004; Schott et al. 2009; Longrich et al., 2010; Watabe et al, 2011).

Stegoceras validum

Specimen UALVP 2 (Figure 5-1E, F) was collected from the Upper Cretaceous (Campanian) Dinosaur Park Formation of Alberta, Canada, and was first described by Gilmore (1924). This specimen remains the best preserved skull for *Stegoceras* and is one of the few pachycephalosaur species known from a complete skull. Only slight taphonomic distortion was observed for UALVP 2, including slight right skew to the entire skull along with minor dorsal displacement of the vomers and palatines. The nasal passage was well defined in this taxon and well bounded by the bones of the nasal cavity. Metaplastic ossification of the overlying dermis was extensively present in this species. Both the supraorbital membrane and the dermis surrounding the bony nasal aperture, often regarded as "dermal sculpturing" (Witzmann, 2009), were preserved in UALVP 2. The narial dermal ossification provided a hard limit to nostril size and position. As described below, mineralization or ossification of soft tissues extended to portions of the cartilaginous nasal capsule, such as the tectum nasi, septum, and turbinates.

Sphaerotholus edmontonensis

MRF 360 (Figure 5-1B), 361 (Figure 5-1C), 362 are new specimens collected in a poorly lithified iron-rich sandstone in the lower third of the Upper Cretaceous Hell Creek Formation (latest Maastrichtian) of southwestern North Dakota. The most complete and informative specimen, MRF 360, is assigned to *S. edmontonensis* based on the triangular arrangement of three nodes on the caudolateral corner of the squamosal and the placement of the first node over the contact between the parietal and squamosal (Sullivan, 2000). Open sutures on the skull suggest that this specimen represents a juvenile. It is

incompletely preserved in two pieces that were separated along the frontoparietal suture (Figure 5-4). The frontoparietal dome and portions of the braincase are preserved, but the palate, quadrates, and nasals were lost due to erosion, exposing the caudal regions of the nasal cavity, revealing preserved soft-tissue structures. The nasal cavity structures of MRF 360 were preserved by the rapid precipitation of siderite (identified by scanning electron microscopy equipped with energy dispersive X-ray spectroscopy [SEM/EDX]) onto the external surfaces of the structures. Subsequent decay of the cartilage left behind a high-fidelity siderite mould and thin voids, which denote the morphology and location of the presumably cartilaginous turbinates. CT scans indicate that the voids left behind after complete decay of the structures are not merely superficial, but extend well into the skull. The requisite rapid siderite precipitation rate (Allison and Pye, 1994) and slow decay of cartilage (Coe, 1978) for this type of preservation have been noted in modern reducing environments and decaying carcasses, respectively.

Two other pachycephalosaurid specimens found near MRF 360 are also referable to *S. edmontonensis*. MRF 361 is similar to MRF 360 in preserving the dome and some of the braincase, but nasal soft tissues are not preserved. MRF 362 preserves a portion of the nasal bones, and, although it is a very fragmentary specimen, it provides important details on the internal structure of the bony nasal cavity.

Sphaerotholus goodwini

NMMNH P-27403 (Figure 5-1D) is the holotype specimen of *S. goodwini* and was collected from the Upper Cretaceous (Campanian) Kirtland Formation of the San Juan Basin, New Mexico (Williamson and Carr, 2002). It consists of a fairly complete

frontoparietal dome, as well as much of the braincase, and, much like MRF 360, preserves portions of what are here interpreted as mineralized olfactory turbinates.

Prenocephale prenes

ZPAL MgD-1/104 (Figure 5-1A) is the holotype specimen of *P. prenes* and was collected from the Upper Cretaceous Nemegt Formation of Mongolia. The skull is virtually complete. It is the best known skull anatomically (Maryańska and Osmólska, 1974; Sereno, 2000; Maryańska et al., 2004; Sullivan, 2006). Only a cast of the skull was available for CT scanning, but the original specimen was studied by one of the authors (LMW).

CT Scanning Protocols

All principal pachycephalosaur fossils specimens discussed here were scanned at the University of Texas High-Resolution X-ray CT Facility (UTCT) in Austin, Texas, with the exception of MRF 362, which was scanned at the Ohio University MicroCT Scanning facility (OUμCT) in Athens, Ohio. The *Stegoceras validum* specimen (UALVP 2) was scanned axially on the UTCT's ACTIS system at a slice thickness of 250 μm, 450 kV, 1.3 mA, and 1400 views for a total of 514 slices. Both *Sphaerotholus edmontonensis* crania were scanned axially on UTCT's ACTIS system, MRF 360 at a slice thickness of 237 μm, 215 kV, 0.15 mA, and 1800 views for a total of 531 slices, and MRF 361 at a slice thickness of 500 μm, 400 kV, 3.7 mA, and 1000 views for a total of 262 slices. The *S. edmontonensis* nasal fragment (MRF 362) was scanned axially on OUμCT's GE eXplore Locus *in vivo* Small Animal MicroCT Scanner at a slice thickness of 90 μm, 80 kV, 498 μA, 3600 views for a total of 730 slices. The holotype specimen of *S. goodwini*

(NMMNH P-27403) was not a major specimen for this study, but scan data were made available by T. E. Williamson; the specimen was scanned at the State of New Mexico Office of the Medical Investigator on a Philips Brilliance Big-Bore scanner at a slice thickness of 400 μm, 120 kV, and 166 mA for a total of 398 slices. All scan data were imported into Avizo 7 (FEI Visualization Sciences Group, Burlington, MA) on 64-bit PC workstations for analysis. Anatomical features of interest (e.g., nasal cavity, turbinates, cranial endocast, endosseous labyrinth, etc.) were highlighted and digitally extracted using Avizo's segmentation tools for quantification and visualization.

Brief Anatomical Description

We present some brief descriptions here to provide the pertinent anatomical framework for the airflow modeling. The full extent of the nasal cavity is preserved only in *Stegoceras* (UALVP 2) among the specimens analyzed here with CT scanning, supplemented with observations of *Prenocephale*. It is bounded by the premaxillae rostrally and the maxillae and lacrimals laterally (Figure 5-5A). The greatly expanded nasals provide much of the dorsal limit to the nasal cavity, with the prefrontals participating at the caudalmost extent of the nasal cavity. The caudal border is composed of a mineralized ethmoid ossification that separates the nasal cavity from the orbital cavity (Maryańska and Osmólska, 1974). Ventrally the nasal cavity is bordered by medial extensions of the maxillae, the palatines, and the vomer at the midline. Caudally the vomer contacts an unusual ventromedian process as well as the pterygoids, which are sutured to medial extensions of the highly arched palatines (Figure 5-5B, C). This triangular ventromedian process projects ventrally at the rostrocaudal level of the caudal

extremities of the bony choanae and tooth rows. Gilmore (1924) regarded this median process as deriving from the vomer, but could not rule out its being part of the parasphenoid (his "presphenoid"), and Maryańska and Osmólska (1974) agreed with the parasphenoid interpretation. Analysis of the CT scan data, however, does not reveal any clear continuity of this ventromedian process with the vomer, pterygoid, or parasphenoid, but rather appears to be suturally separate from adjacent bones. The other well preserved pachycephalosaurid skull, that of *Prenocephale prenes* (ZPAL MgD-1/104), lacks a ventromedian process, but has a tuberosity on the pterygoids in a similar location. So the process in *Stegoceras* may represent mineralization of a perhaps more widely distributed soft-tissue structure, which is discussed further below in the context of restoration of the soft palate.

The well-constrained nasal cavity of *Stegoceras* allows for interpretation of the extent of the cartilaginous nasal capsule and the locations of the major regions of the nasal cavity. The vestibulum nasi appears to have been fairly short, whereas the CNP comprised the majority of the nasal capsule, extending from the rostral aspect of the maxillae and continuing caudally to the mesethmoid. The border of the bony choana was formed by the maxilla laterally and the vomer and palatine medially (Figure 5-5C). The vaulting of the palatines produced a noticeable concavity within the oral region. A ventral concavity shared by the palatine and pterygoid caudal to the bony choana (here termed the choanal fossa) suggests that the nasal passage continued beyond the bony choanal border, pushing the fleshy choana—that is, the transition from nasopharynx to oropharynx—further toward the throat (Figure 5-5D). We regard the ventromedian

process and choanal fossae as osteological correlates of a soft palate, with the fleshy choanae opening immediately caudal to the ventromedian process. This inference is functionally consistent in that the soft palate would extend caudally to about the distal end of the tooth row. It also receives support from a comparison with extant relatives (birds and lizards) that also have extensive bony choanae with much smaller, caudally placed, fleshy choanae (Rieppel et al., 2008; Crole and Soley, 2010). In these extant species, the much larger bony choana is partially or completely floored over by a tight-fitting sheet of oral mucosa, leaving only slit-like openings for the fleshy choana. A similar situation was likely present in *Stegoceras*. The result of this anatomical arrangement would be an extensive nasopharyngeal duct somewhat similar to the nasopharyngeal duct seen in extant crocodylians (Witmer, 1995b), as well as some mammals and turtles.

As noted above, CT scans of the skull of *Stegoceras* (UALVP 2) revealed the presence of mineralized turbinates within the caudal region of the nasal cavity. This caudal location—recessed dorsally away from the rest of the nasal cavity and adjacent to the olfactory bulbs—indicates that this region was the olfactory recess, which would have housed the olfactory chamber. Thus, the turbinates found here likely supported olfactory conchae, clothed in olfactory epithelium. This specimen also preserved portions of the tectum nasi and lateral nasal wall, providing a clear picture of nasal capsule shape in pachycephalosaurs. Likewise, as noted above, one of the *Sphaerotholus* specimens (MRF 360) preserves very comparable turbinates. Moreover, this specimen also preserves parts of the lateral nasal wall, tectum nasi, and a perforated caudal wall separating the olfactory

bulbs from the olfactory chamber of the nasal cavity. This perforated wall appears equivalent to the cribriform plate seen in mammals and is the first time such a structure has been preserved in a dinosaur fossil. The presence of a cribriform plate so close to the preserved turbinates, coupled with their location within the caudalmost aspect of the nasal cavity, suggests that these turbinates indeed supported olfactory conchae.

The turbinates in *Stegoceras* and *Sphaerotholus* appear very similar to each other, which is significant in that the two taxa are not particularly closely related, suggesting that potentially all pachycephalosaurids had such structures. The nasal septum in *Stegoceras* has a spade-shaped base and is overall wider than in *Sphaerotholus*. In both taxa, the turbinates are vertically oriented, shell-like, lamellar structures that arc convex-medially toward the septum. The turbinates in *Stegoceras* are slightly more dorsoventrally splayed when viewed rostrally (Figure 5-6), but this splaying was likely a preservational artifact of the deteriorating nasal capsule prior to fossilization. Portions of the right olfactory turbinate appear to be torn, whereas the left olfactory turbinate has been completely separated from the rest of the nasal capsule. Reattaching these structures reduces the splay seen in the turbinates, making them approach the shape seen in *Sphaerotholus*. A region of unidentified preserved soft tissue was observed in the nasal cavity of *Sphaerotholus* ventrolateral to the olfactory turbinates. It consists of a coiled shape with the left side preserving more coils than the right. These structures may be a second set of turbinates. Exactly what function these potential turbinates would play has been difficult to assess. Extant archosaurs generally have a single olfactory turbinate (but see Discussion), suggesting that these secondary turbinates may have housed respiratory

conchae. The placement of these potential turbinates, however, is out of the predicted flow region of the airfield (generally between the nasal septum and the next most lateral tissue). Further, the scroll-shaped secondary structures are angled 49° ventral to the olfactory concha (Figure 5-7), which suggests that if air did enter these structures it did so from a steep angle. This situation may indicate that *Sphaerotholus* had a relatively vaulted nasal cavity compared to other pachycephalosaurs. Connections between these extra tissues and the olfactory turbinates occur only at the caudalmost aspect of the olfactory chamber. Unfortunately the lack of facial bones for *Sphaerotholus* hamper any further attempts to reconstruct the shape of its nasal capsule.

Methods for Computational Fluid Dynamic Analyses

Model Creation

As noted above, skulls were CT-scanned and segmented using the 3D visualization software Avizo 7.1. Taphonomic distortion is a common problem with fossilized bones (Dunlavey et al., 2004; Angielczyk and Sheets, 2007), necessitating the use of retrodeformation techniques to restore original shape (Motani et al., 2005; Witmer and Ridgely, 2008b; Arbour and Currie, 2012). The hypermineralized nature of pachycephalosaur skulls made them more resistant to taphonomic distortion than other dinosaurs. For *Stegoceras* (UALVP 2), a slight dorsomedial skew of the right side was present (Figure 5-8). This skew had little effect on the nasal region, requiring minor retrodeformation in Maya (Autodesk 2013) to ameliorate.

A 3-dimensional surface model of the nasal cavity was segmented from the CT data. This surface model was essentially a cast that comprised the negative space between

the bones bounding the nasal cavity and represented the potential spaces through which the respired air field could have moved (Figure 5-9). A distinct septal sulcus could be discerned from the CT data. This sulcus suggested that *Stegoceras validum* had a complete nasal septum similar to its extant relatives. Further evidence for this complete septum could be seen in the olfactory chamber where, as noted above, the septum had become mineralized. The presence of a complete septum would have separated the right and left nasal capsules from one another such that air passing through one nasal capsule would interact independently from air entering the other nasal capsule. This independence allowed for modeling of only one side of the nasal capsule as flow patterns should be basically identical in the opposing side. This first-pass nasal reconstruction took into account only the bony boundaries of the nasal cavity and its associated paranasal sinuses (Figure 5-9). This low-fidelity nasal capsule model was thus referred to as the bony-bounded model (BBM). The presence of mineralized turbinates allowed for further refinement of the nasal capsule. The location of the olfactory turbinates relative to the segmented airway indicated that the caudal portion of the nasal capsule was much more constricted than the BBM model would indicate. The extra space within the nasal capsule likely represented portions of the paranasal sinus system. In this case the expanded caudal region of the nasal capsule likely represented a cavum conchae, inflating the olfactory turbinate as it does in birds and crocodylians (Witmer, 1995b).

CFD Preparation

Before models could be subjected to a fluid dynamic analysis, they first needed to be cleaned of any artifacts of segmentation. These artifacts included low-resolution areas

of segmentation that produced “stair-stepping” regions to the model, as well as areas where an insufficient number of triangles were used to represent parts of the morphology, introducing a high skew (triangles with extremely acute angles) into the model. Surface models were cleaned using the smoothing and noise reduction algorithms in Geomagic Studios 10 (Geomagic). Surface models were then recalculated (remeshed) in Avizo 7.1 to reduce skew by covering the model in as many equilateral triangles as possible.

Models were assigned a series of boundary conditions that would induce physiologically-realistic airflow through the model (Figure 5-10). These boundary conditions consisted of a pressure inlet located at the nostril, a pressure outlet located at the fleshy choana and an impermeable wall boundary over the rest of the model. Surface models were transformed into volumetric meshes for fluid dynamic analysis (Figure 5-10). A hybrid mesh consisting of a tetrahedral shell with a hexahedral core was created for each model. This meshing technique provided the efficiency of hexahedral cells (Aftosmis et al., 1994; Biswas and Strawn, 1998) without the difficulties associated with fitting hexahedra to unstructured grids (Blacker, 2001; Ruiz-Gironés, 2011). Mesh creation was done using the program ICEM CFD (ANSYS Inc.). Fluid dynamic analysis was performed using the fluid dynamics program Fluent 13 (ANSYS Inc.).

Environmental Parameters

Standard sea level atmospheric pressure (101,325 Pa) was used for the area surrounding the nostrils. The wall boundary incorporated a ‘no-slip’ condition indicating a lack of movement at the solid-fluid boundary. Although the mucous and cilia that comprise the respiratory epithelia will contribute to some movement of the air field, these

movements are often so slow (≤1 cm/min) and their thickness so slight that they can essentially be ignored (Craven et al., 2009a). In Fluent the "target-mass-flow-rate" option was used to obtain estimated volumetric flow rates at the pressure outlet, allowing the program to determine the pressure gradient necessary to obtain these rates. A 3D double-precision solver was chosen for model analysis. A segregated pressure-based PISO algorithm was used to solve the steady-state continuity and Navier-Stokes equations. A node-based discretization gradient was used on all models. A second-order accurate spatial discretization scheme was used for both pressure and momentum (Fluent 2006). Iterative models ran until all normalized residuals of error had converged to 1.0×10^{-4}. Point surface monitors placed at various locations on the models were also employed as a secondary means of determining convergence independent of continuity and momentum. Results were analyzed using Fluent 13 and Avizo Wind 7.1. Models were tested during resting inspiration and expiration.

To ensure that grid resolution would not affect the final results, a grid convergence index (GCI) for each model was calculated based on three grid resolutions (grid refinement ratio = 2) for each model of nasal morphology (Figure 5-10). GCI calculations followed the methods of Roache (1994) and Craven et al. (2009a).

Physiological Variables

A key requirement for any simulation of respiration is the necessary empirical data to justify the flow rates being simulated. For many extant taxa, respiratory data are either readily available in the literature or are obtainable via experimentation. Obviously, neither of these options is available for extinct taxa. Certain aspects of the respiratory

system, such as air sac placement (O'Connor, 2006, 2009; O'Connor and Claessens, 2005; Wedel, 2003), respiratory muscles (Carrier and Farmer, 2000a, b), and overall lung mobility (Schachner et al., 2009, 2011b), may be inferred from osteological correlates found on the skeleton. However, they tell us very little of the dynamic variables required to simulate flow rates (i.e., tidal volume and respiratory frequency, which are required to determine respiratory drive), which thus requires respiratory variables to be inferred. To ensure confidence in our inferences, we used the extant phylogenetic bracket (EPB) approach (Witmer 1995a) to aid in estimates of respiration values for pachycephalosaurs. This was accomplished by searching the literature for data on resting respiratory variables in extant diapsids. Although this group is not as well studied as mammals, there are a handful of studies that proved useful for obtaining physiologically viable resting respiration values.

The most comprehensive collection of respiration data on diapsids comes from Frappell et al. (2001), who surveyed resting respiratory variables in 50 species of birds spanning a broad phylogenetic range of extant Neornithes. Their data was corrected for phylogeny, making it the most rigorous look at respiratory variables for any diapsid taxon to date. However, these data only covered one half of the dinosaur EPB. No similar comprehensive study has been performed for crocodylians. The works of Farmer and Carrier (2000a, b) and Farmer (2006), however, come the closest, although the data are limited to one crocodylian taxon (*Alligator mississippiensis*). Farmer (2006) discovered an apparent constraint on tidal volume in extant archosaurs. Taking data from a variety of alligator studies, Farmer (2006) discovered that the equation relating tidal volume to

body mass in crocodylians was almost identical to the same equation in birds obtained by Frappell et al. (2001).

$$V_T = 20.3M^{1.06} \text{ — Frappell et al., 2001}$$

$$V_T = 20.7M^{1.06} \text{ — Farmer, 2006}$$

The differences between the equations are slight enough that they are likely the result of the limited taxon sampling for crocodylians. These data suggest that it may be possible to predict tidal volume in extinct archosaurs such as dinosaurs.

Determining respiratory rate was more difficult due to a general lack of broadly comparative data for diapsids other than birds. Individual respiratory variables have been recorded previously for alligators (Hicks and White, 1992; Farmer and Carrier, 2000a). These data show that alligators between 1.34–3.4 kg at 30°C, had a respiratory frequency of 7.5–7.3 breaths/min respectively. These values fall within the range of values for bird taxa of similar size (e.g., 8.6–8.4 breaths/min for a 1 kg penguin and pheasant respectively [Frappell et al., 2001]). To further aid in reconstructing respiratory physiology, we looked at resting respiratory variables in squamates, the immediate outgroup to archosaurs. To date there has only been one preliminary study of respiratory variables in squamates (Bennett, 1973). This study looked at 16 species of lizards ranging in size from 0.1–1 kg. Results of that study found tidal volume to be shallower in lizards compared to archosaurs. However, respiratory frequency (at 37°C) for the size range studied did fall within the respiratory frequency range of similar sized non-passerine birds (17–35 breaths/min). These data suggest that diapsids, as a group, breathe in a similar manner regardless of thermophysiology. This breathing frequency is substantially

different from that of mammals, which take approximately three times as many breaths during an equal period of time (Frappell et al., 2001). Based on the similarities of these studies, the equations from Frappell et al. (2001) were used, as they provided a physiologically reasonable set of respiratory values (Table 5-1). These equations required an estimate of body mass. To account for the fact that precise body masses of extinct animals are currently unknowable, we used a high and low end for body mass estimates so as to incorporate a range of values that were likely to encompass the "true value" of the living animal (Hutchinson et al., 2011). Minimum and maximum mass estimates for *Stegoceras validum* were obtained from Peczkis (1995).

Model Assumptions

Fluid dynamic modeling—like all modeling—requires initial assumptions be met prior to running an analysis. Two of these assumptions are the viscosity model chosen for the fluid and the steadiness of the flow over time. To determine which viscosity model to use, it was necessary to ascertain the type of fluid flow (laminar or turbulent) that was likely present in the airway, which can be approximated by calculating the Reynolds number throughout the airway. Reynolds numbers are dimensionless ratios of inertial-to-viscous forces within a fluid. Reynolds numbers below 2000 indicate that viscous forces dominate the flow field, making fluid flow laminar (Vogel, 1994). As the Reynolds numbers increase above 2000 the orderliness of the flow deteriorates, resulting in laminar flows that contain partially formed turbulence (Vogel, 1994). At Reynolds numbers of 4000 and higher, inertial forces dominate the flow field resulting in fully formed turbulent flow (Vogel, 1994).

It is difficult to calculate Reynolds numbers for biological systems as the fractal nature of the shapes involved make it difficult to obtain a characteristic length (typically the diameter). A way around this problem is to borrow a technique from civil engineering and use the wetted perimeter of the object, as was performed by Holmes et al. (2011).

$$\mathrm{Re} = \frac{4Q}{Pv}$$

where Q = the volumetric flow rate measured (m^3/s), P = the wetted perimeter in meters (Foss, 1998), and v = the kinematic viscosity of air (1.6036e-05 m^2/s at 30°C).

Using cross sections taken approximately every 3 mm, and assuming the volumetric flow rates obtained from Frappell et al. (2001), the resulting Reynolds numbers suggested that a laminar viscosity model was the best choice for all the models studied (Table 5-2).

The second assumption that needed to be met was the steadiness of the flow field. The steadiness of a flow determines how often it is able to assume the classic parabolic profile under oscillating conditions (e.g., the pulsation of blood flow or the pendular pattern of breathing). To determine this we used the dimensionless Womersley number (Womersley, 1955), as defined for the respiratory system (Craven et al., 2009a).

$$Wo = \frac{Dh}{2}\sqrt{\frac{2\pi f}{v}}$$

Where f = the frequency of oscillation (Hz), and Dh is the hydraulic diameter of the airway defined as:

$$Dh = \frac{4A}{P} \text{ (Foss, 1998)}$$

where A = the area of the cross section being measured (m^2).

The Womersley number is a function of a structure's size, the frequency of oscillation, and the kinematic viscosity of the fluid being moved (Loudon and Tordesillas, 1998). At Wo ≤ 1 the flow field may be considered to exist in a quasi-steady state, which suggests that the fluid is capable of reaching and maintaining the standard parabolic profile. Furthermore, it also implies that instantaneous flow rate can be determined by the corresponding instantaneous pressure gradient (Loudon and Tordesillas, 1998), allowing for a steady-state solution to be modeled. As Wo increasingly deviates from unity, the flow becomes more unsteady. At Wo > 10 inertial forces dominate once more, forcing a flattened "plug" profile to the fluid flow (Ku, 1997). This flow type is considered to be completely unsteady, making its shape for a given pressure gradient unknown *a priori*, necessitating the use of a transient model for flow calculations.

Based on the breathing frequency data obtained from Frappell et al. (2001), Womersley data from all our pachycephalosaur models fell between 0.2–2.6, indicating that a steady-state solution would be a valid modeling scenario (Table 5-2).

Results

Qualitative comparisons of airflow profiles across all of the grid resolutions used here revealed gross overall similarity in airflow patterns. GCI data indicated that the highest grid resolutions were largely independent of grid error at both high and low flow velocities (Table 5-3, Figure 5-11).

Airflow in the Bony-Bounded Model (BBM)

Air movement through the BBM airway consisted of slow moving air traversing the nasal capsule from nostril to choana. Pressure values and associated velocities were exceedingly low (maximum pressure drop < 2 Pa) resulting in a slow moving air stream throughout the nasal capsule. Despite being a largely open space, some slight stratification of the air field was observed. Air entered the nostril where it proceeded through the small vestibulum nasi. The shape of the vestibulum nasi directed air medially as it entered the enlarged CNP. The sudden transition from the relatively confined vestibulum nasi to the larger CNP resulted in a Venturi effect, jetting air further into the nasal capsule where it fanned out to encompass the larger space. This effect created a noticeable pocket of relatively stagnant air within the lateral aspect of the CNP. As the inspired air field approached the olfactory chamber it veered ventrolaterally towards the ductus nasopharyngeus, which imparted a low-velocity swirling motion to the air field. Portions of this swirling forced the lateral-most air streams to flow caudally to rostrally along the ventrolateral aspect of the CNP, filling up this portion of the nasal capsule and creating a barrier to entry for other inspired air (Figure 5-12). This pattern was observed under both estimated flow rates, with the higher flow rate serving only to enforce the pattern observed under the slower flow regime (Figure 5-13). Upon expiration flow spiraled through the CNP to exit through the nostril.

Comparing these data with previously published works on mammals (Craven et al., 2009b; Doorly et al., 2008; Jiang and Zhao, 2010), as well as our own work on sauropsids (Bourke and Witmer, 2010, 2011), some notable differences were observed.

Flow rate in the nasal capsule of *Stegoceras* was substantially slower and more uniform than the inspiratory flows seen in extant amniotes. The near lack of olfactory flow in the BBM of *S. validum* is clearly unrealistic and a sign that the BBM was not accurately capturing the flow pattern within the nose. This determination was based on multiple lines of evidence including the presence of a well-developed olfactory region in this taxon. The preservation of well-developed olfactory turbinates (Figure 5-6) further suggested that olfaction was, if anything, a strong sensory component of this animal's repertoire. Large olfactory bulbs on the endocast of *S. validum* likewise indicated that olfactory sensitivity was, at the very least, not reduced in this specimen. Furthermore, extant amniotes with even moderately developed olfaction (e.g., humans) routinely show air moving through their olfactory chambers during resting respiration (Kimbell et al., 1997; Guilherme et al., 2007; Craven et al., 2009a). In contrast, airflow during resting respiration in the BBM of *S. validum* dropped quickly in velocity shortly upon entering the olfactory chamber. This air did not proceed far before being drawn back into the ductus nasopharyngeus (Figure 5-13). Higher inspiratory flow speeds allowed for greater olfactory chamber penetration, but always at exceedingly low speeds (<1.5 cm/s). That the flow pattern observed in our bony-bounded model was in disagreement with these morphological criteria suggests that the BBM was inadequate for revealing airflow patterns in the living animal. These results were not unexpected in that the bony-bounded airway is largely an empty space with no reconstructed soft tissues (other than the soft palate to provide the position of the fleshy choana). Extant taxa utilize various soft-tissue conformations to manipulate the respired air field, directing it to different regions of the

nasal capsule before exiting the choana. *Stegoceras* would have had similar structures in its nasal capsule, in particular a region near the olfactory chamber that would have aided in pushing air further in. Ultimately, the results of the BBM analyses show that nasal soft tissues must be considered to provide valid tests of hypotheses of nasal airflow and physiology.

Reconstructing Soft-Tissue Structures

All extant diapsids fill the majority of their nasal cavities with mucocartilaginous tissues that come with associated neurovasculature and glands. The current conformation of the bony-bounded nasal capsule in *Stegoceras validum* did not take into account the neurovasculature or glands that would have been present. These structures would have taken up varying amounts of space that would limit the extent of the nasal capsule.

Mineralization/ossification of many of the periorbital elements in pachycephalosaurids provides key information on the broad patterns of blood flow entering and exiting the nasal region. In *Stegoceras*, the nasal region was likely supplied by the ethmoid arteries, similar to extant archosaurs. In crocodylians, the ethmoid arteries are branches of the caudal cerebral arteries, whereas in birds the ethmoid arteries are branches of the rostral cerebral arteries (Baumel, 1993; Sedlmayr, 2002; Almeida and Campos, 2011). During crocodylian development, the connection of the rostral cerebral arteries to the ethmoid arteries obliterates, leaving the caudal cerebral arteries to form the ethmoid arteries (Burda, 1969). The osteological evidence that would inform which condition occurred in *Stegoceras* is currently unavailable, but the ethmoid arteries were restored in *Stegoceras* on a level I′ inferential basis (i.e., a homologous condition present

minimally in both extant outgroups [level I] but lacking osteological correlates, hence the I′ designation; Witmer, 1995a; Figure 5-14). In extant archosaurs, the ethmoid arteries form the nasal vessels rostral to an anastomosis between the ethmoid and supraorbital arteries (Sedlmayr, 2002). In *Stegoceras*, a canal was found that represents the course of the supraorbital vessels as they entered the nasal region and anastomosed with the nasal vessels, similar to *Prenocephale* (Maryańska and Osmólska 1974). Maryańska and Osmólska (1974) reported in *Prenocephale* that two foramina between accessory orbital ossifications 1 and 2 transmitted the ethmoid arteries. Maryańska and Osmólska (1974) reconstructed these blood vessels according to squamate vascular anatomy, where the supraorbital vessels supply a majority of the blood to the nasal region and the cerebral arterial contribution is overshadowed by extracranial blood vessels, specifically, the supraorbital arteries (Burda, 1966; Porter and Witmer, 2012). In *Stegoceras*, we used archosaur vascular anatomy to inform the restoration of the supraorbital vessels anastomosing with one of the nasal vessels. This anastomosis likely occurred with the lateral rather than the common or medial nasal vessels, as canals that transmitted branches of the medial nasal vessels were found within the suture between the nasal bones. These canals indicated that the bifurcation of the common nasal vessels occurred caudal to the supraorbital vessels, excluding the common nasal vessels from the anastomosis. The restoration of this anastomosis is a level I′ inference (Figure 5-14).

The common nasal arteries bifurcate into medial and lateral nasal arteries ventral to the olfactory bulbs in extant archosaurs (Sedlmayr, 2002). The medial nasal vessels (arteries and veins) travel within the mucosa along the nasal septum, leaving few

osteological correlates. They course rostroventrally with the medial nasal nerve along the nasal septum from the olfactory region to canals in the premaxilla, where they usually anastomose with terminal branches of the dorsal alveolar blood vessels. In *Stegoceras*, canals were found between the nasal bones that initially coursed rostrodorsally and then curved caudodorsally. These canals indicated the location of the medial nasal vessels as they passed along the nasal septum and indicated the caudalmost location of the medial nasal vessels after they branched from the common nasal vessels. Canals and grooves within the premaxilla of both *Stegoceras* and *Prenocephale* were found along the ventrolateral aspect of the nasal process. These canals and grooves transmitted the medial nasal neurovascular bundle through the premaxilla, where they ultimately anastomosed with the dorsal alveolar, palatine, and lateral nasal vessels. Based on the presence of these osteological correlates, the medial nasal blood vessels were restored in *Stegoceras* on a level I basis, although parts of the vessels require a level 1′ inference (Figure 5-14).

In extant archosaurs, the lateral nasal arteries branch from the common nasal artery and then join the lateral nasal nerve after it exits the nasal capsule through the foramen epiphaniale (Witmer, 1995b; Sedlmayr, 2002). The lateral nasal neurovascular bundle then courses rostrolaterally along the dorsolateral aspect of the nasal capsule, where it supplies the nasal gland (Witmer, 1995b; Sedlmayr, 2002). After supplying the nasal gland, the lateral nasal neurovascular bundle courses rostroventrally to supply the plexus surrounding the vestibulum nasi. The lateral nasal neurovascular bundle has different osteological correlates in birds (the lateral orbitonasal foramen; Witmer 1995b) and crocodylians (e.g., canals in the nasal bones of alligators). *Stegoceras* resembles the

crocodylian condition in having branches of the lateral nasal vessels passing through canals in the nasal bones to reach the dorsal aspect of the skull. The main trunk of the lateral nasal vessels would connect these branches, indicating the course of the lateral nasal vessels through the nasal region. These vessels were restored in *Stegoceras*, again requiring both level I′ and level II inferences (level II inferences draw phylogenetic support from only one extant outgroup, in this case crocodylians; Figure 5-14).

In extant diapsids, the lateral nasal vessels anastomose with the dorsal alveolar vessels just caudal to the bony narial aperture. They form an anastomotic loop around the vestibulum nasi that has been shown to contain cavernous tissue (Stebbins, 1948; Oelrich, 1956; Witmer, 2001; Sedlmayr, 2002). These blood vessels curve dorsally around the nostril and anastomose with the premaxillary vessels (the continuation of the dorsal alveolar vessels ventrally) and the medial nasal vessels within the premaxilla (Sedlmayr, 2002). In extant diapsids, an anastomosis between the dorsal alveolar, nasal, and palatine vessels was found within a canal near the premaxilla and maxilla articulation. A nerve was not found within this canal in the extant sample and is likely an exclusively vascular osteological correlate. In *Stegoceras*, a similar canal within the premaxilla likely transmitted anastomotic branches of the palatine, dorsal alveolar, and nasal blood vessels. The restoration of this anastomosis was a level I or I′ inference (Figure 5-14).

In extant archosaurs, the veins of the nasal region usually course with the artery of the same name. The medial and lateral nasal veins are tributaries of the olfactory sinus and its caudal continuation, the dorsal sagittal sinus (Baumel, 1993; Sedlmayr, 2002). The venous drainage from the medial and lateral nasal vein that contained cooled blood

from the nasal region could drain directly into the dorsal sagittal sinus. The olfactory sinus was restored in *Stegoceras* as a level I′ inference, and the dorsal sagittal sinus was restored as a level I inference (Figure 5-14).

A closer examination of the CT data for *Stegoceras* revealed the presence of a ridge projecting ventromedially and running along the ventral surface of the nasals. This ridge was observed on both sides of the skull suggesting that it was not an artifact of preservation. It runs from the rostral tip of the nasals, caudally toward the lacrimal in the caudal region of the nasal cavity (Figure 5-15). Further support for this ridge structure came from two other *Sphaerotholus edmontonensis* specimens found near MRF 360 (MRF 361 and MRF 362). Each specimen exhibits similar ridges running down the ventral aspect of the nasals. Finally, a similar ridge is present in *Prenocephale* (ZPAL MgD-1/104) as well, although its full extent cannot be determined without CT scanning. Thus, the presence of these ridges in these three pachycephalosaurid taxa further supports the interpretation that these were not artifacts of preservation. The presence of a ridge running within the length of the nasal cavity suggests that a soft-tissue structure was present. Ridges within the nasal cavities of mammals function as attachment sites for turbinates and have been used as osteological correlates for respiratory turbinates in extinct synapsids (Hillenius, 1992). The turbinates of diapsids rarely mineralize, but the cartilaginous skeleton may still pull on its attaching bone with enough force to form a process or ridge, especially if the animal is large (Figure 5-16). Thus, we hypothesize that the ridges observed within the nasal cavities of pachycephalosaurids supported turbinates, specifically respiratory turbinates, given their location. The exact size and shape of these

turbinates currently cannot be worked out, but comparisons with extant diapsids offer potential shapes that could have been present. Among extant birds, turbinate shapes are typically limited to variations of scrolls or branches (Bang, 1971). Thus, to assess the effects of turbinate placement within the airway of *Stegoceras*, two separate digital models were made. One model contained a scrolling turbinate whereas the other model contained a branched turbinate (Figure 5-17C, D). As we were assessing the effect of these shapes on the respired air field in life, we were actually looking at the effect of the innermost structures of the nasal capsule—the conchae.

In extant archosaur taxa, the conchae are supplied primarily by the medial nasal vessels. The crocodylian concha and avian caudal concha are supplied by branches of the medial nasal vessels and the ventral aspects of these olfactory conchae are supplied by the sphenopalatine artery (Oelrich, 1956; Sedlmayr, 2002). In birds, the lateral nasal vessels supply the rostral concha and the rostral aspect of the middle concha (Sedlmayr, 2002). In crocodylians, only the medial nasal vessels have been found to supply the conchae. In *Stegoceras*, conchal branches of the medial nasal vessels were restored as a level I′ inference. The sphenopalatine artery was restored in *Stegoceras* as a level I inference, based on canals found in extant taxa and in *Prenocephale* within the orbit and passing into the nasal region through the sphenopalatine foramen. This foramen is located "dorsal to the tongue of the pterygoid which underlies the palatine and ventral to several small ossifications" (Maryańska and Osmólska 1974, p. 83). In extant archosaurs and squamates, the sphenopalatine artery supplies the mucosa of the nasal septum. These

blood vessels would have supplied the restored concha, increasing vascularization of soft tissues in the airfield.

Although bony ridges in the nasal cavity and the lateral expansion of the nasal capsule may be related to the presence of turbinates, it is also possible that they might be related to other soft-tissue structures, as well. For example, based on phylogenetics, *Stegoceras*, like almost all archosaurs, should have had a well-developed paranasal air sinus, known as the antorbital sinus (Witmer, 1997b). *Prenocephale* (ZPAL MgD-1/104) has an extensive antorbital sinus running the length of the maxilla (Maryańska and Osmólska, 1974; Witmer, 1997b; Maryańska et al., 2004). Thus, the lateral expansion of the nasal capsule in *Stegoceras* noted above may actually represent the antorbital sinus. If so, the ridge seen in *Stegoceras* may have been associated with a largely unossified or unmineralized wall that separated the nasal capsule from the paranasal sinus. In *Prenocephale*, a medial lamina of the maxilla provides a partial bony wall, but in *Stegoceras* the CT scan data clearly indicate that such a wall, if present, must have been composed of soft tissue (cartilage and/or mucosa). Many extant birds have a largely cartilaginous medial wall of the antorbital sinus (Witmer, 1995b), as did many extinct saurischians (Witmer, 1997a), and so this condition in *Stegoceras* would be not that unusual. As such, it was decided that a third digital model of nasal capsule variation should be made that incorporated an extended paranasal septum (Figure 5-17B).

Finally, a fourth model was created to test the possibility that the ridge seen in *Stegoceras* (UALVP 2) incorporated both a paranasal septum and a nasal turbinate (Figure 5-17E). As noted above, in *Prenocephale* (ZPAL MgD-1/104), the paranasal

septum is preserved as a lamina of maxilla medial to the antorbital sinus. This lamina approaches, and indeed contacts in some areas, a ridge that seems comparable to (and likely homologous with) the ridge in *Stegoceras*. As preserved, the ridge in *Prenocephale* is not associated with the maxillary paranasal septum throughout its entire length, perhaps lending support to the notion that the ridge could simultaneously function to demarcate the walls of the antorbital sinus and to support a respiratory turbinate. Indeed, in many extant amniotes, nasal conchae are closely associated with paranasal air sinuses (Witmer, 1995b, 1997a).

To test the impact of these different soft-tissue hypotheses on nasal airflow, the 3D modeling program Maya (Autodesk 2013) was used to model conchae of different conformations (scrolled and branched), as well as a paranasal septum walling off the antorbital sinus (with and without a turbinate), in *Stegoceras*. These models were converted into fluid dynamic models which were then subjected to CFD analysis following the criteria listed above.

Results of Modeling a Paranasal Septum

As just noted, a paranasal septum was digitally modeled and placed along the path of the nasal ridge (Figure 5-17B). The septum completely separated the lateral expansion of the bony-bounded nasal capsule. Justification for this was based on the relationship of the paranasal sinuses to the air passages of extant amniotes. The antorbital sinus in *Stegoceras* joined with the nasal capsule via an ostium, probably in a position similar to that described for *Prenocephale* (Maryańska and Osmólska, 1974; Witmer, 1997b). However, this ostium would have been fairly small and arranged orthogonal to respired

airflow (Witmer, 1995b; Witmer and Ridgely, 2008a), resulting in very little air exchange taking place during respiration.

Results of CFD analysis revealed a substantial change in airflow pattern. Both pressure drop and flow velocity greatly increased over the BBM (Table 5-4). Similar to the bony-bounded airway, the air field continued to exhibit a medial bias as air moved from the vestibulum nasi to the CNP. However, unlike the BBM, the air field never formed a caudal-to-rostral loop, which represents an advance in that the loop was regarded as being unrealistic. Rather, inspired air arced mediolaterally as it traveled through the CNP to the ductus nasopharyngeus. Air in the dorsalmost portion of the airway moved the slowest, whereas air nearer to the nasal capsule floor—i.e., closer to the ductus nasopharyngeus—moved fastest. These flow patterns were true for both flow rates tested. Under the flow rate estimated for a 10 kg individual, airflow was remarkably slow, with air in the nasal capsule averaging 16 cm/min. This low-velocity air imparted a weak momentum to the air streams entering the olfactory chamber, keeping air from overcoming the relatively high pressure in the olfactory chamber, resulting in stagnation. This pattern changed somewhat under the flow rate estimated for a 40 kg individual. Under this flow regime, some air did enter the olfactory chamber where it circulated dorsally, then rostrally (Figure 5-18). Airflow upon expiration was nearly identical to airflow in the BBM, with air spiraling through the nasal capsule towards the nostril (Figure 5-19).

Results of Modeling a Scrolled Concha

Using the middle concha of turkeys (*Meleagris gallapovo*) as a fairly typical template for conchal shape, a simple scrolled concha was inserted into the nasal capsule of *Stegoceras* along the length of the nasal ridge. The concha scrolled mediolaterally 1.5 times before opening into the ductus nasopharyngeus. The concha left 1–4 mm of space within the nasal capsule for respired air to traverse. These are fairly typical values for extant amniotes.

Pressure drop was uneven across the nasal capsule. Placement of the scrolled concha served to function as a barrier separating a relatively low-pressure gradient medially from a relatively steeper pressure gradient laterally. During inspiration, air followed a path similar to that observed in the BBM, with the vestibulum nasi largely directing the flow of air into the CNP. The concha split the air field into three different channels. One channel took a ventral route to the ductus nasopharyngeus, wrapping around the outside of the concha (Figure 5-20). A second channel entered the concha where it followed a fairly straight path towards the ductus nasopharyngeus (Figure 5-20). Very little twisting or cyclonic motion of the air was observed in the concha at either the estimated low or high flow rates. The final air channel proceeded medially along the outside of the concha toward the olfactory chamber. As with the paranasal septum model, airflow at the estimated low flow rate did not penetrate the olfactory chamber but stopped just short of it before wrapping ventrally around the concha and exiting into the ductus nasopharyngeus. However, under the high flow-rate estimate, air was able to slightly penetrate the olfactory chamber (Figure 5-20). Airflow on expiration initially spiraled out

of the ductus nasopharyngeus where it encountered the concha. Air entering the concha straightened shortly upon entry. Other air channels proceeded ventrally or medially around the concha. Very little air proceeded along the dorsal aspect of the concha.

Results of Modeling a Branched Concha

The middle concha of an ostrich (*Struthio camelus*) was used as a fairly typical template for construction of the branched concha for *Stegoceras*. As with the scrolled concha, the branched concha ran the length of the nasal ridge prior to termination near the ductus nasopharyngeus. The more open nature of the branched shape provided more room for the air field (1–6 mm space between the concha and the capsular walls).

Similar to the scrolled concha, inspired air broke into multiple (3–4) separate channels as it came into contact with the branched concha (Figure 5-21). The first channel proceeded ventrolaterally with occasional air streams noted dorsally along the outside of the concha. These dorsal streams were relatively slow moving as they proceeded caudally towards the ductus nasopharyngeus. The second channel entered the lateral branch of the concha where it proceeded toward the ductus nasopharyngeus in a relatively straight line. The third channel entered the medial branch of the concha where it proceeded caudally towards the olfactory chamber. At 4.4 L/min (10 kg), air moved slowly through the medial branch and was unable to penetrate the olfactory chamber before wrapping around the outside of the concha and dumping into the ductus nasopharyngeus. At 10 L/min (40 kg), effectively no air was found moving through the medial branch of the concha. The fourth and final channel proceeded along the outside of the medial branch where it moved caudally into the olfactory chamber. At 4.4 L/min,

olfactory flow deteriorated 8 mm into the 25 mm deep olfactory chamber. At 10 L/min, this olfactory chamber penetration was slightly better with average olfactory flow faster than before. Airflow upon expiration was more evenly distributed than in the scrolled conchal morphology, with air streams readily passing around and through the branched concha. This included air moving through the olfactory chamber, indicating olfactory washout was taking place.

Results of Modeling a Concha with a Paranasal Septum

This airway model used the antorbital sinus configuration with the modeled paranasal septum described above but with the addition of a mediolaterally scrolled concha. Surprisingly, despite the reduced size of the airway with the combined structures, distance from the center of the air stream to the nearest wall was very comparable to the other conchal arrangements (< 4.5 mm).

Inspired air broke into three channels shortly after entering the CNP. Most air traveled ventrally along the outside of the concha, towards the ductus nasopharyngeus. A second channel moved through the scroll where it followed the contours but never really developed a spiraling motion. The third channel of inspired air ran towards the olfactory chamber between the nasal septum and the medial wall of the concha. This channel exhibited slower airflow than the rest of the nasal capsule, with air meandering towards the olfactory chamber before being drawn ventrally towards the ductus nasopharyngeus. Similarly to the scrolled conchal model, air movement became stagnant upon entry into the olfactory chamber (Figure 5-22). Airflow on expiration jetted out of the ductus nasopharyngeus where it was split into several channels by the concha. A weak spiraling

motion was observed in the air channel that proceeded along the ventral aspect of the concha. The majority of expired air passed ventral to or within the scroll of the concha, leaving most of the medial aspect of the nasal capsule relatively undisturbed (Figure 5-22).

Discussion

Critique of Methods

The results obtained from our airflow simulations are ultimately dependent on the assumptions used to make them. For instance, the use of a laminar viscosity assumption may have placed excessive restrictions on our airflow models, limiting the ability of respired air to mix within the nasal capsule, or push inspired air into the olfactory chamber via the vortex formation. Although laminar flow is considered orderly, the restrictions of our viscosity model would not necessarily negate the formation and shedding of low Reynolds number, laminar vortices such as Von Kármán trails (Vogel 1994, 2003). Contortions within the airway may also produce laminar "mixing" as well as vortex shedding (Vogel 1994). Our work on extant diapsid airways have produced models that exhibit such vortices using the same laminar viscosity assumption used in this study. Thus, we feel confident that the assumptions used in these analyses, while potentially too conservative, should not negate the formation of airflow patterns that would promote olfactory flow. We prefer to err on the side of conservative estimates.

A large caveat for our results comes from the predicted flow rates used, which were based on rates obtained from regression equations relating respiratory variables to body mass in birds. Birds are not pachycephalosaurs, yet still can be informative for

dinosaur studies. Birds are generally small-bodied, volant endotherms. In contrast, pachycephalosaurs were larger-bodied, terrestrial animals of controversial metabolic status. Thus, it is possible that the airflow rates predicted might be overestimated. The metabolism of pachycephalosaurs, or any extinct animal, currently remains, strictly speaking, unknown, but we argue that it would have little bearing on the respiratory parameters used in the modeling methods used here. Although oxygen demand in tachymetabolic, endothermic birds may be over 20 times higher than similar sized bradymetabolic ectotherms (Nagy et al., 1999), the arrangement of the avian respiratory system allows birds to extract more oxygen per breath, and at lower concentrations, than similar sized mammals (Schmidt-Nielsen, 1997), which results in avian breathing frequencies being one-third those of similar sized mammals (Frappell et al., 2001). For non-passerine birds, this breathing frequency falls within the same range as similar sized lizards (Bennett, 1973), assuming a monophasic breathing pattern (Milsom, 1988). In turn, the large tidal volume in birds has been shown to be almost identical to the tidal volume in similar sized crocodylians (Farmer, 2006). Moreover, recent studies indicate that some key aspects of the avian respiratory system, such as unidirectional pulmonary airflow, may be deeply nested within diapsids (Farmer and Sanders, 2010; Schachner et al., 2013). Given all these similarities in respiratory variables, the inspiratory drive estimated for *Stegoceras* likely falls within the range of physiological relevance for an animal its size regardless of its metabolic status.

It remains possible that the volumetric flow rate in *Stegoceras* is underestimated based on the combined nature of the equations from Frappell et al. (2001). The authors

provided several allometric equations for resting respiratory variables, including equations that could have been derived from other variables, in this case breathing frequency and tidal volume. Using the estimates obtained from these individual equations, the calculated volumetric flow rates for a 10 and 40 kg *Stegoceras* would be 1.3 and 1.6 times higher, respectively, than the combined inspiratory drive equation. However, using these higher inspiratory flow rates would have had a negligible effect on the results reported. Our study analyzed airflow through the same nasal morphology at flow rates that differed from each other by a factor of almost three. Despite this large difference in volumetric flow, the overall flow pattern remained essentially the same.

Lastly, the models used in these simulations were based on segmentation of CT scan data. Although likely higher in resolution than wax or latex casts, it still remains likely that the segmented data did not fully capture the shape of the nasal cavity. Vagaries of preservation and preparation, combined with technical factors in the segmentation program (e.g., smoothing algorithms, Hounsfield spectra, and tolerance values), may result in reconstructions that are flawed to some extent. Still, the segmentations, resulting nasal capsule models, and all the CFD analyses constitute a nested series of hypotheses that are amenable to testing via new or better data on pachycephalosaur nasal anatomy. Likewise, although we cannot directly compare the results obtained here with data from a living individual of *S. validum*, the error ranges provided by the grid convergence index do suggest that we are close enough to the original structure that—given the conditions specified by the program—the results obtained from our simulations should not be affected by the resolution of the airway models used.

Flow Analysis

Under all nasal conformations tested the estimated flow rate for a 10 kg *Stegoceras validum* (4.4 L/min) was too slow to be entirely effective at ventilating the nasal capsule, especially the olfactory chamber. As noted at the outset, restoration of credible, phylogenetically constrained airflow patterns, such as appreciable olfactory airflow, is a powerful test of these models. This discrepancy in our results suggests either that 10 kg was too low of a body-mass estimate for this specimen or that, as discussed above, the difference in body shape between birds and pachycephalosaurs was large enough that the predicted estimates provided by the bird equation were not directly comparable to those of the pachycephalosaur. The intent of these analyses was not to iteratively refine the airway models until they precisely matched extant findings. Such an effort would be largely wasted in that the precise conformation of the nasal structures in any extinct animal is ultimately unknowable, and so cannot be tested rigorously. Rather our intent was to explore the general effects of different conformations, and the clear outcome was that an airway modeled with conchae (whether scrolled or branched) provided more realistic flow patterns whereas airways without conchae were less credible or not credible at all.

For example, the bony-bounded airway model (BBM) of *Stegoceras* resulted in greatly reduced airflow velocities through the nasal capsule, complete with some unrealistic flow patterns (e.g., caudal-to-rostral flow in the lateral aspect of the CNP, lack of olfactory flow in the olfactory chamber). Incorporating soft tissue into the nasal capsule produced results more in line with what is seen in extant diapsids. Such

improvements are expected in that living animals have nasal soft tissues that greatly modify airflow, and the BBM essentially revealed that the fossils themselves cannot be taken at face value. Soft tissues matter.

Given that the olfactory chamber was largely devoid of airflow under most nasal configurations, it is tempting to ask how certain we are of the chamber's configuration. For many dinosaurs, the shape of the olfactory chamber can only be partially ascertained. However, due to the remarkable preservation seen in *Stegoceras* and other pachycephalosaurs, the olfactory turbinates and even portions of the nasal capsule wall have remained largely intact. Thus, unlike most other dinosaurs, we are relatively certain of the overall shape of the olfactory chamber in this group. The difficulty of moving air into this region of the nasal capsule was more likely the result of missing soft tissues rostral to the olfactory chamber. Based on our work on extant diapsids, various soft-tissue structures are used to direct air into the olfactory chamber. In birds, conchal shape and a raised ridge known as the crista nasalis help separate flow streams and direct air into the olfactory chamber (Figure 5-23C top). Similarly, in lizards, an airway constriction called the postvestibular ridge reduces the aperture of the nasal capsule just prior to entering the CNP, which results in inspired air jetting into the CNP, allowing air to reach the olfactory chamber (Figure 5-23C bottom). In crocodylians, the junction of the primary choana and ductus nasopharyngeus is highly compressed laterally, which occurs just prior to the entrance to the olfactory chamber. Air in this region shows a similar jetting effect to that of lizards (Figure 5-23C middle). Likewise, in macrosmatic mammals, the lamina transversa and dorsal meatus have been shown to provide similar olfactory segregating

functions (Craven et al. 2007, 2010). The distance between the vestibulum nasi and the olfactory chamber in pachycephalosaurs suggests that some soft-tissue structure must have been present to help guide air towards the olfactory chamber.

Studies on extant taxa have shown that the airway takes up a relatively small amount of space within the nasal capsule (e.g., Jackson and Schmidt-Nielsen, 1964; Murrish and Schmidt-Nielsen 1970; Langman et al., 1979). By reducing the lumen of the nasal conduit, local pressure drops considerably, resulting in an increased flow speed for any given flow rate, which is beneficial for decreasing the travel time for air to pass from the nostril to lungs, ensuring successful ventilation. However, the reduced lumen also increases the resistance of air to movement through the nasal capsule. Resistance of fluid to movement within a pipe is directly proportional to pipe length and inversely proportional to pipe diameter raised to the fourth power (Vogel, 1994). For instance, if a pipe's diameter is decreased by half, its resistance will increase 16 fold. Thus, the upper respiratory tract must balance keeping the airway small enough to maintain high flow rates for efficient lung ventilation and other physiological processes (e.g., thermoregulation), but large enough that resistance to air movement does not require an inordinate amount of muscular effort. Such compromises have been noted in the trachea of giraffes, which are smaller in diameter than equivalent sized mammals (Hugh-Jones et al., 1978), as well as in the often convoluted tracheae of birds, which are wider for a given neck length resulting in the same resistance as an equivalent-sized mammal with a shorter trachea (Hinds and Calder, 1971). Studies on extant taxa have revealed that the distance between the center of the air stream and the nearest wall of the nasal airways is

rarely more than 5 mm (Jackson and Schmidt-Nielsen, 1964; Schmidt-Nielsen et al., 1970; Murrish and Schmidt Nielsen, 1970; Langman et al., 1979). These short distances are required for the efficient transfer of heat and moisture within the nasal capsule (Collins et al., 1971) and thus would be expected to be present within the nasal capsule of *Stegoceras*. Under the BBM, the distance between the center of the air stream and the capsular wall was rarely less than 5 mm (Figure 5-24), except for the region of the olfactory turbinate.

Addition of a paranasal septum reduced airway volume by 23%, slightly increasing the surface area to volume ratio and decreasing the distance to the nearest wall to less than 4 mm in many places. However large portions of the air field still remained above the 5 mm mark, suggesting that the improvements to the airway from this morphology were only slight. In contrast, the incorporation of a respiratory concha greatly changed the composition of the respired air field, contracting the volume by 10–29%, increasing overall surface area, and dividing the nasal capsule into distinct respiratory and olfactory regions. Distance from the center of the airfield was reduced to 0.22–4.3 mm throughout the cavum nasi proprium (Figure 5-24).

Placement of a concha, whether branched or scrolled, created two distinct pressure gradients. A relatively steep, low-pressure gradient pushed the majority of the air field into the lateral aspect of the nasal capsule where it entered the ductus nasopharyngeus. A much shallower gradient formed on the medial aspect of the nasal capsule, leading to the olfactory chamber. This pressure separation was very similar to the pressure distribution observed in extant, concha-filled birds. The scroll-shaped

concha's separation of the medial and lateral sides of the nasal capsule resulted in the medial (olfactory) side having an extended high-pressure zone. This zone posed a barrier to entry for inspired air (Figure 5-25). Olfactory information is acquired mostly on inspiration (Schoenfeld and Cleland, 2005). Thus, for our tests olfactory flow during inspiration was more informative of model effectiveness than flow available upon expiration. These data suggested that the coiled conchal shape was not very effective at moving air into the olfactory chamber. In contrast olfactory flow was highest under the branched concha model. The shape of the branched concha, with its curled medial projection, created a transverse partition to the air field that reduced ventral migration of air around the concha and into the ductus nasopharyngeus (Figure 5-25). This produced a conveyor belt-like function along the medial branch of the branched concha, forcing air to ride along it, pushing air further into the olfactory chamber and producing results more in line with what is seen in extant amniotes. Thus, of the five nasal conformations tested for *Stegoceras validum,* the branched concha conformation produced results that agreed best with airflow patterns in extant diapsids.

Sniffing

Given the lack of realistic olfactory airflow under many of the modeling scenarios just discussed, it must be asked whether sniffing would have been a more appropriate scenario to model. Sniffing is a distinct breathing pattern apart from regular respiration. It consists of rapid, ballistic inspirations and expirations that produce substantially higher airflow rates than observed under resting respiration (Craven et al., 2009b). These rapid oscillations serve to push large volumes of air into the olfactory recess where odorant

molecules differentially settle out along the olfactory epithelium (Mozell, 1970). Perhaps, then, olfactory flow is only substantial during a sniffing bout. Whereas airflow into the olfactory chamber was likely much higher during sniffing in *Stegoceras*, much as it is in extant animals (e.g., Craven et al., 2009b), sniffing is a behavior that typically occurs only after a stimulus has been detected (e.g., Dial and Schwenk, 1996, Craven et al., 2010). Thus, air must still first reach the olfactory epithelium in order to stimulate sniffing behavior. Although classically viewed as being restricted to the olfactory chamber, olfactory epithelium may extend far rostrally from the olfactory chamber (e.g., Saint-Girons, 1976), thus allowing an olfactory stimulus to be detected earlier, and perhaps reducing the need to push air first into the olfactory chamber. Olfactory epithelium has been observed to be distributed differentially along the nasal capsule of extant tetrapods (Schoenfeld and Cleland, 2005). More rostrally located olfactory receptor neurons are sensitive to highly sorptive odorant molecules, whereas less sorptive molecules require more retention time in the airway and are not absorbed until much farther into the olfactory recess (Schoenfeld and Cleland, 2005). Although ultimately dependent on the concentrations and types of odorants being inspired, given the regional sorptivity of olfactory epithelia, a full, or at least partial, pass through the olfactory chamber may still be necessary to stimulate sniffing behavior, which could explain why olfactory chamber airflow was observed in all extant diapsids during restful respiration that we have modeled using CFD (Figure 5-23). Other computational analyses have also observed airflow within the olfactory chamber during restful breathing (Zhao et al. 2006, Jiang and Zhao, 2010). Thus, the flow patterns observed in many of our modeled

Stegoceras nasal morphologies still appear valid as tests of overall nasal conformation despite using flow patterns associated with resting respiration rather than sniffing. That is, although models incorporating sniffing might have produced even greater, more realistic olfactory flow, our intent again was not to restore airflow exactly (which is an unattainable goal) but rather to assess whether conchal structures attached to the preserved ridges had a positive impact on airflow, which could be done using resting respiration rather than invoking new assumptions about the airflow dynamics of dinosaur sniffing.

Osteological Evidence for Turbinates and its Implications

Turbinates—olfactory or respiratory—are delicate structures that rarely mineralize in extant diapsids and even more rarely preserve in the fossil record. The systemic hypermineralization observed in pachycephalosaurids resulted in a relatively clear picture of the olfactory turbinates, implying an at least moderate if not well-developed sense of smell, which is concordant with the neurological finding of relatively large olfactory bulbs in the brain endocast. Evidence for respiratory turbinates in extinct taxa usually relies on proxies for their existence, namely, the presence of internal ridges along the bones of the nasal cavity (Hillenius, 1992, 1994; Ruben, 1996). The ridges noted on the ventral aspect of the nasal bones in *Stegoceras*, *Sphaerotholus*, and *Prenocephale* appear to meet the criteria used to assess turbinate placement in mammals, and to a lesser extent, birds (Figure 5-16). Another criterion used to assess the presence of turbinates is the overall cross-sectional area of the nasal cavity (Ruben et al., 1996). It has been argued that animals lacking respiratory turbinates have nasal cavities that are

smaller in cross-sectional area. However, this relationship is highly dependent on both the estimated mass of the individual, as well as the location within the nasal capsule in which the cross section was taken. Based on the data used to make the graph in Ruben et al. (1996), *Stegoceras* variably falls on the ectotherm line, the endotherm line, or above both lines depending on the mass estimate used and the location of the cross section. As a predictor of metabolic physiology, cross-sectional area of the nasal cavity currently appears problematic.

The results presented here suggest that the nasal capsule of *Stegoceras*—and presumably other pachycephalosaurids given the similar morphology of *Prenocephale*—housed well-developed nasal (presumably respiratory) turbinates for at least two reasons. First, the acknowledged osteological correlates of turbinates are present in the form of longitudinal ridges on the bones surrounding the cavum nasi proprium. And second, the CFD modeling analyses reveal that reasonably realistic nasal airflow can be restored when nasal conchae are included in the models. Respiratory conchae have been physiologically linked to reducing respiratory evaporative water loss (REWL), which is a critical function for endotherms due to their elevated ventilation rates, and thus have been used as prima facie evidence for elevated resting metabolic rates in the animals housing them (Hillenius, 1992; Ruben et al., 1996; Geist, 2000; Chinsamy and Hillenius, 2004). This apparent causal link has led to the intriguing proposition that respiratory conchae (or turbinates) may be used as indicators of metabolic status for extinct animals (Hillenius, 1994; Ruben, 1995; Ruben et al., 1996; Hillenius and Ruben, 2004). Given this line of reasoning, the inference of respiratory conchae in pachycephalosaurids would suggest

that these dinosaurs had elevated rates of metabolism. The relatively recent discovery of potential respiratory turbinates in the distantly related tyrannosaur CMNH 7541 (Witmer and Ridgely, 2010) suggests that respiratory conchae may have been widespread within Dinosauria, with the implication being that perhaps all dinosaurs had elevated metabolic rates.

However, this view of respiratory conchae as indicators of resting metabolism is not without contention (Seymour, 2004a, b; Padian and Horner, 2004). Opponents have noted examples of extant mammals and birds with reduced or absent respiratory conchae, indicating that not all tachymetabolic endotherms require respiratory conchae to offset heat and water loss. It is worth noting that opposition to the respiratory concha argument comes from the view that conchae are not absolutely necessary for tachymetabolic endothermy and so their presumed absence cannot absolutely refute hypotheses of endothermy in extinct taxa. Conversely, the uniqueness of respiratory conchae to endotherms has not been questioned. The original argument for respiratory turbinates/conchae and elevated metabolism (Hillenius, 1992) posited that the conchae in extant bradymetabolic reptiles were solely olfactory in nature. The function of turbinates, or, more correctly, the mucosa-covered conchae that reside on turbinates, is dependent on both the location of the concha within the airway as well as the epithelium that covers the conchae. Of these two criteria, only the former is accessible to paleontology. Conchae obtain respiratory status if they lie within the main flow of the respired air field (Ruben et al., 1998). This can be grossly determined by looking at the shape of the nasal capsule and determining the general direction of flow from nostril to choana. In general, the

olfactory chamber and paranasal sinuses are considered to be the two portions of the nasal passage that lie outside of the main air field (more so for the latter). Thus, any conchal structure within the olfactory chamber would be considered to be olfactory-only in function, whereas structures lying within the main air field have been considered respiratory-only in function. This black and white view of conchal function starts to blur upon viewing the histology of the mucosa on the conchae. For instance, the middle concha of birds is generally considered to be respiratory-only in function, based on its location within the nasal capsule (Ruben et al., 1998; Geist, 2000). However, histologically, this structure may be partly or largely covered in olfactory epithelium as is seen in some Columbiformes (Bang, 1971) as well as ostriches (Jin et al., 2008; Figure 5-26).

The argument that extant reptiles lack respiratory conchae—or at least conchal structures that play a physiological role in heat and water balance—is questioned by our work on the conchal anatomy and histology in extant reptiles. Using only the criterion of position within the nasal capsule it becomes apparent that the preconcha of crocodylians should be classified as a respiratory concha. It lies directly in the line of the respired air field as determined by gross analyses of airway shape as well as detailed CFD analysis of respired airflow (Bourke and Witmer, 2010; Figure 5-27). Histologically, this region of the nasal capsule has been found to contain olfactory epithelia mixed with respiratory epithelium (Saint-Girons, 1976; Hansen, 2007). However, the extent of the olfactory epithelium is less pronounced on the preconcha than on the more caudally located concha. An extensive plexus along the ventral side of the airway, and a well vascularized

preconcha mainly supplied by the medial nasal and sphenopalatine vessels offer further support for a thermoregulatory function of the crocodylian preconcha (Porter and Witmer 2011; Figure 5-27). The position of these well-vascularized surfaces in the airstream would have allowed evaporative cooling to cool blood within them and support physiological thermoregulation. The avian caudal concha and the crocodylian concha and postconcha are not as well vascularized, indicating a lesser role in physiological thermoregulation, likely due to reduced airspeeds decreasing the ability to support evaporation. Therefore, the preconcha of crocodylians based on anatomical location, relative vasculature, and potentially histology, warrants classification as a respiratory concha, pending experimental validation.

The single concha of squamates has routinely been cited as having solely an olfactory function (Ruben, 1995; Ruben et al., 1996, 1998; Hillenius and Ruben, 2004). However, much like the preconcha of crocodylians, this structure at least partially lies within the respiratory air field. Our CFD analyses on iguanas and varanids have shown that the rostral and ventral portion of the squamate concha lies within the main airfield during both phases of respiration (Figure 5-28). This rostral portion of the concha is more vascular than the caudal portion in iguanas (Figure 5-28). Extensive studies on squamate nasal histology (Stebbins, 1948; Bellairs, 1949; Duvdevani, 1972; Gabe and Saint-Girons, 1976; Rehorek et al., 2000) have shown that this area of the nasal capsule is composed of respiratory epithelium, whereas olfactory epithelium makes up the caudal portion of the concha. Thus, the single concha of squamates must be viewed as a regionally segregated respiratory and olfactory turbinate.

Lastly, it is pertinent to note that the original argument for the role that respiratory conchae play in the evolution of endothermy was based on the presumably requisite coupling of high ventilation (respiration) rates with the high oxygen requirements of endothermy, as seen in mammals (Hillenius, 1994; Ruben et al., 1996; 1998). However, extant birds—which may have average basal metabolic rates up to twice those of similarly sized mammals (McNab, 2009)—are able to meet these high oxygen demands not with high ventilation rates but rather through a respiratory system that is more efficient at extracting more oxygen per breath. As a result, birds breathe, on average, one- to two-thirds as often as similarly sized mammals (Calder, 1968; Frappell et al., 2001). Although comparable respiratory data are relatively few for reptiles, these low respiratory frequencies for birds are not that different from those of similarly sized—continuously breathing—lizards (Bennett 1973) and alligators (see Methods above). These disparate respiratory parameters call into question how important respiratory conchae are for endothermy in birds, and are reflected in the conflicting results of empirical studies on avian respiratory conchae (Tieleman et al., 1999; Geist, 2000; Michaeli & Pinshow, 2001).

In light of our findings on the diversity of nasal conchal structure, histology, blood flow, and airflow in diapsids, it is appropriate to be cautious about the physiological implications of the inference of respiratory conchae in pachycephalosaurids or other dinosaurs. More experimental work is needed to explore the physiological significance of these intriguing anatomical findings in nonavian diapsids. It is possible that heat exchange in these conchal structures could play a more local role in selective

brain temperature regulation (Witmer, 2001; Porter and Witmer, 2011), as either an alternative or an adjunct to a broader respiratory role in mitigating REWL.

Acknowledgments

For useful discussions over the course of the project we thank B. Andres, D. Brinkman, D. Cerio, B. Craven, J. Davis, C. Early, R. Felice, J. Gauthier, E. Gorscak, A. Morhardt, M. Norell, H. O'Brien, E. Snively, and E. Vrba Thanks to S. Anderson, D. Briggs, P. Dodson, and J. Lyson for comments on an early version of portions of the manuscript. M. Caldwell and P. Manning graciously carried specimens to Austin, Texas, for CT scanning. At UTCT, we thank M. Colbert and J. Maisano. We also thank H. Rockhold and OhioHealth O'Bleness Hospital (Athens, OH) for CT scanning. For scanning and providing the scan data of NMMNH P-27403, we thank C. Gerrard, G. Hatch, C. Pilbro, and especially T. Williamson. We thank M. and J. Sonsalla for donating MRF 360–362 to the Marmarth Research Foundation, and B. Benty and M. Fox for preparing them. We thank Michael Habib and Brent Craven for useful advice and critique on the manuscript.

Funding

This project made possible through National Science Foundation (NSF) Graduate Research Fellowships to J.M.B. and T.R.L., as well as a Jurassic Foundation grant to J.M.B. and The University of Pennsylvania Summer Research Stipend in Palaeontology to E.R.S. This project is an extension of the Visible Interactive Dinosaur Project, funded by NSF grant IOR-1050154 to L.M.W. and R.C.R.

References

Aftosmis, M., Gaitonde, D., Tavares, T.S. 1994. On the accuracy, stability and monotonicity of various reconstruction algorithms for unstructured meshes. AIAA Pap. 94–0415.

Agarwal, R. 1999. Computational fluid dynamics of whole body aircraft. Annu Rev Fluid Mech. 31:125–169.

Allison, P.A., Pye, K. 1994 Early diagenetic mineralization and fossil preservation in modern carbonate concretions. Palaios. 9:561–575.

Almeida, L., Campos, R. 2011. Systematization, description and territory of the caudal cerebral artery of the brain in broad-snouted caiman (*Caiman latirostris*). Pesq Vet Bras. 31(9):817–822.

Angielczyk, K.D., Sheets, H.D. 2007. Investigation of simulated tectonic deformation in fossils using geometric morphometrics. Paleobiology. 33:125–148.

Arbour, V.M., Currie, P.J. 2012. Analyzing taphonomic deformation of ankylosaur skulls using retro-deformation and Finite Element Analysis. PLOS ONE. 7:e39323 doi,10.1371/journal.pone.0039323.

Bang, B.G. 1960. Anatomical evidence for olfactory function in some species of birds. Nature. 188:547–549.

Bang, B.G. 1971. Functional anatomy of the olfactory system in 23 orders of birds. Acta Anat. 79(58):1–76.

Bang, B.G., Wenzel, B.M. 1985. Nasal cavity and olfactory system. In: King AS., McLelland J, editors. Form and Function in Birds Volume 3. Elsevier. p 195–225.

Baumel, J.J. 1993. Systema cardiovasculare. In: Baumel, JJ, editor. Handbook of Avian Anatomy: Nomina Anatomica Avium. Cambridge, MA: Nuttall Ornithological Club. p. 407–476.

Baumel, J.J., Witmer, L.M. 1993. Osteologia. In: Baumel, J.J., King, A.S., Breazile, J.E., Evans, H.E., Vanden Berge, J.C., editors. Handbook of Avian Anatomy: Nomina Anatomica Avium. Publications of the Nuttall Ornithological Club. No. 23. p 45–132.

Bellairs, A D'A. 1949. Observations on the snout of *Varanus*, and a comparison with that of other lizards and snakes. J Anat. 83 Pt.2:116–146.

Bennett, A.F. 1973. Ventilation in two species of lizards during rest and activity. Comp Biochem Physiol. 46A:653–671.

Biswas, R., Strawn, R.C. 1998. Tetrahedral and hexahedral mesh adaptation for CFD problems. App Num Math. 26:135–151.

Blacker, T. 2001. Automated conformal hexahedral meshing constraints, challenges and opportunities. Engin Comp. 17:201–210.

Bourke, J.M., Witmer, L.M. 2010. The nose knows: the effects of nasal cavity anatomy on airflow in alligators. JVP. 30(2 supp): 63A.

Bourke, J.M., Witmer, L.M. 2011. Computer modeling of nasal airflow in two extant avian dinosaurs (turkey and ostrich), with implications for modeling airflow in extinct theropods. JVP. 31(2 supp):75A.

Bourke, J.M., Witmer, L.M. 2012. Dorsal or rostral nostrils? Testing fleshy nostril position and airflow in sauropods using computational fluid dynamics. JVP. 32(1 supp):66A.

Brown, C., Russel, A.P. 2012. Homology and architecture of the caudal basket of Pachycephalosauria (Dinosauria: Ornithischia): The first occurrence of myorhabdoi in Tetrapoda. PLOS ONE. 7(1):e30212.

Brzustowicz, J.P., Lounsberry, T.H., Esclafer de la Rode, J.M. 2002. Experimental and computational simulations utilized during the aerodynamic development of the Dodge Intrepid R/T race car. SAE. 2002-01–3334.

Brzustowicz, J., Lounsberry, T., Esclafer de la Rode, J.M. 2003. Improving racecar aerodynamics. SAE Automot Eng. 111(5):95–98.

Burda, D.J. 1966. Embryonic modifications of lacertilian intracranial arteries. Am J Anat. 118(3):743-754.

Burda, D.J. 1969. Developmental aspects of intracranial arterial supply in the alligator brain. J Comp Neuro. 135(4):369–380.

Carrano, M.T., Hutchinson, J.R. 2002. Pelvic and hindlimb musculature of *Tyrannosaurus rex* (Dinosauria: Theropoda). J Morph. 253:207–228.

Carrier, D.R., Farmer, C.G. 2000a. The evolution of pelvic aspiration in archosaurs. Paleobiology. 26(2):271–293.

Carrier, D.R., Farmer, C.G. 2000b. The integration of ventilation and locomotion in archosaurs. Amer Zool. 40:87–100.

Chen, XBBE., Lee, P.H., Chong, V.F.H., Wang, D.Y. 2009. Assessment of septal deviation effects on nasal air flow; A computational fluid dynamics model. Laryngoscope. 119:1730–1736.

Chinsamy, A., Hillenius, W.J. 2004. Physiology of nonavian dinosaurs. In: Weishampel DB, Dodson P. Osmólska H, editors. The Dinosauria 2nd edition. U California Press: Berkeley. p 643–659.

Coe, M. 1978. The decomposition of elephant carcasses in the Tsavo (East) National Park, Kenya. J Arid Env. 1:71–86.

Colbert, E.H. 1946. *Sebecus*, representative of a peculiar suborder of fossil Crocodilia from Patagonia. Bull Am Mus Nat Hist. 87(4):221–270.

Collins, J.C., Pilkington, T.C., Schmidt-Nielsen, K. 1971. A model of respiratory heat transfer in a small mammal. Biophys J. 11: 886–914.

Coombs, W.P. Jr. 1975. Sauropod habits and habitats. Palaeogeography, Palaeoclimatology, Palaeoecology. 17:1–33.

Coombs, W.P. Jr. 1978. The families of the ornithischian dinosaur order Ankylosauria. Palaeontology. 21:143–170.

Craven, B.A., Neuberger, T., Paterson, E.G., Webb, A.G., Josephson, E.M., Morrison, E.E., Settles, G.S. 2007. Reconstruction and morphometric analysis of the nasal airway of the dog (*Canis familiaris*) and implications regarding olfactory airflow. Anat Rec. 290:1325–1340.

Craven, B.A., Paterson, E.G., Settles, G.S. 2010. The fluid dynamics of canine olfaction: Unique nasal airflow patterns as an explanation of macrosmia. J R Soc Interface. 7:933–943.

Craven, B.A., Patterson, E.G., Settles, G.S., Lawson, M.J. 2009a. Development and verification of a high-fidelity computational fluid dynamics models of canine nasal airflow. J Biomech Engin. 131:091002-1.

Craven, B.A., Paterson, E.G., Settles, G.S. 2009b. The fluid dynamics of canine olfaction, unique nasal airflow patterns as an explanation of macrosmia. J R Soc Interface. 7(47):933–943.

Crole, M.R., Soley, J.T. 2010. Gross morphology of the intra-oral rhampotheca, oropharynx and proximal oesophagus of the emu (*Dromaius novaehollandiae*). Anat Hist Embryol. 39:207–218.

Dial, B.E., Schwenk, K. 1996. Olfaction and predator detection in *Coleonyx brevis* (Squamata: Eublepharidae), with comments on the functional significance of buccal pulsing in geckos. J Exp Zool. 276:415–424.

Doorly, D.J., Taylor, D.J., Schroter, R.C. 2008. Mechanics of airflow in the human nasal airways. Resp Phys Neuro. 163:100–110.

Dunlavey, T., Mitchell, C., Sheets, H.D. 2004. Retro-deformation is paramount to the accurate description of fossil taxa. Geo Soc America Abstracts. 36:422.

Duvdevani, I. 1972. The anatomy and histology of the nasal cavities and the nasal salt gland in four species of fringed-toed lizards, *Acanthodactylus* (Lacertidae). J Morph. 137:353–364.

Evans, D.C., Schott, R.K., Larson, D.W., Brown, C.M., Ryan, M.J. 2013. The oldest North American pachycephalosaurid and the hidden diversity of small-bodied ornithischian dinosaurs. Nature Communications. 4(1828). doi: 10.1038/ncomms2749.

Evans, D., Witmer, L.M., Ridgely,, R.C. 2009. Endocranial anatomy of lambeosaurine dinosaurs: A sensorineural perspective on cranial crest function. Anat Rec. 292:1315–1337.

Farmer, C.G., Sanders, K. 2010. Unidirectional airflow in the lungs of alligators. Science. 327:338–340.

Farmer, C.G. 2006. On the origin of avian air sacs. Resp Phys Neuro. 154:89–106.

Farmer. C.G., Carrier. D.R. 2000a. Pelvic aspiration in the American alligator (*Alligator mississippiensis*). J Exp Biol. 203:1679–1687.

Farmer, C.G., Carrier, D.R. 2000b. Ventilation and gas exchange during treadmill locomotion in the American alligator (*Alligator mississippiensis*). J Exp Biol. 203:1671–1678.

Fastovsky, D.F., Weishampel, D.B. 2005. The Evolution and Extinction of the Dinosaurs. Cambridge: Cambridge University Press.

Foss, J.F. 1998. Basic engineering fluid mechanics. In Johnson RW, editor. The Handbook of Fluid Dynamics. CRC Press. Florida. p 5-1–5-99.

Frappell, P.B., Hinds, D.S, Boggs, D.F. 2001. Scaling of respiratory variables and the breathing pattern in birds: An allometric and phylogenetic approach. Phys Biochem Zool. 74(1):75–89.

Gabe, M., Saint-Girons, H. 1976. Contribution a la morphologie comparee des fosses nasales et leurs annexes chez les lepidosoriens. Mem du Mus Nat d'HIst Naturelle. 98(A):1–87.

Garcia, G.J.M., Bailie, N., Martins, D.A., Kimbell, J.S. 2007. Atrophic rhinitis: A CFD study of air conditioning in the nasal cavity. J Appl Physiol. 103:1082–1092.

Geist, N.R. 2000. Nasal respiratory turbinate function in birds. Physiol Biochem Zool. 73(5):581–589.

Gilmore, C.W. 1924. On *Troodon validus* An orthopodous dinosaur from the Belly River Cretaceous of Alberta, Canada. Bull Alberta Univ. 1:1–43.

Guilherme, J.M.G., Bailie, N., Martins, D.A., Kimbell, J.S. 2007. Atrophic rhinitis: A CFD study of air conditioning in the nasal cavity. J Appl Physiol. 103:1082–1092.

Haas, G. 1955. The jaw musculature in *Protoceratops* and in other ceratopsians. Am Mus Nov. 1729:1–24.

Hansen, A. 2007. Olfactory and solitary chemosensory cells: Two different chemosensory systems in the nasal cavity of the American alligator, *Alligator mississippiensis*. BMC Neuro. 8:64.

Hicks, J.W., White, F.N. 1992. Pulmonary gas exchange during intermittent ventilation in the American alligator. Resp Physiol. 88:23–36.

Hieronymus, T.L., Witmer, L.M., Tanke, D.H., Currie, P.J. 2009. The facial integument of centrosaurine ceratopsids: Morphological and histological correlates of novel skin structures. Anat Rec. 292:1370–1396.

Hillenius, W. 1992. The evolution of nasal turbinates and mammalian endothermy. Paleobiology. 18(1):17–29.

Hillenius, W.J. 1994. Turbinates in therapsids: Evidence for Late Permian origins of mammalian endothermy. Evolution. 48(2):207–229.

Hillenius, W.J., Ruben, J.A. 2004. The evolution of endothermy in terrestrial vertebrates: Who? When? Why? Phys Biochem Zool. 77(6):1019–1042.

Hinds, D.S., Calder, W.A. 1971. Tracheal dead space in the respiration of birds. Evolution. 25(2):429–440.

Hoi, Y., Meng, H., Woodward, S.H., Bendok, B.R., Hanel, R.A., Guterman, L.R., Hopkins, L.N. 2004. Effects of arterial geometry on aneurysm growth: Three-dimensional computational fluid dynamics study. J Neurosurg. 101:676–681.

Holliday, C.M. 2009. New insights into dinosaur jaw muscle anatomy. Anat Rec. 292:1246–1265.

Holliday, C.M., Witmer, L.M. 2008. Cranial kinesis in dinosaurs: intracranial joints, protractor muscles, and their significance for cranial evolution and function in diapsids. JVP. 28(4):1073–1088.

Holmes, W.M., Cotton, R., Xuan, V.B., Rygg, A.D., Craven, B.A., Abel, R.L., Slack, R., Cox, J.P.L. 2011. Three-dimensional structure of the nasal passageway of a hagfish and its implications for olfaction. Anat Rec. 294:1045-1056.

Hopson, J.A. 1979. Paleoneurology. In: Gans C, editor. Biology of the Reptilia. Vol. IX: Neurology. A. New York: Academic Press. p 39–146.

Horner, J.R., Goodwin, M.B. 2009. Extreme cranial ontogeny in the Upper Cretaceous dinosaur Pachycephalosaurus. PLOS ONE. 4(10):e7652. doi:10.1371/journal.pone.0007626.

Hugh-Jones, P., Barter, C.E., Hime,, J.M., Rusbridge, M.M. 1978. Dead space and tidal volume of the giraffe compared with some other mammals. Resp Phys. 35:53–58.

Hutchinson, J.R., Bates, K.T., Molnar, J., Allen, V., Makovicky. P.J. 2011. A computational analysis of limb and body dimensions in *Tyrannosaurus rex* with implications for locomotion, ontogeny, and growth. PLOS ONE. 6(10):e26037.

Jackson, D.C., Schmidt-Nielsen, K. 1964. Countercurrent heat exchange in the respiratory passages. Physiology. 51:1192–1197.

Jarvik, E. 1942. On the structure of the snout of crossopterygians and lower gnathostomes in general. Zool Bidr Upsala. 21:235–675.

Jiang, J., Zhao, K. 2010. Airflow and nanoparticle deposition in rat nose under various breathing and sniffing conditions. J Aerosol Sci. 41(11):1030–1043.

Jin, E.J, Peng, K.M., Wang, J.X., Du, AN., Tang, L., Wei, L., Wang, Y., Li, S.H., Song, H. 2008. Study of the morphology of the olfactory organ of African ostrich chick. Anat Histol Embryol. 37:161–165.

Kimbell, J.S., Godo, M.N., Gross, E.A., Joyner, D.R., Richardson, R.B., Morgan, K.T. 1997. Computer simulation of inspiratory airflow in all regions of the F344 rat nasal passages. Tox App Pharm. 145:388–398.

Ku, D.N. 1997. Blood flow in arteries. Annu Rev Fluid Mech. 29:399–434.

Langman, V.A., Maloiy, G.M.O., Schmidt-Nielsen, K., Schroter, R.C. 1979. Nasal heat exchange in the giraffe and other large mammals. Resp Physiol. 37:325–333.

Lauder, G.V., Drucker, E.G., Nauen, J.C., Wilga, C.D. 2003. Experimental hydrodynamics and evolution: Caudal fin locomotion in fishes. In: Bels VL, Gasc J-P, Casinos A, editors. Vertebrate Biomechanics and Evolution. Oxford: BIOS Scientific Publishers. p 117–135.

Lehman, T.M. 1996. A horned dinosaur from the El Picacho formation of west Texas, and review of ceratopsian dinosaurs from the American southwest. J Paleont. 70(3):494–508.

Longrich, N.R., Sankey, J., Tanke, D. 2010. *Texacephale langstoni*, a new genus of pachycephalosaurid (Dinosauria: Ornithischia) from the upper Campanian Aguja Formation, Southern Texas, USA. Cretaceous Research. 31(2): 274–284.

Loudon, C., Tordesillas, A. 1998. The use of the dimensionless Womersley number to characterize the unsteady nature of internal flow. J Theor Biol. 191(1):63–78.

Maidment, S.C.R., Porro, L.B. 2009. Homology of the palpebral and origin of supraorbital ossification in ornithischian dinosaurs. Lethaia. 43(1):95–111.

Maryańska, T., Chapman, R.E., Weishampel, D.B. 2004. Pachycephalosauria. In: Weishampel, D.B., Dodson, P., Osmólska, H., editors. The Dinosauria 2nd edition. U California Press: Berkeley. p. 464–477.

Maryańska, T. 1977. Ankylosauridae (Dinosauria) from Mongolia. Palaeontologia Polonica. 37:85–151.

Maryańska, T., Osmólska, H. 1974. Pachycephalosauria, a new suborder of ornithischian dinosaurs. Palaeontologia Polonica. 30:45–102.

Milsom, W.K. 1988. Control of arrhythmic breathing in aerial breathers. Can J Zool. 66(1):99–108.

Mirade, P.S., Daudin, J-D. 2006. Computational fluid dynamics prediction and validation of gas circulation in a cheese-ripening room. Int Dairy J. 16(8):920–930.

Miyashita, T., Arbour, V.M., Witmer, L.M., Currie, P.J. 2011. The internal cranial morphology of an armoured dinosaur *Euoplocephalus* corroborated by X-ray computed tomographic reconstruction. J Anat. 219(6):661–675.

Motani, R., Amenta, N., Wiley, D.F. 2005. Possibilities and limitations of three dimensional retrodeformation of a trilobite and plesiosaur vertebrae. Paleo Bios. 25:88.

Mozell, M.M. 1970. Evidence for a chromatographic model of olfaction. J Gen Physiol. 56(1):46–63.

Murrish, D.E., Schmidt-Nielsen, K. 1970. Exhaled air temperature and water conservation in lizards. Resp Phys. 10(2):151-158.

Nagy, K.A., Girard, I.A., Brown, T.K. 1999. Energetics of free-ranging mammals, reptiles, and birds. Annu Rev Nutr. 19:247–277.

O'Connor, P.M. 2006. Postcranial pneumaticity: An evaluation of soft-tisssue influences on the postcranial skeleton and the reconstruction of pulmonary anatomy in archosaurs. J Morph. 267:1199–1266.

O'Connor, P.M. 2009. Evolution of archosaurian body plans: Skeletal adaptation of an air-sac-based breathing apparatus in birds and other archosaurs. J Int Biol. 311A:629–646.

O'Connor, P.M., Claessens, L.P.A.M. 2005. Basic avian pulmonary design and flow-through ventilation in non-avian theropod dinosaurs. 2005. Nature. 436:253–256.

Oelrich, T.M. 1956. The anatomy of the head of *Ctenosauria pectinata* (Iguanidae). Misc Pub Mus Zool University of Michigan 94:1–122.

O'Gorman, E.J., Hone, D.W.E. 2012. Body size distribution of the dinosaurs. PLOS ONE. 7(12):e51925. doi:10.1371/journal.pone.0051925.

Osborn, H.F. 1898. Additional characters of the great herbivorous dinosaur *Camarasaurus*. Bull Am Mus Nat His. 10:219–233.

Osmólska, H. 1974.Nasal salt glands in dinosaurs. Acta Palaeo Polo. 24:205–215.

Ostrom, J.H. 1961. Cranial morphology of the hadrosaurian dinosaurs of North America. Bull Am Mus Nat Hist. 122(2):1–78.

Ostrom, J.H. 1962.The cranial crests of hadrosaurian dinosaurs. Postilla. 62:1–29.

Padian, K., Horner, J.R. 2004. Dinosaur physiology. In: Weishampel, D.B., Dodson, P., Osmólska, H., editors. The Dinosauria 2nd Edition. Berkeley: University of California Press. p 660–671.

Parsons, T.S. 1959.Nasal anatomy and the phylogeny of reptiles. Evolution. 13:175-187.

Parsons, T.S. 1967. Evolution of the nasal structure in the lower tetrapods. Am Zool. 7:397–413.

Parsons, T.S. 1970. The nose and Jacobson's organ. In: Gans C, Parsons TS, editors: Biology of the Reptilia 2. New York: Academic Press, p 99–191.

Peczkis, J. 1995. Implications for body-mass estimates for dinosaurs. JVP. 14(4):520–533.

Porter, W.P, Witmer LM. 2011. Vascular anatomy and its physiological implications in extant and extinct dinosaurs and other diapsids. JVP. 31 (supp 2):176A.

Porter, W.P., Witmer, L.M. 2012. Vascular patterns in iguanas: Blood vessels and cephalic sites of thermal exchange. Annual Meeting of the Society of Integrative and Comparative Biology, Charleston, South Carolina.

Rehorek, S.J., Firth, B.T., Hutchinson, M.N. 2000. The structure of the nasal chemosensory system in squamate reptiles. 1. The olfactory organ, with special reference to olfaction in geckos. J Biosci. 25(2):173–179.

Rieppel, O., Gauthier, J., Maisano, J. 2008. Comparative morphology of the dermal palate in squamate reptiles, with comments on phylogenetic implications. Zool J Linn Soc. 152:131–152.

Roache, P.J. 1994. Perspective: A method for uniform reporting of grid refinement studies. J Fluid Engin. 116:405–413.

Romer, A.S. 1922. The locomotor apparatus of certain primitive and mammal-like reptiles. Bull Am Mus Nat Hist. 46:517–603.

Romer, A.S. 1924. Pectoral limb musculature and shoulder-girdle structure in fish and tetrapods. Anat Rec. 27(2):119–143.

Romer, A.S. 1933. Vertebrate Paleontology. Chicago: University of Chicago Press.

Ruben, J.A. 1995. The evolution of endothermy in mammals and birds: From physiology to fossils. Annu Rev Physiol. 57:69–95.

Ruben, J.A. 1996. Evolution of endothermy in mammals, birds and their ancestors. In: Johnston IA, Bennett AF, editors. Animals and Temperature: Phenotypic and Evolutionary Adaptation. Cambridge: Cambridge University Press. p 347–376.

Ruben, J.A., Hillenius, W.J., Geist, N.R., Leitch, A., Jones, T.D., Currie, P.J., Horner, J.R., Espe III, G. 1996.The metabolic status of some late Cretaceous dinosaurs. Science. 273(5279):1204–1207.

Ruben, J.A., Jones, T.D., Geist, N.R. 1998. Respiratory physiology of the dinosaurs. BioEssays. 20:852–859.

Rudwick, M.J.S. 1964. The inference of function from structure in fossils. Br J Phil Sci. 15:27–40.

Ruiz-Gironés, E. 2011. Automatic hexahedral meshing algorithms: From structured to unstructured meshes. Ph.D. Dissertation, Universitat Politècnica de Catalunya, Barcelona Spain.

Saint-Girons, H. 1976. Données histologiques sur les fosses nasales et leurs annexes chez *Crocodylus niloticus* Laurenti et *Caiman crocodilus* (Linnaeus) (Reptilia, Crocodylidae). Zoomorphologie. 84(3):301–318.

Schachner, E.R., Cieri, R.L., Butler, J.P., Farmer, C.G. 2013. Unidirectional pulmonary airflow patterns in the savannah monitor lizard. Nature. doi:10.1038/nature12871.

Schachner, E.R., Farmer, C.G., McDonald, A.T., Dodson, P. 2011a. Evolution of the dinosauriform respiratory apparatus: New evidence from the postcranial axial skeleton. Anat Rec. 294:1532–1547.

Schachner, E.R., Manning, P.L., Dodson, P.D. 2011b. Pelvic and hindlimb myology of the basal archosaur *Poposaurus gracilis* (Archosauria: Poposauroidea. J Morph. 272:1464–1491.

Schachner, E.R., Lyson, T.R., Dodson, P. 2009. Evolution of the respiratory system in nonavian theropods: Evidence from rib and vertebral morphology. Anat Rec. 292:1501–1513.

Schmidt-Nielsen, K. 1997. Animal Physiology. 5th ed. Cambridge: Cambridge University Press.

Schmidt-Nielsen, K., Hainsworth, R.F., Murrish, D. 1970. Counter-current heat exchange in the respiratory passages: Effect on water and heat balance. Resp Physiol. 9:263–276.

Schoenfeld, T.A., Cleland, T.A. 2005. The anatomical logic of smell. Trend Neuro. 28(11):620–627.

Schott, R.K., Evans, D.C., Goodwin, M.B., Horner, J.R., Brown, C.M., Longrich, N.R. 2011. Cranial Ontogeny in *Stegoceras validum* (Dinosauria: Pachycephalosauria): A quantitative model of pachycephalosaur dome growth and variation. PLOS ONE. 6(6):e21092. doi:10.1371/journal.pone.0021092.

Schott, R.K., Evans, D.C., Williamson, T.E., Carr, T.D., Goodwin, M.B. 2009.The anatomy and systematics of *Colepiocephale lambei* (Dinosauria: Pachycephalosauridae). JVP. 29(3):771–786.

Sedlmayr, J.C. 2002. Anatomy, evolution, and functional significance of cephalic vasculature in Archosauria. Ph.D. Dissertation, Ohio University, Athens, OH.

Sereno, P.C. 2000. The fossil record, systematics and evolution of pachycephalosaurs and ceratopsians from Asia. In: Benton MJ, Shishkin MA, Unwin DM, Kurochkin EN, editors. The Age of Dinosaurs in Russia and Mongolia. Cambridge: Cambridge University Press. p. 480–560.

Seymour, R.S. 2004a. Evidence for endothermic ancestors of crocodiles at the stem of archosaur evolution. Physiol Biochem Zool. 77(6):1051–1067.

Seymour, R.S. 2004b. Reply to Hillenius and Ruben. Physiol Biochem Zool. 77(6):1073–1075.

Simpson, G.G., Elftman, H.O. 1928. Hind limb musculature and habits of a Paleocene multituberculate. Am Mus Nov. 333:l–19.

Snively, E., Cox, A. 2008. Structural Mechanics of Pachycephalosaur Crania Permitted Head-Butting Behavior. Paleontologica Electronica. 11(1):3A17.

Snively, E., Russell, A.P. 2007. Functional variation of neck muscles and their relation to feeding style in Tyrannosauridae and other large theropod dinosaurs. Anat Rec. 290:934–957.

Snively, E., Theodor, J.M. 2011. Common functional correlates of head-strike behavior in the pachycephalosaur *Stegoceras validum* (Ornithischia, Dinosauria) and

combative artiodactyls. PLOS ONE. 6(6): e21422. doi:10.1371/journal.pone.0021422.

Stebbins, R.C. 1948. Nasal structure in lizards with reference to olfaction and conditioning of the inspired air. Am J Anat. 83(2):183–221.

Sullivan, R.M. 2000 *Prenocephale edmontonensis* (Brown and Schlaikjer) new comb. and *P. brevis* (Lambe) new comb. (Dinosauria: Ornithischia: Pachycephalosauria) from the Upper Cretaceous of North America. NM Mus Nat Hist Bull. 17:177–190.

Sullivan, R.M. 2003. Revision of the dinosaur Stegoceras Lambe (Ornithischia, Pachycephalosauridae). JVP. 23(1):181–207.

Sullivan, R.M. 2006. A taxonomic review of the Pachycephalosauridae (Dinosauria: Ornithischia). NMMNH Sci Bull. 35:347–365.

Tsuihiji, T. 2010. Reconstructions of the axial muscle insertions in the occipital region of dinosaurs: Evaluations of past hypotheses on Marginocephalia and Tyrannosauridae using the extant phylogenetic bracket approach. Anat Rec. 293:1360–1386.

Vickaryous, M.K., Russell, A.P. 2003. A redescription of the skull of *Euoplocephalus tutus* (Archosauria: Ornithischia): a foundation for comparative and systematic studies of ankylosaurian dinosaurs. Zool J Linn Soc. 137:157–186.

Vogel, S. 1994. Life in Moving Fluids. 2nd ed. New Jersey, Princeton University Press.

Vogel, S. 2003. Viscosity and the patterns of flow. In Vogel S, editor. Comparative Biomechanics: Life's Physical World. New Jersey: Princeton University Press. p 117–138.

Waibl, H., Gasse, H., Hashimoto, Y., Burdas, K-D., Constantinescu, G.M., Saber, A.S., Simoens, P., Salazar, I., Sotonyi, P., Augsburger, H., Bragulla, H. 2012. Nomina anatomica veterinaria. 5th edition. International Committee on Veterinary Gross Anatomical Nomenclature. World Association of Veterinary Anatomists.

Watabe, M., Tsogtbaatar, K., Sullivan, R.M. 2011. A new pachycephalosaurid from the Baynshire formation (Cenomanian-Late Santonian), Gobi Desert, Mongolia. NMMNH Bull. 53:489–497.

Wedel, M.J. 2003. Vertebral pneumaticity, air sacs, and the physiology of sauropod dinosaurs. Paleobiology. 29(2):243–255.

Weishampel, D.B. 1981. The nasal cavity of lambeosaurine hadrosaurids (Reptilia: Ornithischia): comparative anatomy and homologies. J Paleo. 55(5):1046–1057.

Wheeler, P. 1978. Elaborate CNS cooling structures in large dinosaurs. Nature. 275:441–443.

Williamson, T.E., Carr, T.D. 2002. A new genus of derived pachycephalosaurian from Western North America. JVP. 22(4):779–801.

Witmer, L.M. 1995a. The extant phylogenetic bracket and the importance of reconstructing soft tissues in fossils. In: Thomason JJ, editor. Functional Morphology in Vertebrate Paleontology. New York: Cambridge University Press. p. 19–33.

Witmer, L.M. 1995b. Homology of facial structures in extant archosaurs (birds and crocodilians), with special reference to paranasal pneumaticity and nasal conchae. J Morph. 225:269–327.

Witmer, L.M. 1997a. The evolution of the antorbital cavity of archosaurs: A study in soft-tissue reconstruction in the fossil record with an analysis of the function of pneumaticity. JVP. 17 (1:Supp):1–73.

Witmer, L.M. 1997b. Craniofacial air sinus systems. In: Currie P.J., Padian, K., editors. The Encyclopedia of Dinosaurs. New York: Academic Press. p 151–159.

Witmer, L.M. 2001. Nostril position in dinosaurs and other vertebrates and its significance for nasal function. Science. 293:850–853.

Witmer, L.M., Ridgely, R.C. 2008a. The paranasal air sinuses of predatory and armored dinosaurs(Archosauria: Theropoda and Ankylosauria)and their contribution to cephalic architecture. Anat Rec. 291:1362–1388.

Witmer, L.M., Ridgely, R.C. 2008b. Structure of the brain cavity and inner ear of the centrosaurine ceratopsid *Pachyrhinosaurus* based on CT scanning and 3D visualization. In Currie PJ, editor. A New Horned Dinosaur From an Upper Cretaceous Bone Bed in Alberta. National Research Council Research Press, Ottawa. p. 117–144.

Witmer, L.M., Ridgely, R.C. 2009. New insights into the brain, braincase, and ear region of tyrannosaurs (Dinosauria, Theropoda), with implications for sensory organization and behavior. Anat Rec. 292:1266–1296.

Witmer, L.M., Ridgely, R.C. 2010. The Cleveland tyrannosaur skull (*Nanotyrannus* or *Tyrannosaurus*): New findings based on CT scanning, with special reference to the braincase. Kirtlandia. 57:61–81.

Witmer, L.M., Sampson, S.D. 1999. Nasal conchae and blood supply in some dinosaurs: Physiological implications. JVP. 19(3:Supp.):85A.

Witmer, L.M., Ridgely, R.C., Dufeau, D.L., Semones, M.C. 2008. Using CT to Peer into the Past: 3D visualization of the brain and ear regions of birds, crocodiles, and nonavian dinosaurs. In: Endo H, Frey R, editors. Anatomical Imaging: Towards a New Morphology. Springer. p 67–87.

Witzmann, F. 2009. Comparative histology of sculptured dermal bones in basal tetrapods, and the implications for the soft tissue dermis. Paleodiversity. 2:233–270.

Womersley, J.R. 1955. Method for the calculation of velocity, rate of flow and viscous drag in arteries when the pressure gradient is known. J Physiol. 127:553–563.

Yam, R., Yuen, P.L., Yung, R., Choy, T. 2011. Rethinking hospital general ward ventilation design using computational fluid dynamics. J Hosp Inf. 77(1):31–36.

Zhao, K., Dalton, P., Yang, G.C., Scherer, P.W. 2006. Numerical modeling of turbulent and laminar airflow and odorant transport during sniffing in the human and rat nose. Chem Senses. 31:107–118.

CHAPTER 6 : THE CONVOLUTED AIRWAYS OF ANKYLOSAURIAN DINOSAURS WERE EFFICIENT AIR CONDITIONERS

Abstract

Complicated, labyrinthine nasal passages are an enigmatic hallmark of Ankylosauria, a group of armored ornithischian dinosaurs. Previous research has suggested that such convoluted nasal passages potentially could have functioned as efficient heat exchangers analogous to the respiratory turbinates of mammals and birds. We tested this hypothesis by performing a computational fluid dynamic analysis on the elaborate nasal passages of the nodosaurid *Panoplosaurus mirus* and the ankylosaurid *Euoplocephalus tutus*. Our models predicted that an 1100 kg *Panoplosaurus* and 2000 kg *Euoplocephalus* would require approximately 833 and 1568 thermal calories, respectively, to warm a single breath of air by 20°C at 50% relative humidity. Air temperature drop during exhalation resulted in an energy savings of 65% for *Panoplosaurus* and 84% for *Euoplocephalus,* with water savings of 63% and 79%, respectively. These results fall well within the range of heat and water savings in extant terrestrial amniotes. Tests of alternate airway reconstructions (e.g., simple nasal vestibule, elongate but completely straight nasal vestibule) revealed that the extensive elaboration observed in the nasal vestibule of ankylosaurs is a viable alternative to respiratory turbinates when it comes to conditioning respired air. Our results further indicate that the larger *Euoplocephalus* required a more efficient nasal passage to offset the higher heat loads associated with its larger mass. The unique combination of large

bodies with small brains may have necessitated the evolution of complicated airways in dinosaurs as a means of buffering increased heat loads coming from the body.

Anatomical Abbreviations

a nas, apertura nasalis; air, airway; ant sin, antorbital sinus; bone, bone of nasal cavity; cap, cartilaginous nasal capsule; ch, choana; ch f, choanal fossa; ch fd, choanal fold; ch fp, choanal flap; ch g, choanal groove; cnp, cavum nasi proprium; co, concha; ept, ectopterygoid; f ex, fenestra exochoanalis; j, jugal; lam, lamina transversa; max, maxilla; mnca, median nasal caputegulum; mu, mucosa; nar, naris; ns, nasal; olf turb, olfactory turbinate; p2, secondary palate; pal, palatine; pmax, premaxilla; pt, pterygoid; q, quadrate; tr, tracheal extension; turb, turbinate; v, vomer; vest, nasal vestibule.

Introduction

Ankylosaurs were a successful group of ornithischians that had a near global distribution throughout the Cretaceous (Vickaryous et al. 2004). Ankylosaurs are best known for their well-armored hides, afforded by extensive osteoderm coverage across the back, sides, and tail, as well as the skull (Coombs 1971; Vickaryous et al. 2001, 2004). In members of Ankylosauridae these osteoderms ended in an expanded—and ankylosed—tail club. The process behind dermal ossification in ankylosaurs has attracted much interest over the years (Scheyer and Sander 2004; Main et al. 2005; Hayashi et al. 2009; Vickaryous and Sire 2009). The method of mineralizing soft tissues into a toughened, armored hide appears to have been a somatically global one that had the side effect of mineralizing unrelated soft tissues throughout the body, such as potential eyelids in *Euoplocephalus tutus* (Coombs 1972). This tendency to mineralize soft tissues extended

into the nasal passage where Maryańska (1971) first observed structures in the nose of *Pinacosaurus grangeri* that were typically cartilaginous or mucosal in other clades. She interpreted these structures within the nasal cavity of *P. grangeri* and other ankylosaurs as turbinates or conchae (Maryańska 1971, 1977). Brown (1908) was perhaps the first to report the complexity of the nasal cavities of ankylosaurs, pointing to a symmetrical series of air spaces in snout of *Ankylosaurus magniventris*. Coombs (1978) later uncovered a similarly elaborate series of chambers within the nasal cavity of *Euoplocephalus tutus* which were interpreted as an extensive set of paranasal sinuses surrounding the nasal capsule (Coombs 1978; Coombs and Maryańska 1990; Witmer 1997). Osmólska (1979) suggested a rostral placement of the nasal gland in ankylosaurs based on a sectioned off recess within the nasal vestibule of *P. grangeri*. Later work challenged this interpretation in favor of an enlarged paranasal sinus system (Hill et al. 2003) somewhat akin to that described by Coombs for *Euoplocephalus*. Similar observations of paranasal pneumaticity were suggested for other ankylosaurs as well based on the extensive excavations repeatedly uncovered within the nasal cavities of these dinosaurs (Witmer 1997; Vickaryous and Russell 2003; Carpenter 2004; Vickaryous 2006). It was only after a detailed computed tomographic (CT) scan of various ankylosaur skulls that it became apparent that many of the structures initially interpreted as running parallel to a rather simplistic respiratory passage were in fact parts of bony laminae that braced and separated loops of a remarkably complicated nasal vestibule (Witmer and Ridgely 2008, Miyashita et al. 2011).

Such a complicated structure begs a functional explanation. The nasal passage in extant animals offers a variety of functions that amniotes have emphasized in different ways. The nasal passage is a large component of the conducting portion of the respiratory system (Kierszenbaum 2007), delivering air from the environment to the lungs. The nasal passage functions in modulating air coming into the lungs by filtering out dust and pathogens. It conditions respired air, warming and humidifying it upon inspiration and then cooling and drying it on expiration. This conditioning capacity of the nasal passage received extensive study in the latter part of the 20th century (Jackson and Schmidt-Nielsen 1964; Schmidt-Nielsen et al. 1970; Murrish and Schmidt-Nielsen 1970; Collins et al. 1971; Murrish 1973; Langman et al. 1979), especially in relation to respiratory turbinates/conchae and their association with tachymetabolic endothermy (Hillenius 1992, 1994; Ruben et al. 1996, 1998; Geist 2000; Ruben and Hillenius 2004). Only a specific portion of the nasal passage functions in odorant analysis. The requirements of olfaction run counter to the need to oxygenate the body, requiring regional separation of the nasal passage into a respiratory region and a slower moving olfactory region. The latter region may be expanded into a blind space referred to as the olfactory recess or olfactory chamber in macrosmatic species such as dogs and crocodylians (Weldon and Ferguson 1993; Craven et al. 2007; Chapter 2). Lastly, the nasal passage may also function in phonation, providing vocal resonance to sound coming from the pharynx and even providing primary sound production in certain animals such as saiga antelope and male gharials (Martin and Bellairs 1977; Frey et al. 2007; Dinets 2013).

Witmer and Ridgely (2008) briefly suggested that the elongated airways of ankylosaurs may have functioned in thermoregulation or in vocal resonance. Miyashita et al (2011) expanded on this argument, offering evidence against an olfactory explanation and for either a thermoregulatory function and/or a vocal resonance function. Regarding the former, Miyashita et al. described the extensive surface area that a looping nasal passage offers, and coupled this enhanced surface area with extensive vascular irrigation surrounding the elongated nasal vestibule (Witmer & Ridgely 2008, Miyashita et al. 2011). Such a combination would result in heat transfer from the body to the air regardless of whether or not this was the primary function of the nasal passage (Miyashita et al. 2011). Until now, the thermoregulatory capacity of these elaborate nasal passages had been inferred based on anatomy alone.

We sought to test the functional hypothesis that the nasal passage in ankylosaurs was an efficient heat exchanger by modeling the airways of a nodosaurid and an ankylosaurid. To simulate the flow of heat between the nasal passage and the air, we performed a computational fluid dynamic (CFD) analysis. Digital simulation of fluid movement via CFD is routinely performed in the fields of aeronautics (Luckring et al. 2014), automobile engineering (Katz 2006), and building ventilation (Yam et al. 2011). Using digital models alleviates the costs associated with physical models, such as choice of material, as well as the costs and complications associated with physical experiments such as flume systems and wind tunnels. Digital simulation of fluid movement via CFD provides a cost-effective means of testing multiple flow speeds, which is difficult to obtain in extant animals and impossible for our long-extinct taxa. Further, the use of

digital simulations provided the opportunity to digitally manipulate the nasal passages, allowing us to test the preserved, convoluted airways against digitally manipulated airways that were either shorter or straighter (see Methods below). In addition to general airflow characteristics, we further modeled the heat-transfer potential within the nasal passages of these two dinosaurs. Results were compared to each other and to previously published results on extant animals to determine if the effectiveness of the nasal passage in ankylosaurs was within the range observed in extant animals. We were particularly interested in seeing how well a non-turbinate filled nasal passage would compare to the extensive, turbinate-filled noses of various mammals and birds.

Institutional Abbreviations

AMNH, American Museum of Natural History, New York, USA; CMN, Canadian Museum of Nature, Ottawa, CA; ROM, Royal Ontario Museum, Ontario, CA; ZPAL, Institute of Paleobiology (Zaklad Paleobiolgii) of the Polish Academy of Sciences, Warsaw, PL.

Materials and Methods

Specimens

We analyzed airflow in two species of ankylosaur, the nodosaurid *Panoplosaurus mirus* (ROM 1215) and the ankylosaurid *Euoplocephalus tutus* (AMNH 5405). CT data and initial 3D models were obtained from previous work conducted by Witmer and Ridgely (2008). To aid with soft-tissue reconstruction we further looked at other specimens of *Euoplocephalus* (AMNH 5403, ROM 1930) and *Panoplosaurus* (CMN 2759) as well as the related species: *Edmontonia rugosidens* (AMNH 5381),

Ankylosaurus magniventris (AMNH 5214), and *Pinacosaurus granger* (ZPAL MgD-II/1).

Model Construction

Segmentation

Osteological evidence for a complete nasal septum (septal sulcus or partially mineralized septum) meant that each nasal passage acted independently of the other. This allowed for modeling of one side of the nose only, which saved on computational costs. Initial segmentation of the airways produced a rough approximation of the nasal passage in life, complete with a rostral and caudal vestibular loop (Witmer and Ridgely 2008) and an enlarged olfactory recess. The vestibulum and the cavum nasi proprium were unattached in the original segmentations, requiring further segmentation and attachment to produce a single surface model. The nasopharyngeal duct was not segmented in the original models and required segmentation for this region. Although Witmer and Ridgely (2008) as well as Miyashita et al. (2011) discussed the presence of well-preserved olfactory turbinates within the olfactory recess of these dinosaurs, neither study published images of the segmented structures. For our study, these structures and their effect on the airway (i.e., the impressions they left on the digital airway cast) were segmented out using the program Avizo 7.1 (FEI Visualization Sciences Group, Burlington, MA). As with the initial airway segmentation the final product was a cast of the inside of the nasal cavity, revealing the potential space in which air could reside within the nasal passage. Examination of the CT data within the olfactory recess revealed both the presence of the mineralized olfactory turbinate as well as the outer boundary to the nasal capsule. These

data provided insight into the limit of the airway in life, which was substantially more restricted than initial segmentations suggested (Figure 6-1). Extra space lateral to our interpretations of the nasal passage wall, was interpreted as housing the antorbital sinus. Its placement near the olfactory chamber, adjacent to the cavum nasi proprium, is consistent with antorbital sinus placement in extant archosaurs (Witmer 1997). In preparation for meshing the segmented models were cleaned of segmentation artifacts using the program Geomagic 10 (3D Systems Geomagic, Rock Hill, SC).

Fleshy nostril placement and soft palate

Although ROM 1215 and AMNH 5405 both contained well preserved nasal passages, the terminal regions of the nose—the fleshy nostril and choana—were not preserved. To aid with these soft-tissue reconstructions we turned to other specimens of the same species along with well-preserved specimens of related ankylosaurs to better determine the location of the nostril and choana. *Fleshy nostril*—For *Panoplosaurus*, we used the well-preserved skull of CMN 2759 to determine the location of the nostril. CMN 2759 preserved the rostral wall of the bony narial aperture, which was composed of the rostral-most cranial osteoderm, most similar to the median nasal caputegulum of *Euoplocephalus* (Arbour and Currie 2013). These anatomical structures strongly suggested that the nostril of *Panoplosaurus* deviated laterally (Figure 6-2). Laterally-facing nostrils are fairly commonplace in diapsids and thus such a placement in *Panoplosaurus* was not unexpected.

For *Euoplocephalus,* AMNH 5405 did not present a well-preserved rostral-most portion of the cranium. To assist with nostril positioning, we compared bony narial

aperture shape in AMNH 5405 with ROM 1930 (Figure 6-2). In the latter, preservation of the rostral-most region of the cranium revealed an enlarged bony narial aperture that faced forward suggesting terminal nostril placement. However, the width of the bony narial aperture encompassed both the rostral-most portion of the cranium as well as a lateral portion of the cranium. Thus it remains possible that the nostril in *Euoplocephalus* could have been deviated laterally, or had a rostrolateral combination thereof. This position would be consistent with fleshy nostril placement in *Ankylosaurus* (AMNH 5214) where dermal ossification is extensive and indicates unambiguously that the nostril was located rostroventrolaterally. In contrast, *Anodontosaurus lambei* (CMN 8530) is closely related to *Euoplocephalus* and shows a well constrained bony narial aperture that would limit the nostril to a terminal position on the snout (Arbour and Currie 2013). All known skulls of *Euoplocephalus* that preserve the rostral-tip of the snout show a much less constrained bony narial aperture. This could indicate that the caputegula covering the cranium were less extensive in this species and that terminal fleshy nostrils were present, but were constrained only by soft-tissues. AMNH 5405 has a fossa on the premaxillae (apertura nasalis, Vickaryous and Russell 2003) that has previously been interpreted as a portion of the nasal vestibule (Vickaryous and Russell 2003; Witmer and Ridgely 2008; Figure 6-2). This fossa is wide enough that it could have easily housed a laterally deviating nasal vestibule that terminated rostrally in a laterally-facing nostril. For the purposes of our analysis we fit *Euoplocephalus* with such a nostril, with the caveat that the osteological evidence for it was equivocal (Figure 6-2). Such a position is consistent

with the general finding in amniotes that fleshy nostrils tend to be rostroventrally situated within the nasal vestibule (Witmer 2001).

Choana—The choana is the fleshy, "internal nostrils" for the nasal passage. It represents the terminus of the airway within the nasal passage as the airway passes into the throat. Much like the fleshy nostril is within a larger narial fossa, the choana also is often associated with a much larger structure called the fenestra exochoanalis (Jarvik 1942, Bellairs 1949) or bony choana (Bourke et al. 2014). The difference in shape between the fleshy and bony structures varies across species. In birds, the fenestra exochoanalis is extensive. It is bordered by the palatines laterally and caudally, the vomers medially, and the maxilla rostrally (Baumel and Witmer 1993). The choana opens as a fleshy slit at the caudal terminus of the fenestra exochoanalis in birds, and is often covered in life by "choanal flaps" that keep food particles out of the nasal passage during ingestion (Zusi and Livezey 2006; Crole and Soley 2010). Osteologically, the choana is associated with a depression in the palatines referred to as the choanal fossa (Zusi and Livezey 2006; Figure 6-3). Lizards have a choanal morphology similar to birds. Their extensive fenestra exochoanalis is bounded by the maxillae rostrally and laterally, the palatines caudally and medially, and the vomers medially. As with birds, the choana resides at the caudal-most extent of the fenestra exochoanalis (Parsons 1970; Rieppel et al. 2008). However, unlike birds, the fleshy covering of much of the fenestra exochoanalis is less extensive and food appears to be prevented from entering the nasal passage partially by the more lateral placement of the choana on the oral roof along with a well developed choanal fold that runs the majority of the length of the fenestra

exochoanalis (Rieppel et al. 2008; Figure 6-3). As with birds, lizard choanae are associated with a choanal fossa (choanal groove, Parsons 1970; Rieppel et al. 2008) situated at the caudal-most extent of the fenestra exochoanalis. Depending on the lizard species, the choana either opens or is greatly expanded in this region of the fenestra exochoanalis (Figure 6-3). Crocodylians have an apomorphic choana placement referred to as the secondary choana (Witmer 1995a). It is produced via elongation of the nasopharyngeal duct through the palatines and into the pterygoids. The original or primary choana is still present and can be viewed internally within the dried skulls of extant crocodylians, where Witmer (1995) observed it bounded medially by the vomer, caudally by the palatines and vomer, and laterally by the palatines and maxilla. These bony associations agree with choana placement in birds and lizards, thus suggesting that the primary choana is the location of the fenestra exochoanalis. The soft-tissue of the secondary choana is essentially an identical outline of the underlying bone, negating the need for a separate term for this region. Thus the exit of the nasal cavity in crocodylians, regardless of soft-tissue presence, is the secondary choana (Figure 6-3). Using the extant phylogenetic bracket approach (EPB, Witmer 1995b), the presence of a choanal groove/fossa in both birds and lizards, can be considered a shared trait for diapsids that was later lost in crocodylians, making the choanal groove/fossa a level 1 inference for placement of the choana in the fenestra exochoanalis (Bourke et al. 2014).

Both *Panoplosaurus* and *Euoplocephalus* had extensive fenestrae exochoanales (Figure 6-4–Figure 6-5). The shape of the soft palate in ankylosaurs has not been extensively studied. However, details on the hard-tissue anatomy indicate that despite an

enlarged fenestra exochoanalis, there is evidence of bony secondary palate formation (Coombs and Maryańska 1990; Vickaryous 2001; Vickaryous and Russell 2003; Vickaryous et al. 2004). The secondary palate of ankylosaurs has traditionally been viewed as a bipartite structure (Coombs and Maryańska 1990). Rostrally, elongated vomers contact the premaxilla, which sends out medial processes along with the maxilla to form palatal shelves, making a structure referred to as the "rostrodorsal secondary palate" (Coombs and Maryańska 1990; Vickaryous 2001). Caudally, the palatines join with the vomers and pterygoids to form a structure called the "caudodorsal secondary palate" (Coombs and Maryańska 1990; Vickaryous 2001; Vickaryous and Russell 2003). In light of new information on the shape of the nasal passage in ankylosaurs, the terminology for the palatal region of ankylosaurs should be revised. The rostrodorsal secondary palate in ankylosaurs such as *Euoplocephalus* should be viewed as the secondary palate (Figure 6-4), which is consistent with the usage of the term in other tetrapods in which the premaxillae and maxillae (and sometimes even palatines) meet rostral to the choanae (Romer 1953). The "caudodorsal secondary palate" serves to separate the olfactory recess from the rest of the nasal cavity. This structure is equivalent to the nasal structure known in mammals as the lamina transversa (Negus 1958; Cave 1967, Craven et al. 2010) and thus takes no part in the formation of the definitive palate (Figure 6-4C). A large depression in the caudal aspect of the palatines appears equivalent to the choanal fossa or choanal groove seen in most extant diapsids (Figure 6-3). As such, we interpret this region as the opening of the choana into the throat. This interpretation makes the lamina transversa the bony boundary for an elongate nasopharyngeal duct. In

nodosaurs such as *Panoplosaurus*, the distinction between the secondary palate and the choana is more evident (Carpenter 1990; Vickaryous 2006; Figure 6-5). As with *Euoplocephalus*, there is evidence of a choanal fossa on the caudal aspect of the palatines, suggesting that the choana opened caudally in this taxon as well (Figure 6-5).

Soft-tissue correction

Airways segmented from the skulls represented the outer limits of the nasal passage, referred to here as the bony-bounded (BB) airway. In life, soft tissues within the nasal passage such as the nasal capsule cartilages, mucosa, nerves, and vasculature would have been present and would have occupied space within these well-constrained nasal passages (Figure 6-6). Previous surveys of airway calibers in the nasal passages of extant amniotes showed that airway calibers (the distance spanned between mucosal walls) did not exceed 10 mm in diameter regardless of the size (0.1–600kg) or phylogenetic position (from squamate reptiles to artiodactyl mammals) of the animal (Langman et al. 1979; Bourke et al. 2014). This constraint appears to be dictated by the biophysical limitations of diffusion, which effectively works across only very small distances (Vogel 1994). The thermoregulatory and olfactory functions of the nasal cavity are both diffusion-dependent functions (Schmidt-Nielsen et al. 1970; Collins et al. 1970; Schoenfeld and Cleland 2005). In contrast to data from extant animals, the average BB airway calibers in *Panoplosaurus* and *Euoplocephalus* were 15.8 mm and 22.9 mm, respectively. These were significantly larger calibers than that observed in the mucosa-lined airways of extant amniotes. To bring airway calibers within the range observed in extant amniotes, we imported airway models of *Panoplosaurus* and *Euoplocephalus* into the 3D modeling and

animation program Maya (Autodesk, San Rafael, CA) where the airways were compressed using the program's 3D deformation tools. Airway calibers were reduced until the average diameter was ~10 mm, which is the upper limit observed in extant amniotes, making this a conservative estimate for ankylosaurs. Airway compression followed the natural contours of the nasal passage such that the refined airways resembled a more compressed version of the original segmentation (Figure 6-7–Figure 6-8). These soft-tissue-corrected airways are here referred to as the ST airways. An extension off the choana was added to all models tested. This extension served to replicate the connection of the nasal airway to the larynx and trachea. This extension was added in large measure to address technical aspects of the software (see below) and to ensure that fully developed airflow would be present at the choana during expiration, thus removing any potential heat flow artifacts created by having the program initialize airflow at the choana during expiration (Figure 6-7–Figure 6-8).

To further test the hypothesis that the convoluted airways in our two ankylosaur taxa, were conferring a heat-transfer benefit, we digitally manipulated duplicates of our ST airways to remove either the length or the convolutions from the nasal vestibule (Figure 6-9–Figure 6-10). One version had a nasal vestibule that ran the straight-line distance between the nostril and the cavum nasi proprium. This model, referred to as the basic airway (Figure 6-9B, Figure 6-10B), was used to represent what a "standard" or plesiomorphic nasal vestibule would look like. The second version of the ST airway retained the total length of the nasal vestibule but had the curvature of the airway removed (Figure 6-9A, Figure 6-10A). This model was referred to as the straightened

airway. It represented the effects of airway distance alone on heat transfer through the nasal passage.

Boundary conditions

Prior to volumetric meshing, the airway models were assigned a series of boundary conditions, comprising a set of criteria that described this region of the model to the CFD program. Boundary condition assignment was done to elicit physiologically realistic airflow within the nasal passage (i.e., pressure driven air movement between nostril and choana). These conditions consisted of a pressure inlet located at the fleshy nostril and a pressure outlet located at the end of the artificial trachea (Figure 6-11). During expiration, the assignment of these boundary conditions (inlet and outlet) was swapped. A series of impermeable wall boundaries covered the rest of the nasal passage model. Wall boundaries were demarcated based on anatomical location (Figure 6-11), which was done to better control for regional variation in heat transfer across the nasal passage. Each wall boundary was considered rigid and incorporated a "no-slip" condition that states that air at the fluid-solid interface would be static, an assumption based on known properties of fluid movement through enclosed structures (Vogel 1994). It is pertinent to appreciate that amniote nasal passages do not have a truly rigid boundary layer between the mucosa and the air field. Boundary layers act as an obstacle to diffusion based processes, thus it is beneficial for amniotes to have means of reducing the size of these boundary layers. In extant amniotes, there is a mucociliary "conveyor belt" composed of ciliated epithelium that beats in unison towards the nostril or choana (Lucas and Douglas 1934; Winet et al. 1982). This conveyor belt serves to break up the

boundary layer between the mucosa and the air field, which aids in diffusion of heat and odorant molecules across the air-mucosa boundary. However, the speed of cilial movement is extremely slow (≤ 1 cm/min) compared to airflow and can be considered negligible for the purposes of airflow and heat-transfer modeling (Craven et al. 2009). Thus, our use of a no-slip boundary condition should not hamper or otherwise reduce the quality of our results.

Meshing

Volumetric meshing was performed using the meshing program ICEM CFD (ANSYS Inc., Canonsburg, PA). Models consisted of a tetrahedral-hexahedral (tet-hex) hybrid mesh. First, an unstructured tetrahedral mesh was constructed using the robust OCTREE method (Yerry and Shephard 1984). After mesh reconstruction, the core of the mesh was deleted and then flooded with hexahedra wherever possible. This hybrid construction offers the versatility of tetrahedra for unstructured mesh reconstruction (Georges et al., 1988; Shephard and Georges, 1991), coupled with the computational efficiency of hexahedra (Biswas and Strawn, 1998; Longest and Vinchurkar 2007). To better resolve wall boundary effects on heat transfer, we incorporated a prism layer along the wall of the nasal passage. This layer consisted of four cells that grew in size from the wall by 1.5 times their parent cell, producing a thickness of approximately 0.7 mm (Figure 6-11).

Computational Fluid Dynamic Analysis

Meshes were imported into the CFD program Fluent (ANSYS Inc., Canonsburg, PA) for analysis. To determine the appropriate fluid dynamic model to apply to our

airway models, we first took cross sections throughout the nasal passages to determine the dimensionless Reynolds and Womersley numbers for the airway. The Reynolds number is a staple of fluid dynamic analyses (Vogel 1994, 2003), representing the mathematical relationship between the viscous and inertial forces within a fluid. Low Reynolds numbers (< 2000) indicate that viscous forces dominate the system and that orderly (i.e, laminar) flow will be the dominant flow type expected. Reynolds numbers between 2000–4000 are a transitionary zone in which laminar flow may be punctuated with periods of turbulence that manifest in the form of secondary flows such as Von Kármán trails (Vogel 1994). Reynolds numbers above 4000 indicate that inertial forces dominate the system and that flow will be chaotic or turbulent (Vogel 1994, 2003). We used the following equation to calculate the Reynolds number for the airway (Holmes et al. 2011):

$$(1)\ Re = \frac{4Q}{Pv}\ ,$$

where Q = volumetric flow rate (m^3/sec), P = the wetted perimeter in meters (Foss 1998), and v = the kinematic viscosity of air at 15°C ($1.412e^{-5}$ m^2/sec).

We used the dimensionless Womersley number (Womersley 1955) to determine the steadiness of the flow field, or in other words, how often airflow was able to produce a parabolic flow profile. This profile is related to the size of the airway, viscosity of the fluid, and frequency of the oscillation (i.e., breathing rate). Womersley numbers < 1 indicate a quasi-steady flow field that can be modeled using as time independent, or steady-state. As the Womersley number climbs above unity, steadiness decreases. At Womersley numbers > 10 the oscillation of the flow is too high for flow to completely

develop (Ku 1997) and is considered unsteady, thus requiring a transient or time-step-based modeling approach. We calculated the Womersley number using Eq. 2 (Craven et al. 2009):

$$(2)\ o = \frac{Dh}{2}\sqrt{\frac{2\pi f}{v}},$$

where f = the frequency of oscillation (Hz), Dh is the hydraulic diameter of the airway, and *v* is the same as Eq. 1. Hydraulic diameter was calculated using Eq. 3 (Foss 1998):

$$(3)\ h = \frac{4A}{P},$$

where A = the area of the cross section measured (m^2) and P is the same as Eq. 1.

Physiological Variables

Following our previous methodology (Bourke et al. 2014), we used the phylogenetically corrected allometric equation for resting respiration in birds by Frappell et al. (2001) to estimate flow rates during inspiration and expiration (Table 6-1). Mass estimates for both ankylosaurs were taken from the supplementary data in Brown et al. (2013). Estimated masses for the two ankylosaurs were over 20 times larger than the largest animal in the Frappell et al. dataset (an 88 kg ostrich), and thus using their regression equations required extending the regression line well beyond the initial scope of the data. To alleviate the effects of this approach we used the lightest mass estimates for *Panoplosaurus* and *Euoplocephalus* as provided by Brown et al. (2013, Table 6-1).

Respiratory flow variables were input into the Reynolds and Womersley equations above, which indicated that both taxa would have had steady flow, but air would been largely transitional, if not completely turbulent, within the nasal passages during simulated respiration. The latter result seemed at odds with previously published

results on resting respiration in amniotes. In extant amniotes measured during restful breathing, laminar flow dominates the air field (Zhao et al. 2006; Hörschler et al. 2006; Jiang and Zhao 2010; Craven et al. 2010). Laminar flow is less energetically expensive (due to lower resistance) than turbulent flow, and can be expected in animals that are not undergoing strenuous exercise. Our two ankylosaurs did not show this pattern, suggesting that the regression equations we used may not be viable at such large body masses or that our ankylosaurs' body plans were not appropriate for the avian-based equation of Frappell et al. (2001). To reduce the effects of poor flow rate choice, we recalculated airflow rates by rearranging the Eq. 1:

$$(4)\ Q = \frac{(Re)Pv}{4}$$

We refer to this new method as the Reversed-Reynolds approach. It provides an upper limit to volumetric flow through the nasal passage under relaxed conditions. We set the Reynolds number at 2000 (corresponding to the transition into turbulence) as our constant and recalculated flow rate across the nasal passages. The lowest flow rate obtained from this Reversed-Reynolds equation was chosen as the new flow rate (Table 6-1). This approach, the first of its kind as far as we know, ensures that laminar flow will dominate the air field under simulated respiration.

As flow rate has been shown to be the primary variable affecting the efficiency of the nasal passage at managing heat flow (Schmidt-Nielsen et al. 1970; Naftali et al. 2005), we chose to run the ST and BB models under both flow rate estimates. The initial flow rate, estimated from the regression by Frappell et al. 2001, was deemed the "high flow rate" model. Our revised flow rate estimate, calculated using our Reverse-Reynolds

method, was deemed the “low flow rate” model. For the high flow rate model, we used the Wilcox two equation κ–ω turbulence model with low Reynolds corrections and shear stress transport. For the low flow rate model, we used the standard laminar viscosity model.

Environmental Conditions

We simulated sea-level air at 15°C and 50% relative humidity (r.h.), which was within the range of expected conditions that these dinosaurs would have experienced in their environment (Barrick et al. 1999). We gave the nasal passages an estimated body temperature of 35°C. This body temperature fell within the range of body temperatures typically observed in extant large terrestrial mammals, birds, and reptiles (Table 6-2). Density (1102 kg/m^3), thermal conductivity (0.34 w/mK), and specific heat for the mucosal walls (3150 j/kgK) were obtained from the database provided by the Foundation for Research on Information Technologies in Society (IT'IS).

By default, Fluent gives all walls a thickness of zero, which is unrealistic for our heat transfer analysis. In extant amniotes, heat transfers to the nose via conduction between the blood vessel walls and the surrounding mucosa. To more accurately simulate this transfer, we used a procedurally generated wall (known as a shell conduction zone) of 0.5 mm to simulate the distance between the nasal passage and the adjacent blood vessels.

Pressure and velocity coupling used the SIMPLEC algorithm along with a node-based discretization gradient. We used a second order accurate spatial discretization scheme for pressure, momentum, turbulence (when applicable), and energy.

Models ran until the results obtained from each analysis had reached a specified level of stability and consistency referred to as convergence (Tu et al. 2013), which indicated that the numerical process used to solve the problem had asymptotically approached the "true" solution (i.e., airflow and heat transfer through a real nasal passage) given the conditions provided to the program. In CFD, convergence may be determined based on the global imbalances in the values for each node within the mesh between steps, or iterations, of the model. Imbalances, or errors, between each iteration are referred to as residuals (Tu et al. 2013). The smaller these residuals are, the smaller the error is and the more converged the solution becomes. Global variables for momentum, pressure, and continuity (the conservation of fluid mass) are generally considered solved when their residuals have fallen below $1.0e^{-3}$ (Tu et al. 2013). However, for physiological studies such as ours we applied the stricter criterion of $1.0e^{-4}$ (Craven et al., 2009; Bourke et al., 2014). For energy (heat flow), convergence is determined when the residuals of error had fallen below $1.0e^{-6}$. To further aid in determining convergence we monitored special surfaces placed throughout regions of the model. These surfaces were designed to output data from a single location only. They provided localized measures of convergence and were used in conjunction with standard convergence measures for continuity, momentum, and energy to determine when models had been sufficiently solved.

Post Processing and Heat Flow Measurements

Solved models were exported to the CFD module of Avizo (Avizo Wind) where qualitative and quantitative measurements were taken. For heat flow, we took

measurements from cross sections of the nasal passage. These cross sections were taken orthogonal to the curvature of the nasal passage so as to get a cross section of the air field as it traversed that portion of the nasal passage. Multiple measurements were taken from each cross section and the mean was recorded for each cross section.

Validation Study

Prior to running our analysis on the ankylosaur models, we sought first to validate our methodology using empirically obtained data on heat transfer in pigeons (Geist 2000). We used CT data from a large adult domestic pigeon (*Columba livia*) and followed the methodology outlined above to simulate heat transfer within the nasal passage (Table 6-3, Figure 6-12). As with the ankylosaurs we only modeled heat transfer through the left nasal passage. Data obtained during inspiration were used to inform the expiration model under the assumption that warming of the air by the nasal walls came at the expense of an equal reduction in mucosal wall temperature. Environmental temperature and humidity were set to 15°C and 50% relative humidity, respectively, reflecting the conditions used by Geist (2000).

Results

Validation Test

Upon inspiration, the nasal passage of our pigeon model warmed air by 22°C, almost reaching body temperature by the time air had reached the throat. This 22°C drop in temperature was applied to the nasal walls of the expiration model. Air within the trachea was set to a temperature of 38°C, reflecting empirically obtained data on tracheal temperature in pigeons during expiration (Geist 2000). The converged expiration model

revealed a drop in air temperature from 38°C to 21.6°C at the nostril (Figure 6-12). This 16.4°C drop in temperature was well within the range of values obtained by Geist (Table 6-3), suggesting that our methodology was valid.

Panoplosaurus mirus

BB airway

Under the high flow rate model, the BB airway was able to successfully increase inhaled air temperature by 18.2°C (Figure 6-13). Most (93%) of this heating took place inside the elongate nasal vestibule. The larger volume of the nasal passage produced slower-moving air with a fair amount of vorticity present inside the CNP. Inspired air left the choana at 33.2°C. Upon expiration, air left the nostrils at 22.7°C. Under the low flow rate model the BB nasal passage was able to warm air to 18.6°C, with 92% of airway heating limited to the nasal vestibule. The low flow rate model exhibited more laminarity in airflow compared to the more turbulent high flow model. On expiration, the BB airway reduced air temperature down to 20.5°C before it left the nostrils.

ST airway

Under the high flow rate model, the nasal passage of *Panoplosaurus* was able to heat inspired air up by 17.9°C. The convoluted nasal vestibule was responsible for the majority of the heat transfer (94%, Figure 6-14). Air left the choana at 32.9°C. Vortices were observed in the first portion of the nasal vestibule (rostral loop of Witmer and Ridgely 2008) as well as the cavum nasi proprium near the olfactory recess. Upon expiration, air passed into the choana at 35°C and left the nostril at 21.6°C. Expiratory flow was more laminar than inspiratory flow, with very few vortices observed throughout

the nasal passage. Under the low flow rate model the nasal passage of *Panoplosaurus* warmed inspired air by 19.3°C. As with the high flow rate model, most of the heat transfer (89%) occurred within the convoluted nasal vestibule (Figure 6-14). The cavum nasi proprium contributed slightly more to airway heating under this scenario than under the high flow rate scenario. Similar vortices were observed in the low flow rate model as in the high flow rate model (Figure 6-14). On expiration air in the low flow rate model left the nostril at 19.5°C.

Basic airway

The basic airway consisted of a plesiomorphic truncated nasal vestibule that ran in a straight line from the nostril to the opening of the CNP. This reduced the nasal vestibule length by 55%. As this basic airway was strictly a hypothetical construct, we only ran the model under the more conservative, Reversed-Reynolds low flow scenario. The lower flow rate associated with this scenario provided the shorter airway the best opportunity to transfer heat from the nasal passage. Despite this lower flow rate, the basic airway still had difficulty transferring a substantial amount of heat from the nasal passage to the inspired air. On the outset, this difficulty was not entirely clear as the entire nasal passage was able to warm the inspired air by 17.6°C (Figure 6-15). However, only 63% of that heat exchange took place inside the truncated nasal vestibule. This was evident upon examining the temperature distribution through the nasal passage. Sagittal cross sections of the nasal passage revealed a consistent, low-temperature central stream of air that traveled through the nasal vestibule largely unchanged by the surrounding nasal mucosa, resulting in a cool stream of air entering the CNP (Figure 6-15A). Placing a greater

emphasis on the CNP to heat the remainder of the air field proved detrimental to heat savings as the final expired air temperature at the nostril was a relatively high 26.5°C (Figure 6-15B).

Straightened airway

Removing the curvature from the lengthened nasal vestibule resulted in removal of all of the vorticity observed in the BB and ST airway models. Under our low flow scenario the straightened airway was able to heat air up to 18.3°C prior to leaving through the choana (Figure 6-16). 78% of that heating occurred in the much elongated nasal vestibule. On expiration, the nasal passage was able to reduce the heat of the expired air by 11°C, resulting in expired air leaving the nostril at 23.9°C.

Euoplocephalus tutus

BB airway

Under the high flow rate model the BB airway was able to heat up respired air by 18.8°C, with 82% of that heating taking place within the confines of the nasal vestibule (Figure 6-17). Vorticity was evident in most of the bends of the nasal vestibule as well as inside the spacious cavum nasi proprium. On expiration, the nasal passage was able to reduce the expired air temperature by 13.9°C, resulting in air leaving the nostrils at 21.1°C. Under the low flow rate scenario, the BB airway was capable of heating up inspired air by 18.8°C, with 88% of the heat exchange occurring inside the convoluted nasal vestibule (Figure 6-17). Despite a lower flow rate, standing vortices along the curves of the nasal vestibule were still present. On expiration at this low flow rate, the

nasal passage was able to reduce the temperature of expired air by 15.6°C, resulting in air leaving the nostrils at 19.4°C.

ST airway

The high flow rate model for *Euoplocephalus* was able to warm air by 19.7°C with essentially all of that heat transfer (97%) occurring in the convoluted nasal vestibule (Figure 6-18). Extensive vorticity was observed throughout the nasal passage. These vortices were often concentrated around the multiple convolutions within the nasal passage. Upon expiration, air entered the choana at 35°C and left at 17.3°C. As with *Panoplosaurus,* there were fewer vortices upon expiration than inspiration. The low flow rate model for *Euoplocephalus* warmed inspired air up to body temperature (15°C–35°C). Almost all of that heat transfer occurred within the extensively convoluted nasal vestibule (99%). Similar flow patterns were observed under the low flow rate scenario as the high flow rate scenario (Figure 6-18). Under the expiration model, air left the nostril at 15.9°C, just slightly above ambient temperature.

Basic airway

As with *Panoplosaurus*, the basic airway for *Euoplocephalus* consisted of a simple, straight nasal vestibule that ran in a straight line from the nostril to the cavum nasi proprium (Figure 6-19). The total length of this simplified nasal vestibule was 162.14 mm, which was an 80% reduction in length from the original 808.74 mm nasal vestibule. As with the basic *Panoplosaurus* airway model, we ran this model under our most conservative, Reversed-Reynolds flow estimates. Under this low flow scenario the basic airway of *Euoplocephalus* was able to warm up inspired air by 15.3°C, which

appeared impressive initially. However, much like the *Panoplosaurus* model, closer examination of the airway revealed distinct differences between this basic airway and the ST airway. As with the basic airway of *Panoplosaurus*, the basic airway of *Euoplocephalus* had a fairly ineffective nasal vestibule. The nasal vestibule was able to contribute approximately 45% to the heating of the air field, resulting in a steady stream of cool air moving through the nasal vestibule and into the CNP (Figure 6-19). The majority of heating was provided by the CNP. Similarly to the basic airway of *Panoplosaurus*, this reliance on the CNP to deliver heat to the inspired air field had direct consequences for the nasal passage during expiration, where the nasal passage was only capable of reducing airway temperature by a miniscule 4.7°C. The resulting expired air left the nasal passage at only 5°C below body temperature (30.3°C).

Straightened airway

As with *Panoplosaurus*, the removal of nasal vestibule curvature resulted in vortex-free, laminar air traversing the much elongated nasal vestibule (Figure 6-20). Under the low flow scenario the straightened airway of *Euoplocephalus* was able to raise the temperature of inspired air by an impressive 19.3°C, with 89% of that heating occurring in the elongated nasal vestibule. On expiration, the straightened airway was able to reduce the temperature of the expired air by 12.2°C, resulting in air leaving the nostrils at 22.8°C.

Discussion

Both ankylosaur nasal passages revealed a substantial capacity to modify the properties of the existing air. By using our assumptions of tidal volume, it is possible to

calculate the efficiency of these convoluted nasal passages at heating and cooling respired air. We can then compare these results to data collected on heat recovery efficiency in the nasal passages of extant animals. The specific heat capacity of air across the majority of physiological temperatures is 0.24 cal/g°C (Schmidt-Nielsen 1997). Using the equation for tidal volume by Frappell et al. (2001), the estimated volume of air that would have been inspired during one breath for *Panoplosaurus* and *Euoplocephalus* is 34 and 64 liters, respectively (Table 6-4). To determine how much air must be heated to body temperature prior to reaching the lungs, we multiplied our estimated tidal volumes by the density of air at the assigned body temperature (1.146 g/L at 35°C). From these data, we calculated that *Panoplosaurus* and *Euoplocephalus* would have required 187 and 350 thermal calories per breath, respectively, to warm environmental air (15°C) up to body temperature (35°C, Table 6-4). These results only accounted for the change in temperature of the air. To account for the caloric cost associated with humidifying the air from 50% relative humidity to 100% relative humidity, we used a saturated steam table to determine the latent heat of vaporization of air at body temperature (556 kcal/kg, Table 6-4). Adding the latent heat of vaporization to our initial caloric analyses revealed that *Panoplosaurus* and *Euoplocephalus* would have required 833 and 1568 thermal calories per breath, respectively, to heat and humidify air from 15°C and 50% r.h., to 35°C and 100% r.h.

To determine energy and water savings, we used the simulated expired air temperatures from all models, coupled with our estimated tidal volumes. As heat is a form of energy, the same equations used to calculated the heating of air can be used to

determine its cooling, with only the signs changing to indicated direction of energy flow. Similarly, the energy recovered in the phase state change of water uses the same equation, albeit with the caloric savings changing with lower temperatures (cooler air can hold less water). The ratio of energy costs to energy savings reveals the overall efficiency of the nasal passages at conditioning respired air. Comparing the energetic savings across all six models for *Panoplosaurus* (Table 6-5, Figure 6-21 top) and *Euoplocephalus* (Table 6-6, Figure 6-21 bottom) revealed striking differences between the airway models. The ST airways under the low flow rate scenario, recouped the most energy for both dinosaur taxa (73% and 84% for *Panoplosaurus* and *Euoplocephalus*, respectively). This version of the nasal passage was meant to most closely represent what the original nasal passage would have been like in life. In contrast, the nasal passages as they were preserved in the fossils (i.e., the BB airways) and placed under the same low flow rate scenario, were not able to recoup as much heat energy (69% and 73% of inspiratory cost for *Panoplosaurus* and *Euoplocephalus*, respectively). Despite the remarkably well preserved nasal passages of both dinosaurs, accounting for soft tissue still resulted in profound differences in heat transfer efficiency. Comparing the energy savings calculated for the ST airways *Panoplosaurus* and *Euoplocephalus* to experimentally obtained energy and water recovery values for extant amniotes, we found that both dinosaurs had energy and water recovery values on par with many extant animals (Figure 6-22).

Airflow rate did have a noticeable effect on heat transfer efficiency, with lower flow rates resulting in more effective heat transfer (11–14% and 6–9% greater efficiency for *Panoplosaurus* and *Euoplocephalus*, respectively; Figure 6-21). These results agree

with previous measurements (Michaeli and Pinshow 2001) and simulations (Naftali et al. 2005) that indicate flow rate is the largest factor affecting heat transfer between air and the nasal passage.

That the heat transfer efficiency of the dinosaur nasal passages was a result of their great length was made evident upon comparison with the artificially shortened basic airways (Figure 6-15, Figure 6-19, Figure 6-21). These basic airways represented a minimalistic trek of the nasal vestibule from the nostril to the cavum nasi proprium. Achieving this ultra-conservative anatomical structuring required excising most of the preserved nasal vestibule (55% and 80% of the nasal vestibule in *Panoplosaurus* and *Euoplocephalus,* respectively). These truncated nasal vestibules offered very little surface area for heat to transfer from the respired air to the nasal mucosa (Figure 6-15, Figure 6-19). Although the cavum nasi proprium did offer some sizeable heat transfer capacity during inspiration, this was largely bypassed on expiration, requiring the nasal vestibule for most of the heat transfer. As such, the basic airways showed extremely reduced heat recovery abilities (62–32% of the respective ST airway heat recovery for *Panoplosaurus* and *Euoplocephalus,* Tables 5–6, Figure 6-21). These results strongly suggest that airway elaboration has a strong thermoregulatory component to its function.

Maintaining the length but removing curvature (convolutions) from the nasal vestibule proved to have a negative effect on heat and water recovery ability (Figure 6-21), albeit not as prominent as the basic airway. When compared to the low flow rate ST airways, curvature removal resulted in a 23% drop in heat transfer efficiency for *Panoplosaurus* and a 28% drop in heat transfer efficiency for *Euoplocephalus*. The

removal of airway curvature removed with it the presence of standing vortices in the nasal vestibules of both taxa (Figure 6-16, Figure 6-20). This reduction in heat transfer efficiency makes sense in light of this fact. As fluid flows within an object (e.g., air in the nasal passage) the portions of the flow field closest to the object's surface will have a tendency to stick to that surface, imparting drag on the fluid as a whole (Vogel 1994). As streamlines move further and further from these surfaces this wall drag is minimized, resulting in fluid at the center of the flow field moving at the highest velocities and producing the classic fluid dynamic parabolic profile (Vogel 1994). Since fluids at the fluid-surface boundary are essentially static they create a non-motile boundary layer that acts as a barrier to diffusion. Finding ways to reduce the size of this boundary layer can increase the speed at which diffusion takes place (Vogel 1994). Placing sharp turns and contortions within the nasal passage acts to break up this boundary layer, allowing cooler air to come into closer contact with the surrounding mucosa. The presence of standing vortices at multiple curves within the nasal passage of both *Panoplosaurus* and *Euoplocephalus* (Figure 6-16, Figure 6-20) reveals multiple regions where that boundary layer was broken up. Further, the presence of vortices slows down the passage of the air molecules through the nasal passage, providing more time for air to reach thermal equilibrium with the body. By coiling the nasal passage within the skull, ankylosaurs were able to take advantage of the extra surface area for air to interact with the mucosa. This surface area, coupled with the adjacent location of large nasal vasculature (Witmer and Ridgely 2008, Porter 2015) and boundary-layer-breaking effects caused by forcing

the air field to radically change direction as it moves through the nasal passage, resulted in these nasal passages greatly affecting the heat content of the respired air.

Water savings can partially be calculated using the data obtained from this study (Figure 6-21). As with heat transfer efficiency, the ST airway reconstructions under the low flow rate scenarios, produced the highest water savings (69% and 79% for *Panoplosaurus* and *Euoplocephalus*), whereas the truncated, basic airways were the least effective (44% and 27%). Overall water flux (amount of water used per day) cannot be calculated for extinct animals, and thus we cannot be certain of how important reducing respiratory evaporative water loss (REWL) was for ankylosaurs. Nonetheless, our data do suggest that the nasal passages in both ankylosaurs functioned effectively as water reclaimers as well as air conditioners.

Of the two ankylosaurs, *Euoplocephalus* showed greater air conditioning efficiency (Tables 5, 6, Figure 6-21, Figure 6-22). Under both high and low flow rate scenarios, both the BB and ST airways of *Euoplocephalus* were able to bring inspired air closer to simulated body temperature than *Panoplosaurus*. Upon expiration, the ST-corrected nasal passage of *Euoplocephalus* was able to lower air temperatures 3.6–4.2°C lower than air temperatures in the ST-corrected nasal passage of *Panoplosaurus*. This translated into an 15–22% greater energy savings and a 14–19% greater water recovery. The more elaborately convoluted nasal vestibule in *Euoplocephalus* compared to *Panoplosaurus* (Witmer & Ridgely 2008; Figure 6-7–10) was likely responsible for these greater energy savings despite the larger flow rates and tidal volumes. The nasal vestibule played the largest role in air conditioning for both models. These results suggest that

Euoplocephalus may have needed a more efficient nasal passage than *Panoplosaurus*. Why was that? Both ankylosaurs come from the same stratigraphic level of the Dinosaur Park Formation (Brown et al. 2013) indicating that they were likely contemporaneous animals. This suggests that environmental factors were not the cause for the more elaborate nasal passage of *Euoplocephalus*. Phylogenetically, both are relatively closely related, despite being representatives of the two major branches of Ankylosauria (Vickaryous et al. 2004; Thompson et al. 2012). We suspect that the larger size of *Euoplocephalus* (900–1500 kg more massive than *Panoplosaurus* based on estimates from Brown et al. 2013) necessitated a more efficient nasal passage. Larger animals—with their lower surface-to-volume ratios—absorb, produce, and retain more heat than smaller animals (Schmidt-Nielsen 1984). As a substantially more massive animal, *Euoplocephalus* would have had to cope with higher heat loads than its relatively smaller relative. Elaborating the nasal apparatus could have been a response to this higher heat load. Alternatively, the more elaborate nasal passage of *Euoplocephalus* could be related to the generally more elaborate nasal passages of ankylosaurids compared to nodosaurids (Witmer and Ridgely 2008). At the moment our knowledge of nasal passage shape in ankylosaurs is largely limited to the two taxa used in this study. However, if the more extensive "paranasal sinus system" of ankylosaurids is an indication of a more convoluted nasal vestibule, then it would seem that ankylosaurids had apomorphically elaborated their nasal passages more than nodosaurids (Hill et al. 2003; Carpenter 2004). That ankylosaurids tended to get larger than nodosaurids suggests a potential causal relationship between the nasal passage and body size, and would agree with our

physiological interpretations of the more elaborate nasal passage of *Euoplocephalus*. Interestingly, this finding appears to be the first time that such a correlation has been observed. Previous attempts to quantify nasal elaboration with body size (Van Valkenburgh et al. 2004) did not uncover such a relationship and we suspect that this may be due to the way in which a parallel system can scale compared to a serial system (see below). Whether nasal elaboration opened up opportunities for larger body sizes or if large body size spurred the evolution of nasal passage elaboration cannot be determined at this point. It is important to note that the results presented in this study do not negate potential other functions of the nasal passage, especially in regard to vocal resonance. These results simply indicate that these elaborate nasal passages were capable and efficient at the one nasal function we tested.

It is worth noting that regardless of the relative efficiency between these two ankylosaurs, both animals seemed to have been quite capable of modifying the respired air. That both animals were able to modify air apparently without the aid of respiratory turbinates or conchae is particularly intriguing. Respiratory turbinates, and the physiologically active mucosal conchae that reside on them, have been hypothesized to have evolved strictly for the function of increasing the water reclaiming ability of the nasal passage, mitigating the effects of high ventilation rates as seen in mammalian endotherms (Hillenius 1992, 1994; Geist 2000; Ruben and Hillenius 2004). However, as has been previously suggested (Bourke et al. 2014), this necessity for respiratory turbinates appears to be truer for mammals than for sauropsids, which have markedly lower ventilation rates than equivalently sized mammals (Frappell et al. 2001, Bourke et

al. 2014). The estimated resting breathing frequency of *Panoplosaurus* and *Euoplocephalus* was 1.5 and1.2 breaths/minute, respectively. Such slow breathing would result in naturally low REWL rates regardless of whether respiratory turbinates were present. As such, the need for a water recovery mechanism may not be as strong a selective force as it appears to be in mammals, allowing for alternate means of solving the REWL problem, such as evolving a long, winding nasal passage. Our results indicate that an elongated, convoluted nasal passage produces equivalent results to a turbinate-filled airway. Both anatomical organizations appear to offer the same results albeit with different tradeoffs. A single, winding airway warms and transports air in a stepwise, serial fashion whereas a turbinate-filled airway breaks the air field into multiple, parallel-running air streams. The latter approach appears to function well at warming large volumes of air in a relatively small space, allowing a short airway to act like a long airway (see Chapter 3). However, by breaking the airfield into a series of smaller streams, turbinates also decrease the caliber of the airway in these regions. Intuitively we should expect to see a concomitant, and rather large, increase in airflow resistance as determined from a derivation of the Hagen-Poiseuille equation (Vogel 1994):

$$(5)\mathrm{R} = \frac{8\mu l}{\pi r^4},$$

where R = resistance, μ = dynamic viscosity, l = the length of the "pipe" and r = the radius of the "pipe." As indicated by the exponent in the equation, resistance is highly sensitive to the radius of the structure through which a fluid flows. Separating the airfield into a series of smaller air channels should result in a substantial increase in airway resistance. However, even though turbinates break up the airway into multiple channels,

these channels are all running in parallel to each other. Unlike resistance in a serial system of pipes the cumulative resistance in a turbinate-filled airway—much like in an electrical circuit—is best calculated by taking the reciprocals of resistance for each parallel channel (Vogel 1994):

$$(6)\ R_{total} = \sum \frac{1}{\frac{1}{R_1}+\frac{1}{R_2}+\frac{1}{R_3}\ldots},$$

where R is the same as in Eq. 5. Thus an airway split into multiple parallel channels will increase in resistance much slower than it would appear at the outset, which makes the filling of nasal passages with turbinates an energetically viable option (Figure 6-23). Standard scaling rules indicate that an isometric increase in body size will increase the volume of the nasal passage (Schmidt-Nielsen 1984). Van Valkenburgh et al. (2004) found the turbinate-filled nasal passages of carnivorans to scale positively allometrically, thus indicating even larger increases in airway volume with body size than predicted from isometry. Increasing nasal passage volume should reduce the efficacy of the nasal passage at transferring heat, due to the diffusion limited nature of heat transfer discussed earlier. However, increasing the volume of a turbinate-filled nasal passage results in a relatively minor increase in the gap distance between opposing turbinate walls. Thus, an increase in nasal cavity volume results in only modest increases in individual channel volume. The larger size of the nasal cavity may further be compensated for by changing the arrangement of individual turbinates (e.g., increased scrolling) or increasing the thickness of the mucosa that resides on them (conchae). This ability to slow the rate of radial distance increase within the air field, appears to make nasal turbinates more resilient to changes in body size than a serially-arranged nasal passage may be. This

resilience may explain why turbinate density appears to not scale with body size in carnivoran mammals (Van Valkenburgh et al. 2004). In contrast, a single long airway offers lower resistance, but it does impose a limit on how much air can be processed at any one time. Increasing efficiency requires more contortions of the nasal passage. If one is a slow breather, then this limitation on airflow processing is unlikely to cause a problem. Among extant diapsids, the nasal passages of ankylosaurs are reminiscent of the winding airways recorded in some lizards, such as *Uromastyx* (Stebbins 1948; Figure 6-24). Lizards, much like birds, are rather slow breathers compared to similar sized mammals (Bennett 1973), and the limitation on air processing imposed by a long, serial airway does not seem to affect them.

Although much has been written on the heat and water retaining function of respiratory turbinates (Hillenius 1992, 1994; Ruben et al. 1996, 1998; Geist 2000; Ruben and Hillenius 2004) as well as the nasal passage itself (Jackson and Schmidt-Nielsen 1964; Schmidt-Nielsen et al. 1970; Collins et al. 1971; Langman et al. 1979), fewer studies have looked at the other side of this nasal function, its ability to dump excess heat from the body core. Inspired air is heated in the nasal passage by pulling heat away from warm blood coursing beneath the adjacent mucosa. As such, the nasal passage not only warms and humidifies inspired air, but it also acts as a heat sink for hot blood coming from the body core. Blood vessels that detour through the nasal passage have the potential to shed excess heat, thus providing a source of cooled blood. An extensive survey of blood vasculature in extant sauropsids (Porter 2015) found that the nasal passage receives branches from major arteries coming from the body core via the internal

and external carotid arteries. These arterial branches dump into capillary beds that transition into major venous pathways that course caudally towards the brain. Reconstructed vasculature in dinosaurs, including the ankylosaurs used in this study (Witmer and Ridgely 2008), has revealed extensive nasal vasculature in large-bodied dinosaurs, and blood vessel pathways similar to those of extant diapsids (Porter 2015). Having hot blood coming from the body core, shed excess heat in the nasal passages prior to entering the brain, provides a means for sauropsids to keep their brains from overheating. Studies on extant amniotes have observed that head temperature tends to be more strictly regulated than body temperature (Heath 1964; Johnson 1973, 1974; Pough & McFarland 1976; Tattersall et al. 2006). The oronasal apparatus has long been implicated in controlling these body temperature differences (Baker et al. 1974; Crawford et al. 1976; Baker 1982; Caputa 2004; Tattersall et al. 2006). Many studies have focused solely on the role of the oronasal apparatus in avoiding heat stress (Caputa 2004). These studies tended to observe other signs of heat stress (e.g., panting) that have been shown to offer a means of locally cooling the cephalic region of the body (Crawford et al. 1976; Baker 1982; Caputa 2004; Tattersall et al. 2006). Our ankylosaur data, however, indicate that a substantial blood cooling capacity in the nasal passage was present even under "relaxed" or resting conditions (i.e., not heat stress). We speculate that heat dumping in these enhanced nasal passages may have been more obligate as the large size of these dinosaurs would have resulted in a very high heat load that, when transferred to remarkably small brains (Witmer et al. 2008), would have created a scenario that placed these animals at near constant risk of brain overheating. Similar nasal elaborations have

been observed in sauropods, ornithopods, and ceratopsians (Witmer and Sampson 1999). All of these groups are composed of mostly large bodied (multi-tonne) animals. Nasal elaboration may have evolved for brain cooling in these taxa as well. Future work looking at more basal members of these dinosaur groups (e.g., *Minmi paravertebra* for ankylosaurs) will provide greater insight into the role of nasal passage elaboration and body size evolution in dinosaurs.

Acknowledgments

We would like to thank the National Science Foundation (NSF) Graduate Research Fellowship, Doris O. and Samuel P. Welles Research Fund, and Jurassic Foundation for funding to JMB, and NSF grants (IBN-0343744, IOB-0517257, IOS-1050154) to LMW. Thanks to C. Mehling and M. Norell for AMNH material. Thanks to D. Evans and K. Seymour for access to ROM material. For assistance with CT scanning of ankylosaur fossils, we thank H. Rockhold, RT, and OhioHealth O'Bleness Hospital, Athens, Ohio. Thanks to Wm. R. Porter for useful discussions and interpretations of vascular data. Thanks to B. Van Valkenburgh and B. A. Craven for discussions on turbinate anatomy and general CFD questions. Thanks to Ryan Ridgely for initial segmentation and help with CT interpretation. Thanks to Ashley Morhardt, Don Cerio, and Catherine Early for useful discussions.

References

Arbour, V.M., Currie, P.J. 2013. *Euoplocephalus tutus* and the diversity of ankylosaurid dinosaurs in the Late Cretaceous of Alberta, Canada, and Montana, USA. PLOS One. 8(5):e62421.

Baker, M.A. 1982. Brain cooling in endotherms in heat and exercise. Ann Rev Physiol. 44:85–96.

Baker, M.A., Chapman, L.W., Nathanson, M. 1974. Control of brain temperature in dogs: Effects of tracheostomy. Resp Physiol. 22:325–333.

Barrick, R., Fischer, A.G., Showers, W.J. 1999. Oxygen isotopes from turtle bone: Applications for terrestrial paleoclimates? Palaios. 14(2):186–191.

Baumel, J.J., Witmer, L.M. 1993. Osteologia. in: Baumel, J.J., King, A.S,, Breazile, J.E., Evans H.E., Vanden Berge, J.C, (eds). Handbook of Avian Anatomy: Nomina Anatomica Avium. Publications of the Nuttall Ornithological Club. No. 23. pp:45–132.

Bellairs, A D'A. 1949. Observations on the snout of *Varanus*, and a comparison with that of other lizards and snakes. J Anat. 83 (Pt.2):116–146.

Bennett, A.F. 1973. Ventilation in two species of lizards during rest and activity. Comp Biochem Physiol. 46A:653–671.

Biswas R., Strawn R.C., 1998. Tetrahedral and hexahedral mesh adaptation for CFD problems. App Num Math. 26:135–151.

Bourke, J.M., Porter, W.M., Ridgely, R.C., Lyson, T.R., Schachner, E.R., Bell, P.R., Witmer, L.M. 2014. Breathing life into dinosaurs: Tackling challenges of soft-tissue restoration and nasal airflow in extinct species. Anat Rec. 297:2148–2186.

Brown, B. 1908. The Ankylosauridae, a new family of armored dinosaurs from the Upper Cretaceous. Bull Am Mus Nat Hist. 24:187–201.

Brown, C.M., Evans, D.C., Campione, N.E., O'Brien, L.J., Eberth, D.A. 2013. Evidence for taphonomic size bias in the Dinosaur Park Formation (Campanian, Alberta), a model Mesozoic terrestrial alluvial-paralic system. Palaeogeo Palaeoclim Palaeoeco. 372:108–122.

Caputa, M. 2004. Selective brain cooling: A multiple regulatory mechanism. J Therm Biol. 29:691–702.

Carpenter, K. 2004. Redescription of *Ankylosaurus magniventris* Brown 1908 (Ankylosauridae) from the Upper Cretaceous of the Western Interior of North America. Can J Earth Sci. 41:961–986.

Carpenter, K. 1990. Ankylosaur systematics: Example using *Panoplosaurus* and *Edmontonia* (Ankylosauria: Nodosauridae). in Carpenter, K., Currie, P.J. (eds). Dinosaur Systematics Approaches and Perspectives. New York, NY Cambridge U Press. pps:281–298.

Cave, A.J.E. 1967. The nature and function of the mammalian epipharynx. J Zool Lond. 153:277–289.

Collins, J.C., Pilkington, T.C., Schmidt-Nielsen, K. 1971. A model of respiratory heat transfer in a small mammal. Biophys J. 11:886–914.

Coombs W.P. 1978. The families of the ornithischian dinosaur order Ankylosauria. Palaeontology. 21:143–170.

Coombs, W.P. 1972. The bony eyelid of *Euoplocephalus* (Reptilia, Ornithischia). J. Paleo. 46(2):637–650.

Coombs, W.P Jr. 1971. The Ankylosauria. Ph.D Dissertation. New York, Columbia University

Coombs, W.P., Maryańska, T. 1990. Ankylosauria. in: Weishampel, D.B., Dodson, P., Osmólska, H. (eds). The Dinosauria: First Edition. Berkeley. UC Press. pps:456–483.

Craven, B.A., Neuberger, T., Paterson, E.G., Webb, A.G., Josephson, E.M., Morrison, E.E., Settles, G.S. 2007. Reconstruction and morphometric analysis of the nasal airway of the dog (*Canis familiaris*) and implications regarding olfactory airflow. Anat Rec. 290:1325–1340.

Craven, B.A., Paterson, E.G., Settles, G.S. 2010. The fluid dynamics of canine olfaction: Unique nasal airflow patterns as an explanation of macrosmia. J R Soc Interface. 7:933–943.

Craven, B.A., Paterson, E.G., Settles, G.S., Lawson, M.J. 2009. Development and verification of a high-fidelity computational fluid dynamics models of canine nasal airflow. J Biomech Eng. 131: 091002–1.

Crawford, E.C., Palomeque, J., Barber, B.J. 1977. A physiological basis for head-body temperature differe1nces in a panting lizard. Comp Biochem Physiol. 56A: 161–163.

Crole, M.R., Soley, J.T. 2010. Gross morphology of the intra-oral rhampotheca, oropharynx and proximal oesophagus of the emu (*Dromaius novaehollandiae*). Anat Hist Embryol. 39:207–218.

Dinets, V. 2013. Long-distance signaling in Crocodylia. Copeia. 3:517–526.

Foss, J.F. 1998. Basic engineering fluid mechanics. in Johnson, R.W. (ed) The Handbook of Fluid Dynamics. Florida: CRC Press. p:5-1–5-99.

Frappell, P.B., Hinds, D.S., Boggs, D.F. 2001. Scaling of respiratory variables and the breathing pattern in birds: an allometric and phylogenetic approach. Phys Biochem Zool. 74:75–89.

Frey, R., Volodin, I., Volodina, E. 2007. A nose that roars: Anatomical specializations and behavioural features of rutting male saiga. J Anat. 211 , 717–736.

Geist, N.R. 2000. Nasal respiratory turbinate function in birds. Physiol Biochem Zool. 73:581–589.

Georges, P., Hecht, F., Saltel, E., 1988. Constraint of the boundary and automatic mesh generation. In: Sengupta, S., Håuser, J., Eiseman, P.R., and J.F. Thompson (eds). Numerical Grid Generation in Computational Fluid Mechanics. Pineridge, Swansea, UK.

Hayashi, S., Carpenter, K., Scheyer, T.M., Watabe, M., Suzuki, D. 2009. Function and evolution of ankylosaur dermal armor. Acta Paleo Polon. 55(2):213–228.

Heath, J.E. 1964. Head-body temperature differences in horned lizards. Physiol Zool 37(3):279–279.

Hill, R.V., Witmer, L.M., Norell, M.A. 2003. A new specimen of *Pinacosaurus grangeri* (Dinosauria: Ornithischia) from the Late Cretaceous of Mongolia: Ontogeny and phylogeny of ankylosaurs. Am Mus Novit. 3395:1–29.

Hillenius, W.J. 1994. Turbinates in therapsids: evidence for Late Permian origins of mammalian endothermy. Evolution. 48:207–229.

Hillenius, W. 1992. The evolution of nasal turbinates and mammalian endothermy. Paleobiology. 18:17–29.

Hillenius, W.J., Ruben, J.A. 2004. The evolution of endothermy in terrestrial vertebrates: who? when? why? Phys Biochem Zool. 77:1019–1042.

Holmes, W.M., Cotton, R., Xuan, V.B., Rygg, A.D., Craven, B.A., Abel, R.L., Slack, R., Cox, J.P.L. 2011. Three-dimensional structure of the nasal passageway of a hagfish and its implications for olfaction. Anat Rec. 294:1045–1056.

Hörschler, I., Brücker, Ch., Schröder, W., Meinke, M. 2006. Investigation of the impact of the geometry on the nose flow. Eu J Mech B/Fluids. 25:471–490.

Jackson, D.C., Schmidt-Nielsen, K. 1964. Countercurrent heat exchange in the respiratory passages. Physiology. 51:1192–1197.

Jarvik, E. 1942. On the structure of the snout of crossopterygians and lower gnathostomes in general. Zool Bidr Upsala. 21:235–675.

Jiang, J., Zhao, K. 2010. Airflow and nanoparticle deposition in rat nose under various breathing and sniffing conditions—A computational evaluation of the unsteady and turbulent effect. J Aerosol Sci. 41:1030–1043.

Johnson, C.R. 1974. Thermoregulation in crocodilians-I. Head-body temperature control in the Papuan-New Guinean crocodiles, *Crocodylus novaeguineae* and *Crocodylus porosus*. Comp Biochem Physiol. 49A:3–28.

Johnson, C.R. 1973. Thermoregulation in pythons-II. Head-body temperature differences and thermal preferenda in Australian pythons. Comp Biochem Physiol. 45A:1065–1087.

Katz, J. 2006. Aerodynamics of race cars. Annu. Rev. Fluid Mech. 38:27-63.

Kierszenbaum, A.L. 2007. "Respiratory System" in Histology and Cell Biology: An Introduction to Pathology. 2nd ed. Elsevier. Philadelphia, PA. p.437.

Langman, V.A, Maloiy, G.M.O., Schmidt-Nielsen, K., Schroter, R.C. 1979. Nasal heat exchange in the giraffe and other large mammals. Respir Physiol. 37:325–333.

Longest, P.W., Vinchurkar, S. 2007. Effects of mesh style and grid convergence on particle deposition in bifurcating airway models with comparisons to experimental data. Med Engin Phys. 29:350–366.

Lucas, A.M., Douglas, L.C. 1934. Principles underlying ciliary activity in the respiratory tract. Archiv Otolaryng. 20518-541.

Luckring, J.M., Rizzi, A., Davis, M.B. 2014. Toward improved CFD predictions of slender airframe aerodynamics using the F-16XL aircraft (CAWAPI-2). AIAA. 419:1-14.

Main, R.P., de Ricqlès, A., Horner, J.R., Padian, K. 2005. The evolution and function of thyreophoran dinosaur scutes: implications for plate function in stegosaurs. Paleobiology. 31:291–314.

Martin, B.G.H., Bellairs, A.d'A. 1977. The narial excrescence and pterygoid bulla of the gharial, *Gavialis gangeticus* (Crocodilia). J Zool Lond. 182:541–558.

Maryańska, T. 1977. Ankylosauridae (Dinosauria) from Mongolia. Palaeontologia Polonica. 37:85–151.

Maryańska, T. 1971. New data on the skull of *Pinacosaurus grangeri* (Ankylosauria). Palaeontologia Polonica. 25: 45–53.

Michaeli, G., Pinshow, B. 2001. Respiratory water loss in free-flying pigeons. J Exp Biol. 204:3803–3814.

Miyashita, T., Arbour, V.M., Witmer, L.M., Currie, P.J. 2011. The internal cranial morphology of an armoured dinosaur *Euoplocephalus* corroborated by X-ray computed tomographic reconstruction. J Anat. 219(6):661–675.

Murrish, D.E. 1973. Respiratory heat and water exchange in penguins. Resp Physiol. 19:262–270.

Murrish , D.E., Schmidt-Nielsen, K. 1970. Exhaled air temperature and water conservation in lizards. Resp Physiol. 10:151–158.

Naftali, S., Rosenfeld, M., Wolf, M., Elad, D. 2005. The air-conditioning capacity of the human nose. Ann Biomed Engin. 33(4):545–553.

Negus, V.E., 1958. The comparative anatomy and physiology of the nose and paranasal sinuses. Livingstone, London, England.

Osmólska, H. 1979. Nasal salt glands in dinosaurs. Acta Palaeontologica Polonica. 24: 205–215.

Pough, F.H., McFarland, W.N. 1976. A physical basis for head-body temperature differences in reptiles. Comp Biochem Physiol. 53A:301–303.

Porter, W. R. 2015. Physiological implications of dinosaur cephalic vascular systems. Unpublished doctoral dissertation, Ohio University. 433 pp.

Rieppel, O., Gauthier, J., Maisano. J. 2008. Comparative morphology of the dermal palate in squamate reptiles, with comments on phylogenetic implications. Zool J Linn Soc. 152:131–152.

Romer, A.S. 1953. Osteology of the Reptiles. Malabar, FL. Krieger Publishing Company.

Ruben, J.A., Jones, T.D., Geist, N.R. 1998. Respiratory physiology of the dinosaurs. BioEssays. 20:852–859.

Ruben, J.A., Hillenius, W.J., Geist, N.R., Leitch, A., Jones, T.D., Currie, P.J.,Horner, J.R., Espe III, G. 1996. The metabolic status of some Late Cretaceous dinosaurs. Science. 273:1204–1207.

Scheyer, T.M., Sander, P.M. 2004. Histology of ankylosaur osteoderms: implications for systematics and function. JVP. 24:874–893.

Schoenfeld, T.A., Cleland, T.A. 2005. The anatomical logic of smell.Trends Neurosci. 28:620–627.

Schmidt-Nielsen, K. 1997. Animal Physiology. 5th ed. Cambridge: Cambridge University Press.

Schmidt-Nielsen, K. 1984. Scaling: Why is animal size so important? Cambridge, MA. Cambridge U Press.

Schmidt-Nielsen, K., Hainsworth, R.F., Murrish, D. 1970. Counter-current heat exchange in the respiratory passages: Effect on water and heat balance. Resp Physiol. 9:263–276.

Shephard, M., Georges, M., 1991. Automatic three-dimensional mesh generation by the finite octree technique. Int. J Num Meth Engin. 32:709–749.

Stebbins, R.C. 1948. Nasal structure in lizards with reference to olfaction and conditioning of the respired air. Am J Anat. 83(2):183–221.

Tattersall, G.J., Cadena, V., Skinner, M.C. 2006. Respiratory cooling and thermoregulatory coupling in reptiles. Resp Physiol Neurobio. 154:302–318.

Tu, J., Yeoh, G.H., Liu, C. 2012. Computational Fluid Dynamics, Second Edition: A practical Approach. United Kingdom: Butterworth-Heinemann.

Vickaryous, M.K. 2006. New information on the cranial anatomy of *Edmontonia rugosidens* Gilmore, a Late Cretaceous nodosaurid dinosaur from Dinosaur Provincial Park, Alberta. JVP. 26:1011–1013.

Vickaryous, M.K. 2001. Skull morphology of the Ankylosauria. Masters Thesis. U Calgary.

Vickaryous, M.K., Maryanska, T., Weishampel, D.B. 2004 in Weishampel, D.B., Dodson, P., Osmolska, H. (eds) Dinosauria 2nd Edition. Los Angeles, CA UC Press. pps: 363–392.

Vickaryous, M.K., Russell, A.P. 2003. A redescription of the skull of *Euoplocephalus tutus* (Archosauria: Ornithischia): a foundation for comparative and systematic studies of ankylosaurian dinosaurs. Zool J Linn Soc. 137:157–186.

Vickaryous, M.K., Russell, A.P., Currie, P.J.. 2001. Cranial ornamentation of ankylosaurs (Ornithischia: Thyreophora): Reappraisal of developmental hypotheses. in Carpenter, K. (ed) The Armored Dinosaurs. Indianapolis, ID. IUP pps: 318–340.

Vickaryous, M., Sire, J.−Y. 2009. The integumentary skeleton of tetrapods: Origin, evolution, and development. J Anat. 214:407–644.

Vogel, S. 2003. Viscosity and the patterns of flow. In Vogel, S. (ed) Comparative Biomechanics: Life's Physical World. New Jersey. Princeton University Press. p:117–138.

Vogel, S. 1994. Life in Moving Fluids. 2nd ed. New Jersey: Princeton University Press.

Weldon, P.J., Ferguson, M.W.J. 1993. Chemoreception in crocodilians: Anatomy, natural history, and empirical results. Brain Behav Evol. 41(3–5):239–245.

Winet, H., Yates, G.T., Wu, T.Y., Head, J. 1982. On the mechanics of mucociliary flows. II. A fluorescent tracer method for obtaining flow velocity profiles in mucus. Cell Motility. Supp. 1:29–34.

Witmer, L.M. 2001. Nostril position in dinosaurs and other vertebrates and its significance for nasal function. Science. 293:850–853.

Witmer, L. M. 1997. The evolution of the antorbital cavity of archosaurs: A study in soft-tissue reconstruction in the fossil record with an analysis of the function of pneumaticity. Mem SVP. 3:1-73.

Witmer, L.M. 1995a. Homology of facial structures in extant archosaurs (birds and crocodilians), with special reference to paranasal pneumaticity and nasal conchae. J Morphol. 225:269–327.

Witmer, L.M. 1995b. The extant phylogenetic bracket and the importance of reconstructing soft tissues in fossils. in: Thomason, J.J. (ed). Functional morphology in vertebrate paleontology. New York: Cambridge University Press. pp:19–33.

Witmer, L.M., Ridgely, R.C. 2008. The paranasal air sinuses of predatory and armored dinosaurs(Archosauria: Theropoda and Ankylosauria)and their contribution to cephalic architecture. Anat Rec. 291:1362–1388.

Witmer, L.M., Ridgely, R.C., Dufeau, D.L., Semones, M.C.. 2008. Using CT to peer into the past: 3D visualization of the brain and ear regions of birds, crocodiles, and nonavian dinosaurs. in: Endo H, Frey R, (eds).Anatomical Imaging: Towards a New Morphology. Springer. p 67–87.

Witmer, L.M., Sampson, S.D. 1999. Nasal conchae and blood supply in some dinosaurs: physiological implications. JVP. 19 (3 supp):85A.

Womersley, J.R. 1955. Method for the calculation of velocity, rate of flow and viscous drag in arteries when the pressure gradient is known. J Physiol. 127:553–563.

Yam, R., Yuen, P.L., Yung, R., Choy, T. 2011. Rethinking hospital general ward ventilation design using computational fluid dynamics. J Hosp Infect. 77:31-36.

Yerry, M., Shephard, M., 1984. Automatic three-dimensional mesh generation by the modified-octree technique. Int. J Num Meth Engin. 20:1965–1990.

Zhao, K., Dalton, P., Yang, G.C., Scherer, P.W. 2006. Numerical modeling of turbulent and laminar airflow and odorant transport during sniffing in the human and rat nose. Chem Senses. 31:107–118.

Zusi, R.L. Livezey, B.C. 2006. Variation in the os palatinum and its structural relation to the palatum ossseum of birds (Aves). Annals Carnegie Museum. 75(3):137–180.

APPENDIX FOR CHAPTER 6

Heat Savings Graph

To compare the results from our two ankylosaur models (*Panoplosaurus mirus*, *Euoplocephalus tutus*) to extant animals we surveyed the literature for data on heat and water savings within the nasal passages of extant birds, mammals, and reptiles. Taxa and their references are listed in Appendix Table 1.

Appendix Table 1.

Taxa used for comparative energy savings graph

Taxon	**Reference**
Cactus wren (*Campylorhynchus brunneicapillus*)	Schmidt-Nelsen et al. 1970
Kangaroo rat (*Dipodomys merriami*)	Schmidt-Nelsen et al. 1970
Giraffe (*Giraffa camelopardalis*)	Langman et al. 1979
Donkey (*Equus africanus*)	Langman et al. 1979
Desert iguana (*Dipsosaurus dorsalis*)	Murrish and Schmidt-Nielsen 1970
Crow (*Corvus brachyrhynchos*)	Geist 2000
Pigeon (*Columba livia*)	Geist 2000

With the exception of the cactus wren and kangaroo rat, all of these studies only reported estimated water recovery from respiration. Heat savings had to be calculated manually, which required knowledge of how much air was inspired during one breath.

For most of the studies we considered, this number was not given. To obtain a reasonable estimate, we used the equations for tidal volume in mammals and lizards from Stahl (1967) and Bennett (1973), respectively.

Calculating heat costs required knowing the density of air at each given temperature. This was used to calculate the mass of air in that tidal volume. This value was multiplied by the specific heat of air at a given temperature (0.24 cal/g°C) to determine the heat capacity of that bolus of air. Appendix Table 2 lists these values for inspiration.

Appendix Table 2.

Inspiratory values for taxa studied *data from references cited in Appendix Table 1

Taxon	**Tidal volume (ml)**	**Mass of air (g)**	**Heat capacity (cal/°C)**	**Temperature increase (°C)***	**Total energy (cal)**
Giraffe (*Giraffa camelopardalis*)	5,959	6.78	1.63	16.2	26.4
Donkey (*Equus africanus*)	1,605	1.82	0.44	14	6.16
Desert iguana (*Dipsosaurus dorsalis*)	0.457	$5.12e^{-4}$	$1.23e^{-4}$	12	$1.5e^{-3}$
Crow (*Corvus brachyrhynchos*)	7.25*	$8.14e^{-3}$	$1.95e^{-3}$	26.1	$5.1e^{-2}$
Pigeon (*Columba livia*)	5.24*	$5.90e^{-3}$	$1.41e^{-3}$	25.7	$3.6e^{-2}$

Calculation of heat saving followed the same approach, but used the final expired temperature to determine the mass of air that would have been expelled during expiration. Total heat energy recouped is shown in Appendix Table 3 Comparing heat costs to heat savings produced the percentage results shown in Figure 6-22 of the manuscript.

Appendix Table 3.

Heat energy savings among taxa studied. * data from references in Appendix Table 1

Taxon	**Expired temp (°C)***	**Mass of air (g)**	**Heat capacity (cal/°C)**	**Temp decrease (°C)**	**Energy saved (cal)**
Giraffe (*Giraffa camelopardalis*)	28.0	6.98	1.7	9.3	15.8
Donkey (*Equus africanus*)	32.3	1.86	0.45	5.3	2.4
Desert iguana (*Dipsosaurus dorsalis*)	35	$5.24e^{-4}$	$1.3e^{-4}$	7	$9.1e^{-4}$
Crow (*Corvus brachyrhynchos*)	21.9	$8.68e^{-3}$	$2.1e^{-3}$	19.2	$4.0e^{-2}$
Pigeon (*Columba livia*)	21.4	$6.28e^{-3}$	$1.5e^{-3}$	19.3	$3.0e^{-2}$

Comparability of the Data

As mentioned in the caption for Figure 6-22, these results provided a "ballpark" comparison among taxa. They allow us to see the overall energy recovery capacity within the nasal passage. However, since these data came from three different studies that had very different protocols, these results should not be looked at as being perfectly comparable. For instance, the study on the desert iguana (currently the only reptile to have such a study done) had measurements of inspiration and expiration at a variety of body temperatures. To make the results from that paper more compatible with the mammal and bird data, we took the largest exhaled temperature drop observed, which was 7°C when the animal had a body temperature of 42°C in an ambient temperature of 30°C (note: Murrish and Schmidt-Nielsen [1970] had a typographical error in their discussion that stated the lizards reduced air temperature by only 5°C, but their results section and data graph indicate that 7°C is the correct number). Murrish and Schmidt-Nielsen (1970) did not test their lizards at an ambient temperature of 15°C, nor a relative humidity of 50%, thus making direct comparisons between Langman et al. (1979) and Geist (2000) impossible. Similarly, the data from Schmidt-Nielsen et al. (1970) were for animals breathing in air at 25% relative humidity, and the data from Langman et al. (1979) did not specify humidity, nor did they test at air temperatures of 15°C. Of the data used for comparisons, the data from Geist 2000 are the most equivalent for comparison with our dinosaur models.

References

Bennett, A.F. 1973. Ventilation in two species of lizards during rest and activity. Comp Biochem Physiol. 46A:653–671.

Frappell, P.B., Hinds, D.S., Boggs, D.F. 2001. Scaling of respiratory variables and the breathing pattern in birds: an allometric and phylogenetic approach. Phys Biochem Zool. 74:75–89.

Geist, N.R. 2000. Nasal respiratory turbinate function in birds. Physiol Biochem Zool. 73:581–589.

Langman, V.A, Maloiy, G.M.O., Schmidt-Nielsen, K., Schroter, R.C. 1979. Nasal heat exchange in the giraffe and other large mammals. Respir Physiol. 37:325–333.

Murrish , D.E., Schmidt-Nielsen, K. 1970. Exhaled air temperature and water conservation in lizards. Resp Physiol. 10:151–158.

Schmidt-Nielsen, K., Hainsworth, R.F., Murrish, D. 1970. Counter-current heat exchange in the respiratory passages: Effect on water and heat balance. Resp Physiol. 9:263–276.

Stahl, W. 1967. Scaling of respiratory variables in mammal. J Appl Physiol. 22(3):453–460.

TABLES

Table 2-1. Masses and estimated resting respiration rates for specimens used in this study.

Taxon	Mass (kg)	Inspiration rate (ml/min)	Expiration rate (ml/min)
Alligator (OUVC 10389)	0.468[a]	173.2[b]	172.7[b]
Turkey (OUVC 10599)	4.94[c]	2832[d]	1560[d]
Ostrich (OUVC 10636)	74[c]	14800[d]	7200[d]
Iguana (OUVC 10603)	0.870[e]	1014[f]	1014[f]
Monitor lizard (OUVC 10675)	1.73[e]	720[g]	720[g]

a = Coulson et al. 1973; b = Farmer & Carrier 2000b; c = Hinds and Calder 1971; d = Frappell et al. 2001; e = direct measurement; f = Scaled from Giordano & Jackson 1973, and incorporation of an estimated 80% NVP; g = Scaled from Hopkins et al. 1995 and incorporation of an estimated 80% NVP

Table 2-2. Reynolds and Womersley numbers for airways of the study taxa.

Taxon	Reynolds Number	Womersley Number
Alligator (OUVC 10389)	8–88	0.08–0.35
Turkey (OUVC 10599)	89–1915	0.12–0.52
Ostrich (OUVC 10636	119–2253	0.24–0.70
Iguana (OUVC 10603)	36–208	0.64–1.5
Monitor lizard (OUVC 10675)	25–175	0.39–2.6

Table 2-3. Grid convergence index results

Soft tissue		
Taxon	**Finest grid (elements)**	**GCI Result**
Alligator	1,825,942	$2.46e^{-4}$
Turkey	2,758,391	2.96
Ostrich	2,147,583	1.32
Iguana	1,627,539	6.41
Monitor lizard	1,495,848	0.38
Bony Bounded		
Taxon	**Finest grid (elements)**	**GCI Result**
Alligator	1,104,782	$9.6e^{-3}$
Turkey	2,600,494	4.8
Ostrich	1,153,120	9.82
Iguana	1,035,088	23.93
Monitor lizard	1,721,400	0.14

Table 2-4. Average radial distance from the center of the air field to the nearest mucosal wall (mm) in the soft-tissue nasal capsules of the study specimens.

Taxon	Vestibulum nasi	Cavum nasi proprium	Ductus nasopharyngeus
Alligator	0.05	0.07	0.08
Turkey	0.71	0.58	0.68
Ostrich	2.12	1.71	1.65
Iguana	1.20	0.80	1.08
Monitor lizard	1.44	1.17	1.45

Table 3-1. Initial cell resolution and final cell resolution from solution-based AMR.

Model	Initial cell resolution	Final (AMR) cell resolution
Wild type	946,441	992,514
A model	939,065	879,000
R model	1,482,662	885,316
AR model	807,671	684,801
M model	1,093,607	1,081,371
C model	1,846,181	1,306,554
MC model	1,098,911	1,085,445
CN model	867,919	300,298

Table 3-2. Nasal passage permutations tested in this study.

Model	Atrial concha	Rostral concha	Middle concha	Caudal concha	Crista nasalis
Wild type	✓	✓	✓	✓	✓
A model	×	✓	✓	✓	✓
R model	✓	×	✓	✓	✓
AR model	×	×	✓	✓	✓
M model	✓	✓	×	✓	✓
C model	✓	✓	✓	×	✓
MC model	✓	✓	×	×	✓
CN model	×	×	×	×	✓
BB model*	×	×	×	×	×

*Model taken from Chapter 2.

Table 3-3. Pressure drop differences between the various permutations of the turkey nasal passage. Pressure information was calculated from area-weighted average surface integrals taken from the choana.

Model	**Δ Pressure (Pa)**
Wild type	17.8
A model	15.1
R model	17.8
AR model	15.5
M model	14.5
C model	21.7
MC model	14.8
CN model	7.2
BB model	3.1

Table 4-1. Taxa used in analysis and associated scan resolutions

Crocodylia		
Taxon	**N**	**Scan resolutions**
Alligator mississippiensis	4	92 µm, 200 µm, 600 µm
Crocodylus siamensis	1	300 µm
Osteolaemus tetraspis	2	90 µm
Aves		
Taxon	**N**	**Scan resolutions**
Morus bassanus	1	90 µm
Buceros sp.	1	90 µm
Calypte anna	3	90 µm
Threskiornithinae	1	400 µm
Phoebastria immutabilis	1	90 µm
Pelacanus sp.	2	400 µm, 600 µm
Columba livia	2	90 µm, 45 µm
Meleagris gallopavo	3	90 µm
Coragyps atratus	2	90 µm, 600 µm
Laridae	1	600 µm
Podicipedidae	1	600 µm
Struthio camelus	5	90 µm
Squamata		
Taxon	**N**	**Scan resolutions**
Anolis cristatellus	2	45 µm
Anolis evermanni	2	45 µm
Gekko gekko	1	45 µm
Iguana iguana	3	90 µm, 600 µm
Varanus exanthematicus	3	90 µm 400 µm
Varanus albigularis	1	500 µm
Varanus niloticus	2	500 µm
Varanus gouldii	2	90 µm, 45 µm
Uromastyx aegyptia	1	90 µm

Table 4-2. Regional volumetric comparisons between ST and BB airways

Taxon	**Airway volumes (ml)**			
Alligator	**Vestibule**	**Cavum nasi proprium**	**Nasopharyngeal duct**	**Global**
ST	0.011	0.558	0.250	$8.2e^{-4}$
BB	0.192	1.166	0.274	$1.4e^{-3}$
Turkey				
ST	0.846	0.410	0.107	2.67
BB	1.257	0.878	0.170	5.75
Ostrich				
ST	8.814	6.148	2.281	33.92
BB	11.291	10.934	4.441	63.58
Iguana				
ST	0.170	0.274	0.214	0.532
BB	0.145	0.796	0.054	0.987
Monitor lizard				
ST	1.105	0.429	0.204	1.74
BB	1.234	1.003	0.314	2.79

Table 5-1. Estimated resting respiratory variables for *Stegoceras validum* based on data from Frappell et al. 2001.

Estimated mass (kg)	**Frequency (breaths/min)**	**Tidal volume (ml)**	**Inspiratory drive (ml/s)**
10	7.64	233	73
40	4.67	1013	169

Table 5-2. Average Reynolds and Womersley numbers across all the nasal capsule morphologies in *Stegoceras validum* under two estimated flow rates. Data range in parentheses.

Mass (kg)	Flow Rate (L/min)	Reynolds number	Womersley number
10	4.4	128 (43–214)	1.2 (0.6–2.2)
40	10	297 (100–496)	0.9 (0.4–1.7)

Table 5-3. Grid Convergence Index (GCI) for the finest grid

Nasal morphology	Converged variable	GCI_{finest} (4.4 L/min)	GCI_{finest} 10 L/min
Bony bounded	ΔP	0.1698	0.149
Paranasal septum	ΔP	1.3087	8.9628
Scrolled turbinate	ΔP	1.0628	1.6692
Branched turbinate	ΔP	1.5421	4.4215
Septum and concha	ΔP	0.045	0.04

Table 5-4. Maximum pressure and velocity magnitudes in different configurations of the nasal capsule at 10 L/min.

Model	Max Pressure (Pa)	Max velocity (m/s)	Resistance (Pa*s/ml)
Bony-bounded	1.807289	1.39497	0.010841566
Paranasal septum	5.419671	2.283075	0.032511524
Scrolled concha	3.001694	1.693192	0.018006563
Branched concha	4.424924	2.286139	0.026544235
Septum + concha	4.108988	2.14766	0.024648998

Table 6-1. Respiratory values for the ankylosaurs *Panoplosaurus mirus* and *Euoplocephalus tutus.*

Taxon	Mass (kg)*	Tidal volume (ml)†	Breathing frequency†	High flow rate†	Low flow rate‡
Panoplosaurus	1100	34,000	1.5 breaths/min	77 L/min	37 L/min
Euoplocephalus	2000	64,000	1.2 breaths/min)	110 L/min	48 L/min

*Brown et al. 2013 supplementary table. †Frappell et al. 2001 table 2. ‡Reversed-Reynolds equation: $Q = \frac{2000(Pv)}{4}$. See methods for explanation of variable abbreviations.

Table 6-2. Core body temperatures recorded for a variety of large, terrestrial amniotes

Taxon	Body Temperature (°C)	Reference
African elephant (*Loxodonta Africana*)	36.2–36.6	Kinahan et al. 2007; Phillips & Heath 1995
Asian elephant (*Elephas maximus*)	35.7–36.8	Weissenbock et al. 2011; Rowe et al. 2013
Black rhinoceros (*Diceros bicornis*)	31.8–41.9	Langman 1985; Kock et al. 1990
White rhinoceros (*Ceratotherium simum*)	33.6–37.5	Harthoorn et al. 1958; Citino and Bush 2006
Masai giraffe (*Giraffa camelopardalis*)	35.7–39.1	Bligh and Hathoorn 1965; Langman et al. 1979, 1982
Grizzly bear (*Ursus arctos*)	36.5–38.5	Schwartz et al. 2003
Emu (*Dromaius novaehollandiae*)	37.4–39.2	Prinzinger et al. 1991; Maloney and Dawson 1993
Ostrich (*Struthio camelus*)	38.0–40.2	Bligh and Hartley 1965; Prinzinger et al. 1991
Galapagos tortoise (*Chelonoidis nigra*)	28–31	Mackay 1964
Komodo dragon (*Varanus komodoensis*)	36–40	McNab and Auffenberg 1976

Temperature data comes from rectal/cloacal measurements or from telemetry data.

Table 6-3. Comparison of values for heat transfer in domestic pigeons (*Columba livia*) between experimental data from Geist (2000) and simulation (this study).

Study	Mass (g)	Body temp (°C)	Ambient air (°C)	Oral temp (°C)	Exhaled temp (°C)
Geist 2000	319 (+/- 45.2)	40.7	15	38.2 +/- 0.5	21.4 +/- 0.5
This study	455	40.7	15	38	21.6

Table 6-4. Energetic cost of heating one bolus of air by 20°C at 50% relative humidity for *Panoplosaurus mirus* and *Euoplocephalus tutus.*

Taxon	Tidal volume (ml)	Mass of air (g)	Cost of heating air 20°C (cal)	Latent heat of evaporation (cal)	Total energy cost (cal)
P. mirus	34000	39	187	646	833
E. tutus	64000	73	350	1218	1568

Table 6-5. Energy savings from reducing expired air temperature in all airway models for *Panoplosaurus mirus.*

Model	Expired temp (°C)	Heat savings (cal)	Latent heat of condensation (cal)	Total energy recovered (cal)
BB airway (high)	22.67	115	392	507
BB airway (low)	20.46	136	441	577
ST airway (high)	21.57	126	419	545
ST airway (low)	19.48	145	460	605
Basic airway	26.5	79.5	294	374
Straightened airway	23.93	103	363	466

Table 6-6. Table 6. Energy savings from reducing expired air temperature in all airway models for *Euoplocephalus tutus*.

Model	Expired temp (°C)	Heat savings (cal)	Latent heat of condensation (cal)	Total energy recovered (cal)
BB airway (high)	21.11	244	803	1047
BB airway (low)	19.42	274	868	1142
ST airway (high)	17.34	311	934	1245
ST airway (low)	15.87	337	980	1317
Basic airway	30.3	83	335	418
Straightened airway	22.77	214	738	952

FIGURES

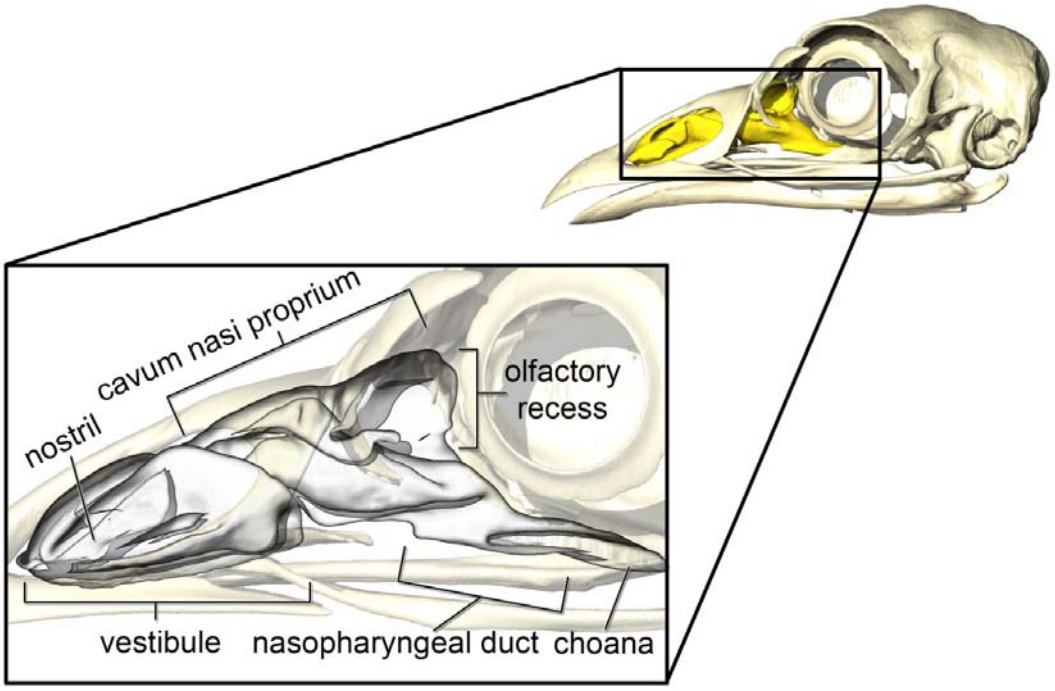

Figure 1-1.Basic anatomy of the nasal passage as shown in a turkey (*Meleagris gallopavo*, OUVC 10599).

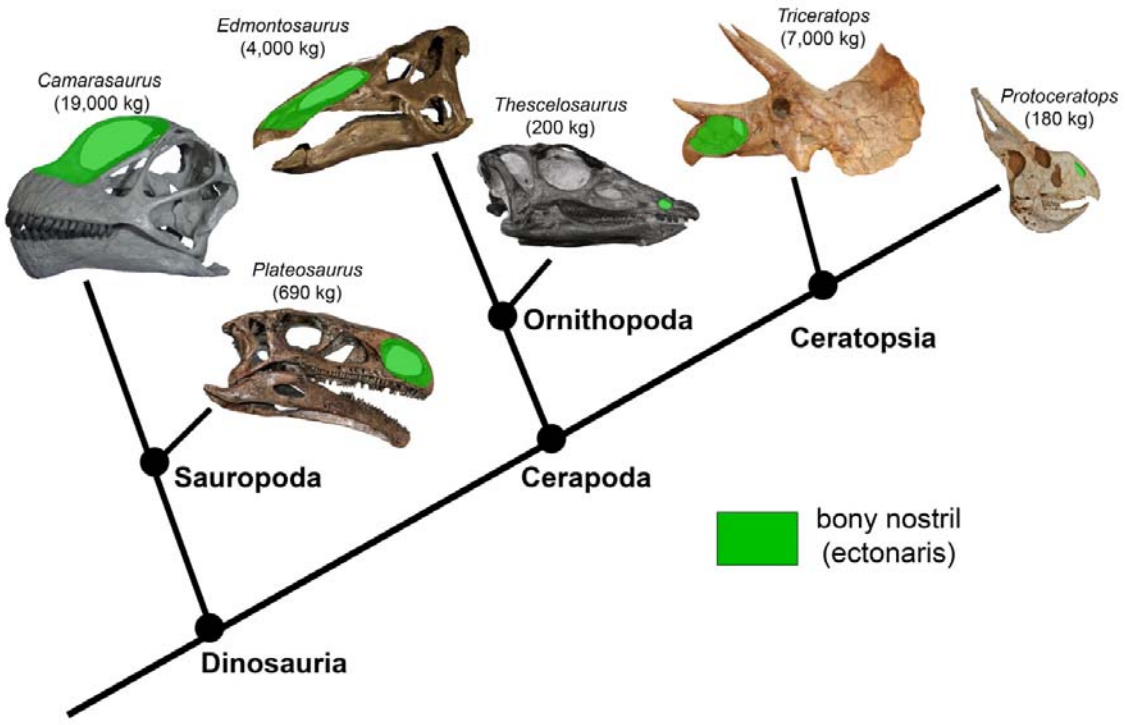

Figure 1-2. Nasal passage elaboration in various dinosaur taxa (as shown by size of ectonaris). Each lineage contained basal members with small body size (< 1 tonne) and concomitantly small nasal passages. Each lineage shows allometric increase in the size of the rostral nasal passage (nasal vestibule) as body mass increases.

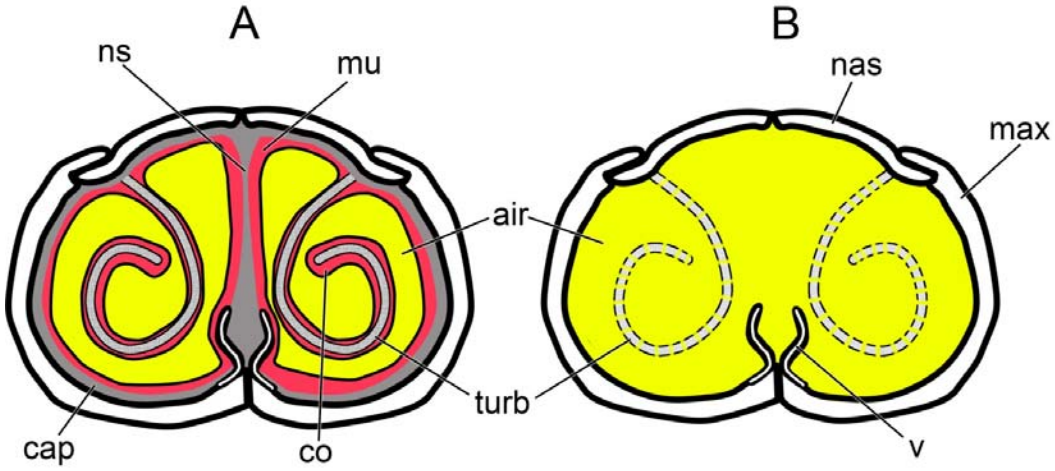

Figure 1-3. Axial cross section of a generic diapsid nasal passage showcasing the differences in airway morphology between soft tissues (A) and the bony-bounded airways typically preserved in the fossil record (B). Dashed lines are used for turbinates to represent the delicate nature of the structures, which affects their preservation. air, airway; cap, cartilaginous nasal capsule; co; mucocartilaginous concha; max, maxilla; mu, mucosa; nas, nasal; ns, nasal septum; turb, nasal turbinate; v, vomer.

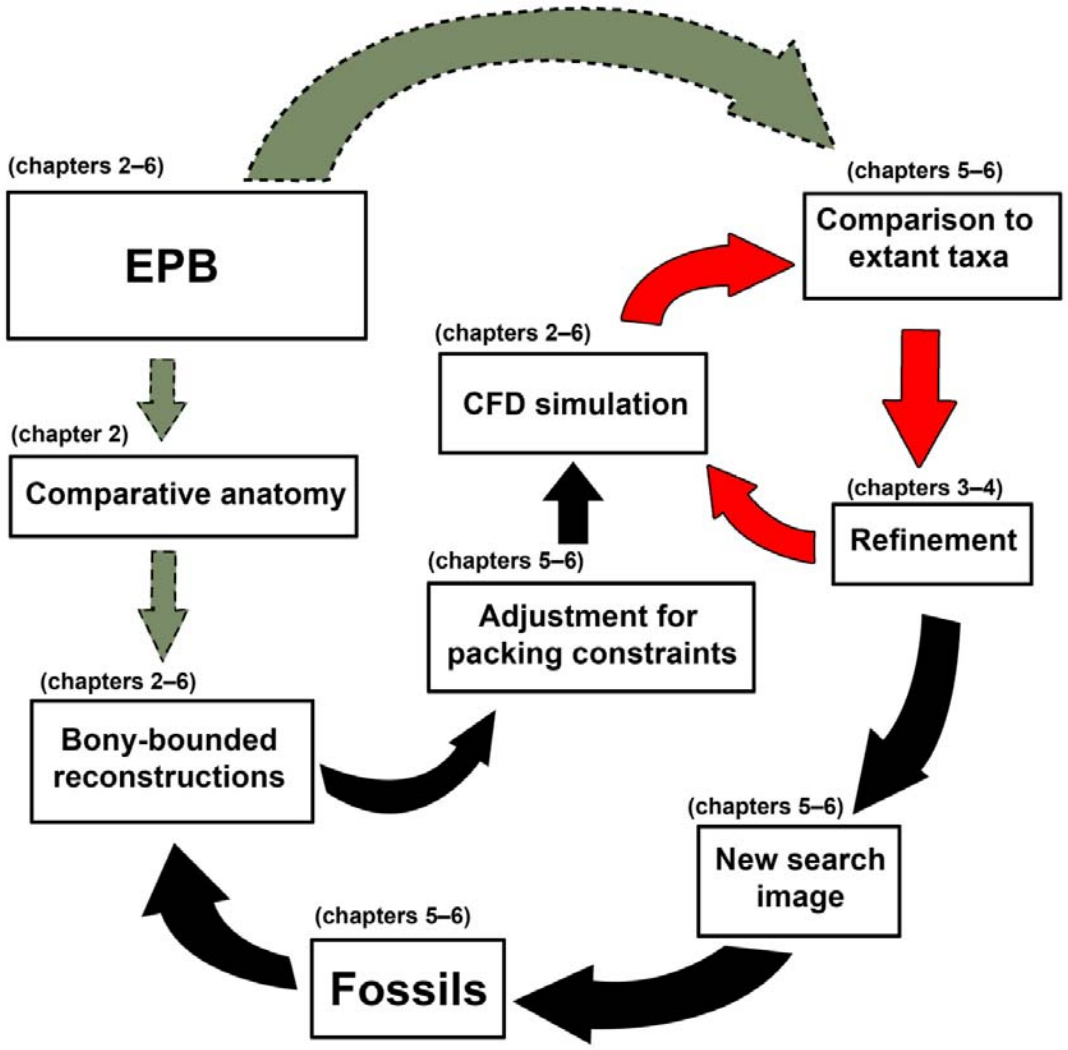

Figure 1-4.Workflow for soft-tissue reconstruction in extinct animals. Starting with fossils, a bony-bounded (BB) nasal passage is constructed using data obtained from comparative anatomy under the umbrella of the EPB (grey arrows). BB airways are adjusted to account for the presence of other soft tissues sharing the same space (e.g., neurovasculature, glands, and even muscles). Adjusted BB airways then undergo a CFD analysis. Flow results for the BB airways are compared to CFD results from extant, soft-tissue airways (ST). Disconnects in fluid patterns between the BB and ST airways get highlighted for refinement. This process is repeated (red arrows) until results of the BB airway more closely reflect what is seen in the ST airway. Refined airways provide new search images that can be taken back to the fossils to look for evidence of these soft tissues. Relevant chapters for each step in the workflow have been highlighted (parentheses).

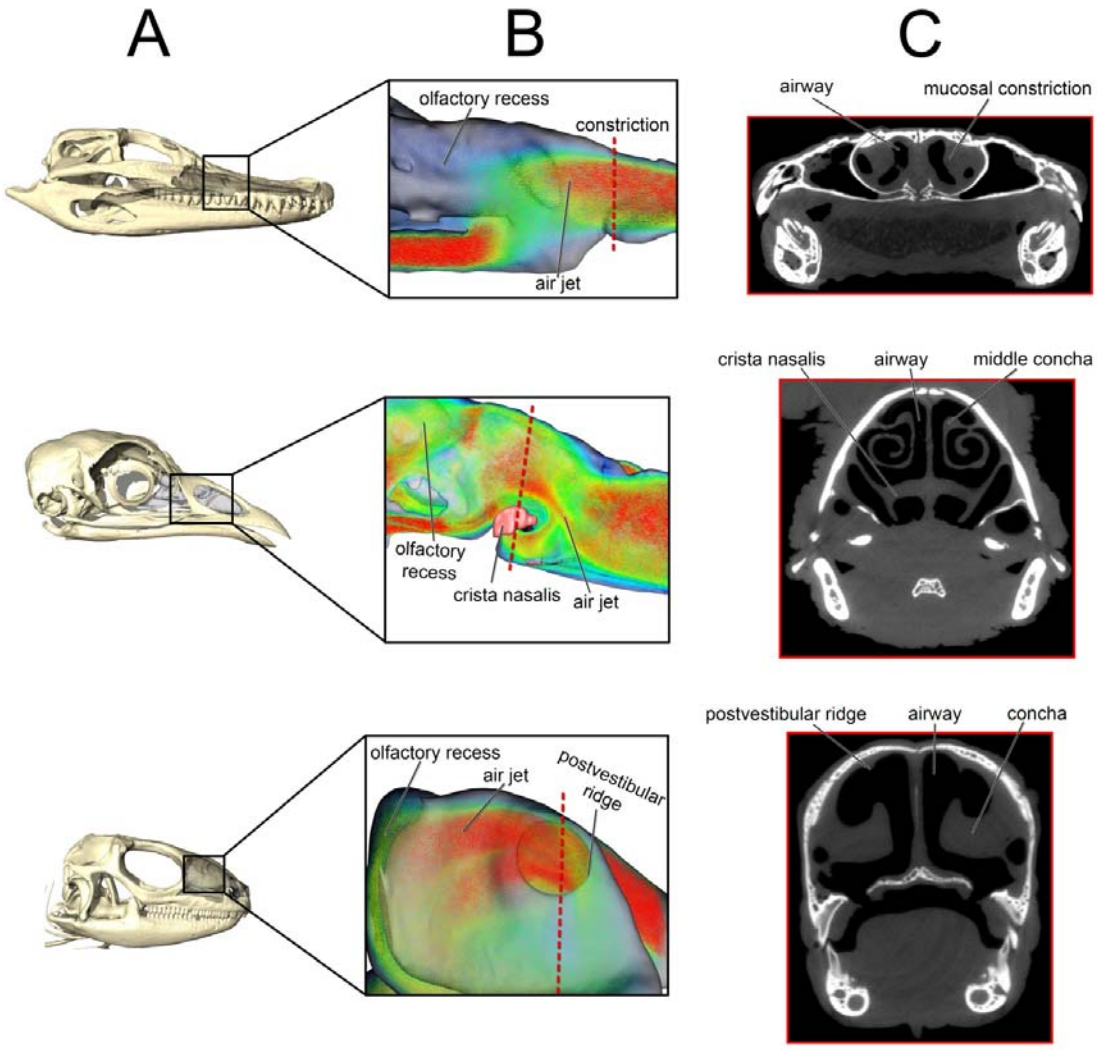

Figure 1-5. CFD models of the nasal passages in extant diapsids showing locations of nasal constrictions that aid airflow through the nose. (A) Skulls of an American alligator (*Alligator mississippiensis*, OUVC 10389, top), wild turkey (*Meleagris gallopavo*, OUVC 10599, middle), and green iguana (*Iguana iguana*, OUVC 10603, bottom) with their in situ, left nasal passages shown in medial view. (B) Focused regions of the nasal passage showing a vector plot of the air field during resting inspiration. The vector plot is color coded for velocity, with higher velocities represented by hotter colors. Red dashed line indicates the location of (C) axial CT slices showing the soft-tissue constrictions labeled in B.

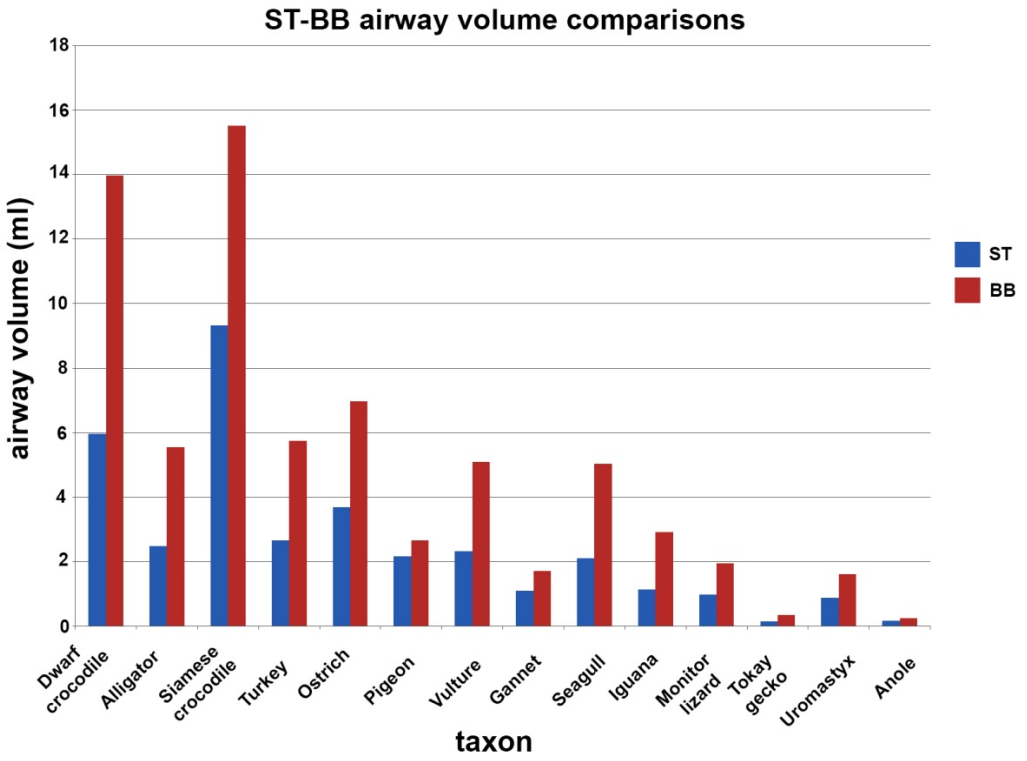

Figure 1-6. Graph of soft-tissue (ST) and bony-bounded (BB) airway volumes for a variety of extant diapsids.

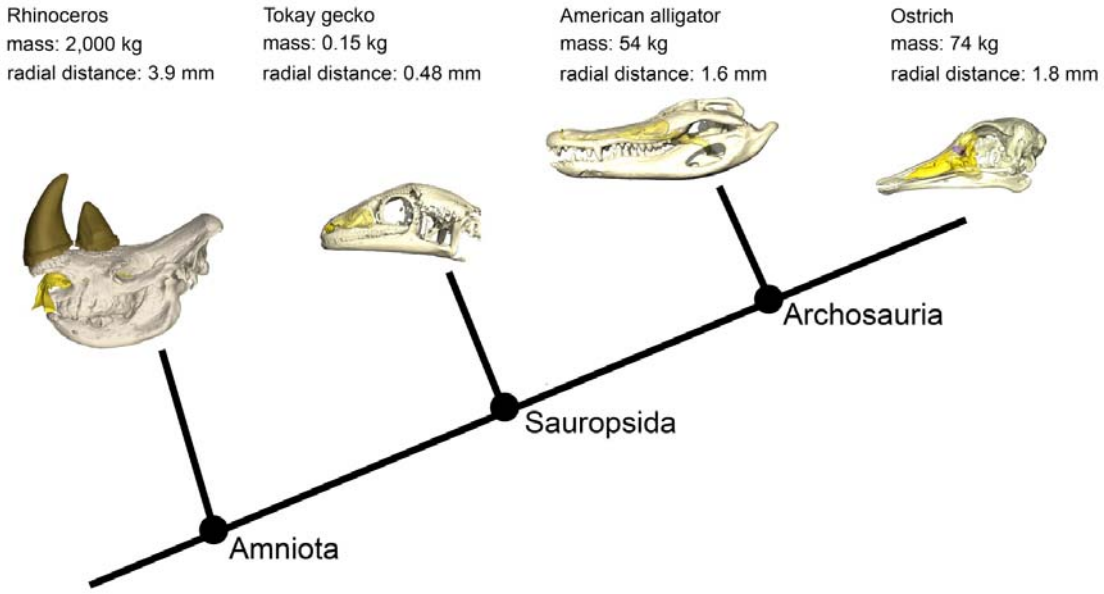

Figure 1-7. Cladogram showing similarity of radial airway distances within the nasal passages of various amniote species varying in size across four orders of magnitude. Radial distance numbers are averages taken throughout the nasal passage.

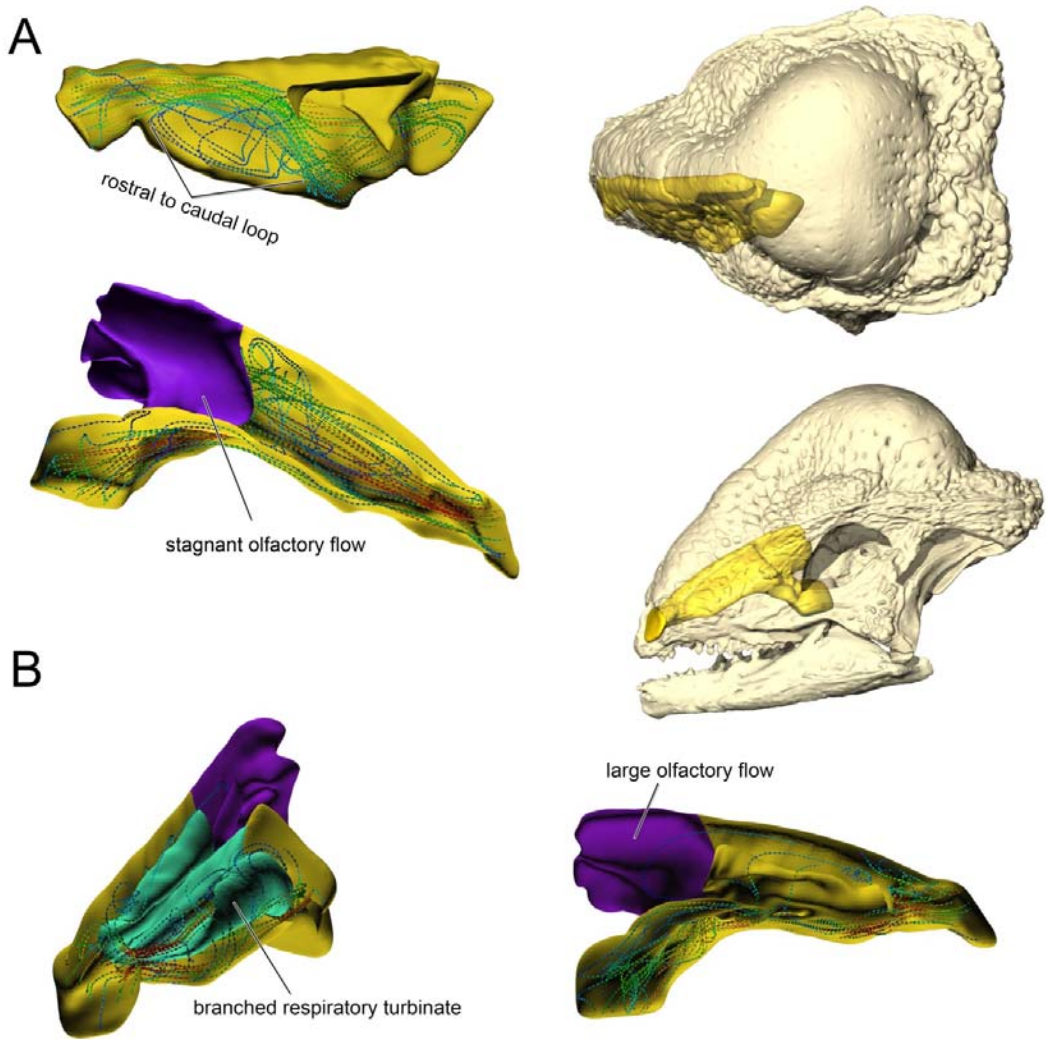

Figure 1-8. Airflow through the left nasal passage of *Stegoceras validum* (UALVP-2). (A) Airflow through the bony-bounded (BB) nasal passage during inspiration. BB airway shown in dorsal (top) and medial (bottom) views. (B) Airflow through the nasal airway model featuring a branched nasal turbinate. Nasal passage shown in left rostrolateral view (left) and left medial view (right).

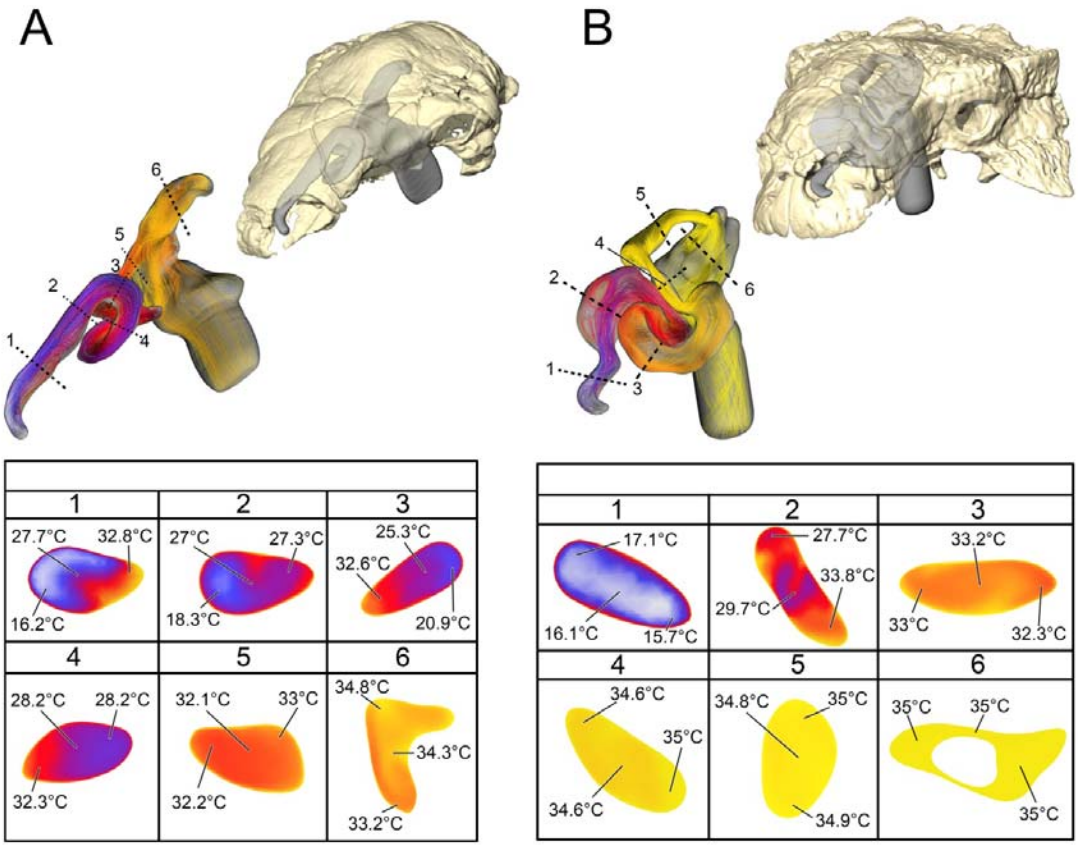

Figure 1-9. Heat transfer within the soft-tissue corrected nasal passages of the ankylosaurs (A) *Panoplosaurus mirus* and (B) *Euoplocephalus tutus*. Cross sections were taken from comparable regions of both nasal passages. Note the slightly higher temperatures per region in *Euoplocephalus* vs. *Panoplosaurus*.

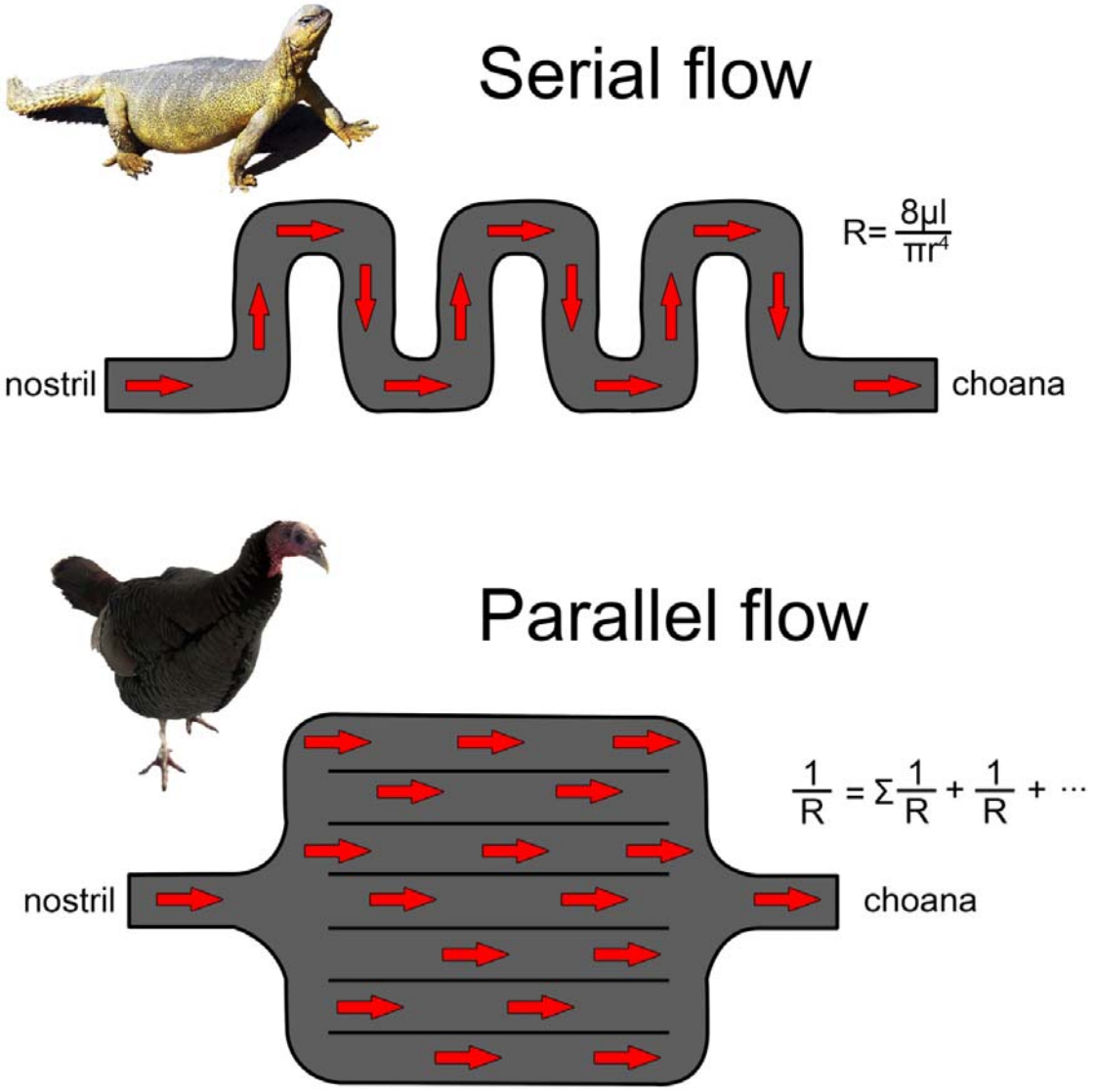

Figure 1-10. Visual comparisons of two different means of conditioning respired air. Serially-aligned nasal passages are comprised of a single, elongate and contorted nasal vestibule such as those found in lizards such as mastigures (*Uromastyx*). Parallel-aligned nasal passages are comprised of a large space within the nasal passage, partitioned into multiple smaller spaces via respiratory turbinates such as those in turkeys (*Meleagris*). Both evolutionary approaches offer different benefits and drawbacks (see text) Mastigure photo by Kathleen A. Hoard. Turkey photo by Jona Thunder.

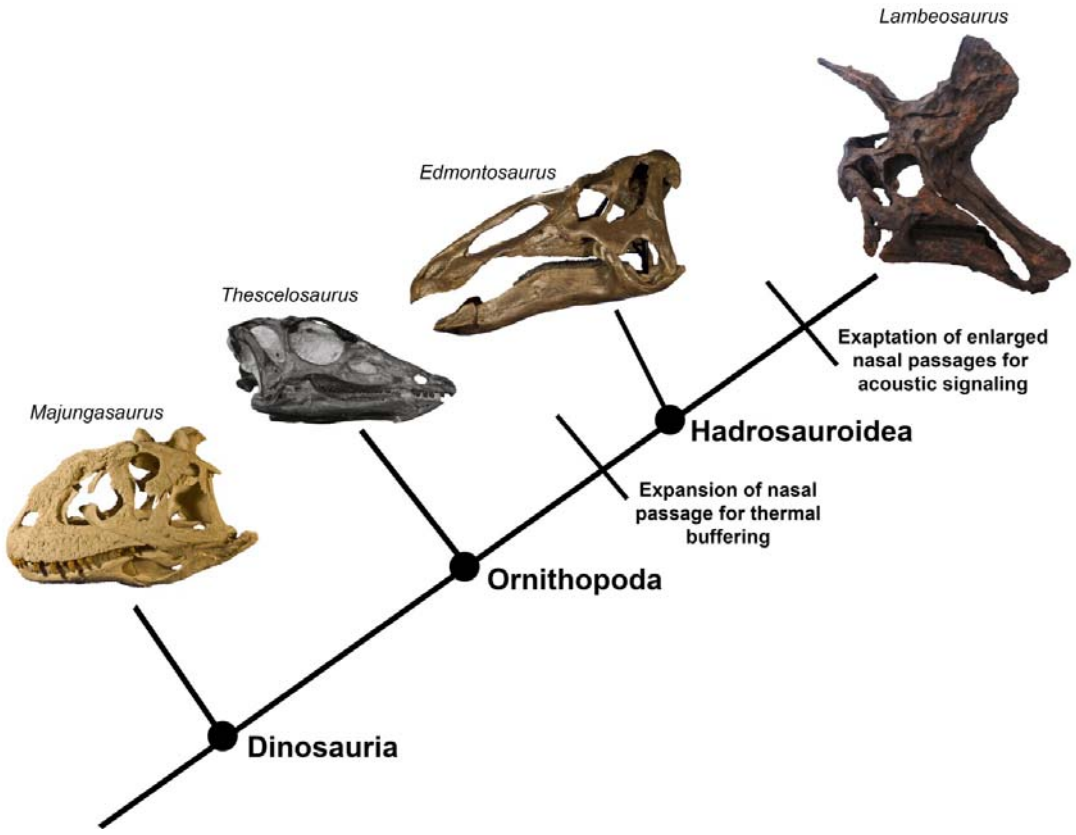

Figure 1-11. Potential evolutionary scenario for the enlarged nasal crests in lambeosaurine hadrosaurs.

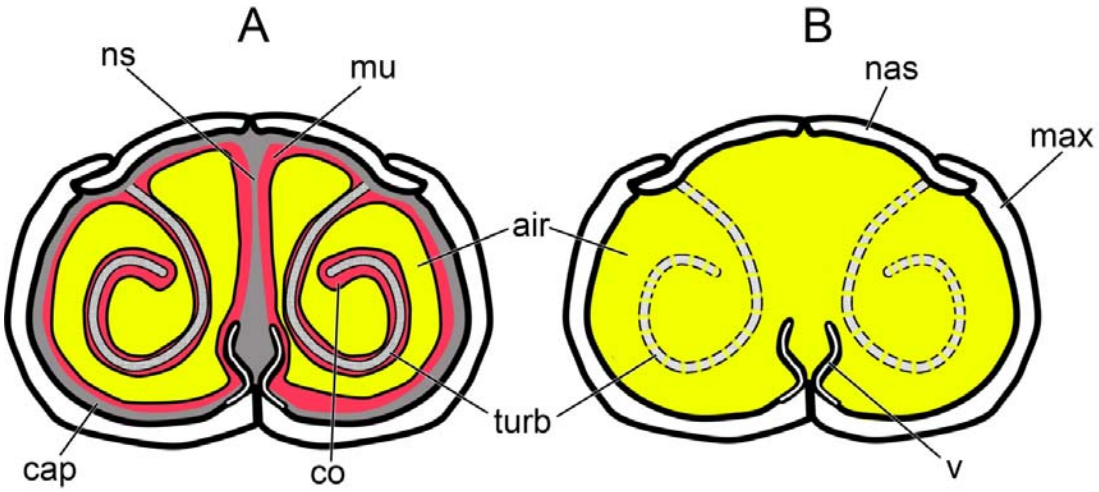

Figure 2-1.Comparisons of soft-tissue (A) and bony-bounded (B) nasal passages in a generalized diapsid nasal cavity. Much of the geometry of the nasal passage is formed from soft-tissue structures that rarely fossilize. Even mineralized structures such as nasal turbinates, may be lost to fossilization due to their fragile construction.

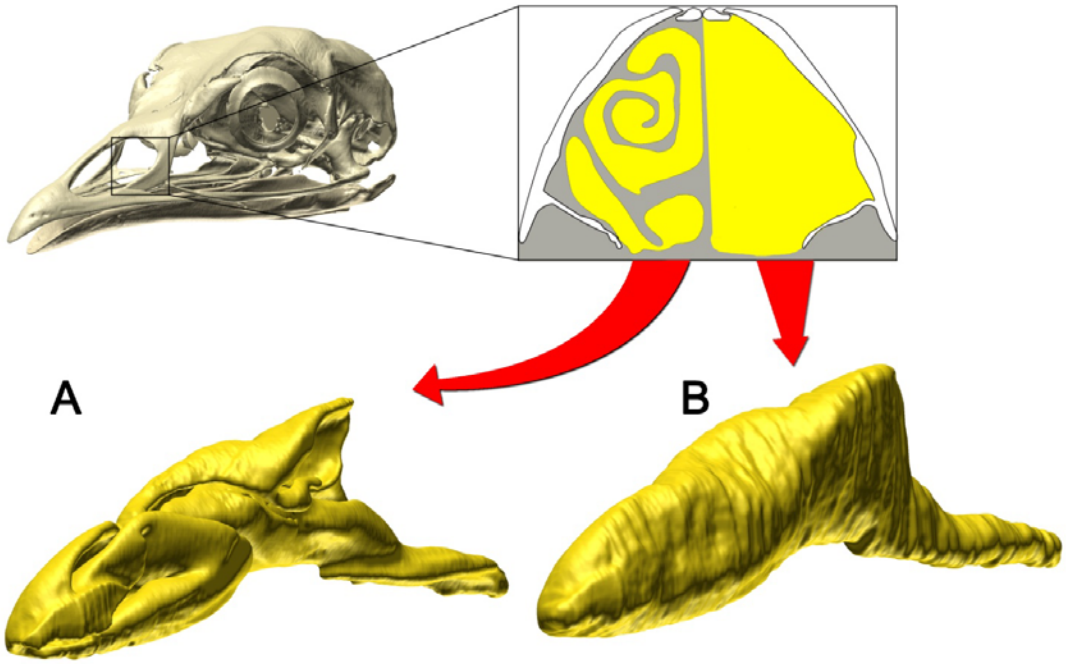

Figure 2-2. Example of airway segmentation based on that of a wild turkey (*Meleagris gallopavo*, OUVC 10599). Heads are CT scanned and these data are used to segment out the airway based on either its soft-tissue (A) or bony boundaries (B).

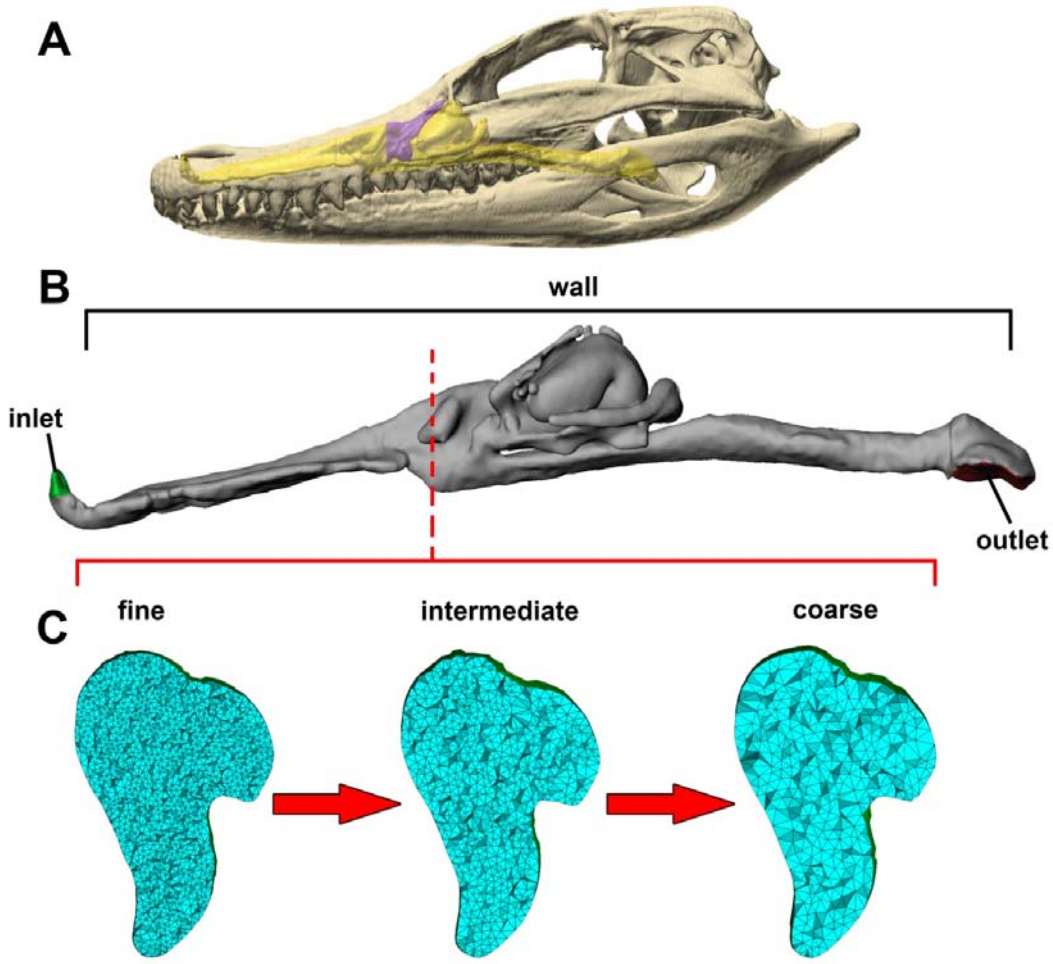

Figure 2-3. Example of workflow using (A) the skull of an American alligator (*Alligator mississippiensis*, OUVC 10389). Segmented airways were assigned a series of boundary conditions (B) prior to tetrahedral conversion. Three different model resolutions (C), coarse (321 thousand elements), intermediate (766 thousand elements), and fine (1.8 million elements), were created to test for grid independence.

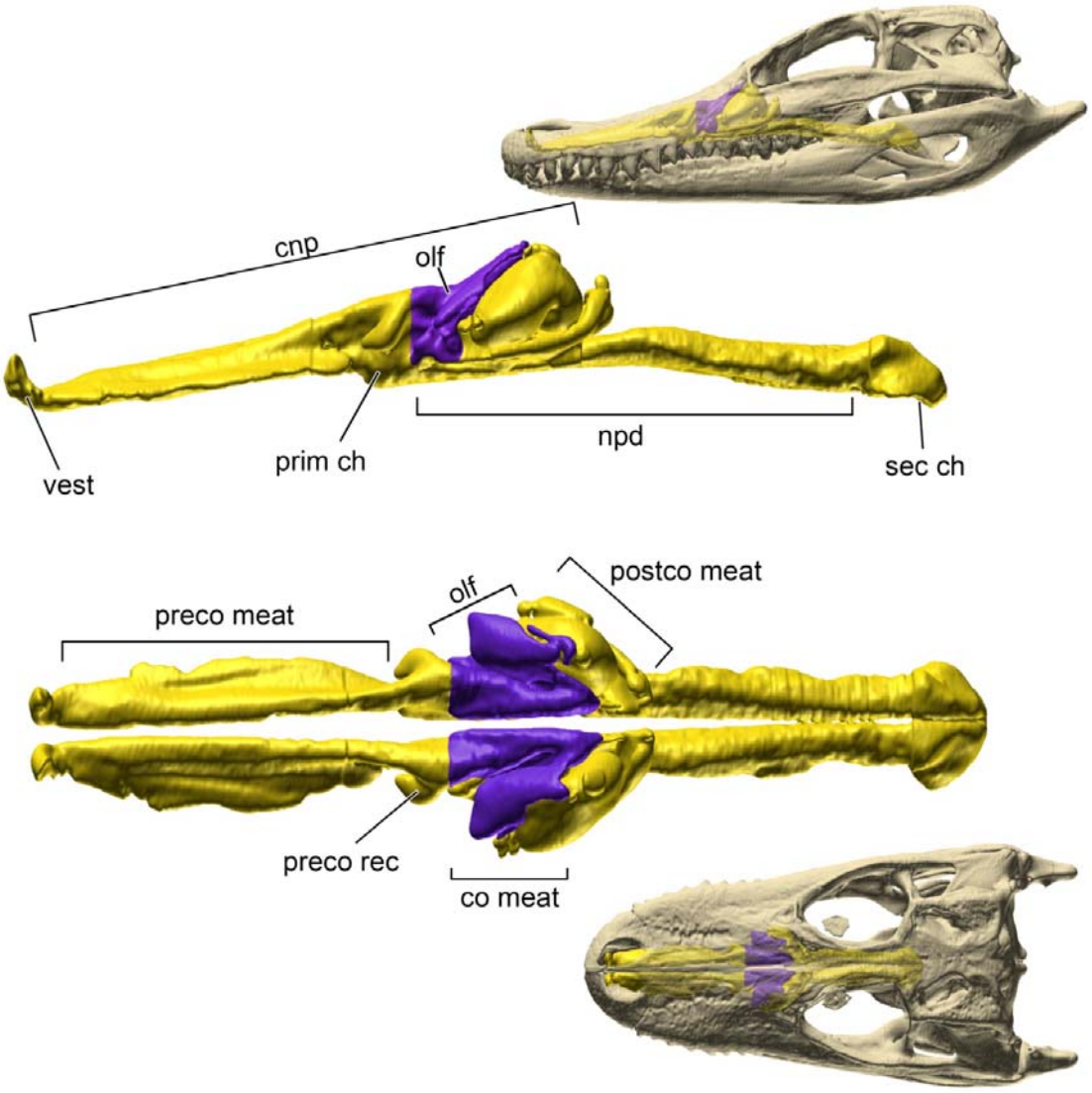

Figure 2-4. Morphology of the airway in an American alligator (*Alligator mississippiensis,* OUVC 10389). Top: Left airway in lateral view. Bottom: Complete airway in dorsal view.

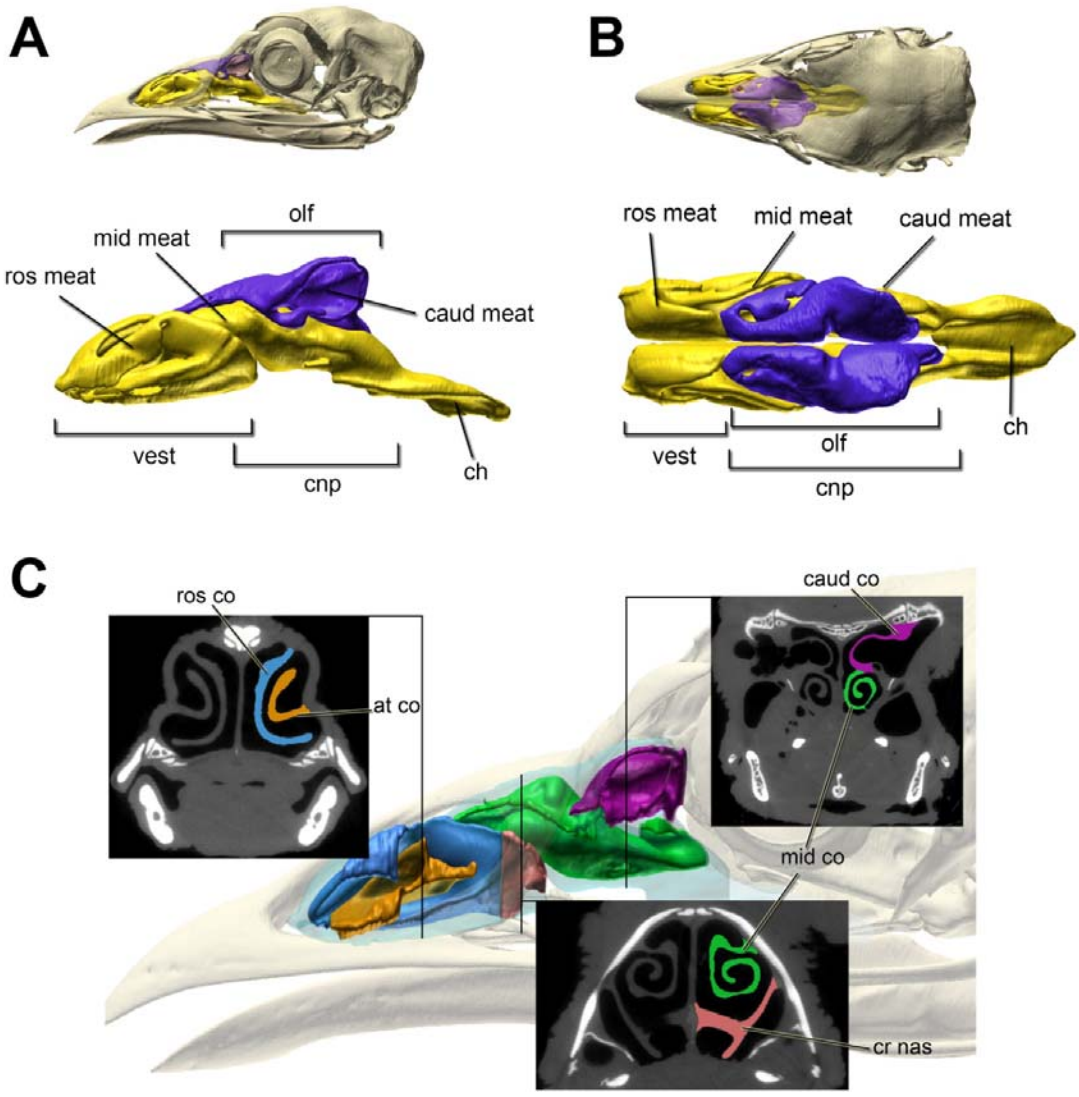

Figure 2-5. Morphology of the airway in a turkey (*Meleagris gallopavo,* OUVC 10599). (A) Left airway in lateral view. (B) Nasal capsule in dorsal view. (C) Cross sections highlight the locations and shape of the various conchae within the nasal capsule.

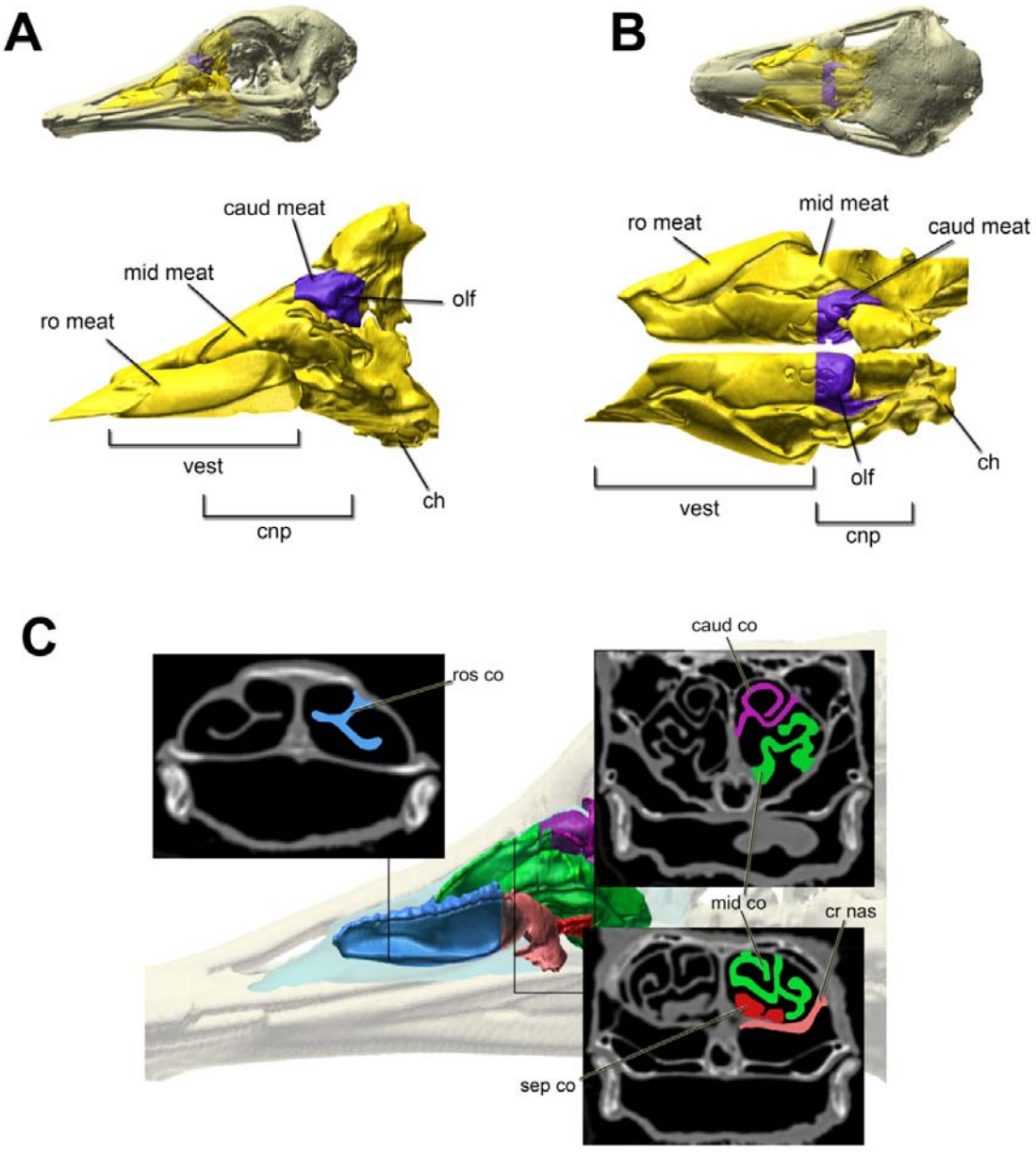

Figure 2-6. Morphology of the airway in an ostrich (*Struthio camelus,* OUVC 10636). (A) Left airway in lateral view. (B) Nasal capsule in dorsal view. (C) Cross sections highlight the locations and shape of the various conchae within the nasal capsule.

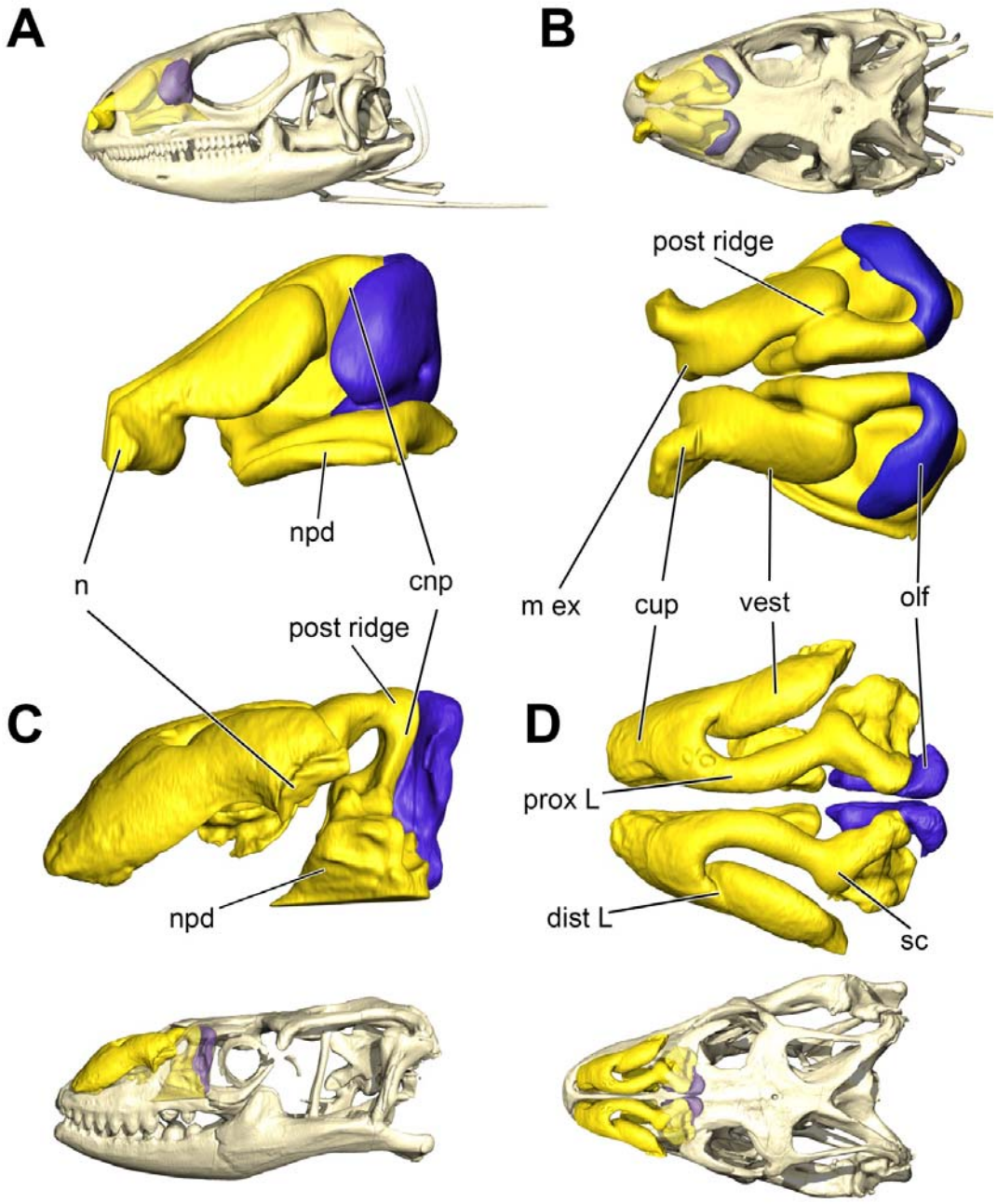

Figure 2-7. Airway morphologies of an iguana (*Iguana iguana,* OUVC 10603, A–B), and savannah monitor (*Varanus exanthematicus*, OUVC 10675, C–D). A, C: Nasal capsules in left lateral view. B, D: Nasal capsules in dorsal view. Savannah monitor skull and airway in C have been mirrored so that the right airway aligns with the left airway of the iguana.

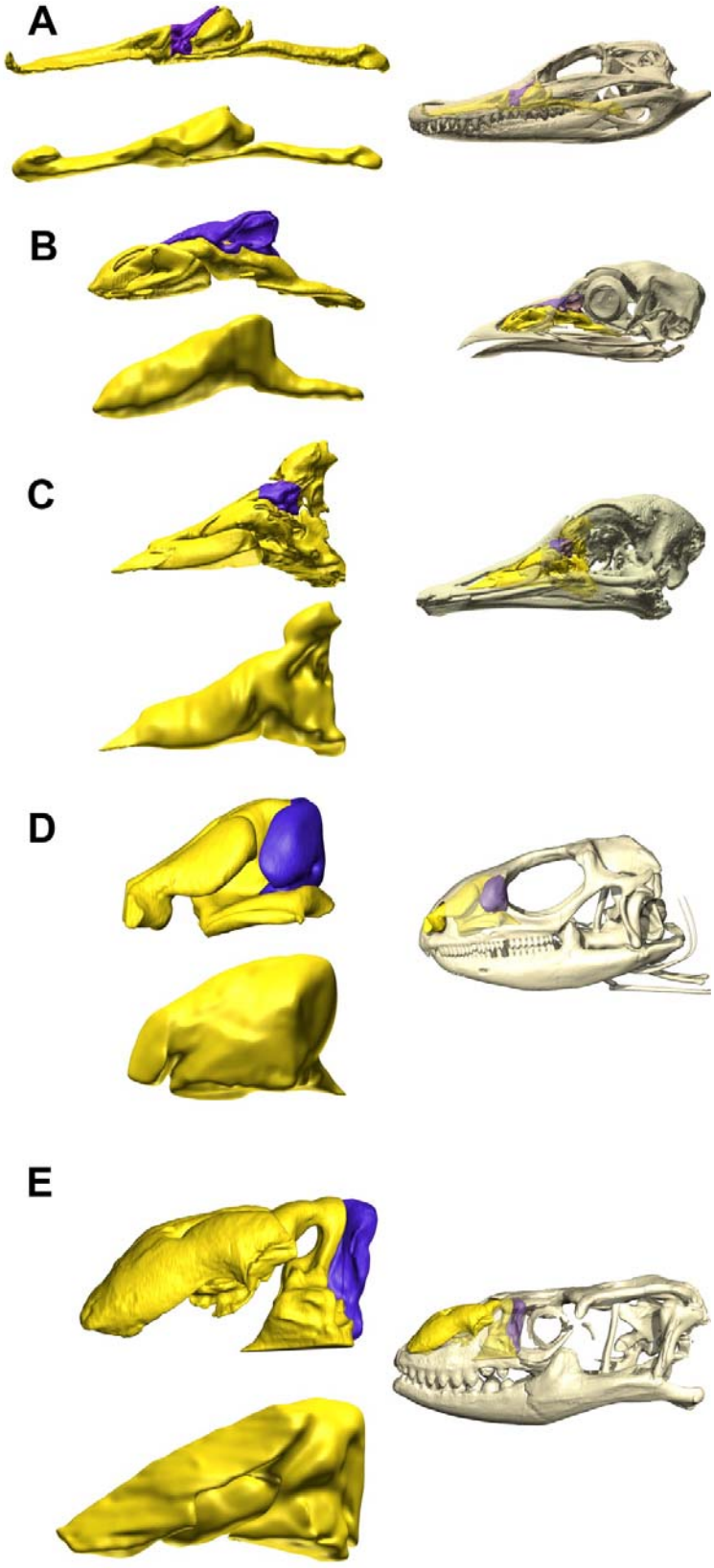
A
B
C
D
E

Figure 2-8. Soft-tissue (top) and bony-bounded (bottom) airways of study taxa. (A) alligator (*Alligator mississippiensis*, OUVC 10389), (B) turkey (*Meleagris gallopavo*, OUVC 10599), (C) ostrich (*Struthio camelus,* OUVC 10636), (D) iguana (*Iguana iguana*, OUVC 10603), and (E) monitor lizard (*Varanus exanthematicus*, OUVC 10675).

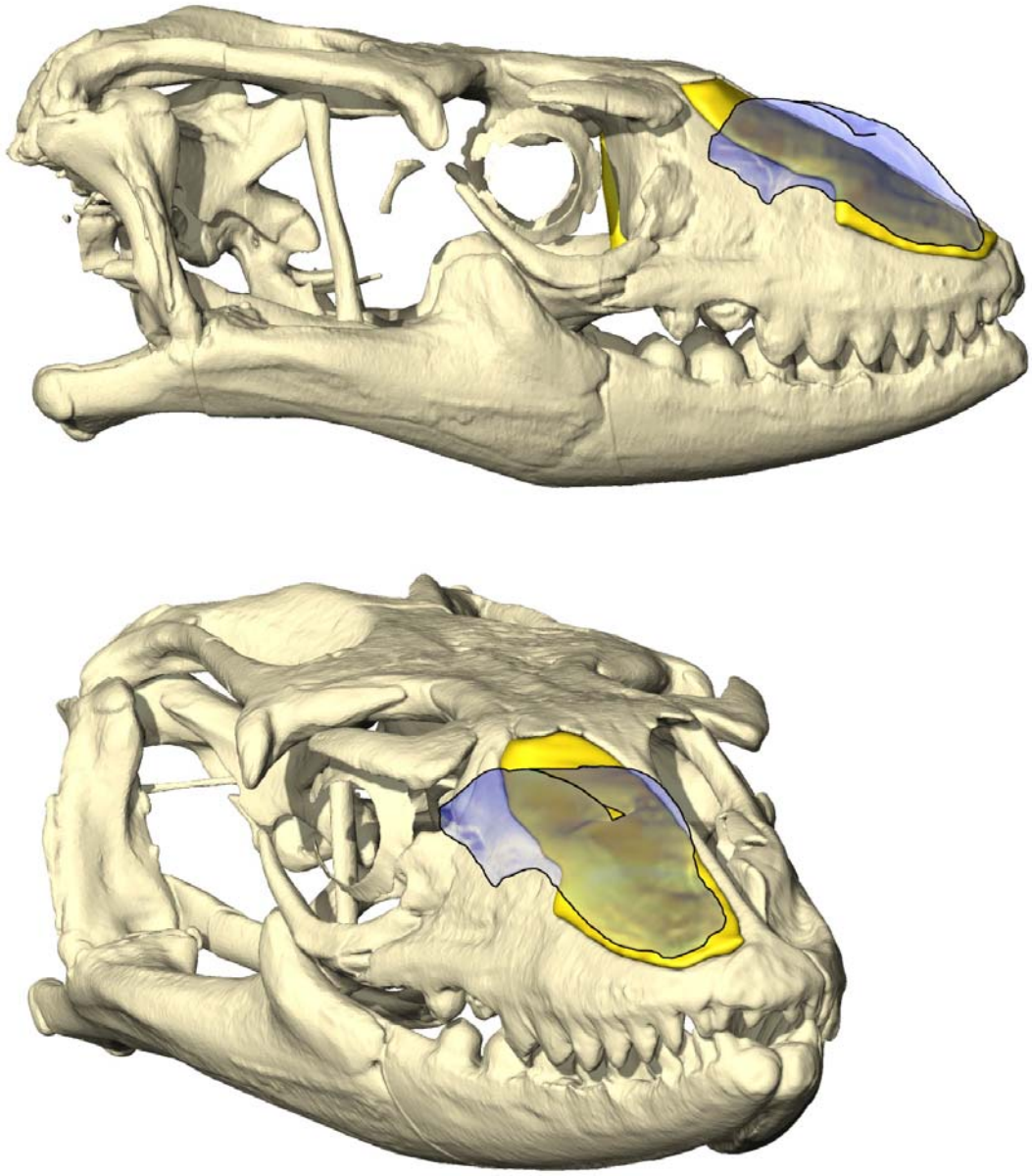

Figure 2-9. Savannah monitor (*Varanus exanthematicus*, OUVC 10675) skull with soft-tissue and bony-bounded airways in life position. Large portions of the soft-tissue vestibulum nasi (transparent outline) extended beyond the limits of the bony-bounded airway.

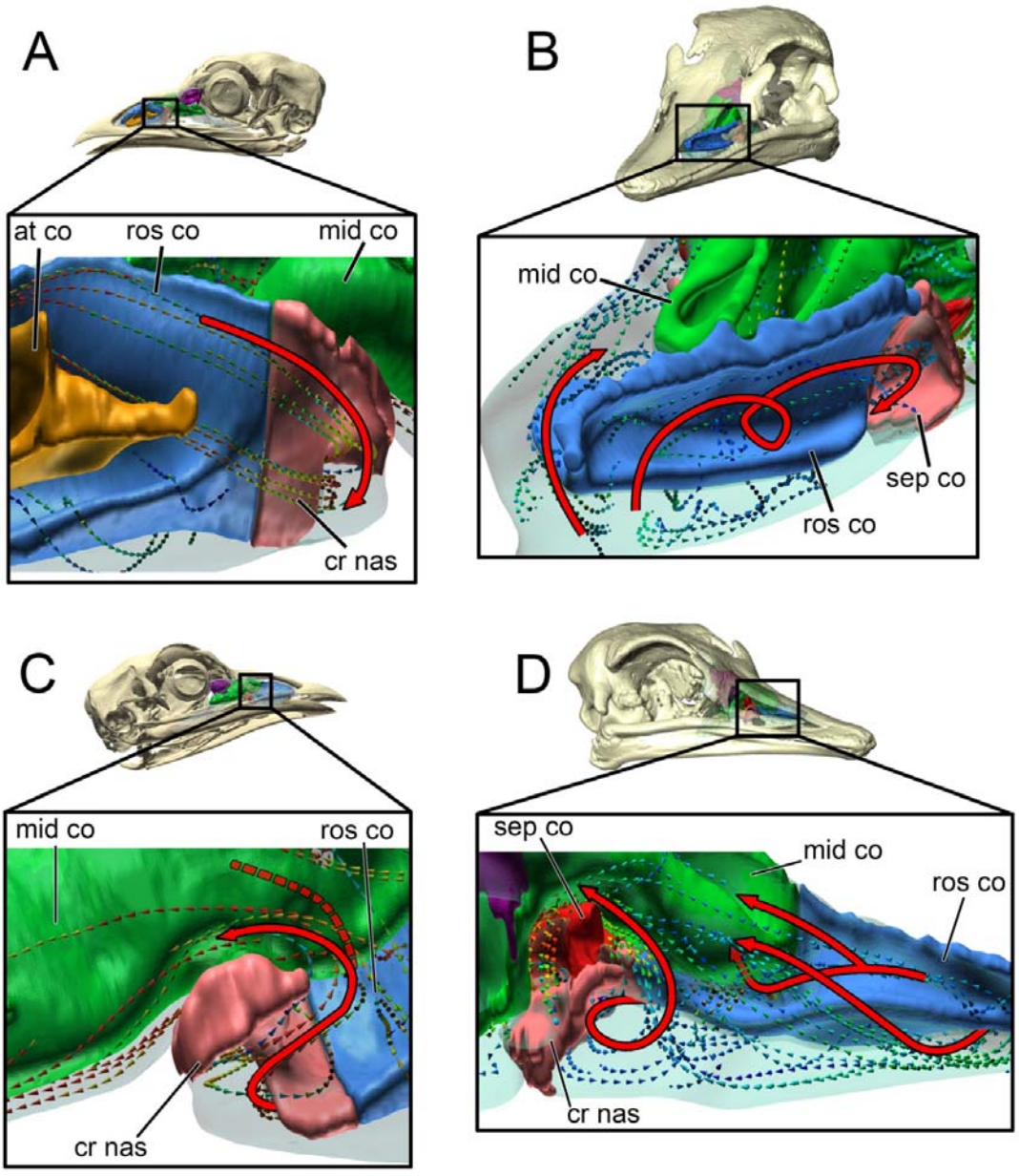

Figure 2-10. Inspiratory airflow through the vestibulum nasi of a turkey (*Meleagris gallopavo,* OUVC 10599, A, C) and an ostrich (*Struthio camelus,* OUVC 10636, B,D). (A) Lateral view of vestibulum nasi in turkey. (B) Rostrolateral view of inspiratory airflow through vestibulum nasi in an ostrich. (C) Ventromedial view of inspiratory airflow in the vestibulum nasi of a turkey. (D) Medial view of airflow in the vestibulum nasi of an ostrich.

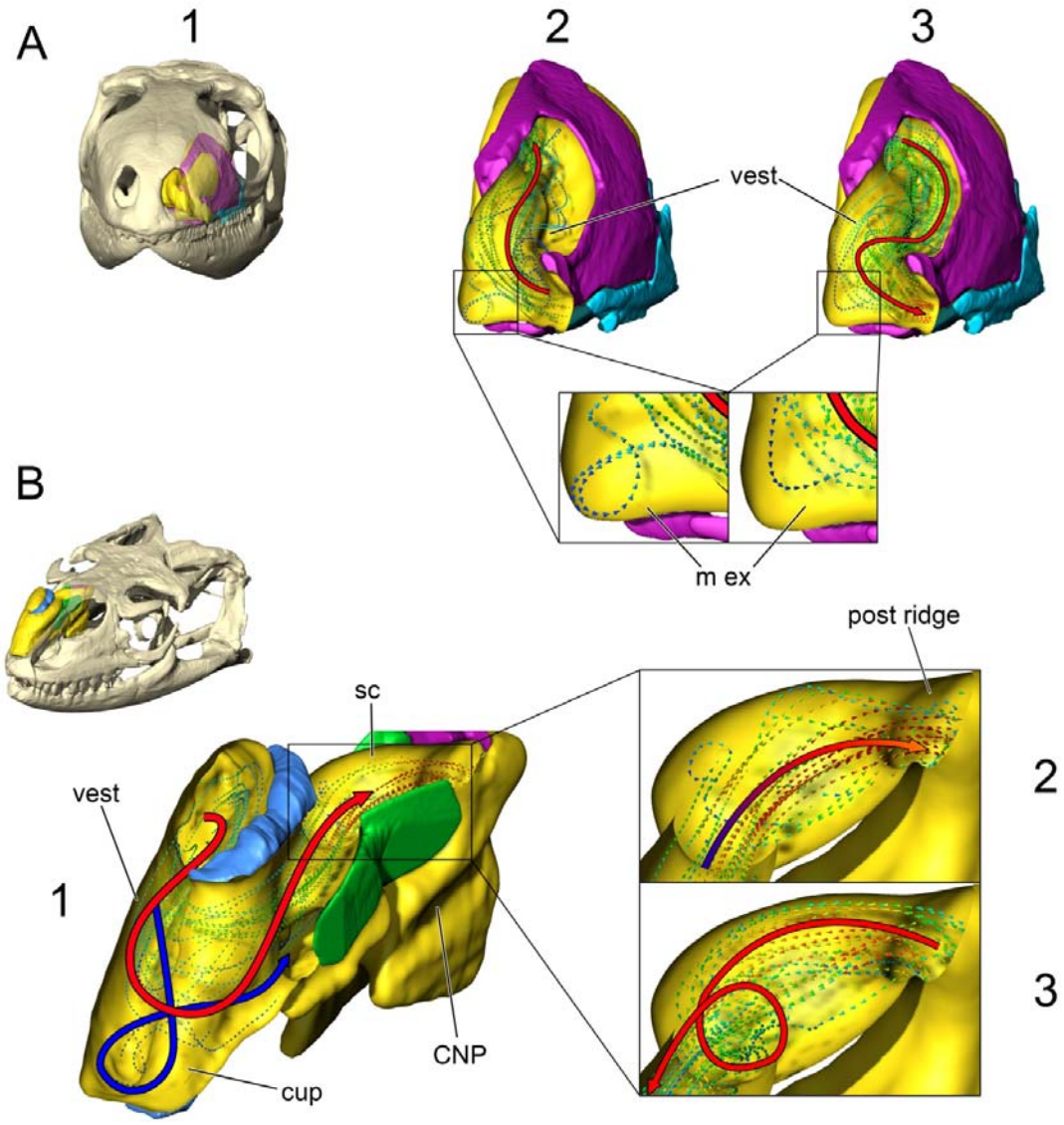

Figure 2-11. Airflow in the vestibulum nasi of both squamates. (A1) Iguana (*Iguana iguana*, OUVC 10603) skull with in situ nasal capsule. (A2) Airflow during inspiration. (A3) Airflow during expiration. (A inset): close up of the medial expansion in the iguana during inspiration (left) and expiration (right). (B1) Nasal capsule of monitor lizard (*Varanus exanthematicus*, OUVC 10675) showing airflow during inspiration. Arrows are color-coded for velocity. Warmer colors indicate faster moving air. (B2) Close up of rounded expansion at terminus of vestibulum nasi during inspiration and (B3) during expiration.

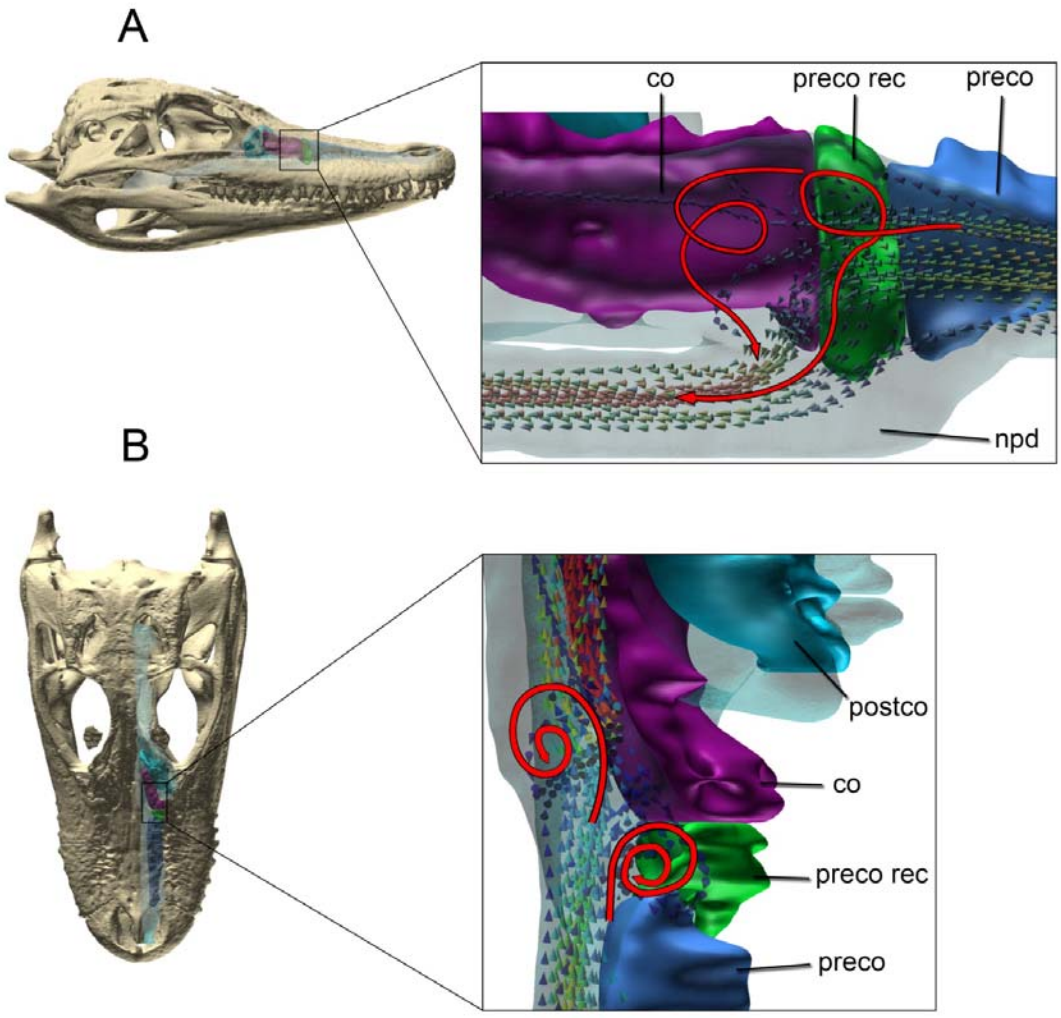

Figure 2-12. Inspiratory airflow through the CNP of the alligator (*Alligator mississippiensis*, OUVC 10389). Medial (A) and dorsal (B) views of air streams as they entered the junction of the primary choana and the olfactory chamber.

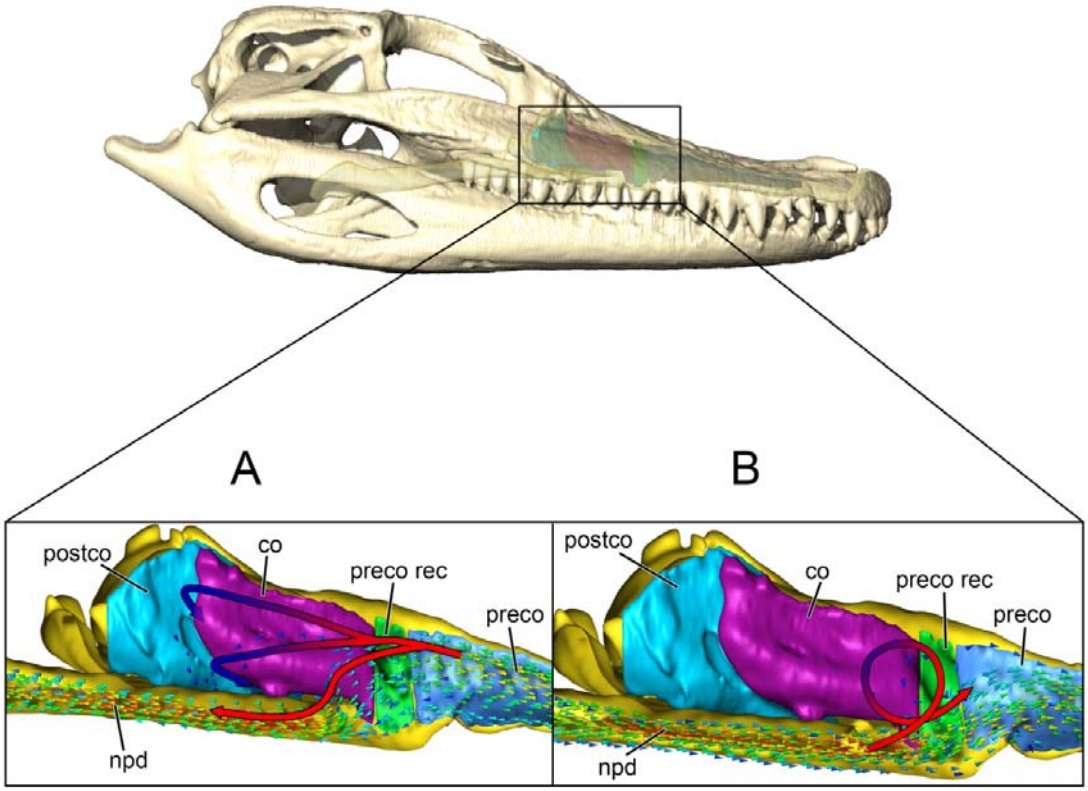

Figure 2-13. Olfactory flow in the alligator (*Alligator mississippiensis*, OUVC 10389) during inspiration (A) and expiration (B).

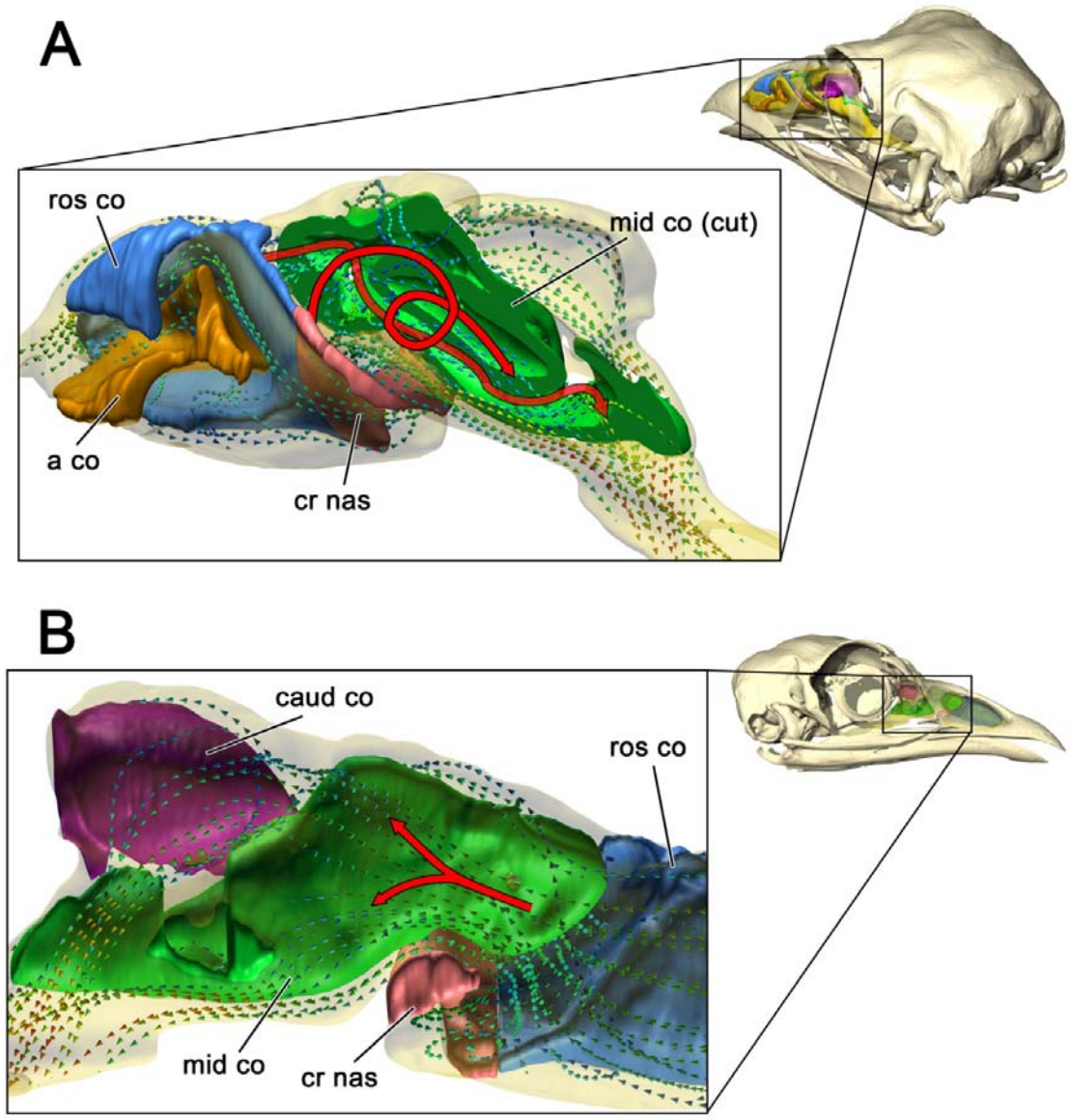

Figure 2-14. Airflow through the middle concha of a turkey (*Meleagris gallopavo*, OUVC 10599) during inspiration. (A) caudolateral view of airway. (B) Medial view of airway.

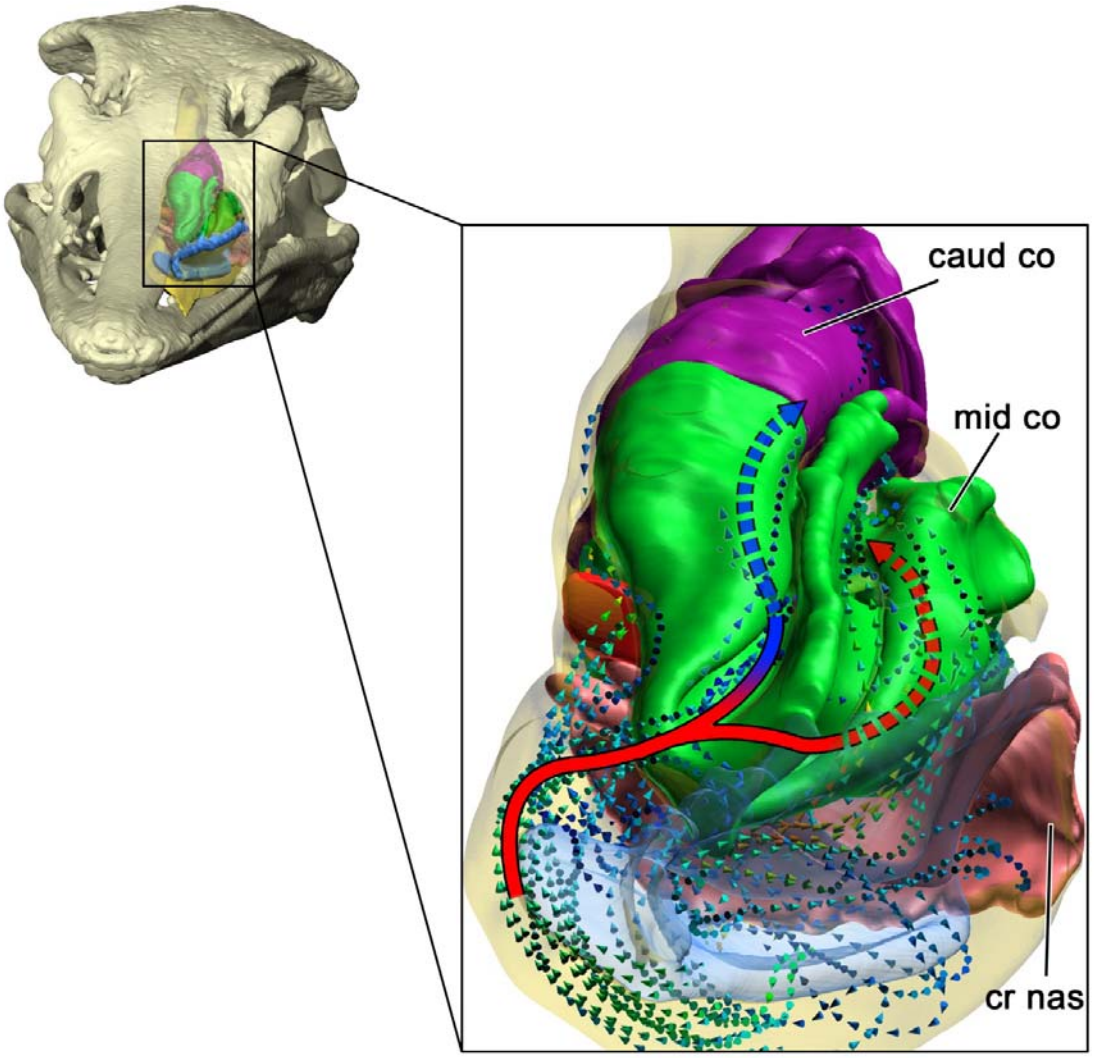

Figure 2-15. Oblique rostral view of airflow through the CNP of an ostrich (*Struthio camelus*, OUVC 10636) during inspiration. Airflow arrows are color-coded for speed. Warmer colors = faster air velocities. Dotted arrows represent air travel within the concha.

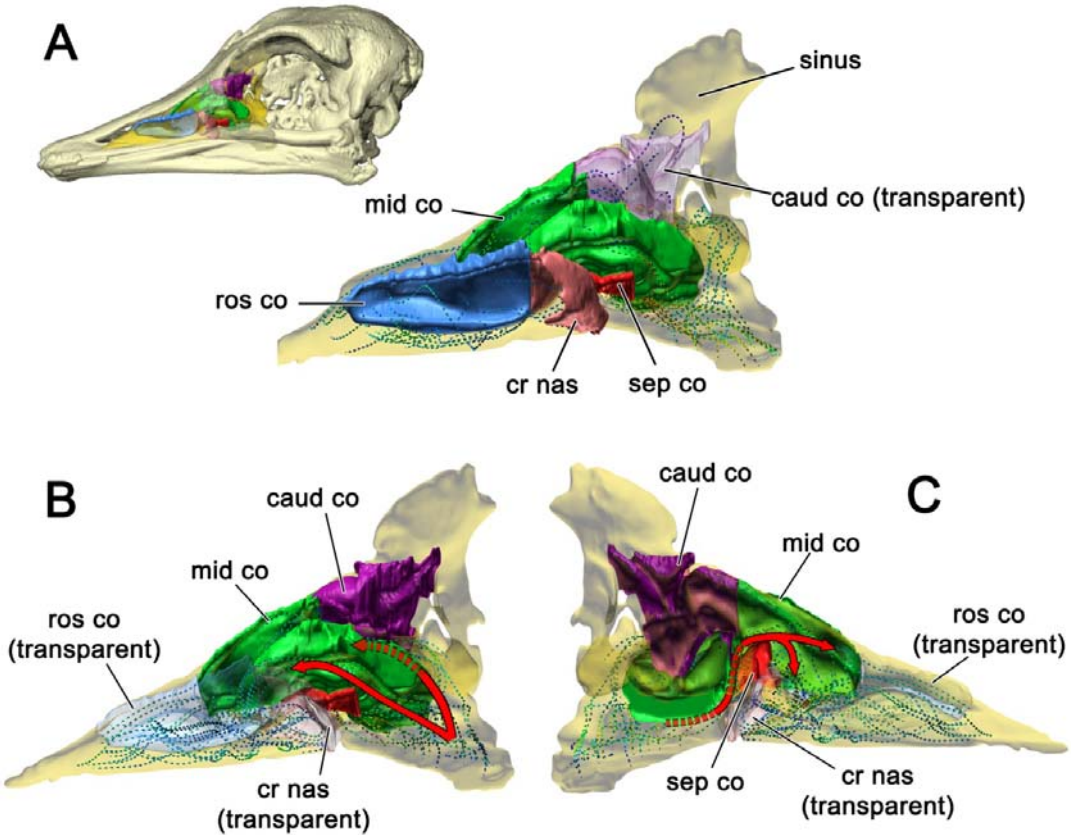

Figure 2-16. (A) Left lateral view of airflow within the ostrich nasal capsule (*Struthio camelus*, OUVC 10636) during inspiration. (B) Left lateral and (C) medial views of airflow in the ostrich nasal capsule during expiration.

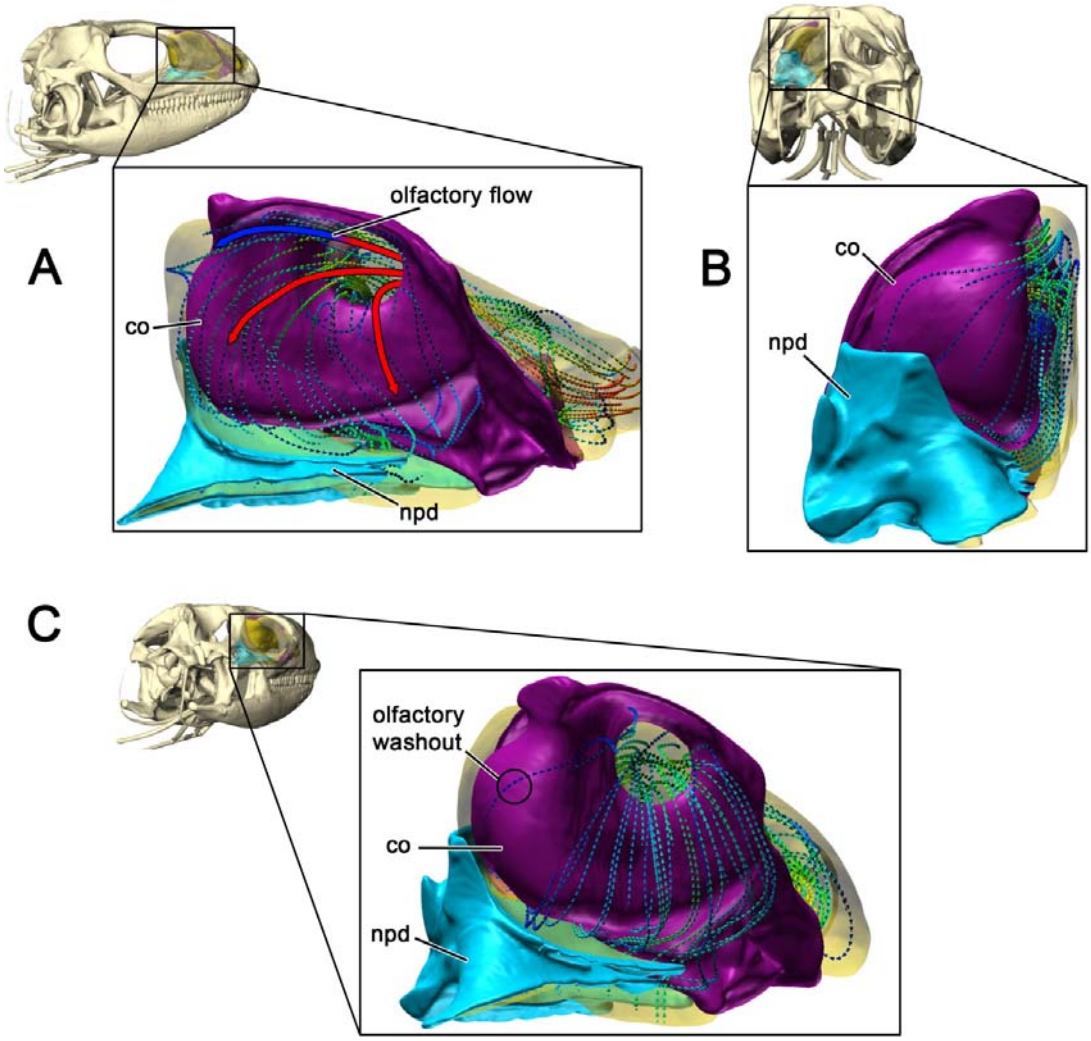

Figure 2-17. Airflow through the CNP of an iguana (*Iguana iguana*, OUVC 10603). (A) Left lateral view of inspired air as it entered and traversed the enlarged concha of the CNP. (B) Caudal view of the olfactory chamber showing slower air movements. (C) Caudomedial view of left airway during expiration. Note the presence of some olfactory washout. Arrows are color-coded for speed with warmer arrows = higher air velocities.

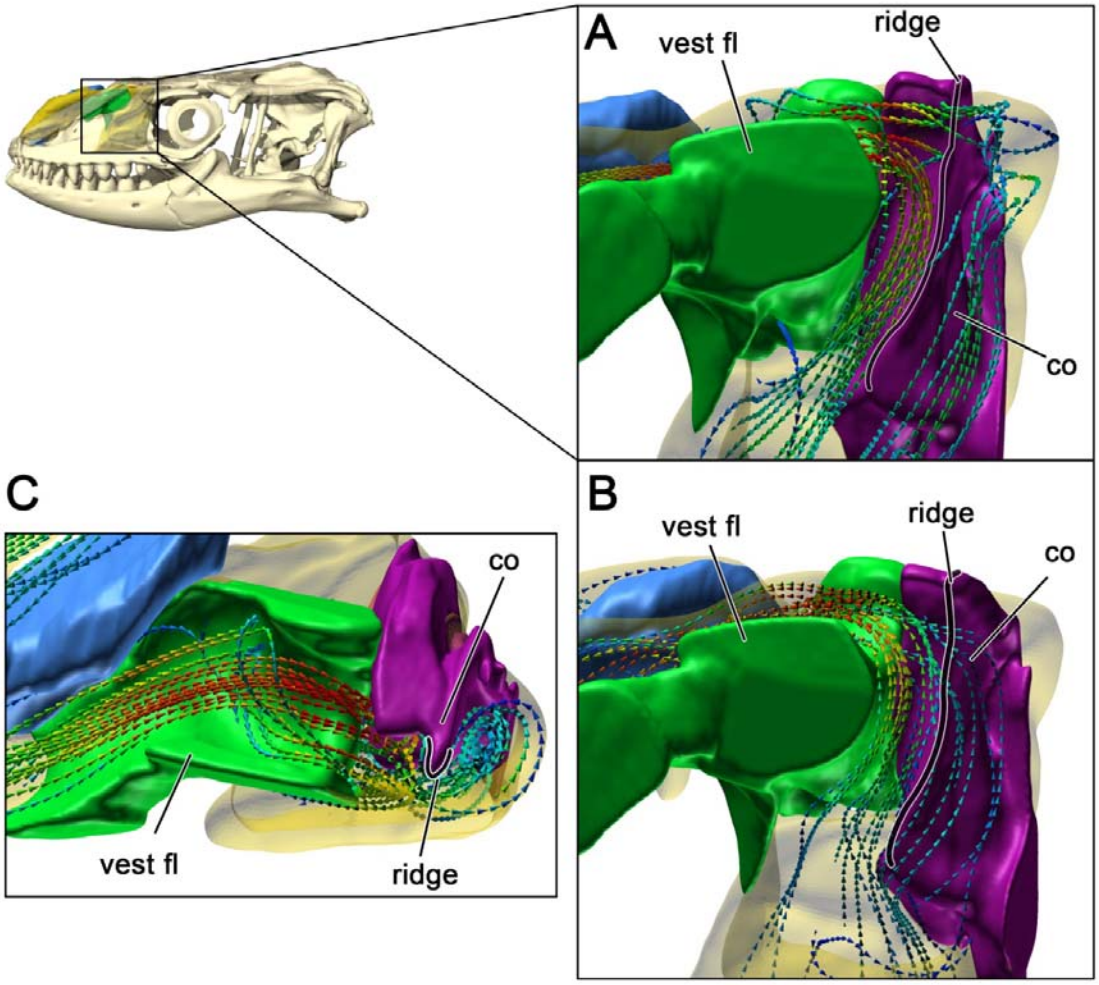

Figure 2-18. Airflow through the CNP of a savannah monitor (*Varanus exanthematicus*, OUVC 10675). Medial view of inspired (A) and expired (B) air moving through the CNP. (C) Dorsal view of air entering the CNP from the vestibulum nasi. Note the presence of a conchal ridge that functioned as a barrier separating respiratory from olfactory air flow.

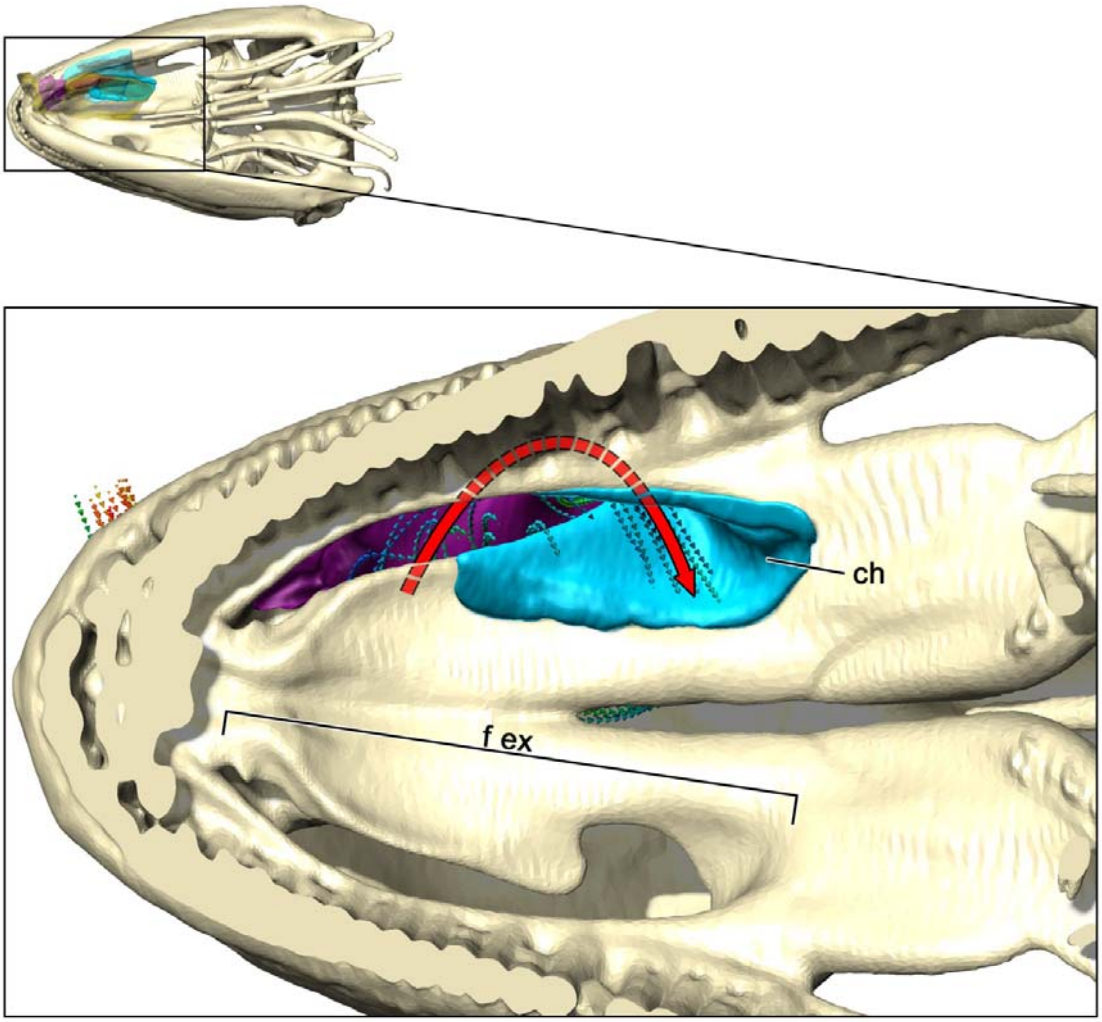

Figure 2-19. Ventral view of inspired airflow in the ductus nasopharyngeus of an iguana (*Iguana iguana*, OUVC 10603). Note the presence of a distinct arch coming from the CNP. This arch forces most inspired air to exit via the caudally placed choana, bypassing most of the fenestra exochoanalis.

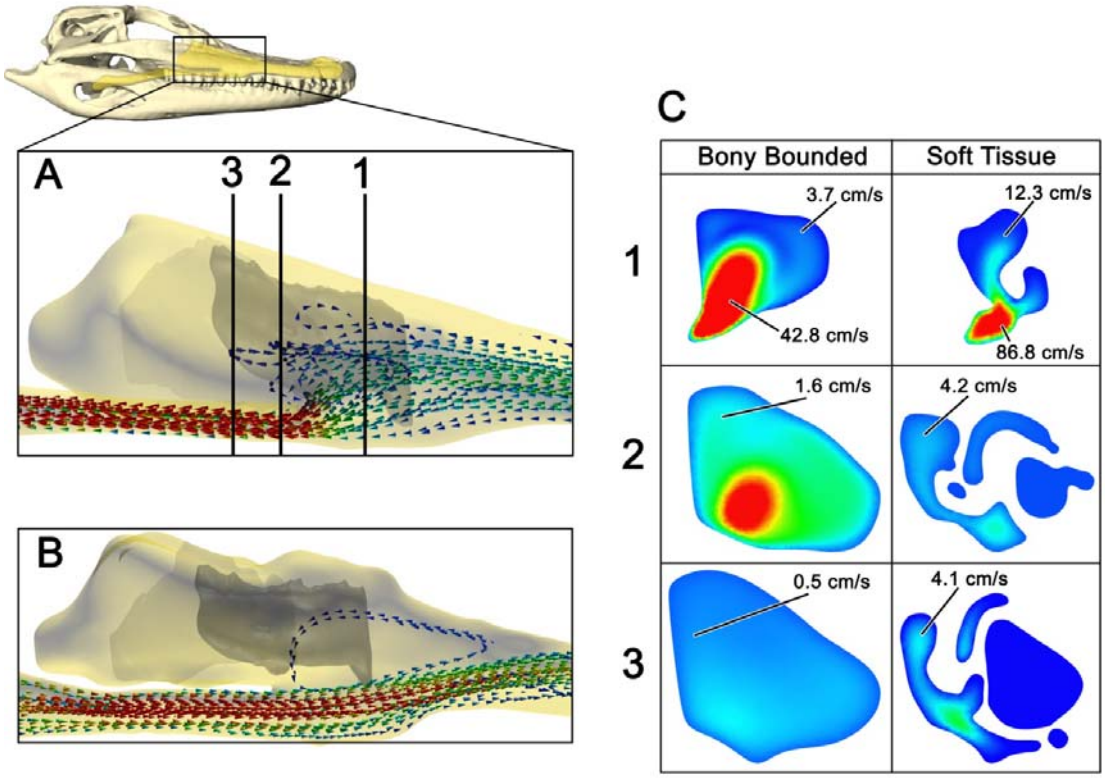

Figure 2-20. (A) Left medial view of airflow through the caudal CNP of the bony-bounded alligator model (*Alligator mississippiensis*, OUVC 10389) during inspiration and (B) expiration. Transparent conchae are placed within the BB airway to show relative airflow positions compared to the soft-tissue counterpart. (C) Airflow velocities through the same cross sections in the bony-bounded and soft-tissue airway. Numbers correspond to slice locations shown in A.

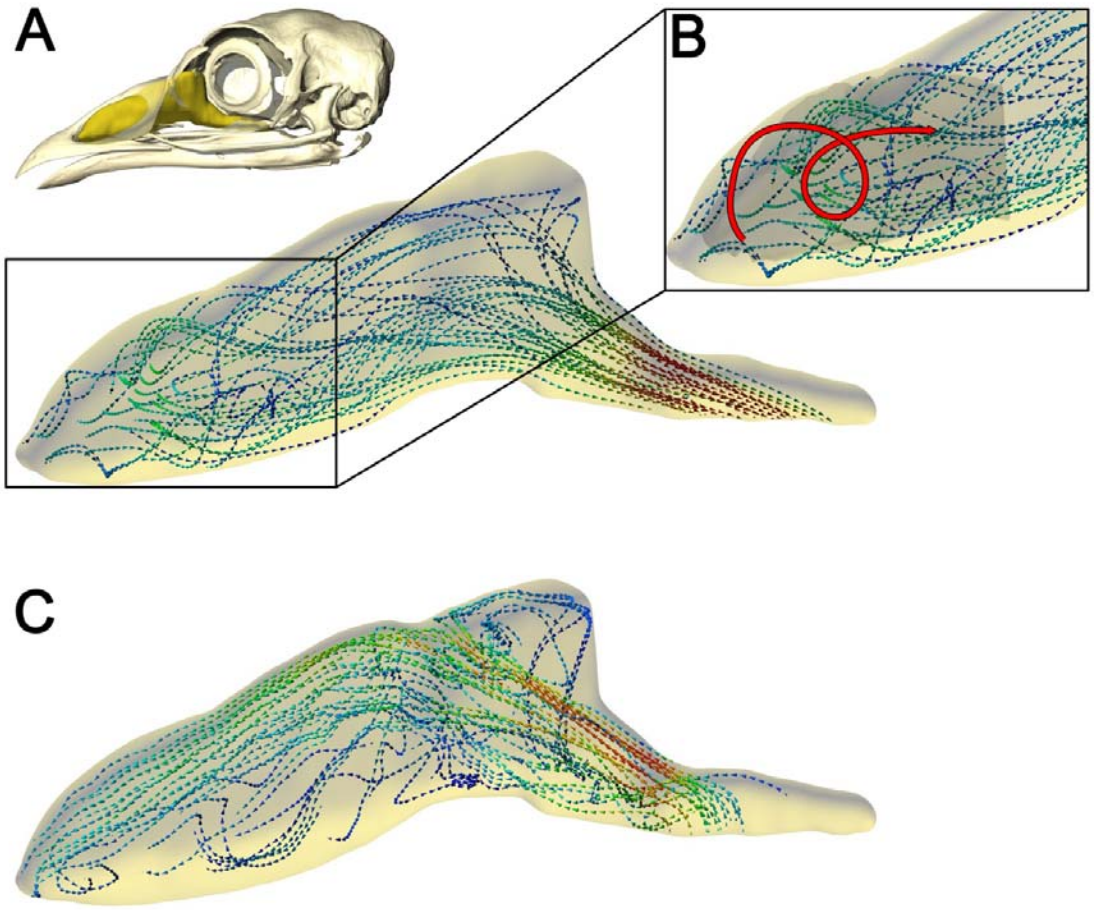

Figure 2-21. Airflow in the bony-bounded airway of the turkey (*Meleagris gallopavo*, OUVC 10599). (A) left lateral view of airflow during inspiration. (B) zoomed in vestibulum nasi region reveals presence of vortices that are similar to those seen in the soft-tissue airway. (C) Airflow pattern during expiration. Transparent rostral concha in B is placed in BB airway to indicate relative position of air streams compared to the soft-tissue counterpart.

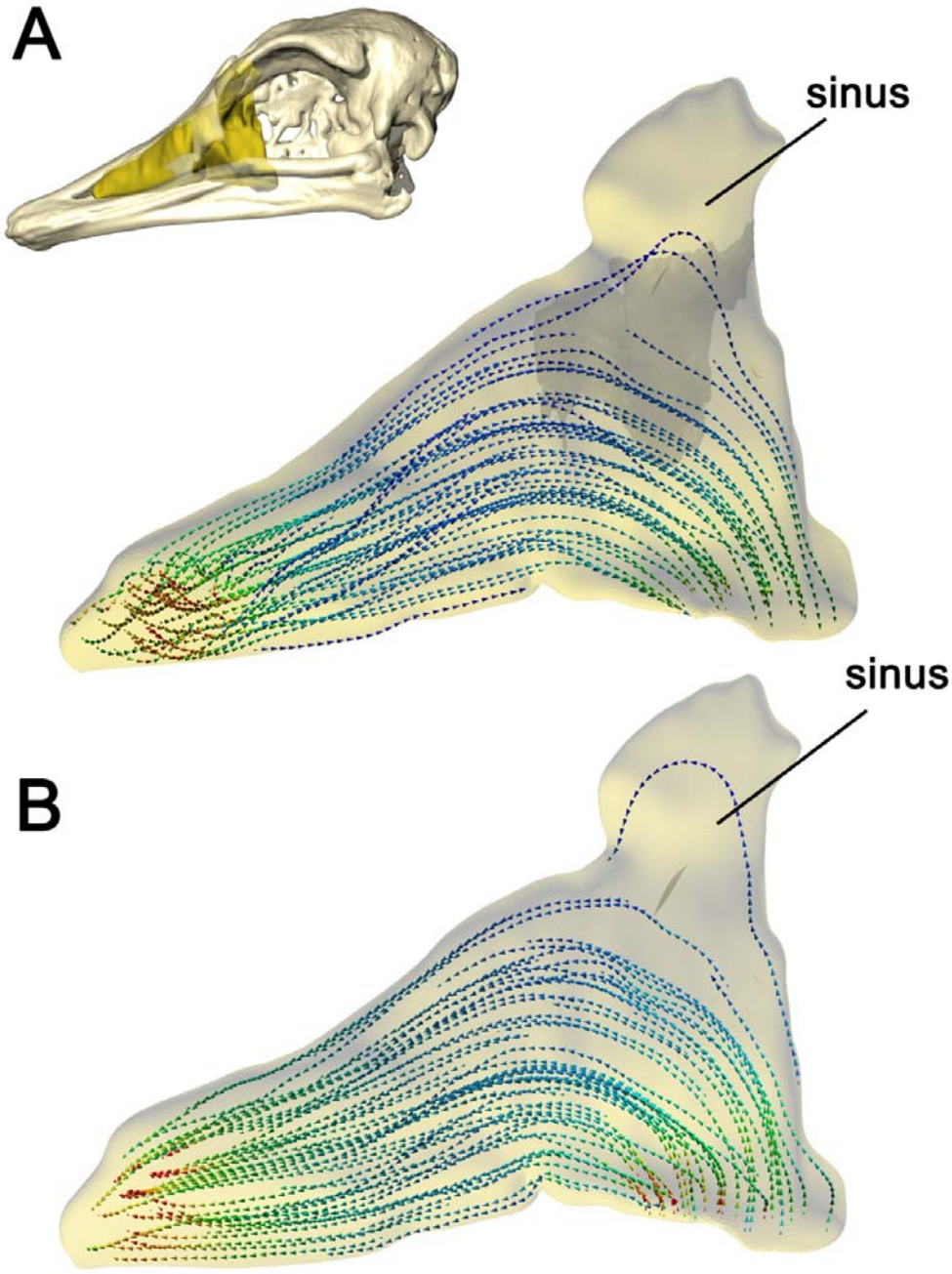

Figure 2-22. Airflow patterns in BB model of an ostrich airway (*Struthio camelus,* OUVC 10636) during inspiration (A) and expiration (B). Note the relative lack of airflow to the dorsal expansion (paranasal sinus). Transparent caudal concha in A is placed in BB airway for comparison to its soft-tissue counterpart.

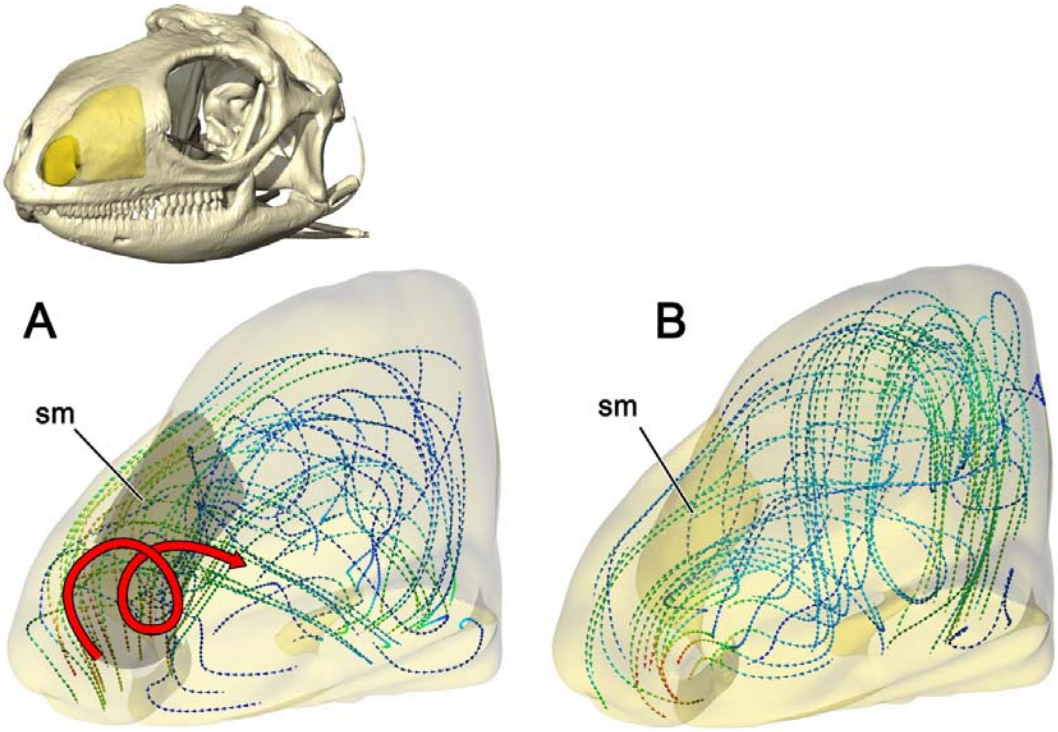

Figure 2-23. Rostrolateral view of airflow through the bony-bounded nasal capsule of an iguana (*Iguana iguana*, OUVC 10603) during inspiration (A) and expiration (B). Septomaxilla is made in transparent in A, so as to better illustrate the origin of the inspired vortex.

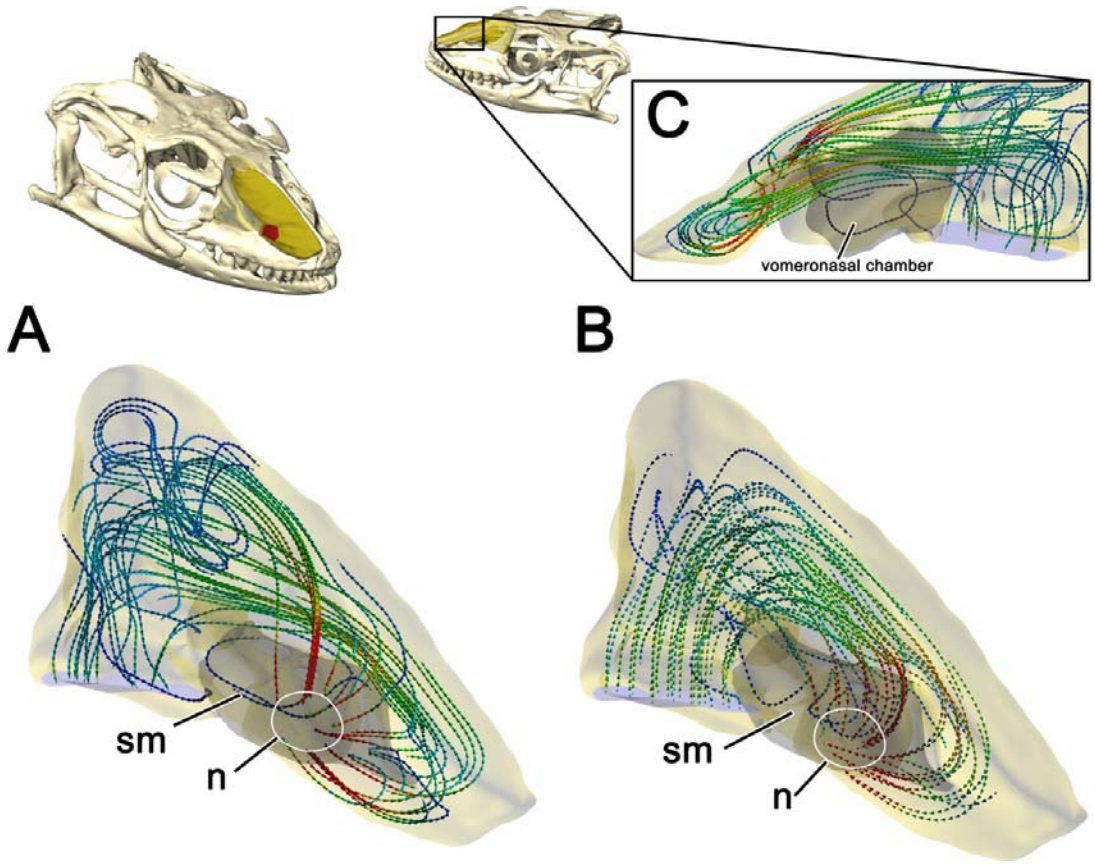

Figure 2-24. Rostrodorsolateral view of airflow in the bony-bounded nasal capsule of the monitor lizard (*Varanus exanthematicus,* OUVC 10675) during inspiration (A) and expiration (B). Dorsomedial view of airflow through the vomeronasal chamber during inspiration (C). Colors correspond to air speed with warmer colors indicating higher velocities. Vomeronasal flow arrows are desaturated to indicate negligible flow and deeper location relative to other air streams. The white circle indicates the location of the naris for the bony-bounded airway.

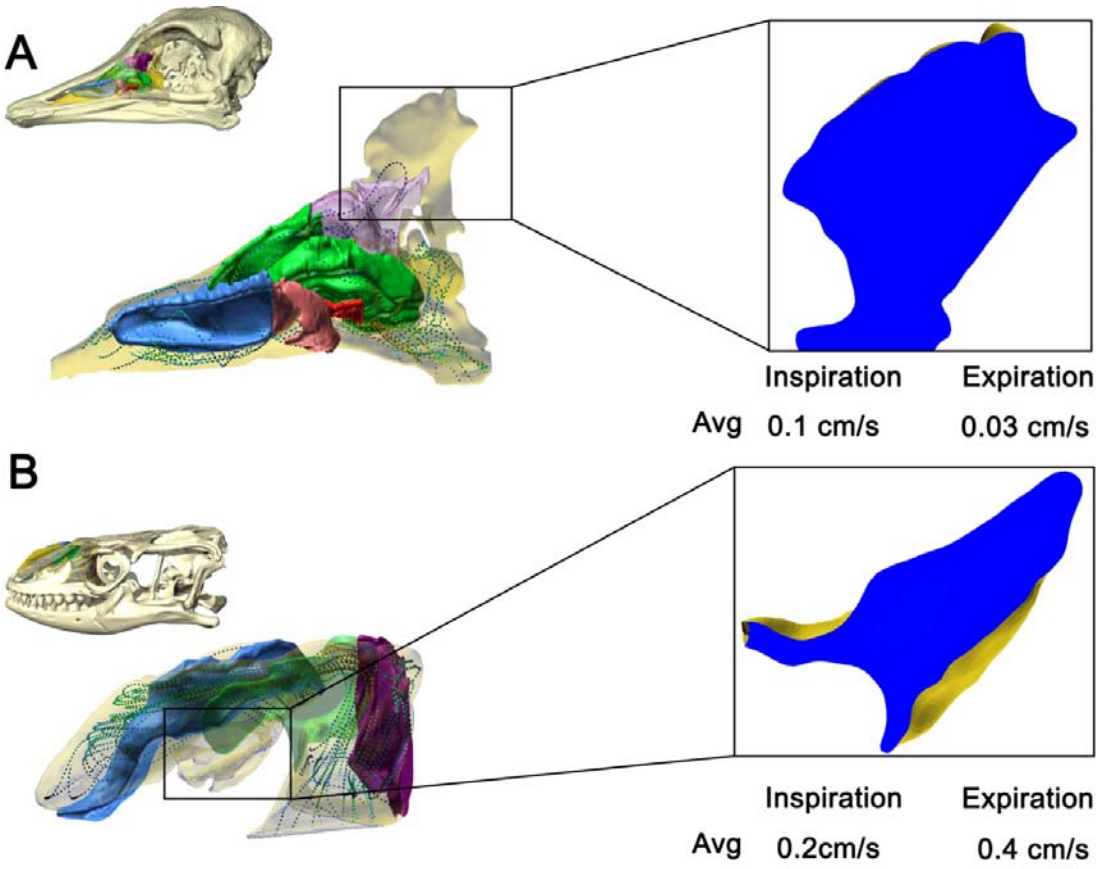

Figure 2-25. Potential paranasal sinuses in the ostrich (*Struthio camelus,* OUVC 10636, A) and monitor lizard (*Varanus exanthematicus*, OUVC 10675, B). *Insets:* Presence of near stagnant airflow in selected regions during both phases of respiration.

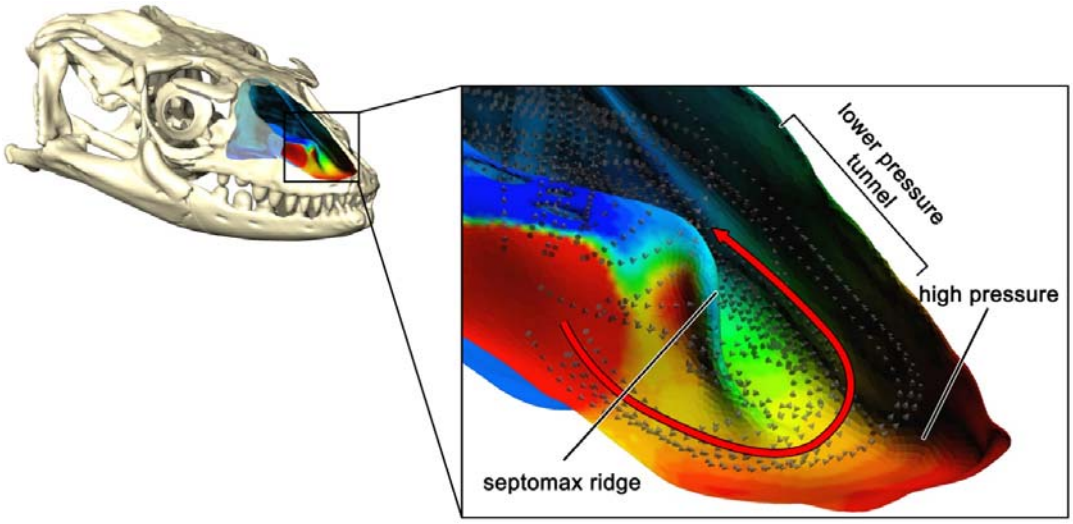

Figure 2-26. Pressure map of the bony-bounded airway in the savannah monitor (*Varanus exanthematicus*, OUVC 10675). Hotter colors correspond to higher pressures. Note how the ridge on the septomaxilla acts to create a high-pressure zone with low-pressure tunnel.

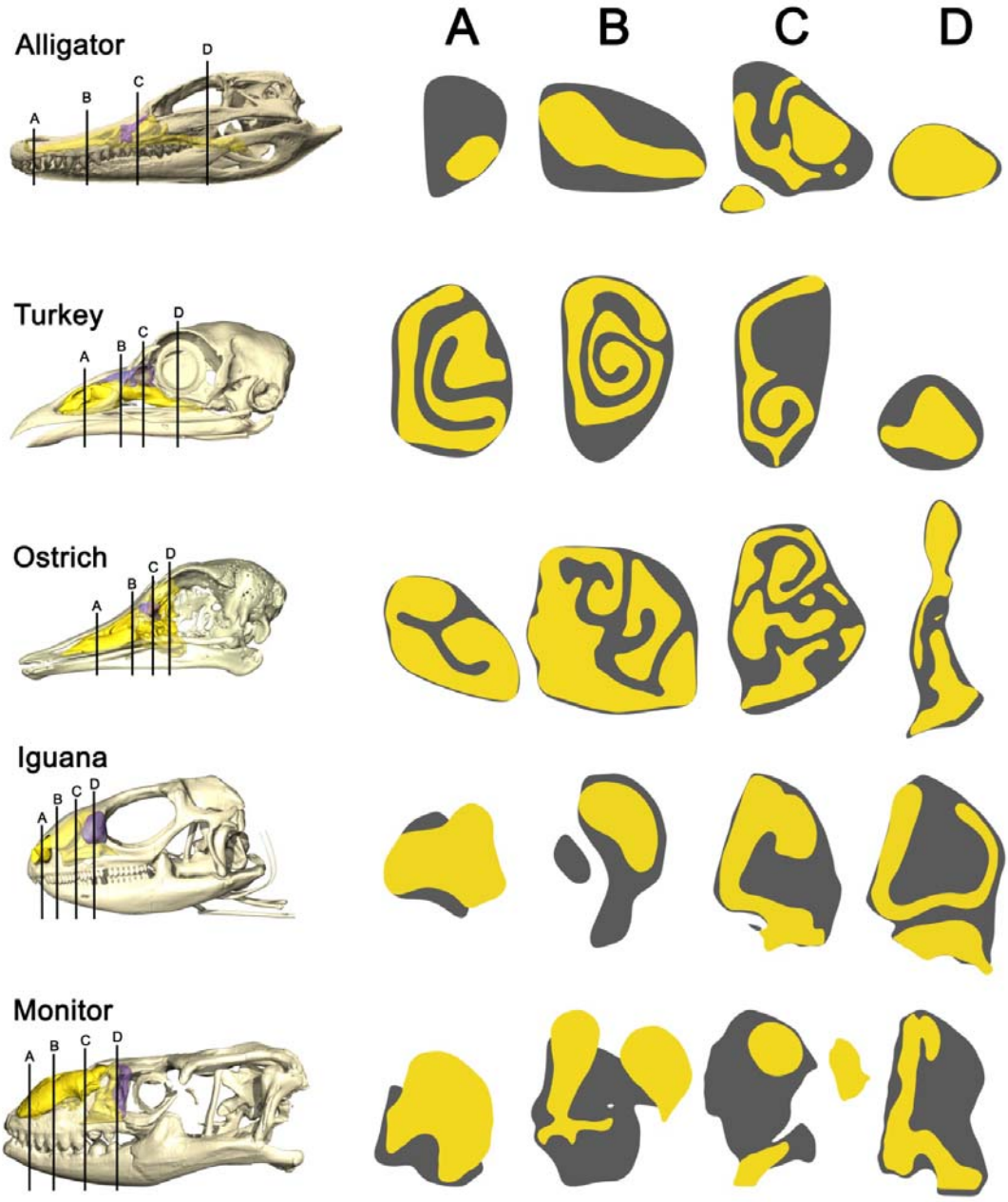

Figure 2-27. Comparison of soft-tissue (yellow) and bony-bounded (grey) airway morphologies across the taxa in this study. Numbers correspond to cross section locations on the skulls. The savannah monitor skull and cross sections were mirrored to align with the other four taxa.

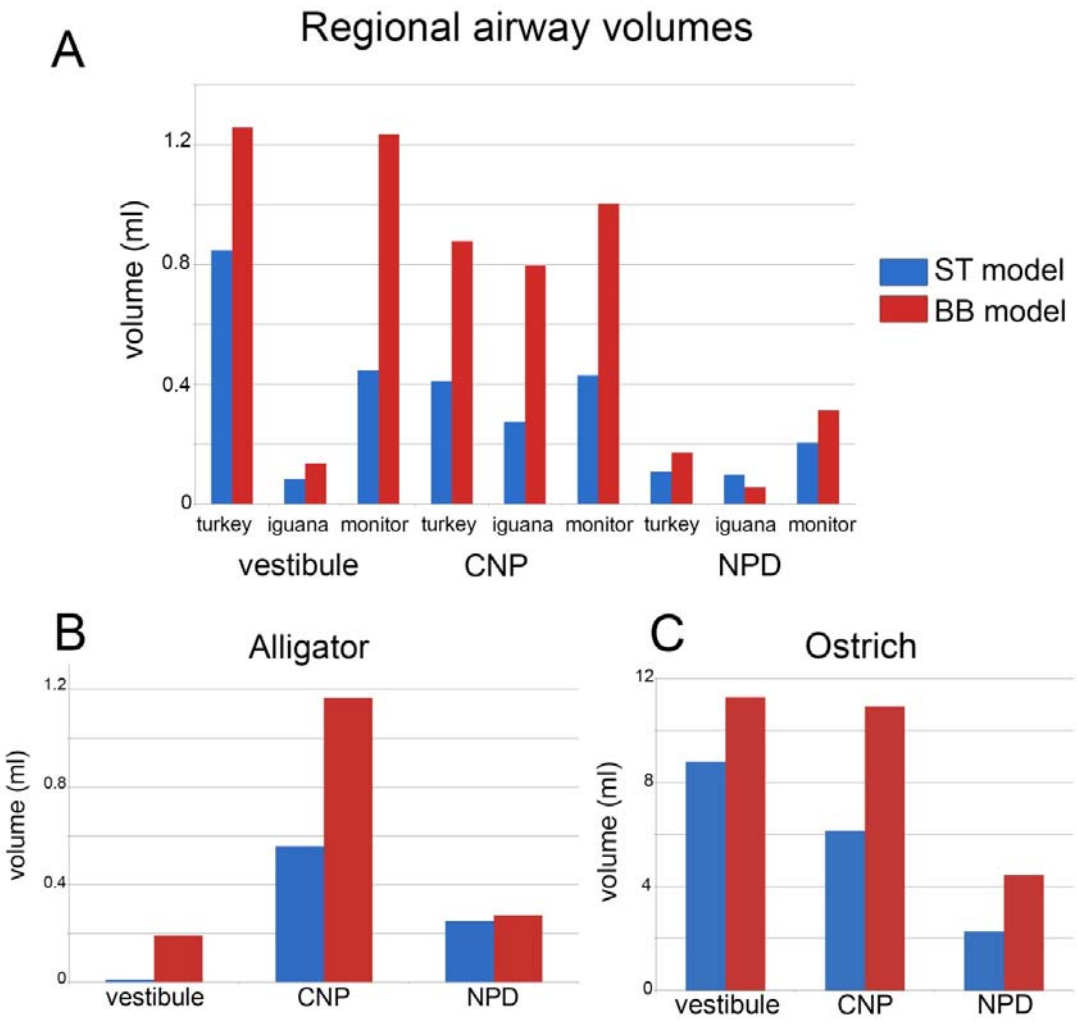

Figure 2-28. (A) Chart of airway volumes in different regions of the nasal passage. Bony-bounded airways (BB model) consistently showed higher volumes than their soft-tissue counterparts (ST model). Separate charts were made for the alligator (B) and ostrich (C) models to maintain legibility of chart A.

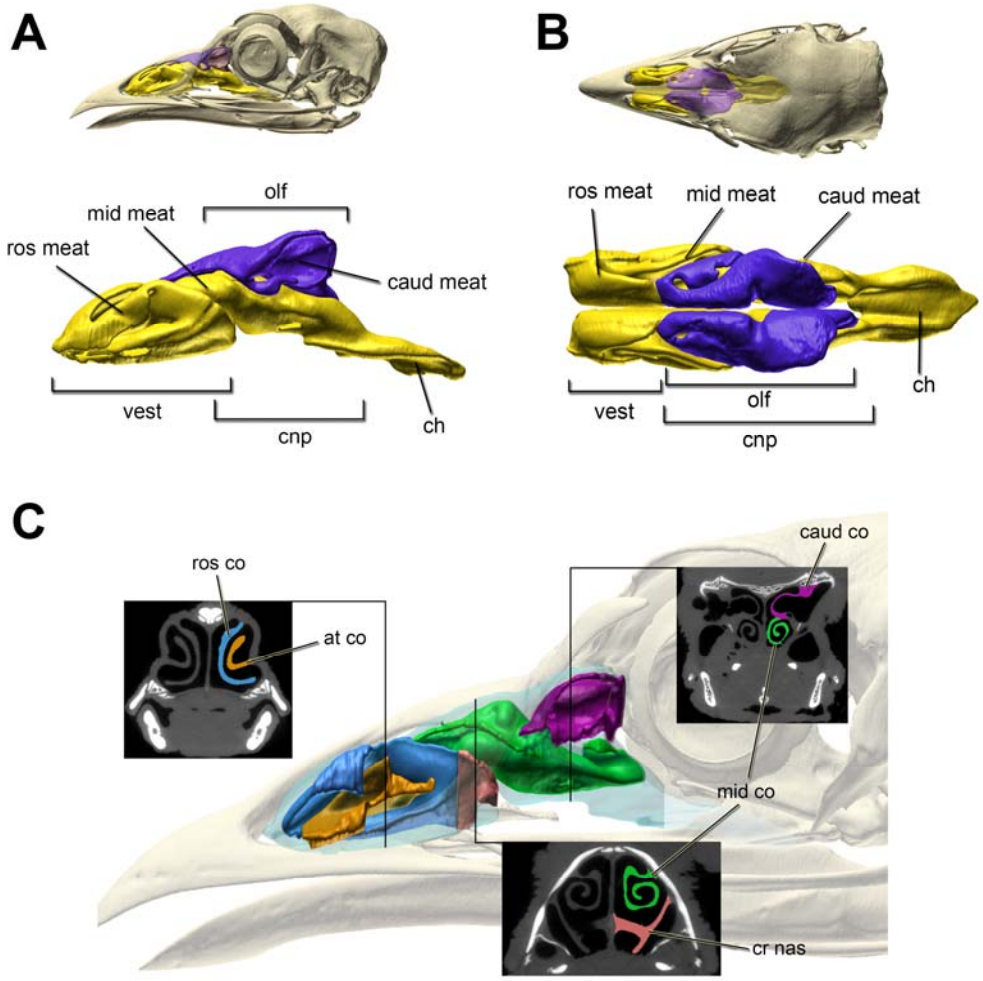

Figure 3-1. Segmented airway cast of wild turkey (*Meleagris gallopavo*, OUVC 10599) showing the location of the various meatuses within the nasal capsule as shown in (A) lateral and (B) dorsal views. (C) Cross sections showing the location of color-coded conchae, and crista nasalis, within the nasal capsule.

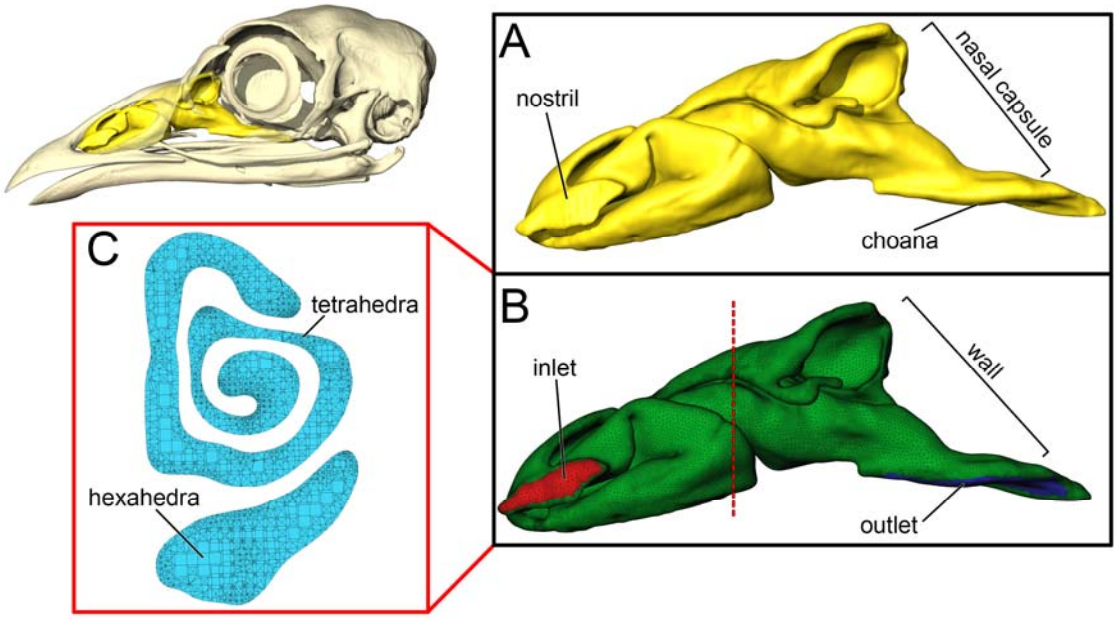

Figure 3-2. Workflow for model creation from OUVC 10599. (A) Cast of left nasal capsule is segmented out in 3D. (B) Model is cleaned of segmentation artifacts and given a series of boundary conditions that promote realistic airflow prior to volumetric mesh generation. The vertical red line indicates the axial cross section location in (C), showing the tetrahedral-hexahedral (tet-hex) hybrid mesh interior.

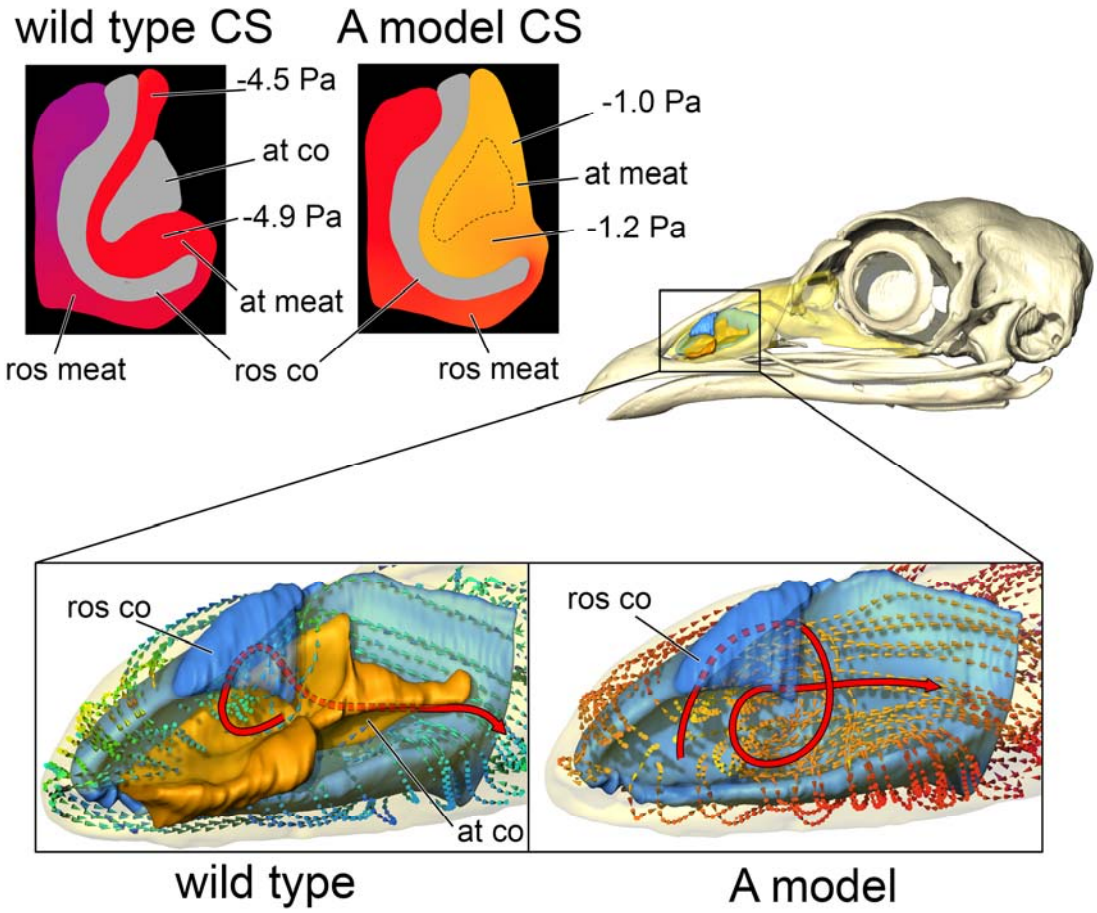

Figure 3-3. Airflow and pressure comparisons between the A model (removal of the atrial concha) versus the wild type model of a wild turkey (*Meleagris gallopavo*, OUVC 10599). *Upper left*: Cross sections (CS) reveal the change in the pressure gradient across the vestibulum nasi upon atrial concha ablation. *Bottom insets*: Particle plots within the vestibulum nasi reveal substantial differences in airflow patterns, with atrial concha ablation resulting in the formation of a vortex along the lateral aspect of the rostral concha.

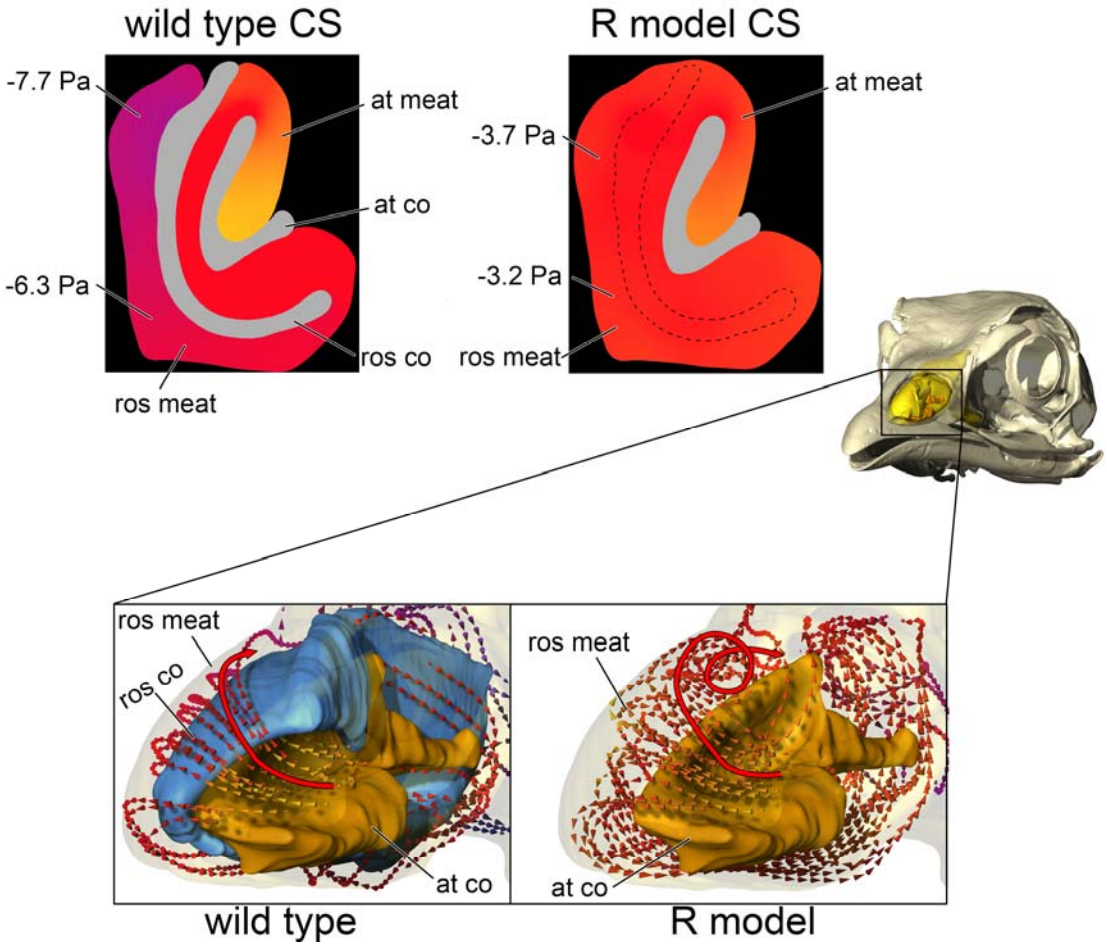

Figure 3-4. Airflow and pressure comparisons between wildtype and R model (removal of the rostral concha) of a wild turkey (*Meleagris gallopavo*, OUVC 10599). *Top*: Axial cross sections (CS) through the vestibulum nasi showing changes in pressure distribution between models. *Bottom*: Rostrolateral view through vestibulum nasi showing increased vorticity within the R model as opposed to the wild type.

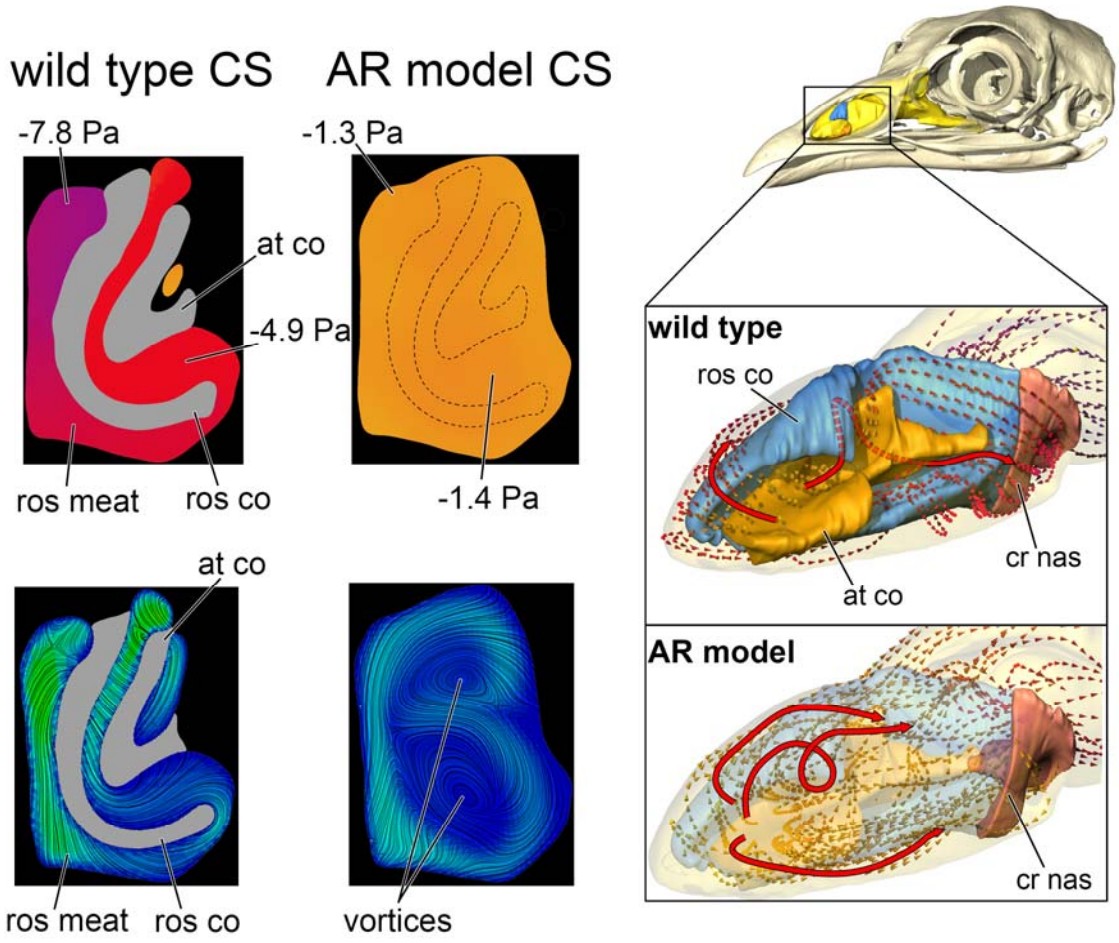

Figure 3-5. Airflow and pressure comparisons between the wild type and AR model (removal of both atrial and rostral conchae) of a wild turkey (*Meleagris gallopavo*, OUVC 10599). *Left top:* Axial cross sections (CS) through the vestibulum nasi showing homogenization of pressure in the AR model compared to the wild type. *Left bottom:* Cross section of velocity streamlines passing through the vestibulum nasi show enhanced vorticity within the AR model. *Right:* Particle plots showing general airflow patterns in the wild type and AR models during inspiration.

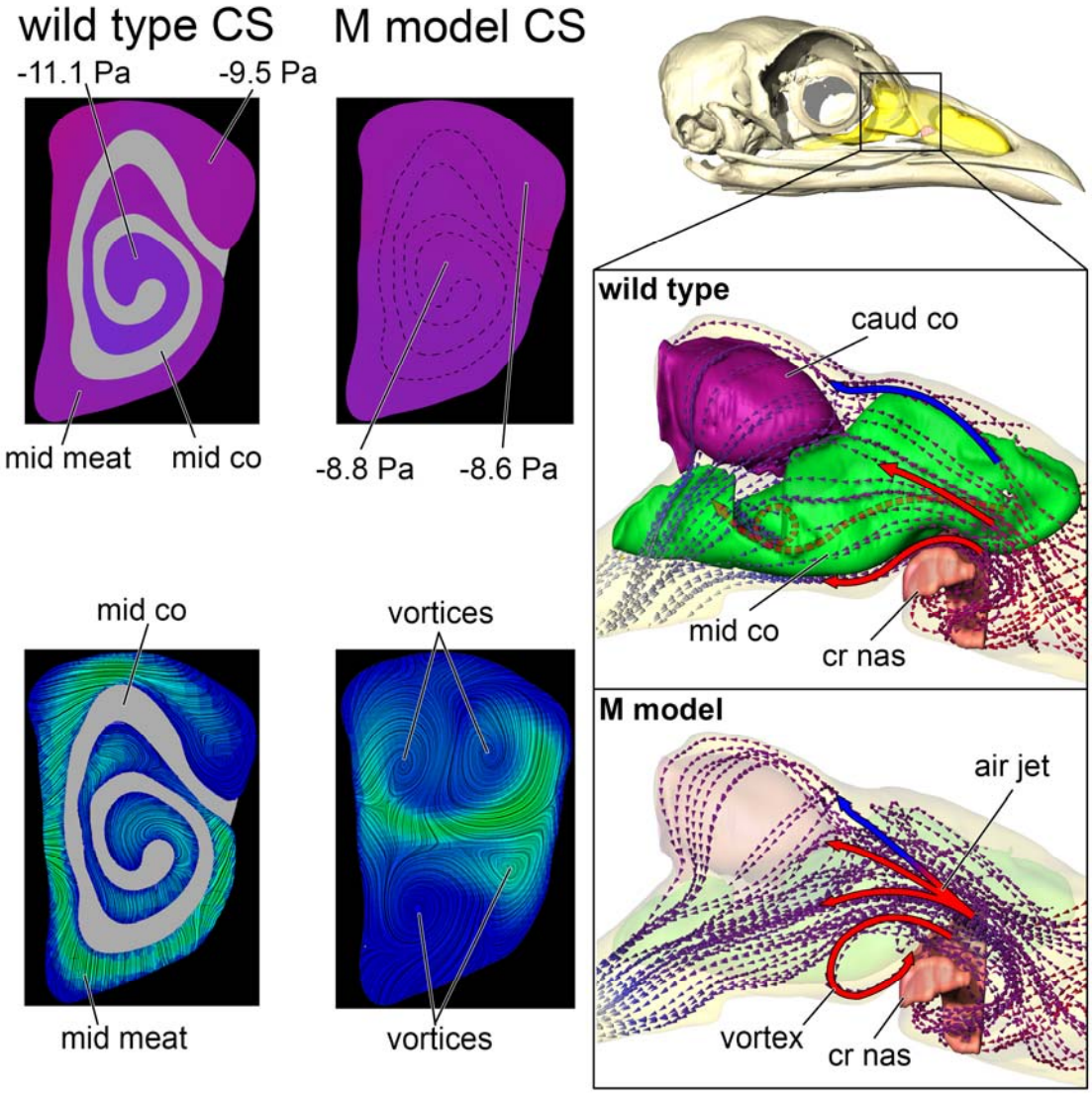

Figure 3-6. Airflow and pressure comparisons between wild type and M model (removal of the middle concha) of a wild turkey (*Meleagris gallopavo*, OUVC 10599). *Left top:* Axial cross sections (CS) showing total pressure in the wild type and M model. *Left bottom:* Velocity streamline cross sections showing changes in air field shape between the wild type and M model. *Right:* Medial view of nasal capsule with inspiratory airflow in the wild type and M model. Note the distinct jetting and vorticity present in the M model when the middle concha is removed. Arrows color-coded for flow type. Red = Respiratory flow Blue = Olfactory flow.

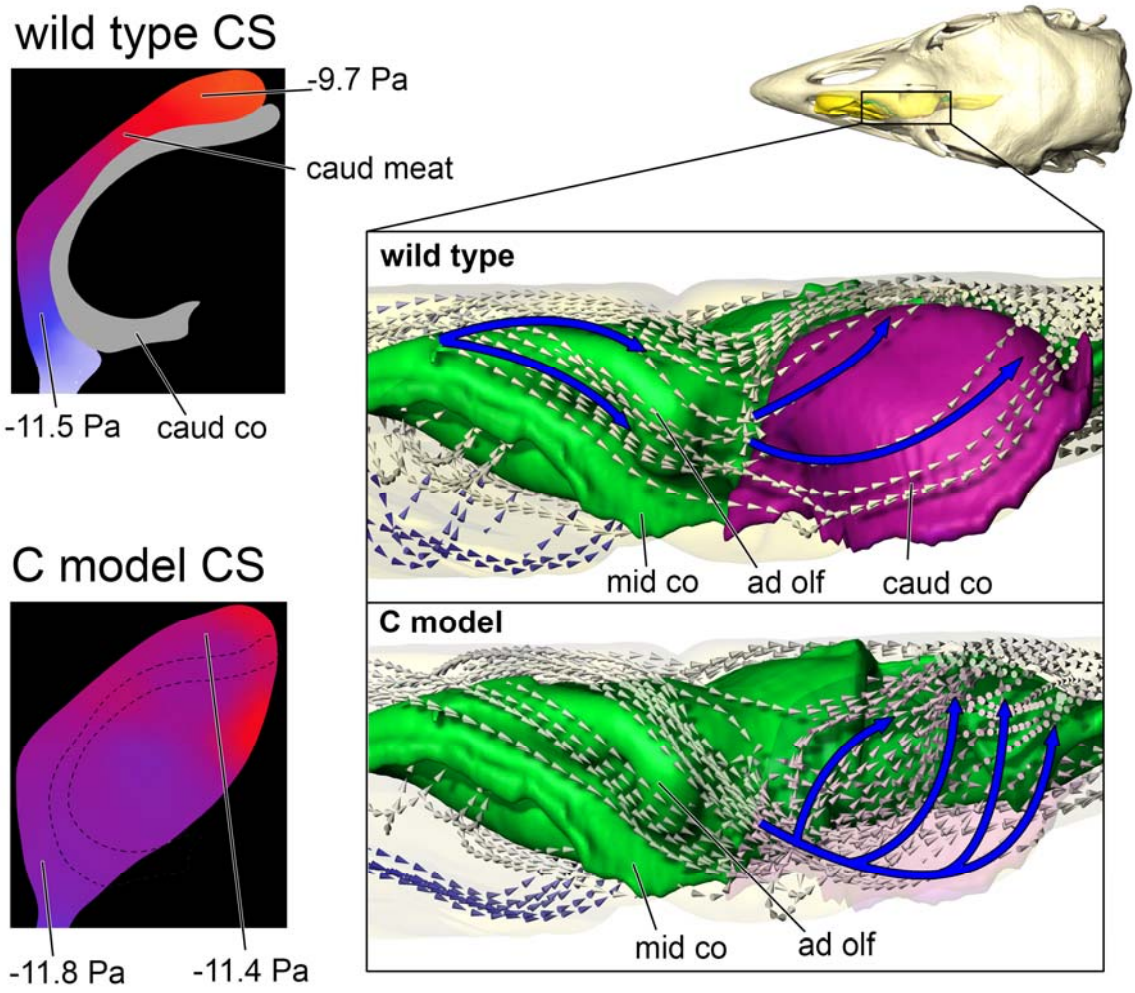

Figure 3-7. Airflow and pressure comparison between the wild type and C models (removal of the caudal concha) of a wild turkey (*Meleagris gallopavo*, OUVC 10599). *Left:* Axial cross sections (CS) through the olfactory chamber showing the increased volume of the C model compared to the wild type along with the corresponding pressure decrease in the former. *Right:* Dorsal view of the nasal capsule comparing inspiratory flow in the wild type and C model. Wild type olfactory flow covered a greater mediolateral arc than the C model, which stayed largely in the lateral portion of the olfactory chamber.

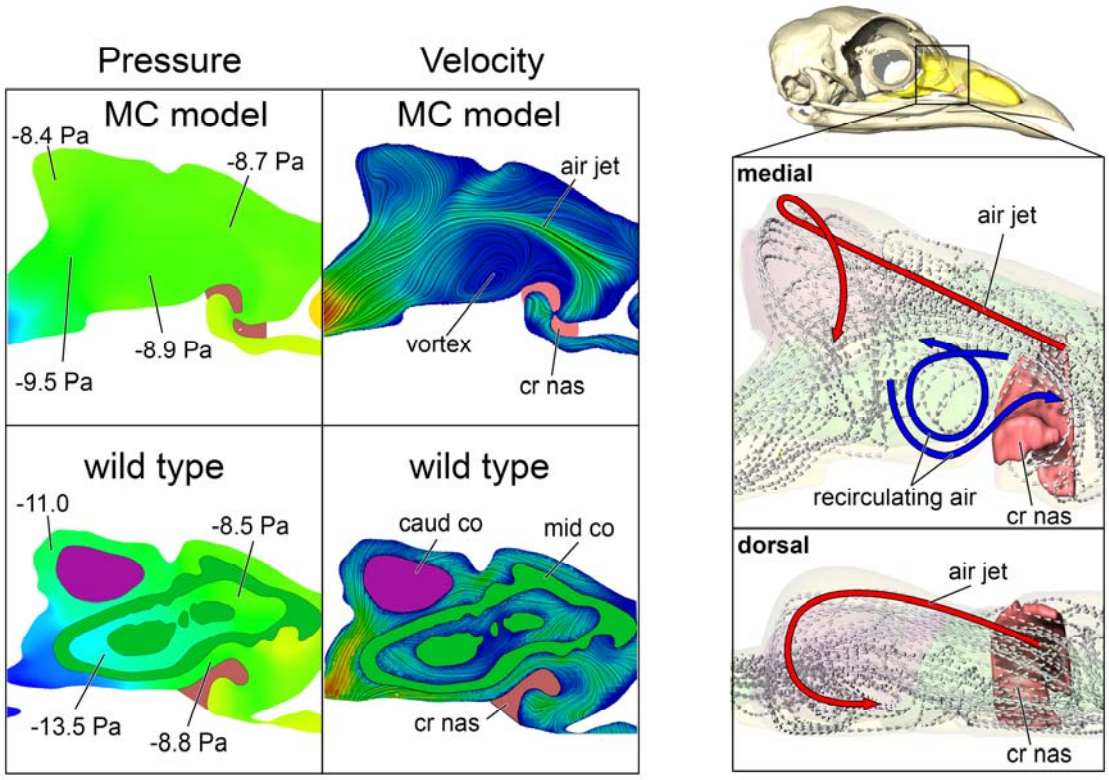

Figure 3-8. Airflow and pressure distribution within the MC model (removal of both middle and caudal conchae) of a wild turkey (*Meleagris gallopavo*, OUVC 10599) during inspiration. *Left:* Medial sagittal sections through the highlighted region shown on the turkey skull. Cross sections show pressure distribution and air streams through this region of the nasal capsule. Air streams are color coded for velocity (hotter colors = faster flow). Flow is compared to the wild type model. *Right:* Inset showing flow pattern in the MC model from a medial and dorsal perspective.

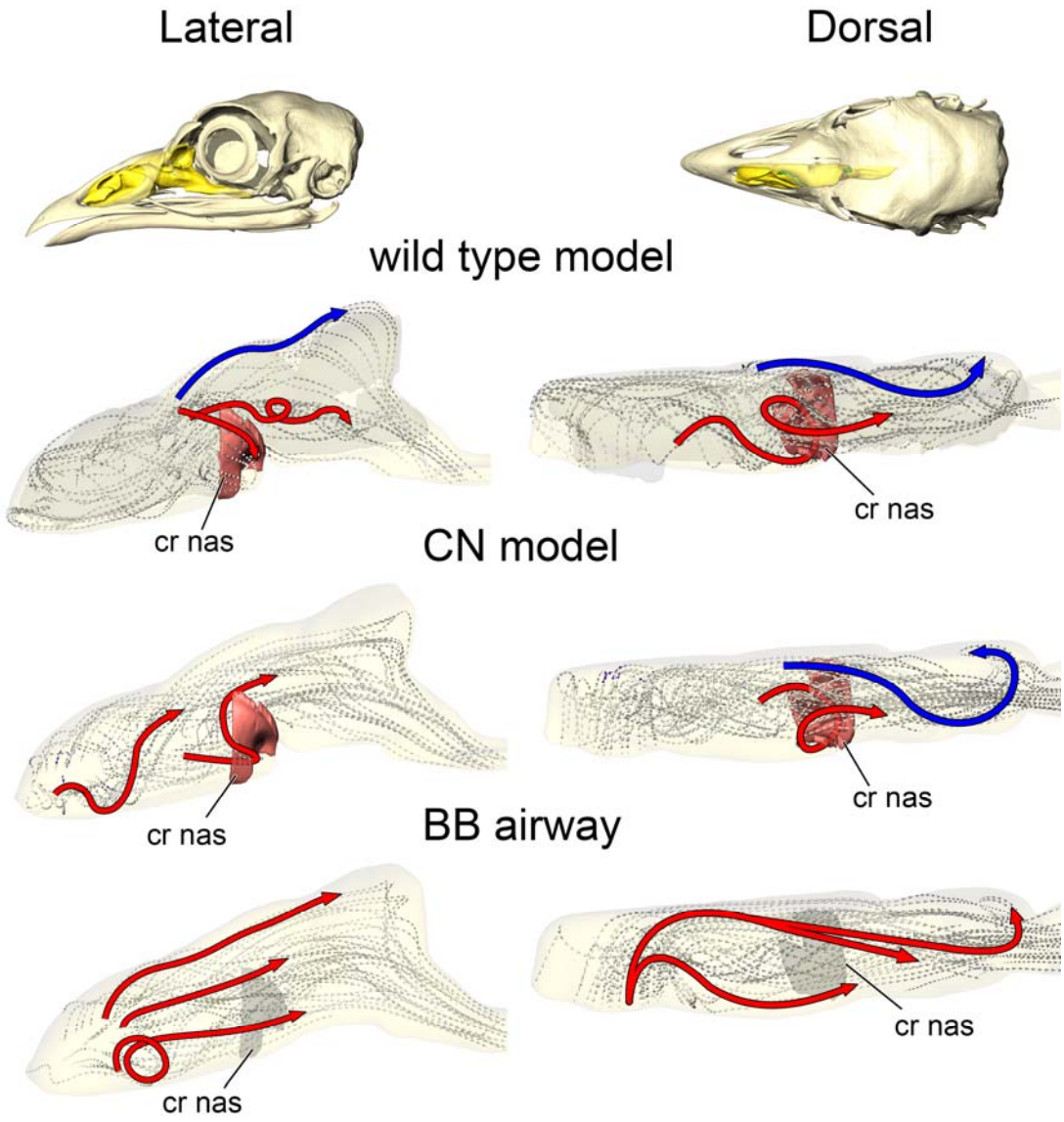

Figure 3-9. Airflow comparison between the wild type airway, CN model (removal of the crista nasalis), and the BB airway (removal of all soft-tissue structures) from Chapter 2. Arrows show major flow patterns and are color coded for flow type (Red = respiratory, Blue = olfactory).

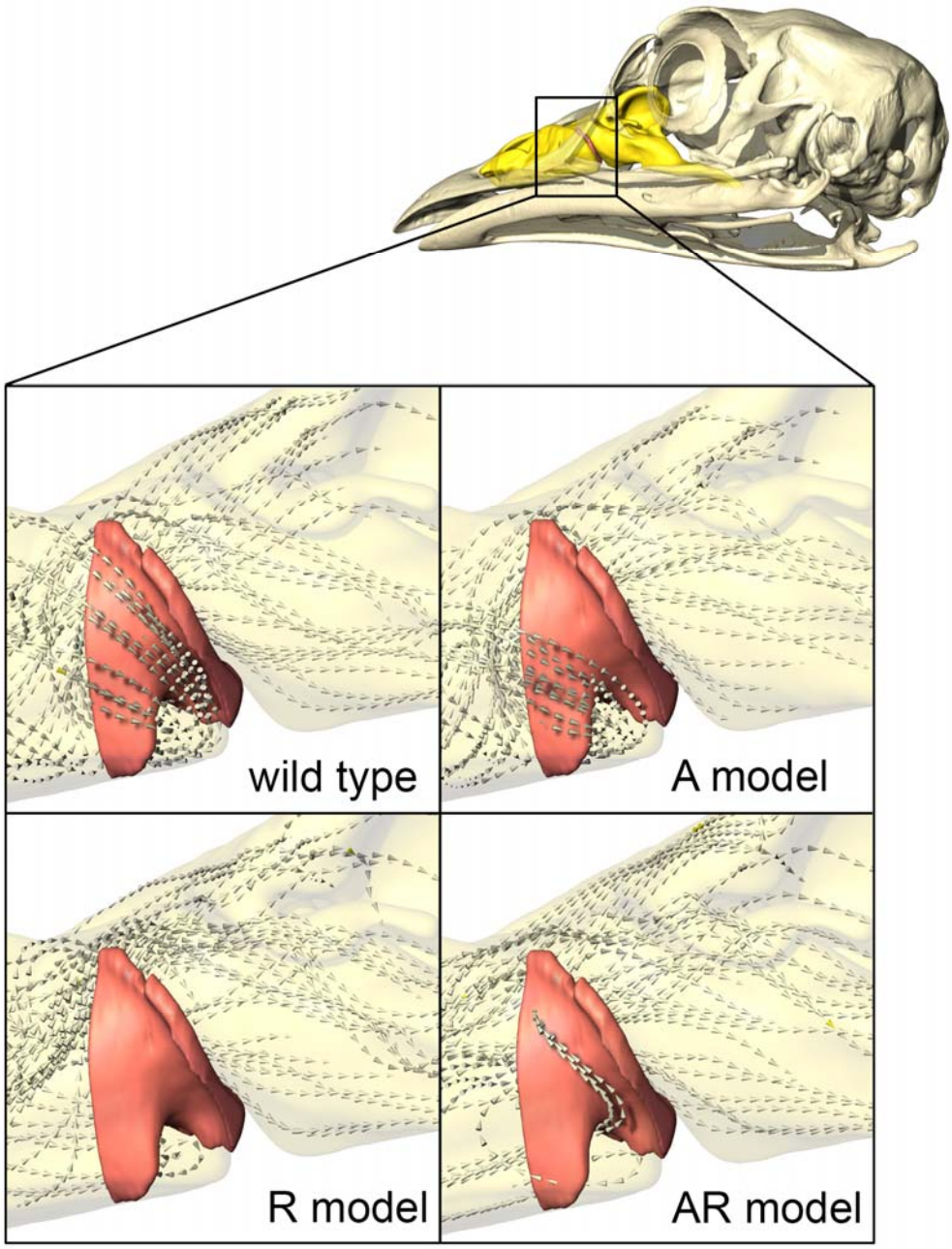

Figure 3-10. Comparison of airflow around the base of the crista nasalis of a wild turkey (*Meleagris gallopavo*, OUVC 10599) in the relevant airway models during resting inspiration.

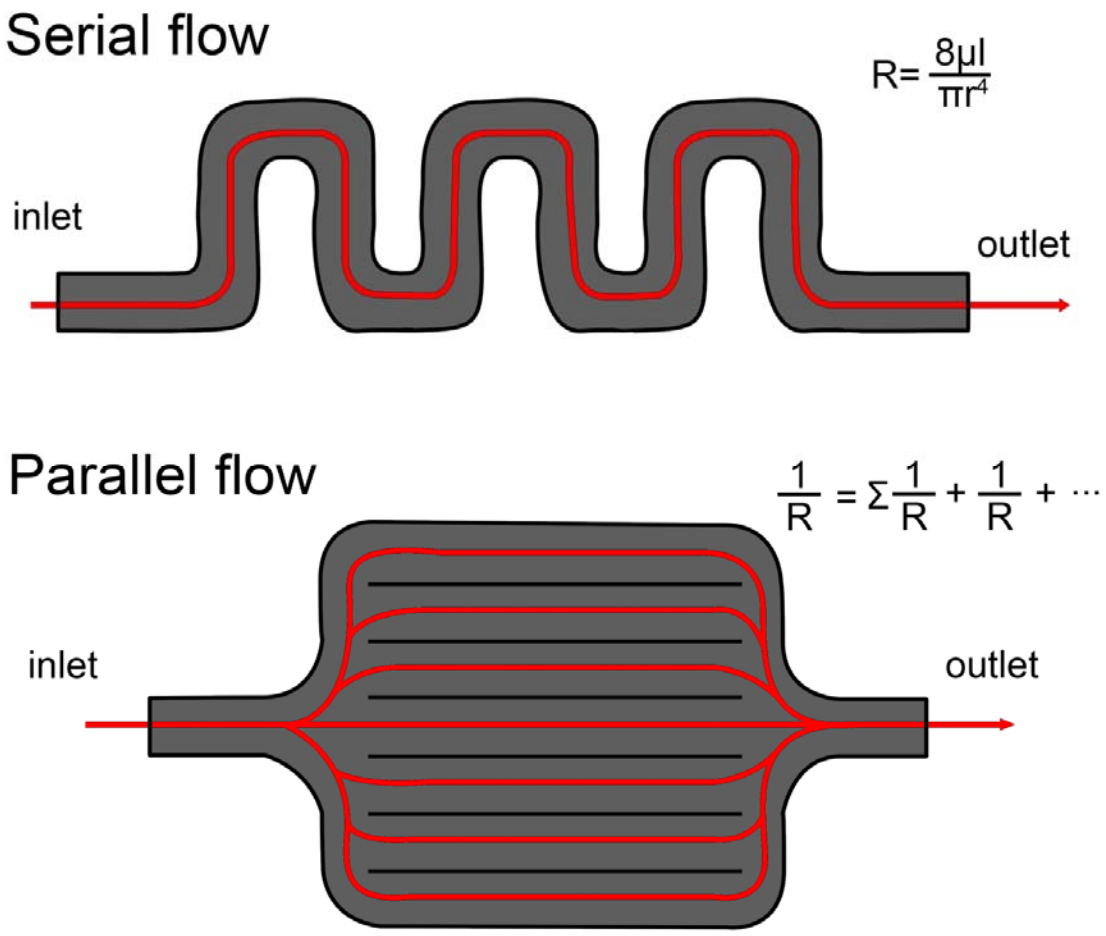

Figure 3-11. Diagram showing two different means of transferring heat and odorant molecules in a nasal passage. Parallel segmentation of the air field (red arrow) may be advantageous over serial air flow when the cost in anatomical space is great.

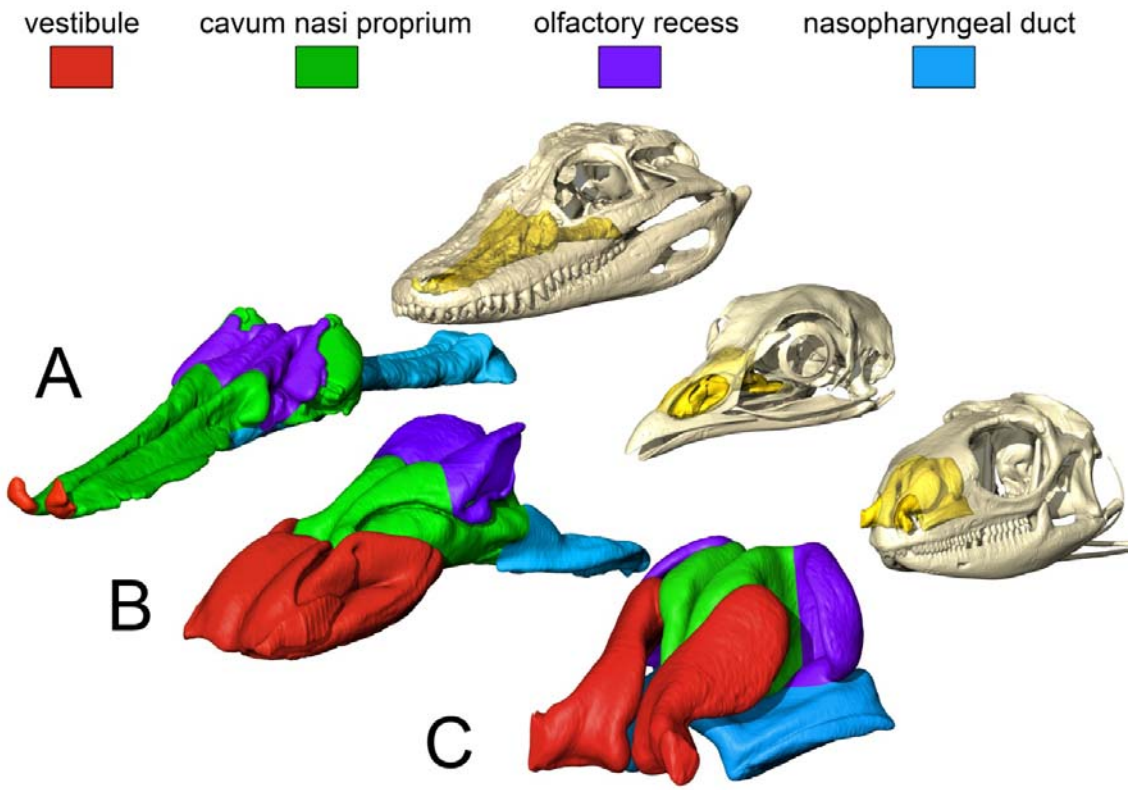

Figure 4-1. Nasal airway anatomy shown next to associated skulls of (A) a crocodylian (*Alligator mississippiensis*, OUVC 10389), (B) a bird (*Meleagris gallopavo*, OUVC 10599), and (C) a lizard (*Iguana iguana*, OUVC 10603). Note that the olfactory recess is part of the CNP and has been colored differently only to highlight its approximate location within the nasal passage.

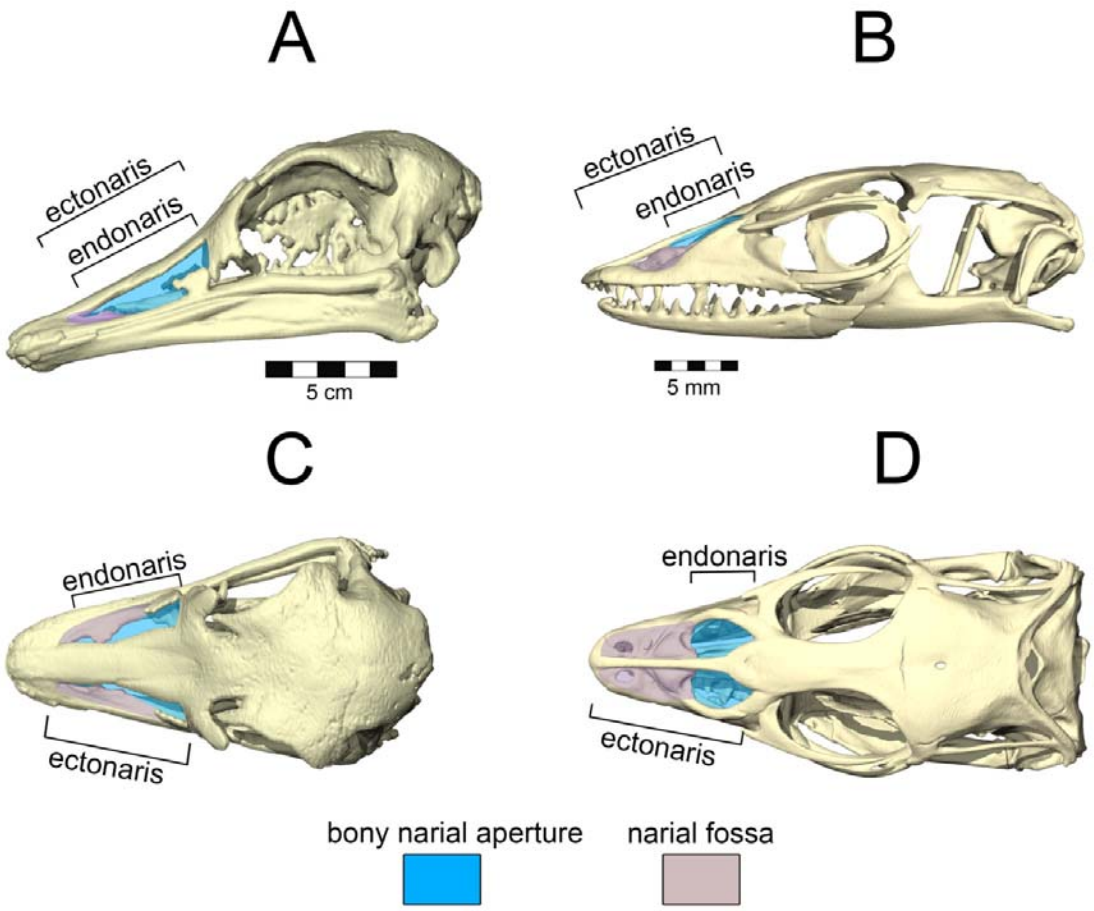

Figure 4-2. Anatomical location of the bony nostril (ectonaris) in (A, C) an ostrich (*Struthio camelus*, OUVC 10636) and (B, D) a Gould's monitor lizard (*Varanus gouldii*, YPM R 4093). (A–B) Left lateral view of skulls. (C–D) Dorsal view of skulls.

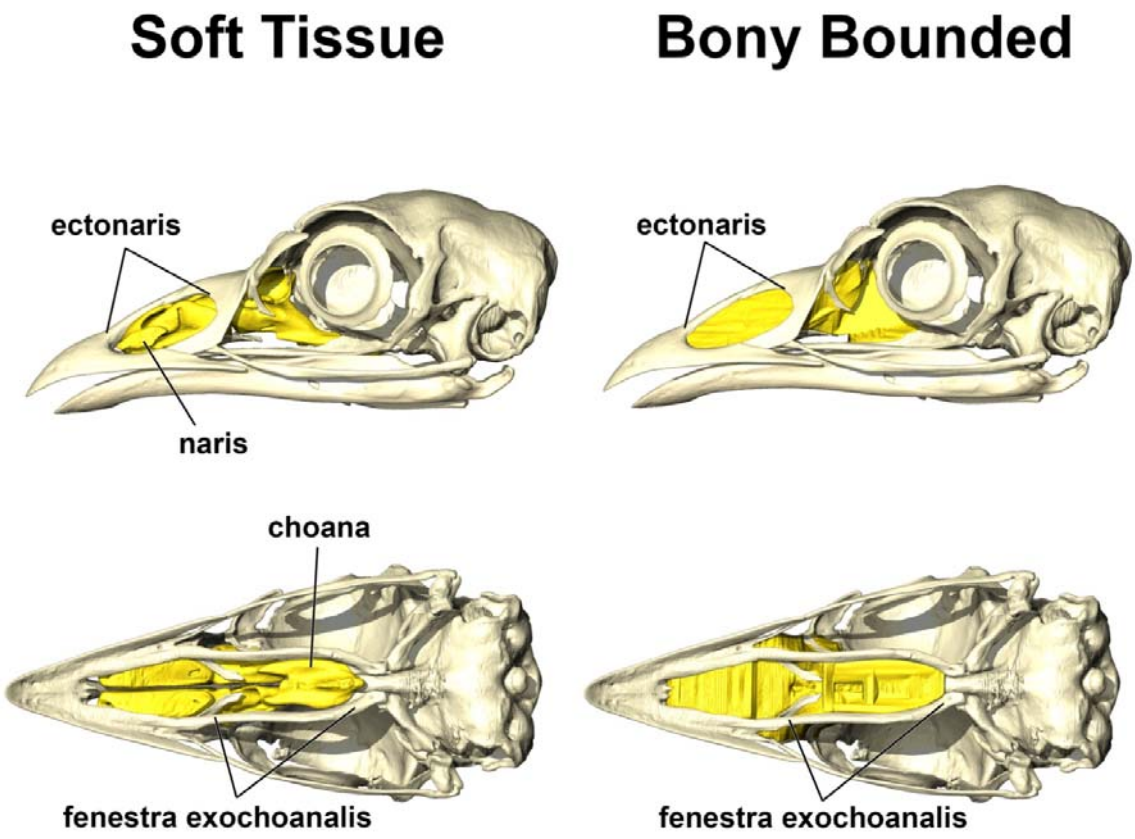

Figure 4-3. An adult wild turkey (*Meleagris gallopavo*, OUVC 10599) is used to illustrate the difference in segmentation models between the soft-tissue and bony-bounded airway interpretations. Skulls and in situ nasal passages shown in left lateral (top) and ventral (bottom) views.

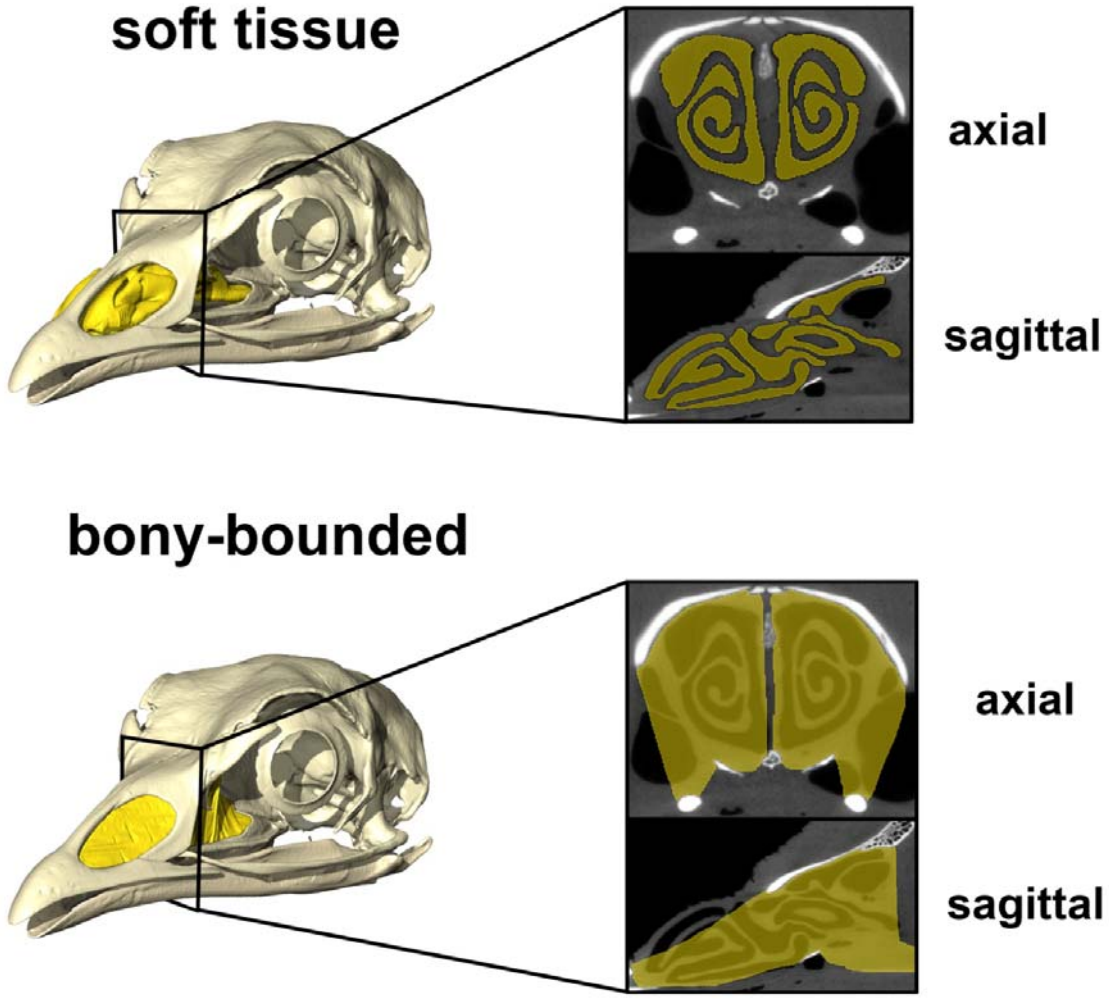

Figure 4-4. Adult wild turkey (*Meleagris gallopavo*, OUVC 10599) shown in oblique view (left). CT slices (right) of the airways taken from the same location show the difference in segmentation criteria between a soft-tissue segmentation (top) and a bony-bounded segmentation (bottom).

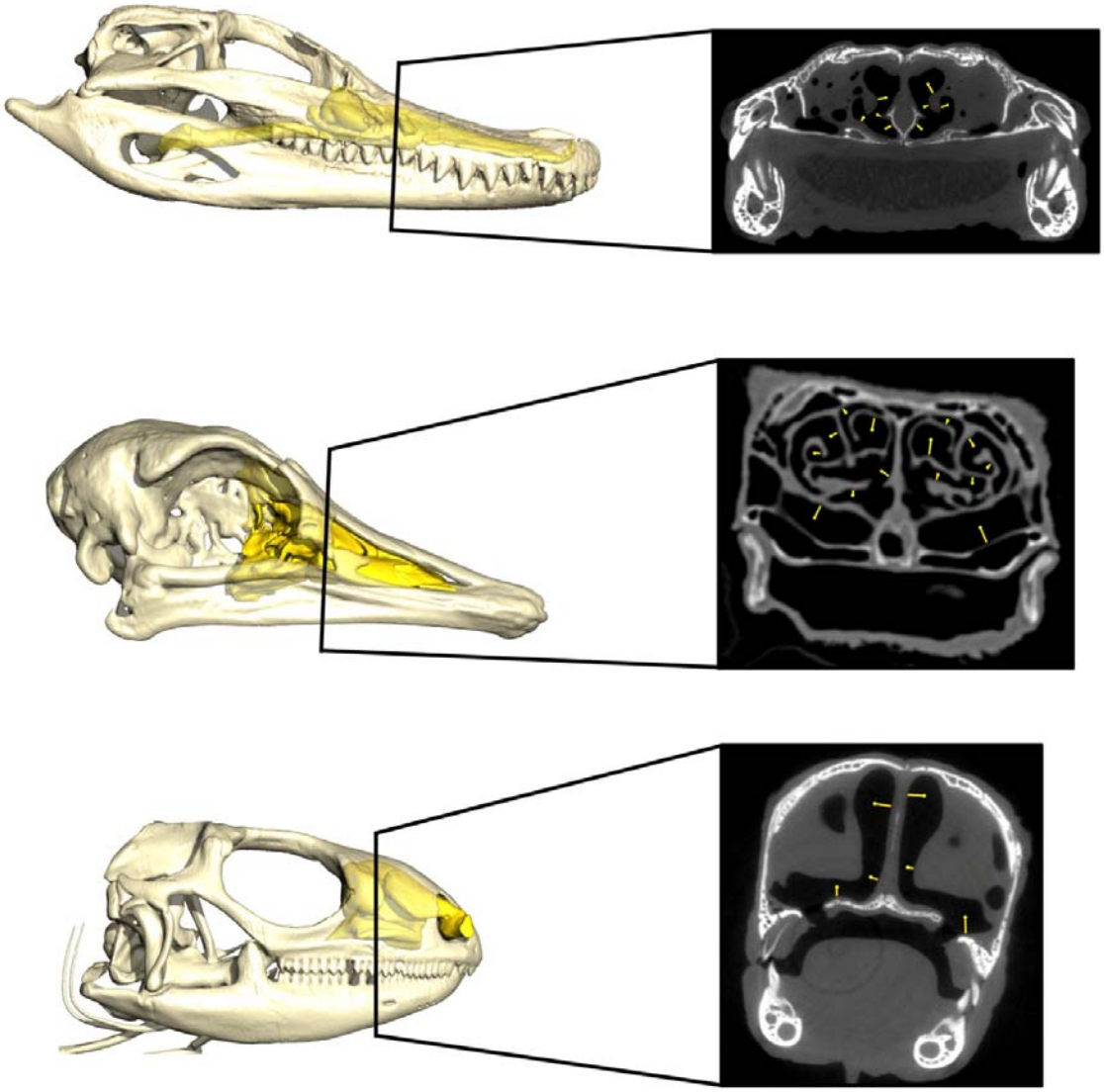

Figure 4-5. Example airway measurements taken from each specimen. The skulls and airways of an Alligator (*Alligator mississippiensis*, OUVC 10389, top), ostrich (*Struthio camelus*, OUVC 10636, middle), and iguana (*Iguana iguana*, OUVC 10603, bottom) are shown with their respective, axial CT slices. Multiple measurements were taken from the center of the air field to the nearest nasal wall. The amount of measurements per cross section varied depending on cross section location and anatomical complexity.

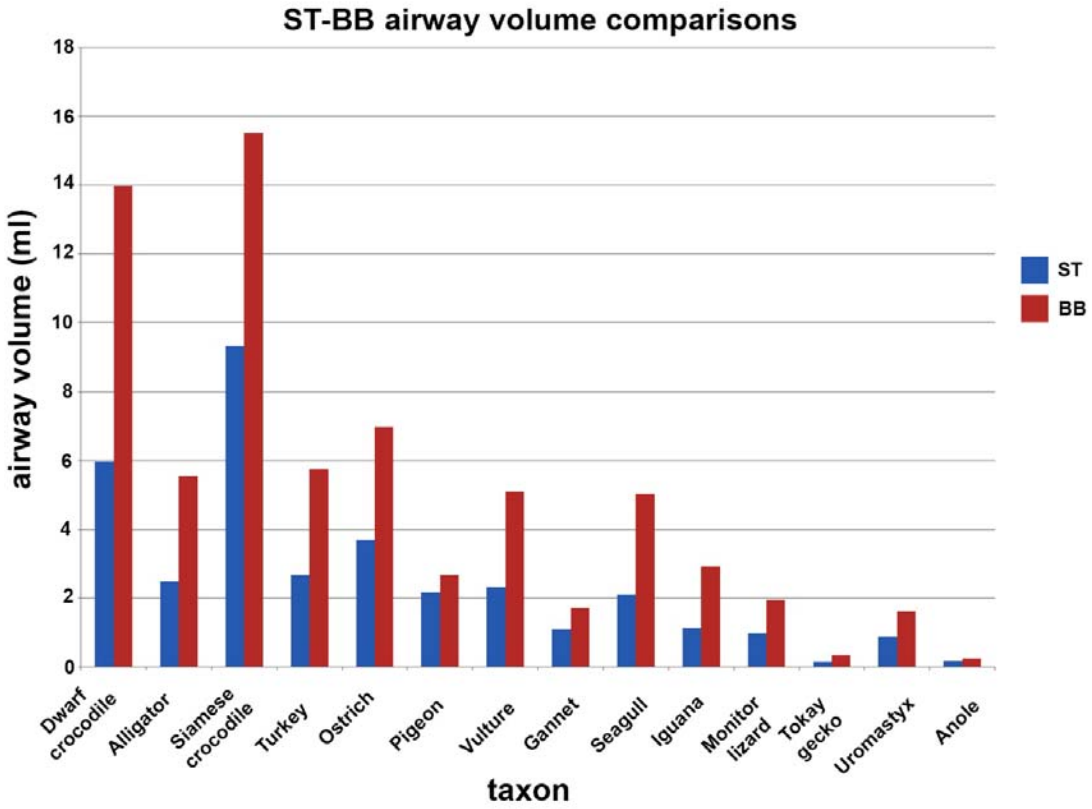

Figure 4-6. Comparison of soft-tissue and bony-bounded airway volumes for taxa used in this study.

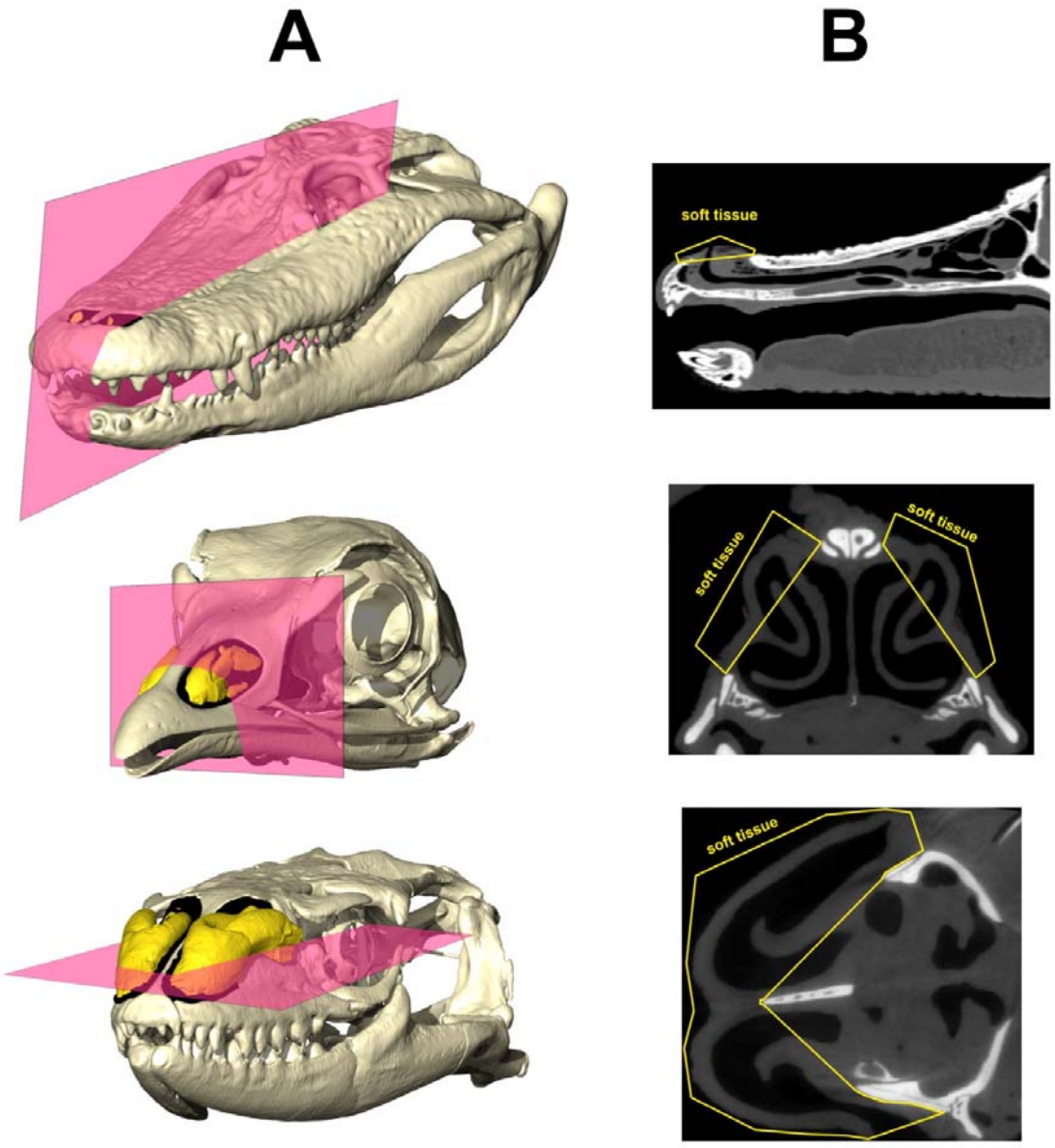

Figure 4-7. Soft-tissue extensions of the airway beyond the limits of the skull. (A) Skulls of (top) an American alligator (*Alligator mississippiensis*, OUVC 9761), (middle) wild turkey (*Meleagris gallopavo*, OUVC 10599), and (bottom) savannah monitor (*Varanus exanthematicus*, OUVC 10675) are shown next to (B) their corresponding CT slice showing the extent of soft-tissue extension beyond the limits of the underlying skull bones. Pink rectangles indicate the location and plane in which the CT image was taken.

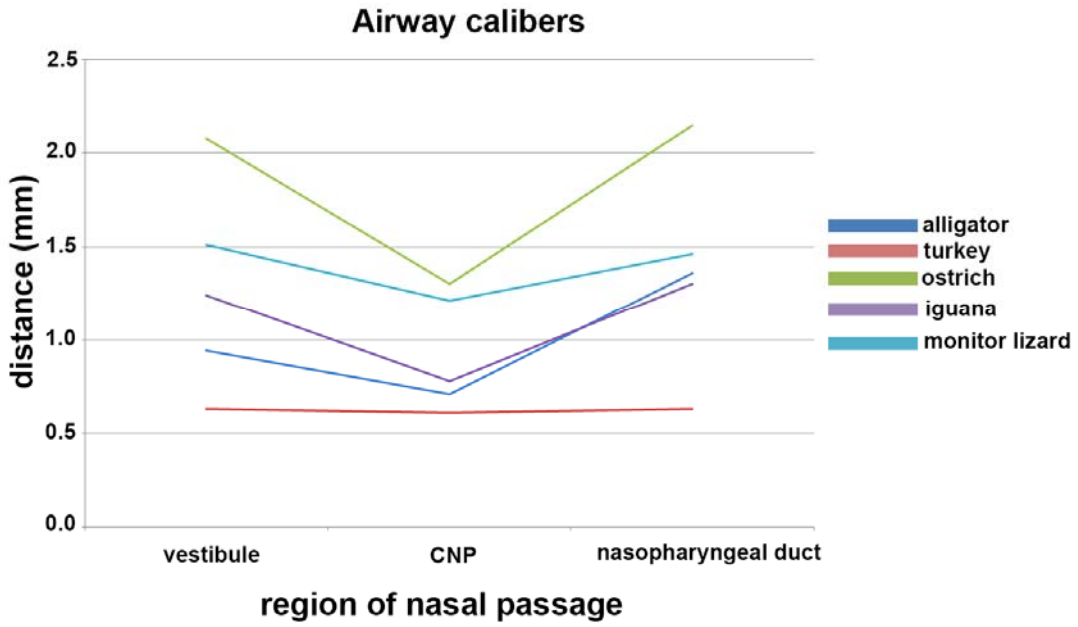

Figure 4-8. Average airway radial distances from the center of the air field to the nearest mucosal wall in some of the taxa used in this study. Measurements are separated by their location throughout the nasal passage.

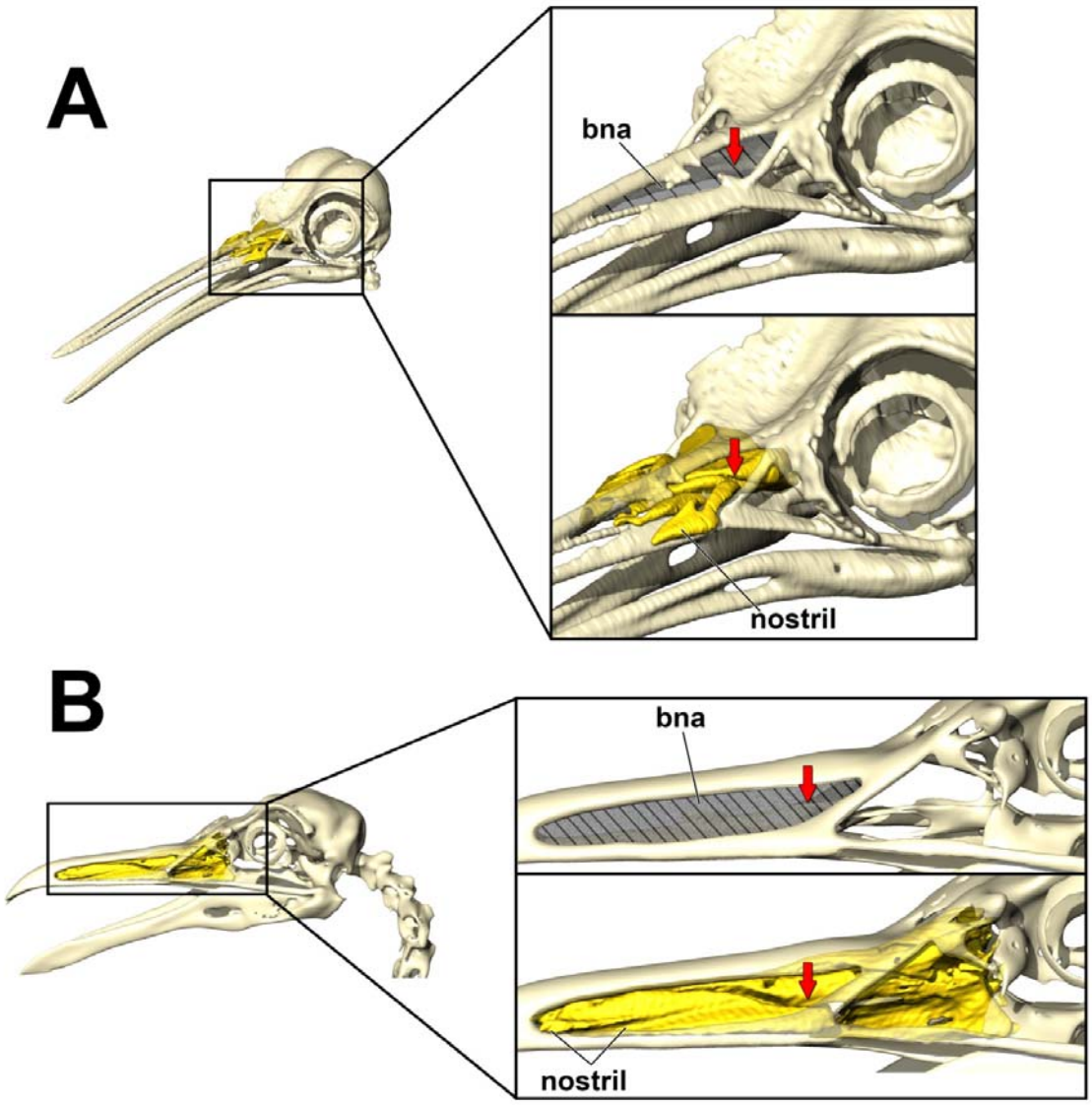

Figure 4-9. Skulls of (A) an Anna's hummingbird (*Calypte anna*), (B) a western gull (*Larus occidentalis*), and their associated airways (in yellow) illustrate the relationship between the bony narial aperture and the nasal vestibule. The rise of the crista nasalis was used to demarcate the location of the terminal vestibule (red arrow). Hatching denotes the span of the bony narial aperture. Note how the caudal terminus of the nasal vestibule falls well within the caudal limits of the bony narial aperture.

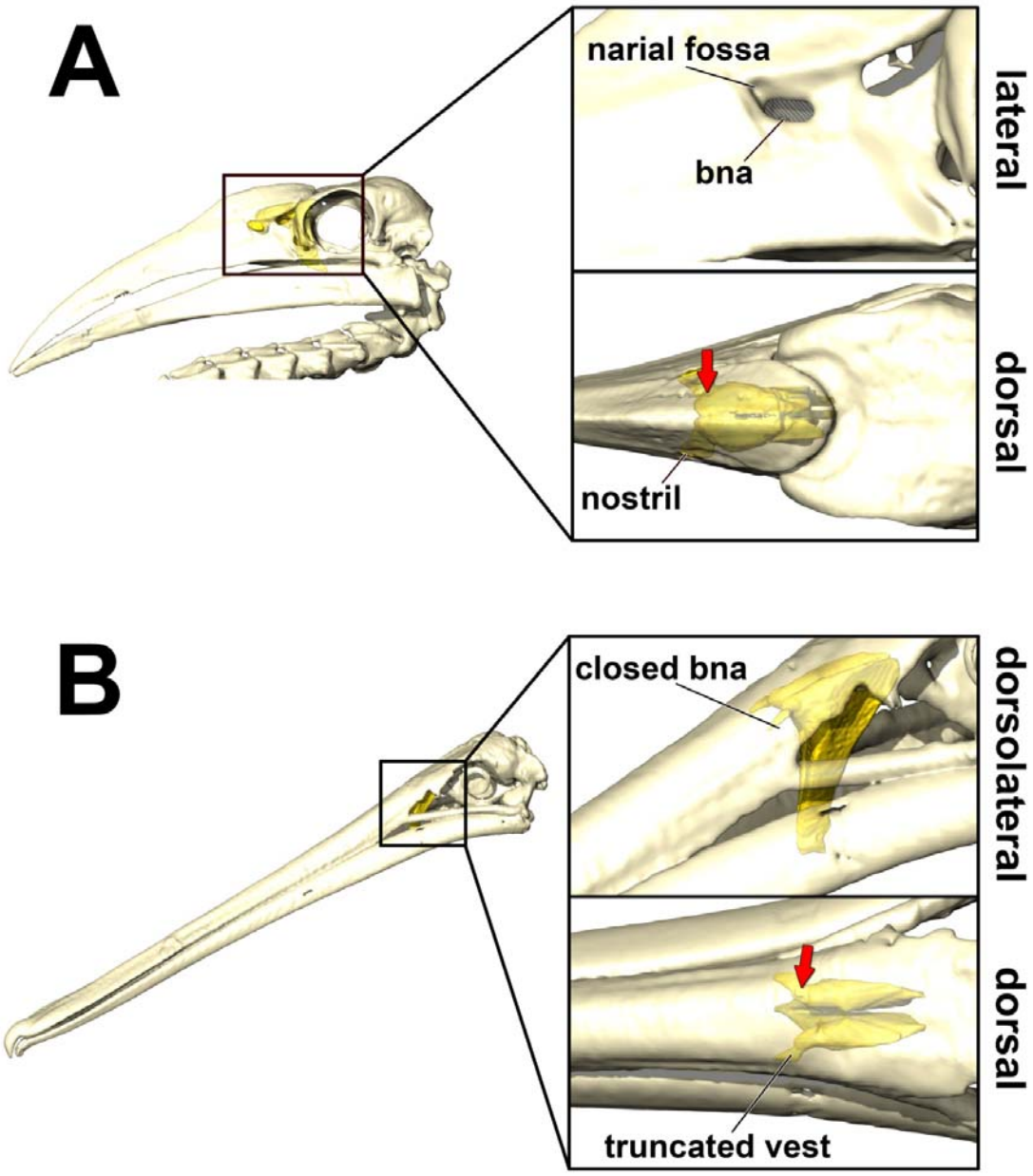

Figure 4-10. Skulls of (A) a southern ground hornbill (*Buceros leadbeateri*, TM 73579) and (B) a brown pelican (*Pelecanus occidentalis*) with their in situ airways (in yellow). Insets illustrate the correspondence of nasal vestibule length to bony nostril width. Pelicans offer a unique case as they have closed their bony nostrils, resulting in truncated, vestigial nasal vestibules. Hatching denotes the span of the bony narial aperture. Red arrow denotes caudal terminus of nasal vestibule.

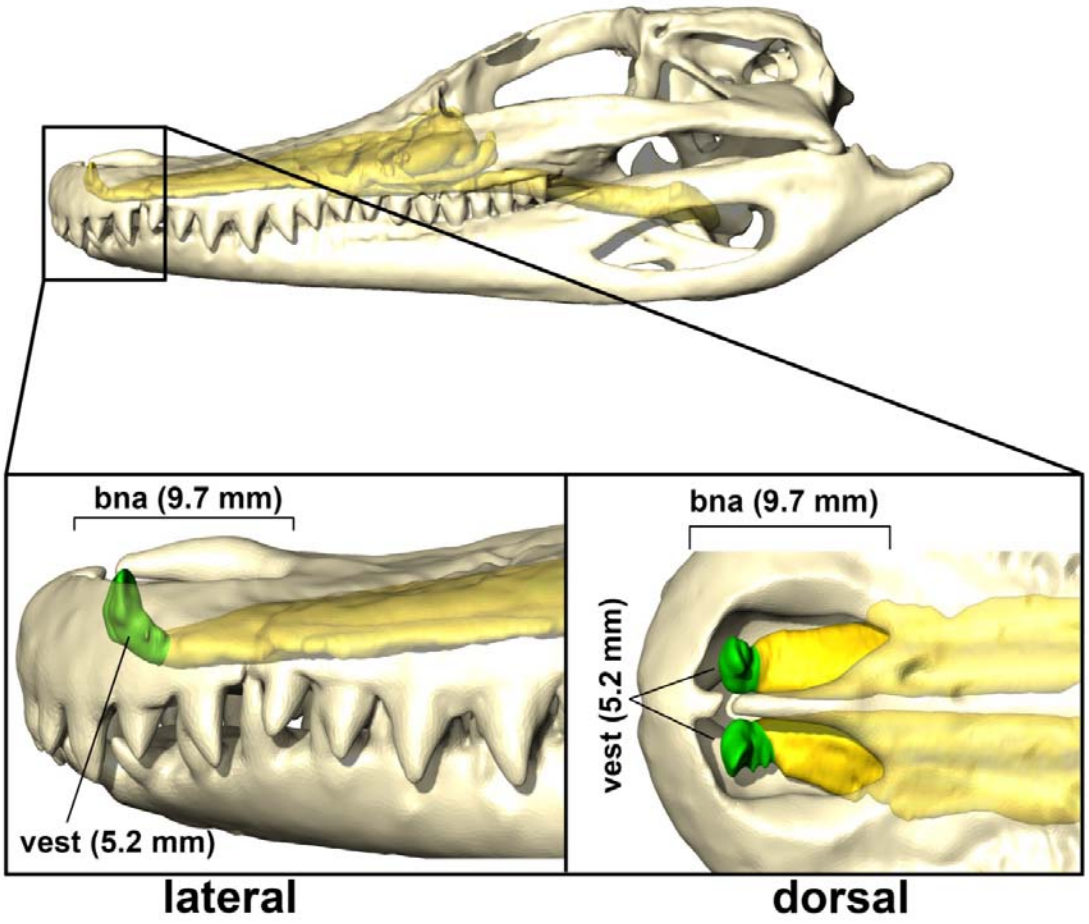

Figure 4-11. Nasal vestibule and bony narial aperture of a young alligator (*Alligator mississippiensis,* OUVC 10389). Although short in relation to the rest of the nasal passage, the vertical descent of the vestibule obscures its total length, which is fairly substantial compared to the associated bony narial aperture.

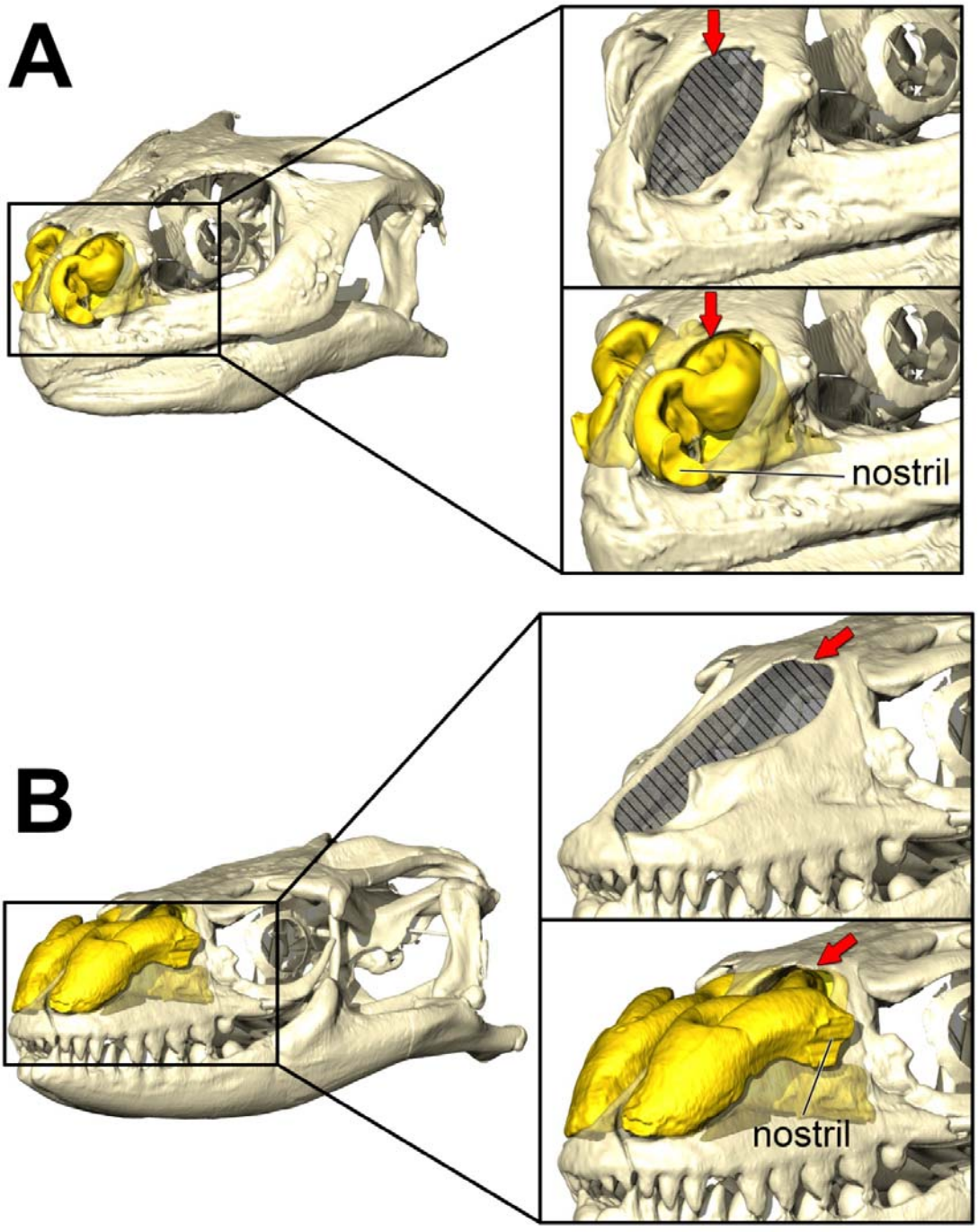

Figure 4-12. Bony narial aperture in relation to the airway in (A) the agamid, *Uromastyx aegyptia* (OUVC 10688), and (B) the varanid, *Varanus exanthematicus* (OUVC 10675). Hatching denotes the span of the bony narial aperture. Red arrow indicates the caudal terminus of the nasal vestibule.

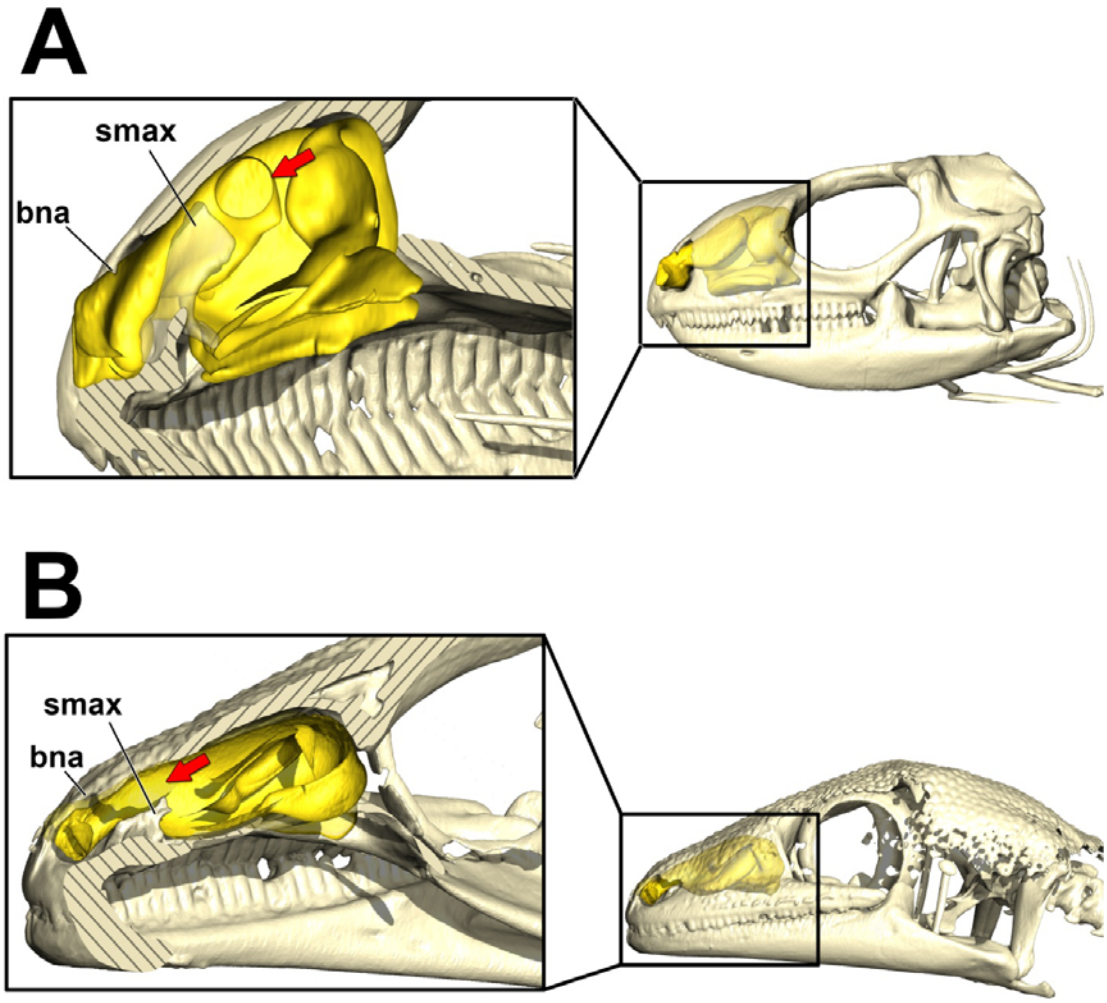

Figure 4-13. Relationship between the bony narial aperture, septomaxilla, and the nasal vestibule in a green iguana (*Iguana iguana*, OUVC 10603), and a tokay gecko (*Gekko gecko*, OUVC xxxxx). Insets show a left sagittal section through the skull and airway. Hatching denotes cut bone.

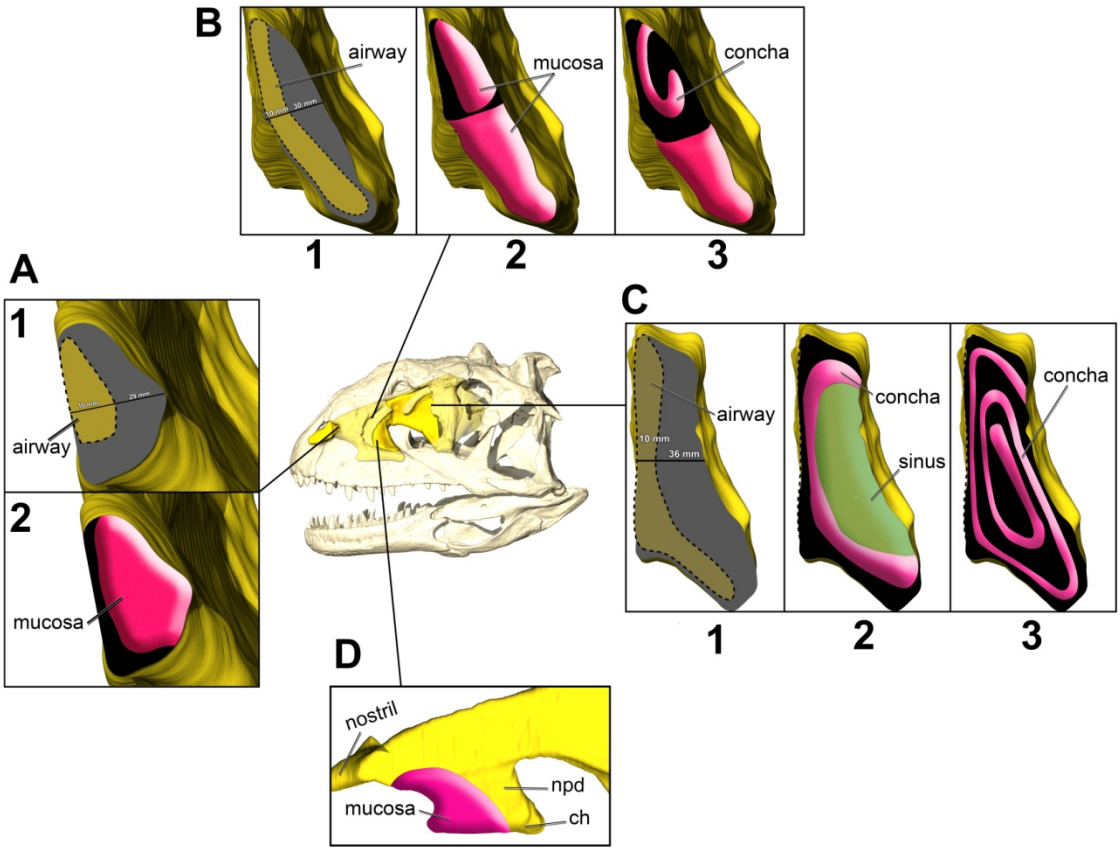

Figure 4-14. Soft-tissue-corrected airway for *Majungasaurus crenatissimus* (FMNH PR 2100). (A) Caudal rim of the bony narial aperture was used to determine the caudal terminus of the nasal vestibule, which would have likely held a mucosal constriction. (A1) Difference in airway diameters between the ST-corrected airway (yellow) and BB airway (grey). (A2) Potential mucosal coverage that could have compressed the airway at this junction. (B) CNP of *M. crenatissimus*. (B1) Comparison of airway diameters as in A1. (B2) Potential mucosal or (B3) conchal shape that could have compressed this region of the airway. (C) Olfactory region. (C1) Comparison of airway diameters as in A1 and B1. (C2) Large, hollow hillock-shaped concha shown effectively compressing this region of the nasal passage. Portion of the antorbital sinus is shown inflating the concha. (C3) Large size of the olfactory region could have alternatively provided room for a coiled olfactory turbinate. (D) Potential soft-tissue constriction of the bony-bounded nasopharyngeal duct. Such a constriction would provide greater separation of olfactory and respiratory air streams.

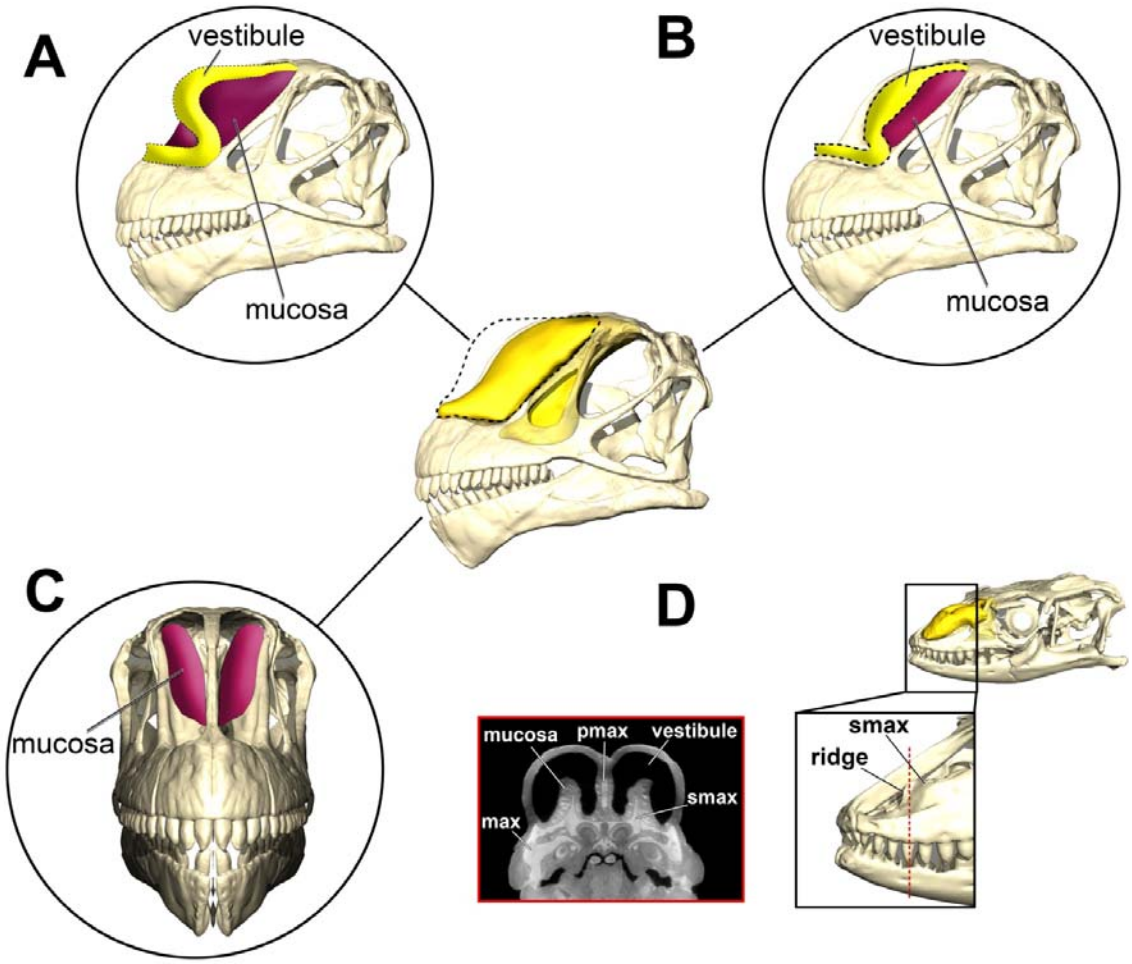

Figure 4-15. Potential soft-tissue corrections for the nasal vestibule in the sauropod *Camarasaurus grandis* (GMNH-PV101). Center: Skull of *C. grandis* with conservatively reconstructed, bony-bounded airway. Dashed lines indicate potential dorsal and rostral extent of the nasal passage in life. (A) Elaborate nasal vestibule enhanced via extensive mucosal coverage (purple). (B) Nasal vestibule constricted and limited to the extent of the associated nasal cavity bones. (C) Rostral view of airway showing potential mucosal extensions coming off the premaxillary processes of the maxilla (purple). (D) Skull of a savannah monitor (*Varanus exanthematicus*, OUVC 10675) with associated airway (yellow). Inset: close up of the rostrum in *V. exanthematicus* showing the dome-shaped septomaxilla with a bony-ridge extending dorsally. Red dashes indicate the location of the rostral axial CT slice shown in the red box. Note the presence of extensive mucosa coming off the ridge on the septomaxilla.

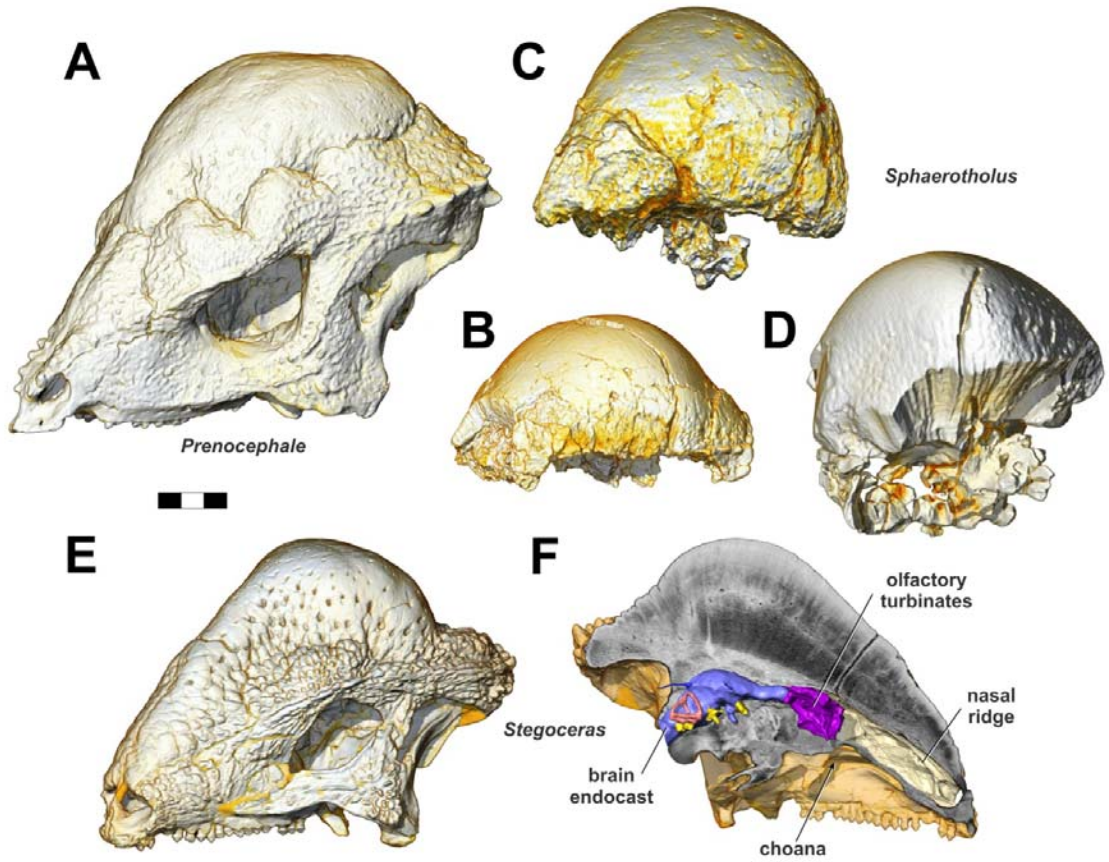

Figure 5-1. Pachycephalosaurid skulls discussed in this article, based on volume-rendered CT-scan data, in oblique left rostrolateral view, except for F which is a medial view of the left half of a sagittally sectioned skull. (A) *Prenocephale prenes*, ZPAL MgD-1/104. (B) *Sphaerotholus edmontonensis,* MRF 360. (C) *S. edmontonensis,* MRF 361. (D) *S. goodwini*, NMMNH P-27403. (E) *Stegoceras validum*, UALVP 2. (F) *S. validum*, UALVP 2, sagittally sectioned to reveal putative respiratory turbinate ridge on the nasal and segmented surfaces of brain endocast and mineralized olfactory turbinates. Scale bar equals 3 cm.

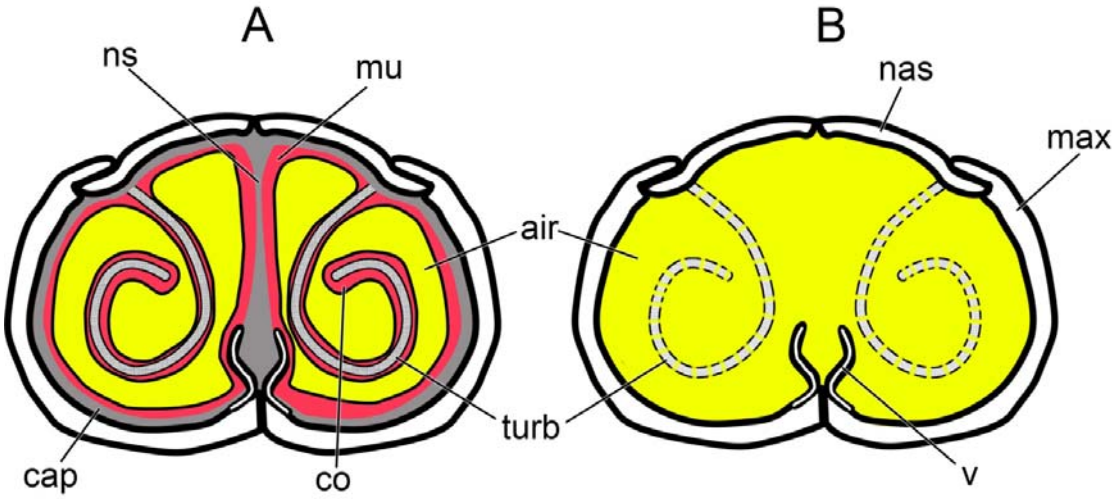

Figure 5-2. Diagrammatic cross sections through the nasal region of a generalized amniote. (A) The nasal passage can be broken down into a series of nested layers starting with the bones surrounding the nasal cavity (white). Deep to the bones of the nasal cavity is the cartilaginous nasal capsule and nasal septum (gray) as well as cartilaginous or mineralized turbinates (hatched). Deep to this layer lies the mucosa (red) and conchae. The deepest region is the open space of the nasal airway where respired air travels (yellow). (B) In contrast, fossilized airways rarely retain evidence of the soft tissue within, resulting in a much lower fidelity, bony-bounded airway. Even mineralized turbinates may not preserve due to their delicate architecture.

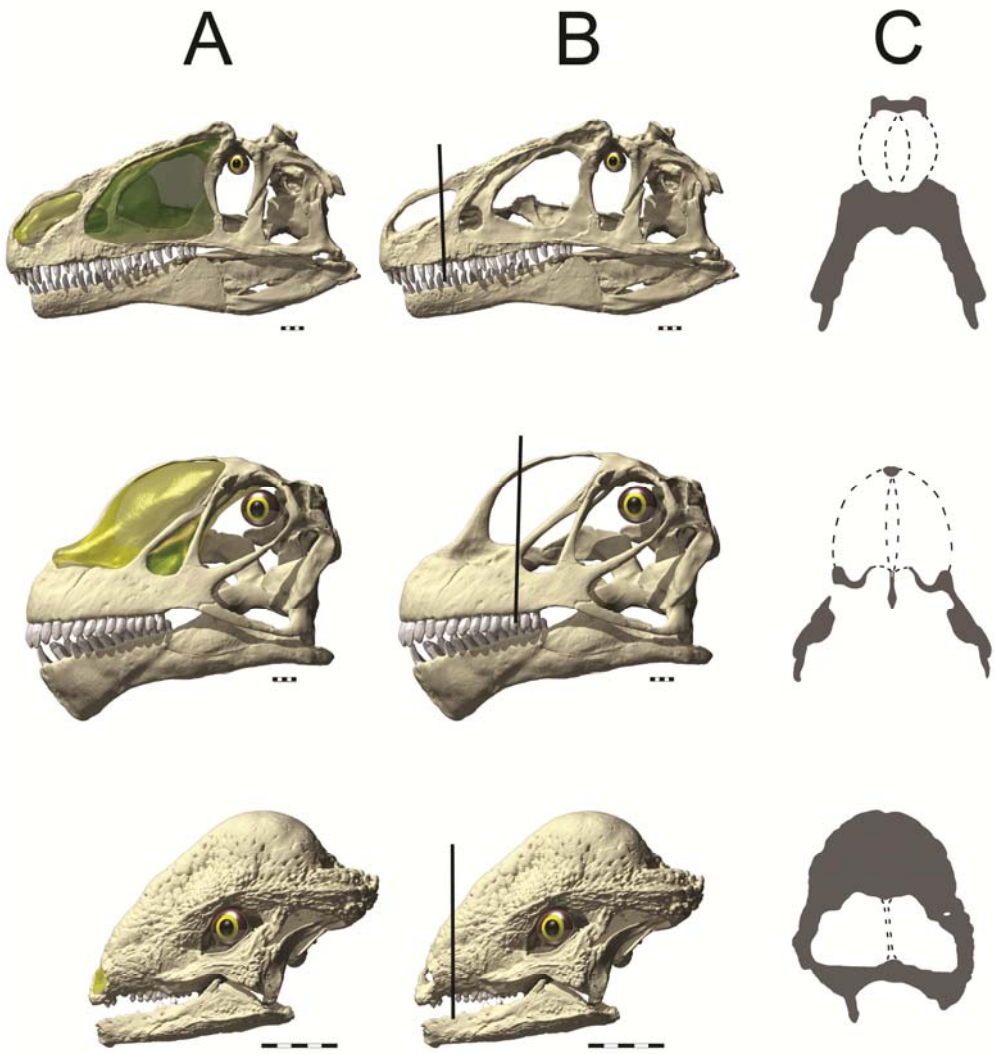

Figure 5-3. Comparison of nasal cavity boundaries in the dinosaur genera *Allosaurus* (top), *Camarasaurus* (middle), and *Stegoceras* (bottom). (A) Skulls with nasal capsule and paranasal sinuses restored. (B) Skulls without restored nasal passages. Black line indicates the location of (C) cross sections taken through the nasal passage. Dotted lines indicate the boundaries of conservatively restored nasal passages. Note the extensive unbounded regions of the nasal cavity in *Allosaurus* and *Camarasaurus* compared to *Stegoceras*. The well-constrained nasal cavity of Stegoceras is more amenable to soft-tissue restoration. Scale bar equals 5 cm.

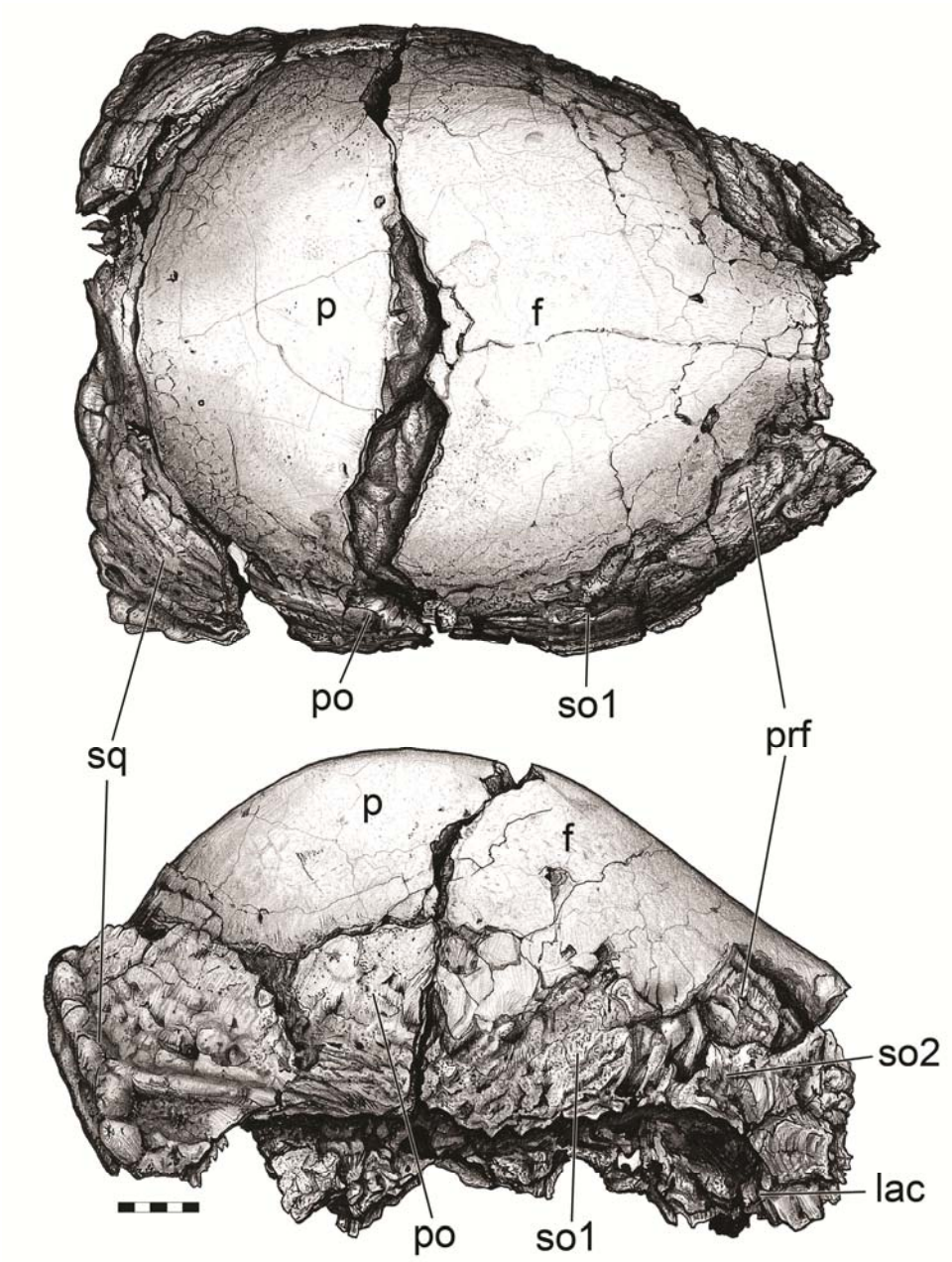

Figure 5-4. Preserved dome of *Sphaerotholus edmontonensis*, MRF 360, in dorsal (top) and right lateral view (bottom).

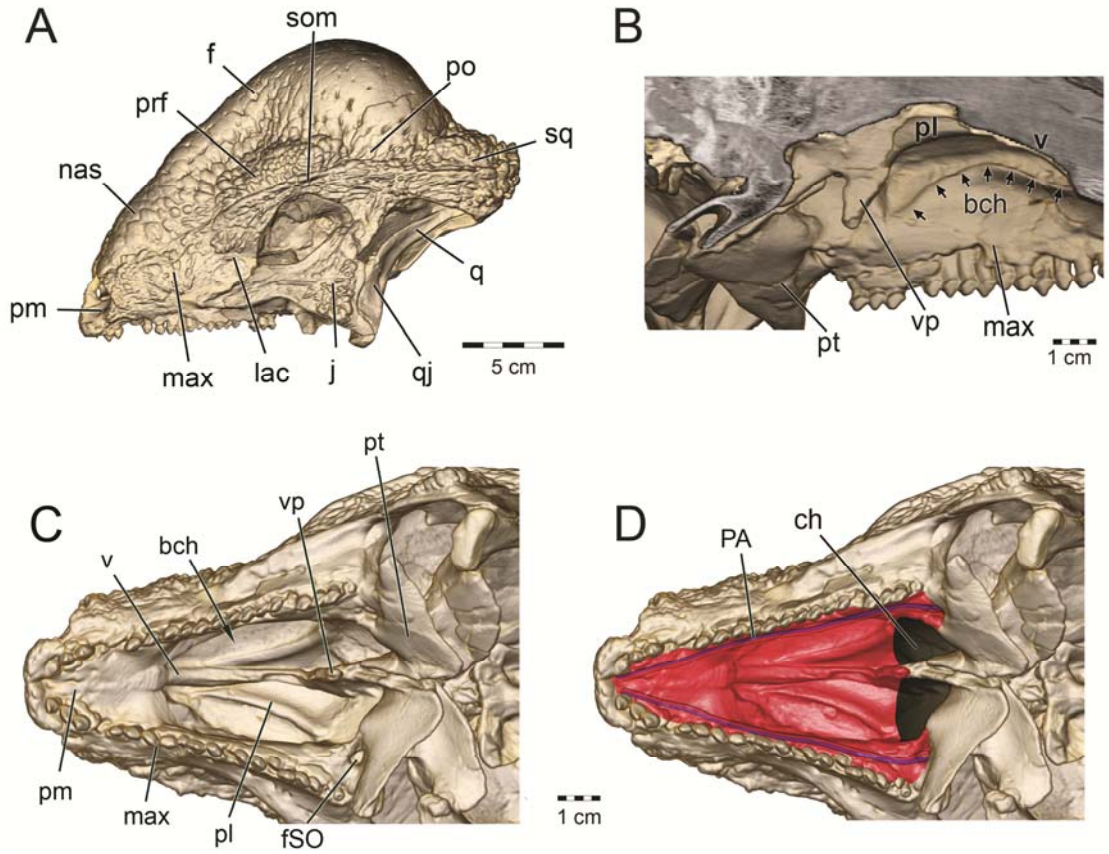

Figure 5-5. *Stegoceras validum*, UALVP 2, cranium. (A) Lateral view. (B) Left medial view of the sagittally sectioned skull highlighting neomorphic ventromedian process of palate. (C) Ventral view of skull (D) Same view as C but with restored soft palate and vasculature.

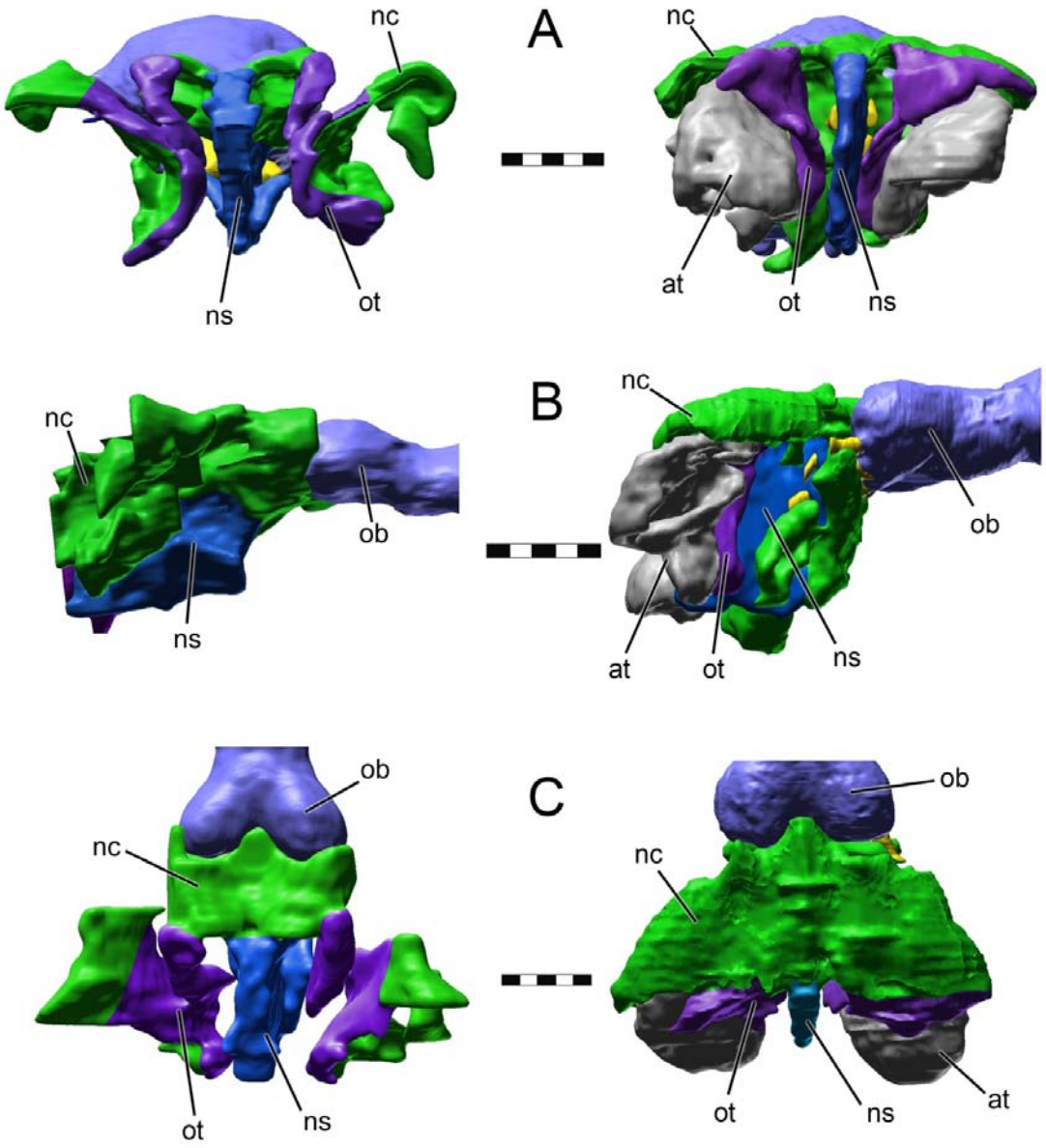

Figure 5-6. Preserved nasal capsule morphology compared between *Stegoceras validum* (UALVP 2) (left) and *Sphaerotholus edmontonensis* (MRF 360) (right) in (A) rostral, (B) left lateral, and (C) dorsal views. Scale bars equal 1 cm.

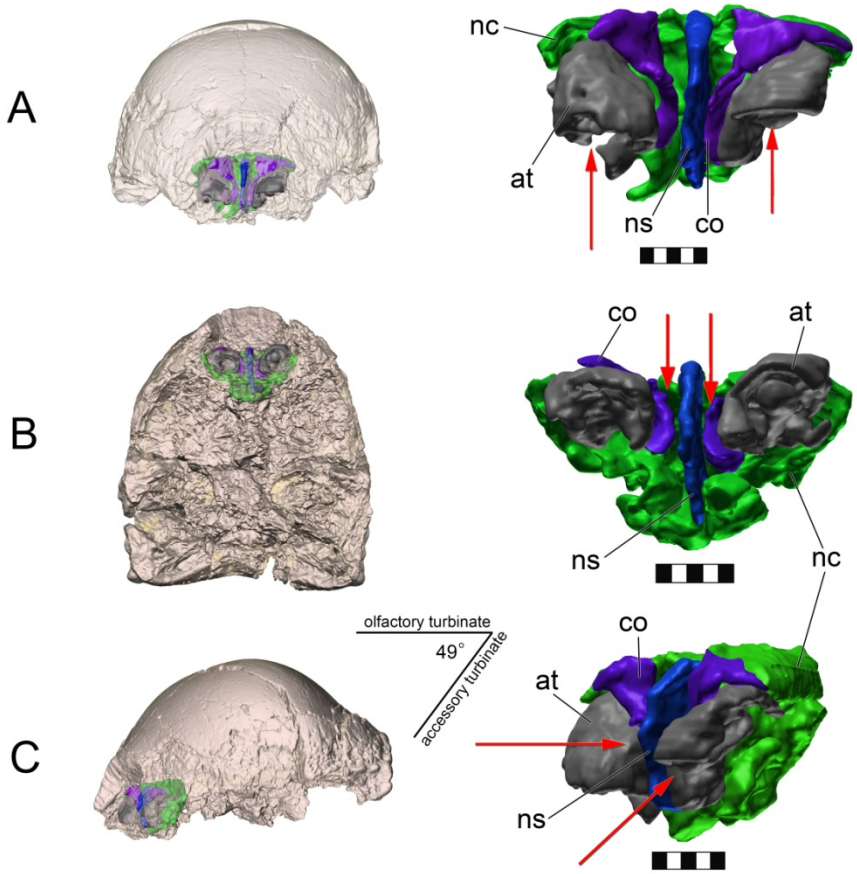

Figure 5-7. Turbinate anatomy for *Sphaerotholus edmontonensis*, MRF 360 shown *in situ* within the semitransparent cranium (left) and isolated (right) in (A) rostral, (B) ventral, and (C) left lateral oblique views. Airflow direction (red arrows) between the olfactory turbinates (purple) and septum (blue) is compared to flow through the potential accessory turbinates (gray), which are offset from the rest of nasal tissues by 49°. Scale bars equal 1 cm.

Figure 5-8. Caudal view of skull for *Stegoceras validum* (UALVP 2). The thinner outline shows the skull as preserved, with taphonomic deformation causing a slight dorsomedial skew of the right side. The thicker outline indicates the corrected, retrodeformed skull. Most deformation occurred on the right side of the skull leaving the left side relatively untouched.

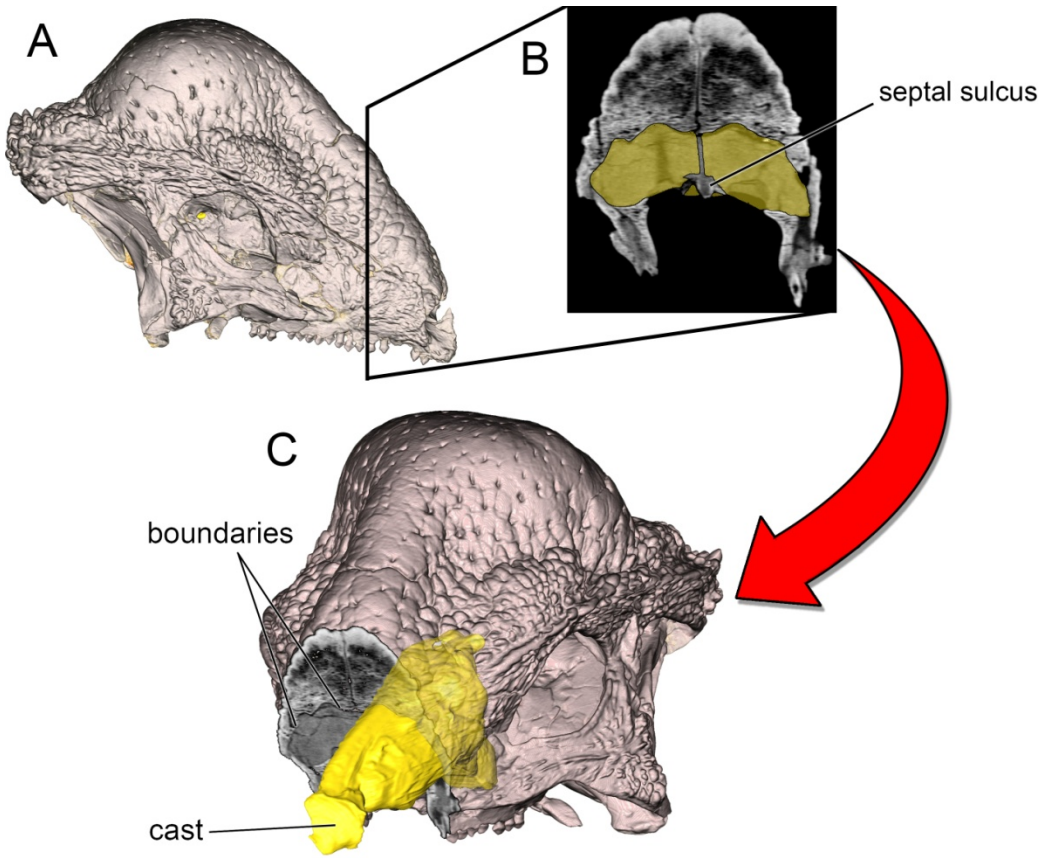

Figure 5-9. Segmentation of the air spaces on the left side of *Stegoceras validum* (UALVP 2). The skull (A) was CT scanned and from the CT data (B) the airway was segmented out using osteological correlates for its boundaries (e.g., the septal sulcus). The presence of a complete septum was used to justify segmentation of only the left side of the airway (C).

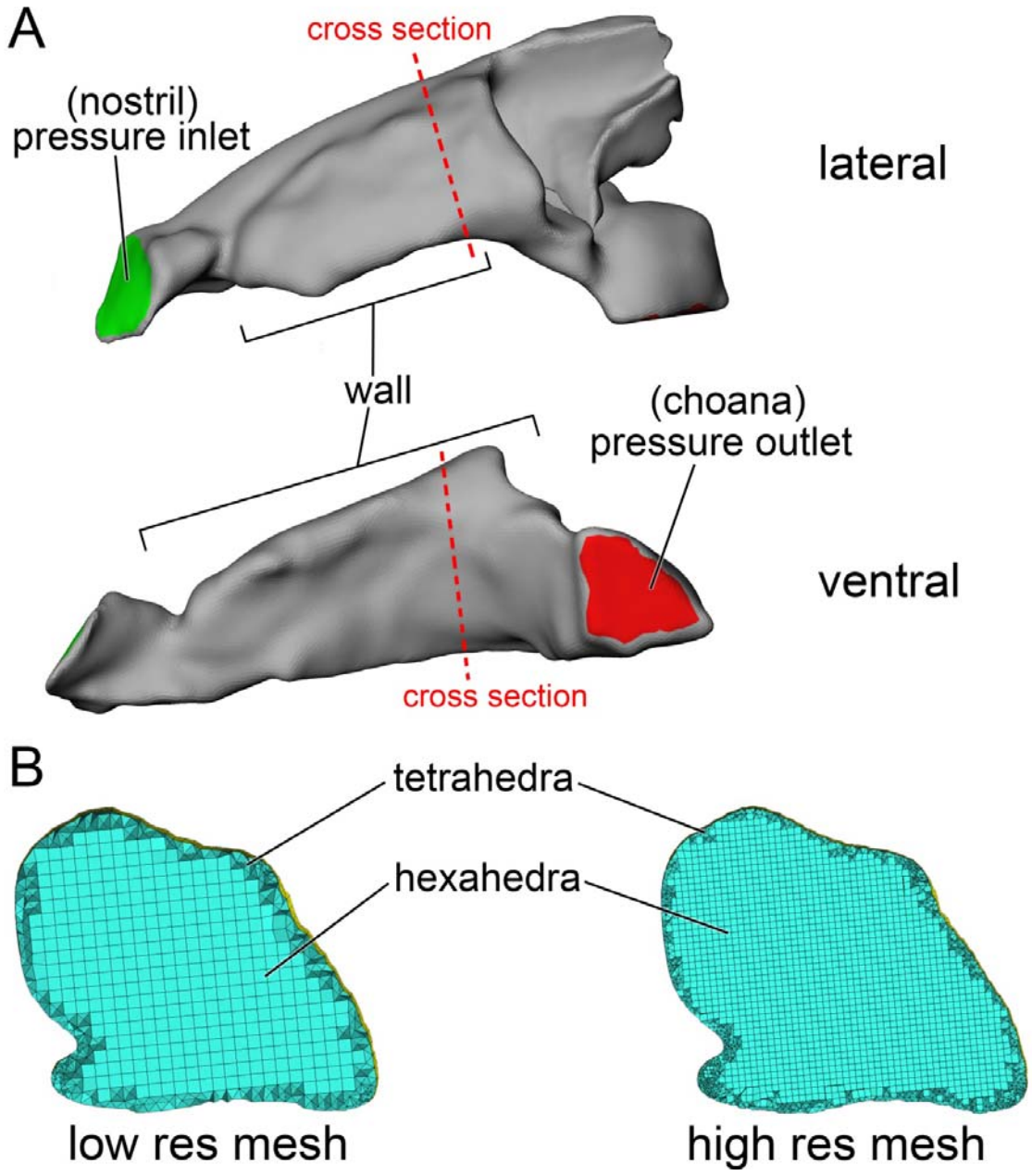

Figure 5-10. (A) Boundary condition placement on models. Boundary setup reflects inspiration. Inlets and outlets were swapped for expiration. (B) Cross sections from location shown in "A" demonstrate the distribution of tetrahedra and hexahedra within models. Multiple resolutions of each model were run to ensure grid independence.

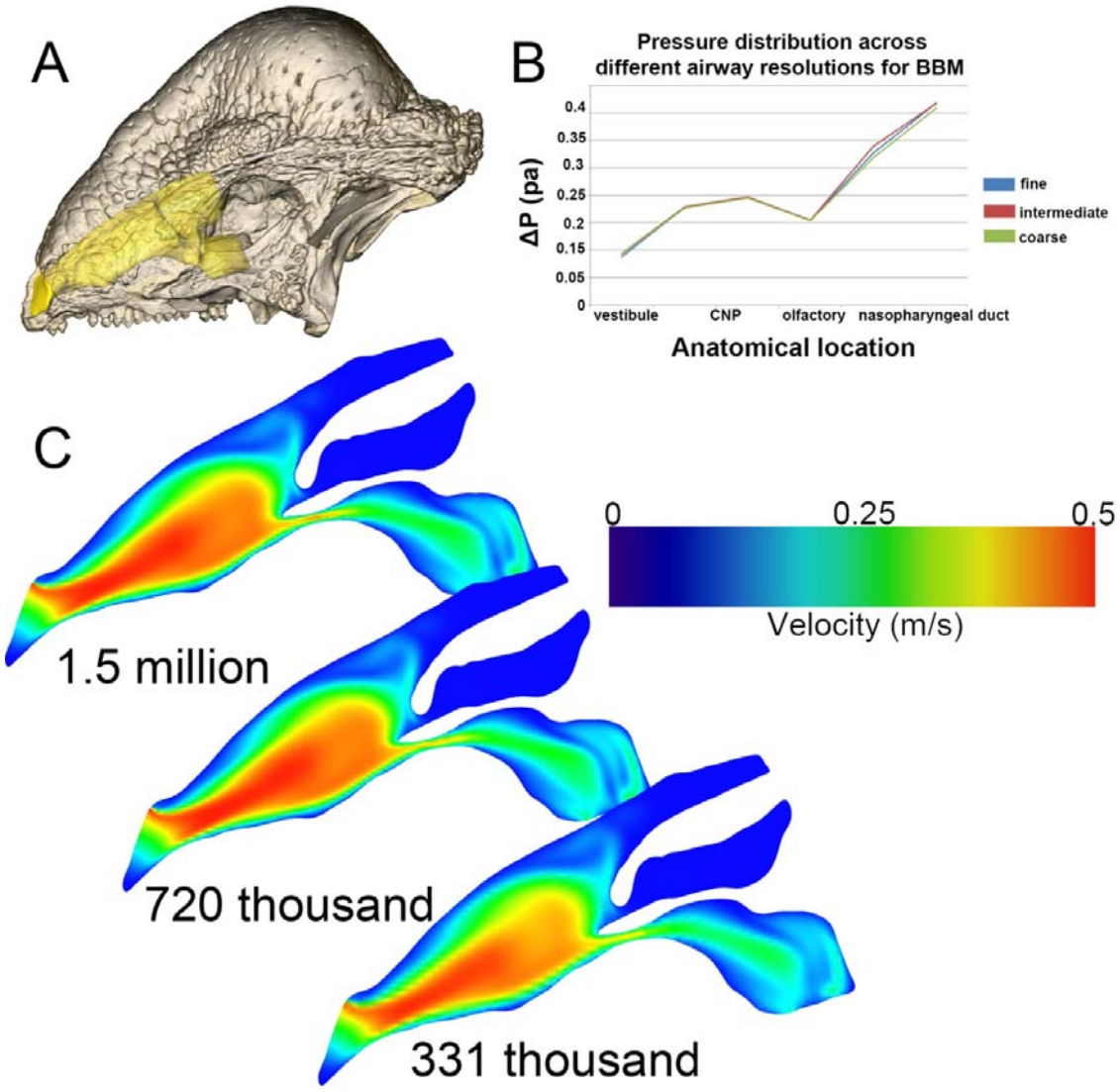

Figure 5-11. Grid Convergence Index (GCI) results from a three grid refinement study to determine solution independence. (A) Sagittal cross sections through the nasal cavity of *Stegoceras* (UALVP 2) were taken from each model resolution. (B) Magnitude of pressure distribution throughout the nasal capsule of the bony bounded airway grids. (C) Velocity profiles taken from the same location along each grid resolution reveal extensive similarity between grids, indicating that the solution obtained was largely free of grid error.

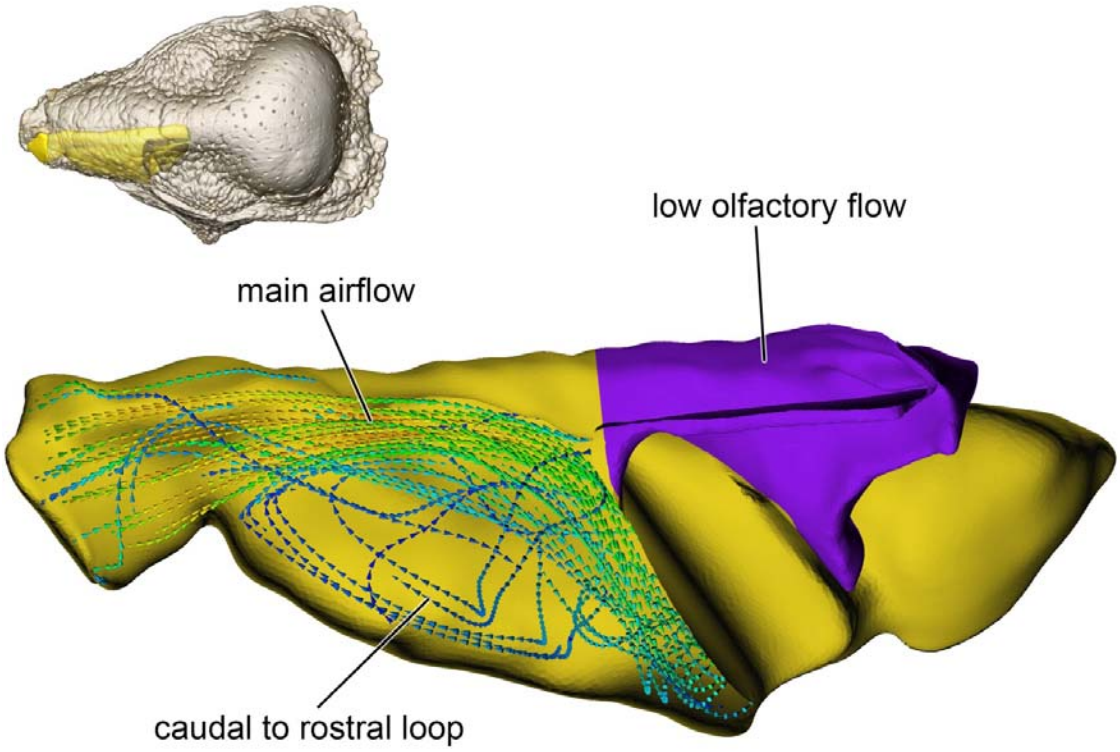

Figure 5-12. Dorsal view of bony-bounded airway in *Stegoceras validum* (UALVP 2). Little olfactory flow was noted in the airway under both flow rates. Furthermore, a caudal-to-rostral loop was observed in the lateral aspect of the cavum nasi proprium.

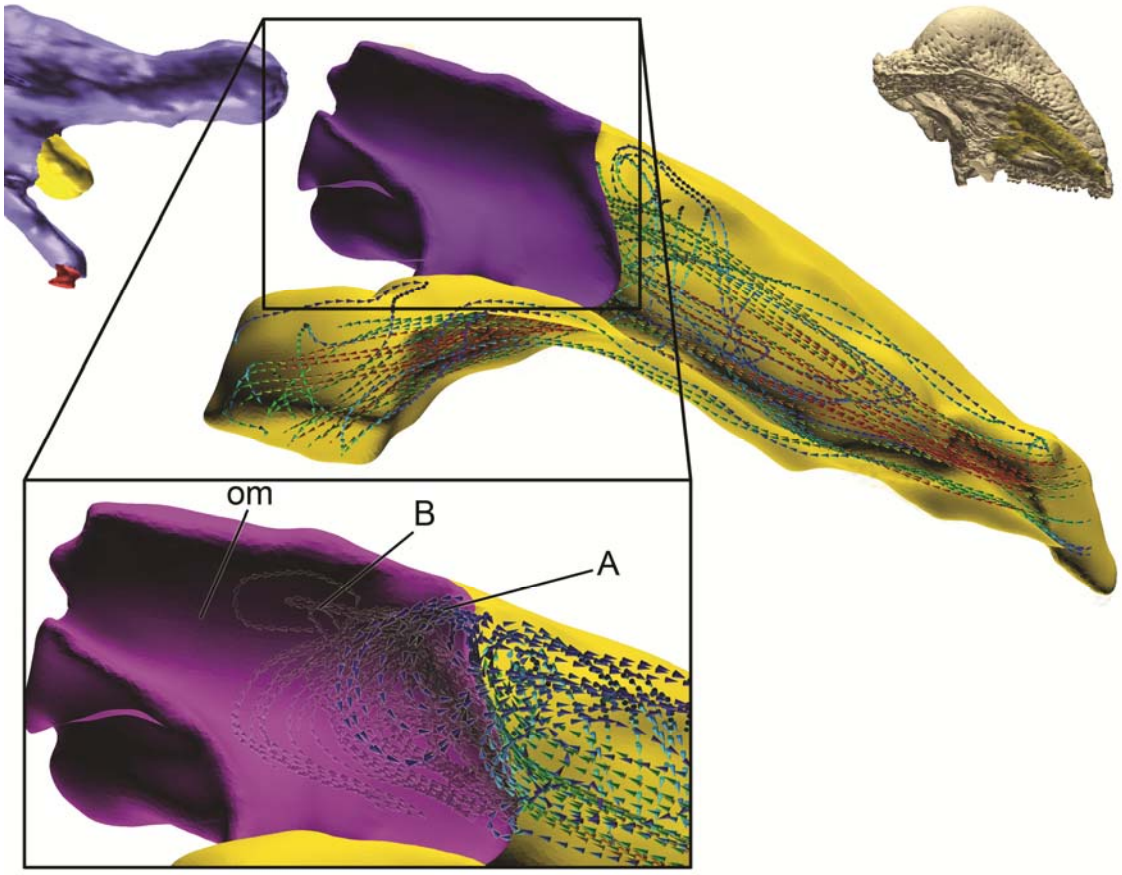

Figure 5-13. Medial view of left bony-bounded airway under inspiratory flow conditions. The brain endocast placement (top left) shows the close association of the olfactory bulbs with the olfactory chamber. Inset: Olfactory flow within the olfactory meatus (om) under a flow regime of (A) 4.4 L/min and (B) 10 L/min.

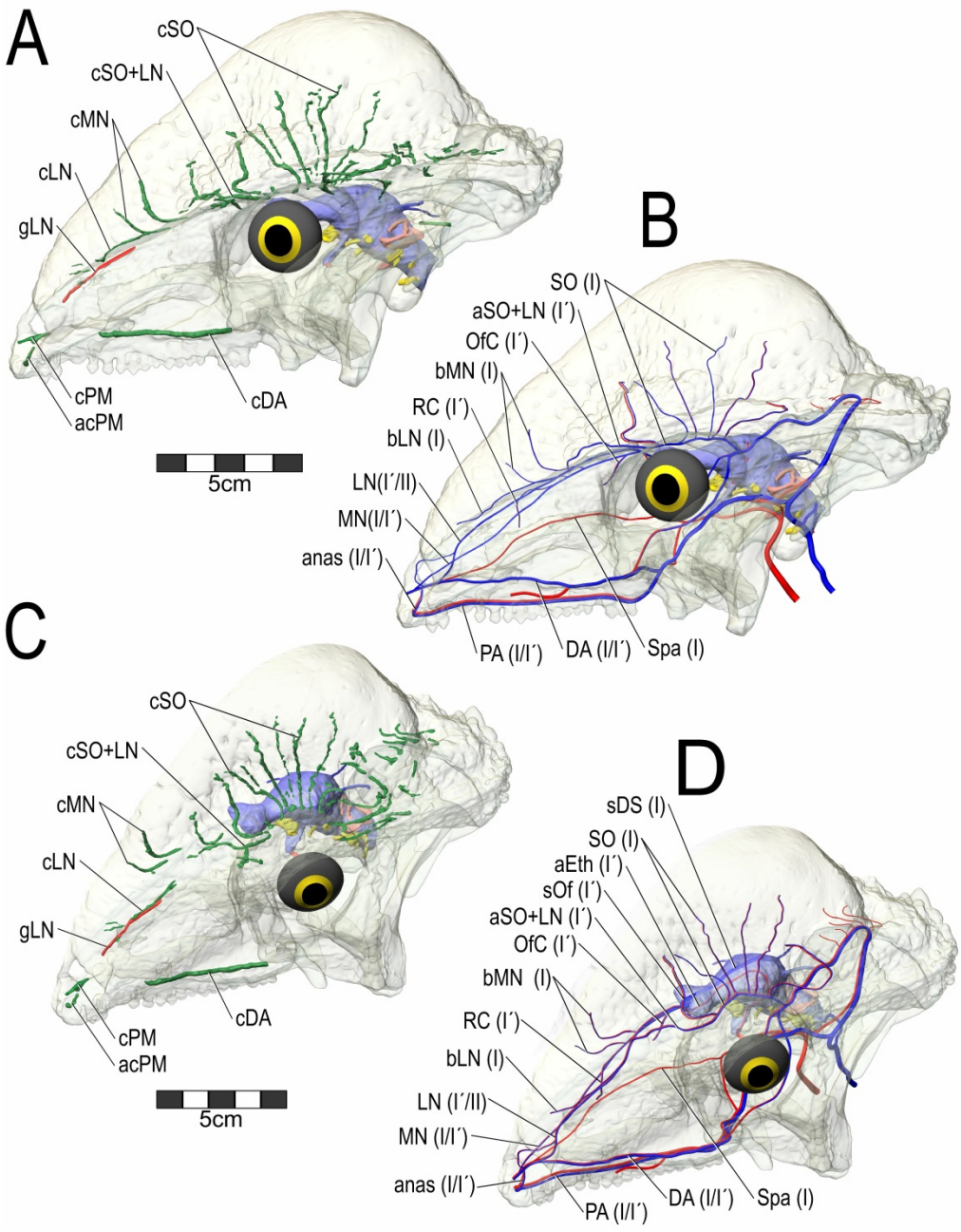

Figure 5-14. Restoration of the blood vessels within the nasal region of *Stegoceras validum* (UALVP 2). (A) Left lateral view and (C) left dorsolateral view, showing osteological correlates (e.g., vascular canals and grooves) found in the nasal region. (B) Left lateral view and (D) left dorsolateral view showing the restored blood vessels that supply and drain the nasal region. Levels of inference follow abbreviations parenthetically.

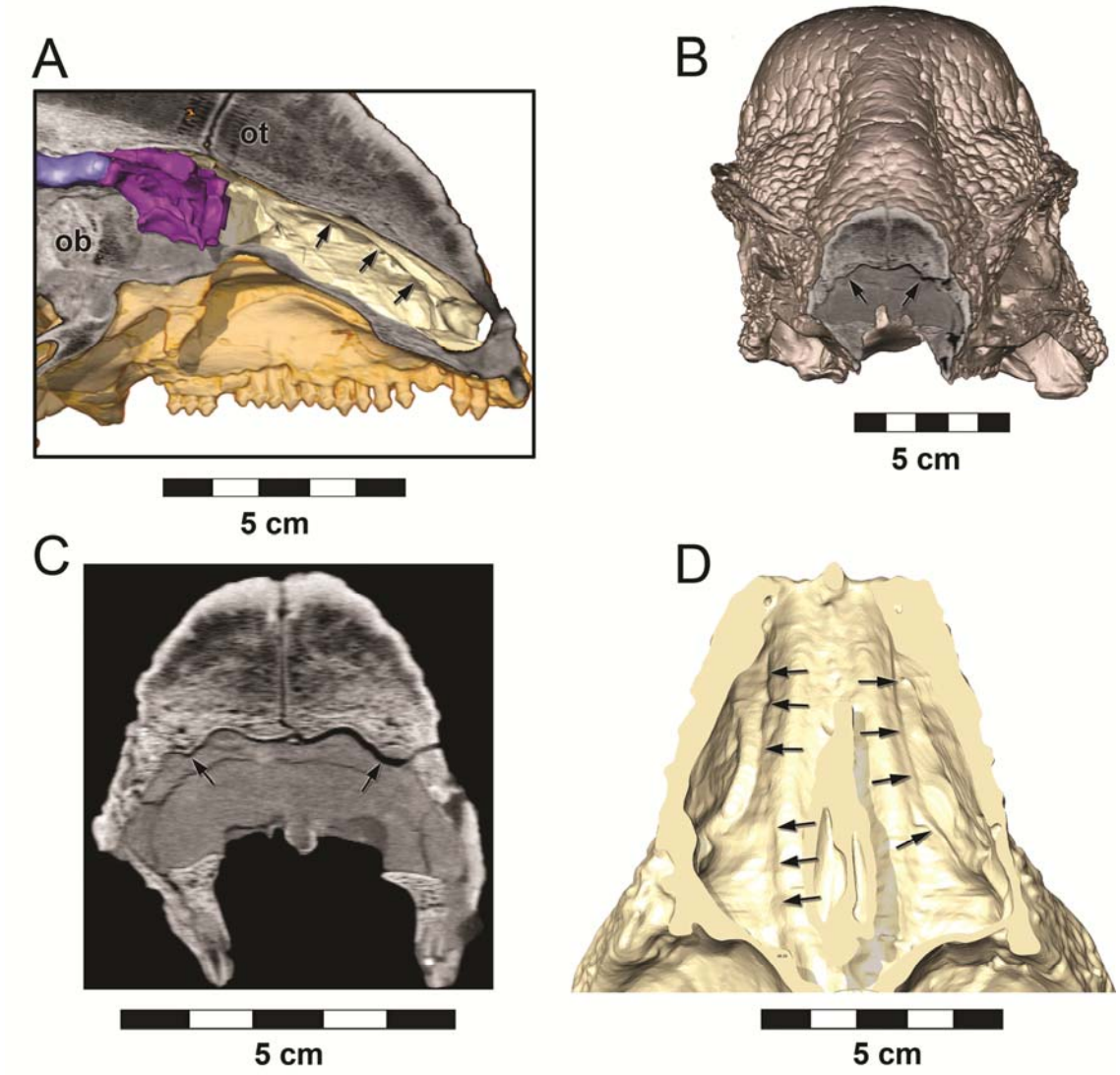

Figure 5-15. Putative turbinate ridge within the nasal cavity of *Stegoceras validum* (UALVP 2). (A) Left medial view with brain endocast and olfactory turbinates in place. (B) Rostral view with axial slice shown. (C) CT image of axial slice from B. (D) Ventral view of the roof of the nasal cavity. Arrows point to the ridge.

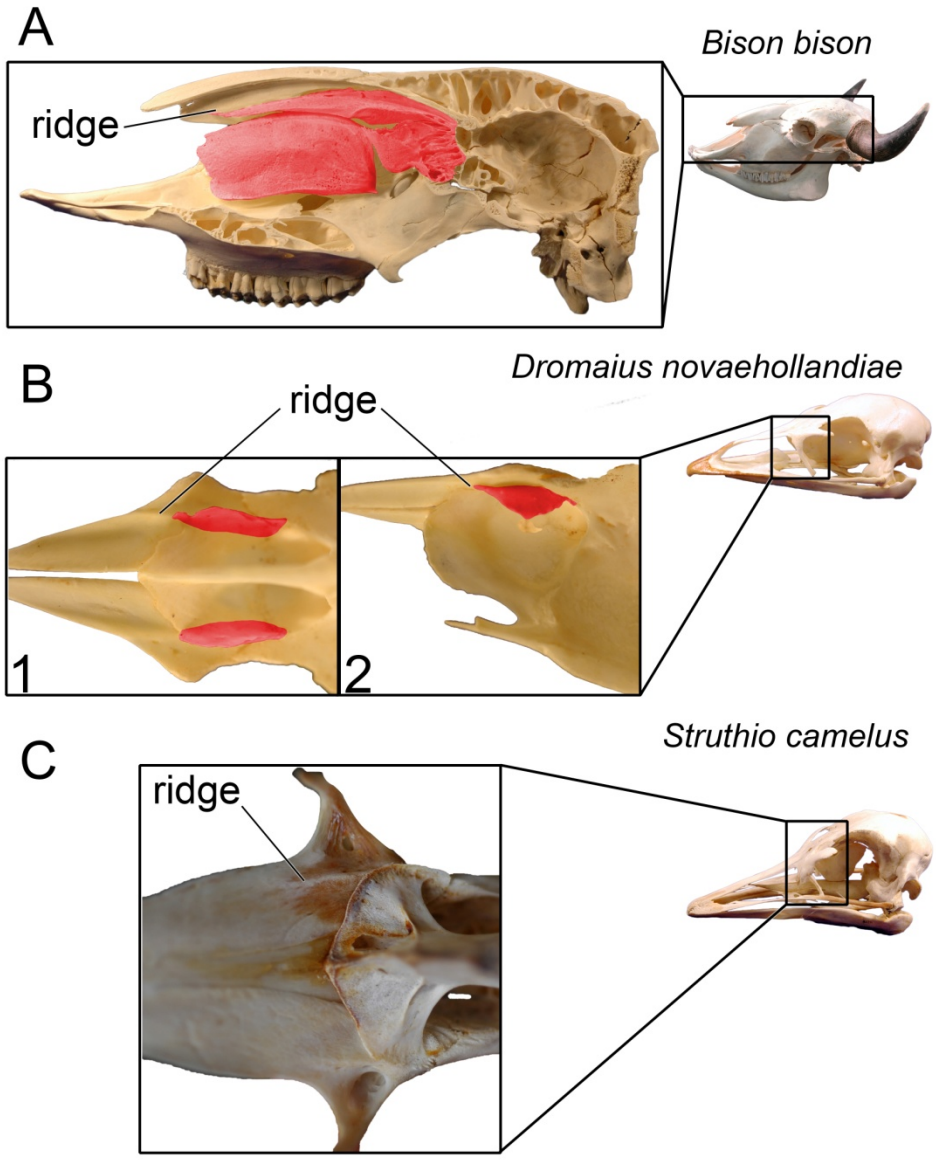

Figure 5-16. (A) Mineralized nasal turbinates (red) in a representative mammal (*Bison bison*, OUVC 9557 [inset], 09489). *(B, C)* Ridges for turbinates are also rare in diapsids, but large paleognaths sometime show turbinate ridges for attachment of their middle and caudal turbinates. (B) Although rarely mineralized, the caudal nasal turbinates (red) in some birds will mineralize. (1) Ventral view of nasals in emu (*Dromaius novaehollandiae*, OUVC 10539 [inset], 10534). (2) Left lateral view of nasals and mesethmoid in the same specimen. (C) Ventral view of nasals and mesethmoid of an ostrich (*Struthio camelus*, OUVC 10464 [inset], 10526).

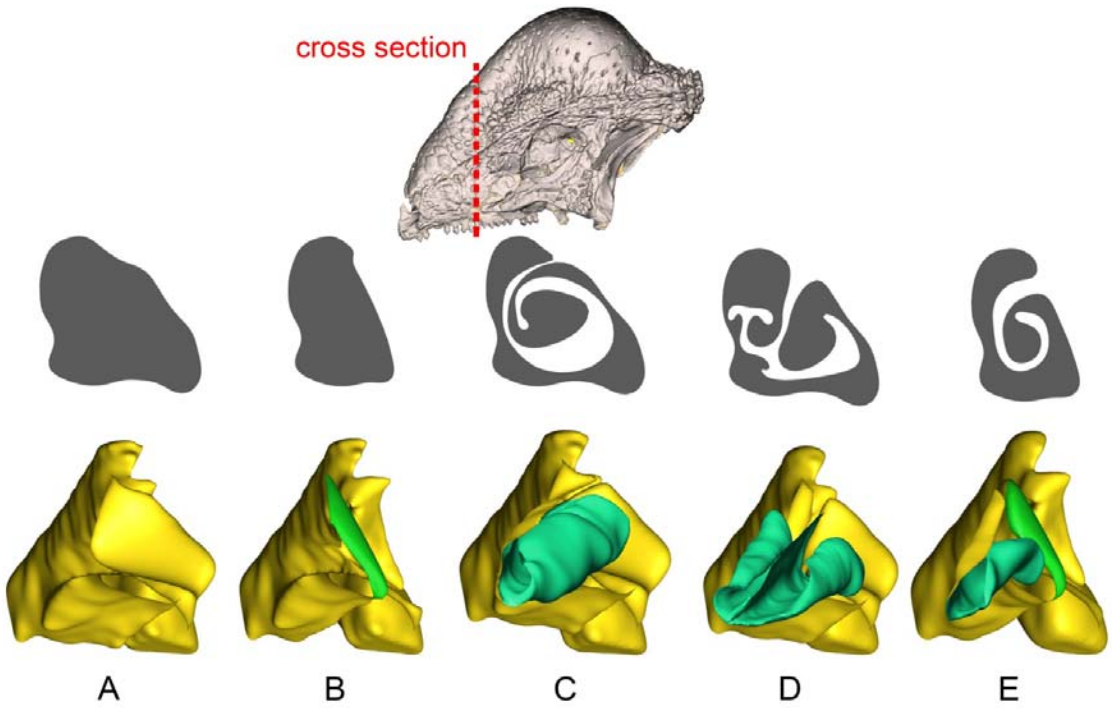

Figure 5-17. Four potential morphologies of *Stegoceras validum* (UALVP 2) were tested and had airflow patterns compared to (A) the bony-bounded airway morphology, which did not take into account any unpreserved soft tissue. (B) Nasal morphology composed of a paranasal septum walling off the antorbital paranasal air sinus from the the CNP. (C) Nasal morphology that incorporated a scrolled nasal concha. (D) Nasal morphology that incorporated a branched nasal concha. (E) Nasal morphology that incorporated both an antorbital septum and a scrolled nasal concha. Models are shown with the front-facing triangles hidden, allowing a view of the inside of the airway. Paranasal septum = green. Conchae = aquamarine.

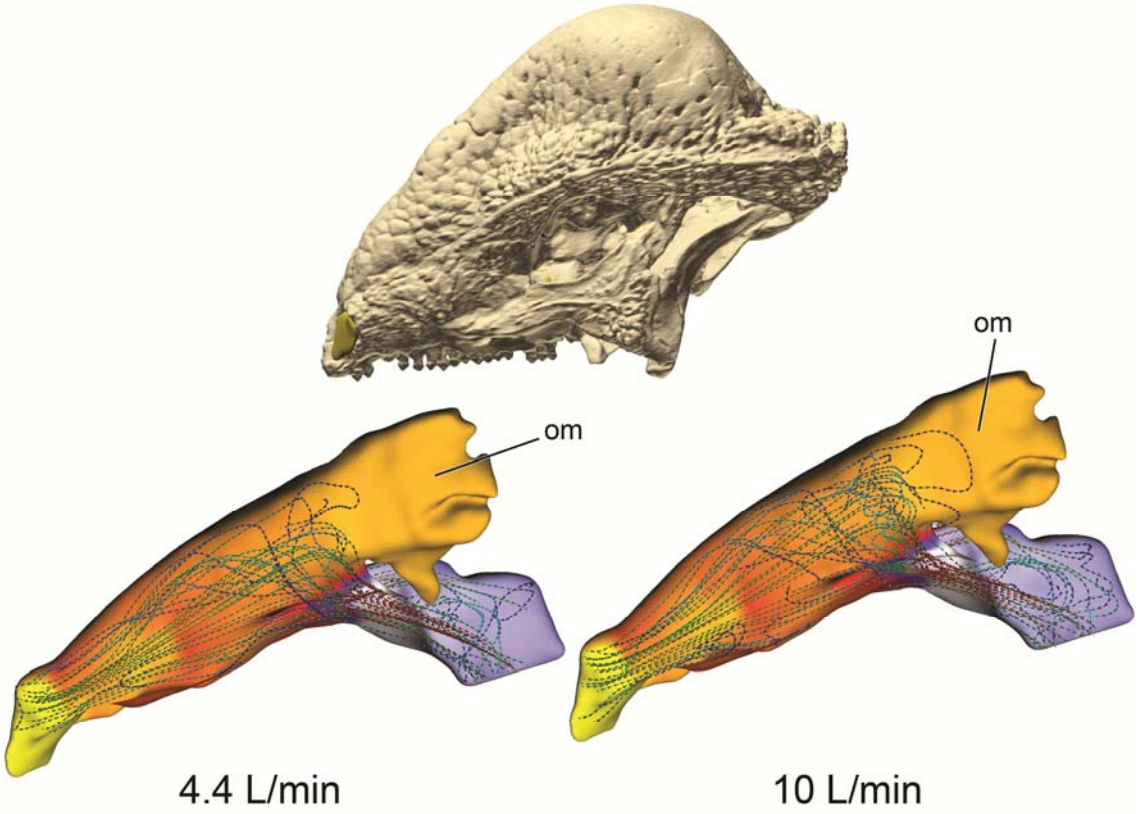

Figure 5-18. Lateral view of the nasal capsule of *Stegoceras validum* (UALVP 2) modeled with a paranasal septum at both high (right) and low (left) flow rates. Nasal capsule is color-coded to reflect the pressure distribution through the airway. Hotter colors represent higher pressures (lower flow velocities).

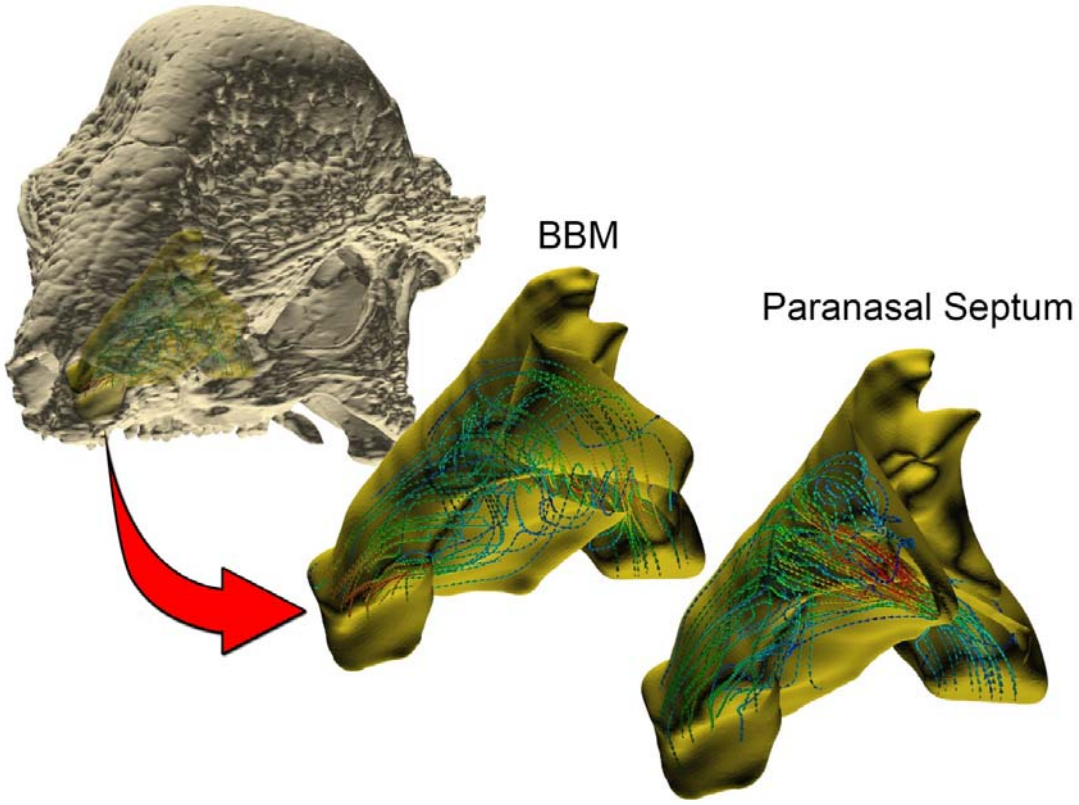

Figure 5-19. Comparison of airflow of *Stegoceras validum* (UALVP 2) during expiration at 10 L/min in the bony-bounded airway model and airway modeled with a paranasal septum. Airways both exhibited a distinct lateromedial swirl to the air field. Swirling was narrower and less developed in the airway modeled with a paranasal septum.

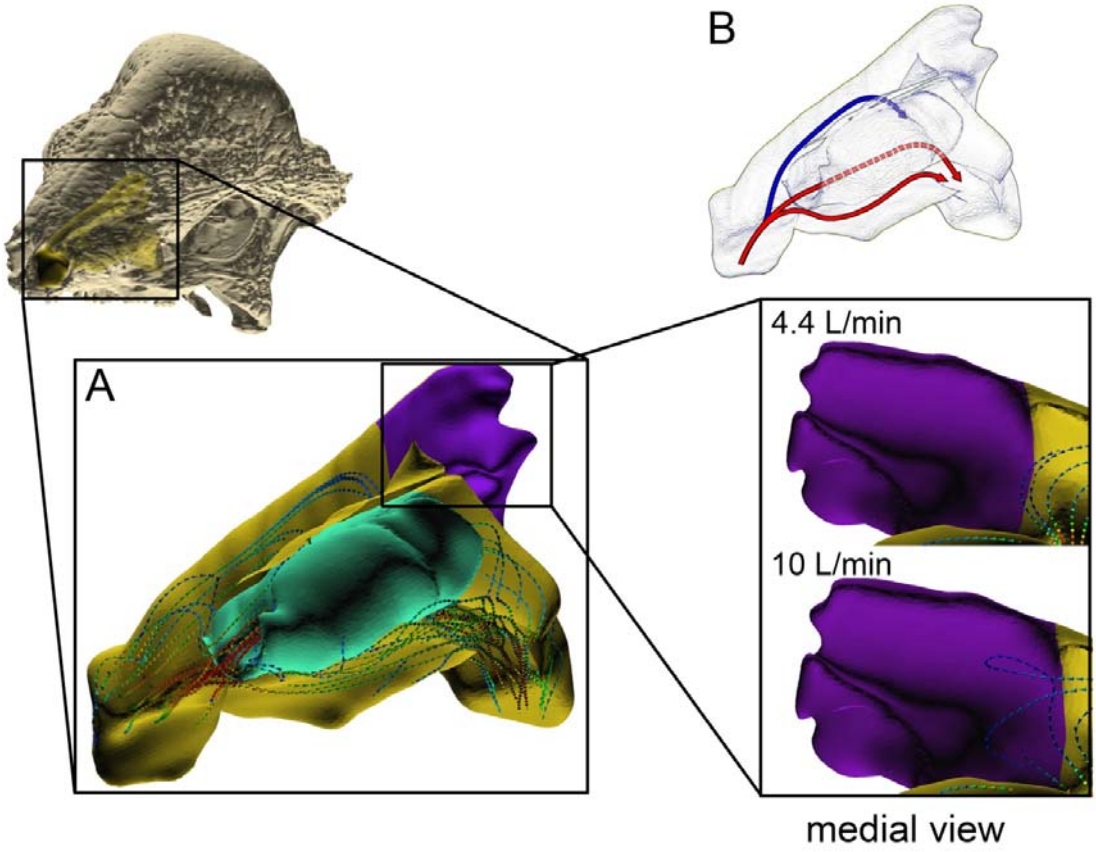

Figure 5-20. Nasal capsule of *Stegoceras validum* (UALVP 2) modeled with a scrolled concha. (A) Inspiratory airflow through the scrolled concha (aqua) model. Arrows are color-coded for velocity with hotter colors representing higher velocities. (B) Inspired air broke into three channels upon entering the CNP. Very little olfactory flow was observed under both flow regimes with olfactory mixing being less at the lower flow rate.

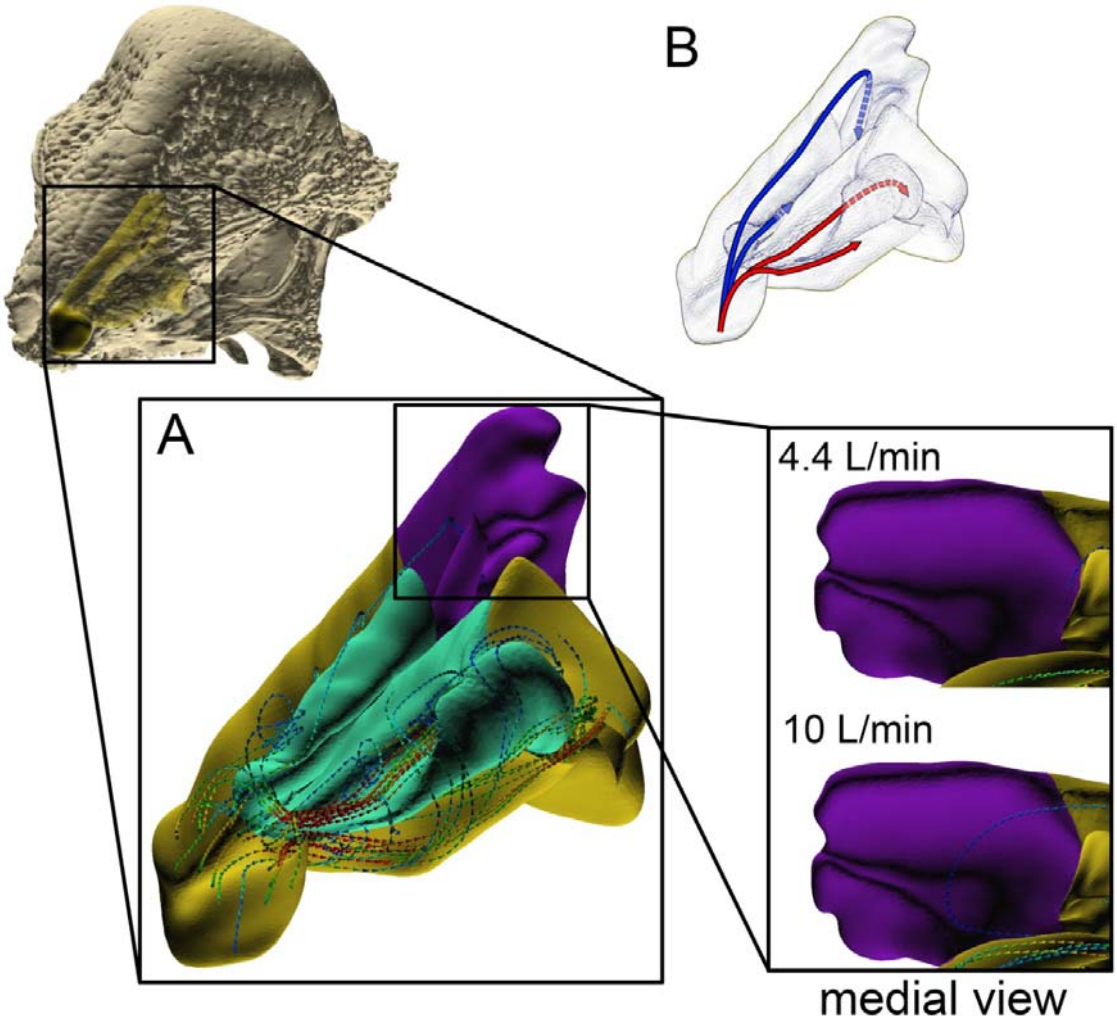

Figure 5-21. Nasal capsule of *Stegoceras validum* (UALVP 2) modeled with a branched concha. (A) Inspiratory airflow in the branched concha (aqua) model. Arrows are color-coded for velocity with hotter colors indicating higher velocity. (B) Inspired air broke into 3–4 separate channels upon entering the CNP. Inset: Some olfactory mixing was observed at the low flow rate whereas substantial mixing was observed at the higher flow rate.

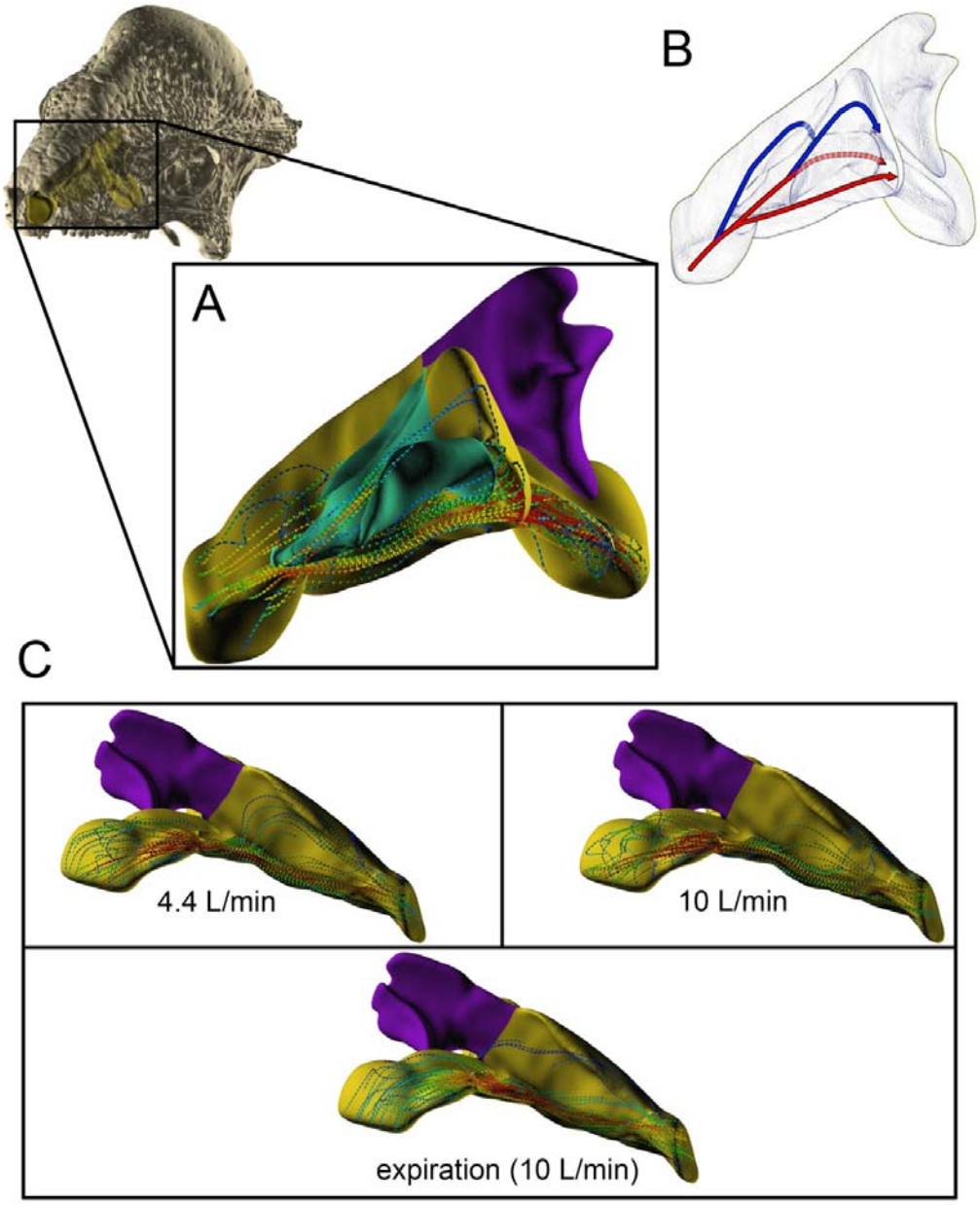

Figure 5-22. Nasal capsule of *Stegoceras validum* (UALVP 2) modeled with a scrolled concha and a paranasal septum. (A) Airflow during resting inspiration through the model with both scrolled concha (aqua) and a paranasal septum. (B) Airflow was observed to break into three different channels during inspiration. Arrows are color-coded for velocity with hotter colors indicating greater velocities. (C) Left medial views of the nasal capsule during high and low volume inspiration. Under both scenarios flow within the olfactory chamber (purple) was essentially stagnant. This pattern was repeated upon expiration as well (regardless of flow rate). This nasal morphology produced very little olfactory flow during all phases of respiration.

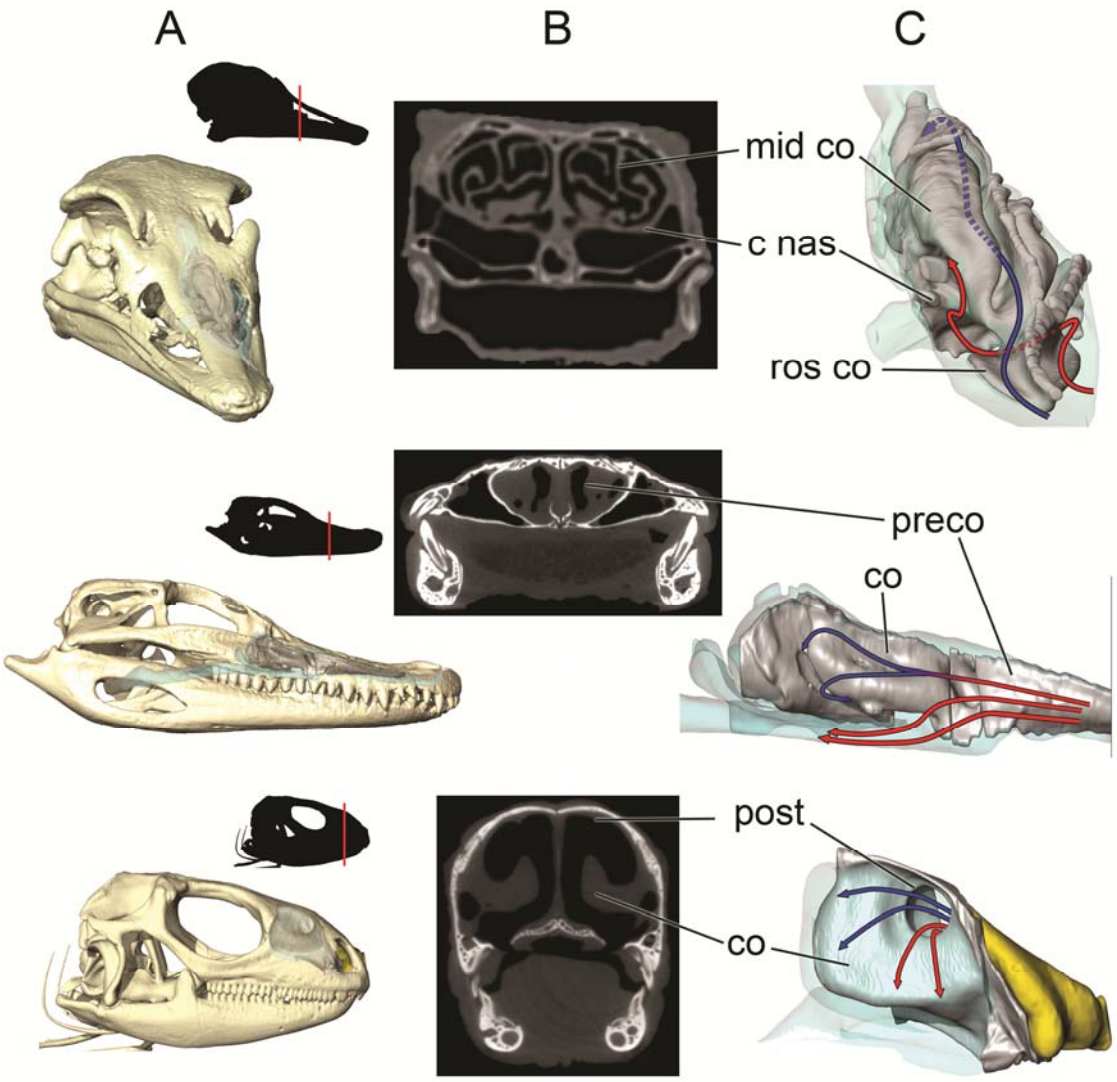

Figure 5-23. Nasal airways in extant diapsids highlighting regions of airway constriction and olfactory segregation. (A) Skulls of an ostrich (*Struthio camelus*, OUVC 10636, top), alligator (*Alligator mississippiensis*, OUVC 10389, middle), and iguana (*Iguana iguana*, OUVC 10603 bottom). (B) Axial cross sections taken at locations shown in the silhouettes in A. (C) Simplified representation of airflow through nasal capsule at regions near airway constrictions. Airways in C reflect skull positions in A.

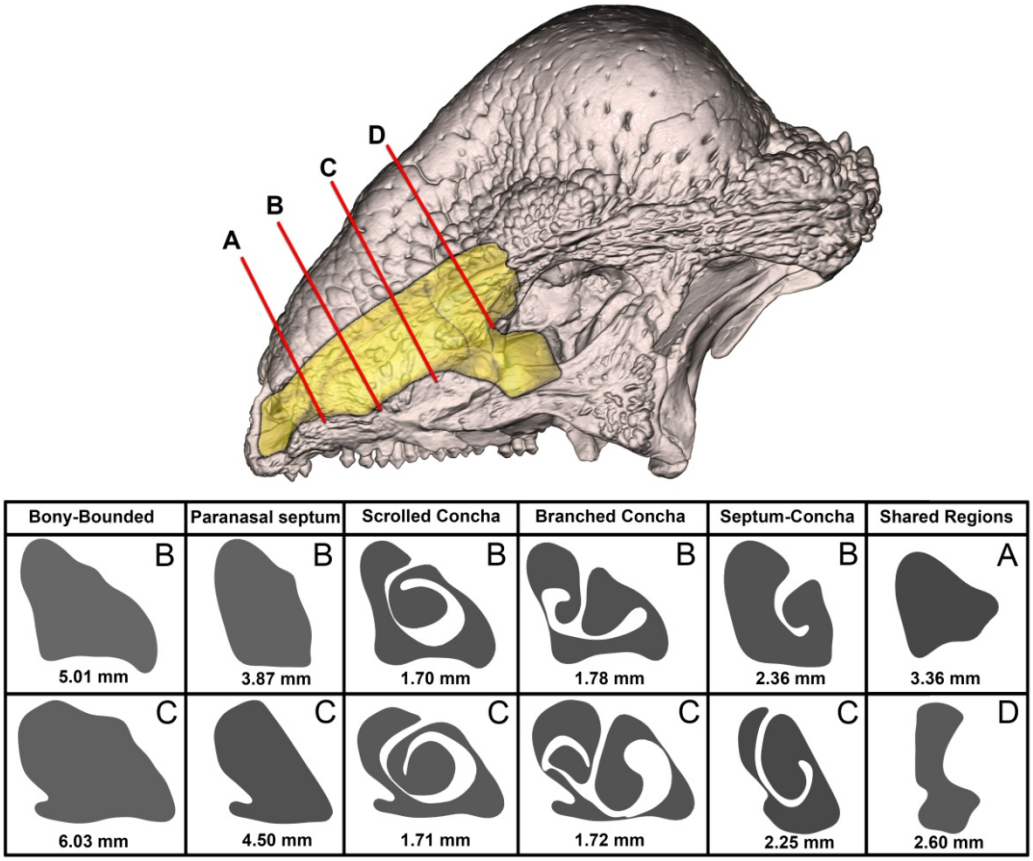

Figure 5-24. Example cross-sectional measurements through the nasal capsule of *Stegoceras validum* (UALVP 2) showing the average distance from the center of the airfield to the nearest wall in all five nasal morphologies. Lettered red lines indicate locations of cross sections throughout the nasal capsule. As nasal morphology changed only within the CNP (B,C) a single average is shown for all five nasal morphologies in their shared regions of interest (A, D).

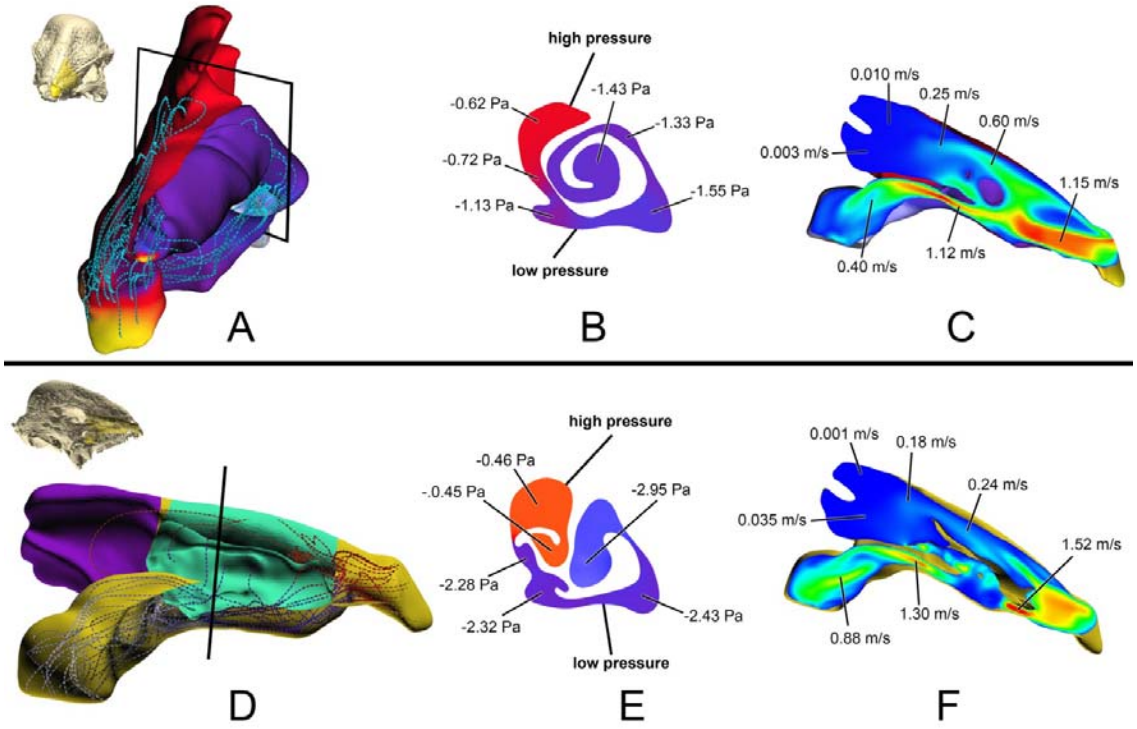

Figure 5-25. Pressure and velocity distribution within the nasal capsule of the scrolled concha model (A–C) and branched concha model (D–F) of *Stegoceras validum* (UALVP 2). (A) Placement of concha split the nasal capsule into a high-pressure medial side and low-pressure lateral side. (B, E) Pressure was always higher in the olfactory chamber than the rest of the nasal capsule, with the connection between the high- and low-pressure regions being less complete in the scrolled model (B) compared to the branched model (E). (D) More complete separation in the branched concha produced a conveyor belt-like effect pushing inspired air further into the olfactory chamber. (C,F) Cross sections through a medial view of the scrolled (C) and branched (F) models. The airfield is capable of maintaining momentum further into the olfactory chamber under the branched model.

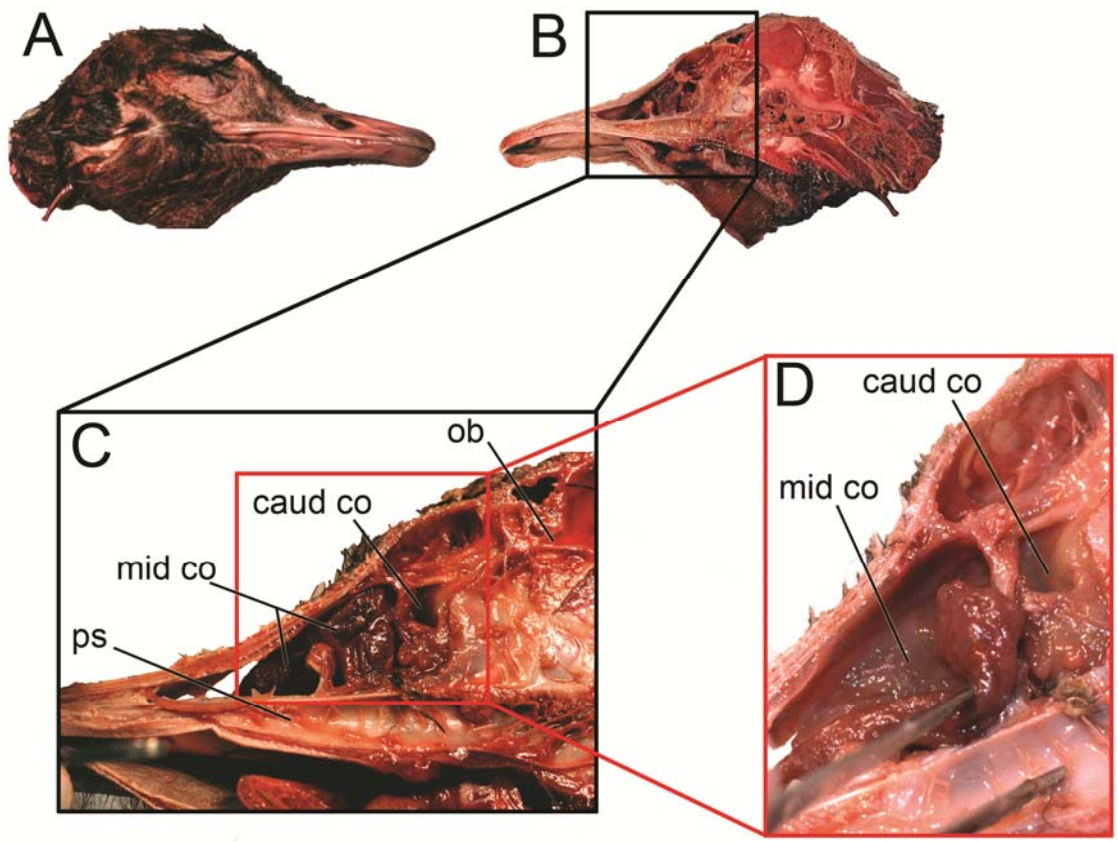

Figure 5-26. Gross analysis of epithelium on the middle concha of an ostrich (*Struthio camelus*, OUVC 10660). (A) Right lateral view of ostrich head. (B) Right medial view of sagittally-sectioned ostrich head. (C) Inset of ostrich nasal passage with nasal septum removed. (D) Inset of cavum nasi proprium with medial branch of middle concha reflected to reveal yellow-colored olfactory epithelium similar to the olfactory epithelium seen on the caudal concha.

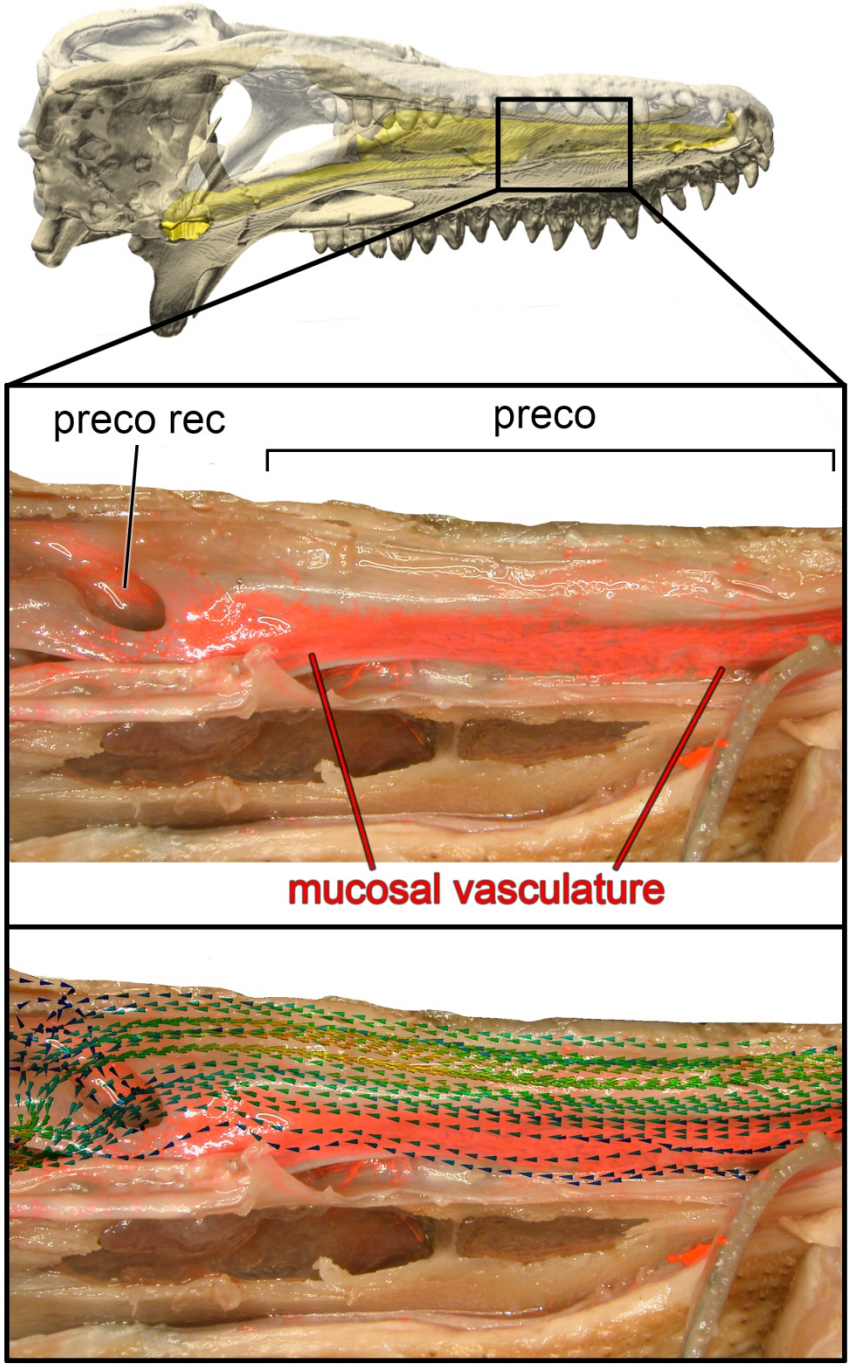

Figure 5-27. Ventromedial view of left airway in *Alligator mississippiensis* (OUVC 10389). Inset: Dissection of injected *Alligator* nasal capsule revealing extensive vasculature within the mucosa of the preconcha and tectum nasi (top). A separate vascular plexus was observed along the solum nasi as well (not shown). This region of the nasal capsule is in direct line with the path of respired air (bottom) suggesting that it serves a thermoregulatory function in *Alligator*.

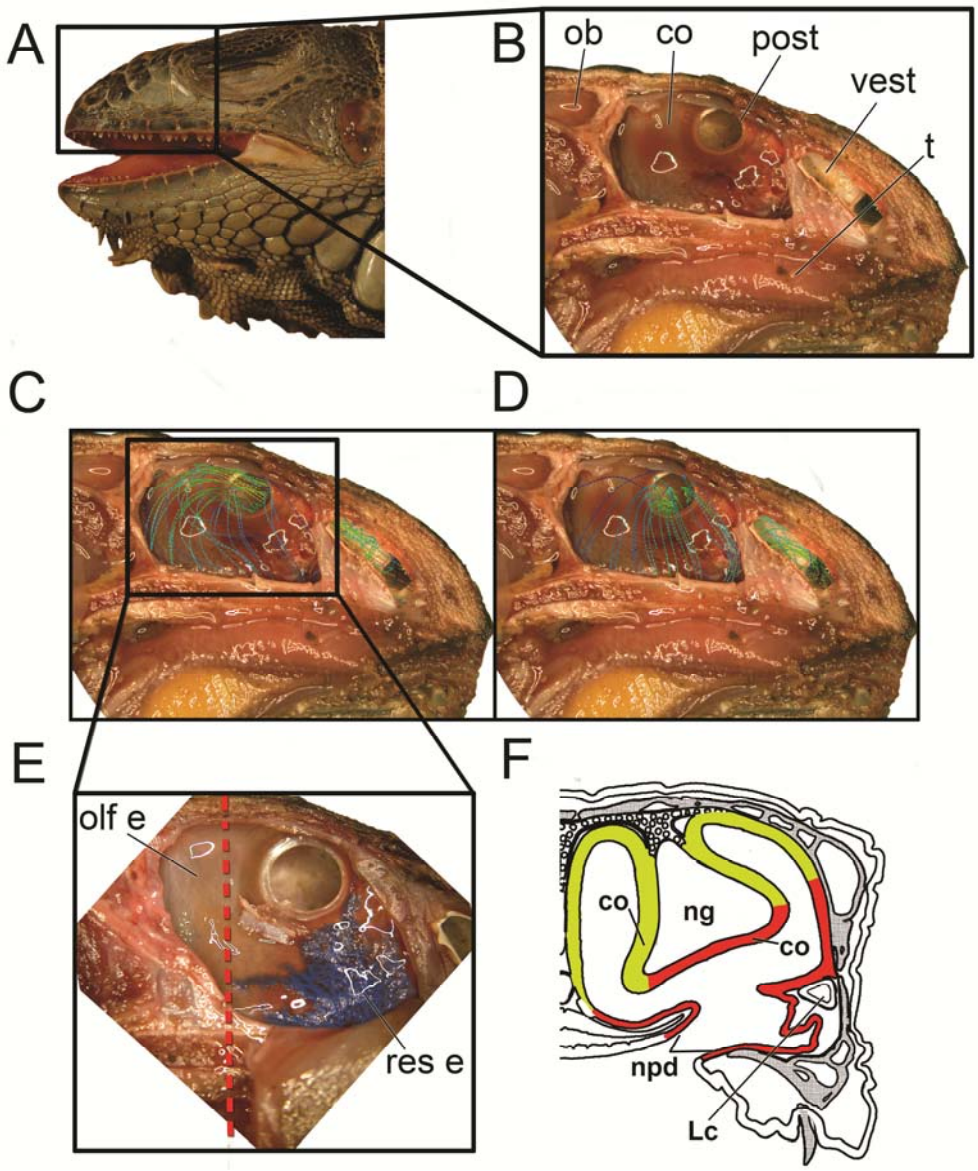

Figure 5-28. Nasal morphology and airflow through the nasal capsule of *Iguana iguana* (OUVC 10684). (A) Left lateral view of head highlighting nasal capsule location. (B) Left medial view of sagittal section through nasal septum. (C) Airflow pattern based on CFD analysis during inspiration and (D) during expiration. (E) Expanded view of concha, showing the gross location of respiratory and olfactory epithelium. Vascular injection (blue) reveals extensive blood flow to the respiratory region of the concha. Red dotted line indicates the location of (F) the diagrammatic cross section through the concha revealing the histological location of epithelia along the nasal capsule. Yellow = olfactory epithelium. Red = respiratory epithelium. Diagram in F based on Gabe and Saint-Girons (1976).

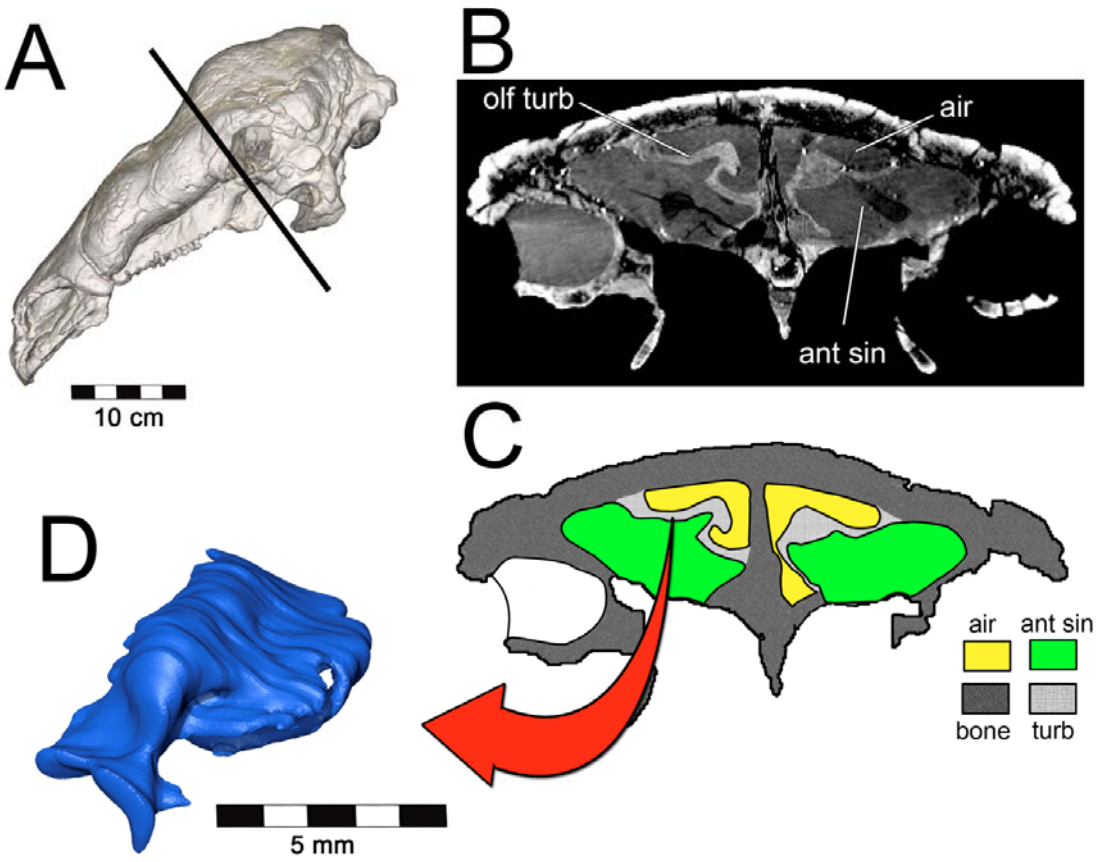

Figure 6-1. Segmentation of the airway in *Panoplosaurus mirus* (ROM 1215). (A) Skull in left lateral view. Line represents the location of (B) axial CT section showing preserved olfactory turbinates. (C) Diagram of CT image showing caliber of airway vs. entire nasal cavity. (D) Segmented olfactory turbinate in same plane as CT image.

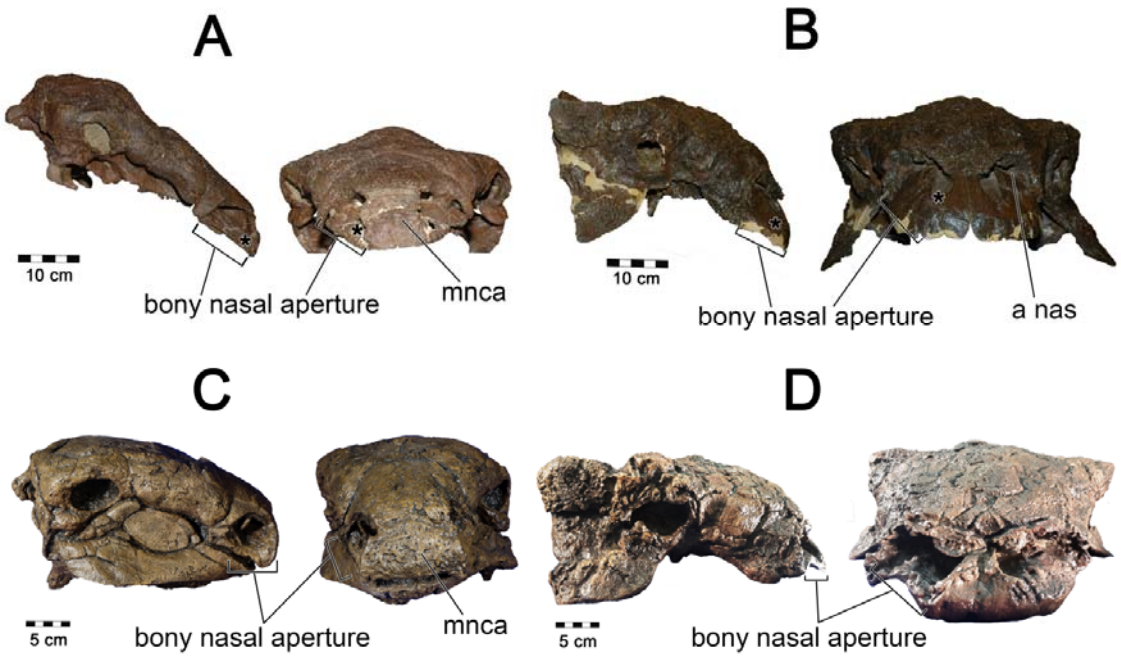

Figure 6-2. Nostril placement in ankylosaur models. All skulls in right lateral and rostral views. For *Panoplosaurus. mirus* (A, C) we used (A) ROM 1215 as our base model with nostril placement informed by (C) CMN 8530. For *Euoplocephalus.tutus* (B, D) we used (B) AMNH 5405 as our base model with the skull of (D) ROM 1930 informing us on the limits to the extent of the nostril. Asterisks in A and B denote location of fleshy nostril in our models.

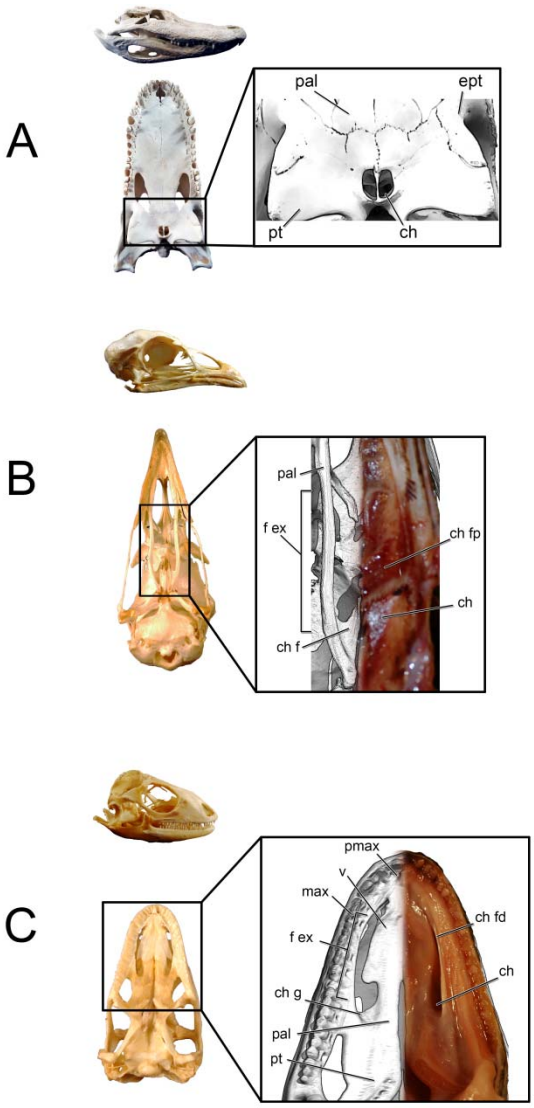

Figure 6-3. Lateral and ventral views of extant diapsid skulls illustrating the location of the choana. Crocodylians such as (A) *Alligator mississippiensis* (OUVC 9412) have a greatly retracted, apomorphic secondary choana. *Inset:* The bony boundaries to the secondary choana correspond to the soft-tissue boundaries. Birds such as (B) *Meleagris gallopavo* (OUVC 9647) retain the plesiomorphic placement of the choana. *Inset:* Magnified palatal region showing the difference between the bony boundaries to the choana (left side of image) and the soft-tissue boundaries (right side of image). Lizards such as (C) *Iguana iguana* (OUVC 10446) similarly show the plesiomorphic position of the choana. *Inset:* Relationship between the bony boundaries to the choana (left side of image) and the more restricted soft-tissue boundaries (right side of image).

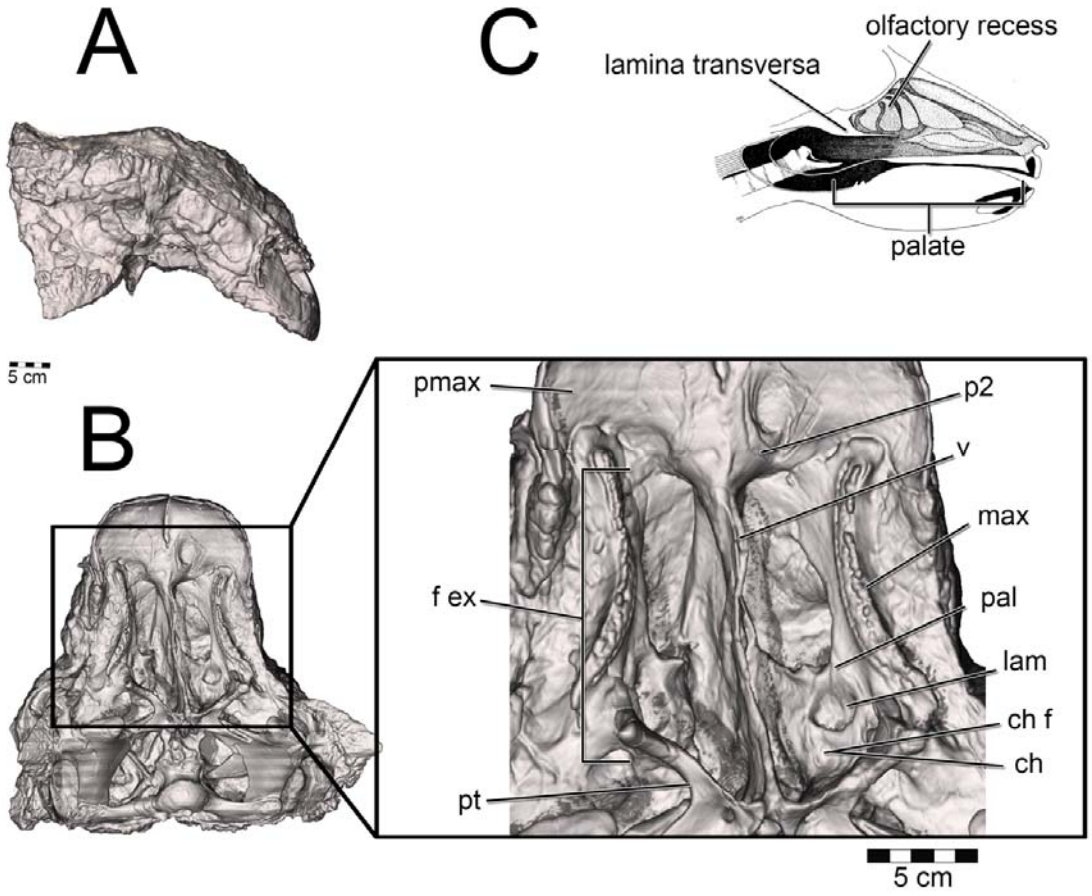

Figure 6-4. Palate identification and placement in *Euoplocephalus tutus* (AMNH 5405). (A) Skull in lateral and (B) ventral view. *Inset:* Major features of the palatal region. We refer to the caudodorsal secondary palate as equivalent to the lamina transversa observed in many mammals (C). Image in C modified from Cave 1967.

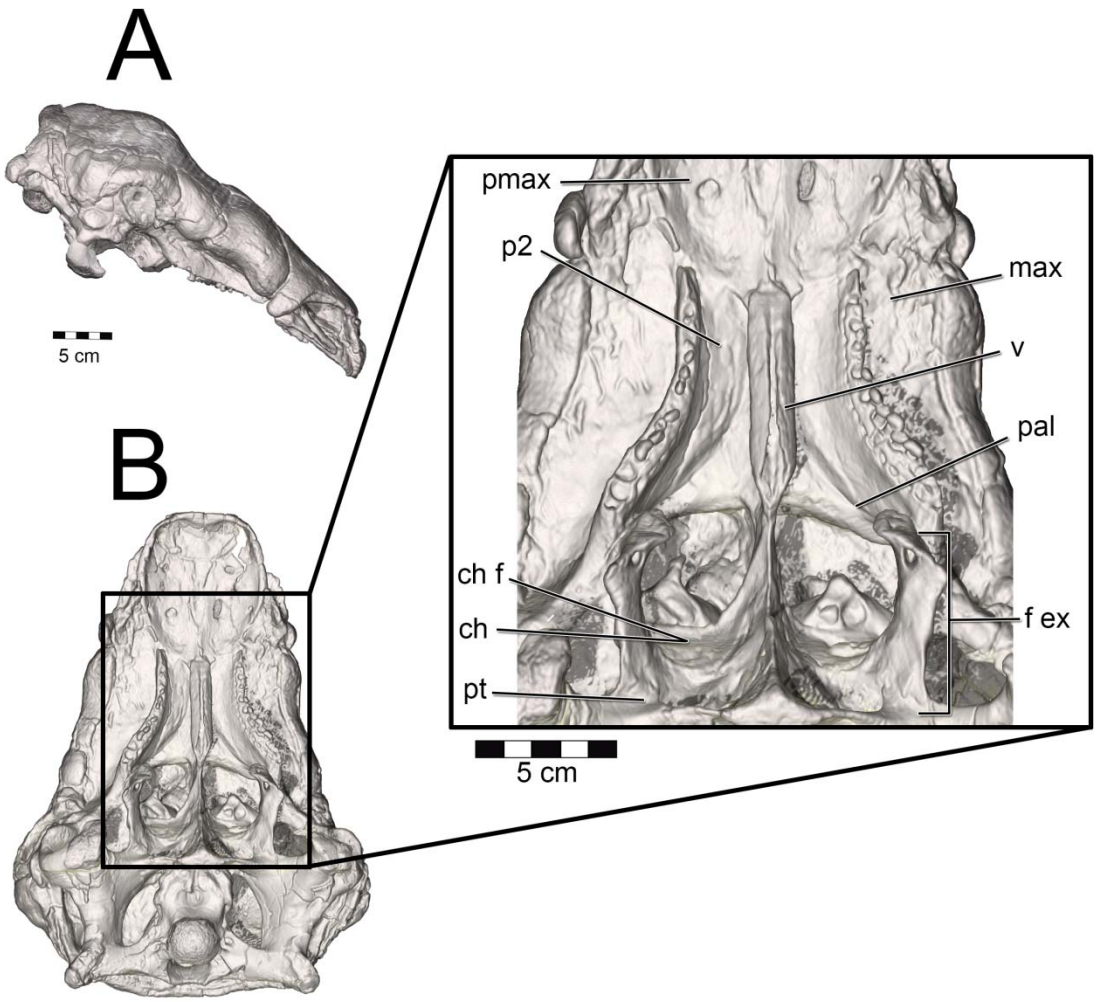

Figure 6-5. Palate identification and choana placement in *Panoplosaurus mirus* (ROM 1215). (A) Skull in lateral and (B) ventral view. *Inset:* Major features of the palatal region.

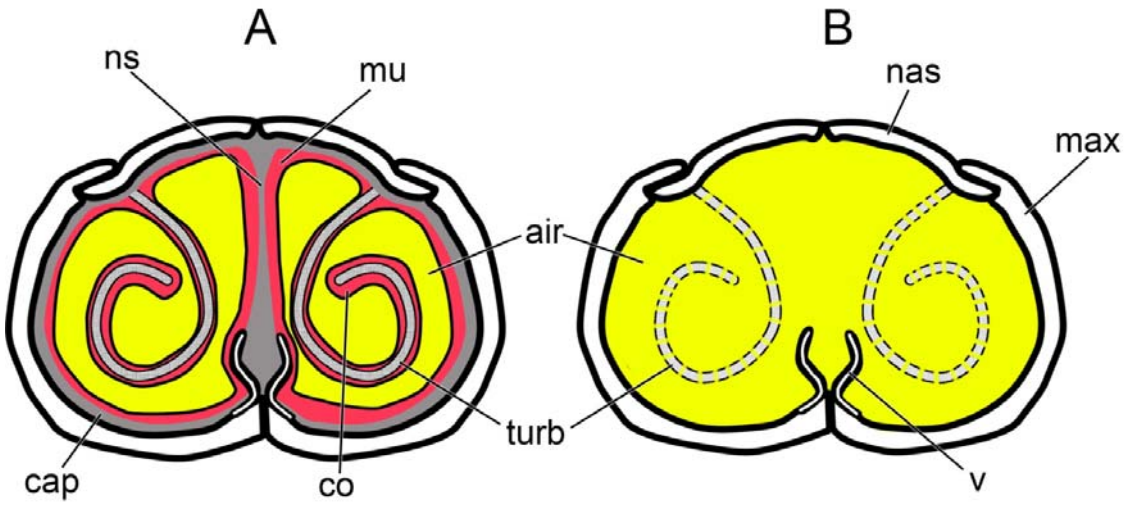

Figure 6-6. Generic airway diagram for diapsids. Note the much more constricted airway in the soft-tissue nasal passage (A) vs. the emptier, bony-bounded nasal passage typically preserved in fossils (B).

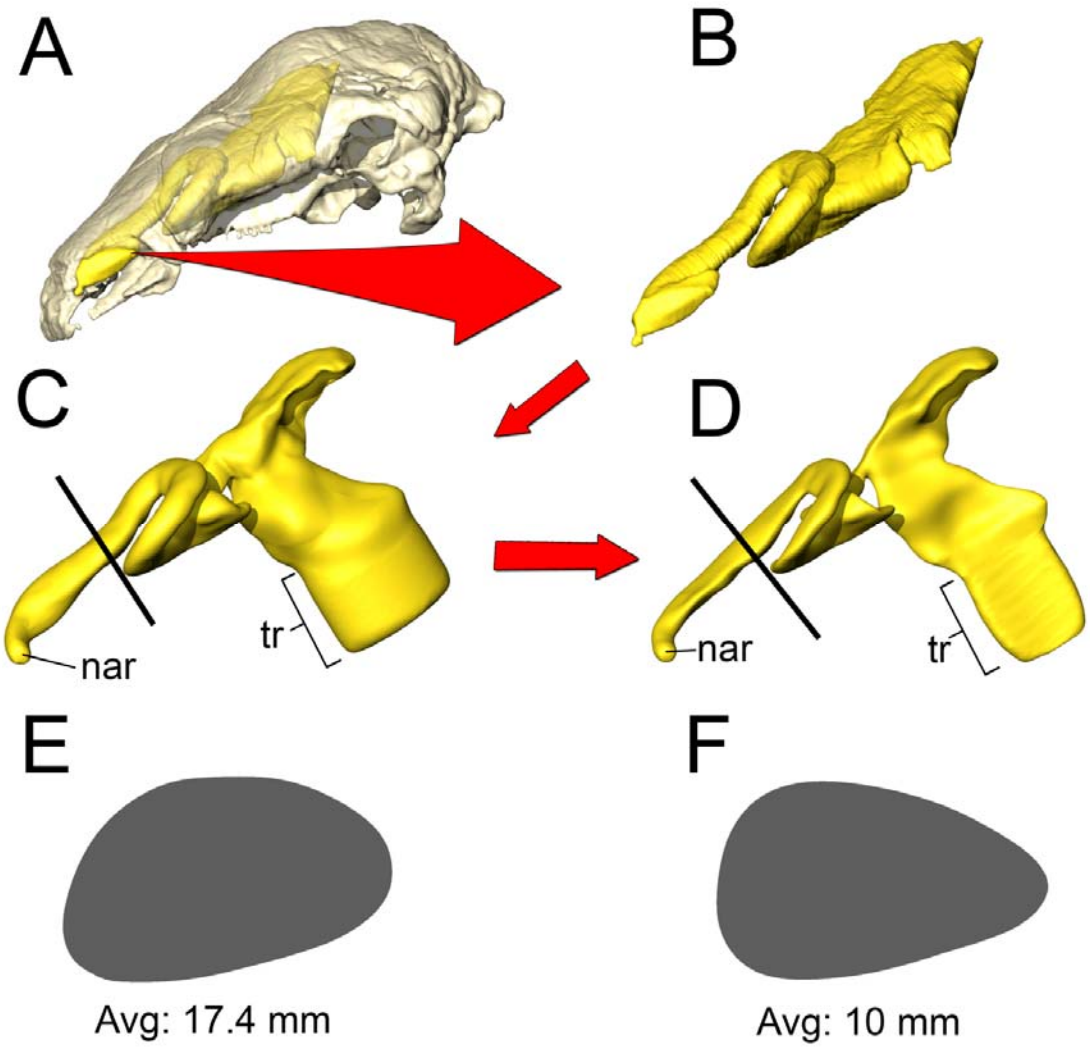

Figure 6-7. Airway reconstruction and soft-tissue correction in *Panoplosaurus mirus*. (A) Initial CT-based bony-bounded segmentation of airway within the skull and (B) isolated. (C) Airway cleaned and separated, with the addition of a soft-tissue naris and nasopharyngeal duct exiting into an artificially created laryngotracheal region. (D) Nasal passage digitally compressed to reduce airway caliber, bringing it closer to what is observed in the mucosa-lined airways of extant amniotes. Black lines indicate locations of cross sections (E–F). (E) Original bony-bounded airway caliber. (F) Airway caliber after soft-tissue correction.

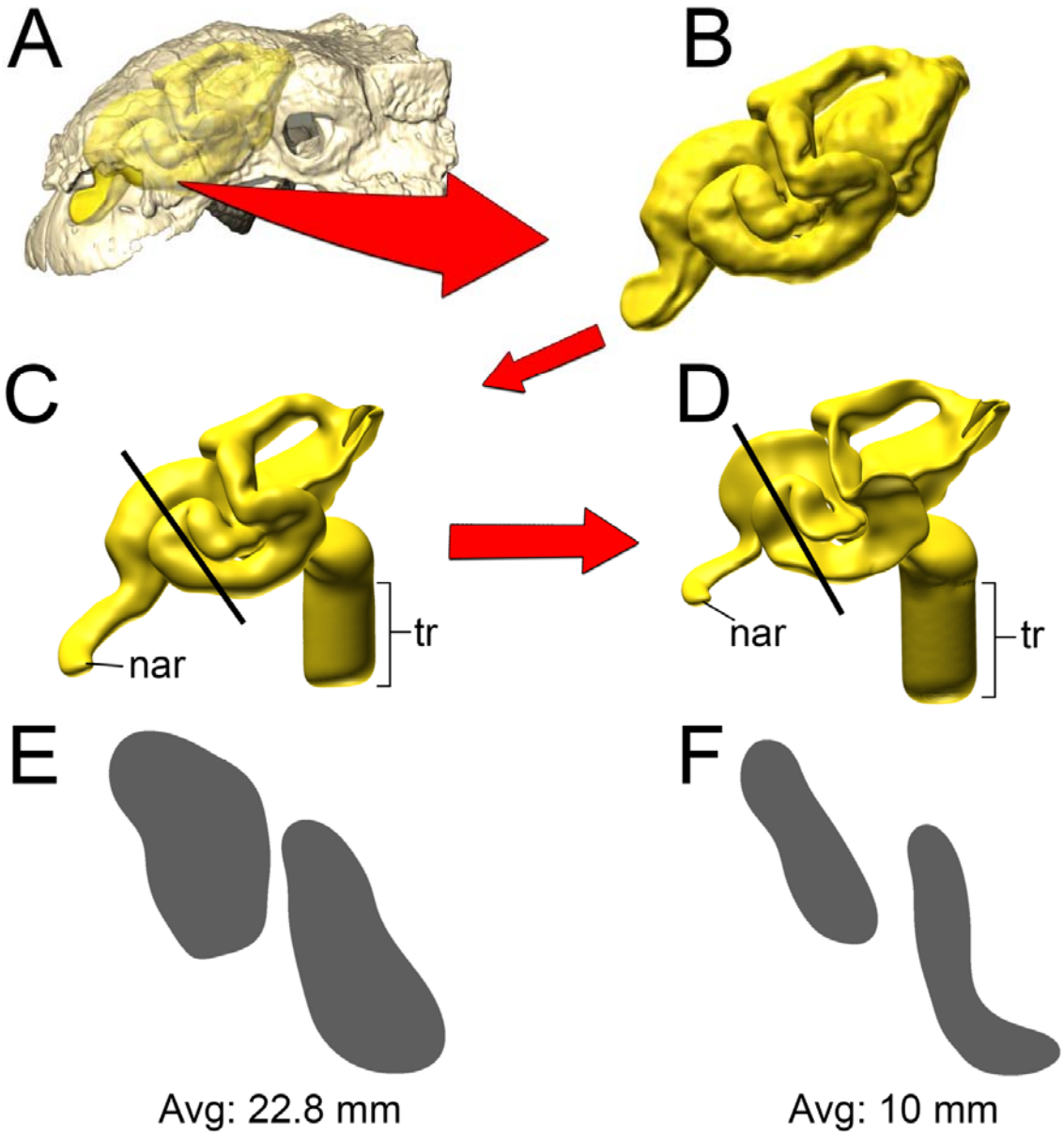

Figure 6-8. Airway reconstruction and soft-tissue correction in *Euoplocephalus tutus*. (A) Initial CT-based bony-bounded segmentation of airway within the skull and (B) isolated. (C) Airway cleaned and separated, with the addition of a soft-tissue naris and nasopharyngeal duct exiting into an artificially created laryngotracheal region. (D) Nasal passage digitally compressed to reduce airway caliber closer to what is observed in the mucosa-lined airways of extant amniotes. Black lines indicate locations of cross sections (E–F). (E) Original bony-bounded airway caliber. (F) Airway caliber after soft-tissue correction.

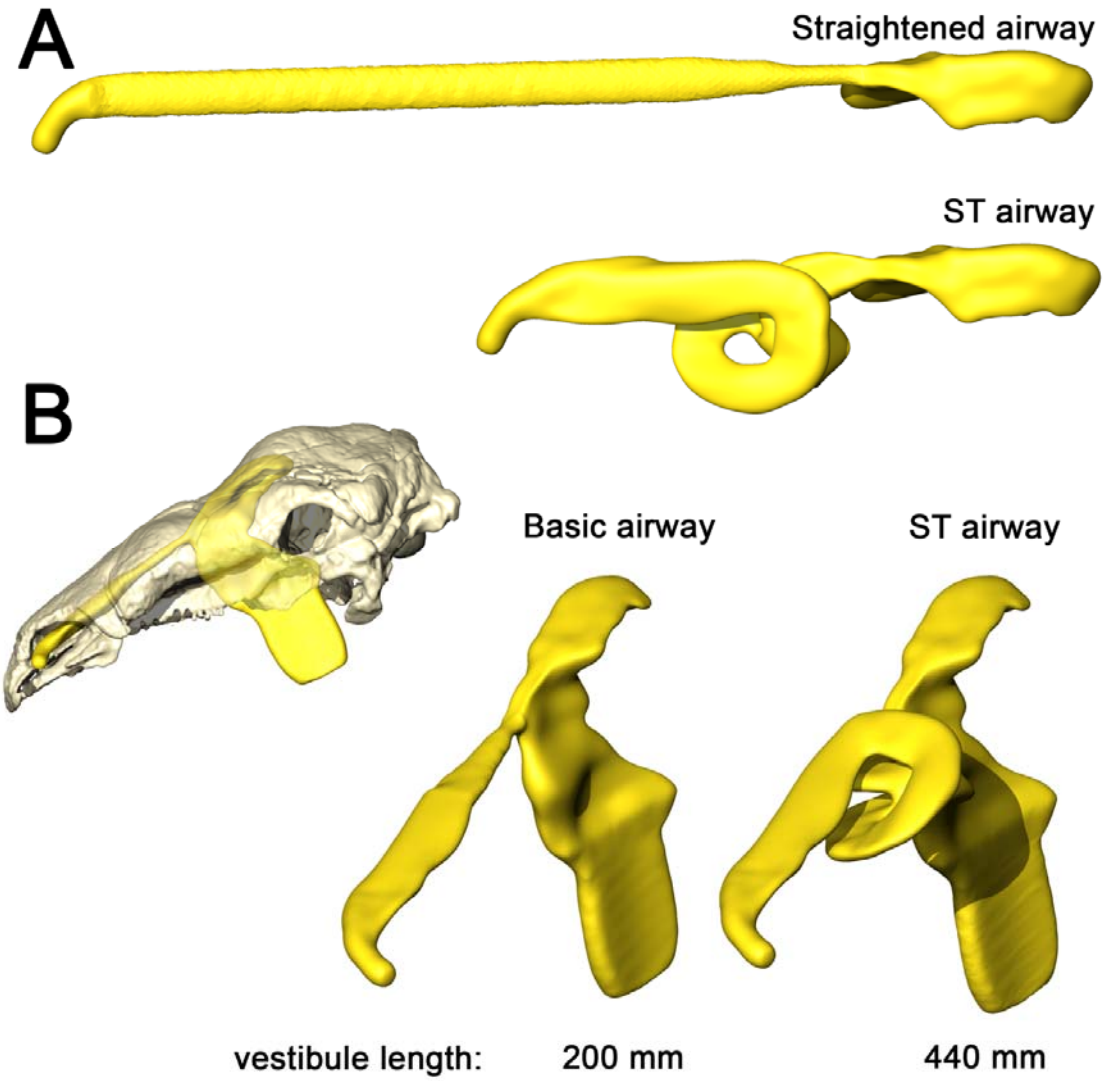

Figure 6-9. Alternate airway models for *Panoplosaurus mirus*. (A) Dorsal view of the straightened airway (removal of nasal vestibule curvature) and the original, ST-corrected airway. (B) Lateral view of skull of *P. mirus* (ROM 1215) with basic airway in situ. Running a straight line connection between nostril and CNP resulted in loss of 55% of the nasal vestibule.

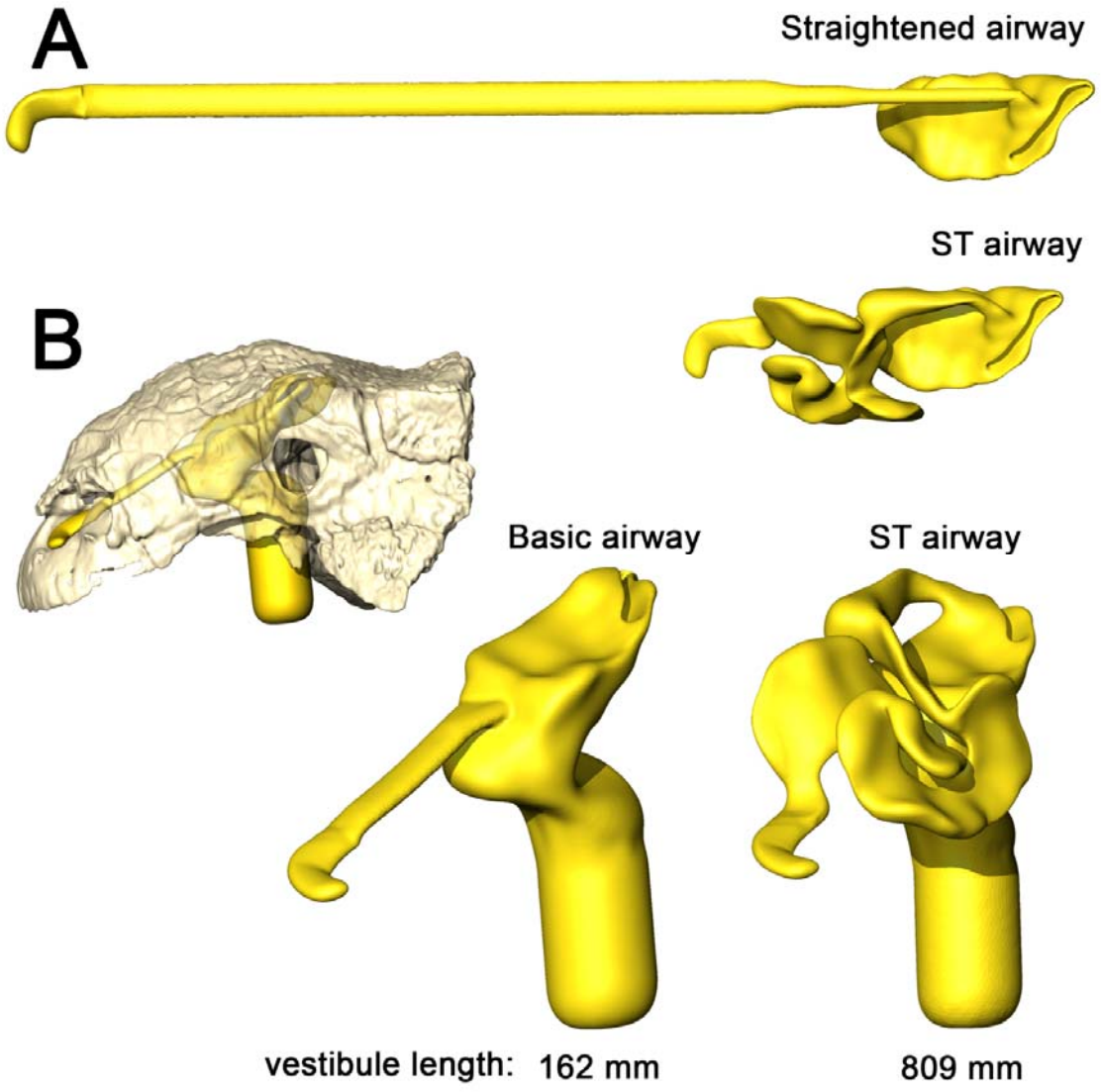

Figure 6-10. Alternate airway models for *Euoplocephalus tutus*. (A) Dorsal view of the straightened airway (removal of nasal vestibule curvature) and the original, ST-corrected airway. (B) Lateral view of skull of *E. tutus* (AMNH 5405) with basic airway in situ. Running a straight line connection between nostril and CNP resulted in loss of 80% of the nasal vestibule.

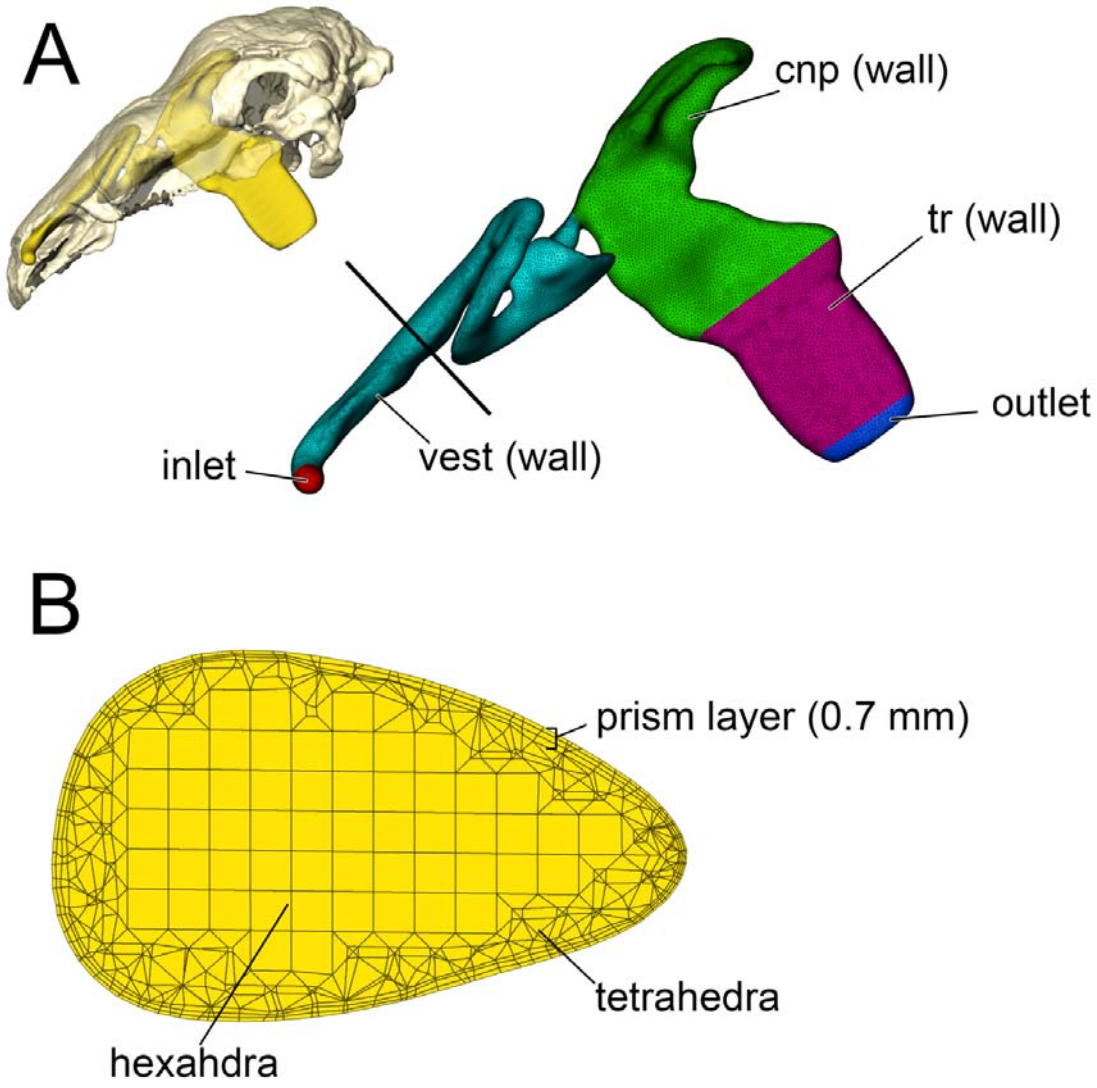

Figure 6-11. Mesh example for *Panoplosaurus mirus*. (A) Nasal passage was assigned a series of boundary conditions (color-coded). Black line indicates location of (B) axial cross section illustrating the distribution of volumetric cells within the nasal passage.

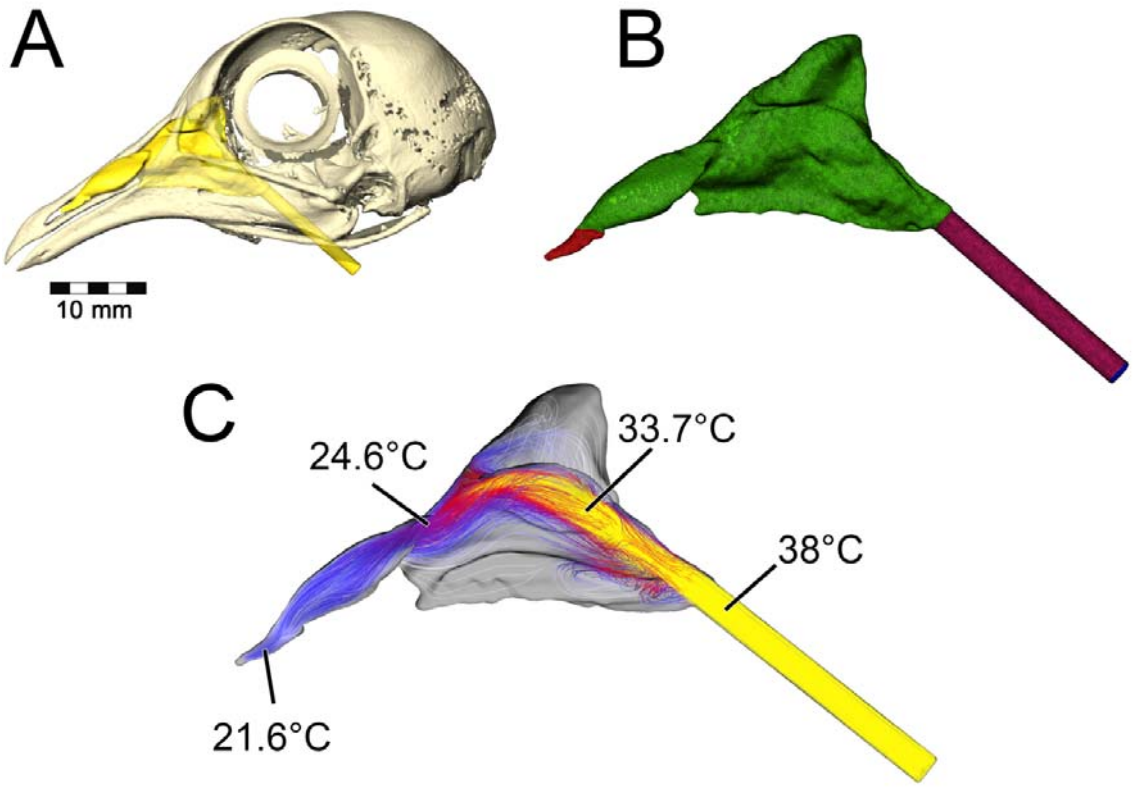

Figure 6-12. Airflow and heat transfer within the left nasal passage of a pigeon (*Columba livia*). (A) Airway was segmented out from the head and (B) converted into a volumetric mesh for CFD analysis. (C) Results of CFD analysis during expiration.

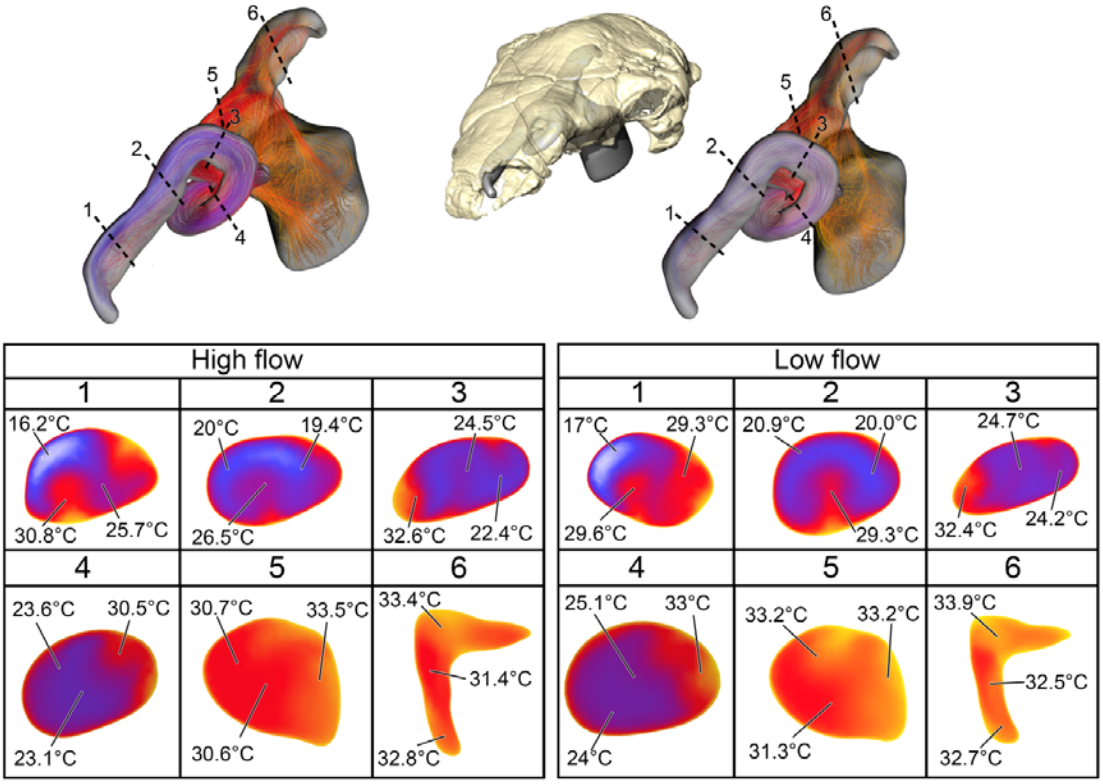

Figure 6-13. Heat flow within the bony-bounded nasal passage of *Panoplosaurus mirus* during inspiration under both high (left) and low (right) flow scenarios. Numbers of dotted lines indicate cross-section numbers. Cross sections were taken at equivalent locations on both models.

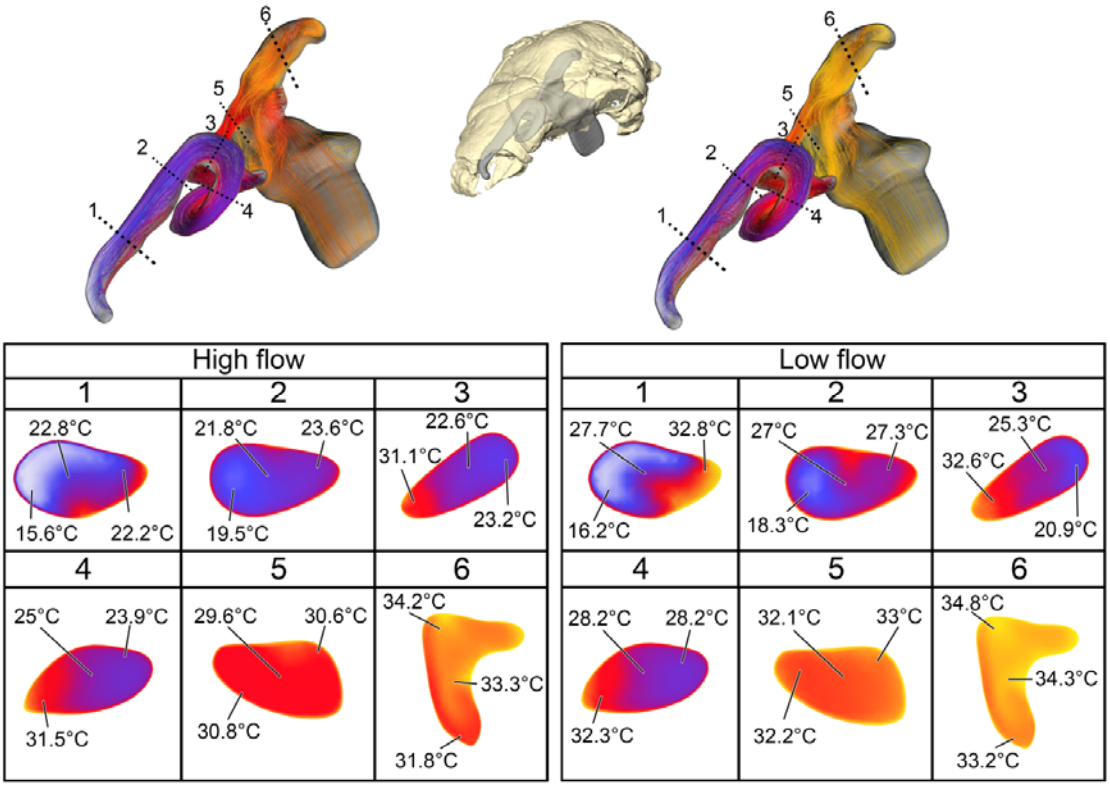

Figure 6-14. Heat flow within the soft-tissue corrected nasal passage of *Panoplosaurus mirus* during inspiration under both high (left) and low (right) flow scenarios. Numbers of dotted lines indicate cross-section numbers. Cross sections were taken at equivalent locations on both models.

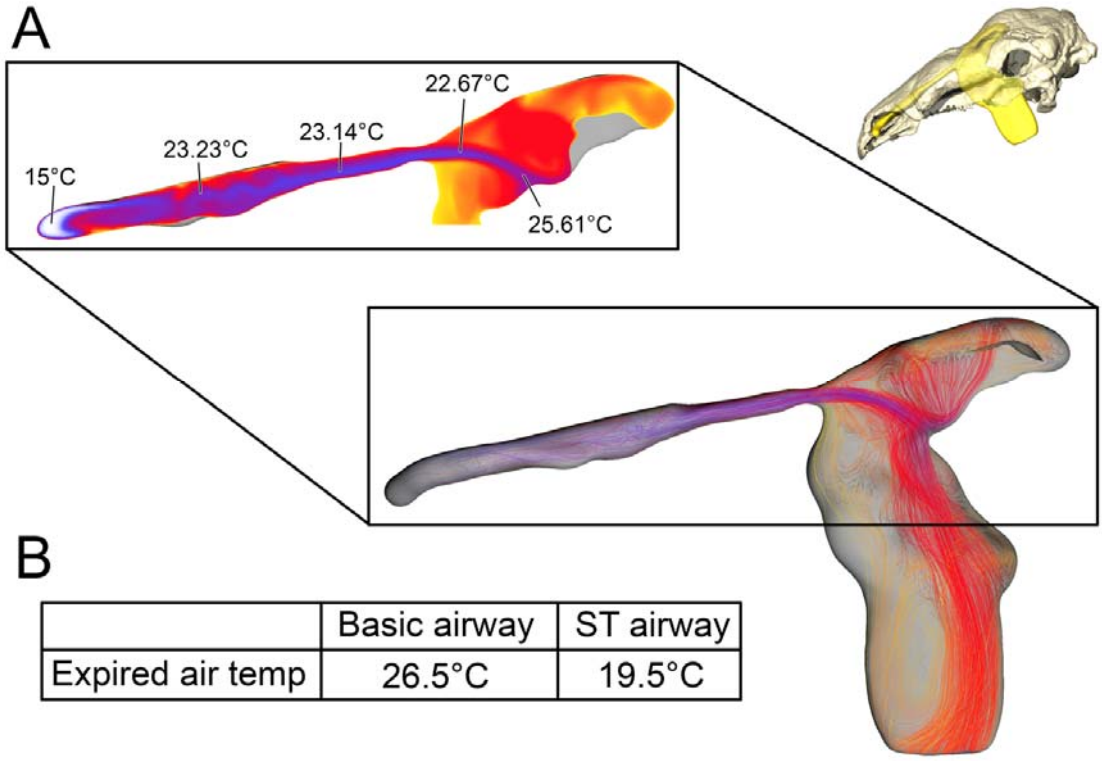

	Basic airway	ST airway
Expired air temp	26.5°C	19.5°C

Figure 6-15. Airflow through the basic airway of *Panoplosaurus mirus*. (A) Left lateral view of nasal passage with air streams showing general air field pattern. Airway is color-coded for temperature (hotter colors = hotter temperatures. *Inset:* Sagittal cross section of the nasal vestibule and CNP showing central stream of cool air passing through the nasal vestibule. (B) Temperature at the nostril during expiration for the basic airway and the ST airway.

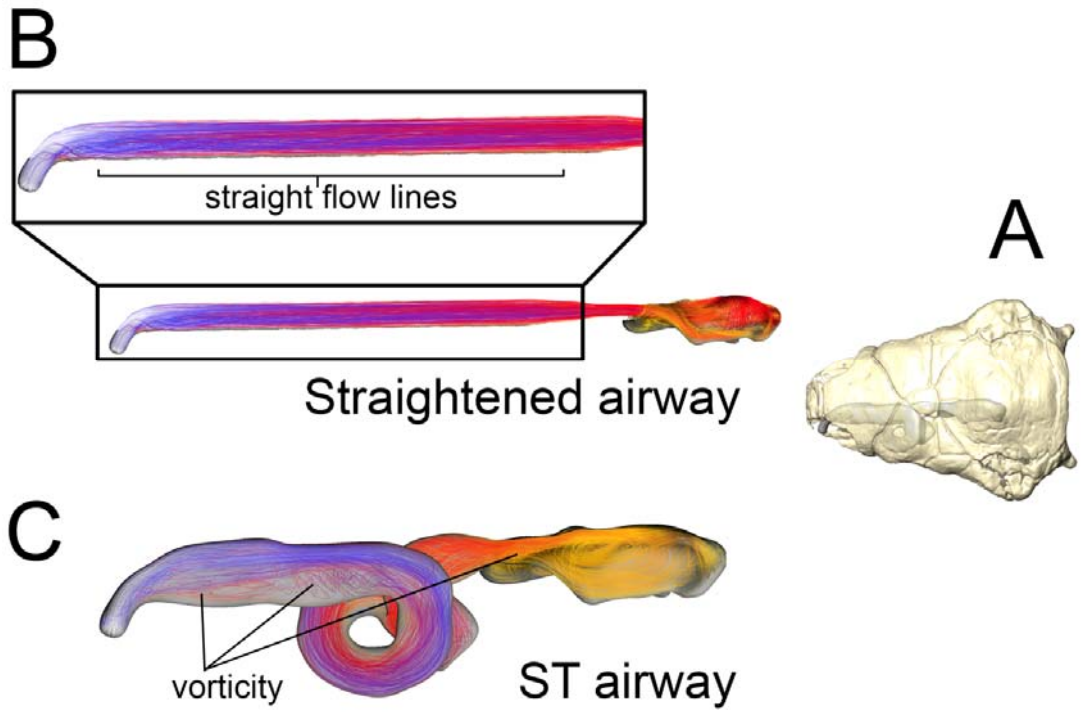

Figure 6-16. Airflow comparison between the straightened airway and the ST airway in *Panoplosaurus mirus*. (A) Dorsal view of the skull of *P. mirus* with ST airway in situ. (B) Dorsal view of the straightened airway with flow lines in place. Airflow lines are color-coded for temperature (hot colors = hotter temperatures). *Inset:* Magnified region of nasal vestibule showing evenly spaced, straight flow lines. (C) Dorsal view of the ST airway under the low flow scenario. Note the presence of vorticity throughout the nasal vestibule. Note: ST airway in C is not to scale with straightened airway B.

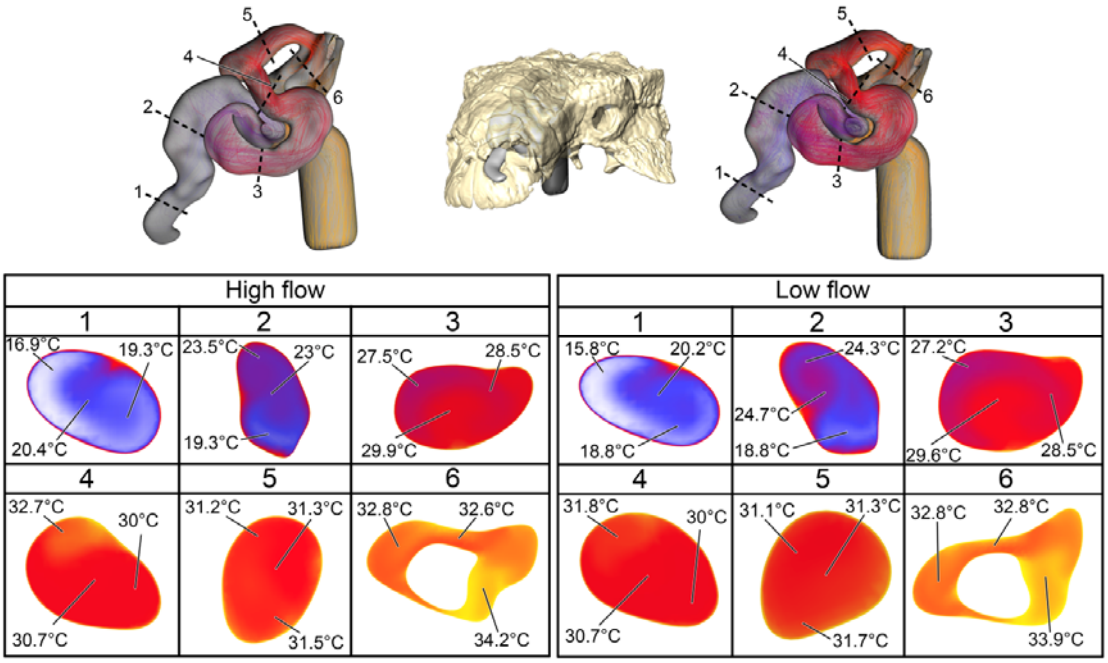

Figure 6-17. Heat flow within the bony-bounded nasal passage of *Euoplocephalus tutus* during inspiration under both high (left) and low (right) flow scenarios. Numbers of dotted lines indicate cross-section numbers. Cross sections were taken at equivalent locations on both models.

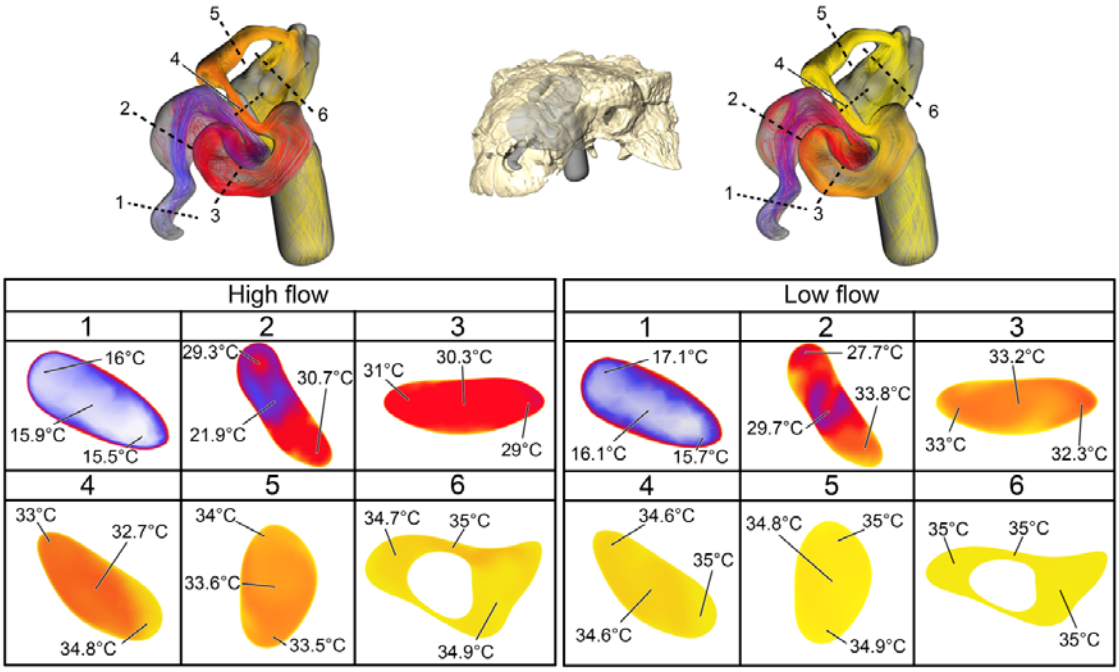

Figure 6-18. Heat flow within the soft-tissue corrected nasal passage of *Euoplocephalus tutus* during inspiration under both high (left) and low (right) flow scenarios. Numbers of dotted lines indicate cross-section numbers. Cross sections were taken at equivalent locations on both models.

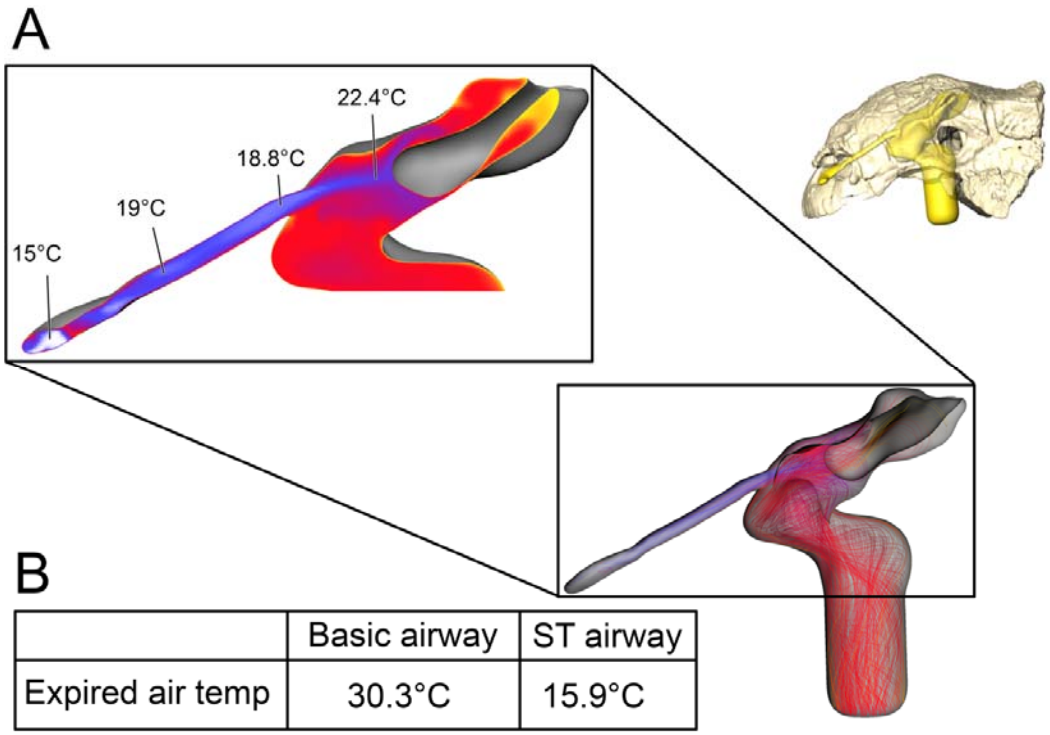

	Basic airway	ST airway
Expired air temp	30.3°C	15.9°C

Figure 6-19. Airflow through the basic airway of *Euoplocephalus tutus*. (A) Left lateral view of basic airway showing airflow. Streamlines are color-coded for heat (hotter colors = hotter temperatures). *Inset*: Sagittal cross section of airway showing persistent stream of cool air traversing the nasal vestibule and interacting with the CNP. (B) Temperature at the nostril during expiration for the basic airway and the ST airway.

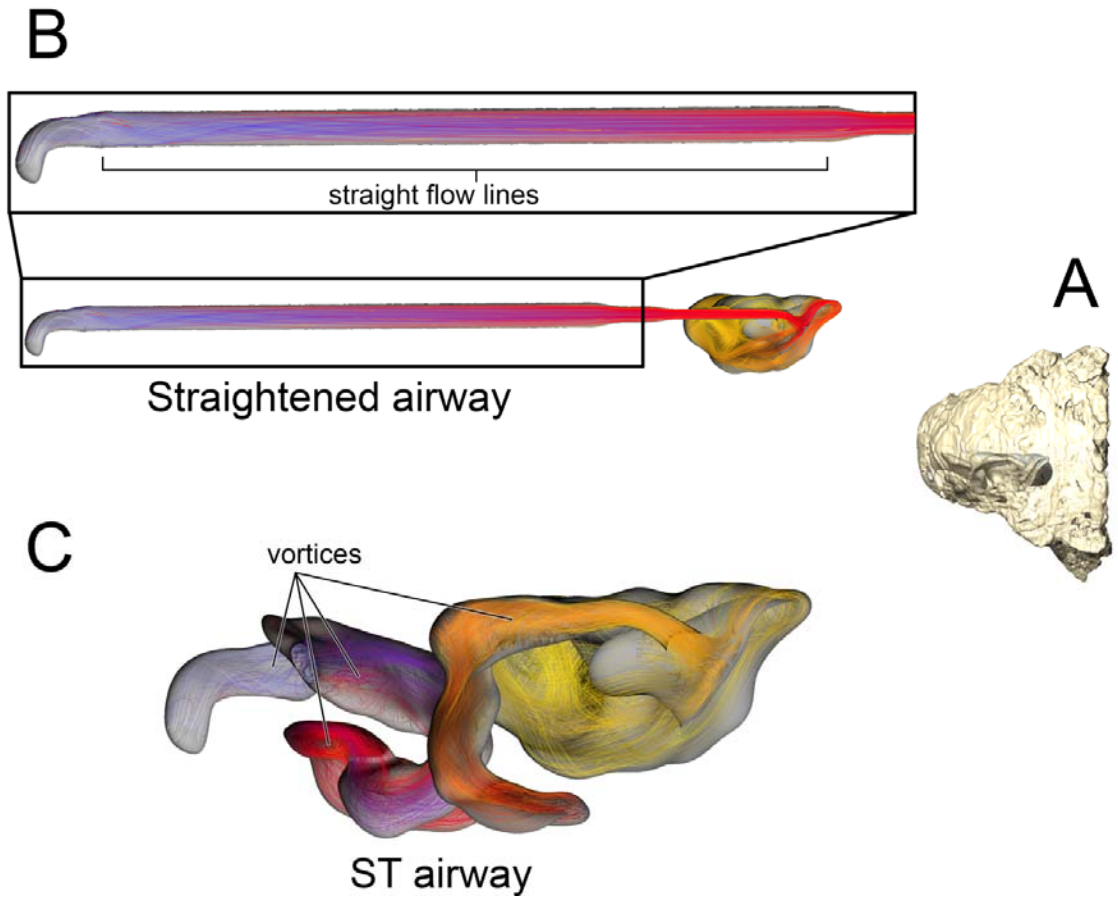

Figure 6-20. Airflow comparison between the straightened airway and the ST airway in *Euoplocephalus tutus*. (A) Dorsal view of the skull of *E. tutus* with ST airway in situ. (B) Dorsal view of the straightened airway with flow lines in place. Airflow lines are color-coded for temperature (hot colors = hotter temperatures). *Inset:* Magnified region of nasal vestibule showing evenly spaced, straight flow lines. (C) Dorsal view of the ST airway under the low flow scenario showing the presence of vorticity throughout the nasal vestibule. Note: ST airway in C is not to scale with straightened airway B.

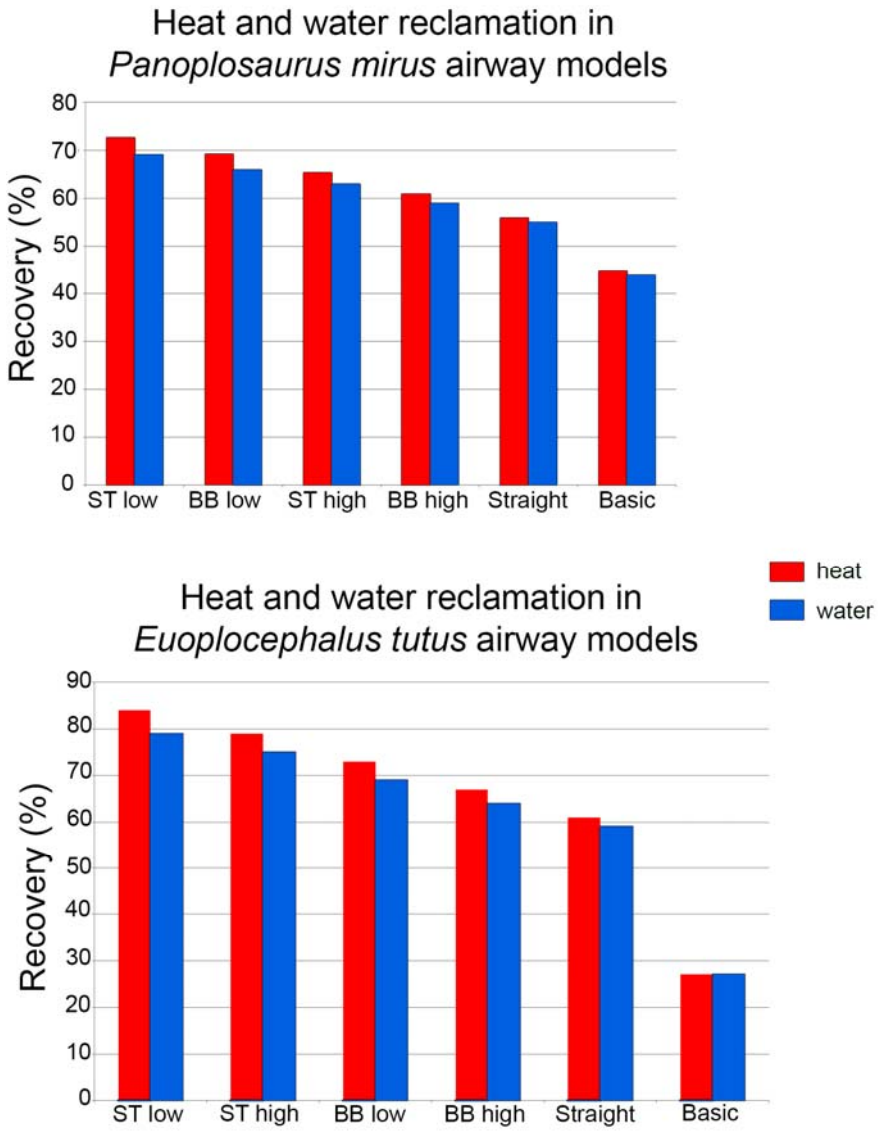

Figure 6-21. Heat and water savings between all nasal airway models for *Panoplosaurus mirus* (top) and *Euoplocephalus tutus* (bottom). Models are organized from greatest savings to least in both graphs.

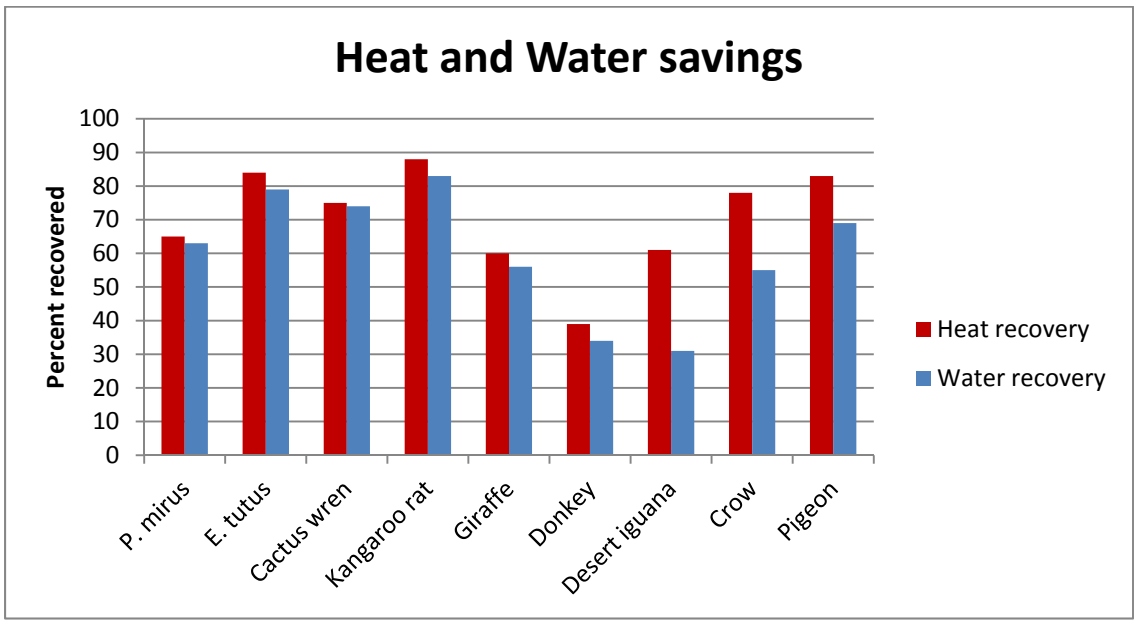

Figure 6-22. Heat and water savings calculated for the most efficient airway models of *Panoplosaurus mirus* and *Euoplocephalus tutus* vs. various extant animals. Note that variations in experimental protocol means that, although these results are comparable, they should not be viewed as fully equivalent. See Appendix for details on graph calculation and references for extant data.

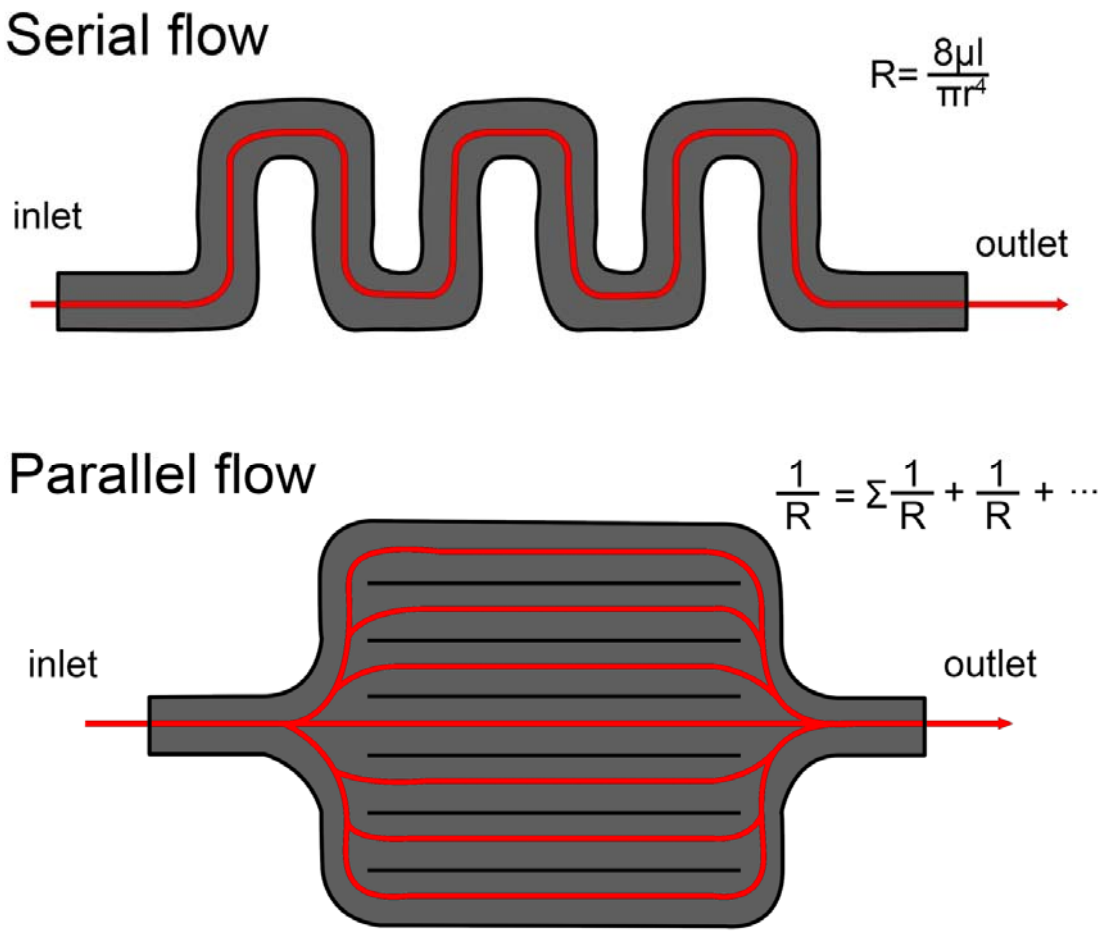

Figure 6-23. Example of flow in a serial pipe (as in convoluted ankylosaur nasal cavities) vs. a parallel pipe (as in turbinate-filled mammalian nasal cavities). Resistance can be calculated using similar methods for calculating resistance in an electrical circuit. Although the pipes in the parallel pipe may be smaller than the serial pipe, they are all running parallel to one another, resulting in a much smaller increase in resistance and a more economical use of available space.

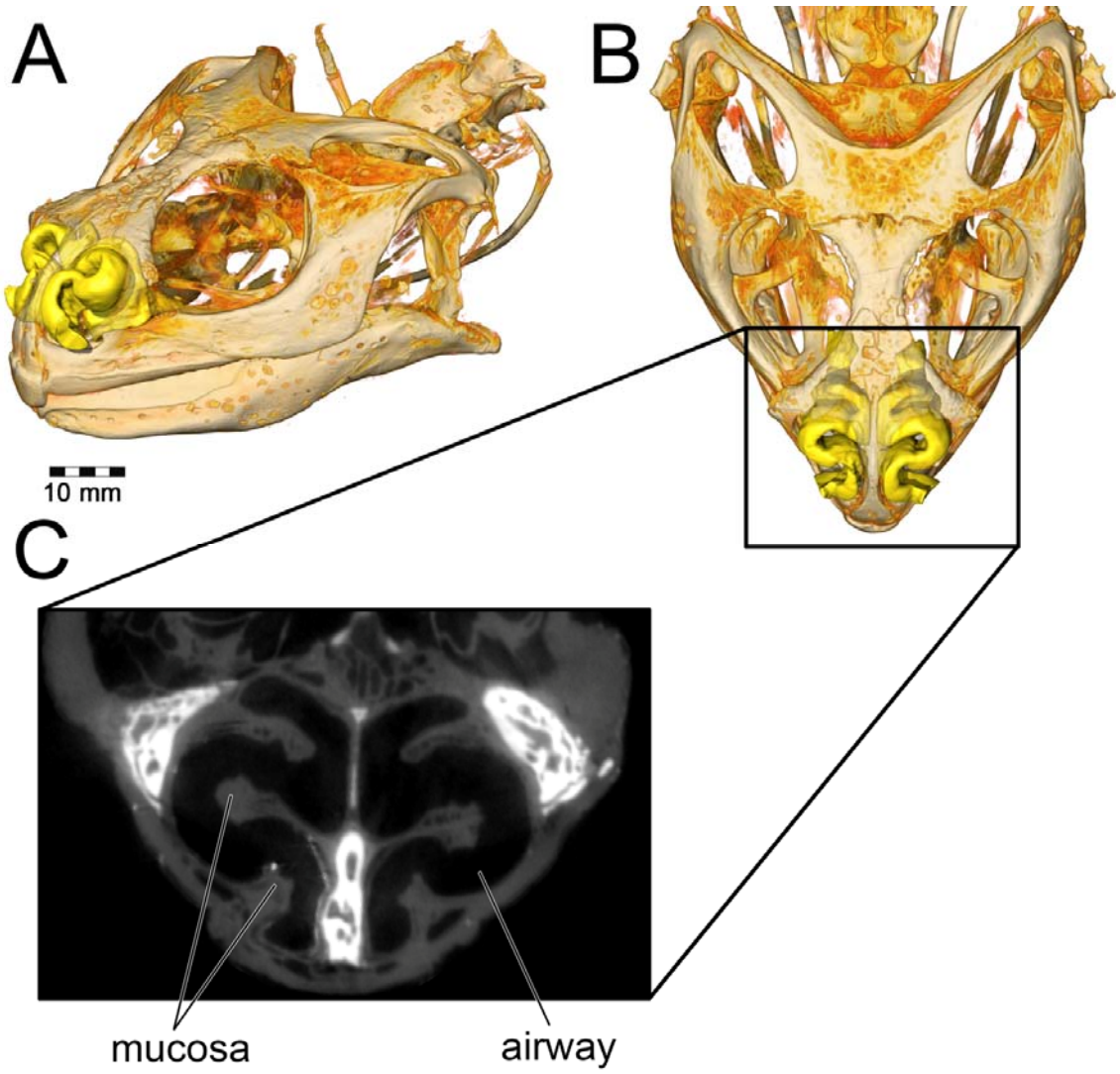

Figure 6-24. Airway of the lizard *Uromastyx aegyptia* (OUVC 10688) in (A) oblique left lateral and (B) dorsal view. As with ankylosaurs, the nasal passage (yellow) exhibits convolutions that increase surface area. (C) Horizontal CT slice image reveals that "slabs" of mucosa are responsible for compressing the airway. It is likely that these mucosal slabs are well vascularized, which would aid in heat and water savings during respiration in this taxon.

Thesis and Dissertation Services